Entanglement and decoherence in cosmology and in analogue gravity experiments

Amaury Micheli

université PARIS-SACLAY

Entanglement and decoherence in cosmology and in analogue gravity experiments

Intrication et décohérence en cosmologie et dans les expériences de gravité analogue

Thèse de doctorat de l'université Paris-Saclay

École doctorale n°564 : physique en Île-de-France (PIF)
Spécialité de doctorat : Physique
Graduate School : Physique. Référent : Faculté des Sciences d'Orsay

Thèse préparée dans l'unité de recherche **IJCLab** (Université Paris-Saclay, CNRS), sous la direction de **Christos CHARMOUSIS**, Directeur de recherche, la co-direction de **Jérôme MARTIN**, Directeur de recherche, et le co-encadrement de **Scott J. ROBERTSON**, Professeur Junior

Thèse soutenue à Paris, le 15 Septembre 2023, par

Amaury MICHELI

Composition du jury

Membres du jury avec voix délibérative

Chris WESTBROOK Directeur de Recherche CNRS, Institut d'Optique Graduate School	**Président**
Ivan AGULLO Professeur associé (eq. HDR), Louisiana State University	**Rapporteur & Examinateur**
Silke WEINFURTNER Professeur, University of Nottingham	**Rapportrice & Examinatrice**
Andreas ALBRECHT Professeur Distingué, University of California, Davis	**Examinateur**
David KAISER Professeur, Massachusetts Institute of Technology	**Examinateur**

THESE DE DOCTORAT
NNT : 2023UPASP078

université PARIS-SACLAY | ÉCOLE DOCTORALE Physique en Île-de-France (PIF)

Titre : Intrication et décohérence en cosmologie et dans les expériences de gravité analogue
Mots clés : Gravité analogue, Cosmologie, Décohérence, Intrication, Espace-temps Courbe.

Résumé :

Cette thèse est consacrée à l'analyse de la création et destruction de corrélations quantiques dans le contexte de l'inflation cosmologique et d'une expérience analogue du préchauffage. L'inflation est une phase d'expansion accélérée de l'Univers, précédant le modèle dit standard de la cosmologie, introduite pour résoudre certaines lacunes du modèle. L'inflation fournit également un mécanisme d'émergence des inhomogénéités primordiales par amplification de fluctuations quantiques initiales. Elle est suivie d'une période de "réchauffement", durant laquelle on s'attend à ce que la plupart des particules soient générées et atteignent l'équilibre thermique, préparant ainsi le terrain pour le déroulement du modèle standard de la cosmologie. Pendant une période de "préchauffage", cette création procède en partie par excitation paramétrique de modes résonants des champs de matière initialement dans leur vide, un véritable processus quantique. La physique de l'inflation cosmologique et du préchauffage est celle d'un champ classique fort agissant sur un champ quantique pour produire des particules intriquées. Lorsque la source est la métrique de l'espace-temps elle-même, comme dans l'inflation, nous sommes dans le cadre de la théorie quantique des champs en espace-temps courbe (TQCEC). L'évolution des corrélations quantiques ainsi générées est le sujet de cette thèse. Dans la première partie du manuscrit, nous présentons le traitement quantique standard des perturbations cosmologiques durant l'inflation. Nous passons ensuite en revue les travaux antérieurs analysant la génération de corrélations quantiques entre des perturbations d'impulsions opposées à l'aide de mesures de «quanticité» telles que la non-séparabilité, la discorde quantique ou une inégalité de Bell. Partant de cette revue, nous présentons un calcul de l'évolution de la discorde quantique pour l'état des modes d'impulsions opposées lorsque la distillation des corrélations aux degrés de liberté environnementaux, appellée décohérence, est prise en compte à l'aide d'un modèle de Caldeira-Leggett. La décohérence place les perturbations dans un état comprimé mixte à deux modes, omniprésent dans le TQCEC et la physique quantique à basse énergie. Nous identifions les régimes dans lesquels les corrélations quantiques persistent malgré la décohérence et les régimes dans lesquels elles disparaissent. Enfin, nous procédons à une comparaison systématique des résultats de trois mesures différentes de quanticité appliquées au même état mixte comprimé à deux modes et démontrons un degré d'inéquivalence entre eux. La seconde partie du manuscrit est dédiée à l'analyse d'une expérience dite de "gravité analogue". La gravité analogue a émergé des travaux fondateurs de W. Unruh qui a proposé de concevoir des expériences de matière condensée pour tester les prédictions de la TQCEC dans un contexte où l'intrication peut, en principe, être mesurée. Depuis 2008, plusieurs groupes ont mené des expériences pour observer les propriétés de quasi-particules émises soit par un trou noir analogue, soit par l'analogue d'un univers en expansion. Nous nous concentrons ici sur une expérience imitant la dynamique du préchauffage à l'aide d'un gaz quasi unidimensionnel d'atomes d'hélium métastables, qui, lors de sa première réalisation, n'a pas pu mettre en évidence l'intrication. Il a ensuite été postulé qu'un degré suffisant d'interactions des quasi-particules pouvait expliquer cette absence. Nous commençons par passer en revue la génération de paires intriquées dans l'expérience et discutons l'absence d'intrication. Nous analysons ensuite les interactions du gaz de Bose unidimensionnel pour démontrer l'existence de nouveaux processus de dissipation pour les excitations générées au cours de l'expérience. Enfin, nous montrons l'effet de ces mêmes processus sur la corrélation. Nous concluons qu'ils pourraient être suffisants pour expliquer l'absence d'intrication dans l'expérience.

université PARIS-SACLAY | ÉCOLE DOCTORALE Physique en Île-de-France (PIF)

Title: Entanglement and decoherence in cosmology and in analogue gravity experiments
Keywords: Analogue gravity, Cosmology, Decoherence, Entanglement, Curved Spacetime.

Abstract:

This thesis is dedicated to analysing the generation and destruction of quantum correlations in the context of inflationary cosmology and an experiment of 'analogue' preheating. Inflation is a phase of accelerated expansion of the Universe, preceding the so-called Standard Model of Big Bang cosmology, introduced to solve some shortcomings of this model. It also provides a mechanism for the emergence of primordial inhomogeneities by amplification of initial quantum fluctuations. Inflation is followed by a 'reheating' period, in which most particles are expected to be generated and reach thermal equilibrium, setting the stage for the standard Big Bang of cosmology. During a 'preheating' period, this creation proceeds partly by parametric excitation of resonant modes of the matter fields initially in their vacuum, a genuine quantum process. The physics of both situations, inflation and preheating, is that of a strong classical field acting on a quantum field to produce entangled (quasi-)particles. When the classical source is the space-time metric itself, as in inflation, we are in the framework of Quantum Field Theory in Curved Space-time (QFTCS). The evolution of the generated quantum correlations is the topic of this PhD.

In the first part of the manuscript, we present the standard quantum treatment of cosmological perturbations during inflation. We then review previous works analysing the generation of quantum correlations between opposite momenta perturbations using measures of 'quantumness' such as non-separability, quantum discord or Bell inequalities. Building upon them, we present a computation of the evolution of quantum discord for the state of opposite momenta modes when the distillation of correlations to environmental degrees of freedom, i.e. decoherence, is taken into account using a Caldeira-Leggett model. Decoherence places the perturbations in a mixed two-mode squeezed state, ubiquitous in QFTCS and low-energy quantum physics. We identify regimes in which quantum correlations persist despite decoherence and regimes in which they disappear. Finally, we systematically compare the results of three different measures of quantumness applied to the same mixed two-mode squeezed state and demonstrate a degree of inequivalence between them.

The second part of the manuscript is devoted to a so-called 'analogue gravity' experiment. Analogue gravity ideas emerged from the seminal works of W. Unruh, who proposed designing condensed matter experiments to test the predictions of QFTCS in a context where entanglement can, in principle, be measured. Since 2008 several groups have performed experiments to observe the properties of quasi-particles emitted either by an analogue black hole or by the analogue of an expanding universe. We here focus on an experiment mimicking the dynamics of preheating using a quasi-one dimensional gas of metastable Helium atoms, which in its first run failed to witness entanglement. It was later postulated that a sufficient degree of quasi-particle interactions could explain its absence. We start by reviewing the generation of entangled pairs in the experiment and the ensuing discussion on the absence of entanglement. We then analyse the interactions of one-dimensional Bose gas and uncover new dissipation processes for the excitations generated during the experiment. Finally, we show the effect of the same processes on correlation. We conclude that they might be sufficient to explain the absence of entanglement in the experiment.

Remerciements

Je souhaiterais remercier toutes les personnes que j'ai côtoyées, rencontrées, croisées au cours des quatre années de préparation de cette thèse. Sa forme et son contenu ne seraient pas les mêmes sans ces innombrables interactions.

En premier lieu, je pense à double titre à Renaud Parentani, avec qui j'ai travaillé pendant les premiers mois de ma thèse. Premièrement, parce que l'étude de la dissipation dans un système analogue réalisée dans la thèse est la poursuite directe d'un axe de recherche qu'il a initié et, il me semble, l'achèvement du sujet de stage que nous avions effectué ensemble avant le début de ma thèse. Également, car lors de mes travaux sur la quanticité des perturbations cosmologiques, la seconde moitié de cette thèse, je n'ai cessé d'être impressionné par l'acuité et le caractère précurseur de ses contributions au domaine.

Je tiens ensuite à remercier toutes les personnes qui m'ont permis de poursuivre ma thèse après une première année difficile. Tout d'abord mes deux directeurs, Jérôme Martin et Scott Robertson, qui ont bien voulu assumer ce rôle alors qu'ils n'avaient rien demandé. Ils ont été des directeurs géniaux d'un point de vue humain et ils sont probablement les personnes avec qui j'apprécie le plus de faire de la physique. À ce titre, je remercie aussi Vincent Vennin, pour sa gentillesse, mais aussi parce que j'ai toujours un immense plaisir à travailler avec lui. Je remercie également Christos Charmousis pour son soutien immédiat et ses conseils constants, ainsi que pour avoir signé tous les papiers administratifs pendant trois ans (sans rechigner).

Évidemment, je ne pourrais remercier suffisamment Hsiao-Yin pour m'avoir soutenu (et supporté) durant des années éprouvantes, et m'avoir aidé à prendre les bonnes décisions. Je remercie mes parents, mon frère et toute ma famille pour leur accompagnement depuis bien plus que quatre ans.

Cette thèse doit beaucoup aux personnes qui ont contribué à ce que ses conditions de réalisation soient agréables. Je remercie énormément l'IAP (Institut d'Astrophysique de Paris) dans son ensemble pour son accueil, notamment le groupe $\mathcal{GR}\varepsilon\mathbb{C}\mathcal{O}$ et l'équipe informatique. Un immense merci à tou.te.s les doctorant.e.s de l'IAP qui ont joué un rôle essentiel dans ma motivation et mon épanouissement. Merci à Aline, Louis et Nai qui ont partagé mon bureau. Merci aux membres du club café de l'IAP Étienne, Marko et Nai (encore). Merci à celleux

avec qui je n'ai pas partagé un bureau ou une machine à café, mais avec qui j'ai passé des moments formidables, notamment Alix, Axel, Clément, Denis, Eduardo, Emma, Emilie, Ira, Julien, Louise, Matthieu, Marie, Marko, Pierre, Quentin.

À l'extérieur de l'IAP, je remercie Thomas, un autre membre de la petite équipe intéressée par les aspects quantiques des perturbations cosmologiques et maintenant un bel ami, Victor, un autre amateur d'intrication qui subit mes délires de théoriciens dans la bonne humeur, ainsi que Chris, Denis et Quentin, le reste de la sympathique équipe collaborant sur COSQUA, Giulia, Florian et Tim, mes codoctorant.e.s de feu le LPT, Bartjan, Eugeny (in particular for explaining clearly the mapping between scalar-tensor theory and $f(R)$ gravity), Gatien, Karim, Marie et Sarah, toujours du LPT.

Un grand merci à mes ami.e.s Alan, Benjy(s), Cyril, Daniel, Danilo, Dina, Étienne, JB, Léa, Lisheng, Louis, Ludo, Luisa, Matthieu(s), Naïla, Nilo, Virginie.

Je suis également très reconnaissant envers mes professeurs de mathématiques du lycée Bernard Palissy, en particulier M. Akkouche, Mme et M. Puyou, qui, par la diversité de leurs enseignements, m'ont fait découvrir le plaisir de la résolution de problèmes.

A big thank you to David Wands and Greg Kaplanek for their warm reception at ICG and Imperial College.

Finally, I also want to thank the members of the websites Physics Forum and StackExchange, where I have many times find detailed and enlightening contributions, especially when preparing classes.

This work was supported by the French National Research Agency via Grant No. ANR-20-CE47-0001 associated with the project COSQUA (Cosmology and Quantum Simulation).

Synthèse en français

Cette thèse est consacrée à l'analyse de la création et destruction de corrélations quantiques dans le contexte de l'inflation cosmologique et d'une expérience analogue du préchauffage.

L'inflation est une phase d'expansion accélérée de l'Univers, précédant le modèle dit standard de la cosmologie, introduite pour résoudre certaines lacunes du modèle. L'inflation fournit également un mécanisme d'émergence des inhomogénéités primordiales par amplification de fluctuations quantiques initiales. Elle est suivie d'une période de "réchauffement", durant laquelle on s'attend à ce que la plupart des particules soient générées et atteignent l'équilibre thermique, préparant ainsi le terrain pour le déroulement du modèle standard de la cosmologie. Pendant une période de "préchauffage", cette création procède en partie par excitation paramétrique de modes résonants des champs de matière initialement dans leur vide, un véritable processus quantique. La physique de l'inflation cosmologique et du préchauffage est celle d'un champ classique fort agissant sur un champ quantique pour produire des particules intriquées. Lorsque la source est la métrique de l'espace-temps elle-même, comme dans l'inflation, nous sommes dans le cadre de la théorie quantique des champs en espace-temps courbe (TQCEC). L'évolution des corrélations quantiques ainsi générées est le sujet de cette thèse.

Le premier chapitre du manuscrit 1 fait office d'introduction aux domaines dans lesquels les contributions de la thèse s'inscrivent : la cosmologie inflationnaire et les expériences dites de "gravité analogue". La première partie du chapitre 1.1 est une présentation de la description standard de l'évolution de l'Univers considéré en première approximation comme homogène. Ce traitement est basé sur la relativité générale dont les fondamentaux nécessaires sont tout d'abord rappelés en section 1.1.1. Nous utilisons ensuite 1.1.2 cette théorie appliquée aux différentes composantes de l'Univers considérées comme homogènes et isotropes, hypothèse justifiée par les observations, pour dériver la géométrie de l'espace-temps (un Univers en expansion décrit par la métrique de Friedmann-Robertson-Lemaitre-Walker) et les équations régissant leur évolution (équations de Friedmann et équation d'état). En se basant sur ces équations et sur les observations donnant la composition actuelle de l'Univers, nous présentons 1.1.3 le modèle standard de la cosmologie décrivant l'histoire de celui-ci comme une succession d'ères. Chacune de ses ères est caractérisée par la domination de la composition de l'Univers par une de ses composantes, et un taux d'expansion qui lui est associé. Cette première partie se conclut 1.1.4 par une explication de certains problèmes associés au modèle standard de la cosmologie: problème de la platitude, de l'horizon et des

monopoles.

Dans la seconde partie du chapitre 1.2 nous présentons le modèle d'inflation cosmique, les prédictions associées pour l'état des inhomogénéités dans l'Univers, ainsi que comment cette période se connecte avec le modèle standard de la cosmologie via une période de (p)réchauffement. L'inflation cosmique correspond à une période d'expansion *accélérée* de l'Univers, par opposition aux périodes du modèle standard où le taux d'expansion est décroissant. Nous commençons 1.2.1 par montrer qu'une période suffisamment longue d'expansion accélérée permet de résoudre les trois problèmes du modèle standard détaillés précédemment. Nous montrons ensuite comment une telle période d'inflation peut survenir si la composition de l'Univers est dominée par un champ scalaire homogène, l'inflaton, avec un potentiel suffisamment plat pour que son évolution soit lente (conditions de roulement lent). Dans 1.2.3, nous introduisons la description perturbative standard des inhomogénéités dans l'Univers, leur caractère perturbatif étant justifié par leur petitesse observée. Nous dérivons ensuite les équations d'évolution des perturbations pendant l'inflation qui prédisent une amplification de celles-ci. De plus, les grandes échelles d'énergie attendues pour l'inflation, suggèrent de décrire les perturbations par des champs quantiques. Nous montrons que ce caractère quantique fixe un niveau minimal pour ces inhomogénéités si nous choisissons de considérer leur champ comme initialement sans particules. L'expansion de l'Univers amplifie ensuite ces fluctuations du vide, un phénomène de TQCEC. Le spectre de puissance des inhomogeneités prédit par ce scénario d'amplification des fluctuations du vide est en parfait accord avec les données du fond diffus cosmologique. À l'issue d'une période d'inflation, l'Univers est essentiellement vide de particule. Afin de connecter cette période avec le modèle standard de la cosmologie, qui suppose un grand nombre de particules à l'équilibre, une période de réchauffement est nécessaire. Nous discutons du réchauffement dans la dernière section de ce chapitre 1.2.4, ainsi que du scénario de préchauffage, mentionné précédemment, dans lequel des particules sont créées par des amplifications paramétriques provoquées par les oscillations de l'inflaton au fond de son potentiel. Il s'agit là encore d'un effet de TQCEC.

La troisième et dernière partie 1.3 du chapitre d'introduction est consacrée à une présentation des expériences de gravité analogue. Tout d'abord 1.3.1, nous motivons l'utilité de telles expériences par quelques calculs d'ordre de grandeur montrant la difficulté d'observer directement un effet de TQCEC où la création de particules depuis le vide quantique médiée par la gravité. Nous démontrons ensuite 1.3.2 que les équations décrivant les perturbations de grande longueur d'onde d'un fluide peuvent être mises sous la forme de celle d'un champ scalaire évoluant dans un espace-temps courbe. La métrique de cet espace-temps est appelée métrique acoustique. Dans 1.3.3 nous passons rapidement en revue les progrès im-

portant effectué dans la conceptualisation et la réalisation d'expérience analogue en général. Enfin, dans 1.3.4, nous procédons à une revue plus exhaustive des expériences faisant une analogie avec une situation cosmologique.

Le second chapitre 2 comprend les travaux effectués durant la thèse sur le caractère quantique ou classique des perturbations cosmologiques. Comme détaillé dans le premier chapitre, dans le scénario standard de formation des structures, les inhomogénéités primordiales sont le résultat de fluctuations du vide quantique amplifiées par la gravité, notamment pendant l'inflation. Il est bien connu que l'état quantique qui en résulte est, pour les variables appropriées, un état comprimé à deux modes (two-mode squeezed state) pour les modes de Fourier de direction opposés $\pm\boldsymbol{k}$. Ces aspects standards des perturbations cosmologiques quantiques sont décrits en détail dans l'article de revue reproduit dans la seconde partie du chapitre 2.2. Cet article passe également en revue l'état de l'art des discussions sur le caractère quantique ou classique des perturbations avant et jusqu'au milieu de la thèse. En particulier, nous revenons sur l'affirmation qu'un état très comprimé serait classique en le présentant rigoureusement et en n'en montrant les limites: cela n'est vrai qu'en considérant la valeur de certains opérateurs. Nous décrivons un certain nombre d'autres mesures de quanticité, basées sur les corrélations au sein de l'état comprimé, qui ont été appliquées aux perturbations cosmologiques (séparabilité, inégalités de Bell, discorde quantique, etc.) et qui montrent au contraire que l'état contient des corrélations quantiques. Enfin, nous discutons les quelques articles prenant en compte l'effet que l'interaction des deux modes avec d'autres champs peut avoir sur les corrélations, phénomène dit de décohérence. Il est attendu que la décohérence affaiblisse les corrélations et leur enlève tout caractère quantique. Les travaux effectués dans le contexte cosmologique tendent à confirmer cette intuition tout en montrant qu'il y a une compétition entre la décohérence et la compression de l'état pour déterminer le niveau de corrélation. Dans la partie suivante 2.3 nous reproduisons l'article rédigé pendant cette thèse consacré à l'évolution de la discorde quantique des perturbations cosmologiques en présence de décohérence. Les premières parties de l'article sont applicables au calcul de la discorde bipartite d'un champ scalaire dans un état gaussien. Nous commençons par montrer la dépendance de la discorde dans le choix de la "partition" du champ en groupe de degrés de libertés. Nous décrivons ensuite l'évolution de la discorde en l'absence de décohérence en utilisant plusieurs formalismes. Le cœur de l'analyse est contenu dans la troisième partie où l'évolution du système est suivie en présence de décohérence décrite par un modèle de Caldeira-Leggett qui préserve le caractère gaussien de l'état. Ceci nous permet de garder un formalisme simple pour le calcul de la discorde tout en autorisant une paramétrisation de l'interaction par sa dépendance temporelle dans le facteur d'échelle. Pour faciliter la compréhension de cette évolution, nous introduisons des paramètres de

compression généralisés qui permettent une représentation géométrique simple de l'état, même en présence de décohérence. Enfin, nous appliquons ces résultats au cas des perturbations cosmologiques qui fixe la dépendance temporelle du champ en absence de décohérence. Nous montrons que deux régimes existent : l'un où la décohérence est suffisamment forte pour effacer toute discorde, l'autre où la discorde, et donc les corrélations quantiques, restent larges à la fin de l'inflation. Dans la dernière partie 2.4, nous reproduisons un article de la thèse comparant différentes mesures de quanticité pour les états comprimés à deux modes décohérés que nous avons étudiés dans l'article précédent. Ces états émergent dans de multiples contextes physique. L'article est en conséquence très générique et rédigé dans un langage de théorique quantique de l'information. Pour ces états, l'effet de la décohérence est paramétrisé simplement par la valeur de la pureté de l'état, qui décroit avec le degré d'interaction avec l'environnement. De tels états sont dits mixtes. Nous montrons que, même pour cette classe simple d'états mixtes, les critères sont inéquivalents, mais que pour tous les critères, la nature classique ou quantique de l'état est le résultat d'une compétition entre le niveau de pureté et le niveau de compression.

Le troisième chapitre décrit les progrès effectués dans la description théorique 3 d'une expérience de préchauffage analogue utilisant un gaz d'Hélium métastable piégé dans un piège magnétique quasi unidimensionnel. Nous commençons 3.2 par décrire l'idée générale de l'expérience et les paramètres du gaz étudié. Nous revenons ensuite 3.3 en détails sur la modélisation de l'expérience. Nous décrivons ce qu'est un état condensé, suivons la dynamique du gaz dans l'approximation d'une condensation complète puis étudions l'évolution de la partie non condensée via l'approche de Bogoliubov-de Gennes. Le rôle des oscillations de l'inflaton dans le préchauffage qui produit une amplification paramétrique des autres champs dans l'Univers est joué dans l'expérience par l'oscillation radiale de la partie condensée du gaz qui génère des excitations longitudinales dans la partie non condensée. L'oscillation radiale est produite par une modulation de la fréquence de piégeage radiale. Nous étudions la dynamique des excitations longitudinales en absence, puis en présence de modulation. Nous montrons dans ce dernier cas que la modulation produit une compression des modes normaux de direction opposées $\pm k$ en espace de Fourier. Cette compression se traduit par une création de paires de quasi-particules corrélées. L'analogie avec le préchauffage et les moyens de mesurer cette production sont détaillés dans la partie suivante 3.3.3. En particulier, nous insistons sur la nécessité de mesurer la non-séparabilité des paires produites afin de certifier qu'elles ont émergés du vide quantique et non d'une stimulation de la population thermique préexistante. Nous revenons également dans cette partie sur les résultats expérimentaux obtenus dans la première réalisation de l'expérience qui n'avait pas réussi à démontrer la non-séparabilité des paires. Il avait alors été

suggéré que des interactions entre les paires produites pouvaient détruire les corrélations quantiques. La suite de ce chapitre consiste précisément en l'étude de ces interactions afin d'évaluer leur capacité à faire disparaitre les corrélations quantiques générées dans l'expérience. Nous commençons 3.3.4 par expliquer que le caractère unidimensionnel du gaz nous oblige à adopter un schéma perturbatif en termes de densité et de phase pour pouvoir utiliser l'approche de Bogoliubov-de Gennes. Ce schéma perturbatif est ensuite utilisé dans l'article reproduit dans la partie suivante 3.4 dans lequel il est montré que les interactions entre modes normaux peuvent mener au transfert des excitations produites vers d'autres modes, faisant effectivement décroitre le nombre et la corrélation des modes normaux produits. Les interactions dominantes sont des processus dit de Beliaev et Landau stimulés par la population thermique de quasi-particules. Une quasi-particule créée dans un mode donné peut-être transférée dans un mode voisin par collision avec une quasi-particule thermique. Nous calculons le temps de vie des quasi-particules dans un mode donné dû à ces processus. L'article s'appuie largement sur des simulations numériques basées sur l'approximation de Wigner tronquée pour modéliser l'évolution du gaz. Ces simulations confirment nos prédictions analytiques et en particulier le temps de vie calculé pour les modes normaux. Nous donnons des détails supplémentaires sur ces simulations dans la partie 3.5. Enfin, dans la dernière partie 3.6 nous présentons nos derniers résultats sur le temps de vie de la corrélation entre les modes normaux. Ce temps de vie apparait égal à celui de la population des modes. Cette égalité des temps de vie était une hypothèse du modèle effectif utilisé dans la littérature pour décrire l'effet des interactions sur la production de quasi-particules. En se basant sur un seuil estimé dans la littérature, nous montrons que les processus que nous avons identifiés semblent suffisants pour expliquer l'absence de corrélation quantique dans la première réalisation de l'expérience. Il s'agit du résultat majeur pour cette partie de la thèse.

La dernière partie revient sur les résultats obtenus durant la thèse et proposent quelques directions possibles de poursuite directe des travaux ainsi que des perspectives plus larges pour les domaines dans lesquels ils s'insèrent.

Contents

Structure of the manuscript

In this thesis, we have considered time-dependent scenarios relevant to cosmology and considered the amplification of quantum fluctuations in such scenarios. The analysis focused on the evolution of the 'quantumness' of the amplified fluctuations. We conducted this study in the case of inflationary cosmology and an 'analogue' preheating experiment. In order to make this thesis by published works as self-contained as possible, we start in Chapt. 1 with a long introduction. It first goes over the necessary basics of relativistic cosmology in Sec. 1.1. In Sec. 1.2, we then review the motivations for cosmic inflation, its simplest implementation via single field slow-roll inflation and the consequences for the statistics of primordial inhomogeneities as well as, very briefly, for the production of particles in the early Universe. In the latest part of the introduction, Sec. 1.3, we briefly introduce analogue gravity experiments. Following this introduction, in Sec. 2, we reproduce the articles published during the PhD about quantum aspects of cosmological perturbations [1, 2, 3]. The following chapter, Chapt. 3, is then dedicated to the analogue preheating experiment studied during this PhD. The first sections explain in detail the set-up of the experiment. We also review the results of a series of publications of which the contribution of this PhD [4] is a continuation. Finally, in the last chapter Chapt. 4, we draw some conclusions on the work done and give possible directions for what could be investigated next.

1 - Introduction

1.1 Homogeneous cosmology

We start this manuscript with a general presentation of cosmology. This presentation is relatively standard and inspired by several textbooks [5, 6], as well as lectures given at the ICFP master in Paris by Jérôme Martin, Sébastien Renaux-Petel and Marios Petropoulos.

1.1.1 Gravity described by general relativity

Cosmology is the study of the history of the universe on large scales, typically scales larger than the typical distance in between galaxies i.e. $d \gg 1\text{Mpc} \approx 10^{22}\text{m}$ [6]. What are the relevant physical ingredients to take into account over these scales? Of the four fundamental interactions (gravity, electromagnetic, weak and strong forces), gravity is the one that dominates on cosmological scales. First, the two latter have a very short range of interaction, while electromagnetic force and gravity have an infinite range. Of these two, gravity is by far the weakest. For instance the gravitational attraction between an electron and a proton is 40 orders of magnitude smaller than the electromagnetic one. Still, electromagnetic charges can be positive and negative, leading to the phenomenon of screening. Therefore, on cosmological scales, assuming the universe to be charge neutral, the electromagnetic force plays no role, and gravity will be the main player in defining the evolution of cosmological structures. Currently, the most accurate theory describing the gravity force is General Relativity (GR) formulated by Einstein [7]. We briefly recap the mathematical and physical concepts of GR necessary for the discussions in this manuscript and refer to [8, 5, 6] for further details. In GR, events, e.g. the emission/reception of a particle, are represented as points on a 4-dimensional Lorentzian manifold $\mathcal{M}$. A manifold is a space for which the neighbourhood of any event looks like that of Special Relativity: events $\mathcal{E}$ are represented by 4-vectors $x_{\mathcal{E}} = (ct, \boldsymbol{x})$ in $\mathbb{R} \times \mathbb{R}^3$ and the spacetime distance in between two infinitesimally close events $\mathcal{E}_1$ and $\mathcal{E}_2$ such that $x^\mu_{\mathcal{E}_2} = x^\mu_{\mathcal{E}_1} + \mathrm{d}x^\mu$ is given by

$$\mathrm{d}s^2 = \eta_{\mu\nu}\mathrm{d}x^\mu \mathrm{d}x^\nu \,, \tag{1.1}$$

where the 2-tensor $\eta_{\mu\nu}$ is the Minkowski metric

$$\eta_{\mu\nu} = \begin{pmatrix} -1 & 0 & 0 & 0 \\ 0 & 1 & 0 & 0 \\ 0 & 0 & 1 & 0 \\ 0 & 0 & 0 & 1 \end{pmatrix} . \tag{1.2}$$

We adopt for the rest of this manuscript the mostly-pluses convention $(-+++)$ for the signature of the metric [6]. The Lorentzian manifolds used in GR are precisely equipped with a globally defined metric tensor $g_{\mu\nu}$ that locally, by choosing an appropriate system of coordinates, reads like the Minkowski metric $\eta_{\mu\nu}$. $g_{\mu\nu}$ dictates how distances and time duration between events are measured at a given manifold point. Generically the spacetime distance between infinitesimally close events reads

$$\mathrm{d}s^2 = g_{\mu\nu}(x)\,\mathrm{d}x^\mu \mathrm{d}x^\nu\,. \tag{1.3}$$

In GR the metric encodes all the information about the geometry of spacetime. It is a *dynamical* quantity, which is affected by the matter-energy content of spacetime. Einstein's field equations give the relation in between the two

$$G_{\mu\nu} = \frac{8\pi G_\mathrm{N}}{c^4} T_{\mu\nu}\,, \tag{1.4}$$

where $G_{\mu\nu}$ is the Einstein tensor, and $T_{\mu\nu}$ is the stress-energy tensor characterising the matter-energy content. $G_{\mu\nu}$ is related to the Ricci tensor $R_{\mu\nu}$, and the scalar curvature R, by

$$G_{\mu\nu} = R_{\mu\nu} - \frac{1}{2} R g_{\mu\nu}\,. \tag{1.5}$$

These two quantities are related to the Riemann tensor $R^\mu{}_{\nu\rho\sigma}$ by

$$R = R^\mu{}_\mu; \quad R_{\mu\nu} = R^\alpha{}_{\mu\alpha\nu} \tag{1.6}$$

The Riemann tensor itself is completely built from second-derivatives of the metric[1]

$$R^\mu{}_{\nu\rho\sigma} = \partial_\rho \Gamma^\mu_{\nu\sigma} - \partial_\sigma \Gamma^\mu_{\nu\rho} + \Gamma^\mu_{\rho\lambda}\Gamma^\lambda_{\nu\sigma} - \Gamma^\mu_{\sigma\lambda}\Gamma^\lambda_{\nu\rho} \tag{1.7}$$

where

$$\Gamma^\mu_{\nu\rho} = \frac{1}{2} g^{\mu\lambda}\left(\partial_\nu g_{\rho\lambda} + \partial_\rho g_{\nu\lambda} - \partial_\lambda g_{\nu\rho}\right)\,, \tag{1.8}$$

is the Levi-Civita connection. Einstein's field equations (1.4) can be derived from an action principle. The evolution of the metric is described by the Einstein-Hilbert action

$$S_\mathrm{EH} = \frac{c^3}{16\pi G}\int \mathrm{d}^4x\sqrt{-g}\,R\,, \tag{1.9}$$

where g is the determinant of the metric $g_{\mu\nu}$, while that of matter is described by the action

$$S_\mathrm{m} = \frac{1}{c}\int \mathrm{d}^4x\sqrt{-g}\,\mathcal{L}_\mathrm{m}\,, \tag{1.10}$$

[1] Different conventions exist for the expression of the components of the Riemann tensor. We follow the conventions of [6].

where $\mathcal{L}_m$ is a Lagrangian describing the behaviour of matter fields. Defining

$$T_{\mu\nu} = \frac{-2}{\sqrt{-g}} \frac{\delta \sqrt{-g}\, \mathcal{L}_{\mathrm{m}}}{\delta g^{\mu\nu}} \,, \tag{1.11}$$

Eq. (1.4) is equivalent to the Euler-Lagrange equations for the total action $S = S_{\mathrm{EH}} + S_{\mathrm{m}}$ varied with respect to $g^{\mu\nu}$. Once the metric of spacetime is known, we can compute the trajectories of test bodies i.e. bodies whose energy is small enough so that the modification they induce on the local metric can be neglected as a first approximation e.g. photons, dust grains or satellites. The spacetime trajectories $\underline{X}(u) = \{x^\mu(u)\}$ of such test bodies, where u is an affine parameter, are given by the *geodesics* curves of this spacetime. Affinely parameterised geodesics are solutions of

$$\frac{\mathrm{d}^2 x^\mu}{\mathrm{d}u^2} + \Gamma^\mu_{\nu\lambda} \frac{\mathrm{d}x^\nu}{\mathrm{d}u} \frac{\mathrm{d}x^\lambda}{\mathrm{d}u} = 0 \,. \tag{1.12}$$

This equation is a generalisation to curved spacetime of Newton's second law (in a gravitational field), and there are several ways to derive it. Eq. (1.12) can, for instance, be derived by requiring that test bodies going from $\underline{X}(u_1)$ to $\underline{X}(u_2)$ follow trajectories whose spacetime length is locally extremal in the sense that this length $\ell = \int_{u_1}^{u_2} \mathrm{d}s(u)$ is stationary under infinitesimal changes around the trajectory [5]. For massive particles, the 4-velocity $\mathrm{d}\underline{X}(u)/\mathrm{d}u$ is time-like, i.e. $g_{\mu\nu} \frac{\mathrm{d}x^\mu}{\mathrm{d}u} \frac{\mathrm{d}x^\nu}{\mathrm{d}u} < 0$, and u can be chosen to be the proper time τ associated to the particle rescaled by its mass $u = c\tau/m$ (which changes the dimension of this parameter) so that

$$g_{\mu\nu} \frac{\mathrm{d}x^\mu}{\mathrm{d}\tau} \frac{\mathrm{d}x^\nu}{\mathrm{d}\tau} = -m^2 \,. \tag{1.13}$$

Then

$$\underline{P} = m \frac{\mathrm{d}\underline{X}(\tau)}{\mathrm{d}\tau} = \left(\frac{E}{c}, P^i \right) \,, \tag{1.14}$$

is the energy-momentum vector of the particle. E is the energy of the particle, while $p = \sqrt{g_{ij} P^i P^j}$ is its physical three-momentum, such that $E^2 = p^2 c^2 + m^2 c^4$ by normalisation of the vector. For massless particles, e.g. photons, there is no notion of proper time and $\mathrm{d}\underline{X}(u)/\mathrm{d}u$ is such that

$$g_{\mu\nu} \frac{\mathrm{d}x^\mu}{\mathrm{d}\tau} \frac{\mathrm{d}x^\nu}{\mathrm{d}\tau} = 0 \,. \tag{1.15}$$

The parameter u can still be chosen so that $\underline{P} = \mathrm{d}\underline{X}(u)/\mathrm{d}u$ is the energy-momentum vector of the particle [6, 5]. The normalisation of the 4-vector then gives $E = pc$. The geodesic equation Eq. (1.12) can be conveniently rewritten as

$$P^\mu \nabla_\mu P^\nu = 0 \,, \tag{1.16}$$

valid for massive and massless particles, where ∇_μ is the covariant derivative with respect to the Levi-Civita connection.

1.1.2 General relativistic cosmology

Having reviewed the necessary basics of general relativity, we can apply the theory to the distributions of energy and matter in the Universe on large scales.

1.1.2-a Geometry of the Universe: FLRW

It is an observational fact that the distribution of matter in the (observable) Universe is isotropic on large scales, larger than 100Mpc [5].[2] We assume, in addition, that we, human observers, do not occupy a specific spatial position in the Universe and that the Universe, therefore, would appear as isotropic from any other location. It is the so-called cosmological principle [8], and implies that the Universe is also homogeneous. The isotropy and homogeneity of the Universe translate in the mathematical framework of GR as the existence of a class of coordinate systems i.e. of observers, in which the metric is invariant by translation and rotation. One can show that the metric in such coordinates is then of the Friedmann-Lemaître-Robertson-Walker (FLRW) form [8]. The line element reads

$$\mathrm{d}s^2 = -c^2\mathrm{d}t^2 + a^2(t)\left(\frac{\mathrm{d}r^2}{1-\mathcal{K}r^2} + r^2\mathrm{d}\theta^2 + r^2\sin^2\theta\mathrm{d}\varphi^2\right), \tag{1.17}$$

where the time coordinate t is referred to as cosmic time, (r, θ, φ) are the spherical *co-moving* coordinates, $\mathcal{K}$ is called the spatial curvature, and $a(t)$ is the scale factor. The scale factor is the only dynamical quantity in Eq. (1.17). The evolution of the homogeneous cosmological spacetime thus boils down to that of $a(t)$.

1.1.2-b Time and distances in expanding Universe

Let us briefly discuss how to describe distances and time intervals in cosmology with the FLRW metric. We start with the spatial curvature $\mathcal{K}$. First, notice that if $\mathcal{K} = 0$ and $a(t) = 1$, the FLRW metric reduces to the Minkowski metric in spherical coordinates. For $\mathcal{K} \neq 0$, we can always set $\mathcal{K} = \pm 1$ by re-parameterising the comoving coordinates $\boldsymbol{r}' = \sqrt{\mathcal{K}}\,\boldsymbol{r}$ and $a' = a/\sqrt{\mathcal{K}}$. Notice that the density parameter for curvature $\Omega_\mathcal{K} = \mathcal{K}/a^2$, see Sec. 1.1.2-d for the origin of this quantity, is invariant under such re-parameterisation. Generically, the spatial metric induced by the metric (1.17) on $t = \text{cst}$ hypersurfaces lead to the standard 3-dimensional Euclidian distance for $\mathcal{K} = 0$, and to the geodesic distance over a unit sphere (respectively hyperbola) for $\mathcal{K} = +1$ (resp. $\mathcal{K} = -1$). $\mathcal{K}$ thus encodes the geometry of the spatial sections of the Universe. Let us now consider an arbitrary scale factor $a(t)$ and assumes $\mathcal{K} = 0$ for simplicity. We compute the *physical* distance in between two points located at fixed co-moving coordinates $\boldsymbol{r}_1 = (r_1, 0, 0)$ and $\boldsymbol{r}_2 = (r_2, 0, 0)$, as a function of cosmic time t. This physical distance is given

[2] We ignore the CMB dipole attributed to the peculiar velocity of our local group, or we work in a coordinate system boosted with respect to Earth so that this dipole is eliminated.

by integrating the induced metric on $t = cst$ hypersurfaces in between these two points

$$d = \int_{r_1}^{r_2} \sqrt{g_{ij} \mathrm{d}x^i \mathrm{d}x^j} = a(t) \left| r_1 - r_2 \right| , \tag{1.18}$$

where the summation using Latin indices, such as i, is limited to spatial indices, as opposed to summation using Greek indices, such as μ, which covers all spacetime coordinates. The scale factor $a(t)$, which evolves as a function of cosmic time, leads to dilation or contraction of the physical distances in the Universe. We come back to this point at the end of this part. What are the trajectories of test bodies in such an expanding Universe? To answer, we have to solve the geodesics equation, Eq. (1.16). The Christoffel symbols for the FLRW metric and the computation details are given in Appendix A.1. Two special cases are worth mentioning. First, test bodies at rest in co-moving coordinates i.e. with no peculiar velocity $\mathrm{d}x^r/\mathrm{d}u = 0$, follow geodesics curves. Such bodies are called *co-moving* observers. Their proper time τ corresponds to cosmic time t. A second important case is that of photons. In Appendix A.1, it is shown that if we consider a photon received today at t_0 and trace back its evolution until an earlier time t, we find that

$$E(t) = \frac{a_0}{a(t)} E_0 \, , \tag{1.19}$$

where E_0 is its energy, as seen by a co-moving observer, when received. The energy of a photon is directly related to its frequency via $E = h\nu$ where h is the Planck constant. Therefore, independently of its reception frequency ν_0, the photon was redshifted by an amount given by

$$\frac{\nu}{\nu_0} = \frac{a_0}{a} = 1 + z \, , \tag{1.20}$$

where z is called the redshift. z is a convenient proxy to parameterise the evolution of quantities in the FLRW metric. First, the redshift of a light source can be directly measured by spectroscopy i.e. by comparing the frequencies of lines in the spectrum of the source to their tabulated values e.g. [9]. Additionally, contrary to cosmic time t, the use of the redshift z to label the time of occurrence of different events, e.g. emission of lights from different astrophysical objects, does not depend on the details of the evolution of $a\,(t)$. Therefore, in the rest of this text, we often refer to the redshift of events rather than their time of occurrence. We give a list of approximate redshifts used in the manuscript in Tab. 1.1.

We close this discussion with a few words on the notion of distances in cosmology. Notably, neither the physical nor the co-moving distance between two objects can be directly measured in cosmology. The information we have about objects in astrophysics and cosmology comes from the light (and, in a few instances, the gravitational waves) that they emit. By measuring it, we try to infer the distance

z_{GUT} (without inflation)	$z_{\mathrm{dec}\,\nu}$	z_{BBN}	z_{LSS}	z_{eq}	z_{m}
10^{29}	6×10^9	4×10^8	1090	3400	0.297

Table 1.1: Approximate values of redshift used in the manuscript. The approximation z_{GUT} is computed in Sec. 1.1.3-c. $z_{\mathrm{dec}\,\nu}$ and z_{BBN} are taken from Tab. 3.1 of [6]. z_{LSS} is reported in [10, 11] where it is named $z_\star$. The approximations z_{eq} and z_{m} are computed in Sec. 1.1.3-a.

to the object. For instance, in a Newtonian spacetime, the perceived flux L_{R} of a static object located at a distance d from us decays as

$$L_{\mathrm{R}} = \frac{L_{\mathrm{E}}}{4\pi d^2}\,, \tag{1.21}$$

where L_{E} is the luminosity emitted, and we assumed the emission to be isotropic. Therefore, if we know L_{E}, by measuring L_{R}, we can infer the distance to the object d. Because light propagation from the source is affected by the expansion of the Universe, this relation breaks down in FLRW Universe. If we define the luminosity distance d_{L} by

$$L_{\mathrm{R}} = \frac{L_{\mathrm{E}}}{4\pi d_{\mathrm{L}}^2}\,, \tag{1.22}$$

we find that [5]

$$d_{\mathrm{L}}(t_{\mathrm{R}}) = d_{\mathrm{E/R}}(t_{\mathrm{E}})\left(1 + z_{\mathrm{E/R}}\right)^2\,, \tag{1.23}$$

where $d_{\mathrm{E/R}}(t_{\mathrm{E}}) = a(t_{\mathrm{E}})r_{\mathrm{E/R}}$ is the physical distance to the source at the time of emission, and $z_{\mathrm{E/R}} = a(t_{\mathrm{R}})/a(t_{\mathrm{E}}) - 1$ is the redshift to the source. Therefore, if we trust the description of cosmology based on GR, in order to compute the physical distance to an object we also need an independent measure of its redshift $z_{\mathrm{E/R}}$. We can also view Eq. (1.23) as a prediction of cosmological models with an expanding/contracting Universe which can be tested. Generically, $z_{\mathrm{E/R}}$ depends on the time of emission and reception of light, so on the distance to object $d_{\mathrm{E/R}}$. This relation depends on the details of the evolution of $a(t)$ i.e. on the considered cosmological model. Still, for sources close enough such that $z_{\mathrm{E/R}} \ll 1$, we can derive the approximate relation

$$d_{\mathrm{L}}(t_{\mathrm{R}}) \approx \frac{z_{\mathrm{E/R}}}{cH\left(t_{\mathrm{R}}\right)}\,, \tag{1.24}$$

where

$$H = \frac{\dot{a}}{a}\,, \tag{1.25}$$

is the rate of expansion of the Universe and is called the Hubble parameter. Eq. (1.24) can be tested by plotting the luminosity distance of objects as a function of their measured redshifts (correcting for any Doppler effect). The first to put forward this linear relationship and to use observational data to extract the rate was Lemaître in 1927 [12]. It was also identified by Hubble in [13], whose name is now given to the relation of Eq (1.24). The analysis was later repeated with more accurate data and confirmed the result. The expansion of the Universe is the first confirmed prediction of GR-based cosmology. We will present others later on.

1.1.2-c Energy-matter content of the Universe

Having detailed the basic features of the FLRW metric in full generality, we want to compute the precise dynamics of the scale factor $a(t)$ in cosmology. It is given by Einstein's field equations (1.4). The Einstein tensor on the left-hand side is entirely determined by the metric and Eqs. (1.5-1.8). The right-hand side depends on the matter-energy content of the Universe, which we now specify. The average distribution of matter, represented by the stress-energy tensor $T_{\mu\nu}$, has to be compatible with the homogeneity and isotropy observed. One can show [6] that the matter must then be described by a *perfect fluid*. The stress-energy tensor of a generic perfect fluid reads

$$T^{\mu\nu} = (\rho + p)\,\frac{u^\mu u^\nu}{c^2} + p g^{\mu\nu}\,, \tag{1.26}$$

where ρ is the energy density of the fluid, p its pressure and u^μ its 4-velocity vector normalised to $g_{\mu\nu}u^\mu u^\nu = -c^2$. Notice that this expression is covariant. Imposing that the fluids composing the Universe appear isotropic and homogeneous to co-moving observers further requires that the fluid is co-moving i.e. $u^\mu = (c, \mathbf{0})$ in co-moving coordinates; the fluid is at rest and the energy density ρ and pressure p are a function of time t but independent of $\boldsymbol{x}$. Then $T^{\mu\nu}$ assumes the simple form

$$T^{\mu\nu} = \begin{pmatrix} \rho & 0 & 0 & 0 \\ 0 & p & 0 & 0 \\ 0 & 0 & p & 0 \\ 0 & 0 & 0 & p \end{pmatrix}\,. \tag{1.27}$$

1.1.2-d Friedmann's equations

In the presence of a collection of perfect fluids, Einstein's field equations (1.4) reduce to the two Friedmann equations [5, 6]

$$H^2 = \frac{8\pi G_{\rm N}}{3c^2}\sum_i \rho_i - \frac{\mathcal{K}c^2}{a^2}\,, \tag{1.28}$$

$$\frac{\ddot{a}}{a} = -\frac{4\pi G_{\rm N}}{3c^2}\sum_i (\rho_i + 3p_i)\,. \tag{1.29}$$

where H was defined in Eq (1.25). Additionally, we assume that each perfect fluid is separately covariantly conserved i.e. we neglect conversion between the different species of fluid

$$\nabla_\mu T_i^{\mu\nu} = 0 \iff \dot{\rho}_i + 3H\left(\rho_i + p_i\right) = 0\,, \tag{1.30}$$

where $T_i^{\mu\nu}$ is the stress-energy tensor associated to the ith fluid.[3] To close the system of equations, we have to specify the relation between the energy density of the fluid and its pressure. This relation is called the equation of state of the fluid and depends on the nature of each fluid. The linear ansatz

$$p = w\rho\,, \tag{1.31}$$

where w is called the equation of state parameter, covers most of the relevant cases, e.g. pressure-less matter corresponds to $w = 0$, and radiation to $w = 1/3$. Combining Eq. (1.30) and Eq. (1.31), we get the evolution of the energy density of the fluid

$$\rho\left(t\right) = \rho_0 \left[\frac{a_0}{a\left(t\right)}\right]^{3(1+w)}\,, \tag{1.32}$$

where ρ_0 and a_0 are the quantities evaluated at present time.

1.1.3 Standard model of Big Bang cosmology

1.1.3-a Composition of the Universe

In the standard model of cosmology, we summarise the Universe's composition in four components: baryonic matter, cold dark matter, radiation and dark energy. We will denote respectively ρ_b, ρ_cdm, ρ_γ and ρ_Λ their densities. The same subscripts are used for the pressure and all quantities related to a specific form of matter. Baryonic and cold dark matters are taken to be pressure-less perfect fluids with $w_\mathrm{m} = 0$.[4] Because they dilute identically, we gather them in a single energy density ρ_m. Radiation is a perfect fluid with $w_\gamma = 1/3$. Dark energy is modelled by a *cosmological constant* Λ added to the spatial curvature in the action (1.9) such that

$$S_\Lambda = \frac{c^3}{16\pi G_\mathrm{N}} \int \mathrm{d}^4x\sqrt{-g}\left(R - 2\Lambda\right)\,. \tag{1.33}$$

This results in the modified field equations

$$G_{\mu\nu} + \Lambda g_{\mu\nu} = \frac{8\pi G_\mathrm{N}}{c^4} T_{\mu\nu}\,. \tag{1.34}$$

[3] The covariant conservation of the total stress-energy tensor is a consequence of Einstein's field equations and not an additional assumption. In the case of a single fluid Eq. (1.30) can then be derived from Eqs. (1.28)-(1.29).

[4] The adjective 'cold' precisely refers to the fact that this unknown form of matter behaves as a pressure-less fluid as opposed to a relativistic one $w \sim 1/3$ [6].

H_0	$\Omega_{\rm b}^{(0)}h^2$	$\Omega_{\rm cdm}^{(0)}h^2$
67.36 ± 0.54	0.02237 ± 0.00015	0.1200 ± 0.0012
$\Omega_\Lambda^{(0)}$	$\Omega_\mathcal{K}^{(0)}$	$T_\gamma^{(0)}$
0.6847 ± 0.0073	0.0007 ± 0.0019	2.72548 ± 0.00057

Table 1.2: Values of the cosmological parameters given at 68% confidence. The values for H_0, $\Omega_{\rm b}^{(0)}h^2$, $\Omega_{\rm cdm}^{(0)}h^2$, $\Omega_\Lambda^{(0)}$ and $\Omega_\mathcal{K}^{(0)}$ are based on the results of the mission *Planck* [11] where $h = H_0\,(100\,\mathrm{km}\times\mathrm{s}^{-1}\times\mathrm{Mpc}^{-1})^{-1}$. They are obtained by performing a Markov Chain Monte Carlo (MCMC) analysis on the temperature and polarisation power spectra of the CMB, see Sec. 1.2.3, combined with lensing information. The first four values are obtained by assuming a spatially-flat, $\Omega_\mathcal{K}^{(0)} = 0$, ΛCDM model with adiabatic, Gaussian initial fluctuations. H_0 and $\Omega_\Lambda^{(0)}$ are best-fit directly quoted from the paper. The value of $\Omega_\mathcal{K}^{(0)}$ comes from an MCMC analysis performed over *Planck* data combined with BAO data, where the curvature is included as an extra parameter. The value of the CMB photons' temperature $T_\gamma^{(0)}$ is reported from [14].

While the cosmological constant in this presentation appears in the 'geometry' part of the action, the $\Lambda g_{\mu\nu}$ term can be moved to the right-hand side of the field equations and understood as the stress-energy tensor of a perfect fluid with energy density $\rho_\Lambda = \Lambda c^4/8\pi G$ and equation of state parameter $w_\Lambda = -1$. Dark energy is then seen as a type of matter with *negative* pressure. The standard model of Big Bang cosmology is often referred to as the Lambda-CDM model precisely because it features a cosmological constant Λ as dark energy and cold dark matter in addition to ordinary matter. We will come back to the necessity of introducing dark matter and dark energy in Sec. 1.1.3-c, and focus here on describing the physical content of the Lambda-CDM model.

The first Friedmann equation (1.28) can be rewritten by dividing by the critical energy density

$$\rho_{\rm c}(t) = \frac{3H^2(t)c^2}{8\pi G_{\rm N}}\,. \tag{1.35}$$

It reads

$$\Omega_{\rm b} + \Omega_{\rm cdm} + \Omega_\gamma + \Omega_\Lambda + \Omega_\mathcal{K} = 1\,, \tag{1.36}$$

where we have defined the density parameters for each fluid $\Omega_X = \rho_X/\rho_{\rm c}$. Each density parameter can then be understood as the contribution of the fluid to the total density of energy in the Universe. Let us say a few words about the contribution of the spatial curvature. We can treat the spatial curvature as a fictitious perfect

fluid at the level of Friedmann equations by taking its contribution to Eq. (1.28) to be its energy density $\rho_\mathcal{K} = -3M_{\rm Pl}^2\mathcal{K}/a^2$. Accordingly we take $w_\mathcal{K} = -1/3$ so that (1.32) is verified and that the contribution of curvature to Eq. (1.29) vanishes. Still, notice that the resulting density parameter can contribute positively or negatively to (1.36) depending on whether the Universe is closed or open $\mathcal{K} = \mp 1$. The measured values of the cosmological parameters at present time[5] are given in the table Tab. 1.1.3-a. From these, we can compute the values of all density parameters at present time. From the values of $\Omega_{\rm b}^{(0)}h^2$, $\Omega_{\rm cdm}^{(0)}h^2$ and H_0, we find $\Omega_{\rm b}^{(0)} \approx 0.049$ and $\Omega_{\rm cdm}^{(0)} \approx 0.264$. Finally, radiation encompasses all types of relativistic species. We assume that neutrinos are still relativistic today and we assume that their number is dominated by that in the Cosmic Neutrino Background, and similarly for photons, see Sec. 1.2.3. Then we have a simple relation between the density of photons and that of neutrinos [11]

$$\rho_\nu = 3.046 \times \frac{7}{8} \times \left(\frac{7}{11}\right)^{4/3} \rho_\gamma \,. \tag{1.37}$$

In general, the energy density of relativistic fluid at thermal equilibrium is directly related to its temperature

$$\rho = \frac{\pi^2}{30} g X \frac{(k_{\rm B}T)^4}{(\hbar c)^3} \,. \tag{1.38}$$

g is the number of degrees of freedom of the particle, e.g. $g_\gamma = 2$ for the two helicities of the photons, or $g_{e-} = 2$ because the electron has spin 1/2 and so two spin states. The factor X differentiates between bosons $X = 1$ and fermions $X = 7/8$. Using the relation of Eq. (1.38) for the photons of the CMB at temperature $T_\gamma^{(0)}$ we can compute ρ_γ, and deduce ρ_ν. Combining the two and taking the value of H_0 given in Tab. 1.1.3-a we find the density parameter of radiation $\Omega_\gamma^{(0)} = 9.21 \times 10^{-5}$; the contribution of radiation is negligible at present time.

From the present-day values of the density parameters, and knowing how each fluid dilutes (1.32), we can infer the composition of the Universe at any past time as a function of the redshift z, see Fig. 1.1. We observe a succession of three different 'eras', where the energy density of one fluid is orders of magnitude larger than that of the others. First, we have the present-day dark-energy-dominated era. Before that, we had a matter-dominated era and, even earlier, a radiation-dominated era. We can compute the redshifts of transition between these different eras by equating the density parameters of the relevant dominant contributions, e.g. between dark energy and matter, to find the redshift at which the matter

[5] All quantities evaluated at present time will be shown with an exponent (0) or an index 0.

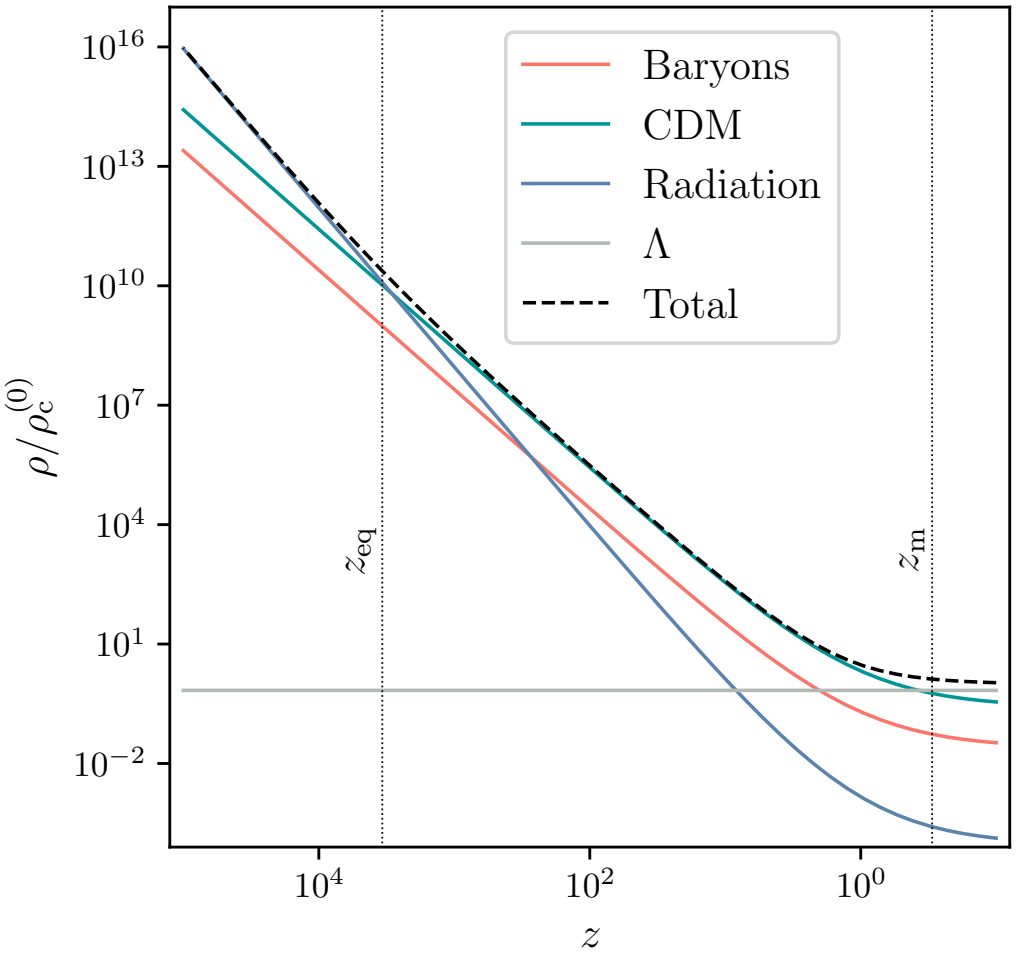

Figure 1.1: Energy densities of the different constituents ρ_i as a function of the redshift z in logarithmic scale. The dominant constituent is seen to vary with redshift. The dotted lines show the approximate transition redshifts given in Tab. 1.1.

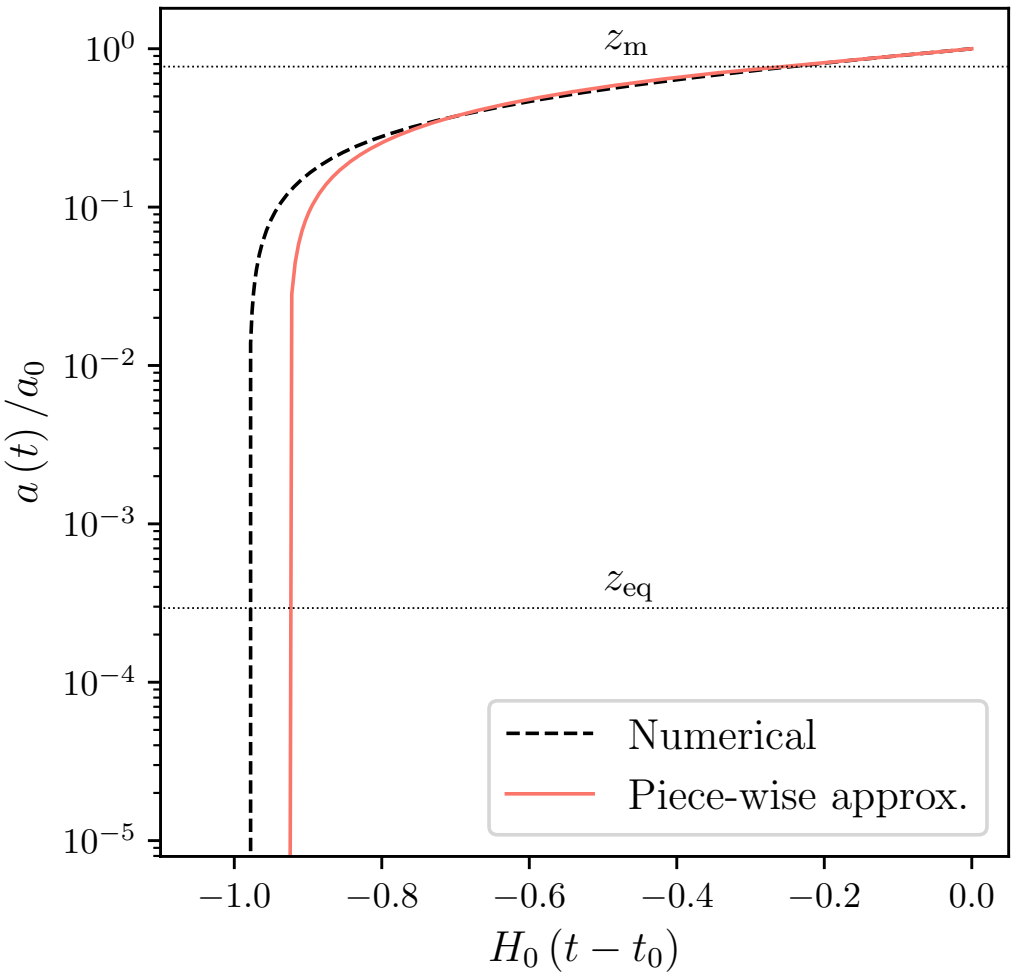

Figure 1.2: Evolution of the scale factor $a(t)$ as a function of cosmic time t. The dashed curve is obtained by numerically solving Eq. (1.28) backwards in time starting from present-day values given in Tab. 1.1.3-a. The red curve shows the piece-wise approximation computed in Eq. (1.40). The dotted lines show the approximate redshifts of transition given in Tab. 1.1.

domination era ended. We have

$$z_{\rm m} = \left[\frac{\Omega_\Lambda^{(0)}}{\Omega_{\rm m}^{(0)}}\right]^{1/3} - 1\,, \tag{1.39a}$$

$$z_{\rm eq} = \frac{\Omega_{\rm m}^{(0)}}{\Omega_\gamma^{(0)}} - 1\,, \tag{1.39b}$$

where $z_{\rm m}$ (resp. $z_{\rm eq}$) is the redshift when the contributions of dark energy and matter (resp. matter and radiation) are equal. This last time is often referred to as 'equality' time, hence its label. The numerical values obtained using the values of cosmological parameters given in Tab. 1.1.3-a are given in Tab. 1.1 Notice that the curvature is measured to be negligible at present time. In fact, since its value is currently small compared to that of matter and radiation, then it has always been negligible and will always be. Indeed, as we go back in time to smaller values of $a(t)$, the contributions of matter and radiation grow faster than that of curvature, respectively, as $\rho_{\rm m} \approx a^{-3}(t)$ for matter, and $\rho_\gamma \approx a^{-4}(t)$ for radiation, versus $\rho_\mathcal{K} \approx a^{-2}(t)$ for curvature. In addition, since the budget is now dominated by dark energy, whose energy density is constant, while curvature's contribution dilutes, it will not dominate in the future as well.

One may wish to describe the evolution of the composition of the Universe as a function of cosmic time t, rather than as a function of the scale factor a. That requires solving the dynamics of the scale factor $a(t)$ as a function of t given by Eq. (1.28). In the case where a single fluid X dominates and we can neglect the other contributions in (1.28), the equation is easily solved. For a collection of fluids, it can either be solved numerically or by assuming instantaneous transitions between the different eras where a single fluid dominates the energy budget. Following the second route, and requiring the scale factor a and the overall energy density ρ to be continuous at the transitions[6], we get a piece-wise approximation of the dynamics. It reads

$$\frac{a(t)}{a_0} = \begin{cases} e^{-H_0(t_0-t)} & \text{for } t > t_{\rm m}\,, \\ \frac{1}{1+z_{\rm m}}\left[1+\frac{3}{2}H_0\,(t-t_{\rm m})\right]^{2/3} & \text{for } t_{\rm m} > t > t_{\rm eq}\,, \\ \frac{1}{1+z_{\rm eq}}\left[1+2H_0\left(\frac{1+z_{\rm eq}}{1+z_{\rm m}}\right)^{3/2}(t-t_{\rm eq})\right]^{1/2} & \text{for } t_{\rm eq} > t > t_{\rm BB}\,, \end{cases} \tag{1.40}$$

where $t_{\rm m}$ is the time when the contributions of dark energy and matter are equal, and $t_{\rm eq}$ is the time of equality. $t_{\rm BB}$ is the time of Big Bang defined by $a(t_{\rm BB}) = 0$. $t_0 - t_{\rm BB}$ is then the age of the Universe. We emphasise that the value of these times depends on the precise dynamics of the scale factor. In the piece-wise

[6]Notice that by Eq. (1.28) it implies that H is continuous as well.

approximation above, their expressions in terms of the redshift of transition can be obtained by evaluating the above equations at transition time. Using the dynamics of the scale factor in Eq. (1.40) and the dilution equation, Eq. (1.32), we get the dynamics of the total energy density

$$\frac{\rho(t)}{\rho_{\rm c}^{(0)}} = \begin{cases} 1 & \text{for } z_{\rm m} \geq z\,, \\ \left(\frac{1+z}{1+z_{\rm m}}\right)^3 & \text{for } z_{\rm eq} \geq z \geq z_{\rm m}\,, \\ \left(\frac{1+z_{\rm eq}}{1+z_{\rm m}}\right)^3 \left(\frac{1+z}{1+z_{\rm eq}}\right)^4 & \text{for } z \geq z_{\rm eq}\,. \end{cases} \tag{1.41}$$

This evolution of the scale factor and density from present time is plotted in Fig. 1.2.

1.1.3-b Thermal history of the Universe

According to Eq. (1.40), as we go back in time, the scale factor decreases, and the energy density of the fluids in the Universe increases, see Fig. 1.2. Earlier times are therefore associated with larger energies. Generically we can associate an energy scale E to a given total energy density ρ via [6]

$$E = \left(\hbar^3 c^3 \rho\right)^{1/4} = \sqrt{\hbar}\, c \left(3H^2 M_{\rm Pl}^2\right)^{1/4} = \left(24\pi H_{\rm in}^2 t_{\rm Pl}^2\right)^{1/4} M_{\rm Pl} c^2\,, \tag{1.42}$$

where we have used Eq. (1.28) to rewrite the energy scale in terms of the Hubble parameter and introduced the reduced Planck mass $M_{\rm Pl} = \sqrt{\hbar c/8\pi G_{\rm N}}$ and Planck time $t_{\rm Pl} = \sqrt{\hbar G_{\rm N}/c^5}$. In particular, notice that at a finite value of cosmic time $t_{\rm BB}$, the scale factor vanishes so that the energy density of the fluids in the Universe becomes infinite. This is the initial singularity in the Big Bang model. By analogy with the form of the energy density of a single relativistic fluid in Eq. (1.38), and neglecting the energy of curvature and of non-relativistic fluids, we can write [6]

$$\rho = \frac{\pi^2}{30} g_\star(T) \frac{(k_{\rm B}T)^4}{(\hbar c)^3}\,, \tag{1.43}$$

where T is a reference temperature (typically chosen to be that of photons T_γ), and

$$g_\star(T) = \sum_i g_i X_i \left(\frac{T_i}{T}\right)^4\,, \tag{1.44}$$

is called the effective number of degrees of freedom. The sum is over all the fluids making up the budget of the Universe. Notice that here, different species of particles would be treated as a separate fluid, e.g. proton and neutrons, and not summarised in a common baryonic fluid. At early enough time, when the energy is large enough, the constituents of the Universe were in thermal equilibrium in a

primordial plasma at a common temperature T [6]. Then, $g_\star$ is just a weighted sum of the degrees of freedom of the different fluids. Since the density of relativistic species dilutes as a^{-4}, Eq. (1.43) gives an inverse proportionality relation between the temperature and the scale factor $T \propto a^{-1}$.[7] Note that the energy scale E of Eq. (1.42) is then proportional to the temperature. This allows us to discuss the order of occurrence of the different events in the early Universe by referring directly to the temperature and energy of the Universe at that time rather than its redshift.

We follow closely the account of these events made in Chapter 3 of [6]. Unless specified, the order of magnitude of the different quantities are also taken from this reference. First, the proportionality coefficient in Eq. (1.43) is not strictly a constant of time. The composition of the plasma changes, and so does $g_\star(T)$. As the energy increases, atoms and nuclei are shattered by collisions with highly energetic particles. Even the protons and neutrons are eventually shattered into fundamental particles; the larger the energies of the collision, the larger the masses of the particles that can be produced. Ultimately, when the temperature is around 100 GeV, the plasma contains all the fundamental particles of the Standard Model of particle physics. They are then relativistic and at thermal equilibrium. If we consider an extension of the Standard Model, such as Grand Unification Theories (GUT) [15], then at even larger temperature, around $T_{\text{GUT}} \approx 10^{16}$ GeV for GUT [5], other particles would also be present.

We here start our account of the events with Standard Model particles at equilibrium. As temperature decreases, the heaviest particles stop being produced by particle-antiparticle pair creation, and they gradually decay until we are only left with electrons, positrons, protons, neutrons, photons, neutrinos and anti-neutrinos. Initially, photons are trapped in the plasma due to Thompson scattering on electrons, while neutrinos are trapped due to interaction via weak nuclear force. As temperature drops, $T_{\text{dec}\,\nu} \approx 1\,\text{MeV}$ the interaction rate of neutrinos with other species Γ_ν drops below the expansion rate H^{-1} leading to a decoupling of the neutrinos from the plasma. Intuitively, the expansion is pulling away the reagents too fast compared to their typical interaction time for them to have time to interact. After decoupling, the neutrinos free-stream in the Universe. Therefore, the hot Big Bang model predicts a background radiation of neutrinos emitted in the early Universe. Since these neutrinos were at thermal equilibrium, this radiation should be that of a black body at temperature $(1 + z_{\text{dec}\,\nu})^{-1} T_{\text{dec}\,\nu} \approx 1.9\,\text{K}$, where we have redshifted it to its value at present time. Later, when the temperature is below the MeV, around $T_{\text{BBN}} \sim 0.1\,\text{Mev}$ [16], the so-called Big Bang Nucle-

[7] A more correct relation $T \propto g_\star^{-1/3}(T) a^{-1}$ can be obtained by considering the total entropy density [6]. The extra factor of $g_\star^{-1/3}$ accounts for species becoming non-relativistic, so that they drop out of the sum Eq. (1.44), and transferring their entropy to other species.

osynthesis (BBN) [17] starts taking place i.e. protons and neutrons fuse to form nuclei of the lightest atoms, essentially up to the lithium. Only a little bit later, at $T_{\text{rec.}} \approx 0.25 - 0.3\,\text{eV}$, did the free electrons start to combine with protons to form actual hydrogen atoms. Then, since the photons were mainly interacting with free electrons via Thomson scattering, the decrease in the density of free electrons strongly reduced their interaction rate, eventually leading to their decoupling from the plasma at $T_{\text{dec}} \approx 0.25\,\text{eV}$, and $z_{\text{dec}} = 1100$. The hot Big Bang model thus also predicts a background black-body radiation of photons at temperature $(1 + z_{\text{dec}})^{-1} T_{\text{dec}} \approx T_\gamma^{(0)}$ today.

1.1.3-c Experimental confirmation and validity of the Lambda-CDM model

Several predictions of the hot Big Bang model described above have been tested. We mention briefly a few of them in connection with the different aspects discussed previously. First, we already mentioned in Sec. 1.1.2-b that the predicted dynamical character of the distances in the Universe was observed as early as [12, 13]. Second, the model predicts the existence of two background thermal radiations, one made of neutrinos and one of photons, emitted when these particles decouple from the postulated primordial plasma. The Cosmic Neutrino Background (CνB) has not been detected yet, as it is notoriously difficult to measure neutrinos, all the more with such small energies. On the other hand, the Cosmic Microwave Background (CMB) of photons, where microwave refers to the current wavelength of these photons, was detected by Penzias and Wilson in 1965 [18, 19]. It was increasingly better studied by several missions, culminating with the Planck satellite [10]. The temperature of CMB photons is measured [14] to be $T_\gamma^{(0)} \approx 2.7K$, in accordance with the prediction of the hot Big Bang model. The CMB is currently the best window we have in the conditions of the very early Universe, and we will come back to it repeatedly in the rest of this text. Third, the hot Big Bang model, in combination with the standard model of particle physics, predicts the abundance of the different elements produced during BBN. These predictions are in excellent agreement with the abundance measured (except for the abundance of Lithium, the so-called 'cosmological lithium problem') [16]. The hot Big Bang model thus allows us to explain most of the cosmological observations consistently. However, it requires the introduction of dark energy and dark matter, the microphysical nature of which remains elusive [20]. We briefly explain how observations lead to the introduction of dark energy and dark matter in the model. In 1998, the authors of [21, 22] extended the Hubble diagram to larger redshifts by measuring the luminosity distance and the redshift of distant supernovae. Based on a more general version of Eq. (1.24) valid for large redshifts and that parametrically depends on the density parameters of the different fluids $\Omega_i^{(0)}$, they demonstrated that expansion *accelerates* and that some fluid behaving as a cosmological constant

had to be introduced to account for it. This fluid is what we now refer to as dark energy. On the other hand, the existence of dark matter can be seen as coming from observations at three different scales [20]. First, at the galactic scale, where the observed rotation curves of galaxies are in tension with Newtonian dynamics if we consider that the galaxies are only made up of luminous matter. This problem is solved by introducing supplementary matter, which is non-luminous, behaves like a pressure-less fluid and interacts only gravitationally with ordinary matter. Second, at the level of galaxy clusters, a comparison with total mass and luminous mass shows a deficit of gravitating mass that can be made up for by adding dark matter. Finally, at cosmological scales, the measures of the CMB spectra allow us to differentiate between ordinary and dark matter and to constrain their abundances separately.

Despite its multiple successes, the hot Big Bang model cannot be valid until arbitrarily large energies. At the very least, when energies are of the order of the Planck Mass $M_{\rm Pl}c^2 \approx 10^{19}\,\mathrm{GeV}$, we expect quantum gravitational effects to become relevant, and Einstein's equation should not be expected to be valid anymore [23]. Therefore, if we wish to discuss the 'initial conditions' of the model, it is appropriate to set them at energies lower than this Planck scale, but the precise choice is arbitrary. In this manuscript, we choose to set the initial conditions at a temperature close to these where the unification of the fundamental forces is postulated $T_{\rm GUT} \approx 10^{16}\,\mathrm{GeV}$. We can compute the associated redshift using the behaviour of the energy density in a radiation-domination era from Eq. (1.41) and equating it to the energy density at GUT scale given by Eq. (1.43) evaluated at $T_{\rm GUT}$. We take $g_\star\left(T_{\rm GUT}\right) \sim 160$, given for a GUT based on SU_5 in [23], and find

$$z_{\rm GUT} = (1+z_{\rm eq})^{1/4}\,(1+z_{\rm m})^{3/4}\left(\frac{\rho_{\rm GUT}}{\rho_{\rm tot}}\right)^{1/4} - 1 \approx 10^{29}\,. \tag{1.45}$$

1.1.4 The hot Big Bang puzzles

Additionally, the hot Big Bang model still leaves unexplained a few observational facts; these are often referred to as the Big Bang puzzles.

1.1.4-a Horizon problem

First, the CMB is observed to be very isotropic $\Delta T/T \sim 10^{-5}$ once the dipole anisotropy of order $\Delta T_{\rm dip}/T \sim 10^{-3}$, attributed to the motion of the Solar system with respect ot the CMB, is removed [24, 6]. A map of the CMB by Planck is given for illustration in Fig. 1.3. However, based on the Lambda-CDM model, any two points on this map separated by more than 1 degree should correspond to regions that were *causally disconnected* at the time of emission. Indeed, at any cosmic time t, two points are causally connected if they have been able to exchange a photon since Big Bang time. The distance travelled by such a photon is called

the particle horizon $d_{\rm H}$. Its value is computed by following a photon (which we can always arrange to be radial) emitted at Big Bang time $t_{\rm BB}$ and received at time t

$$d_{\rm H}(t) = ca(t)\int_{t_{\rm BB}}^{t}\frac{{\rm d}t'}{a\left(t'\right)}\,. \tag{1.46}$$

Assuming an instantaneous matter-radiation decoupling, all the photons received from the CMB come from the same 3D sphere called the Last Scattering Surface (LSS). If we consider the particle horizon at LSS time $t_{\rm LSS}$ we have

$$d_{\rm H}\left(t_{\rm LSS}\right) = \frac{c\left(1+z_{\rm m}\right)^{3/2}}{H_0}\left(\frac{2}{\sqrt{1+z_{\rm LSS}}}-\frac{1}{\sqrt{1+z_{\rm eq}}}\right)\,. \tag{1.47}$$

We now compute the size of the particle horizon at LSS time using Eq. (1.47). Given the current distance from us to LSS

$$d_{\rm LSS} = ca_0\int_{t_{\rm LSS}}^{t_0}\frac{{\rm d}t'}{a\left(t'\right)} = \frac{c\left(1+z_{\rm m}\right)^{3/2}}{H_0}\left[\frac{2\left(1+z_{\rm m}\right)^2+z_{\rm m}}{\left(1+z_{\rm m}\right)^{3/2}}-\frac{2}{\sqrt{1+z_{\rm LSS}}}\right]\,. \tag{1.48}$$

Combining Eq. (1.47) and Eq. (1.48) we can compute the angular size separating these two points on the CMB

$$\delta\theta_{\rm H} = \arctan\left[\frac{d_{\rm H}(t_{\rm LSS})}{d_{\rm LSS}}\right] \approx \frac{\dfrac{2}{\sqrt{1+z_{\rm LSS}}}-\dfrac{1}{\sqrt{1+z_{\rm eq}}}}{\dfrac{2\left(1+z_{\rm m}\right)^2+z_{\rm m}}{\left(1+z_{\rm m}\right)^{3/2}}-\dfrac{2}{\sqrt{1+z_{\rm LSS}}}}\,, \tag{1.49}$$

where we expanded the arctan at first order, because the angle is small, and computed all the other expressions using Eqs. (1.40). Using the values of Tab 1.1, we find $\delta\theta_{\rm H} \approx 0.017\,{\rm rad.} \approx 1\,{\rm deg.}$ as announced[8]. This corresponds to a solid angle of $4\pi\sin^2\left(\delta\theta_{\rm H}/4\right)$, that is, we have $\sin^{-2}\left(\delta\theta_{\rm H}/4\right) \approx 50000$ regions emitting photons at nearly identical temperatures, while any non-adjacent ones have not enjoyed any physical exchange allowing for equilibrium processes. We would then have to impose by hand that the initial conditions in these different regions were the same or accept that they have been set by processes violating causality. This is the horizon problem.

1.1.4-b Flatness problem

A second puzzle comes from the low value of the spatial curvature density parameter $\Omega_{\mathcal{K}}$. Its value is constrained to be small today $\Omega_{\mathcal{K}}^{(0)} = 0.0007 \pm 0.0019$

[8]For comparison, Moon's angular size seen from Earth is 0.5 deg..

and is compatible with 0. Nevertheless, as detailed above, the contribution of spatial curvature to the energy budget is expected to grow with time compared to that of matter and radiation. Therefore, the fact that curvature is negligible today implies that it has to be fine-tuned to an even tinier value at earlier times. Using Eqs. (1.40), we can compute the evolution of the Hubble parameter and so of the critical energy density as well as the evolution of the curvature energy density. We find that the density fraction of curvature reads

$$\Omega_{\mathcal{K}} = \Omega_{\mathcal{K}}^{(0)} \frac{(1+z_{\rm eq})\,(1+z_{\rm m})^3}{(1+z)^2} \quad \text{for } t_{\rm eq} > t > t_{\rm BB}\,. \tag{1.50}$$

We can then, for instance, evaluate the curvature density parameter at GUT scale $z_{\rm GUT}$ and we find $\Omega_{\mathcal{K}}(z_{\rm GUT}) \approx 10^{-58}$. There is a large degree of arbitrariness in the choice of considering this time rather than a later one. In any case, even if evaluated at much lower energies, the fact still stands that the contribution of curvature is tiny. One could argue that the curvature is simply vanishing $\mathcal{K} = 0$ and that it is to be taken as another initial condition. However, as pointed out in [23], the Universe is not *exactly* described by an FLRW metric, and so the spatial curvature is not a parameter in the model that could be fixed to be vanishing by some symmetry principle justifying that the effect is just not actually realised in the physics we observe. FLRW is an effective description of spacetime on large scales, and the value of the spatial curvature $\mathcal{K}$ is the result of some underlying physical processes. It would thus be more satisfactory to see the flatness of the Universe emerging as the result of a physical process. This is the flatness problem.

1.1.4-c Monopole problem

Finally, the non-observation of magnetic monopoles is also considered a shortcoming of the model. Although absent in the standard model of particle physics, monopoles are present in high-energy extensions of it, e.g. Grand Unification Theories. They are expected to be produced in large numbers [25, 26, 27, 28] in the early Universe when the energy densities get very large so that an observable number should persist until today. Monopoles form upon symmetry breaking when a field transition from a 'fake' vacuum, which has become unstable, to a 'true' vacuum, which is stable. When this vacuum has residual symmetry, the field can be found in different configurations of the new vacuum at different locations in space, forming bubbles of different configurations. Topological defects then appear at the boundaries between these bubbles, and monopoles are part of them. The transition is a causal process, so the size of the region with a given field configuration cannot exceed the size of the particle horizon at that time $d_{\rm H}(t_{\rm GUT})$. We can then put a lower bound on the number density of the monopoles forming on the boundaries of these regions $n_{\rm mon} > d_{\rm H}(t_{\rm GUT})^{-3}$. Monopoles can only annihilate by combining with anti-monopoles, and these interactions are expected to be rapidly suppressed

by the expansion of space [25, 26] so that the number of monopoles is effectively conserved until today. We can then compute the present-time density parameter of monopoles

$$\Omega_{\rm mon}^{(0)} = m_{\rm mon}c^2 \frac{H_0^3}{\rho_{\rm c}} \frac{\left(1+z_{\rm GUT}\right)^3}{\left(1+z_{\rm eq}\right)^{3/2}\left(1+z_{\rm m}\right)^{9/2}}\,, \tag{1.51}$$

where $m_{\rm mon}$ is the mass of a monopole. Taking $m_{\rm mon}c^2 \approx 10^{18}\,$GeV and $z_{\rm GUT} \approx 10^{29}$ we have $\Omega_{\rm mon}^{(0)} \approx 10^{20}$ i.e. monopoles would largely dominate the energy budget of the Universe today! We know it is not the case and that the energy budget is dominated by dark energy. Worse, we have yet to observe any such monopole. Searches for monopoles have constrained their number to 10^{-29} per nucleons [29, 30]. Taking all baryonic matter to be nucleons and assimilating all nucleons to protons of mass $m_{\rm p}c^2 = 938$MeV we get a ratio of monopoles to nucleons of

$$\eta_{\rm mon/b} = \frac{\Omega_{\rm mon}^{(0)}}{\Omega_{\rm b}^{(0)}} \frac{m_{\rm p}}{m_{\rm mon}} \approx 2.5 \times 10^3\,, \tag{1.52}$$

more than 30 orders of magnitude larger than the experimental upper limit. GUT models are then in clear tension with the standard hot Big-Bang model.

1.2 Cosmic Inflation

The idea of cosmic inflation appeared in the study of phase transitions in the early Universe from GUT to the Standard Model [23, 32, 33]. Guth [23] recognised that a period of exponential expansion in the early Universe was a way to solve altogether the three puzzles of the Big Bang model that we detailed in the previous sub-section, Sec. 1.1.4. Shortly after, Linde [32] and Albrecht and Steinhardt [33] proposed a 'new inflation' model to solve some problems related to the end of inflation in Guth's original formulation. This section will present cosmic inflation as a generic possible cosmic era outside its initial study context. First, in Sec. 1.2.1, we show how a sufficiently long period of accelerated expansion solves the Big-Bang puzzles. In Sec. 1.2.2, we then present a standard way to realise inflation using a single field slowly rolling on top of its potential. In Sec. 1.2.3, we show, considering cosmological perturbations, that cosmic inflation gives testable and tested predictions for the statistics of inhomogeneities in the early Universe. Finally, in Sec. 1.2.4, we say a few words about the connection between a period of inflation and the standard succession of eras of the hot Big Bang model.

1.2.1 A solution to Big Bang puzzles

We had previously inferred from the present time values of the different density parameters Ω_i that the Universe was successively dominated by radiation, matter

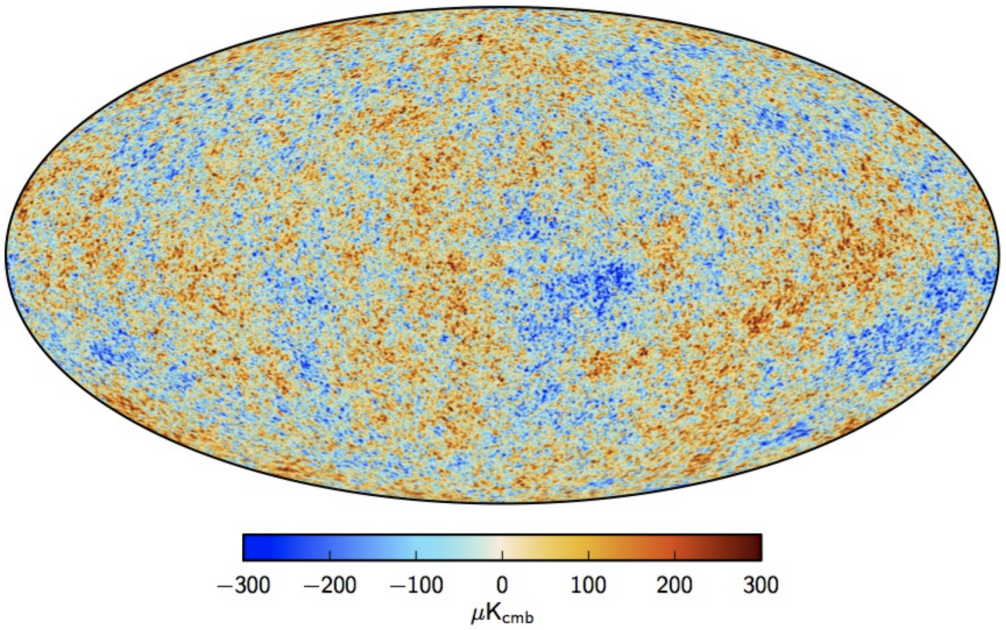

Figure 1.3: CMB map as measured by the satellite Planck [31]. In this map the dipole, attributed to our peculiar velocity with respect to the CMB [24], and the monopole, corresponding to the average thermal emission at $T_\gamma^{(0)} = 2.72548 \pm 0.00057\,\mathrm{K}$ [14], have been subtracted. This map shows the anisotropies of the CMB which reflects the inhomogeneities in the underlying energy-matter content of the Universe at the time of emission.

and finally, dark energy. Let us introduce, during radiation dominated era, a period when another perfect fluid X dominates the energy budget of the Universe between $t_{\rm in}$ and $t_{\rm f}$ so that the scale factor dynamics is modified to

$$\frac{a(t)}{a_0} = \begin{cases} e^{H_0(t_0-t)} & \text{for } t \geq t_{\rm m}, \\ \frac{1}{1+z_{\rm m}}\left[1+\frac{3}{2}H_0(t-t_{\rm m})\right]^{2/3} & \text{for } t_{\rm m} \geq t \geq t_{\rm eq}, \\ \frac{1}{1+z_{\rm eq}}\left[1+2H_0\left(\frac{1+z_{\rm eq}}{1+z_{\rm m}}\right)^{3/2}(t-t_{\rm eq})\right]^{1/2} & \text{for } t_{\rm eq} \geq t \geq t_{\rm f}, \\ \frac{1}{1+z_{\rm f}}\Bigg[1+\frac{3}{2}(w_X+1)H_0 & \\ \qquad \left(\frac{1+z_{\rm eq}}{1+z_{\rm m}}\right)^{3/2}\left(\frac{1+z_{\rm f}}{1+z_{\rm eq}}\right)^{2}(t-t_{\rm f})\Bigg]^{\frac{2}{3(w_X+1)}} & \text{for } t_{\rm f} \geq t \geq t_{\rm in}, \\ \frac{1}{1+z_{\rm in}}\Bigg[1+2H_0\left(\frac{1+z_{\rm eq}}{1+z_{\rm m}}\right)^{3/2} & \\ \qquad \left(\frac{1+z_{\rm f}}{1+z_{\rm eq}}\right)^{2}\left(\frac{1+z_{\rm in}}{1+z_{\rm f}}\right)^{\frac{3}{2}(w_X+1)}(t-t_{\rm f})\Bigg]^{1/2} & \text{for } t_{\rm in} \geq t \geq t_{\rm BB}. \end{cases} \tag{1.53}$$

The evolution of the total energy density is accordingly changed to

$$\frac{\rho(t)}{\rho_{\rm c}^{(0)}} = \begin{cases} 1 & \text{for } z_{\rm m} \geq z\,, \\ \left(\frac{1+z}{1+z_{\rm m}}\right)^3 & \text{for } z_{\rm eq} \geq z \geq z_{\rm m}\,, \\ \left(\frac{1+z_{\rm eq}}{1+z_{\rm m}}\right)^3\left(\frac{1+z}{1+z_{\rm eq}}\right)^4 & \text{for } z_{\rm f} \geq z \geq z_{\rm eq}\,, \\ \left(\frac{1+z_{\rm eq}}{1+z_{\rm m}}\right)^3\left(\frac{1+z_{\rm f}}{1+z_{\rm eq}}\right)^4\left(\frac{1+z}{1+z_{\rm f}}\right)^{3(1+w_X)} & \text{for } z_{\rm in} \geq z \geq z_{\rm f}\,, \\ \left(\frac{1+z_{\rm eq}}{1+z_{\rm m}}\right)^3\left(\frac{1+z_{\rm f}}{1+z_{\rm eq}}\right)^4\left(\frac{1+z_{\rm in}}{1+z_{\rm f}}\right)^{3(1+w_X)}\left(\frac{1+z}{1+z_{\rm in}}\right)^4 & \text{for } z \geq z_{\rm in}\,. \end{cases} \tag{1.54}$$

Notice that the redshift $z(E)$, associated with a certain energy scale E larger than that of inflation, is now pushed to a larger value $z^{\rm infl}(E)$, to account for the extra degree of expansion during inflation. The link between the two can be obtained by equating the energy density of the Universe with and without the inclusion of inflation using Eq. (1.41) and Eq. (1.54). We have

$$1+z^{\rm infl}(E) = [1+z(E)]\, e^{\frac{N}{4}(1-3w_X)}\,, \tag{1.55}$$

where we have introduced the number of e-folds

$$N = \ln\left(\frac{1+z_{\rm f}}{1+z_{\rm in}}\right) = \ln\left(\frac{a_{\rm f}}{a_{\rm in}}\right)\,, \tag{1.56}$$

as a measure of the duration of inflation. We will have to take this change into account to keep fixing the initial condition at GUT scale, now corresponding to

$z_{\mathrm{GUT}}^{\mathrm{infl}}$, to be consistent with our previous computations. We will see that if, during this inflation period, the Universe undergoes an accelerated expansion, then we can solve the three puzzles of the hot Big Bang model. The intuitive reason behind it is that if we start from a locally homogeneous Universe over small regions and blow up any of these regions to be the size of our observable Universe, then the *whole* Universe will appear homogeneous. Additionally, even if initially spatially curved, it will now appear flat as we have 'zoomed in' on a relatively small section of it, making the curvature unnoticeable. Finally, suppose monopoles are produced before or during this period of inflation, and their production rate is small compared to that of expansion. In that case, their density is diluted down to tiny values.

1.2.1-a Horizon problem

First, let us reconsider the particle horizon's angular size today in the CMB. Since the expansion history is unmodified until the radiation domination era, the expression Eq. (1.48) of the co-moving distance to the LSS r_{LSS} is unchanged. Only the expression Eq. (1.47) of the particle horizon r_{H} is modified to

$$\begin{aligned} d_{\mathrm{H}}^{\mathrm{infl}}\left(t_{\mathrm{LSS}}\right) &= \frac{c\left(1+z_{\mathrm{m}}\right)^{3/2}}{H_0}\left\{\frac{2}{\sqrt{1+z_{\mathrm{LSS}}}}-\frac{1}{\sqrt{1+z_{\mathrm{eq}}}}\right. \\ &\left.+\frac{\sqrt{1+z_{\mathrm{eq}}}}{1+z_{\mathrm{f}}}\frac{1-3w_X}{1+3w_X}\left[1-\left(\frac{1+z_{\mathrm{f}}}{1+z_{\mathrm{in}}}\right)^{\frac{3w_X+1}{2}}\right]\right\}, \\ &= d_{\mathrm{H}}\left(t_{\mathrm{LSS}}\right)+\frac{c\left(1+z_{\mathrm{m}}\right)^{3/2}}{H_0}\frac{\sqrt{1+z_{\mathrm{eq}}}}{1+z_{\mathrm{f}}}\frac{1-3w_X}{1+3w_X}\left(1-e^{-\frac{3w_X+1}{2}N}\right). \end{aligned} \tag{1.57}$$

First, notice that if the radiation domination era is uninterrupted i.e. if the additional perfect fluid dominating from $t_{\mathrm{in},}$ to t_{f} behaves as radiation i.e. $w_X = 1/3$, or if the duration of inflation is negligible $N = 0$, then the additional contribution vanishes as it should. Second, for the angular size of the horizon to grow, we need the fluid X to be less stiff than radiation, i.e. $w_X < 1/3$, or else the contribution of the term is negative. In addition, if $w_X > -1/3$, then the term in the exponential is negative, and the term in brackets is bounded by one. The extra contribution will then be negligible because it is suppressed by z_{f} expected to be larger than $z_{\mathrm{BBN}} \sim 10^9$. On the other hand, if $w_X < -1/3$, the contribution is exponential in N. Then, if inflation lasts long enough, we can make the angular horizon $\delta\theta_{\mathrm{H}}$ defined in Eq. (1.49) arbitrarily large. For $w_X < -1/3$, the second Friedmann equation Eq. (1.29) shows that expansion accelerates. Thus, solving the horizon problem requires a phase of *accelerated* expansion. How long should this period last? Let us compute the modification induced by inflation to the size

of the angular horizon at present

$$\delta\theta_{\rm H}^{\rm infl} = \arctan\left[\frac{d_{\rm H}^{\rm infl}(t_{\rm LSS})}{d_{\rm LSS}}\right], \tag{1.58}$$

$$\approx \delta\theta_{\rm H} + \frac{\sqrt{1+z_{\rm eq}}}{1+z_{\rm in}}\frac{1-3w_X}{1+3w_X}e^N\left(1-e^{-\frac{3w_X+1}{2}N}\right) \times \left[\frac{2\left(1+z_{\rm m}\right)^2+z_{\rm m}}{\left(1+z_{\rm m}\right)^{3/2}} - \frac{2}{\sqrt{1+z_{\rm LSS}}}\right]^{-1}. \tag{1.59}$$

We require that this size is larger than the celestial sphere i.e. $\delta\theta_{\rm H}^{\rm infl} > 4\pi$. Assuming that the inflation starts around GUT scale $z_{\rm in} = z_{\rm GUT}^{\rm infl}$, and using Eq. (1.55), we find a lower bound on the number of e-folds that inflation should last. Neglecting $\delta\theta_{\rm H}$, and the 1 in front of the exponential, the condition reads

$$N > 1 + \frac{4}{1-3w_X}\log\left\{4\pi\left[\frac{2\left(1+z_{\rm m}\right)^2+z_{\rm m}}{\left(1+z_{\rm m}\right)^{3/2}} - \frac{2}{\sqrt{1+z_{\rm LSS}}}\right]\frac{1+z_{\rm GUT}}{\sqrt{1+z_{\rm eq}}}\frac{1+3w_X}{1-3w_X}\right\},$$
$$\gtrsim \frac{4}{1-3w_X}\log\left(-10\pi\frac{1+3w_X}{1-3w_X}\frac{z_{\rm GUT}}{\sqrt{z_{\rm eq}}}\right), \tag{1.60}$$

where, in the second line, we have used the values of the different redshifts in Tab. 1.1 to get a simpler estimate of the required number of e-folds. Although the precise number depends on the details of the phase of inflation, in particular on its energy scale, it only does so logarithmically so the order of magnitude will not be modified. Using our estimate $z_{\rm GUT} = 10^{29}$ and assuming that the phase of inflation is powered by a cosmological constant-like fluid $w_X = -1$, we get $N \gtrsim 65$. We will find that roughly the same number of e-folds is required to solve the other Big Bang puzzles.

1.2.1-b Flatness problem

We move on to compute how the curvature density fraction at early times is modified when inflation is included. We had previously computed its value at a certain energy scale in the early Universe and found it to be un-naturally small. With the modified evolution, the curvature density parameter before inflation now reads

$$\Omega_{\mathcal{K}}(z) = \Omega_{\mathcal{K}}^{(0)} e^{(1-3w_X)N}\frac{\left(1+z_{\rm eq}\right)\left(1+z_{\rm m}\right)^3}{\left(1+z\right)^2} \quad \text{for} \quad z \geq z_{\rm in}. \tag{1.61}$$

We want to allow the curvature to be of order unity before the period of inflation starts and compute how much e-folds of inflation this requires. Starting inflation

around GUT scale again we take $\Omega_{\mathcal{K}}\left(z_{\rm GUT}^{\rm infl}\right) \approx 1$, which requires

$$N > \frac{2}{1-3w_X} \ln\left[\frac{1}{\Omega_{\mathcal{K}}^{(0)}} \frac{\left(1+z_{\rm GUT}\right)^2}{\left(1+z_{\rm eq}\right)\left(1+z_{\rm m}\right)^3}\right] \approx 66\,, \tag{1.62}$$

which is almost the same duration as the one required to solve the horizon problem.

1.2.1-c Monopole problem

Finally, we review the monopole problem as well. We assume that the monopole formed after a symmetry breaking before inflation proceeds. We can then repeat the computations of Sec. 1.1.4 to have a lower bound on the density of monopoles, and we have

$$\begin{aligned}\Omega_{\rm mon}^{(0),\rm infl} &= m_{\rm mon}c^2 \frac{H_0^3}{\rho_{\rm c}} \frac{\left(1+z_{\rm GUT}^{\rm infl}\right)^3}{\left(1+z_{\rm eq}\right)^{3/2}\left(1+z_{\rm m}\right)^{9/2}} e^{-\frac{3}{2}N(1-3w_X)}\,, \\ &= \Omega_{\rm mon}^{(0)} e^{-\frac{3}{4}N(1-3w_X)}\,.\end{aligned} \tag{1.63}$$

The estimate of the ratio of the number of monopoles to that of baryons changes to

$$\eta_{\rm mon/b}^{\rm infl} = \eta_{\rm mon/b}\, e^{-\frac{3}{4}N(1-3w_X)}\,. \tag{1.64}$$

To agree with the current observations, we then have to require

$$N > -\frac{4}{3}\frac{1}{1-3w_X} \ln\left(\frac{10^{-29}}{\eta_{\rm mon/b}}\right)\,. \tag{1.65}$$

Evaluating this for a period of inflation powered by a cosmological constant-like fluid, i.e. $w_X = -1$, we find that $N \gtrsim 25$ e-folds of inflation are required, which is the same order of magnitude found for the other problems. Again, changing the fluid parameter w_X, the energy scale of inflation by changing $z_{\rm in}$, or the scale at which we fix the initial condition for curvature, would only marginally change this result as the dependence is logarithmic. The outcome of these computations is that a period of inflation lasting for roughly a 60 e-folds can simultaneously solve the three Big-bang puzzles. This initially constituted the main motivation to introduce such a period [23]. In the next sub-section Sec. 1.2.2 we demonstrate a simple way to realise such a period of inflation.

1.2.2 Single field slow-roll inflation

We have effectively modelled inflation as the interruption of radiation domination era by a phase of domination by another fluid with an equation of state parameter w_X. We then showed that provided this domination is long-enough and leads to an accelerated expansion, i.e. $w_X < -1/3$, we can solve the three

Big-Bang puzzles. We now refer to this period as (cosmic) inflation. We stress that this requires the fluid to behave much differently from matter or radiation, mainly to have a negative pressure. We now show a way to realise such a fluid. It turns out to be sufficient to consider that this fluid is modelled by a scalar field φ with a flat-enough potential $V(\varphi)$ [32, 33], a scenario called single field slow-roll inflation. They are other ways to realise inflation using multiple scalar fields [34], but single field slow-roll inflation is perfectly compatible with observations, so in the rest of this manuscript we will restrict to this simple scenario.

1.2.2-a Scalar field in FLRW

We consider the action of a scalar field minimally coupled to gravity with a standard kinetic term

$$S_\varphi = -\frac{1}{c}\int \mathrm{d}^4x\sqrt{-g}\left[\frac{1}{2}g^{\mu\nu}\partial_\mu\varphi\partial_\nu\varphi + V(\varphi)\right] . \tag{1.66}$$

The field φ will be referred to as the inflaton. We can compute the stress-energy tensor of the field using the formula (1.11), details are given in Appendix B.1,

$$T_{\mu\nu} = \partial_\mu\varphi\partial_\nu\varphi - g_{\mu\nu}\left[\frac{1}{2}g^{\alpha\beta}\partial_\alpha\varphi\partial_\beta\varphi + V(\varphi)\right] . \tag{1.67}$$

Imposing that the scalar field distribution is homogeneous and isotropic, the spatial derivatives must vanish. We then find that the stress-energy tensor (1.67) assumes the perfect fluid form of Eq. (1.27) for

$$\rho = \frac{\dot\varphi^2}{2c^2} + V(\varphi) , \tag{1.68a}$$

$$p = \frac{\dot\varphi^2}{2c^2} - V(\varphi) . \tag{1.68b}$$

There is *a priori* no simple equation of state relating these two parameters, and we have to solve for the dynamics of the fluid to find out how its energy and pressure evolve as the Universe expands. Eq. (1.30), the conservation of the stress-energy tensor $T_{\mu\nu}$, gives a first equation of evolution. For the scalar field, it gives the curved spacetime form of the Klein-Gordon equation [35, 36]

$$\Box\varphi - V'(\varphi)\,c^2 = 0 , \tag{1.69}$$

where we introduced the d'Alembertian operator $\Box = g_{\mu\nu}\nabla^\mu\nabla^\nu$, and used the relation

$$\Box\varphi = -\frac{1}{\sqrt{-g}}\partial_\mu\left(\sqrt{-g}\,g^{\mu\nu}\partial_\nu\varphi\right) . \tag{1.70}$$

valid for scalar fields. Notice the minus sign in Eq. (1.69) in the mostly pluses signature convention. For the FLRW metric we have

$$\ddot{\varphi} + 3H\dot{\varphi} + V'(\varphi)\, c^2 = 0\,. \tag{1.71}$$

The effect of the expansion appears in the friction term proportional to the Hubble parameter. Assuming that the scalar field dominates the energy budget of the Universe, Eq. (1.28), which now reads

$$H^2 = \frac{8\pi G_{\mathrm{N}}}{3c^2}\left[\frac{\dot{\varphi}^2}{2c^2} + V(\varphi)\right], \tag{1.72}$$

and Eq. (1.69) form a closed system of equations completely describing the dynamics of the scalar field once the potential $V(\varphi)$ is fixed. It only features two degrees of freedom so that initial conditions for the system are fixed by a choice of the initial field value and of its derivative $(\varphi_{\mathrm{in}}, \dot{\varphi}_{\mathrm{in}})$, and the subsequent evolution can be represented in a $(\varphi, \dot{\varphi})$-plane.

1.2.2-b de Sitter and slow-roll

In order to get an accelerated expansion of the Universe, Eq. (1.29) shows that we have to require $\rho + 3p < 0$, which translates for the scalar field in a domination of the potential energy over the kinetic one

$$\dot{\varphi}^2 < V(\varphi)\, c^2\,. \tag{1.73}$$

Intuitively, we need the field to evolve slowly in a region of large potential energy. To solve the Big Bang puzzles, this regime should be sustained for at least 60 e-folds. An important limiting case is when the kinetic energy is negligible compared to the potential one $V(\varphi)c^2 \gg \dot{\varphi}^2$ in which case Eqs. (1.68a)-(1.68b) give $p \approx -\rho$ i.e. $w \approx -1$. In such phase the Hubble parameter is a constant $H \approx H_{\mathrm{in}}$ and the expansion is exponential $a(t) = a_{\mathrm{in}} \exp[H(t - t_{\mathrm{in}})]$; just as in the latest stage of the evolution (1.40) when a cosmological constant dominate the energy-budget. The geometry of spacetime is then that of a de Sitter Universe. We now consider the possibility to realise inflation by a phase of *quasi*-de Sitter expansion. Indeed, in a de Sitter spacetime, the exponential expansion never ends, while inflation ends eventually at z_{f}, and the Universe becomes radiation-dominated. Inflation can, therefore, only be close to a de Sitter expansion phase for a finite duration. We will require this phase to be long enough and parameterise the deviations from such a situation. To that end, we introduce the hierarchy of Hubble flow functions $\{\epsilon_n\}$ defined by

$$\epsilon_{n+1} = \frac{\mathrm{d}\ln|\epsilon_n|}{\mathrm{d}N}\,, \tag{1.74}$$

where $\epsilon_0 = H_{\rm in}/H$ and the number of e-folds is computed from the start of inflation $N = \ln(a/a_{\rm in})$. In de Sitter $\epsilon_0 = 1$ and all the other flow functions vanish. Close to de Sitter we have $\epsilon_0 \approx 1$, and for this regime to persist over a few e-folds, we need this slow-roll parameter not to vary much i.e. $\epsilon_1 = \frac{{\rm d}\ln|\epsilon_0|}{{\rm d}N} \ll 1$. We can iterate this reasoning and require all flow functions $n \geq 1$ to be small $\epsilon_n \ll 1$. All flow functions in the hierarchy are of the same order. These are the slow-roll conditions, and the flow functions are often called the slow-roll parameters. Satisfying the slow-roll conditions imposes constraints on the initial conditions and the potential's form. We illustrate that by computing the two first flow functions. The first one reads

$$\epsilon_1 = -\frac{\dot{H}}{H^2} = 1 - \frac{\ddot{a}}{aH^2} = 3\frac{\frac{\dot{\varphi}^2}{2c^2}}{\frac{\dot{\varphi}^2}{2c^2} + V(\varphi)}\,, \tag{1.75}$$

where we have used Friedmann equations to express $\dot{H}$ in terms of the kinetic energy of the field

$$\dot{H} = -\frac{4\pi G_{\rm N}}{c^4}\dot{\varphi}^2\,. \tag{1.76}$$

Notice that the Hubble parameter can only decrease $\dot{H} < 0$, so $\epsilon_1 > 0$. Since inflation happens when $\ddot{a} > 0$, the second equality shows that the condition for inflation is $\epsilon_1 < 1$. Inflation ends for $\epsilon_1 = 1$. On the other hand, the slow-roll condition $\epsilon_1 \ll 1$, required to be close to de Sitter, is stronger than requiring inflation. The kinetic energy must be negligible compared to the potential one, not only smaller. Similarly, the second flow function can be expressed as

$$\epsilon_2 = 6\left[\frac{\epsilon_1}{3} - 1 - \frac{V'(\varphi)\,c^2}{3H\dot{\varphi}}\right]\,. \tag{1.77}$$

Since $\epsilon_1 \ll 1$ and $\epsilon_2 \ll 1$, we get the relation

$$\dot{\varphi} \approx -\frac{V'(\varphi)\,c^2}{3H}\,. \tag{1.78}$$

This last relation corresponds to neglecting $\ddot{\varphi}$ in the Klein-Gordon equation (1.69). It reduces the dynamics to a first-order equation, thereby reducing the space of allowed initial conditions to a choice of $\varphi_{\rm in}$ rather than a couple $(\varphi_{\rm in}, \dot{\varphi}_{\rm in})$. In the slow-roll regime, Eq. (1.78) can then be used to re-express the flow functions in terms of the derivative of the potential. We have

$$\epsilon_1 \approx \frac{\dot{\varphi}^2}{2V(\varphi)\,c^2} = \frac{c^4}{16\pi G_{\rm N}}\left(\frac{V'}{V}\right)^2\,, \tag{1.79}$$

where we have used the first Friedmann equation in the slow-roll limit

$$H^2 \approx \frac{8\pi G_{\mathrm{N}}}{3c^2} V(\varphi) \ . \tag{1.80}$$

The second flow function can similarly be written in terms of the derivatives of the potential. We can approximate $\ddot{\varphi}$ by taking the time derivative of Eq. (1.78) and use Eq. (1.69) and Eq. (1.80) to get

$$\epsilon_2 \approx \frac{c^4}{4\pi G_{\mathrm{N}}} \left[\left(\frac{V'}{V} \right)^2 - \frac{V''}{V} \right] \ . \tag{1.81}$$

To summarise, Eqs. (1.79-1.81) formalise our intuition that the potential should be flat enough in some regions to sustain a slow-roll evolution, and Eq. (1.78) singles out a specific trajectory, i.e. specific initial conditions in this region, for potential energy to dominate over kinetic energy. The conjunction of these two conditions is a generic feature of the slow-roll solution [37] that we have illustrated at leading order in the slow-roll parameters. Generically [37], for a given potential, one can construct order by order an analytic solution of the equations of motion that will satisfy the slow-roll conditions. The series converges towards a single trajectory in the phase-plane $(\varphi, \dot{\varphi})$, the slow-roll solution. An essential feature is that, when the potential supports inflation, the different trajectories in this phase-space will get closer exponentially fast in the number of e-folds. Therefore, provided we consider a scenario with more than a few e-folds of inflation, the slow-roll approximation will be a good approximation of the dynamics of the field *irrespective* of the initial conditions at the start of inflation; it is an attractor solution. This property makes slow-roll inflation partially immune to fine-tuning problems in the initial conditions. The slow-roll approximation is then a powerful method to compute analytically, with an arbitrary level of precision, an inflationary trajectory with somewhat generic properties.

In order to illustrate the described inflationary dynamics and its slow-roll behaviour, we briefly study the case of R^2 inflation, also known as Starobinsky inflation [38]. Similar computations for other common inflationary models can be found in [39]. The potential of this model reads

$$V_{\mathrm{S}}(\varphi) = \frac{3}{4} \left(\frac{mc}{\sqrt{\kappa}\hbar} \right)^2 \left[1 - \exp\left(-\sqrt{\frac{2}{3}} \sqrt{\kappa}\varphi \right) \right]^2 \ , \tag{1.82}$$

where $\kappa = 8\pi G/c^4$. The computation details for this case are given in Appendix B.2. For the potential of Eq (1.82), the slow-roll conditions are satisfied in the large field regime $\sqrt{\kappa}\varphi \gg 1$. In Fig. 1.5, the trajectories are shown to get close to the slow-roll trajectory in this regime, illustrating the attractor property.

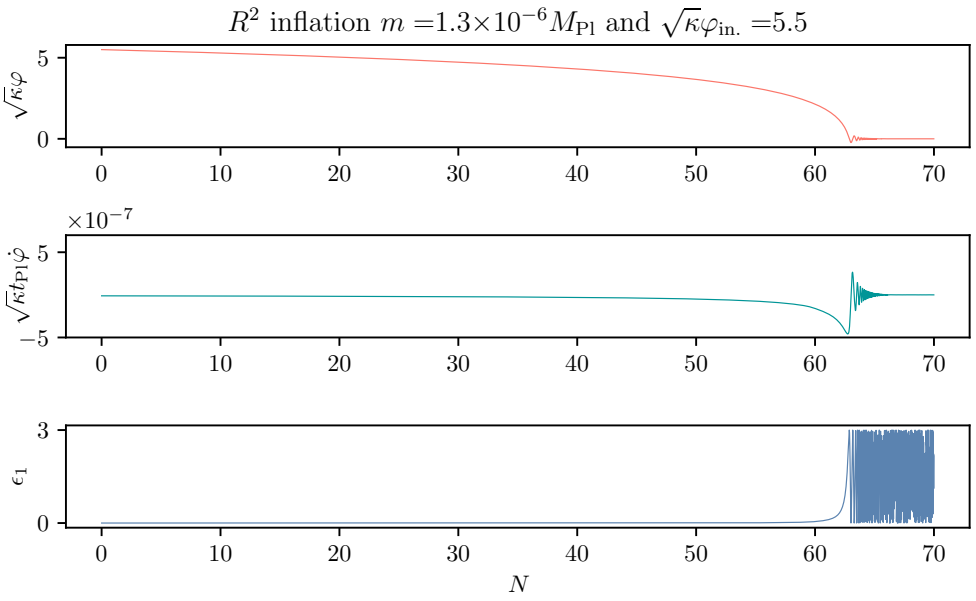

Figure 1.4: Evolution of the field φ, its time-derivative $\dot{\varphi}$ and the first flow function ϵ_1, as a function of the number of e-folds N in R^2-inflation with potential (1.82). Inflation is taken to start at $N = 0$ where $\sqrt{\kappa}\varphi_{\rm in} = 5.5$ while $\dot{\varphi}_{\rm in}$ is given by Eq. (1.78) evaluated at first order in slow-roll. For these values, the end of inflation $\epsilon_1 = 1$ is reached after $N = 64$ e-folds, compatible with the estimate from the first-order slow-roll $N_{\rm e} - \frac{3}{4} - \sqrt{\frac{3}{4}} \approx 65$.

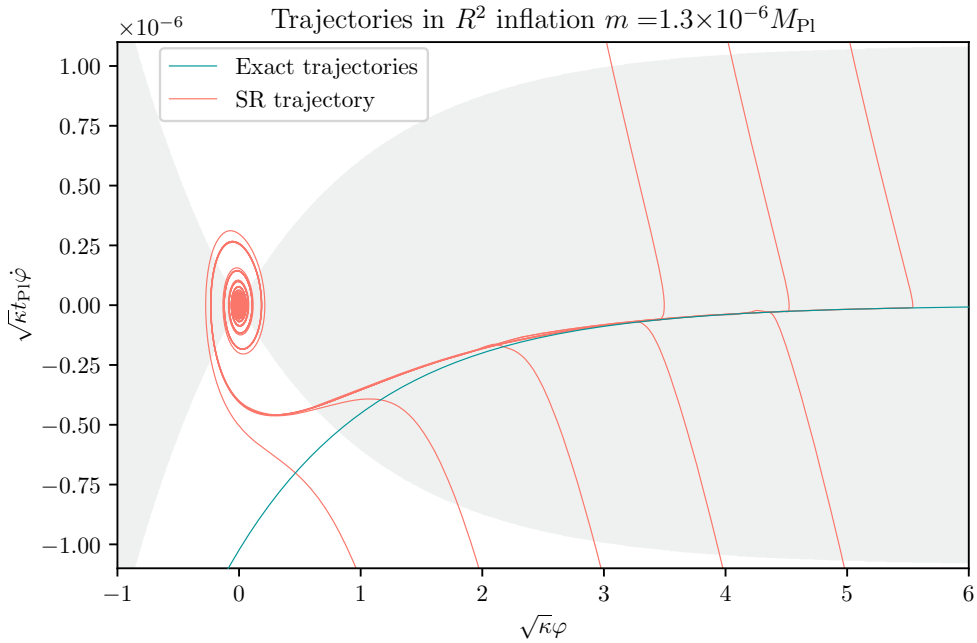

Figure 1.5: Trajectories in the phase-plane $(\varphi, \dot{\varphi})$ in R^2-inflation with potential (1.82). The red lines show the exact trajectories obtained by numerically solving Eq. (1.69) and Eqs. (1.72) for different initial conditions. The green line shows the slow-roll trajectory evaluated at first-order, see Eq. (4.25). The grey areas correspond to $\epsilon_1 \leq 1$ i.e. values for which inflation proceeds. Once they leave the slow-roll attractor, the trajectories spiral towards the origin of the figure. This corresponds to the oscillations of the field, damped by Hubble friction, which can lead to preheating, see Sec. 1.2.4.

Defining the number of e-folds to be 0 at the start of inflation $N = \ln(a_{\rm in}/a)$ and the initial value of the field to be $\varphi_{\rm in}$, the equation of motion is easily integrated to find the evolution of the field as a function of the number of e-folds at first order in slow-roll

$$\varphi(N) = \sqrt{\frac{3}{2}}\frac{1}{\sqrt{\kappa}}\ln\left[\frac{4}{3}(N_e - N)\right], \tag{1.83}$$

where

$$N_{\rm e} = \frac{3}{4}e^{\sqrt{\frac{2}{3}}\sqrt{\kappa}\varphi_{\rm in.}}. \tag{1.84}$$

Using the slow-roll approximation to find when ϵ_1 reaches unity, we find that inflation lasts approximately $\Delta N = N_{\rm e} - \frac{3}{4} - \sqrt{\frac{3}{4}}$, a value controlled by the field's initial value. Comparing with the exact evolution of ϵ_1 shown in Fig. 1.4, it is seen to be a good approximation.

The energy scale of inflation is given by the value of the potential . Using Eq. (1.42), and evaluating the energy at the beginning of inflation, we find

$$E_{\rm infl} \approx \sqrt{\frac{m}{M_{\rm Pl}}}\left(\frac{3}{4}\right)^{1/4} M_{\rm Pl}c^2, \tag{1.85}$$

making it obvious that the mass scale m in the potential controls the energy scale of inflation. For Starobinsky inflation, the field's initial value is decoupled from the energy scale. We can tune the duration of inflation to be long enough to solve the Big Bang puzzles without requiring that the energy scale of inflation is super-Planckian $E_{\rm infl} > M_{\rm Pl}c^2$, a regime in which our classical description is not expected to be accurate anymore. In Figs. 1.4 and 1.5, we chose m such that $E_{\rm infl} = E_{\rm GUT}$, also used for illustration when considering Big-Bang puzzles, and chose the initial value of the field accordingly in order to have roughly 65 e-folds of inflation. Therefore, we have constructed an explicit example of a model of inflation able to solve the Big Bang puzzles without requiring super-Planckian energies or fine-tuning in the initial values of the field. Many such models exist, but they are constrained by the observed properties of inhomogeneities in the early Universe. We review these aspects in the next sub-section Sec. 1.2.3.

We close this sub-section by pointing out that the inflationary scenario we presented is not devoid of problems. For instance, although the attractor property removes some degree of fine-tuning in the initial conditions, we still have assumed that the inflaton field, and so Universe was homogeneous *before* inflation starts. If for inflation to start, we need to require that the Universe is homogeneous across a-causal scales, then we have not solved the Horizon problem. The intuition here is that we only need to require homogeneity initially over a small patch, which is then inflated to our whole observable Universe. Numerical simulations have analysed the beginning of inflation in an inhomogeneous Universe, e.g. [40, 41, 42, 43, 44, 45],

showing that, under certain conditions, in large field models, inflation can start even in a very inhomogeneous environment, see however [45]. We refer to [46, 6] for a discussion of this initial condition problem and others.

1.2.3 Inhomogeneous Universe

In the previous sections, we have only discussed the physics of a homogeneous Universe. Although on very large scales, when coarse-graining the distribution of matter, the Universe appears isotropic, it is only an approximation. On smaller scales, the Universe is obviously inhomogeneous, being made up of galaxy clusters separated by large voids. Soon after the first papers on cosmic inflation as a solution to Big Bang puzzles, it was realised that inflation also offers a mechanism for generating primordial inhomogeneities. In [47], Mukhanov and Chibisov proposed that quantum fluctuations amplified by an intermediate stage of de Sitter expansion could explain inhomogeneities in the Universe. Their work was independent of that of other authors working on inflation. They were building on the work of Starobinsky [38], who showed that quantum-corrected Einstein's field equation admitted a non-singular de Sitter Universe as a solution. This work provided the basis for R^2-inflation used as an example in the last sub-section, Sec. 1.2.2. The analysis of matter inhomogeneities in the context of inflation was first done by [48, 49, 50, 51, 52]. The generation of gravitational waves in the context of inflation was first considered in [53], see Sec. 2.2 for more details. In this sub-section, we start by briefly explaining how to describe small inhomogeneities in cosmology. The CMB's temperature anisotropies are measured to be of order $\delta T/T \sim 10^{-5}$ [31], which directly reflects the small degree of inhomogeneities at LSS time [54]. We expect the inhomogeneities to be even smaller during inflation, which proceeded earlier, so the perturbative treatment should be perfectly valid then. In this sub-section, we will show how a quantum theory of inflation can prescribe some initial conditions for structure formation, which were observationally confirmed and allow us to constrain the specifics of the inflationary model.

1.2.3-a SVT decomposition

To account for the presence of inhomogeneities, we need to go beyond the description of the Universe in terms of the FLRW metric Eq. (1.17). In the standard structure formation scenario, small primordial inhomogeneities are gradually amplified by gravitational collapse. In this work dealing with early Universe physics, we restrict attention to the early phase of this process when the inhomogeneities are still small compared to the background densities. For this exposition, we follow the conventions and discussion of [55], except that we use the mostly-pluses convention for the signature. We start by considering perturbations around the

flat $\mathcal{K} = 0$ FLRW metric

$$\mathrm{d}s^2 = a^2(\eta)\left[-c^2\left(1+2\phi\right)\mathrm{d}\eta^2 + 2B_i \mathrm{d}x^i \mathrm{d}\eta + \left(\gamma_{ij} + E_{ij}\right)\mathrm{d}x^i \mathrm{d}x^j\right] , \tag{1.86}$$

where we work with 3D Cartesian coordinates x^i, γ_{ij} is the Euclidian three-dimensional metric in Cartesian coordinates. We have introduced the conformal time η related to cosmic time by $a^2(\eta)\mathrm{d}\eta^2 = \mathrm{d}t^2$. During inflation the conformal time is negative $\eta < 0$, and the end of inflation corresponds to $\eta \to 0^-$. There are 10 perturbations parameterised by ϕ, the spatial vector B_i and the spatial 2-tensor E_{ij}. It is useful to perform a scalar-vector-tensor (SVT) decomposition of these perturbations. We decompose each of these terms in objects having a well-defined transformation under the group of 3D spatial rotations, which is a symmetry of the (flat) background metric. To avoid confusion, we will refer to these objects as *helicity* scalar-vector-tensors [56, 57]. Therefore, although B_i transforms as a vector under a change of coordinates, we can decompose it in a helicity scalar and a helicity vector as

$$B_i = S_i - \partial_i B \,, \tag{1.87}$$

where B is an helicity scalar and S_i is a divergence-free helicity vector $\partial^i S_i = 0$. Eq. (1.87) is nothing else than the Helmholtz decomposition of a vector. We have a similar decomposition for the tensor

$$E_{ij} = -2\psi\gamma_{ij} + 2\partial_i\partial_j E + 2\partial_{(i}F_{j)} + h_{ij} \,, \tag{1.88}$$

where $\partial_{(i}F_{j)} = \left(\partial_i F_j + \partial_j F_i\right)/2$ is the symmetrised derivative. In this decomposition ψ and E are helicity scalars, F_j is an helicity vector and h_{ij} an helicity tensor. We have $\partial^i F_i = \partial^i h_{ij} = 0$ and the tensor is trace-less $h^i{}_i = 0$. We go to Fourier space to see the effect of rotations on these objects. For any wave-vector $\boldsymbol{k}$, the divergence-free condition reads $k^i S_i(\boldsymbol{k}) = 0$ i.e. $S_i(\boldsymbol{k})$ is transverse, while $\partial_i B(\boldsymbol{k}) \parallel \boldsymbol{k}$. Then under a rotation $R(\theta)$ around the direction $\boldsymbol{k}$, $\partial_i B(\boldsymbol{k})$ will be unaffected, while $S_i(\boldsymbol{k})$ will be rotated. In the helicity basis [56, 57] it would pick up a factor of $e^{\pm i\theta}$. This justifies the terminology of helicity SVT. The same reasoning applies to the components of E_{ij} in Fourier space where $h_{ij}(\boldsymbol{k})$ would instead pick up a factor of $e^{\pm 2i\theta}$ in the helicity basis. In total we have four scalars ψ, ϕ, B, E, two vectors S_i, F_i, and one tensor h_{ij}. No vector perturbations are produced during inflation, and any pre-existing ones would quickly decay [58]. They are thus conveniently ignored in the rest of this text. We can repeat the SVT decomposition for the energy-momentum tensor by perturbing that of a perfect fluid. The two sets of perturbations are related by the perturbed Einstein field equations, which, combined with the perturbed conservation equation, give the equations of motion of the perturbations. We will not discuss the general case here and refer to [55] for details. The main purpose of the SVT decomposition is that scalar, vector and tensors do not mix in the equations of motion at linear order in perturbation theory, see Appendix A of [57] for a proof.

1.2.3-b Gauge invariant variables

There are some ambiguities in the definition of these perturbations. General covariance is a basic property of General Relativity, and equations are generally formulated in a covariant way. This symmetry under coordinate transformations is broken in cosmology by working in coordinates where the distribution of matter is homogeneous and isotropic. Still, we could work with coordinates where the same Universe would no longer look homogeneous. For instance, starting from coordinates where the metric reads as in Eq. (1.17), consider a small shift of the original spatial coordinates $\tilde{x}^i = x^i + \xi^i(\eta, \boldsymbol{x})$. The metric reads

$$\begin{aligned} \mathrm{d}s^2 &= a^2(\eta)\left(-c^2\mathrm{d}\eta^2 + \gamma_{ij}\mathrm{d}x^i\mathrm{d}x^j\right) , \\ &= a^2(\eta)\left\{-c^2\mathrm{d}\eta^2 - 2\xi_i'\mathrm{d}\tilde{x}^i\mathrm{d}\eta + \left[\gamma_{ij} - 2\partial_{(i}\xi_{j)}\right]\mathrm{d}\tilde{x}^i\mathrm{d}\tilde{x}^j\right\} . \end{aligned} \tag{1.89}$$

where $'$ denote derivatives with respect to conformal time η. In the new coordinates, the metric looks like a perturbed FLRW metric, and a direct comparison with the ansatz (1.86) gives non-vanishing values for the perturbation parameters. These perturbations are spurious since the Universe is still manifestly homogeneous by adopting the right system of coordinates (the old ones). This illustrates the *gauge dependence* of the perturbations and of the quantities ϕ,B_i,γ_{ij} and E_{ij}. To avoid mistaking an effect of coordinate choice for a true deviation from FLRW, we can introduce gauge-invariant combinations of them. To build them, one should consider how each type of perturbation transforms under a small coordinate change $\tilde{x}^\mu = x^\mu + \xi^\mu(\eta, \boldsymbol{x})$. In general, it is found that the transverse trace-less perturbations h_{ij} are gauge-invariant and that two gauge-invariant scalars, the so-called Bardeen variables [59], can be constructed

$$\Phi_{(\mathrm{B})} = \phi - \mathcal{H}\left(B - E'\right) + \left(B - E'\right)' , \tag{1.90a}$$

$$\Psi_{(\mathrm{B})} = \psi - \mathcal{H}\left(B - E'\right) , \tag{1.90b}$$

where $\mathcal{H} = a'/a$. We are interested specifically in the case of single field inflation where the situation is simpler and these two variables are equal $\Psi_{(\mathrm{B})} = \Phi_{(\mathrm{B})}$ [55]. Additionally, the perturbations around the background trajectory $\varphi_0(\eta)$ of the field $\varphi = \varphi_0(\eta) + \delta\varphi(\eta, \boldsymbol{x})$ only leads to scalar perturbations that can be gathered with metric perturbations in the gauge invariant combination [55]

$$\delta\varphi_{(\mathrm{gi})} = \delta\varphi + \varphi_0'\left(B - E'\right) . \tag{1.91}$$

The scalar field perturbation $\delta\varphi_{(\mathrm{gi})}$ and the Bardeen variable $\Psi_{(\mathrm{B})}$ are related by the perturbed Einstein equation

$$\mathcal{H}\Phi_{(\mathrm{B})} + \Phi'_{(\mathrm{B})} = \frac{\kappa}{2}\varphi_0'\delta\varphi_{(\mathrm{gi})} \tag{1.92}$$

It is found after lengthy computations [55] that the perturbed actions of Einstein-Hilbert and of the scalar field can be rewritten over a single scalar quantity v, called the Mukhanov-Sasaki variable [47, 60], which is a combination of these two

$$v = a\left[\delta\varphi_{(\mathrm{gi})} + \mathfrak{z}\Phi_{(\mathrm{B})}\right] , \tag{1.93}$$

where

$$\mathfrak{z} = \frac{a\varphi_0'}{\mathcal{H}} = a\sqrt{\frac{2\epsilon_1}{\kappa}} . \tag{1.94}$$

We use the fraktur font $\mathfrak{z}$ to distinguish this quantity from the redshift z. The perturbed action reads [55]

$$\begin{aligned}\delta^{(2)}S_{\mathrm{S}} &= \frac{1}{2c^3}\int \mathrm{d}^4x\left[(v')^2 - \gamma^{ij}c^2\partial_i v\partial_j v + \frac{\mathfrak{z}''}{\mathfrak{z}}v^2\right] ,\\ &= \frac{1}{c^2}\int \mathrm{d}\eta\int_{\mathbb{R}^{3+}}\mathrm{d}^3\boldsymbol{k}\left[v_{\boldsymbol{k}}'v_{-\boldsymbol{k}}' - c^2k^2v_{\boldsymbol{k}}v_{-\boldsymbol{k}} + \frac{\mathfrak{z}''}{\mathfrak{z}}v_{\boldsymbol{k}}v_{-\boldsymbol{k}}\right] ,\end{aligned} \tag{1.95}$$

where in the second line we transformed the action to Fourier space

$$v\left(\boldsymbol{x},\eta\right) = \int\frac{\mathrm{d}^3\boldsymbol{k}}{\left(2\pi\right)^{3/2}}e^{i\boldsymbol{k}.\boldsymbol{x}}v_{\boldsymbol{k}}\left(\eta\right) , \tag{1.96}$$

and folded the integration over $\mathbb{R}^{3+} = \{\boldsymbol{k}|k_{\mathrm{z}} > 0\}$. Since v is real, we have $v^\star_{-\boldsymbol{k}} = v_{\boldsymbol{k}}$. It is more convenient to work in Fourier space because, at the linear level in perturbation theory, different pair of modes $\pm\boldsymbol{k}$ evolve independently as seen from Eq. (1.95). The case of tensor perturbations is studied in detail in [1] reproduced in Sec. 2.2, where the perturbed action is derived, and their evolution is followed during inflation and after. We thus only quote relevant results for comparison with the scalar case. First, the tensor perturbations h_{ij} can be decomposed in two real scalar fields μ_λ, representing its two polarisations $\pm$ in helicity basis, via

$$h_{ij}(\boldsymbol{x},\eta) = \sqrt{32\pi G_{\mathrm{N}}}\sum_{\lambda=\pm}\int\frac{\mathrm{d}^3\boldsymbol{k}}{(2\pi)^{3/2}a(\eta)}\varepsilon_{ij}^{(\lambda)}(\hat{\boldsymbol{k}})\mu_\lambda(\boldsymbol{k},\eta)e^{i\boldsymbol{k}\cdot\boldsymbol{x}} , \tag{1.97}$$

where $\varepsilon_{ij}^{(\lambda)}(\hat{\boldsymbol{k}})$ is the polarisation tensor for a wave in the direction $\hat{\boldsymbol{k}}$ defined in Sec. 2.2. Using this expansion, the perturbed Einstein-Hilbert action for the tensor sector reads

$$\begin{aligned}\delta^{(2)}S_{\mathrm{T}} &= \int\mathrm{d}\eta\sum_{\lambda=\pm}\frac{1}{2}\int\mathrm{d}^3\boldsymbol{x}\left[\left(\mu_\lambda'\right)^2 - c^2\gamma^{ij}\partial_i\mu_\lambda\partial_j\mu_\lambda + \frac{a''}{a}\mu_\lambda^2\right] ,\\ &= \int\mathrm{d}\eta\sum_{\lambda=\pm}\int_{\mathbb{R}^{3+}}\mathrm{d}^3\boldsymbol{k}\left[\mu_\lambda'\left(\boldsymbol{k}\right)\mu_\lambda'\left(-\boldsymbol{k}\right) - \left(c^2k^2 - \frac{a''}{a}\right)\mu_\lambda\left(\boldsymbol{k}\right)\mu_\lambda\left(-\boldsymbol{k}\right)\right] .\end{aligned} \tag{1.98}$$

It is made of two copies of the action of scalar perturbations, up to the substitution $\mathfrak{z} \to a$. Finally, although the Mukhanov-Sasaki variable v allows having the most compact form for the equations of motion, $\delta\varphi$ loses its meaning after inflation so that the definition Eq. (1.93) is not valid anymore[9]. A convenient quantity to work with is ζ defined as

$$\zeta = \frac{2}{3}\frac{\mathcal{H}^{-1}\Phi'_{(\mathrm{B})} + \Phi_{(\mathrm{B})}}{1+w} + \Phi_{(\mathrm{B})}\,, \tag{1.99}$$

where $w = \rho/p$ is the effective equation of state parameter for the total pressure and energy density. The definition (1.99) only contains geometrical quantities and is therefore valid in any background spacetime, in particular when entering radiation domination at the end of inflation. During inflation, ζ can be related to the Mukhanov-Sasaki variable. First, using the expression of energy and pressure density Eqs. (1.68a)-(1.68b) and the definition of the first slow-roll parameter Eq. (1.75), we find

$$w_{\mathrm{infl}} = \frac{2}{3}\epsilon_1 - 1\,. \tag{1.100}$$

We then use the perturbed Einstein equation Eq. (1.92) and the definition Eq. (1.99) to get the simple relation

$$\zeta = \frac{v}{\mathfrak{z}}\,. \tag{1.101}$$

A crucial property of ζ is that when a single perfect fluid dominates, e.g. during inflation or radiation domination, it is conserved on large scales [52, 55, 61]. It thus allows smoothly connecting the evolution of gravitational potentials from inflation to later times, for example at LSS, and to compute the CMB power spectrum. The fluctuations of temperature measured in the CMB photons are related to Bardeen potentials by the Sachs-Wolfe effect [54], which is directly connected to ζ by definition. Similarly, the physical quantity to compute for tensor is h_{ij} rather than μ_λ. However, being intrinsically geometrical, they are always well-defined and differ merely by a factor of a.

1.2.3-c Evolution of inflationary perturbations

We will now solve the equations of motion and describe the evolution of the perturbations during inflation. The equation of motion of the scalar perturbation is straightforwardly derived from the action (1.95)

$$v''_{\pm\boldsymbol{k}} + \left(c^2k^2 - \frac{\mathfrak{z}''}{\mathfrak{z}}\right) v_{\pm\boldsymbol{k}} = 0\,. \tag{1.102}$$

It is the equation of an oscillator with a time-dependent frequency

$$\omega^2_{k\,\mathrm{S}} = c^2k^2 - \frac{\mathfrak{z}''}{\mathfrak{z}}\,. \tag{1.103}$$

[9] Another definition valid for a perfect fluid can be given [55].

The behaviour of the mode $\boldsymbol{k}$ will be different when $\omega_{k\,\mathrm{S}}^2$ is positive or negative. When $\omega_{k\,\mathrm{S}}^2 > 0$, we expect the mode to oscillate, and when $\omega_{k\,\mathrm{S}}^2 < 0$, we expect the mode to be amplified. To understand the evolution of $\mathfrak{z}''/\mathfrak{z}$, we will work again in the slow-roll approximation where the background is a quasi-de Sitter expansion. We express the time-dependent part of the frequency in slow-roll parameters

$$\frac{\mathfrak{z}''}{\mathfrak{z}} = \frac{a''}{a} + \frac{\epsilon_2}{2}\left(\frac{a''}{a} + \mathcal{H}^2\right) + \frac{\mathcal{H}^2}{2}\left(\epsilon_2\epsilon_3 + \frac{\epsilon_2^2}{2}\right) . \tag{1.104}$$

The terms a''/a and $\mathcal{H}$ must also be expanded in slow-roll parameters to be consistent. To understand the mode evolution qualitatively, let us first consider the de Sitter case, where the flow functions vanish. We have $a = -1/H\eta$, then $\mathfrak{z}''/\mathfrak{z} = a''/a = 2/\eta^2$. First, notice that, in de Sitter, the frequency for scalar and tensor perturbations coincide[10]. Second, the sign of $\omega_{k\,\mathrm{S}}^2$ is then directly obtained by a comparison between the physical size of the Hubble radius $c/aH = -c\eta$ and the wavelength of the mode k^{-1}. When the mode is *super-Hubble* i.e. its wavelength is larger than the Hubble radius, then $k\,(aH)^{-1} = -ck\eta \ll 1$ and $\omega_{k\,\mathrm{S}}^2$ is negative: the mode is amplified. On the other hand, when the mode is *sub-Hubble* then $k\,(aH)^{-1} = -ck\eta \gg 1$ and the mode oscillates $\omega_{k\,\mathrm{S}}^2 > 0$. Since the physical size of the Hubble radius decreases as time passes, more modes $\boldsymbol{k}$ will become super-Hubble and be amplified during inflation. The picture is similar in slow-roll, but the amplification condition must be corrected to include the slow-roll parameters and have a precise estimate of the amount of amplification undergone by a mode. Let us follow the evolution of one mode $\boldsymbol{k}$ which is initially sub-Hubble. Starting in the regime $c^2k^2 \gg \mathfrak{z}''/\mathfrak{z}$, since $\omega_{k\,\mathrm{S}} \approx ck$, we have

$$v_{\boldsymbol{k}}(\eta) \approx A_{\boldsymbol{k}} e^{ick\eta} + B_{\boldsymbol{k}} e^{-ick\eta} , \tag{1.105}$$

where $A_{\boldsymbol{k}}$ and $B_{\boldsymbol{k}}$ are two constants fixing the initial conditions for the evolution of the mode. Then in the regime $c^2k^2 \ll \mathfrak{z}''/\mathfrak{z}$ where $\omega_{k\,\mathrm{S}} \approx \mathfrak{z}''/\mathfrak{z}$, we have the following general solution

$$v_{\boldsymbol{k}}(\eta) \approx \alpha_{\boldsymbol{k}}\mathfrak{z}(\eta) + \beta_{\boldsymbol{k}}\mathfrak{z}(\eta)\int_\eta^0 \frac{\mathrm{d}\eta'}{\mathfrak{z}^2(\eta')} , \tag{1.106}$$

where $\alpha_{\boldsymbol{k}}$ and $\beta_{\boldsymbol{k}}$ are two complex coefficients. Dividing by $\mathfrak{z}$, we find the corresponding super-Hubble expression for ζ

$$\zeta_{\boldsymbol{k}} \approx \alpha_{\boldsymbol{k}} + \beta_{\boldsymbol{k}}\int_\eta^0 \frac{\mathrm{d}\eta'}{\mathfrak{z}^2(\eta')} . \tag{1.107}$$

[10] This is a general feature of power law inflation models of which de Sitter is a special case [39]

Since $\mathfrak{z}^2 > 0$, the second term will decay; it is called the decaying mode. In contrast, the first term is a constant and is called the growing mode. As announced when introducing it, we find that ζ goes to a constant $\zeta_{\boldsymbol{k}} \approx \alpha_{\boldsymbol{k}}$ when $\eta \to 0^-$ on large scales. Therefore, to connect computations made for v during inflation to CMB observations, we only need to extract the value $\alpha_{\boldsymbol{k}}$ from the evolution of the Mukhanov-Sasaki variable. This is done by continuously joining the two solutions given in Eq. (1.105) and Eq. (1.106) in the regime $c^2k^2 \approx \mathfrak{z}''/\mathfrak{z}$. The number of e-folds corresponding to this regime depends on the scales considered. We here are interested in the range of modes $\boldsymbol{k}$ corresponding to that measured by CMB experiments like Planck. By tracing back the evolution of their physical size from today to the inflationary period, we can estimate (assuming certain values for energy scale of inflation and reheating) that they crossed out the Hubble radius from 60 to 53 e-folds before the end of inflation [62]. In the next part Sec. 1.2.3-d, we first fix the initial conditions to derive the coefficients $A_{\boldsymbol{k}}$ and $B_{\boldsymbol{k}}$. We then compute an approximate solution for the evolution of the Mukhanov-Sasaki variable valid during this period of 7 e-folds and extract from it the $\alpha_{\boldsymbol{k}}$ coefficient of Eq. (1.107).

1.2.3-d Quantum initial conditions for structure formation

A good way to characterise the properties of the observed CMB temperature fluctuations $\delta T/T$ is to view them as the result of a random process. Intuitively, each patch of a large enough size in a given direction $\hat{\boldsymbol{n}}$ is considered as an independent realisation of the process $\delta T/T(\hat{\boldsymbol{n}})$ [63]. We can then deduce the statistical properties of the underlying process by computing n-point correlation functions. Following this strategy, it is found [64] that the fluctuations are Gaussian within an excellent approximation i.e. all the information is contained in the 2-point correlation function also known as the power spectrum $\langle \delta T/T(\hat{\boldsymbol{n}}) \delta T/T(\hat{\boldsymbol{n}}') \rangle$. These correlation functions are usually decomposed in spherical harmonics to be analysed and are related to that of curvature perturbations $\langle \zeta_{\boldsymbol{k}} \zeta_{\boldsymbol{k}'} \rangle$ by the Sachs-Wolfe effect [54]. In this picture, the curvature perturbations are also seen as a result of an initial random process, the characteristics of which are fixed by the initial conditions. These conditions are fixed in the very early Universe at the beginning of inflation, where the energy scale at play, e.g. around the GUT scale, makes the description of matter in terms of *quantum* fields relevant. We can therefore consider a quantum version of the scalar field theory developed so far. The quantisation procedure is reviewed in detail in [1], reproduced in Sec. 2.2, for the tensor perturbations. The procedure for scalar perturbations proceeds in the same fashion; we do not detail it here. However, for completeness, we present the conclusions of the quantisation procedure for both scalar and tensor. Our goal in this part is to derive the standard results for the spectra of the tensor and scalar perturbations, which can be compared to cosmological observations. The quantum aspects of

the perturbations are one of the two topics of this manuscript, and we relegate in-depth discussions of the quantum aspects to later sections.

First, the Mukhanov-Sasaki variable is promoted to an operator $\hat{v}_{\boldsymbol{k}}$ whose canonically conjugated operator

$$\hat{p}_{\pm\boldsymbol{k}} = \hat{v}'_{\pm\boldsymbol{k}} \,, \tag{1.108}$$

is computed from the action Eq. (1.95), and we impose canonical commutation relation

$$[\hat{v}_{\boldsymbol{k}}, \hat{p}_{\boldsymbol{k}'}] = i\hbar\delta\left(\boldsymbol{k} + \boldsymbol{k}'\right) \,. \tag{1.109}$$

Using these operators, we can compute quantum expectation values for the different quantities, e.g. $\langle\hat{\zeta}(\boldsymbol{x},\eta)\hat{\zeta}(\boldsymbol{x}',\eta)\rangle$. They would match the average value of the quantity if we measured it repeatedly after having prepared the state multiple times with the same initial conditions. However, we have only access to a single realisation of our Universe. Still, under an ergodicity assumption [63], these quantum expectation values are assumed to match the measured statistical expectation values computed over different patches of the Universe at that time. To compare them with the correlation functions measured in the CMB, the expectation values at the end of inflation have to be evolved to LLS time. This evolution is summarised in transfer functions [6]. Using this correspondence, we have to compute the quantum evolution of the operators and evaluate their expectation values at the end of inflation. For that, we can easily compute from Eq. (1.95) the Hamiltonian of the theory. As the action is quadratic, and only mixes the modes $\pm k$, we restrict to a pair of modes

$$\hat{H}_{\pm\boldsymbol{k},\mathrm{S}} = \hat{p}_{\boldsymbol{k}}\hat{p}_{-\boldsymbol{k}} + \left(c^2k^2 - \frac{\mathfrak{z}''}{\mathfrak{z}}\right)\hat{v}_{\boldsymbol{k}}\hat{v}_{-\boldsymbol{k}} \,, \tag{1.110}$$

and write the associated Schrödinger equation. To solve this equation, we are then back to the problem of specifying the initial conditions. The simplest and minimal choice we can make is that initially, there were only *vacuum* fluctuations. When a mode $\boldsymbol{k}$ is very sub-Hubble $ck\eta \to -\infty$ it does not feel the expansion of spacetime, and the quantisation procedure is that of a simple harmonic oscillator of frequencies k. We can introduce the standard creation/annihilation operators

$$\hat{v}_{\boldsymbol{k}}(-\infty) = \sqrt{\frac{\hbar c}{2k}}\left[\hat{a}_{\boldsymbol{k}}(-\infty) + \hat{a}^\dagger_{-\boldsymbol{k}}(-\infty)\right] \,, \tag{1.111a}$$

$$\hat{p}_{\boldsymbol{k}}(-\infty) = -i\sqrt{\frac{\hbar k}{2c}}\left[\hat{a}_{\boldsymbol{k}}(-\infty) - \hat{a}^\dagger_{-\boldsymbol{k}}(-\infty)\right] . \tag{1.111b}$$

The vacuum state in the sub-Hubble limit is then defined as the state annihilated by both operators $\hat{a}_{\pm\boldsymbol{k}}(-\infty)\left|0\right\rangle_{\pm\boldsymbol{k}}$, and is a well-know Gaussian wave-function,

see Sec. 2.2. Evolving the mode under the quadratic Hamiltonian (1.110) from this initial Gaussian vacuum state preserves the Gaussianity of the wave function. The expectation values will then satisfy the observed Gaussian character of the correlation functions. The choice of initial vacuum state for all modes $\boldsymbol{k}$ in the sub-Hubble regime is called the Bunch-Davies vacuum [65]. Working in the Heisenberg picture, the evolution can be summarised using a mode function u_k, such that

$$\hat{v}\left(\boldsymbol{x},\eta\right)=\int\frac{\mathrm{d}^{3}\boldsymbol{k}}{\left(2\pi\right)^{3/2}}\left[e^{i\boldsymbol{k}.\boldsymbol{x}}u_{k}\left(\eta\right)\hat{a}_{\boldsymbol{k}}\left(-\infty\right)+e^{-i\boldsymbol{k}.\boldsymbol{x}}u_{k}^{\star}\left(\eta\right)\hat{a}_{\boldsymbol{k}}^{\dagger}\left(-\infty\right)\right]\,. \tag{1.112}$$

Using Eq. (1.112), one can show that $\hat{v}$ is a solution of the Heisenberg equation if and only if the mode function u_k is a solution of the Mukhanov-Sasaki equation, Eq. (1.102). We have then reduced the quantum evolution to the classical one. Note that this reduction is a general feature of the evolution under a quadratic Hamiltonians, see Sec. 2.2. The considerations of Sec. 1.2.3-c on the evolution of the classical solution $v_{\boldsymbol{k}}$ are then mapped completely to the mode function u_k. Recall that, to solve the dynamics, we have to first find the coefficients in the sub-Hubble limit Eq. (1.105), fixing the initial conditions, and then join the obtained sub-Hubble solution to the super-Hubble one in the regime $k^2\approx\mathfrak{z}''/\mathfrak{z}$. First, the initial conditions are uniquely fixed by choice of the Bunch-Davies vacuum as an initial state. It imposes that the mode function u_k matches in the asymptotic past $ck\eta\to-\infty$ the Minkowski mode function i.e.

$$u_{k}\xrightarrow[ck\eta\to-\infty]{}\sqrt{\frac{\hbar c}{2k}}\,e^{-ick\eta}\,. \tag{1.113}$$

Comparing with Eq. (1.105) it fixes the coefficients to be $A_{\boldsymbol{k}}=\sqrt{\hbar c/2k}$ and $B_{\boldsymbol{k}}=0$. The quantum origin of the perturbations is then reflected in the k-dependence, which is that of the quantum vacuum. Second, to connect with the super-Hubble solution, we have to solve the Mukhanov-Sasaki equation Eq. (1.102) in the regime $k^2\approx\mathfrak{z}''/\mathfrak{z}$ with these initial conditions in the past. In general, the expression of $\mathfrak{z}''/\mathfrak{z}$ given by Eq. (1.104) is too complicated to solve the equation when the flow functions are time-dependent. However, their evolution is itself slow-roll suppressed. Therefore, if we focus on a narrow enough time window around a reference time $\eta_\star$, we can Taylor expand the flow functions. Since we focus on CMB scales, we consider a typical pivot scale $k_\star$ and define its Hubble crossing time by $\eta_\star$ such that $a_\star H_\star=ck_\star$. We denote by a $\star$ quantities evaluated at $\eta_\star$. We Taylor expand the flow-function about $\eta_\star$

$$\epsilon_{n}\left(\eta\right)=\epsilon_{n\star}\left\{1+\epsilon_{n+1\star}\left(N-N_{\star}\right)+\mathcal{O}\left[\left(N-N_{\star}\right)^{2}\epsilon_{n}^{2}\right]\right\}\,. \tag{1.114}$$

All other CMB scales $k\neq k_\star$ will exit the Hubble radius at times η such that $|N-N_\star|\approx 3.5$ [62]. Since we expect $\epsilon_1(\eta_\star)\ll 1$, the expansion is expected to

be valid for a sufficiently large time window to describe all CMB scales. To solve the dynamics, we first compute the dynamics of the scale factor at first order in slow-roll. By definition of the first slow-roll parameter, we have

$$\mathcal{H} \approx -\frac{1}{\eta}\left(1+\epsilon_{1\star}\right) , \tag{1.115}$$

which, by integration, gives

$$\ln\left(\frac{a}{a_\star}\right) = -\left(1+\epsilon_{1\star}\right)\ln\left(\frac{\eta}{\eta_\star}\right) . \tag{1.116}$$

Using $\mathcal{H}_\star \approx -(1+\epsilon_{1\star})/\eta_\star$ we get

$$a\left(\eta\right) \approx \frac{1}{H_\star \eta}\left[1+\epsilon_{1\star}-\epsilon_{1\star}\ln\left(\frac{\eta}{\eta_\star}\right)\right] . \tag{1.117}$$

We can then use Eq. (1.117), and Eq. (1.114) for ϵ_1, to get the expansion of $\mathfrak{z}$ around $\eta_\star$. We have

$$\mathfrak{z}\left(\eta\right) \approx \sqrt{\frac{2\epsilon_{1\star}}{\kappa}}\frac{1}{H_\star\eta}\left[1+\epsilon_{1\star}-\left(\epsilon_{1\star}+\frac{\epsilon_{2\star}}{2}\right)\ln\left(\frac{\eta}{\eta_\star}\right)\right] , \tag{1.118}$$

where we have used $N - N_\star \approx -\ln(\eta/\eta_\star)$. We can then compute the time-dependent parts of the frequencies driving the evolution of scalar and tensor perturbations

$$\frac{a''}{a} = \frac{2+3\epsilon_{1\star}}{\eta^2} , \tag{1.119}$$

and

$$\frac{\mathfrak{z}''}{\mathfrak{z}} = \frac{2+3\epsilon_{1\star}+\frac{3}{2}\epsilon_{2\star}}{\eta^2} , \tag{1.120}$$

where the terms in the logarithm of the conformal time have cancelled out. Due to these cancellations, and the simple remaining time-dependence, the equation of motions, Eq. (1.102), and the equivalent for tensor perturbations, can be integrated in terms of Hankel functions. For Eq. (1.102) we have

$$u_k\left(\eta\right) = C_k\sqrt{\frac{-c^2\hbar\eta\pi}{4}}H^{(1)}_{\frac{3}{2}+\epsilon_{1\star}+\frac{\epsilon_{2\star}}{2}}\left(-ck\eta\right) + D_k\sqrt{\frac{-c^2\hbar\eta\pi}{4}}H^{(2)}_{\frac{3}{2}+\epsilon_{1\star}+\frac{\epsilon_{2\star}}{2}}\left(-ck\eta\right) , \tag{1.121}$$

where C_k and D_k fix the initial conditions. Considering the limit of the Hankel functions in the asymptotic past[11], we have

$$H^{(1/2)}_\nu\left(-ck\eta\right) \xrightarrow[k\eta\to-\infty]{} \sqrt{\frac{2}{-ck\eta\pi}}\,e^{\pm i(ck\eta-\nu\pi/2-\pi/4)} , \tag{1.122}$$

[11]Implicitly, we assume that this asymptotic behaviour is reached sufficiently quickly to be within the range of validity of the expansion around $\eta_\star$. The same assumption is made when looking at the asymptotic future limit below.

so that the Bunch-Davies vacuum corresponds to $C_k = -e^{i\frac{\pi}{2}\left(\epsilon_1+\frac{\epsilon_2}{2}\right)}$, and $D_k = 0$. The mode function is now completely specified. We want to extract from it the value of the coefficient $\alpha_{\boldsymbol{k}}$ in front of the growing mode in Eq. (1.106). To do so, we consider $u_k/\mathfrak{z}(\eta)$, effectively the mode function of ζ, and we take the asymptotic future limit. Generically

$$H_\nu^{(1)}\left(-ck\eta\right) \xrightarrow[ck\eta\to 0^+]{} -\frac{i}{\pi}\Gamma\left(\nu\right)\left(\frac{2}{-ck\eta}\right)^\nu , \tag{1.123}$$

where we have introduced the Gamma function $\Gamma(\nu)$. Using the expansion of $\mathfrak{z}(\eta)$ of Eq. (1.118) we get

$$\begin{aligned}\frac{u_k}{\mathfrak{z}} \underset{ck\eta\to 0^+}{\sim} i\frac{C_k}{2}\sqrt{\frac{\hbar\kappa H_\star^2}{k^3 c\epsilon_{1\star}}}\Bigg[1+\left(1-\ln 2-\gamma_{\rm E}\right)\epsilon_{1\star} \\ +\left(2-\ln 2-\gamma_{\rm E}\right)\frac{\epsilon_{2\star}}{2}-\left(2\epsilon_{1\star}+\epsilon_{2\star}\right)\ln\left(\frac{k}{k_\star}\right)\Bigg] ,\end{aligned} \tag{1.124}$$

where we have used $\Gamma\left(3/2+\nu\right) \approx \sqrt{\pi}[1+(2-2\ln 2-\gamma_{\rm E})\nu]/2$, $\gamma_{\rm E}$ being the Euler constant, and used $ck_\star = -\left(1+\epsilon_{1\star}\right)/\eta_\star$ to replace $\eta_\star$. We find that $u_k/\mathfrak{z}$ is constant in the super-Hubble limit so that the matching to the super-Hubble solution is trivial in this case: we set $\alpha_{\boldsymbol{k}}$ equal to the right of Eq. (1.124). At first order in slow-roll, we thus found that for scales close to $k_\star$, $u_k \approx \alpha_{\boldsymbol{k}}\mathfrak{z}(\eta)$ in the super-Hubble limit.

1.2.3-e Connection to observations

Using Eq. (1.112) we can compute the 2-point function related to the CMB temperature fluctuations. We have

$$\left\langle\hat{v}\left(\boldsymbol{x},\eta\right)\hat{v}\left(\boldsymbol{x}+\boldsymbol{r},\eta\right)\right\rangle = \int_0^{+\infty}\mathrm{d}\ln k\,\frac{\sin\left(kr\right)}{kr}\frac{k^3}{2\pi^2}\left|u_k\right|^2 , \tag{1.125}$$

where we have used homogeneity and isotropy of the mode function to obtain the expression on the right-hand side. The power spectrum is then conventionally defined as

$$\mathcal{P}_v\left(k,\eta\right) = \frac{k^3}{2\pi^2}\left|u_k\right|^2 . \tag{1.126}$$

From Eq. (1.126), we deduce the power spectrum of ζ

$$\mathcal{P}_\zeta\left(k,\eta\right) = \frac{k^3}{2\pi^2}\frac{\left|u_k\right|^2}{\mathfrak{z}^2} , \tag{1.127}$$

which is a dimensionless quantity. These expressions are true at any time. We are interested in the value of $\mathcal{P}_\zeta(k)$ for CMB scales at the end of inflation. In the

previous part, we have derived the asymptotic value of $u_k/\mathfrak{z}$, given in Eq. (1.124), which combined with Eq. (1.127) gives

$$\begin{aligned}\mathcal{P}_\zeta(k) = \frac{H_\star^2 \kappa \hbar}{8\pi^2 \epsilon_{1\star} c}\Big[1 + 2(1 - \ln 2 - \gamma_{\rm E})\,\epsilon_{1\star} \\ + (2 - \ln 2 - \gamma_{\rm E})\,\epsilon_{2\star} - (2\epsilon_{1\star} + \epsilon_{2\star}) \ln\left(\frac{k}{k_\star}\right)\Big]\,.\end{aligned} \tag{1.128}$$

It is the standard formula for the power spectrum of scalar perturbations on CMB scales at the end of inflation [55]. We can perform similar computations for tensor perturbations, see Sec. 2.2. We introduce a mode function $u^{\rm T}_{k,\lambda}$ for each scalar polarisation which will satisfy Eq. (1.102) where $\mathfrak{z}''/\mathfrak{z}$ is replaced by a''/a. The power spectrum for tensor perturbations then reads

$$\mathcal{P}_{\rm T}(k,\eta) = \frac{4\pi\kappa}{\pi^2 a^2 c} k^3 \left|u^{\rm T}_{k,\lambda}\right|^2\,. \tag{1.129}$$

A direct comparison of Eq. (1.119) and Eq. (1.120) then shows that the equation are equal under the substitution $\epsilon_{1\star} \to \epsilon_{1\star} + \epsilon_{2\star}/2$. Therefore, we can repeat the same procedure of matching sub and super-Hubble limits using an intermediate slow-roll approximation. For CMB scales at the end of inflation, we then have

$$\mathcal{P}_{\rm T}(k) = 2\frac{H_\star^2 \kappa \hbar}{\pi^2 c}\left[1 + 2(1 - \ln 2 - \gamma_{\rm E})\,\epsilon_{1\star} - 2\epsilon_{1\star}\ln\left(\frac{k}{k_\star}\right)\right]\,. \tag{1.130}$$

The spectra Eq. (1.128) and Eq. (1.130) are the key predictions of the theory of inflationary perturbations. We briefly discuss how we can extract information about inflation by measuring them. First, if we neglect the slow-roll corrections, both power spectra Eq. (1.128) and Eq. (1.130) are scale invariant. The deviations from scale invariance appear in the first order in the slow-roll parameter due to departure from an exact de Sitter expansion. These deviations are customarily parameterised by introducing the spectral indices

$$n_{\rm S} = 1 + \frac{{\rm d}\ln\mathcal{P}_\zeta}{{\rm d}\ln k}\,, \tag{1.131}$$

and

$$n_{\rm T} = \frac{{\rm d}\ln\mathcal{P}_{\rm T}}{{\rm d}\ln k}\,. \tag{1.132}$$

Further deviations could be parameterised by higher derivatives of the power spectra, e.g. the so-called running of the spectral index. Truncating at the spectral index we can write $\mathcal{P}_\zeta = A_{\rm s}(k/k_\star)^{n_{\rm S}-1}$ and $\mathcal{P}_{\rm T} = A_{\rm T}(k/k_\star)^{n_{\rm T}}$. Scale invariance corresponds to $n_{\rm S} = 1$ and $n_{\rm T} = 0$. Eq. (1.128) and Eq. (1.130) gives in the first

order in slow-roll $n_{\mathrm{S}} = 1 - 2\epsilon_{1\star} - \epsilon_{2\star}$ and $n_{\mathrm{T}} = -2\epsilon_{1\star}$. The behaviour of the spectra thus depends on the values of the slow-roll parameters, which are model-dependent quantities. Nevertheless, since $\epsilon_1 > 0$ for any inflation model, inflation generically predicts a slightly *red-tilted* spectrum for tensor perturbations $n_{\mathrm{T}} < 0$, i.e. a spectrum with an amplitude decreasing with k. On the other hand, the scalar spectrum can be blue-tilted $n_{\mathrm{S}} > 1$ in specific inflationary models where ϵ_2 becomes negative [39]. The experimental measures of the power spectra constrain the values of the spectral indices n_{S} and n_{T}, and so constrain the space of allowed inflationary models to that which can give rise to these values. Another important quantity is the tensor-to-scalar ratio

$$r = \frac{A_{\mathrm{T}}}{A_{\mathrm{S}}} \approx 16\epsilon_{1\star}\,, \tag{1.133}$$

where we have evaluated the expression in the first order in slow-roll parameters. The level of tensor perturbations is slow-roll suppressed compared to scalar perturbations.

So far, only the dominant scalar perturbations have been identified in the CMB, and only an upper bound for the ratio is known $r < 0.036$ at 95% confidence level [66]. The latest measurement of the CMB by Planck has provided significant support for the prediction of single field inflation. It found no trace of non-Gaussianity in the inhomogeneities at its level of precision [64], and the spectrum of scalar perturbations which was found to be slightly red-tilted with a spectral index measured [11] to $n_{\mathrm{S}} = 0.9649 \pm 0.0042$. The overall amplitude was measured to be $A_{\mathrm{S}} = 2.101^{+0.031}_{-0.034} \times 10^{-9}$. The measure of the index constrains the value of the slow-roll parameters at the Hubble crossing for the cosmological scale. A measure of the tensor perturbations would allow direct access to the value of the first slow-roll parameter via the index n_{T}, and then to the value of the Hubble parameter $H_\star$. We recall that its value is directly related to the energy scale of inflation via Eq. (1.42). We get

$$E_\star = \left(\frac{3\pi^2}{2} r A_{\mathrm{S}}\right)^{1/4} M_{\mathrm{Pl}} c^2\,, \tag{1.134}$$

so the observational upper bound on r gives an upper bound on the energy scale of inflation. We find roughly $E_\star \leq 10^{16}\,\mathrm{GeV}$.

To close this sub-section, we want to emphasise that the tremendous practical success of the inflationary mechanism to predict the CMB observations rests on the assumption that these cosmological-scale inhomogeneities emerged from initial vacuum fluctuations, a purely quantum phenomenon. Therefore the CMB temperature fluctuations would be a trace of quantum physics playing a role on cosmological scales, an observation at odds with the common lore that quantum

physics is only relevant on very short scales. This, albeit commonly accepted, surprising feature of the model is worth a deeper analysis. First, in the treatment we presented previously, it was unclear when the physics described stopped being quantum and became completely classical. This is the quantum-to-classical transition problem. Second, although the measure of the power spectrum matched the one predicted from amplified vacuum fluctuations, this only constitutes indirect proof of the quantum origin of the perturbations. We could provide an *ad-hoc* initial stochastic Gaussian distribution that would reproduce the final measured power spectrum, see Sec. 2.2. One might thus want to seek other features in the final distribution that initial classical inhomogeneities would not be able to reproduce. Finally, finding such a feature would demonstrate that a quantum treatment of the fluctuations of geometry is required in the early Universe, so that gravity (at least at a linear level) has to acquire the status of a quantum theory. These are the motivations for the analysis conducted in Chapt. 2.

1.2.4 (P)reheating: connecting inflation to the standard model of cosmology

1.2.4-a Reheating processes

In Sec. 1.2.1, we introduced a transitory phase of inflation within the radiation domination era. We have explained that such a phase allows us to solve the hot Big Bang puzzles while giving a generation mechanism for inhomogeneities in the early Universe, the seeds for structure formation. During inflation, the Universe's energy budget is entirely dominated by the inflaton field φ (and its perturbations $\delta\hat{\varphi}$). Any pre-existing form of matter is expected to be highly diluted by the expansion so that most of the Universe's matter content must be produced after inflation [67, 68]. At the end of inflation, the energy of the inflaton must be somehow transferred to particles in other fields and eventually into the particles of the Standard Model. In addition, to allow BBN to proceed as predicted and observed, these particles must thermalise and do so at a temperature $T_{\rm reheat}$ at least as large as the temperature then: $T_{\rm reheat} \geq T_{\rm BBN} \approx 1\,\text{MeV}$. The processes leading to the initial radiation domination of the standard Hot Big Bang model, and the period during which they unfold, are commonly referred to as *reheating*[12] [69]. We give a brief overview of reheating to connect with the work on an 'analogue preheating experiment' presented in Chapt. 3. We refer to the review [70] for details.

The generation of particles in reheating is expected to proceed in two ways. First, by perturbative decays of inflaton particles φ, to particles of other matter

[12]Since we expect inflation to break any pre-existing thermal equilibrium and dilute the existing forms of matter, the Universe at the end of inflation would be empty and cold. Hence, we must (re)heat it.

fields χ. An example of such a process is a 3-body interaction $\varphi \to \chi\chi$, corresponding to the annihilation of φ-particles in pairs of χ particles . In the first papers on reheating, such perturbative decay processes were considered by adding an effective decay rate in the Klein-Gordon equation (1.69) of the inflaton. Additionally, it was later realised [71, 68, 72] that the oscillations of the inflaton at the end of inflation, see Fig. 1.4, effectively acting as a strong classical field, could trigger an exponential production of particles in modes of other fields χ, within some energy range related to the frequency of the oscillations. This is the phenomenon of parametric amplification. The parametric processes can initially be much more efficient than the perturbative ones [73]. This phase of parametric growth is referred to as *preheating* [72]. However, reheating never completes at this stage [73]. First, parametric resonances produce particles in a very non-thermal state. Interactions between the produced particles are thus necessary to drive the distribution to a thermal one. Second, the parametric resonance process is going to become inefficient as the oscillations of the inflaton are damped by the energy transfer to other particles. Perturbative channels are necessary to ensure in the late stages a total decay of the inflaton and completion of reheating [73, 70]. In [4], reproduced in Sec. 3.4, we consider some interactions between quasi-particles produced in an analogue preheating experiment. However, this analysis focuses on how these interactions affect the production of quantum coherence in the early stage of parametric resonance rather than on how they could lead to the thermalisation of the excitations.

1.2.4-b Illustration of preheating

To close this sub-section, we illustrate the phenomenology of parametric resonance by considering a simple model of preheating used in [73]. Assume that the potential of the inflaton field has a minimum at $\varphi = 0$. We approximate the potential to be quadratic around its minimum

$$V_\varphi(\varphi) \approx \frac{m^2c^2}{2\hbar^2}\varphi^2 , \tag{1.135}$$

and assume that this approximation represents well the part probed by the inflaton in its late-time oscillations. Assume now that the inflaton is coupled to a quantum scalar field $\hat{\chi}$. We assume $\hat{\chi}$ to be massless for simplicity. We take the coupling to the inflaton of the form $\lambda^2\varphi^2\hat{\chi}^2$. The action for χ reads

$$S_\chi = -\frac{1}{c}\int \mathrm{d}^4x\sqrt{-g}\left(\frac{1}{2}g^{\mu\nu}\partial_\mu\hat{\chi}\partial_\nu\hat{\chi} + \frac{1}{2}\lambda^2\varphi^2\hat{\chi}^2\right) . \tag{1.136}$$

As we did previously for $\hat{v}$, we can perform a mode expansion of the scalar field

$$\hat{\chi}(\boldsymbol{x}, t) = \int \frac{\mathrm{d}^3\boldsymbol{k}}{(2\pi)^{3/2}}\left[e^{i\boldsymbol{k}.\boldsymbol{x}}\chi_k(t)\,\hat{c}_{\boldsymbol{k}} + e^{-i\boldsymbol{k}.\boldsymbol{x}}\chi_k^\star(t)\,\hat{c}_{\boldsymbol{k}}^\dagger\right] . \tag{1.137}$$

The mode functions χ_k are going to satisfy the equation of motion of the Fourier modes of the classical version of the field

$$\ddot{\chi}_{\boldsymbol{k}} + 3\frac{\dot{a}}{a}\dot{\chi}_{\boldsymbol{k}} + \left[\frac{c^2k^2}{a^2(t)} + \lambda^2\varphi^2(t)\right]\chi_{\boldsymbol{k}} = 0 \tag{1.138}$$

We make the simplifying assumption that, over the characteristic time scale of the expected growth, we can neglect the expansion of space and take $a = 1$ in Eq (1.138). As a second simplifying assumption, we assume that the inflaton φ oscillates at constant amplitude fixed by its mass $\varphi(t) = \varphi\sin(mc^2t/\hbar)$. This assumption eventually breaks down because the oscillations are damped by the expansion of space and the transfer of energy to $\hat{\chi}$. Under these assumptions Eq. (1.138) can be recast in the form of a Mathieu equation [73]

$$\frac{\partial^2\chi_{\boldsymbol{k}}}{\partial z^2} + \left[\mathcal{A}_k + 2q\cos\left(2\theta\right)\right]\chi_{\boldsymbol{k}} = 0\,, \tag{1.139}$$

where $\mathcal{A}_k = 2q + c^2k^2/m^2$, $q = \lambda^2\varphi^2/2m^2$ and $\theta = mc^2t/\hbar$. Eq. (1.139) is a well-known equation. Its analysis [74] shows that for some q-dependent ranges of $\mathcal{A}_k$ around specific values $\mathcal{A}_k^{(l)}$, the solution will exhibit exponential growth. Outside of these instability bands, the modes oscillate. In the narrow resonance regime, $q \ll 1$, the instability bands are located around $\mathcal{A}_k^{(l)} \approx l^2$ and of size $\sim q^l$. Therefore, the primary band $\mathcal{A}_k^{(1)} \approx 1$ is the largest one, and the resonant modes have frequencies $ck \approx mc^2/\hbar$ i.e. half of the driving frequency. We refer to [74] for more on the instability regime. Notice that in a classical setting, where the Fourier modes of the classical field satisfy Eq. (1.138), an initial vacuum of $\hat{\chi}$ excitation corresponds to $\chi_{\boldsymbol{k}} = 0$. In this case, the solution of Eq. (1.138) gives $\chi_{\boldsymbol{k}} = 0$ at all times. In the quantum case, however, the vacuum corresponds to the normalisation Eq. (1.113), which leads to an amplification of vacuum fluctuations, a pure quantum phenomenon. As we will detail in Sec. 1.3.4-b, a signature of this quantum origin is that the generated pairs are entangled. The entanglement can be generated even if a small incoherent population is initially present.

Note the similarity of this process with the vacuum amplification of scalar and tensor perturbations during the slow-roll part of the evolution. The different dynamics of the background, growing for inflation and oscillating for preheating, lead to different excitation spectra. While any super-Hubble mode is amplified during inflation, only modes in well-defined resonant modes are produced during preheating. Both of these effects fit in a large class of phenomena where a quantum field is excited by a strong classical field such as the Schwinger effect [75] or the Hawking effect [76, 77]. These effects are described using the formalism of quantum field theories in curved spacetimes (QFTCS). We see that such QFTCS effects have significant cosmological consequences. Yet, they are hard to demonstrate experimentally. These effects are small, and the field strengths accessible in laboratories

are often insufficient to generate a signal strong enough to be detected. Therefore, a first avenue to explore is to look for signatures of such quantum effects directly in cosmology. This is the topic of Chapt. 2 for the generation of inflationary perturbations. A second possible avenue is to rely on analogue systems, which are described by the same equations of motion as a QFTCS situation while being experimentally realisable. This perspective led to the development of the *analogue gravity* community, which we present in the next section, Sec. 1.3.

1.3 Analogue gravity

1.3.1 Motivations

The idea of analogue gravity first emerged in the study of Hawking radiation [76, 77, 78]. By studying the evolution of modes of a field in the geometry of a star collapsing to a black hole, Hawking predicted that the black hole would emit a thermal black-body spectrum of the particles associated with that field. The temperature of such radiation was predicted to be inversely proportional to M, the mass of the black-hole

$$T_{\mathrm{H}} = \frac{\hbar c^3}{8\pi G M k_{\mathrm{B}}} \approx \frac{M_\odot}{M} 60\mathrm{nK}\,. \tag{1.140}$$

For astrophysical black holes of mass typically larger than a few solar masses [79], this temperature is much smaller than that of the cosmic microwave background $T_{\mathrm{CMB}} \approx 3\,\mathrm{K}$ [14], so that the hole effectively absorbs energy rather than emits. The temperature is even smaller than the CMB temperature anisotropies $\delta T/T_{\mathrm{CMB}} \approx 10^{-5}$ [24]. Thus, even if the prediction of Hawking is correct, the radiation of astrophysical black holes seems too small to be detected [77].[13]

The Hawking effect illustrates the difficulty of observing QFTCS effects directly. A similar illustration can be found in the Unruh effect [78]. It predicts that a uniformly accelerating observer in the Minkowski vacuum would observe thermal radiations of particles at a temperature

$$T_{\mathrm{U}} = \frac{\hbar}{c}\frac{\alpha}{2\pi k_{\mathrm{B}}}\,, \tag{1.141}$$

where α is the proper acceleration of the observer. Getting a temperature of 1 K in Eq. (1.141), with peak radiation in the microwave, requires accelerating the detector to $\alpha \approx 10^{20}\mathrm{m/s^2}$. To get a reference, we consider the initial linear

[13] As already mentioned in [77], smaller black-holes could have formed as *primordial black-holes* from the collapse of large density fluctuations at the end inflation [80, 81]. If they exist, such black holes can be of all masses, and the smallest ones would emit at a high rate.

accelerator Linac4 at the LHC [82] that takes H^- ions, that we will assume to be protons, from rest to 160 MeV of kinetic energy over 80 m. To get a very rough estimate, we assume the acceleration to be uniform throughout and compute the proper acceleration of the particle (which, for these velocities, does not differ much from the acceleration in the laboratory frame). We get $a \approx 5.70 \times 10^{14} \mathrm{m/s^2}$ i.e. six orders of magnitude lower than the acceleration necessary even to get microwave radiation. Other estimates and a proposition to indirectly observe the Unruh effect can be found in [83].

Still, a few years after the predictions of Hawking radiation, Unruh realised that the equations describing the propagation of linear perturbations (i.e. sound waves) in a trans-sonic fluid could be recast in the form of the equation of motions of a scalar field in a black-hole metric [84]. The intuition behind this result is that in a trans-sonic fluid, there is a sonic horizon. Past this horizon, the flow velocity is larger than the speed of sound, and sound waves can only propagate downstream, like particles beyond the horizon of a black hole. Unruh coined the word 'dumb'-holes for these geometries where sound is trapped. Following the same reasoning leading to Hawking radiation, a quantum fluid with such a sonic horizon would emit thermal radiation of sound waves. Unruh found the temperature to be typically small

$$T \approx 3 \times 10^{-7} \, \frac{c_\mathrm{s}}{c} \left(\frac{R}{1\mathrm{mm}} \right)^{-1} \mathrm{K} \,, \tag{1.142}$$

where c_s is the speed of sound in the fluid and R the size of the horizon. Nevertheless, to quote his words, observing the radiation in this fluid is still 'a much simpler experimental task than creating a 10^{-8} cm black hole'.

In addition to opening up the possibility for the experimental observation of an effect akin to Hawking radiation, the study of this *analogue* system was also acknowledged as a means to assess the robustness to UV modifications of QFT above the Planck scale [84]. Indeed, the derivation assumes no back-reaction of the produced particles on the background metric, and also that there are similar quantum fluctuations available until arbitrarily larger energy, even beyond the Planck scale, to fuel the radiation indefinitely [85]. This is the so-called trans-planckian problem [86, 87, 88]. While the physics beyond the Planck scale i.e. a theory of quantum gravity, is unknown, we know the fluid theory breakdowns when considering scales close to the inter-particle separation. Therefore, the analogue fluid can be used to investigate how a modified UV theory affects the predicted radiation. Ref. [84] marks the beginning of the analogue gravity programme, initially focused on the analogue of the Hawking effect. Before reviewing the field's main achievements, we demonstrate the advertised correspondence between the propagation of sound waves on a fluid and that of a scalar field in curved spacetime.

1.3.2 Sound-waves on a fluid as scalar field in curved spacetime

We closely follow the demonstration made in [89]. Consider a fluid not submitted to any external force described by a pressure field p, a mass density field ρ and a velocity field $\boldsymbol{v}$. We work in the laboratory frame $(ct, \boldsymbol{x})$ and the motion of the fluid is described by the continuity and Euler's equations

$$\partial_t \rho + \vec{\nabla} \cdot (\rho \boldsymbol{v}) = 0\,, \tag{1.143a}$$

$$\partial_t \boldsymbol{v} + \boldsymbol{v}\left(\vec{\nabla} \cdot \boldsymbol{v}\right) = -\frac{1}{\rho}\vec{\nabla} p\,. \tag{1.143b}$$

The continuity equation expresses the local conservation of the mass density, while Euler's equation comes from applying Newton's third law to a mesoscopic volume element. Assuming the fluid to be irrotational and making a Helmholtz decomposition of the velocity field, we have $\boldsymbol{v} = -\vec{\nabla}\phi$, where ϕ is the velocity potential. Then $\vec{\nabla} \cdot \boldsymbol{v} = -\boldsymbol{v} \times (\vec{\nabla} \times \boldsymbol{v}) + \vec{\nabla}(v^2)/2 = \vec{\nabla}(v^2)/2$. Assuming now the fluid to be barotropic i.e. the energy density field is a function of the pressure field $\rho = \rho(p)$, we can define the specific enthalpy of the fluid

$$h\,(p) = \int_0^p \frac{\mathrm{d}p'}{\rho\,(p')}\,, \tag{1.144}$$

such that $\vec{\nabla} h = \vec{\nabla}(p)/\rho$.[14] Euler equation (1.143a) then reads

$$\vec{\nabla}\left(-\partial_t \phi + h + \frac{v^2}{2}\right) = 0\,, \tag{1.145}$$

which can be integrated to

$$-\partial_t \phi + h + \frac{v^2}{2} = 0\,. \tag{1.146}$$

The integration constant C can always be absorbed by redefining the velocity potential $\phi \to \phi + Ct$, which does not affect the velocity field. We set it to 0 in Eq. (1.146). Once the functional link between the density ρ and pressure field p is fixed, the equations Eq. (1.143b) and Eq. (1.146) form a closed system for two dynamical degrees of freedom, the velocity potential ϕ and the pressure field p.

[14] The enthalpy of a thermodynamic system of volume V is defined as the sum of its internal energy U and the energy due to external pressure P exerted on it $H = U + PV$. Consider the enthalpy variation in the system to see how Eq. (1.144) is related to the enthalpy. It reads $\mathrm{d}H = T\mathrm{d}S + V\mathrm{d}P$. If we consider an isentropic system $\mathrm{d}S = 0$, then $\mathrm{d}H = V\mathrm{d}P$. The specific enthalpy h is the enthalpy per unit of mass, so $\mathrm{d}h = \mathrm{d}P/\rho$ since the volume divided by the mass is the inverse mass density. Integrating this equation gives back Eq. (1.144).

We now consider the propagation of perturbations on top of a background solution ϕ_0 and p_0 of these equations; this is the definition of sound waves. We have

$$p = p_0 + \delta p\,, \tag{1.147a}$$
$$\phi = \phi_0 + \delta\phi\,, \tag{1.147b}$$
$$\boldsymbol{v} = -\vec{\nabla}\phi_0 - \vec{\nabla}\left(\delta\phi\right) = \boldsymbol{v}_0 + \delta\boldsymbol{v}\,, \tag{1.147c}$$

where we assume the perturbations to be of small amplitude $|\phi_0| \gg |\delta\phi|$ and $|p_0| \gg |\delta p|$. Varying the specific enthalpy Eq. (1.144) we have

$$h\left(p\right) \approx h\left(p_0\right) + \frac{\delta p}{\rho_0}\,. \tag{1.148}$$

The perturbations of Eq. (1.143b) and Eq. (1.146) at linear order, then reads

$$-\partial_t\delta\phi + \frac{\delta p}{\rho_0} + \boldsymbol{v}_0\cdot\delta\boldsymbol{v} = 0\,, \tag{1.149a}$$
$$\partial_t\delta\rho + \vec{\nabla}\left(\delta p\boldsymbol{v}_0\right) + \vec{\nabla}\cdot\left(\rho_0\delta\boldsymbol{v}\right) = 0\,, \tag{1.149b}$$

Using Eq. (1.149a) we get

$$\delta p = \rho_0\left[\partial_t\delta\phi + \boldsymbol{v}_0\cdot\vec{\nabla}\left(\delta\phi\right)\right]\,, \tag{1.150}$$

that completely expresses the pressure perturbation as a function of the velocity potential perturbation. We define the local speed of sound c_0 by

$$c_0^{-2} = \left.\frac{\partial\rho}{\partial p}\right|_{\rho_0}\,. \tag{1.151}$$

Notice that the speed of sound is *a priori* a field that depends on time and position. Using Eq. (1.150), the density perturbation can then be expressed as

$$\delta\rho = \frac{\rho_0}{c_0^2}\left[\partial_t\delta\phi + \boldsymbol{v}_0\cdot\vec{\nabla}\left(\delta\phi\right)\right]\,. \tag{1.152}$$

Combining this equation with Eq. (1.149b) we get an equation for the perturbation of the velocity potential alone

$$-\partial_t\left\{\frac{\rho_0}{c_0^2}\left[\partial_t\delta\phi + \boldsymbol{v}_0\cdot\vec{\nabla}\left(\delta\phi\right)\right]\right\} + \vec{\nabla}\cdot\left\{\partial_t\delta\phi - \frac{\rho_0}{c_0^2}\left[\partial_t\delta\phi + \boldsymbol{v}_0\cdot\vec{\nabla}\left(\delta\phi\right)\right]\right\}\,. \tag{1.153}$$

This last equation can then be rewritten as a Klein-Gordon equation, see Eq. (1.69), for $\delta\phi$ as if it were a minimally coupled scalar field on curved spacetime without a potential [89]

$$\Box\delta\phi = -\frac{1}{\sqrt{-g}}\partial_\mu\left(\sqrt{-g}\,g^{\mu\nu}\partial_\nu\delta\phi\right) = 0\,, \tag{1.154}$$

where the *acoustic* metric is defined in the laboratory coordinates $(t, \boldsymbol{x})$ by

$$g_{\mu\nu} = \frac{\rho_0}{c_0}\begin{pmatrix} -\left(c_0^2 - v_0^2\right) & -\boldsymbol{v}_0 \\ -\boldsymbol{v}_0 & \mathbb{1}_3 \end{pmatrix}, \tag{1.155}$$

where $\mathbb{1}_3$ is the three-dimensional identity matrix. Eq. (1.154) is the basis of the analogy. We give the associated acoustic line-element[15]

$$\mathrm{d}s^2 = \frac{\rho_0}{c_0}\left[-\left(c_0^2 - v_0^2\right)\mathrm{d}t^2 - 2\mathrm{d}t\boldsymbol{v}_0\cdot\mathrm{d}\boldsymbol{x} + \mathrm{d}\boldsymbol{x}\cdot\mathrm{d}\boldsymbol{x}\right]. \tag{1.156}$$

Although we used a classical framework, since Eq. (1.154) is a linear equation, we would obtain the same result by considering a quantum fluid with a large coherent background treated classically and some perturbations on top, e.g. phonons on a Bose-Einstein condensate $\hat{\phi} \approx \phi_0\hat{\mathbb{1}} + \delta\hat{\phi}$, see Sec. 3. Notice [89] that the analogy has limits. First [89], we only reproduce the kinematics of a field on a given spacetime metric and, although this metric could be dynamical, e.g. if ϕ_0 is made time-dependent, its dynamics is *not* described by analogue Einstein's field equations. Second, we can change coordinates, e.g., redefining time $t \to \tau$ to match the form that a curved spacetime metric would have in a specific set of coordinates; see below for an example with Schwarzchild metric. However, measuring devices will ultimately experience the time of the laboratory frame t and not the transformed one τ, see however [90]. Finally, not every metric can be reproduced, at least not in the simple treatment we presented. In particular, a generic $3+1$ spacetime metric is defined by 6 independent functions: the metric can be represented by a symmetric 4×4 matrix in coordinates which has 10 independent coefficients, but these coefficients depend on a choice of coordinate system which we are free to choose, adding 4 constraints. On the other hand, the acoustic metric features three functions p_0, ϕ_0 and c_0. The continuity equation relates the first two; we are only left with 2 functions to fix. Still, tuning these two functions allows us to reproduce many physically relevant spacetimes, see [89] for examples.

To close this discussion, we show, following [84] (while keeping the mostly pluses convention used in this manuscript), how to reproduce the near horizon part of a black-hole metric. First, let us assume that the speed of sound c_0 is everywhere constant and that the background flow is spherically symmetric, stationary and convergent so that $\rho(r)$ and $\boldsymbol{v} = v^r(r)\mathbf{u}_r$, with $v^r(r) < 0$. Going to spherical coordinates the line element (1.156) then reads

$$\mathrm{d}s^2 = \frac{\rho_0}{c_0}\left\{-\left(c_0^2 - v_0^2\right)\mathrm{d}t^2 - 2v_0^r\mathrm{d}t\mathrm{d}r + \mathrm{d}r^2 + r^2\left[\mathrm{d}\theta^2 + \sin^2\theta\mathrm{d}\varphi^2\right]\right\}. \tag{1.157}$$

[15] Notice that the metric is not dimensionless and the line-element does not have the dimension of a length squared. However, since the field obeys a linear equation of motion, the metric can always be rescaled by an arbitrary factor to be made dimensionless.

We define a new time coordinate

$$\tau = t + \int_0^r \frac{v_0^r}{c_0^2 - (v_0^r)^2} \mathrm{d}r' \,, \tag{1.158}$$

and assume that the fluid becomes trans-sonic at a radius R such that $v^r(r) \approx -c_0 + 2\alpha(r-R)$ close to the sonic horizon. The line element close to the horizon $r \approx R$ then reads

$$\mathrm{d}s^2 = \frac{\rho_0}{c_0}\left[-2\alpha\,(r-R)\,c_0 \mathrm{d}\tau^2 + \frac{c_0}{2\alpha\,(r-R)}\mathrm{d}r^2 + r^2\left(\mathrm{d}\theta^2 + \sin^2\theta \mathrm{d}\varphi^2\right)\right] . \tag{1.159}$$

Comparing with Schwarzchild metric in usual spherical coordinates close to the horizon $r \approx r_\mathrm{s} = 2GM/c^2$, where

$$\mathrm{d}s^2_{\mathrm{Sch.}} = -\frac{c^2}{r_\mathrm{s}^2}\,(r - r_\mathrm{s})\,\mathrm{d}t^2 + \frac{r_\mathrm{s}}{r - r_\mathrm{s}}\mathrm{d}r^2 + r^2\left(\mathrm{d}\theta^2 + \sin^2\theta \mathrm{d}\varphi^2\right) , \tag{1.160}$$

we have the mapping $c_0 = c$ and $\alpha = c^3/4GM$ up to the factor ρ_0/c_0 in front. In the analogy, the speed of sound plays the role of the speed of light, and the factor α is related to the mass of the black hole. This analogy at the linear level, with a conformal factor, is sufficient to get the Hawking effect [84, 89]. Here we only use the formula (1.140) to find what the analogue of Hawking's temperature would be

$$T_\mathrm{H} = \frac{\hbar}{2\pi k_\mathrm{B}}\left(\left.\frac{\partial v^r}{\partial r}\right|_{r=R}\right)^{-1} . \tag{1.161}$$

Theoretical refinements of this idea and experimental progress towards observing an analogue Hawking effect have been the central focus in the analogue gravity community until recently.

1.3.3 Progress and achievements in Analogue Gravity

Several accounts of the progress in the study of analogue systems exist in the literature [85, 89, 91, 92]. We limit ourselves here to a short account mainly following [85, 92] to illustrate the diversity of platforms used and highlight the successes of the analogue gravity programme so far. The initial focus was on analogue black holes and the Hawking effect. A first theoretical success was in understanding that the break-down of the fluid model for large frequencies did not preclude the existence of Hawking radiation, and, provided dispersion was weak enough, preserved approximately its thermality at the expected temperature given in Eq. (1.140) [93, 94, 95, 85]. On the experimental side, many systems were considered as possible platforms to realise the analogy. For instance, the possibility of using superfluid He-3 [96, 97, 98], or Bose-Einstein condensates [99],

two typically quantum fluids, was quickly suggested. The opportunity of using electromagnetic radiation in a medium was also analysed [100, 101]. Since, as detailed in Sec. 1.3.2, the analogy stands both for quantum and classical fields depending on the nature of the fluid considered, a classical analogue black-hole in water waves system was also considered [102].

The mechanism behind Hawking radiation is that of a scattering of modes at the horizon of black-hole. The Hawking radiation corresponds to one of the scattered modes of this process. When vacuum fluctuations source the process, it is called *spontaneous*. The same type of scattering leading to Hawking radiation can also be triggered by sending on the horizon a classical wave or by letting external noise impinge on it. We get a *stimulated* Hawking radiation, the analogue of which can be studied in classical systems.

The first experimental results started to be reported in 2007 with experiments in electromagnetic optical fibres [103] and water waves [104]. In the following years, experiments were improved in these platforms, e.g. see [105] in fibres and [106, 107] for water waves, and performed in a growing diversity of platform, e.g. optical crystals [108], polaritons [109], superfluid He-3 [110] or Bose-Einstein condensates (BEC) [111, 112]. New theoretical tools were introduced to analyse them, e.g. 2-point density correlation functions [113]. To conclude this sketch of the landscape of analogue black-hole experiments and analysis, we point out that, as of June 2023, only one group [111, 112] claims to have observed spontaneous analogue Hawking radiation i.e. seeded by vacuum fluctuations.

1.3.4 Cosmological analogues

Despite the initial dominance of analogue black holes in the analogue gravity field, analogies with other systems have also been considered. The analogues of cosmological situations are of particular relevance for this manuscript that presents results on the analysis of an analogue preheating experiment, see Sec. 1.2.4 and Sec. 3. Before moving on to this specific set-up, we review in this sub-section the first analogue cosmology systems that have been considered or realised.

1.3.4-a Early theoretical investigations

Ref [96] is an early example of analogy with cosmology. It investigates analogies between defects in superfluid He-3 and topological defects in the early Universe, such as cosmic strings.

While the Schwarzchild black hole is a time-independent and stationary spacetime, the most relevant cases for cosmology are rather time-dependent and homogeneous spacetime, as represented by the FLRW metric of Eq. (1.17). Analogues of time-dependent spacetimes were also quickly considered by authors.

First, although not an analogue gravity experiment, the 'Bose-nova' experiment [114] was analysed by [115, 116, 117] drawing inspiration from inflationary

cosmology and the analogue gravity endeavour. In the experiment, the interactions between atoms in a Bose gas are changed from repulsive to attractive, leading to a contracting of the BEC. They drew a parallel between the dynamics of certain excitations on top of the condensate and that of perturbations in inflation, which are 'frozen' and amplified when super-Hubble, before oscillating at later times when re-entering the Hubble radius. They attribute some oscillations seen in [114] to these perturbations.

The possibility of simulating time-dependent spacetimes with such Bose gas with tunable interactions was first explored in [118, 119]. The authors showed that in a constant density condensate, with an appropriately modulated speed of sound, phonons i.e. quantised sound waves, behave as a scalar field in an effective expanding FLRW metric. The dynamics then lead to the creation of phonons from the vacuum [119]. Another way to realise an effective FLRW metric is to consider an expanding (or contracting) condensate or to modulate the sound speed and the trapping frequency simultaneously, as suggested by [120]. The authors also generalised the computations of [119] for the creation of phonons and suggested using density-density correlations, described in Sec. 3 of this manuscript, to demonstrate the presence of quasi-particles. Some authors have also considered the physical status of the coordinates in which the analogue metric is derived. In [121], the authors considered an FLRW spacetime in different coordinates and studied the possibility of observing an analogue of the Gibbons-Hawking effect. In [90], the authors suggested building a detector sensitive to different time coordinates to test their different responses to quasi-particle creation. Other authors have considered the analogy of an expanding Universe with a purely expanding Bose gas without modulating the speed of sound. For instance [122] considered a three-dimensional Bose gas, while [123] considered lower dimensional trapped gases with non-standard self-interactions. The authors of [124] argued that the proposed expansion of the gas, or change of its scattering length, comes with difficulties that can be circumvented by considering a two-component gas.

Numerical simulations of the generation of quasi-particles in analogue cosmology were also performed. In [125], the authors performed numerical simulations of a two-dimensional Bose gas with time-dependent scattering length to evaluate particle production for inflationary or cyclic universe analogues. They used the Truncated Wigner Approximation (TWA) method that became quite standard in analogue gravity, see below Sec. 3.5 and e.g. [126]. In a follow-up work [127], the authors study the implications of breaking down the analogue gravity picture beyond the hydrodynamical regime where we have an acoustic metric see Sec. 1.3.2.

Finally, in [128, 129], the authors proposed to use ion traps rather than Bose gases to build analogue cosmology set-ups.

1.3.4-b Analogue cosmology experiments

The first analogue cosmology experiments were performed in the 2010s. We list a few examples of them to give a panorama. In [130], the authors report on the observations of the production of sound waves following the modulation of the trapping frequency of an elongated cigar-shaped gas. The creation proceeds by a parametric transfer of the energy of the condensate to pairs of phonons in resonant modes at half the driving frequency. Initially designed as an analogue dynamical Casimir effect experiment proposed in [131], the results of the experiment were later re-interpreted as an analogue of preheating [132]. In [133], the analogy was extended to the late time dynamics where a redistribution of resonant phonons to other modes, akin to preheating, see Sec. 1.2.4, is conjectured to have happened. The authors of [130] showed that the produced phonons were correlated but not entangled.

Soon after, in [134], the authors performed a quench i.e. a sudden variation, of the scattering length of a two-dimensional BEC. They observed the amplification of density fluctuations attributed to the creation of phonon pairs and the formation of coherent density oscillations, a signature of the (classical) correlation of the pairs, similar to Sakharov oscillations [135, 136] in primordial inhomogeneities. In a recently updated run of the experiment [137], they reported the observation of the quantum entanglement of the pairs. This arguably makes [137] a successful DCE analogue experiment.

Another analogue cosmology experiment using a Bose gas was reported in [138]. There the authors designed a ring-shaped two-dimensional BEC on which they imprinted an azimuthal phonon pattern before expanding the radius of the BEC. They observed a redshifting of the phonons' wavelength akin to that of cosmological perturbations in FLRW and a damping of their amplitude that they partially attribute to an analogue of Hubble friction. At the end of the expansion, they witness the generation of transverse oscillations of the condensate, whose energy then transfers to topological defects (dark solitons, then vortices). They point out that this transfer is analogue to some reheating models. Refined analyses were performed in [139, 140].

Very recently, in [141], the authors report a precise realisation of the suggestion of [119, 120] in a BEC. The authors first observed the propagation of a localised wave packet of phonons in real space. They showed that, by tuning the geometry of the condensate, they could mimic the propagation in positive, flat or negative curvature spacetimes. Then they perform a co-ramp of the scattering length and the trapping frequency to generate phonons in pairs. They report the observation of analogue Sakharov oscillations, as in [142, 137] following a quench of the scattering length but not that of entanglement of the pairs.

Finally, other experimental platforms were also used for analogue cosmology experiments. The authors of [143] considered the relative motion of two trapped

ions. The relative motion is seen as the analogue of a mode of a quantum field. By changing the trap frequency, they managed to squeeze its state without directly evidencing the entanglement of the two ions. Sakharov-like oscillations were observed in a quantum fluid of light [144], but no direct evidence of entanglement was shown.

Lastly, a second analogue preheating experiment was designed and realised using a fluid-fluid interface [145]. The authors predicted how interactions between the different modes of perturbations generically lead to a transfer of energy from the primary resonant modes to other modes. They were able to observe experimentally different signatures of this transfer, distinguishing them from, for instance, extra Floquet resonances.

1.3.4-c Experiments beyond QFTCS?

In the earliest analysis and experiments, the analogue gravity community focused on simulating pure QFTCS effects. There, quantum perturbations are acted upon by a classical background field, produced particles are assumed to be non-interacting and not back-react on the classical background. In contrast, analogues of (p)reheating, during which interactions and backreaction are essential, have recently received much attention. In addition to the experiment [145], several theoretical studies have been published [146, 147, 148, 149]. The interactions between the produced quasi-particles and the backreaction of these quasi-particles on the condensate are both analysed. For instance, in [148], the authors were able to numerically follow the gradual fragmentation of the initially homogeneous condensate into patches of different densities due to the backreaction of the perturbations, and the decay of the initially excited field, the analogue of the inflaton.

In a similar spirit, we study in this manuscript a possible dissipation channel for the excitations produced by the initial parametric amplification in [130]. Contrary to [145], the excitations of the system are quantum. As detailed in Sec. 1.2.4, we expect that (quasi-)particles will be generated from the quantum vacuum, and a signature of this creation out of the vacuum is that they appear in entangled pairs [132]. Unfortunately, the measured correlations in the original experiment were insufficient to demonstrate the entanglement of the pairs. In [132], the authors showed that a small degree of dissipation was sufficient to explain this absence of entanglement. However, a precise microphysical mechanism to explain this dissipation was missing. In Sec. 3, we present the progress made during this PhD in this direction. In particular, we compute the decay rate of the quasi-particle number and pair correlation induced by the first-order interaction between them. We verify the validity of our predictions by comparing them with numerical simulations. These findings could be helpful in optimising the visibility of entanglement in a new run of the experiment [130].

2 - Quantumness and decoherence of cosmological perturbations

2.1 Content of this chapter

In this chapter, we reproduce the references [1, 2, 3]. They are the original works produced during the PhD devoted to finding features in the state of cosmological perturbations that could reveal their quantum origin. The three next sections are made up of a published article which is briefly introduced. In these introductions we give some context, point out possible mismatches between existing conventions, and sometimes add details skipped in the paper.

2.2 Review: 'Quantum cosmological gravitational waves?'

We start this discussion of the search for quantum features in cosmological perturbations with the review article [1]. Although published later than Ref. [2] and Ref. [3], it exposes in detail the formalism used in other references while skipping the technicalities of these specific works. We, therefore, reproduce it first as an introduction to the two other works. The detailed exposition is contained in Sec. 3 of [1], except for Sec. 3.7, written by Patrick Peter, to be considered separately. Although the focus of the review is on tensor perturbations, most of this exposition is equally applicable to scalar perturbations. Still, note that the discussion of the evolution of the perturbations in a simplified cosmological model made in Sec. 3.8 cannot be applied to scalar perturbations. The latter are described by the Mukhanov-Sasaki variable v and the equation Eq. (1.102) *only* during inflation. The considerations on the extreme squeezing of perturbations in de Sitter apply to scalar and tensor. Finally, the core of the analysis in Sec. 4 and the conclusion in Sec. 5 cover both the scalar and tensor cases. We also point out that the Lagrangian considered in Eq. (22) of [1], reproduced below, differs from that in Eq. (1.98) by a total derivative $\mathrm{d}[\mathcal{H}(\mu_\lambda^\star\mu_\lambda)']/\mathrm{d}\eta$. The form used in [1] is more standard in the cosmology literature, e.g. [150]. A canonical transformation relates them, and they give the same results when computing the expectation values of the same operators. Nevertheless, these different conventions result in different definitions for the conjugated field $\pi_\lambda = \partial L/\partial\mu'_\lambda$: in the convention of Eq. (1.98) we have $\pi_\lambda = \mu'_\lambda$, while in that of Eq. (22) of [1] we have $\pi_\lambda = \mu'_\lambda - \mathcal{H}\mu_\lambda$.

An important consequence, as explained in [151], is that the creation/annihilation operators, Bogoliubov coefficients, and so the squeezing parameters, see Eq. (42) of [1], defined from these two different fields will in general be different. This difference is manifest when comparing Fig. 5 of [1] and Fig. 3 of [2], where the direction of squeezing is horizontal in the first case and vertical in the second. This mismatch translates the difference between the fluctuations of $\hat{v}'$, which are asymptotically of order unity, and those of $\hat{v}' - \mathcal{H}\hat{v}$, which, due to the second term, grow faster than those of $\hat{v}$. However, note that they agree when the expansion of the background encoded by $\mathcal{H}$ can be neglected, e.g. in radiation domination for tensor perturbations.

Two additional references [152, 153] would have deserved citation in the literature review, but we were unaware of them at the time of writing. In [152], the authors considered the decoherence induced by isocurvature perturbations on adiabatic perturbations in a two-field model, where the fields are coupled via the gravitational perturbations. They show that the adiabatic perturbations can be efficiently decohered, in the sense that the off-diagonal matrix elements are suppressed, and compute the associated entanglement entropy. In [153], the authors also considered the decoherence caused by one field on another in de Sitter spacetime. In addition, they considered the effect of a modified dispersion relation for the 'measured' scalar field. They showed that there is a competition between squeezing and decoherence to determine whether the final state of the scalar field particles is separable or not.

The observability of the features, in particular using the measures introduced in Refs. [2, 3] reproduced in Secs. 2.3 and 2.4, is discussed at the very end of Sec. 4. The discussion concludes that no viable measurement protocol has been proposed to demonstrate the quantum origin of cosmological perturbations experimentally.

Quantum cosmological gravitational waves?

Amaury Micheli and Patrick Peter *

Abstract General relativity and its cosmological solution predicts the existence of tensor modes of perturbations evolving on top of our Friedman-Lemaître-Robertson-Walker expanding Universe. Being gauge invariant and not necessarily coupled to other quantum sources, they can be seen as representing pure gravity. Unambiguously showing they are indeed to be quantised would thus provide an unquestionable proof of the quantum nature of gravitation. This review will present a summary of the various theoretical issues that could lead to this conclusion.

Keywords

Cosmological perturbation theory, tensor modes, gravitational waves, quantum cosmology, perturbative quantum gravity.

1 Introduction

Cosmology is a major player when it comes to quantum gravity effects. Indeed, on top of our Friedman-Lemaître-Robertson-Walker (FLRW) expanding Universe, one expects various modes of perturbations to be present, whose classical occurrence is believed to result from initial quantum vacuum fluctuations. In the usual linear

Amaury Micheli, Patrick Peter
$\mathscr{GR}\varepsilon\mathbb{C}\mathscr{O}$ – Institut d'Astrophysique de Paris, CNRS & Sorbonne Université, UMR 7095 98 bis boulevard Arago, 75014 Paris, France, e-mail: peter@iap.fr

Amaury Micheli
IJCLab, Laboratoire de Physique des 2 Infinis Irène Joliot-Curie, Bât. 100 et 200, 15 rue Georges Clémenceau, F-91405 Orsay, France e-mail: amaury.micheli@ijclab.in2p3.fr

* corresponding author

formalism [1, 2], using the FLRW underlying symmetry group (isotropy and homogeneity), they can be categorised into three components, namely scalars, vectors and tensors. At this order, upon which we focus attention below, these components decouple. In a different situation with a background endowed with other symmetries, perturbations can still be expanded in the relevant representations of the associated group; they also naturally decouple at linear order (see, e.g. Ref. [3] for Bianchi I).

Scalar modes, detected long ago in the cosmic microwave background, initiating large-scale structure formation, are distributed in a way that is compatible with quantum vacuum fluctuations in the very early times, often during a phase of inflation. This can be seen as requiring quantisation of gravity, and although many authors consider it does, others argue that gauge issues and coupling with matter render the conclusion not as clear as one would wish.

In an ever-expanding FLRW universe with dynamics driven by GR or any local theory of gravity, with no specific source in the matter fields to induce them, vector perturbations are expected to have decayed long ago so as to be mostly undetectable now [4]. One of the above hypothesis needs to be invalidated to potentially render them cosmologically relevant. Non local theories are expected to yield conclusions similar to local ones [5]. A contracting phase in the universe as implemented in bouncing models [6, 7] can lead to some increase of vector modes [8] which are however limited if produced by means of some coupling with scalar modes initially set to quantum vacuum fluctuations [9], leading to the conclusion that bouncing models are generally stable under vector perturbations. For fully quantum cosmological models however, the situation may not be as clear [10]. In any case, the question of their quantum origin would lead to similar doubts regarding the quantumness of gravity itself; they are conveniently ignored in most studies, and likewise in the present review.

Finally, one is left with the tensor modes, which are gauge invariant and with no obvious coupling to other quantum sources. General relativity (GR) applied to primordial cosmology shows their dynamics to be that of two time-dependent massive scalar fields; most models then demand they should be quantised and set in a vacuum state. The observation of their resulting properties in the absence of quantum anisotropic pressure, jointly with those of the scalar modes, could provide an unambiguous and thus indisputable hint that gravitation itself should acquire the status of a quantum theory.

2 Tensor modes in general relativistic cosmology

Before focusing on the quantum features expected from gravitational waves, let us briefly recap the underlying classical theory. The starting point of our discussion is the FLRW background universe, defined by its scale factor function $a(\eta)$ depending on the (conformal) time η and spatial 3D metric γ_{ij}, with tensorial perturbations h_{ij}. In that case, ignoring both scalar and vector modes which are not the subject of this analysis, one sets the metric as

$$\mathrm{d}s^2 = g_{\mu\nu}\mathrm{d}x^\mu \mathrm{d}x^\nu = a^2(\eta)\left[-\mathrm{d}\eta^2 + (\gamma_{ij}+h_{ij})\,\mathrm{d}x^i\mathrm{d}x^j\right], \tag{1}$$

(we use units such that the velocity of light is $c=1$) and with h_{ij} assumed transverse and traceless, i.e.

$$D^i h_{ij} = 0 \quad \text{and} \quad h^i{}_i = \gamma^{ij}h_{ij} = 0,$$

the 3D covariant derivative D^i being derived from the corresponding metric γ_{ij}. Noting $\mathscr{H} = a'/a$ the conformal Hubble function[2] and $\mathscr{K}$ the spatial curvature[3] associated with the background metric γ_{ij}, the equation of motion for h_{ij} is found to be

$$h''_{ij} + 2\mathscr{H}h'_{ij} + (2\mathscr{K} - \Delta)\,h_{ij} = 8\pi G_{\mathrm{N}} a^2 p\pi_{ij}, \tag{2}$$

where $\Delta = \gamma^{ij}\partial_i\partial_j$, p is the background pressure and π_{ij} the anisotropic stress. For many of the known components of matter, it is vanishing (however, see e.g. [11, 12] and references therein), and we shall make the assumption that $\pi_{ij} = 0$ from now on.

In what follows, we set $\mathscr{K} \to 0$ and thus identify the background spatial metric $\gamma^{ij} \to \delta^{ij}$ as the 3D curvature has been measured to be vanishingly small. Technically, considering a non-vanishing curvature merely amounts to changing the spectrum (and eigenfunctions) of the Laplace-Beltrami operator used below for the mode decomposition [13], so that the calculations and discussions presented below can be generalised in a straightforward way if applied to epochs in which the assumption $\mathscr{K} = 0$ may not be valid.

Let us thus first decompose the tensor perturbations in Fourier modes through[4]

$$h_{ij}(\boldsymbol{x},\eta) = \sqrt{32\pi G_{\mathrm{N}}}\int \frac{\mathrm{d}^3\boldsymbol{k}}{(2\pi)^{3/2}a(\eta)} w_{ij}(\boldsymbol{k},\eta)e^{i\boldsymbol{k}\cdot\boldsymbol{x}} \tag{3}$$

with $w^\star_{ij}(-\boldsymbol{k},\eta) = w_{ij}(\boldsymbol{k},\eta)$ to ensure $h_{ij}\in\mathbb{R}$, so that, from Eq. (2), a given mode satisfies

$$w''_{ij} + \omega_k^2 w_{ij} = 0\,, \tag{4}$$

where we defined the module $k := |\boldsymbol{k}| \geq 0$ and the time-varying frequency

$$\omega_k^2 = k^2 - \frac{a''}{a}\,. \tag{5}$$

At this point, one notes that whenever the scale factor behaves as a power-law of the conformal time[5] $a(\eta) \propto |\eta|^\alpha$, then $a''/a = \alpha(\alpha-1)/\eta^{-2} = (\alpha-1)\mathscr{H}^2/\alpha$. This in particular encompasses the cases of cosmological interest where a single fluid

[2] A prime denotes differentiation with respect to conformal time, e.g. $a' := \mathrm{d}a/\mathrm{d}\eta$

[3] In appropriate units for the comoving coordinates x^i, it can be scaled to $\mathscr{K} = 0, \pm 1$. For most of the practical applications we shall deal with in this review, we shall consider the simplest, and inflation-motivated, flat case with $\mathscr{K} = 0$.

[4] The numerical factor $\sqrt{32\pi G_{\mathrm{N}}}$ is included here for later convenience.

[5] We write the absolute value of the conformal time in what follows, as it is negative in many situations, in particular during inflation.

dominates the Friedmann dynamics, as well as the de Sitter inflationary expansion. The condition $k^2 \gg |a''/a|$ then becomes $k\mathscr{H}^{-1} \propto k|\eta| \ll 1$, so that, in terms of the physical wavelength $\lambda \propto a/k$, one has $\lambda \ll H^{-1}$: such a mode, much smaller than the Hubble scale H^{-1}, is said to be sub-Hubble. Conversely, modes with $k^2 \ll |a''/a|$ are called super-Hubble.

Let us temporarily restrict attention to a sub-Hubble mode $k^2 \gg |a''/a|$. Eq. (4) then simplifies to $w_{ij}'' + k^2 w_{ij} = 0$, whose solution reads $w_{ij} = \alpha_{ij}\exp(\pm ik\eta)$. For a mode propagating in the $+\boldsymbol{x^3}-$direction, this yields $h_{ij} = \alpha_{ij}\exp[\pm ik(x^3 - \eta)]/a(\eta)$. The first constraint, namely $\partial^i h_{ij} = 0$, implies $k^i\alpha_{ij} = k\alpha_{zj} = 0$, so that for $k \neq 0$, one is left with α_{11}, α_{12} and α_{22} as the only non vanishing components (the symmetries of w_{ij} are identical to those of h_{ij}). The second constraint, $h^i{}_i = 0$, translates into $\alpha_{22} = -\alpha_{11}$, so the mode has only two independent degrees of freedom. The matrix α_{ij} can be rewritten explicitly as

$$\alpha_{ij} = \begin{pmatrix} \alpha_{11} & \alpha_{12} & 0 \\ \alpha_{12} & -\alpha_{11} & 0 \\ 0 & 0 & 0 \end{pmatrix} = \underbrace{\begin{pmatrix} 1 & 0 & 0 \\ 0 & -1 & 0 \\ 0 & 0 & 0 \end{pmatrix}}_{=\sqrt{2}P^+_{ij}} \alpha_{11} + \underbrace{\begin{pmatrix} 0 & 1 & 0 \\ 1 & 0 & 0 \\ 0 & 0 & 0 \end{pmatrix}}_{=\sqrt{2}P^\times_{ij}} \alpha_{12}. \tag{6}$$

The matrices P^+_{ij} and $P^\times_{ij}$ represent the two polarisations of the gravitational wave, whose associated tensor perturbations read

$$h_{ij}(\boldsymbol{x},\eta) = h_\times(t-z)\,P^\times_{ij} + h_+(t-z)\,P^+_{ij}, \tag{7}$$

with $\{t,x,y,z\} = \{a\eta, ax^1, ax^2, ax^3\}$ the physical coordinates.

Consider a test particle following the trajectory of affine parameter λ, i.e. $x^\mu(\lambda)$, and initially at rest in the TT-frame where the metric has the form (1) with h_{ij} given by (7), namely, assuming the scale factor a to be constant during the passing of the wave,

$$\mathrm{d}s^2 = -\mathrm{d}t^2 + [1+h_+(z-t)]\,\mathrm{d}x^2 + [1-h_+(z-t)]\,\mathrm{d}y^2 + 2h_\times(z-t)\mathrm{d}x\mathrm{d}y + \mathrm{d}z^2. \tag{8}$$

From (8), one can evaluate the connections while the wave passes, and it turns out that $\Gamma^i_{\eta\eta} = 0$, so that the motion of a particle following a geodesic is unaltered as it moves with the reference frame: it appears at rest at all times. It is therefore not possible to detect a gravitational wave using a single particle.

Writing the line element as $\mathrm{d}s^2 = -\mathrm{d}t^2 + \mathrm{d}\ell^2$, we consider two particles located on the TT-x axis (i,.e. $y = z = 0$) with coordinates x and $x+\Delta x$. Their proper distance is obtained from (8): the relation $\mathrm{d}\ell_x = \sqrt{1+\alpha_+(t)}\mathrm{d}x \simeq \left[1+\frac{1}{2}h_+(t)\right]\mathrm{d}x$, can be integrated to yield $\Delta\ell_x = \left[1+\frac{1}{2}h_+(t)\right]\Delta x$. Similarly, considering two particles lying along the y axis, one obtains $\Delta\ell_y = \left[1-\frac{1}{2}h_+(t)\right]\Delta y$, so that as the separation along one direction is elongated, the other is compressed, and vice versa. A similar calculation on particles set on the $y = \pm x$ lines permits to visualize the effect of the $\alpha_\times$ polarisation. Setting our test particles along a ring in the (x,y) plane, such as shown

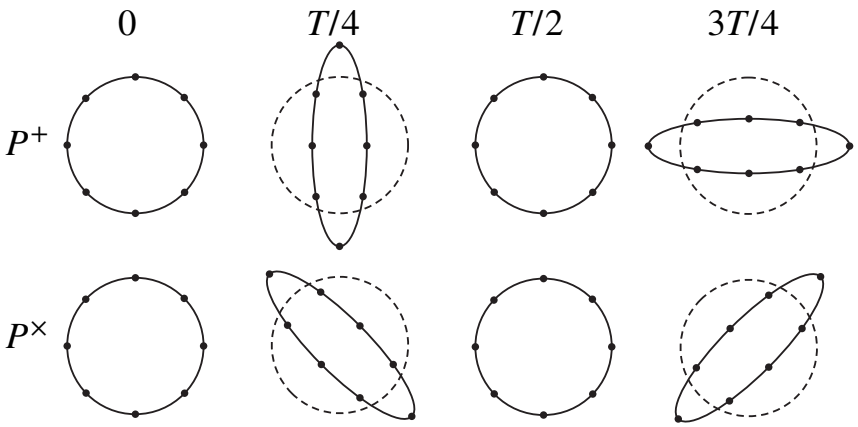

Fig. 1 Effect of a gravitational wave mode P^{+} or $P^{\times}$ as it passes through a ring of test particles, producing '+' or '×' shapes as time goes through a full period of the wave: starting with an initially circular ring at $t = 0$, its shape is modified and shown here for different values of time, namely $T/4$, $T/2$ and $3T/4$ for a period $T = 2\pi/k$.

in Fig. 1, one gets the + and × shapes as the wave propagates in the $\boldsymbol{z}-$direction, hence the names of the polarisation modes.

For a general wave vector $\boldsymbol{k} = k\boldsymbol{n}$ in the arbitrary direction parametrised by the angles φ and θ (see Fig. 2), namely $\boldsymbol{n} = (\cos\varphi\sin\theta, \sin\varphi\sin\theta, \cos\theta)$, one sets

$$w_{ij}(\boldsymbol{k},\eta) = \sum_{\lambda=+,\times} P_{ij}^{(\lambda)}(\boldsymbol{n}) f_{\lambda}(\boldsymbol{k},\eta), \tag{9}$$

with $P_{ij}^{(\lambda)}(\boldsymbol{n})$ the polarisation tensors and f_{λ} the associated functions solutions of the mode equation (4). Fig. 2 shows the vectors $\boldsymbol{e}_a$ ($a = 1,2$) generating the plane orthogonal to the direction of propagation. Defined through

$$\boldsymbol{e}_1 = -\frac{1}{\sin\theta}\frac{\partial \boldsymbol{n}}{\partial\varphi} = \begin{pmatrix} \sin\varphi \\ -\cos\varphi \\ 0 \end{pmatrix} \quad \text{and} \quad \boldsymbol{e}_2 = \frac{\partial \boldsymbol{n}}{\partial\theta} = \begin{pmatrix} \cos\theta\cos\varphi \\ \cos\theta\sin\varphi \\ -\sin\theta \end{pmatrix},$$

so that $\boldsymbol{n} = \boldsymbol{e}_1 \times \boldsymbol{e}_2$, they satisfy $\boldsymbol{e}_a \cdot \boldsymbol{e}_b = \delta_{ab}$ and $\boldsymbol{n} \cdot \boldsymbol{e}_a = 0$. Demanding h_{ij} to be transverse and traceless translates into

$$k^i P_{ij}^{(\lambda)} = 0, \quad \text{and} \quad P_{ij}^{(\lambda)}\delta^{ij} = 0, \tag{10}$$

and one can check that the choice

$$P_{ij}^{+} = \frac{1}{\sqrt{2}}\Big[(\boldsymbol{e}_2)_i(\boldsymbol{e}_2)_j - (\boldsymbol{e}_1)_i(\boldsymbol{e}_1)_j\Big] \quad \text{and} \quad P_{ij}^{\times} = -\frac{1}{\sqrt{2}}\Big[(\boldsymbol{e}_1)_i(\boldsymbol{e}_2)_j + (\boldsymbol{e}_2)_i(\boldsymbol{e}_1)_j\Big] \tag{11}$$

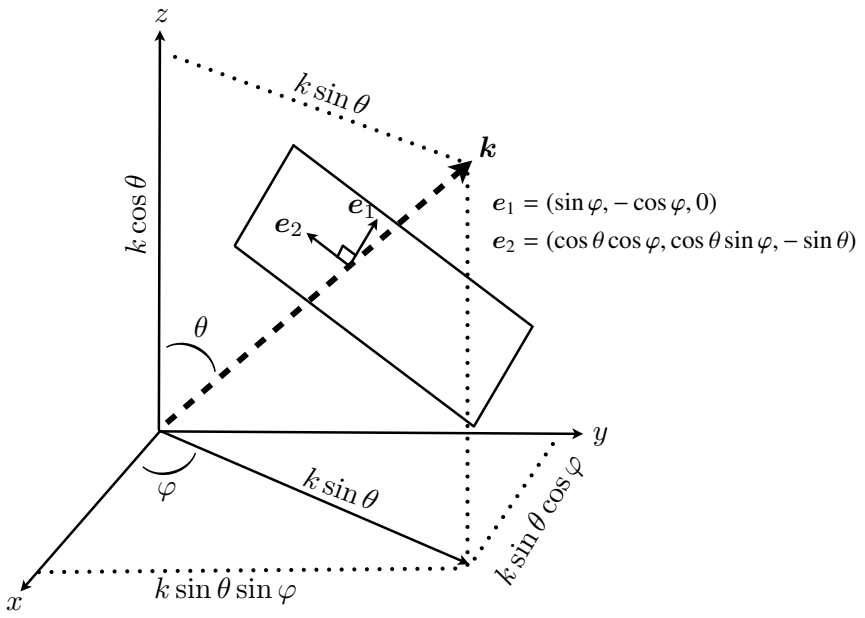

Fig. 2 Definition of the dyad $\boldsymbol{e}_a$ ($a = 1,2$) in the plane orthogonal to the arbitrary direction $\boldsymbol{k}$.

satisfies all the constraints (10); they reduce to those appearing in (6) for $\boldsymbol{k} = k\boldsymbol{z}$ (choosing $\varphi \to 0$ or $\varphi \to \pi$ as it is then undetermined). One can check straightforwardly that the relations

$$P^{i+}_{\ j}(\boldsymbol{n})P^{j+}_{\ i}(\boldsymbol{n}) = P^{i\times}_{\ j}(\boldsymbol{n})P^{j\times}_{\ i}(\boldsymbol{n}) = 1 \quad \text{and} \quad P^{i+}_{\ j}(\boldsymbol{n})P^{j\times}_{\ i}(\boldsymbol{n}) = 0 \tag{12}$$

hold.

Let us note at this point that the transformation $\boldsymbol{n} \to -\boldsymbol{n}$, which amounts to $(\theta,\varphi) \to (\pi-\theta,\varphi+\pi)$, implies $\boldsymbol{e}_1 \to -\boldsymbol{e}_1$ and $\boldsymbol{e}_2 \to \boldsymbol{e}_2$, so that

$$P^{+}_{ij}(-\boldsymbol{n}) = P^{+}_{ij}(\boldsymbol{n}) \quad \text{and} \quad P^{\times}_{ij}(-\boldsymbol{n}) = -P^{\times}_{ij}(\boldsymbol{n}). \tag{13}$$

From (9) and the reality condition below (3), one then finds that

$$f^{\star}_{+}(-\boldsymbol{k},\eta) = f_{+}(\boldsymbol{k},\eta) \quad \text{and} \quad f^{\star}_{\times}(-\boldsymbol{k},\eta) = -f_{\times}(\boldsymbol{k},\eta),$$

the extra minus sign in the cross-polarisation reflecting the fact that the gravitational wave transforms according to a spin-2 representation and not as a scalar. This sign is however inconvenient as it requires the functions f_λ to explicitly depend on the direction of propagation of the gravitational wave.

This issue is solved by considering another basis instead of the $+$ and $\times$ polarisations:

$$\varepsilon_{ij}^{\pm} := \frac{1}{\sqrt{2}}\left(P_{ij}^{+} \pm i P_{ij}^{\times}\right), \tag{14}$$

resulting in the new expansion

$$w_{ij}(\boldsymbol{k},\eta) = \sum_{\lambda=\pm} \varepsilon_{ij}^{(\lambda)}(\boldsymbol{n})\mu_{\lambda}(\boldsymbol{k},\eta), \tag{15}$$

where now one recovers the usual reality conditions in the form

$$\mu_{\pm}^{\star}(-\boldsymbol{k},\eta) = \mu_{\pm}(\boldsymbol{k},\eta), \tag{16}$$

because $\left[\varepsilon_{ij}^{\pm}(-\boldsymbol{n})\right]^{\star} = \varepsilon_{ij}^{\pm}(\boldsymbol{n})$. Note also that the orthogonality relations become $\varepsilon^{i\pm}_{j}(\boldsymbol{n})\varepsilon^{j\mp}_{i}(\boldsymbol{n}) = 1$ and $\varepsilon^{i\pm}_{j}(\boldsymbol{n})\varepsilon^{j\pm}_{i}(\boldsymbol{n}) = 0$ and that the coefficients of the expansion are related via

$$\mu_{\pm}(\boldsymbol{k},\eta) = \frac{1}{\sqrt{2}}\left[f_{+}(\boldsymbol{k},\eta) \mp i f_{-}(\boldsymbol{k},\eta)\right]. \tag{17}$$

Performing a rotation in the plane orthogonal to $\boldsymbol{n}$ by an angle α amounts to rotating $\boldsymbol{e}_a$ through

$$\begin{cases} \boldsymbol{e}_1 \to \boldsymbol{e}_1 \cos\alpha - \boldsymbol{e}_2 \sin\alpha \\ \boldsymbol{e}_2 \to \boldsymbol{e}_1 \sin\alpha + \boldsymbol{e}_2 \cos\alpha \end{cases}$$

and one can check explicitly that the new polarisations transform according to

$$\varepsilon_{ij}^{\pm} \to e^{\pm 2i\alpha}\varepsilon_{ij}^{\pm}, \tag{18}$$

i.e. they transform as tensors with helicity ± 2 and are, therefore referred to as the *helicity* basis. Gathering all the above, one finds that Eq. (15) permits to show that, in general, the modes μ_{+} and μ_{-} both satisfy the same equation of motion, which is nothing but Eq. (4) with the replacement $w_{ij} \to \mu_{\pm}$.

This can be derived directly from Eq. (4) using the expansion on the helicity basis, or going back to the Einstein-Hilbert action and performing an expansion in powers of h_{ij}

$$S_{\rm EH} = \frac{1}{16\pi G_{\rm N}}\int \mathrm{d}^4x\sqrt{-g}R = \frac{1}{16\pi G_{\rm N}}\int \mathrm{d}^4x\sqrt{-\left[g^{(0)}+g^{(2)}\right]}\left[R^{(0)}+R^{(2)}\right] + \cdots,$$

where the dots represent higher-order terms and the determinant is expanded as the exponent of the trace of a logarithm $g = \det\left(g_{\mu\nu}\right) = \det\left(g^{(0)}_{\mu\nu}\right)\det\left(\delta^{\mu}_{\nu} + h^{\mu}_{\nu}\right) = a^4\left[1 - \frac{1}{2}h^{i}_{j}h^{j}_{i} + \mathscr{O}\left(h^3\right)\right]$ and the first term vanishes due to the traceless condition, while the contribution from $R^{(1)}$ vanishes identically if we assume the background to satisfy the equation of motion. The resulting action at second-order reads

$$\delta^{(2)}S_{\rm T} = \frac{1}{64\pi G_{\rm N}}\int a^2(\eta)\left[\frac{\partial h^{i}{}_{j}}{\partial\eta}\frac{\partial h^{j}_{i}}{\partial\eta} - \left(\partial_k h^{i}{}_{j}\right)\partial^k h^{j}_{i}\right]\mathrm{d}^4x. \tag{19}$$

Plugging the expansion (3) and the definition (15) into the action (19), leads to

$$\delta^{(2)}S_{\mathrm{T}} = \int \mathrm{d}\eta \sum_{\lambda=\pm} \frac{1}{2} \int \mathrm{d}^3\boldsymbol{k} \left[\left(\mu_\lambda'^\star - \mathscr{H}\mu_\lambda^\star\right)\left(\mu_\lambda' - \mathscr{H}\mu_\lambda\right) - \boldsymbol{k}^2 \mu_\lambda^\star \mu_\lambda \right]. \tag{20}$$

Upon integrating the $\mathscr{H}(\mu_\lambda^\star\mu_\lambda)'$ by parts, and using Parseval theorem to revert to real space, we get

$$\delta^{(2)}S_{\mathrm{T}} = \int \mathrm{d}\eta \sum_{\lambda=\pm} \frac{1}{2} \int \mathrm{d}^3\boldsymbol{x}\sqrt{\gamma} \left[\left(\mu_\lambda'\right)^2 - \gamma^{ij}\partial_i\mu_\lambda\partial_j\mu_\lambda + \frac{a''}{a}\mu_\lambda^2 \right], \tag{21}$$

where we wrote $\mu_\lambda = \mu_\lambda(\boldsymbol{x},\eta)$ the inverse Fourier transform of $\mu_\lambda(\boldsymbol{k},\eta)$. This is the action for two independent scalar fields μ_+ and μ_-, with identical time-varying masses. One can check that the Euler-Lagrange equation for (21) gives back (4) for both polarisations. The form (20) allows for straightforward quantisation of the gravitational field as a collection of parametric oscillators, which is the subject of the following section.

3 Quantisation and time development

3.1 Historical perspective

Parker, in Ref. [14], was the first to use the above separation of the gravitational wave field into two minimally coupled scalar fields as a simpler route to quantisation, although previous works on (quantum) fields in curved spacetime had already identified the crucial prediction of (vacuum) amplification powered by the expansion of the Universe, including for gravitational waves. Particle creation following a change in boundary conditions of a system was shown in Ref. [15], but creation powered by an expanding Universe was first demonstrated by Parker in his seminal articles [16, 17, 18]. However, it was argued that massless non-zero spin fields, including gravitational waves, had to be conformally coupled to gravity so that no particle creation could occur. The production of gravitons, particles associated with gravitational waves, was studied in anisotropic universes in [19] and hinted at in [20] but Grishchuk [21] was the first to lift the misunderstanding and to compute the ensuing gravitational wave amplification in an isotropic expanding universe. Despite the use of a classical treatment, the corresponding quantum particle pair creation was noted and the existence of a primordial gravitational wave background put forward. Several authors then attempted to compute the spectrum of this background based on spontaneous pair creation from the vacuum still using a classical treatment and different initial conditions and renormalisation procedures as, e.g. in Refs. [22, 23, 24]. Finally, in [24], graviton production due to an early de Sitter phase of expansion, not yet called inflation, was considered with the Bunch-Davies vacuum [25] providing the relevant initial conditions.

Although acknowledged as originating from vacuum fluctuation, the dynamics of primordial gravitational waves was first analysed classically as successive stages of parametric amplifications, either using a classical field and possibly fixing the initial conditions to match quantum vacuum fluctuations [21, 22, 24, 26, 27], or using mode functions [14, 28]. Another presentation, equivalent to the latter, consists in understanding the amplification of the waves as successive Bogoliubov transformations [29] where the initial state is chosen as the vacuum in an asymptotically Minkowski region. Finally, it was latter recognised [30], moving to the Schrödinger picture, that the evolution puts the gravitational waves in a squeezed state. A good parallel presentation of the classical and quantum descriptions can be found in [31].

In this section, we first proceed to the canonical quantisation of the field in the Heisenberg picture following [14]. This is the standard approach; we refer to Refs. [32, 33, 34] for textbooks dealing with scalar fields or gravitational waves. We then review different formal approaches to the evolution of a quantised gravitational wave field on an FLRW background. We begin by using a description in terms of a Bogoliubov transformation, then make the connection with mode functions and finally move to the Schrödinger picture, introducing squeezing parameters and the phase-space representation of the state. We use these different approaches to discuss the mechanism of graviton creation in curved spacetime. This then leads to a discussion of how these particles back-reacts on the geometry. Finally, we use these analyses to compute the properties of primordial gravitational waves produced from the vacuum by the cosmological expansion and discuss their quantum origin [6].

3.2 Canonical quantisation and Bogoliubov transformation

Let us consider one of the two fields μ_λ in Eq. (21). It so happens that for the study of time evolution in terms of Bogoliubov transformations and squeezing, it is useful, and standard [30], to keep the total derivative that was dropped in the process of integration by part between eqs. (20) and (21). The Lagrangian thus obtained reads

$$L_\lambda = \frac{1}{2}\int \mathrm{d}^3\boldsymbol{x}\left[\left(\mu_\lambda'\right)^2 - 2\mathscr{H}\mu_\lambda'\mu_\lambda - \partial_i\mu_\lambda\partial^i\mu_\lambda + \mathscr{H}^2\mu_\lambda^2\right]. \tag{22}$$

The canonically conjugate momentum to μ_λ is

$$\pi_\lambda(\boldsymbol{x},\eta) = \frac{\delta L_\lambda}{\delta\mu_\lambda'} = \mu_\lambda' - \mathscr{H}\mu_\lambda\,, \tag{23}$$

so the Hamiltonian reads

$$H_\lambda = \frac{1}{2}\int \mathrm{d}^3\boldsymbol{x}\left[\pi_\lambda^2 + \mathscr{H}\left(\pi_\lambda\mu_\lambda + \mu_\lambda\pi_\lambda\right) + \partial_i\mu_\lambda\partial^i\mu_\lambda\right], \tag{24}$$

[6] Note that the exact same analyses on quantisation and time evolution can be repeated for scalar perturbations during inflation with the same type of equations [35].

the second term being written in a symmetric way, which is classically irrelevant but prepares for quantisation. We proceed to canonical quantisation by imposing equal-time canonical commutation relations (we now drop the λ subscripts)

$$\left[\hat{\mu}\left(\boldsymbol{x},\eta\right),\hat{\pi}\left(\boldsymbol{x}',\eta\right)\right]=i\hbar\delta\left(\boldsymbol{x}-\boldsymbol{x}'\right), \tag{25a}$$

$$\left[\hat{\mu}\left(\boldsymbol{x},\eta\right),\hat{\mu}\left(\boldsymbol{x}',\eta\right)\right]=\left[\hat{\pi}\left(\boldsymbol{x},\eta\right),\hat{\pi}\left(\boldsymbol{x}',\eta\right)\right]=0. \tag{25b}$$

Going to Fourier-space these relations are equivalent to

$$\left[\hat{\mu}_{\boldsymbol{k}}\left(\eta\right),\hat{\pi}_{\boldsymbol{k}'}\left(\eta\right)\right]=i\hbar\delta\left(\boldsymbol{k}+\boldsymbol{k}'\right), \tag{26a}$$

$$\left[\hat{\mu}_{\boldsymbol{k}}\left(\eta\right),\hat{\mu}_{\boldsymbol{k}'}\left(\eta\right)\right]=\left[\hat{\pi}_{\boldsymbol{k}}\left(\eta\right),\hat{\pi}_{\boldsymbol{k}'}\left(\eta\right)\right]=0, \tag{26b}$$

and the Hamiltonian reads

$$\hat{H}=\int_{\mathbb{R}^{3+}}\mathrm{d}^3\boldsymbol{k}\,\hat{H}_{\pm\boldsymbol{k}}=\int_{\mathbb{R}^{3+}}\mathrm{d}^3\boldsymbol{k}\left[\hat{\pi}_{\boldsymbol{k}}\hat{\pi}_{-\boldsymbol{k}}+\mathscr{H}\left(\hat{\pi}_{\boldsymbol{k}}\hat{\mu}_{-\boldsymbol{k}}+\hat{\mu}_{\boldsymbol{k}}\hat{\pi}_{-\boldsymbol{k}}\right)+k^2\hat{\mu}_{\boldsymbol{k}}\hat{\mu}_{-\boldsymbol{k}}\right], \tag{27}$$

where $\hat{H}_{\pm\boldsymbol{k}}$ is the Hamiltonian for the $\pm\boldsymbol{k}$ sector. Observe that, as required by homogeneity, only the modes $\pm\boldsymbol{k}$ are coupled and the coupling only depends on the norm k, as required by isotropy. In order to expand $\hat{H}$ into a sum of independent Hamiltonians $\hat{H}_{\pm\boldsymbol{k}}$ for the bi-modes $\pm\boldsymbol{k}$, we restrict the integration to be over the top-half half of the Fourier space, denoted by $\mathbb{R}^{3+}$, e.g. by selecting only the vectors $\boldsymbol{k}$ with positive k_z component, and dropping the original global factor of a half.

Let us first analyse the evolution of one such pair of modes $\pm\boldsymbol{k}$ in a situation where the term in $\mathscr{H}$ can be neglected with respect to the others, so that $\hat{\mu}$ is just a free scalar field in Minkowski spacetime. With $\mathscr{H}\to 0$, the Hamiltonian $\hat{H}$ is time-independent and we can introduce the usual creation/annihilation operators for a real scalar field

$$\hat{\mu}_{\boldsymbol{k}}\left(\eta\right)=\sqrt{\frac{\hbar}{2k}}\left[\hat{a}_{\boldsymbol{k}}\left(\eta\right)+\hat{a}^{\dagger}_{-\boldsymbol{k}}\left(\eta\right)\right], \tag{28a}$$

$$\hat{\pi}_{\boldsymbol{k}}\left(\eta\right)=-i\sqrt{\frac{\hbar k}{2}}\left[\hat{a}_{\boldsymbol{k}}\left(\eta\right)-\hat{a}^{\dagger}_{-\boldsymbol{k}}\left(\eta\right)\right]. \tag{28b}$$

The equal-time commutation relations assume the standard form

$$\left[\hat{a}_{\boldsymbol{k}},\hat{a}^{\dagger}_{\boldsymbol{k}'}\right]=\delta\left(\boldsymbol{k}-\boldsymbol{k}'\right)\qquad\text{and}\qquad\left[\hat{a}_{\boldsymbol{k}},\hat{a}_{\boldsymbol{k}'}\right]=\left[\hat{a}^{\dagger}_{\boldsymbol{k}},\hat{a}^{\dagger}_{\boldsymbol{k}'}\right]=0. \tag{29}$$

The Hamiltonian $\hat{H}_{\pm\boldsymbol{k}}$ then separates into two harmonic oscillators of frequency k

$$\hat{H}^{(0)}_{\pm\boldsymbol{k}}=\hbar k\left(\hat{a}^{\dagger}_{\boldsymbol{k}}\hat{a}_{\boldsymbol{k}}+\frac{1}{2}\right)+\hbar k\left(\hat{a}^{\dagger}_{-\boldsymbol{k}}\hat{a}_{-\boldsymbol{k}}+\frac{1}{2}\right), \tag{30}$$

and the Heisenberg equations of motions

$$i\hbar\frac{\mathrm{d}\hat{a}^{(\dagger)}_{\pm\boldsymbol{k}}}{\mathrm{d}\eta} = \left[\hat{a}^{(\dagger)}_{\pm\boldsymbol{k}}, \hat{H}_{\pm\boldsymbol{k}}\right]$$

give $\hat{a}_{\boldsymbol{k}}(\eta) = \hat{a}_{\boldsymbol{k}}(0)e^{-ik\eta}$. Including the friction term proportional to the Hubble function $\mathscr{H}$, the Hamiltonian now reads

$$\hat{H}_{\pm\boldsymbol{k}} = \hbar k\left(\hat{a}^{\dagger}_{\boldsymbol{k}}\hat{a}_{\boldsymbol{k}} + \frac{1}{2}\right) + \hbar k\left(\hat{a}^{\dagger}_{-\boldsymbol{k}}\hat{a}_{-\boldsymbol{k}} + \frac{1}{2}\right) - i\mathscr{H}\hbar\left(\hat{a}_{-\boldsymbol{k}}\hat{a}_{\boldsymbol{k}} - \hat{a}^{\dagger}_{-\boldsymbol{k}}\hat{a}^{\dagger}_{\boldsymbol{k}}\right). \tag{31}$$

The additional term corresponds to an interaction with a time-dependent classical source, the expanding background, acting through $\mathscr{H}$. It couples the $\pm\boldsymbol{k}$ modes by creating/destroying pairs of particles with opposite momentum; $\hat{a}_{\boldsymbol{k}}$ is paired with $\hat{a}_{-\boldsymbol{k}}$ and similarly for their hermitian conjugate. These terms are the only quadratic interactions terms that respect homogeneity. The Heisenberg equations of motions accordingly only mixes $\hat{a}_{\boldsymbol{k}}$ with $\hat{a}^{\dagger}_{\boldsymbol{k}}$

$$\frac{\mathrm{d}}{\mathrm{d}\eta}\begin{pmatrix}\hat{a}_{\boldsymbol{k}}\\ \hat{a}^{\dagger}_{-\boldsymbol{k}}\end{pmatrix} = \begin{pmatrix}-ik & \mathscr{H}\\ \mathscr{H} & ik\end{pmatrix}\begin{pmatrix}\hat{a}_{\boldsymbol{k}}\\ \hat{a}^{\dagger}_{-\boldsymbol{k}}\end{pmatrix}. \tag{32}$$

The operators at any further time η can then be expressed as a linear combination of operators at an earlier time η_{in}

$$\begin{pmatrix}\hat{a}_{\boldsymbol{k}}(\eta)\\ \hat{a}^{\dagger}_{-\boldsymbol{k}}(\eta)\end{pmatrix} = \begin{pmatrix}\alpha_k(\eta) & \beta_k(\eta)\\ \beta^*_k(\eta) & \alpha^*_k(\eta)\end{pmatrix}\begin{pmatrix}\hat{a}_{\boldsymbol{k}}(\eta_{\mathrm{in}})\\ \hat{a}^{\dagger}_{-\boldsymbol{k}}(\eta_{\mathrm{in}})\end{pmatrix}. \tag{33}$$

The system (32) is equivalent to

$$\frac{\mathrm{d}}{\mathrm{d}\eta}\begin{pmatrix}\alpha_k\\ \beta^{\star}_k\end{pmatrix} = \begin{pmatrix}-ik & \mathscr{H}\\ \mathscr{H} & ik\end{pmatrix}\begin{pmatrix}\alpha_k\\ \beta^{\star}_k\end{pmatrix}, \tag{34}$$

with $\alpha_k(\eta_{\mathrm{in}}) = 1$ and $\beta_k(\eta_{\mathrm{in}}) = 0$ as initial conditions. One can check that Eq. (34) implies the quantity $|\alpha_k|^2 - |\beta_k|^2$ is conserved, while the commutation relations (29) impose

$$|\alpha_k|^2 - |\beta_k|^2 = 1\,. \tag{35}$$

At any fixed η, a transformation like (33) respecting the condition (35) is called a Bogoliubov transformation [36]. Notice that the equations of motion, and so the Bogoliubov coefficients, only depend on the norm k. The evolution of the quantum field has thus been reduced to finding the coefficients of a time-dependent Bogoliubov transformation. A convenient way to analyse this situation is to introduce mode functions.

3.3 Mode functions

Having observed that the dynamics only mixes $\hat{a}_{\boldsymbol{k}}$ and $\hat{a}^{\dagger}_{-\boldsymbol{k}}$, we have a basis on which to expand $\hat{\mu}$. Inserting (33) in the Fourier expansion of the field $\hat{\mu}$, we get

$$\hat{\mu}_{\boldsymbol{k}}(\eta) = u_k(\eta)\,\hat{a}_{\boldsymbol{k}}(\eta_{\rm in}) + u_k^{\star}(\eta)\,\hat{a}^{\dagger}_{-\boldsymbol{k}}(\eta_{\rm in})\,, \tag{36a}$$

$$\hat{\pi}_{\boldsymbol{k}}(\eta) = U_k(\eta)\,\hat{a}_{\boldsymbol{k}}(\eta_{\rm in}) + U_k^{\star}(\eta)\,\hat{a}^{\dagger}_{-\boldsymbol{k}}(\eta_{\rm in})\,, \tag{36b}$$

where u_k and U_k are defined by

$$u_k(\eta) = \sqrt{\frac{\hbar}{2k}}\left[\alpha_k(\eta) + \beta_k^{\star}(\eta)\right], \tag{37a}$$

$$U_k(\eta) = -i\sqrt{\frac{\hbar k}{2}}\left[\alpha_k(\eta) - \beta_k^{\star}(\eta)\right]. \tag{37b}$$

Using these functions, we get the so-called mode expansion of the field $\hat{\mu}$

$$\hat{\mu}(\boldsymbol{x},\eta) = \int \frac{{\rm d}^3\boldsymbol{k}}{(2\pi)^{3/2}}\left[e^{i\boldsymbol{k}.\boldsymbol{x}}u_k(\eta)\,\hat{a}_{\boldsymbol{k}}(\eta_{\rm in}) + e^{-i\boldsymbol{k}.\boldsymbol{x}}u_k^{\star}(\eta)\,\hat{a}^{\dagger}_{\boldsymbol{k}}(\eta_{\rm in})\right], \tag{38}$$

and a similar expression for $\hat{\pi}$ with U_k instead of u_k. It can be checked from (33) that u_k simply obeys the same equation of motion (4) as the classical field $\mu(\boldsymbol{k},\eta)$; the momentum mode function U_k is then determined by

$$u_k' = \mathscr{H} u_k + U_k\,. \tag{39}$$

Finally, the conserved quantity $|\alpha_k|^2 - |\beta_k|^2$ maps to the Wronskian $W\left(u_k, u_k^{\star}\right) = u_k^{\star}u_k' - u_k^{\star\prime}u_k$, which is a conserved quantity of (4), so the condition (35) translates in the normalisation

$$W(u_k, u_k^{\star}) = -i\hbar\,. \tag{40}$$

Any function u_k solution of (4) and which satisfies the normalisation condition of the Wronskian is called a mode function.

We now have a dictionnary between the Bogoliubov and mode function presentations. Solving the system (34) with initial conditions $\alpha_k(\eta_{\rm in}) = 1$ and $\beta_k(\eta_{\rm in}) = 0$ is equivalent to solving (4) for u_k with initial conditions $u_k(\eta_{\rm in}) = \sqrt{\hbar/2k}$ and $u_k'(\eta_{\rm in}) = -i\sqrt{\hbar k/2} + \mathscr{H}(\eta_{\rm in})$, U_k being determined by Eq. (39). Using mode functions the quantum dynamics reduces to the classical one. This justifies the classical treatment used in works cited in introduction of this section; it is simply a consequence of working at linear order and we will encounter other manifestations of this fact when studying phase-space representation.

3.4 Squeezed states

The time evolution was described so far in the Heisenberg picture. We now show how to move to the Schrödinger picture and introduce the squeezing formalism. This formulation was initially proposed in Ref. [30] and we use conventions matching those of [37]. Without loss of generality, the Bogoliubov coefficients (33) can be parametrised using three real coefficients r_k, φ_k and θ_k through

$$\alpha_k(\eta) = e^{-i\theta_k(\eta)} \cosh\left[r_k(\eta)\right] , \tag{41a}$$

$$\beta_k(\eta) = -e^{i[\theta_k(\eta)+2\varphi_k(\eta)]} \sinh\left[r_k(\eta)\right] , \tag{41b}$$

where r_k and φ_k are respectively called the squeezing parameter and angle, collectively referred to as the squeezing parameters. We define the 2-mode squeezing and the 2-mode rotation operators by

$$\hat{S}(r_k,\varphi_k) = \exp\left[\int_{\mathbb{R}^{3+}} \mathrm{d}^3\boldsymbol{k} \left(r_k e^{-2i\varphi_k} \hat{a}_{\boldsymbol{k}} \hat{a}_{-\boldsymbol{k}} - r_k e^{2i\varphi_k} \hat{a}^\dagger_{\boldsymbol{k}} \hat{a}^\dagger_{-\boldsymbol{k}}\right)\right] , \tag{42a}$$

$$\hat{R}(\theta_k) = \exp\left[-i\int_{\mathbb{R}^{3+}} \mathrm{d}^3\boldsymbol{k}\theta_k \left(\hat{a}^\dagger_{\boldsymbol{k}} \hat{a}_{\boldsymbol{k}} + \hat{a}^\dagger_{-\boldsymbol{k}} \hat{a}_{-\boldsymbol{k}}\right)\right] , \tag{42b}$$

in which the integrals are again, as in (27), performed over half the Fourier space and the creation and annihilation operators are understood to be evaluated at η_{in}. The operators $\hat{S}$ and $\hat{R}$ defined through (42) are unitary and one can check that

$$\hat{a}^{(\dagger)}_{\pm\boldsymbol{k}}(\eta) = \hat{R}^\dagger(\theta_k)\hat{S}^\dagger(r_k,\varphi_k)\hat{a}^{(\dagger)}_{\pm\boldsymbol{k}}(\eta_{\mathrm{in}})\hat{S}(r_k,\varphi_k)\hat{R}(\theta_k) , \tag{43}$$

where the parameters are that of Eq. (41) and we have made their time dependence implicit for display convenience. The time evolution equation (33) is seen to correspond to the application of a rotation of parameter $\theta_k(\eta)$ followed by a squeezing of parameters $r_k(\eta)$ and $\varphi_k(\eta)$ on the operators.

Any operator $\hat{O}(\eta)$ in the Heisenberg picture can be written as a combination of $\hat{a}^{(\dagger)}_{\pm\boldsymbol{k}}(\eta)$ so we have

$$\begin{aligned} \langle\Psi(\eta_{\mathrm{in}})|\hat{O}(\eta)|\Psi(\eta_{\mathrm{in}})\rangle &= \langle\Psi(\eta_{\mathrm{in}})|\hat{R}^\dagger\hat{S}^\dagger\hat{O}(\eta_{\mathrm{in}})\hat{S}\hat{R}|\Psi(\eta_{\mathrm{in}})\rangle , \\ &= \langle\Psi(\eta)|\hat{O}(\eta_{\mathrm{in}})|\Psi(\eta)\rangle . \end{aligned} \tag{44}$$

where $|\Psi(\eta)\rangle = \hat{S}\hat{R}|\Psi(\eta_{\mathrm{in}})\rangle$ is the Schrödinger evolved state of the system. Choosing the waves to be initially in the vacuum of $\hat{a}^{(\dagger)}_{\pm\boldsymbol{k}}(\eta_{\mathrm{in}})$ for all modes $\boldsymbol{k}$ (we return to this point later) yields

$$|\Psi(\eta)\rangle = \prod_{\mathbb{R}^{3+}} \hat{S}(r_k,\varphi_k)\hat{R}(\theta_k)|0_{\boldsymbol{k}},0_{-\boldsymbol{k}}\rangle = \prod_{\mathbb{R}^{3+}} |2\mathrm{MS},r_k,\varphi_k\rangle , \tag{45}$$

where we have defined the 2-mode squeezed state (2MS) for the modes $\pm\boldsymbol{k}$

$$|2\mathrm{MS}, r_k, \varphi_k\rangle = \hat{S}(r_k, \varphi_k)\,|0_{\boldsymbol{k}}, 0_{-\boldsymbol{k}}\rangle = \frac{1}{\cosh(2r_{\boldsymbol{k}})} \sum_{n=0}^{+\infty} \left(-\tanh 2r_k e^{2i\varphi_k}\right)^n |n_{\boldsymbol{k}}, n_{-\boldsymbol{k}}\rangle\ . \tag{46}$$

The last expression can be computed using a Baker-Campbell-Hausdorff formula on the squeezing operator, now restricted to a single $\pm\boldsymbol{k}$ sector [38] and $|n_{\boldsymbol{k}}, n_{-\boldsymbol{k}}\rangle$ is the state with n particles in the mode $\boldsymbol{k}$ and $-\boldsymbol{k}$. Note that the rotation angle θ_k has dropped from (46) because the vacuum is invariant under the rotation operator and the product involved is over all directions.

Following [39], one can quickly derive the associated wavefunction of a single pair of modes by assuming that, at the initial time, the corresponding state is annihilated by both annihilation operators, i.e.,

$$\hat{a}_{\pm\boldsymbol{k}}(\eta_{\mathrm{in}})\,|0_{\boldsymbol{k}}, 0_{-\boldsymbol{k}}\rangle = 0\,. \tag{47}$$

Since $\hat{S}$ is unitary ($\hat{S}^\dagger\hat{S} = \mathbb{1}$), this is also

$$\begin{aligned} 0 &= \hat{S}(r_k, \varphi_k)\,\hat{a}_{\pm\boldsymbol{k}}\hat{S}^\dagger(r_k, \varphi_k)\,\hat{S}(r_k, \varphi_k)\,|0_{\boldsymbol{k}}, 0_{-\boldsymbol{k}}\rangle\ , \\ &= \hat{S}(r_k, \varphi_k)\,\hat{a}_{\pm\boldsymbol{k}}\hat{S}^\dagger(r_k, \varphi_k)\,|2\mathrm{MS}, r_k, \varphi_k\rangle\,, \end{aligned} \tag{48}$$

where the transformation on the left corresponds to the inverse of Eq. (43) for $\theta_k = 0$. Inverting the Bogoliubov transformation (33) and using (28), the relation (48) becomes

$$\left[\hat{\mu}_{\pm\boldsymbol{k}} + \frac{i}{k}\left(\frac{1 - i\gamma_{12}}{\gamma_{11}}\right)^{-1}\hat{\pi}_{\pm\boldsymbol{k}}\right]|2\mathrm{MS}, r_k, \varphi_k\rangle = 0 \tag{49}$$

where, anticipating the next section, we have introduced the matrix entries

$$\gamma_{11} = \cosh(2r_k) - \cos(2\varphi_k)\sinh(2r_k)\,, \tag{50a}$$

$$\gamma_{12} = -\sin(2\varphi_k)\sinh(2r_k)\,. \tag{50b}$$

Projecting Eq.(49) onto the $\mu_{\pm\boldsymbol{k}}$-representation of the wavefunction[7] by setting $\hat{\mu}_{\pm\boldsymbol{k}} \to \mu_{\pm\boldsymbol{k}}$ and $\hat{\pi}_{\pm\boldsymbol{k}} \to -i\hbar\partial/\partial\mu_{\mp\boldsymbol{k}}$. The wavefunction solution of Eq. (49) reads

$$\Psi(\mu_{\boldsymbol{k}}, \mu_{-\boldsymbol{k}}) = \sqrt{\frac{k}{\pi\hbar\gamma_{11}}}\, e^{-\frac{k}{\hbar}\frac{(1-i\gamma_{12})}{\gamma_{11}}\mu_{\boldsymbol{k}}\mu_{-\boldsymbol{k}}}, \tag{51}$$

which we normalised, using (16), to $\int |\Psi|^2 \mathrm{d}\mu_{\boldsymbol{k}}\mathrm{d}\mu_{-\boldsymbol{k}} = 1$.

When the squeezing parameters are those determined by Eqs. (41), this gives the wavefunction of any $\pm\boldsymbol{k}$ mode of the gravitational waves. One can also provide a description in terms of the squeezed state parameters only by recasting (33) into a set of differential equations involving only r_k, φ_k and θ_k. One finds that the system

[7] Formally, the wavefunction is the projection of the relevant state on the basis $|\{\mu_{\pm\boldsymbol{k}}\}\rangle$, i.e. $\Psi(\mu_{\boldsymbol{k}}, \mu_{-\boldsymbol{k}}) = \langle\mu_{\pm\boldsymbol{k}}|2\mathrm{MS}, r_k, \varphi_k\rangle$.

$$\frac{\mathrm{d}r_k}{\mathrm{d}\eta} = -\mathscr{H}\cos(2\varphi_k)\,, \tag{52a}$$

$$\frac{\mathrm{d}\varphi_k}{\mathrm{d}\eta} = -k + \mathscr{H}\coth(2r_k)\sin(2\varphi_k)\,, \tag{52b}$$

$$\frac{\mathrm{d}\theta_k}{\mathrm{d}\eta} = k - \mathscr{H}\tanh(r_k)\sin(2\varphi_k)\,, \tag{52c}$$

should indeed hold. Note that the equations describing the time evolution of the squeezing parameters r_k and φ_k, namely (52a) and (52b), are independent of θ_k. These equations are however rarely solved directly, as it is easier to first solve Eq. (4) for the mode function, then deduce the Bogoliubov coefficients by inverting (37) and finally, using (41), obtain the expression of the squeezing parameters. The virtue of the squeezing formalism is rather to give a clear phase space representation of the system's evolution. Such representation can be obtained using the Wigner quasi-probability distribution [40] to which we now turn.

3.5 Wigner function

Consider a system described by a density matrix $\hat{\rho}$ and represented by n-pairs of canonically conjugate hermitian operators $\hat{X} = \{(\hat{q}_i, \hat{p}_i)\}_{i\in[1,n]}$ of the same dimension. The Wigner function is a function of $2n$ phase space variables $X = \{(q_i, p_i)\}_{i\in[1,n]}$ defined by

$$W(X) = \frac{1}{(2\pi\hbar)^n}\int \mathrm{d}^n\vec{x}\, e^{-i\frac{\vec{p}\cdot\vec{x}}{\hbar}}\left\langle \vec{q}+\frac{\vec{x}}{2}\right|\hat{\rho}\left|\vec{q}-\frac{\vec{x}}{2}\right\rangle, \tag{53}$$

where the states entering the averaging are product eigenstates of $\hat{q}_i$. The right hand side of (53) is the *Weyl transform* of $\hat{\rho}/(2\pi)^n$. This transform maps any observable $\hat{O}$, which is a function of operators in $\hat{X}$, to a function $\tilde{O}(X)$ of the associated classical variables X. A crucial property is that the expectation value of any such observable $\hat{O}$ can be computed by treating the Wigner function as a probability measure for the Weyl transform

$$\left\langle \hat{O}\right\rangle = \mathbb{E}\left[\tilde{O}(X)\right] = \int W(X)\,\tilde{O}(X)\,\mathscr{D}X, \tag{54}$$

where the integral is over all the relevant variables in X and we denoted $\mathbb{E}$ the stochastic average with respect to the Wigner funcion. Equation (54) then allows to compute averages using the Wigner function as any classical phase-space probability distribution. Finally, the von-Neumann equation of motion for the density matrix can be mapped into an equation of motion for the Wigner function, namely [41]

$$i\hbar\dot{W}(X) = H(\vec{q},\vec{p})\star W - W\star H(\vec{q},\vec{p})\,, \tag{55}$$

where the non-commutative $\star$-product is defined by

$$f(\vec{q},\vec{p})\star g(\vec{q},\vec{p}) = f\left(\vec{q}+\frac{i\hbar}{2}\partial_{\vec{p}},\vec{p}-\frac{i\hbar}{2}\partial_{\vec{q}}\right) g(\vec{q},\vec{p})\,, \tag{56a}$$

$$= f(\vec{q},\vec{p})\, g\left(\vec{q}-\frac{i\hbar}{2}\partial_{\vec{p}},\vec{p}+\frac{i\hbar}{2}\partial_{\vec{q}}\right). \tag{56b}$$

The Wigner function therefore furnishes a complete representation of the state of the system and its evolution in phase space.

Two remarks are in order here. First, in general, the Wigner function is *not* everywhere positive making it only a *quasi*-probability distribution. It can be shown that, for pure states, it is everywhere positive only when it takes the form [42]

$$W(X) = \frac{1}{(\pi\hbar)^n\sqrt{\det\gamma}}\exp\left(-\frac{X^{\mathrm{T}}\gamma^{-1}X}{\hbar}\right), \tag{57}$$

which is completely determined by γ, the covariance matrix, defined by

$$\gamma_{ab} = \langle\hat{X}_a\hat{X}_b+\hat{X}_a\hat{X}_b\rangle. \tag{58}$$

Such states are called Gaussian states and are widely used in quantum optics, see [43] for a review. Second, for evolution under a quadratic Hamiltonian $H\left(\hat{X}\right)$, the dynamics (55) simply reduces to the classical Liouville equation [8]

$$\dot{W}(X) = \{H(X), W(X)\}\,, \tag{59}$$

the curly brackets denoting the usual classical Poisson brackets.

Equation (59) can be solved by the method of characteristics i.e. by evolving the initial distribution along the classical trajectories given by H. This is another manifestation of the fact that, at quadratic order, the quantum dynamics reduces to the classical one. In addition, this implies that an initially Gaussian state will remain Gaussian under a quadratic Hamiltonian and that its evolution is thus summarised in that of its covariance matrix γ.

Both of the above discussed simplifications apply to cosmological perturbations at linear order, to which we return by considering a pair of modes $\pm\boldsymbol{k}$. These two degrees of freedom represented by the four operators $\hat{\mu}_{\pm\boldsymbol{k}}$ and $\hat{\pi}_{\pm\boldsymbol{k}}$. These four operators are *not* hermitian and related to one another by hermitian conjugation. We can however build two such pairs of operators by taking the real and imaginary parts of $\hat{\mu}_{\pm\boldsymbol{k}}$ and $\hat{\pi}_{\pm\boldsymbol{k}}$ (up to a factor of $\sqrt{2}$, introduced for further convenience), namely

[8] For a detailed derivation in the special case of cosmological perturbations see Appendix H of [37].

$$\hat{\mu}^{\mathrm{R}}_{\boldsymbol{k}} = \frac{\hat{\mu}_{\boldsymbol{k}} + \hat{\mu}^{\dagger}_{\boldsymbol{k}}}{\sqrt{2}}, \qquad \hat{\mu}^{\mathrm{I}}_{\boldsymbol{k}} = \frac{\hat{\mu}_{\boldsymbol{k}} - \hat{\mu}^{\dagger}_{\boldsymbol{k}}}{\sqrt{2}i} \tag{60a}$$

$$\hat{\pi}^{\mathrm{R}}_{\boldsymbol{k}} = \frac{\hat{\pi}_{\boldsymbol{k}} + \hat{\pi}^{\dagger}_{\boldsymbol{k}}}{\sqrt{2}}, \qquad \hat{\pi}^{\mathrm{I}}_{\boldsymbol{k}} = \frac{\hat{\pi}_{\boldsymbol{k}} - \hat{\pi}^{\dagger}_{\boldsymbol{k}}}{\sqrt{2}i}. \tag{60b}$$

One can straightforwardly check that those are indeed Hermitian and canonically conjugate i.e. $[\hat{\mu}^{\mathrm{S}}_{\boldsymbol{k}}, \hat{\pi}^{\mathrm{S}'}_{\boldsymbol{k}'}] = i\hbar\delta(\boldsymbol{k}-\boldsymbol{k}')\delta_{\mathrm{S},\mathrm{S}'}$ and $[\hat{\mu}^{\mathrm{S}}_{\boldsymbol{k}}, \hat{\mu}^{\mathrm{S}'}_{\boldsymbol{k}'}] = [\hat{\pi}^{\mathrm{S}}_{\boldsymbol{k}}, \hat{\pi}^{\mathrm{S}'}_{\boldsymbol{k}'}] = 0$ where $\mathrm{S} = \mathrm{R},\mathrm{I}$. We arrange them in the vector $\hat{X}_{\mathrm{R/I}} = \left(k^{1/2}\hat{\mu}^{\mathrm{R}}_{\pm\boldsymbol{k}}, k^{-1/2}\hat{\pi}^{\mathrm{R}}_{-\boldsymbol{k}}, k^{1/2}\hat{\mu}^{\mathrm{I}}_{-\boldsymbol{k}}, k^{-1/2}\hat{\pi}^{\mathrm{R}}_{-\boldsymbol{k}}\right)$, where we have introduced factors of k to give the same dimension to all entries in the vector, whose associate vector of classical variables is denoted $X_{\mathrm{R/I}}$. The Wigner function with respect to these variables is defined by

$$W_{\pm\boldsymbol{k}}(X_{\pm\boldsymbol{k}}) = \frac{1}{(2\pi\hbar)^2}\int e^{-\frac{i}{\hbar}\left(\pi^{\mathrm{R}}_{\boldsymbol{k}}x + \pi^{\mathrm{I}}_{\boldsymbol{k}}y\right)}\left\langle \mu^{\mathrm{R}}_{\boldsymbol{k}} + \frac{x}{2}, \mu^{\mathrm{I}}_{\boldsymbol{k}} + \frac{y}{2}\middle|\,\hat{\rho}_{\boldsymbol{k}}\,\middle|\mu^{\mathrm{R}}_{\boldsymbol{k}} - \frac{x}{2}, \mu^{\mathrm{I}}_{\boldsymbol{k}} - \frac{y}{2}\right\rangle \mathrm{d}x\mathrm{d}y. \tag{61}$$

In terms of the variables (60), the Hamiltonian $\hat{H}_{\pm\boldsymbol{k}}$ separates into two equal Hamiltonian over the R/I sectors that thus evolve independently

$$\hat{H} = \frac{\hbar}{2}\int_{\mathbb{R}^{3+}}\mathrm{d}^3\boldsymbol{k}\sum_{\mathrm{S}=\mathrm{R},\mathrm{I}}\left[(\hat{\pi}^{\mathrm{S}}_{\boldsymbol{k}})^2 + 2\mathscr{H}\left(\hat{\mu}^{\mathrm{S}}_{\boldsymbol{k}}\hat{\pi}^{\mathrm{S}}_{\boldsymbol{k}} + \hat{\pi}^{\mathrm{S}}_{\boldsymbol{k}}\hat{\mu}^{\mathrm{S}}_{\boldsymbol{k}}\right) + k^2(\hat{\mu}^{\mathrm{S}}_{\boldsymbol{k}})^2\right] = \int_{\mathbb{R}^{3+}}\mathrm{d}^3\boldsymbol{k}\sum_{\mathrm{S}=\mathrm{R},\mathrm{I}}\hat{H}^{\mathrm{S}}_{\boldsymbol{k}}. \tag{62}$$

Similarly, the wavefunction (51) factorises into a product of two wavefunctions over each sector $\Psi(\mu_{\boldsymbol{k}}, \mu_{-\boldsymbol{k}}) = \Psi\left(\mu^{\mathrm{R}}_{\boldsymbol{k}}\right)\Psi\left(\mu^{\mathrm{I}}_{\boldsymbol{k}}\right)$ with

$$\Psi\left(\mu^{\mathrm{S}}_{\boldsymbol{k}}\right) = \left(\frac{k}{\pi\hbar\gamma_{11}}\right)^{1/4} e^{-\frac{k}{2\hbar}\frac{(1-i\gamma_{12})}{\gamma_{11}}\left(\mu^{\mathrm{S}}_{\boldsymbol{k}}\right)^2}, \tag{63}$$

and the covariance matrix is block diagonal in the R/I partition $\gamma = \gamma^{\mathrm{R}} \bigoplus \gamma^{\mathrm{I}}$. These separations are in fact imposed by the homogeneity of the state that requires $\left\langle \hat{a}_{\boldsymbol{k}}\hat{a}^{\dagger}_{-\boldsymbol{k}}\right\rangle = \left\langle \hat{a}^2_{\boldsymbol{k}}\right\rangle = 0$, which can be recast in the vanishing of all R/I cross terms [44]. Eq. (63) is nothing else than the wavefunction of a one-mode squeezed state of parameter r_k, φ_k [45]. Going from the $\pm\boldsymbol{k}$ operators to the R/I operators allows to view a 2-mode squeezed state as a product of two 1-mode squeezed states [9]. Such transformations are studied in details in [46].

Since the wavefunction (63) is Gaussian, then so is the associated Wigner function W^{S}; vacuua and squeezed states are indeed Gaussian states. Note that their gaussianity is preserved by the evolution because $\hat{H}^{\mathrm{S}}_{\boldsymbol{k}}$ is quadratic. The Wigner function (61) also factorises into $W_{\pm\boldsymbol{k}} = W^{\mathrm{R}}\left(\hat{\mu}^{\mathrm{R}}_{\boldsymbol{k}}, \hat{\pi}^{\mathrm{R}}_{\boldsymbol{k}}\right)W^{\mathrm{I}}\left(\hat{\mu}^{\mathrm{I}}_{\boldsymbol{k}}, \hat{\pi}^{\mathrm{I}}_{\boldsymbol{k}}\right)$. Both sectors have identical covariance matrix, namely

[9] This fact can be directly seen by factorizing the 2-mode squeezing operator $\hat{S}(r_k, \varphi_k)$ into to two 1-mode squeezing operators for the R/I creation/annihilation operators defined via (28) where $\pm\boldsymbol{k}$ operators are replaced by R/I operators.

$$\gamma^{\mathrm{S}} = \begin{pmatrix} \gamma_{11} & \gamma_{12} \\ \gamma_{21} & \gamma_{22} \end{pmatrix}, \tag{64}$$

with

$$\gamma_{11} = \frac{2k}{\hbar}\left\langle \left(\hat{\mu}^{\mathrm{R}}_{\boldsymbol{k}}\right)^2 \right\rangle = \frac{2k}{\hbar}\left\langle \left(\hat{\mu}^{\mathrm{I}}_{\boldsymbol{k}}\right)^2 \right\rangle = \frac{k}{\hbar}\left\langle \left\{\hat{\mu}_{\boldsymbol{k}}, \hat{\mu}^{\dagger}_{\boldsymbol{k}}\right\} \right\rangle, \tag{65a}$$

$$\gamma_{12} = \gamma_{21} = \frac{1}{\hbar}\left\langle \hat{\mu}^{\mathrm{R}}_{\boldsymbol{k}}\hat{\pi}^{\mathrm{R}}_{\boldsymbol{k}} + \hat{\pi}^{\mathrm{R}}_{\boldsymbol{k}}\hat{\mu}^{\mathrm{R}}_{\boldsymbol{k}} \right\rangle = \frac{1}{\hbar}\left\langle \hat{\mu}^{\mathrm{I}}_{\boldsymbol{k}}\hat{\pi}^{\mathrm{I}}_{\boldsymbol{k}} + \hat{\pi}^{\mathrm{I}}_{\boldsymbol{k}}\hat{\mu}^{\mathrm{I}}_{\boldsymbol{k}} \right\rangle = \frac{1}{\hbar}\left\langle \hat{\mu}_{\boldsymbol{k}}\hat{\pi}^{\dagger}_{\boldsymbol{k}} + \hat{\pi}_{\boldsymbol{k}}\hat{\mu}^{\dagger}_{\boldsymbol{k}} \right\rangle, \tag{65b}$$

$$\gamma_{22} = \frac{2}{\hbar k}\left\langle \left(\hat{\pi}^{\mathrm{R}}_{\boldsymbol{k}}\right)^2 \right\rangle = \frac{2}{\hbar k}\left\langle \left(\hat{\pi}^{\mathrm{I}}_{\boldsymbol{k}}\right)^2 \right\rangle = \frac{1}{\hbar k}\left\langle \left\{\hat{\pi}_{\boldsymbol{k}}, \hat{\pi}^{\dagger}_{\boldsymbol{k}}\right\} \right\rangle, \tag{65c}$$

where we defined the anti-commutator of two operators $\{\hat{A},\hat{B}\} = \hat{A}\hat{B} + \hat{B}\hat{A}$, and we expressed the entries of the covariance matrix in terms of two-point function of the original $\hat{\mu}_{\boldsymbol{k}}$ and $\hat{\pi}_{\boldsymbol{k}}$ operators (one can also check that $\langle \hat{\mu}_{\boldsymbol{k}}\hat{\pi}_{\boldsymbol{k}} + \hat{\pi}^{\dagger}_{\boldsymbol{k}}\hat{\mu}^{\dagger}_{\boldsymbol{k}} \rangle = 0$). Using (65) and the parametrisation (41), the covariance matrix can be conveniently expressed in terms of the squeezing parameters

$$\gamma_{11} = \cosh(2r_k) - \cos(2\varphi_k)\sinh(2r_k), \tag{66a}$$

$$\gamma_{12} = \gamma_{21} = -\sin(2\varphi_k)\sinh(2r_k), \tag{66b}$$

$$\gamma_{22} = \cosh(2r_k) + \cos(2\varphi_k)\sinh(2r_k), \tag{66c}$$

where the expressions for γ_{11} and γ_{12} correspond to those defined earlier when computing the wavefunction. Finally in order to visualize this probability distribution, we compute its contour levels. Owing to gaussianity, those are ellipses whose parameters can be computed through diagonalizing the quadratic form appearing in the argument of the exponential in Eq. (57). It is readily done by performing a rotation in phase space $\widetilde{X}^{\mathrm{S}} = R(-\varphi_k)X^{\mathrm{S}}$ so that the covariance matrix of X^{S} reads

$$(\widetilde{\gamma}^{\mathrm{S}})^{-1} = \begin{pmatrix} e^{2r_k} & 0 \\ 0 & e^{-2r_k} \end{pmatrix}. \tag{67}$$

Some contour levels of W^{S} are plotted in Fig. 3; they provide a geometrical representation of the state of the tensor perturbations in phase space and illustrate the meaning of the squeezing parameters: the ellipse representing the $\sqrt{2}$-σ contour has semi-minor and semi-major axes of length $A_k = \sqrt{\hbar}e^{r_k}$ and $B_k = \sqrt{\hbar}e^{-r_k}$, which are tilted by the angle φ_k in phase space. The fluctuations of the operator in the direction of the semi-major axis are exponentially amplified with respect to the vacuum; this is called a super-fluctuant mode. On the other hand, the fluctuations of the operator related to the semi-major axis are exponentially suppressed, thus defining a sub-fluctuant mode.

The presence of amplification and suppression is a manifestation of the existence of a growing and a decaying solution in Eq. (4) [45]. Their complementary can be traced back to the purity of the state which, for a Gaussian state, can be computed directly in terms of the covariance matrix via [43]

$$p_k = \mathrm{tr}\left(\hat{\rho}^2\right) = \frac{1}{\sqrt{\det\left(\gamma\right)}} = \frac{1}{\gamma_{11}\gamma_{22} - \gamma_{12}^2} = \frac{\hbar^2}{A_k^2 B_k^2} = \frac{\hbar^2\pi^2}{S_k^2}\,, \tag{68}$$

where S_k is the area of the $\sqrt{2}$-σ contour defined by the points where the argument of the exponential in Eq (57) is unity. Since the purity of the state is preserved under Hamiltonian evolution, so is S_k. Therefore, the amplification in a given direction has to be balanced out with squeezing in another. Conversely, if the fluctuations in one direction are reduced, they increase in another. For any quantum state, $p_k \leq 1$ and so the area is minimal for a pure state $p_k = 1$, like the one we consider here, where $S_k = \pi\hbar$; this is a geometrical translation of the Heisenberg uncertainty principle forbidding to localise the system too precisely. Note that in general, due to the rotation φ_k, the product uncertainty of the original pair $(\hat{\mu}_{\boldsymbol{k}}, \hat{\pi}_{\boldsymbol{k}})$ does not saturate the inequality anymore.

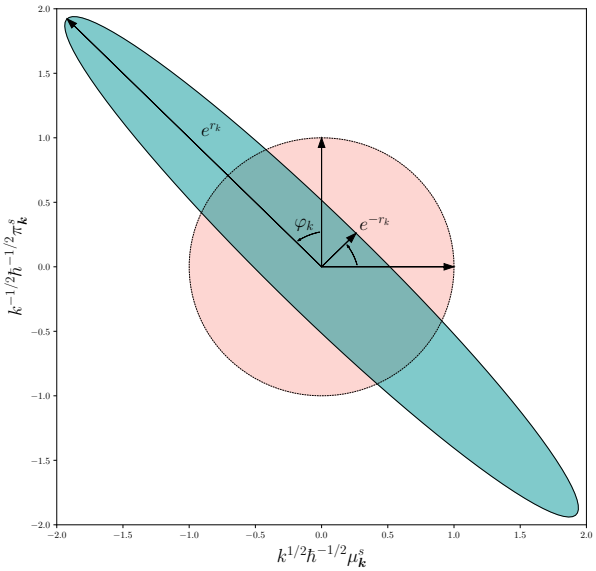

Fig. 3 $\sqrt{2}$-σ contour level of the Wigner function W^{S} for $\varphi_k = \pi/4$, $r_k = 1$ (green ellipse) and the vacuum state $r_k = 0$ (pink circle). This figure is adapted from [46].

In addition to granting an elegant geometrical representation of the state, the presentation in terms of 2-mode squeezed states is often used in the literature to discuss the quantumness of primordial gravitational waves and scalar perturbations alike. These aspects are discussed in Sec. 4.

3.6 Particle production

Having laid out the formalisms to follow the evolution of gravitational waves in cosmology, we want to give more physical insights into the evolution and show that, under certain conditions, it can be understood as a process of particle creation. Bogoliubov transformations and mode functions are the appropriate way to describe this process in curved spacetime. We start by analysing their relation to particle content.

Consider two pairs of operators $\left(\hat{a},\hat{a}^\dagger\right)$ and $\left(\hat{b},\hat{b}^\dagger\right)$ related by a constant Bogoliubov transformation

$$\hat{b} = \alpha\hat{a} + \beta\hat{a}^\dagger\,, \tag{69}$$

with $(\alpha,\beta)\in\mathbb{C}^2$ such that $|\alpha|^2-|\beta|^2=1$. We define two vacua: $|0\rangle_a$ with respect to the $\hat{a}$ operators and $|0\rangle_b$ with respect to the $\hat{b}$ operators. The crucial observation is that these vacua do *not* coincide. The number of b-particles in the a-vacuum is always non-vanishing when the Bogoliubov transformation is non-trivial

$${}_a\langle 0|\hat{b}^\dagger\hat{b}|0\rangle_a = |\beta|^2 > 0\,. \tag{70}$$

The analysis carries over to the study of $\pm\boldsymbol{k}$ modes. Equation (46) shows that the vacuum of the operators $\hat{a}_{\pm\boldsymbol{k}}(\eta)$ is filled with particles associated to $\hat{a}_{\pm\boldsymbol{k}}(\eta_{\rm in})$. We thus already see that the number of particles will be different for the same state using the operators $\hat{a}_{\pm\boldsymbol{k}}(\eta)$ of Eq. (28) at two different times.

What are then the appropriate operators to describe the particle content of the field $\hat{\mu}$ and define a vacuum as we have in Sec. 3.4? We have so far considered operators defined by (28). In Minkowski spacetime ($a'=0$), this form is uniquely selected (up to a phase) by requiring that the Hamiltonian is diagonal and that the vacuum thus defined is invariant under the Poincaré group so that it is shared by all inertial observers, or, equivalently, the vacuum is the ground state of the Hamiltonian [34]. In this situation there *is* a preferred set of operators selected by physical symmetries, which subsequently define preferred notions of vacuum and particle.

The procedure described above breaks down in an expanding Universe, $a'\neq 0$, as the Poincaré group is no longer a symmetry of spacetime, ω_k^2 [see Eq. (27)] is time-dependent and can even become negative so that the existence of an energy minimum is not guaranteed anymore. We are left with no physically preferred vacuum in which no inertial detector would record the presence of particles. In this context, the choice of $\hat{a}_{\boldsymbol{k}}(\eta_{\rm in})$ to perform the expansion (38) appears arbitrary.

A choice of operators in fact corresponds to a choice of mode functions, the latter being more convenient to work with. Consider the operators $\hat{b}_{\pm\boldsymbol{k}}$ related to $\hat{a}_{\pm\boldsymbol{k}}(\eta_{\rm in})$ by the following *time-independent* Bogoliubov transformation

$$\hat{b}_{\boldsymbol{k}} = \rho_k^\star\hat{a}_{\boldsymbol{k}}(\eta_{\rm in}) + \chi_k\hat{a}^\dagger_{-\boldsymbol{k}}(\eta_{\rm in})\,, \tag{71}$$

with $(\rho_k,\chi_k)\in\mathbb{C}^2$ such that $|\rho_k|^2-|\chi_k|^2=1$. Inverting this transformation and inserting in (38), we get

$$\hat{\mu}(\boldsymbol{x},\eta)=\int\frac{\mathrm{d}^3\boldsymbol{k}}{(2\pi)^{3/2}}\left[e^{i\boldsymbol{k}.\boldsymbol{x}}v_k(\eta)\,\hat{b}_{\boldsymbol{k}}+e^{-i\boldsymbol{k}.\boldsymbol{x}}v_k^{\star}(\eta)\,\hat{b}_{\boldsymbol{k}}^{\dagger}\right],$$

where

$$v_k=\rho_k^{\star}u_k-\chi_k u_k^{\star} \tag{72}$$

can be checked to be a mode function, i.e. a solution of (4) with a Wronskian normalised to $W(v_k,v_k^{\star})=\left(|\rho_k|^2-|\chi_k|^2\right)W(u_k,u_k^{\star})=-i\hbar$. A similar expansion is found for $\hat{\pi}$, with v_k replaced by new functions V_k defined as the U_ks through the replacement $u_k\rightarrow v_k$.

We then have an alternative expansion of $\hat{\mu}$ and $\hat{\pi}$ over another set of mode functions and operators. The meaning of the operators in the expansion is set once the associated mode functions are fixed [10], and a choice of mode functions corresponds to a choice of initial conditions for the solutions of (4). The normalisation of the Wronskian fixes one condition, and one is left to choose. For instance, the Minkowski operators (28) are associated to the mode function

$$u_k^{(\mathrm{M})}(\eta)=\sqrt{\frac{\hbar}{2k}}e^{-ik\eta}, \tag{73}$$

corresponding to the initial conditions

$$u_k(\eta_0)=\sqrt{\frac{\hbar}{2k}}e^{-ik\eta_0}\quad\text{and}\quad u_k'(\eta_0)=-i\sqrt{\frac{\hbar k}{2}}e^{-ik\eta_0}. \tag{74}$$

For non-vanishing $\mathscr{H}$, $u_k^{(\mathrm{M})}$ is no longer a solution of (4). Yet, when analysing the evolution of the two helicities of the gravitational field in this context, we have used the associated operators (28). Their time-dependence then does not simply factorise in the running phase of $u_k^{(\mathrm{M})}$ and we have to deal with a continuous change of reference operators parametrised by a *time-dependent* Bogoliubov transformation. These operators correspond at any time η to what would be the Minkowskian definition of particle and vacuum if the modulation were to stop at this instant. Alternatively, we can work with the operators defined at some fixed time η_{in}, as we did in Eq. (36), in which case the time-dependence is that of a mode function satisfying Eq. (4) which differs from that of $u_k^{(\mathrm{M})}$. As just discussed, when the background is time-dependent neither of these two sets of operators can be favoured to discuss the particle content of the field.

There are some situations where one can unambiguously define particles and their properties. One such case [17] is that of a spacetime which is asymptotically Minkowski at both very early and very late times, i.e. one for which the scale factor varies in-between two asymptotic constant values

$$a(\eta)\xrightarrow[\eta\rightarrow-\infty]{}a_{\mathrm{in}}\quad\text{and}\quad a(\eta)\xrightarrow[\eta\rightarrow+\infty]{}a_{\mathrm{out}}\,.$$

[10] This can be seen by expressing $\hat{b}_{\boldsymbol{k}}$ in terms of the mode function and the fields $\hat{b}_{\boldsymbol{k}}=-i\left[V_k^{\star}\hat{\mu}(\boldsymbol{k},\eta)-v_k^{\star}\hat{\pi}(\boldsymbol{k},\eta)\right]$.

We can therefore define asymptotically Minkowski "in" and "out" mode functions $u_k^{(\mathrm{in/out})}$ and associated operators $\hat{a}_{\boldsymbol{k}}^{(\mathrm{in/out})}$ by requiring as initial condition that they match the Minkowski solution

$$u_k^{(\mathrm{in})} \xrightarrow[\eta\to-\infty]{} \sqrt{\frac{\hbar}{2k}} e^{-ik\eta} \quad \text{and} \quad u_k^{(\mathrm{out})} \xrightarrow[\eta\to+\infty]{} \sqrt{\frac{\hbar}{2k}} e^{-ik\eta} \,.$$

These mode functions are both solution of (4) for any time η and are therefore related by a *time-independent* Bogoliubov transformation

$$u_k^{(\mathrm{in})} = \rho_k u_k^{(\mathrm{out})} + \chi_k u_k^{\star(\mathrm{out})} \,, \tag{75}$$

and, via (71), so are $\hat{a}_{\boldsymbol{k}}^{(\mathrm{in/out})}$, and it is straightforward to evaluate the number of particles produced by the non-trivial evolution of the background. We assume that the field is initially (in the "in" region) in the vacuum defined by the "in" operators where there exists a preferred notion of vacuum; we denote $|0\rangle_{\mathrm{in}}$ this "in" vacuum. In order to read the particle content at the end of evolution (in the "out" region) we need to use the "out" operators that define the Minkowski notion of particle there. The number of particles in the "out" region is given by

$$n_{\pm\boldsymbol{k}}^{\mathrm{out}} = {}_{\mathrm{in}}\langle 0| \hat{a}_{\pm\boldsymbol{k}}^{\dagger(\mathrm{out})} \hat{a}_{\pm\boldsymbol{k}}^{(\mathrm{out})} |0\rangle_{\mathrm{in}} = |\chi_k|^2 \,. \tag{76}$$

This number is strictly positive and the same in the modes $\pm\boldsymbol{k}$; this is the well-known phenomenon of pair production out of the vacuum, here powered by the background expansion. To evaluate the extent of this production quantitatively we have to compute the mode equation for both "in" and "out" conditions and match them. This computation can, for example, be done exactly in a 2d model where the scale factor evolves as a hyperbolic tangent between its asymptotic values [47].

Let us make the connection in this idealised case with the time-dependent Bogoliubov coefficients solving the dynamics of (33). First, note that the operators (28) coincide with those defined with respect to a mode function u_k at times η_0 where it satisfies the Minkowski conditions (74). This can be checked directly upon inserting (28) in the expression of the operator in terms of the mode function and the fields at time η_0. This applies in both the "in" and "out" regions

$$\hat{a}_{\pm\boldsymbol{k}}(\eta) \xrightarrow[\eta\to-\infty]{} \hat{a}_{\pm\boldsymbol{k}}^{(\mathrm{in})} \,,$$
$$\hat{a}_{\pm\boldsymbol{k}}(\eta) \xrightarrow[\eta\to+\infty]{} \hat{a}_{\pm\boldsymbol{k}}^{(\mathrm{out})} \,.$$

The time-independent Bogoliubov coefficients between the "in" and the "out" states, therefore, correspond to the late time limit of the time-dependent Bogoliubov coefficients of Eq. (34)

$$\rho_k = \alpha_k(\eta \to +\infty) \quad \text{and} \quad \chi_k = \beta_k(\eta \to +\infty) \,, \tag{77}$$

where the associated number of particles $\left\langle \hat{a}^{\dagger}_{\pm\boldsymbol{k}}(\eta)\,\hat{a}_{\pm\boldsymbol{k}}(\eta)\right\rangle$ and correlations are now meaningful. While it is not *a priori* the case at any intermediate times, since the scale factor is varying, we discuss in Sec. 3.8.2 how it is often possible to identify "in" and "out" regions for certain ranges of modes k in the cosmological evolution.

Anticipating these considerations, we conclude by making a connection with Sec. 3.4 and studying the particle content of a 2-mode squeezed state. Those can also be fully characterised by the following three non-vanishing expectation values (two of them being equal)

$$n_k = \left\langle \hat{a}^{\dagger}_{\boldsymbol{k}}\hat{a}_{\boldsymbol{k}}\right\rangle = \left\langle \hat{a}^{\dagger}_{-\boldsymbol{k}}\hat{a}_{-\boldsymbol{k}}\right\rangle = \frac{\gamma_{11}+\gamma_{22}-2}{4} = \sinh^2(r_k)\,, \tag{78a}$$

$$c_k = \langle \hat{a}_{\boldsymbol{k}}\hat{a}_{-\boldsymbol{k}}\rangle = \frac{\gamma_{11}-\gamma_{22}}{4} + i\frac{\gamma_{12}}{2} = -\frac{1}{2}\sinh(2r_k)\,e^{2i\varphi_k}\,. \tag{78b}$$

These expressions are obtained by inverting Eq. (28) and making use of Eqs. (65) and (66). The first expectation value n_k gives the number of particles in the modes $\boldsymbol{k}$ and $-\boldsymbol{k}$, which must be identical because of isotropy, while c_k encodes the 2-mode coherence of the pairs. Imposing the purity to be less than unity, $p_k = \gamma_{11}\gamma_{22} - \gamma_{12}^2 \leq 1$, yields the following bound on the magnitude of this coherence:

$$|c_k| \leq \sqrt{n_k\,(n_k+1)}. \tag{79}$$

For a pure state like that of the gravitons, the bound is saturated $|c_k| = \sqrt{n_k\,(n_k+1)}$, while for a thermal state $c_k = 0$. In this sense, the modes are uncorrelated in the thermal state and maximally correlated in a 2-mode squeezed state; they are even *entangled* [44]. We come back to this important point in Sec. 4.

3.7 Anomaly-induced semiclassical theory

The concept of particle associated with a quantum field is a global one in the sense that it is defined through modes; somehow, it can be understood, as described above, as the effect of geometry on matter, even when "matter" consists of tensor-like perturbations of the gravitational field itself. When coupled to classical GR in a semiclassical way, the quantum nature of gravitational waves, just like any other particle, may also manifest itself in another way, namely in the back reaction of their quantum fields on geometry; (see, e.g., the historical papers by M. J. Duff [48, 49, 50] who proposed it for the first time, and Refs. [51, 52] as well as the more recent Ref [53]). This approach is, therefore, the opposite of the above, making extensive use of the stress-energy tensor $T_{\mu\nu}(x)$, which is a local quantity.

In this section, for the sake of notational simplicity, we set $\hbar \to 1$ as all the effects are quantum by nature.

3.7.1 Gravity with quantum fields

When quantum fields are described in a geometric background, it is customary to write the corresponding Einstein's equations in the semiclassical form

$$R_{\mu\nu} - \frac{1}{2}Rg_{\mu\nu} + \Lambda g_{\mu\nu} = 8\pi G_{\rm N}\langle T_{\mu\nu}\rangle_{\rm ren}, \tag{80}$$

so that geometry is now sourced by the renormalised stress-energy tensor $\langle T_{\mu\nu}\rangle_{\rm ren}$.

As the classical Einstein equations are derived from a variation of the vacuum Einstein-Hilbert term[11] (possibly including a cosmological constant contribution),

$$S_{\rm EH\Lambda} = \frac{1}{16\pi G_{\rm N}}\int {\rm d}^4x\sqrt{-g}\,(R+2\Lambda)\,, \tag{81}$$

the stress-energy tensor being derived from the classical matter action $\mathscr{S}_{\rm m}$ through

$$T^{\rm class}_{\mu\nu} = -\frac{2}{\sqrt{-g}}\frac{\delta\mathscr{S}_{\rm m}}{\delta g^{\mu\nu}}, \tag{82}$$

one can recover the semiclassical case (80) by similarly defining an effective action $\Gamma[g_{\mu\nu}]$ such that

$$\langle T_{\mu\nu}\rangle = -\frac{2}{\sqrt{-g}}\frac{\delta\Gamma}{\delta g^{\mu\nu}}. \tag{83}$$

It can be shown that for a set of matter fields denoted generically by ϕ, and which can include scalar, gauge and fermion fields, whose dynamics is driven by the action $S[\phi;g_{\mu\nu}]$, one finds

$$e^{i\Gamma[g_{\mu\nu}]} = \int \mathscr{D}\phi\, e^{iS[\phi;g_{\mu\nu}]}, \tag{84}$$

and the expectation value in (83) is then understandable in terms of "in" and "out" vacuum states:

$$\frac{2}{\sqrt{-g}}\frac{\delta\Gamma}{\delta g^{\mu\nu}} = \frac{{}_{\rm out}\langle 0|T_{\mu\nu}|0\rangle_{\rm in}}{{}_{\rm out}\langle 0|0\rangle_{\rm in}}, \tag{85}$$

thereby automatically providing the required normalisation.

In order to integrate explicitly (85) and obtain the relevant effective action, one needs to know the matter content and its corresponding action. Compared to their flat space counterparts, fermionic and vectorial contributions are merely obtained by the minimal coupling, namely making the replacements $\partial \to \nabla$ and using the metric $g_{\mu\nu}$ to integrate. The scalar field case can also include an extra term, not present in the flat Minkowski situation, and one gets

$$S_\varphi = -\frac{1}{2}\int {\rm d}^4x\sqrt{-g}\left[(\partial\boldsymbol{\varphi})^2 + \xi_{ij}\varphi^i\varphi^j R\right], \tag{86}$$

[11] We do not consider the Gibbons–Hawking–York boundary term in these discussions; it can be set to zero by assuming a compact manifold.

where we considered a set of scalars $\{\varphi^i\} = \boldsymbol{\varphi}$; a possible extra potential term $V(\boldsymbol{\varphi})$ can be added to this action. Eq. (86) involves a set of new dimensionless numbers $\{\xi_{ij}\}$ which are called non-minimal parameters. For a single scalar field, this reduces to a single parameter; its special value $\xi = \frac{1}{6}$ yields conformal invariance.

It turns out that the action derived from this procedure contains ultraviolet divergences that thus need to be renormalised. These lead to contributions that are purely geometrical, involving only scalars made out of the Riemann tensor $R_{\mu\nu\alpha\beta}(x)$ and its contractions. This is understandable as short wavelengths are only sensitive to local features of spacetime. Regularising and renormalising forces to introduce counterterms involving higher-order derivatives, and one is naturally led to the conclusion that in order to obtain a renormalisable theory of quantum matter on a classical curved spacetime, one must demand a geometrical framework that goes beyond general relativity.

Applying the procedure described above, the relevant vacuum classical action

$$S_{\rm vac} = S_{\rm EH\Lambda} + S_{\rm HD} \tag{87}$$

is found to include the usual Einstein-Hilbert term (81) in which both $G_{\rm N}$ and Λ are renormalised quantities, but another contribution, containing higher derivatives (HD) terms, needs be included, namely

$$S_{\rm HD} = \int {\rm d}^4x\sqrt{-g}\left(a_1C^2 + a_2E + a_3\Box R + a_4R^2\right), \tag{88}$$

where

$$C^2 = R^2_{\mu\nu\alpha\beta} - 2R^2_{\alpha\beta} + \frac{1}{3}R^2$$

is the square of the Weyl tensor and

$$E = R^2_{\mu\nu\alpha\beta} - 4R^2_{\alpha\beta} + R^2$$

represents the Gauss-Bonnet topological term. The action (87) has been shown [54] to lead to a renormalisable (albeit containing unphysical ghosts or having non-unitarity issues) theory of quantum gravity. Details can be found in particular in [55] in the present volume. The parameter a_3 is irrelevant for the equations of motion since $\Box R$ is a surface term, while the R^2 term is at the origin of the most serious inflation model proposed by Starobinsky [56].

3.7.2 Conformal anomalies

Let us consider a conformally invariant theory, i.e. for which the transformations

$$g_{\mu\nu} \to \bar{g}_{\mu\nu} = \Omega^2(x)g_{\mu\nu} \quad \text{and} \quad \varphi \to \varphi/\Omega(x) \tag{89}$$

(vector fields being left unchanged and spinors transforming with $\Omega^{-3/2}$) leaves the action S unchanged. From this requirement, one finds that the trace of the energy-

momentum tensor [51]

$$T^{\mu}{}_{\mu}[g_{\alpha\beta}(x)] = -\frac{\Omega(x)}{\sqrt{-g(x)}}\frac{\delta S[\bar{g}_{\mu\nu}]}{\delta\Omega(x)}\Big|_{\Omega\to 1}, \tag{90}$$

should vanish if (89) is a symmetry of S. This implies that the scalar fields are massless and $\xi \to \frac{1}{6}$. The identity (90) is true at the classical level, and indeed the conserved Noether current in this case reads

$$\left(2g_{\mu\nu}\frac{\delta}{\delta g_{\mu\nu}} + \sum_i k_i\phi_i\frac{\delta}{\delta\phi_i}\right) S[g_{\alpha\beta}(x),\phi(x)] = 0, \tag{91}$$

in which the weights k_i correspond to the various fields involved, with $k_{\rm s} = -1$ for scalar fields, $k_{\rm f} = -3/2$ for the fermions and $k_{\rm v} = 0$ for the gauge fields.

At the quantum level, however, the trace $\langle T^{\mu}{}_{\mu}\rangle$ is no longer vanishing, as explicitly calculating it with the given matter content (scalar, vector and spinor fields) yields a renormalised expectation value [51]

$$\langle T^{\mu}{}_{\mu}\rangle = -\left(\omega C^2 + bE + c\Box R\right), \tag{92}$$

where the $\beta-$functions ω, b and c depend on the numbers of real scalar degrees of freedom N_0, four-component spinor fermions $N_{1/2}$ and vector fields N_1 in the underlying particle physics model. In practice, they are found to be

$$\begin{pmatrix}\omega\\ b\\ c\end{pmatrix} = \frac{1}{360(4\pi)^2}\begin{pmatrix}3N_0 + 18N_{1/2} + 36N_1\\ -N_0 - 11N_{1/2} - 62N_1\\ 2N_0 + 12N_{1/2} - 36N_1\end{pmatrix}. \tag{93}$$

In the standard model (SM) of particle physics, where the SU(3)×SU(2)×U(1) is broken to SU(3)×U(1) through a Higgs doublet, the relevant numbers are $N_0^{\rm SM} = 4$, $N_1^{\rm SM} = 12$ (eight gluons, the intermediate $W^{\pm}$ and Z^0 and the photon) and $N_{1/2}^{\rm SM} = 24$ (leptons and quarks, assuming a massive neutrino), one finds

$$\omega^{\rm SM} = \frac{73}{480\pi^2}, \quad b^{\rm SM} = -\frac{253}{1440\pi^2} \quad \text{and} \quad c^{\rm SM} = -\frac{17}{720\pi^2}.$$

Note that although b is negative definite, the sign of c depends on the exact matter content: measuring this sign somehow, e.g. through that of the primordial gravitational wave spectrum, could be an indirect way of getting information about the physics that should apply at high energies such as the grand unification (if any) scale. Note for instance that in the case of the minimal supersymmetric extension of the standard model (MSSM), the number of vector modes is unchanged ($N_1^{\rm MSSM} = 12$), while the number of fermions is increased to $N_{1/2}^{\rm MSSM} = 32$ and the proliferation of new scalar modes then yields $N_0^{\rm MSSM} = 104$, leading to $c^{\rm MSSM} = 1/(36\pi^2) > 0$.

Integrating the trace of (83) using (92) is a non-trivial task that has been achieved in Refs. [57, 58]. Ref [59] suggested to rewrite the action in terms of two auxiliary

scalar fields σ and ρ (see also [60] for an independent but equivalent formulation) which happens to be particularly useful for the gravitation wave discussion. It reads

$$\Gamma = S_{\rm c}[g_{\mu\nu}] + \int {\rm d}^4x\sqrt{-g}\left(\frac{1}{2}\sigma\Delta_4\sigma - \frac{1}{2}\rho\Delta_4\rho + \ell_1 C^2\rho\right) + \int {\rm d}^4x\sqrt{-g}\left\{\sigma\left[k_1C^2 + k_2\left(E - \frac{2}{3}\Box R\right)\right] - \frac{1}{12}k_3R^2\right\}, \quad (94)$$

where the integration constant $S_{\rm c}[g_{\mu\nu}]$ is conformally invariant, the covariant conformal fourth-order operator is (see Refs. [57, 58])

$$\Delta_4 = \Box^2 + 2R^{\mu\nu}\nabla_\mu\nabla_\nu - \frac{2}{3}R\Box + \frac{1}{3}R^{;\mu}\nabla_\mu$$

and the coefficients are given in terms of those of (92) through

$$k_1 = -\frac{\omega}{2\sqrt{|b|}}, \quad k_2 = \frac{\sqrt{|b|}}{2}, \quad k_3 = c + \frac{2}{3}b \quad \text{and} \quad \ell_1 = \frac{\omega}{2\sqrt{|b|}} \quad (95)$$

(recall $b < 0$). This effective action stemming from the conformal anomaly (the Noether current is not conserved at the quantum level) should be added to the vacuum term $S_{\rm vac}$ of Eq. (87).

3.7.3 Anomaly-induced cosmology and gravitational waves

Let us apply the above discussion to the specific case of a cosmological framework which is our main subject, first by considering a background FLRW (conformally flat) solution and its tensorial perturbations.

The FLRW metric can be written as a conformal transformation of the Minkowski metric $\eta_{\mu\nu}$ by setting $g_{\mu\nu} = a^2(\eta)\eta_{\mu\nu}$. In this very simple case, variations of (94) with respect to the auxiliary fields σ and ρ yields

$$\left(\partial_t^2 - \boldsymbol{\nabla}^2\right)\left(\sigma + 8\pi\sqrt{|b|}\ln a\right) = 0 \quad \text{and} \quad \left(\partial_t^2 - \boldsymbol{\nabla}^2\right)\rho = 0, \quad (96)$$

with solutions

$$\sigma = \sigma_{\rm h} - 8\pi\sqrt{|b|}\ln a \qquad \text{and} \qquad \rho = \rho_{\rm h}, \quad (97)$$

in which $\sigma_{\rm h}$ and $\rho_{\rm h}$ are solutions of the homogeneous equation, $\left(\partial_t^2 - \boldsymbol{\nabla}^2\right)f_{\rm h} = 0$; they can be set to zero in the cosmological context. In this case, one finds the relation

$$\frac{{\rm d}^n\sigma}{{\rm d}t^n} = -8\pi\sqrt{|b|}\frac{{\rm d}^{n-1}H}{{\rm d}t^{n-1}}$$

where $H = \dot{a}/a$.

The above solution (97) with the FLRW metric can now be inserted into the full theory containing both (94) and the original vacuum (87). It leads to the modified Friedmann equation

$$\frac{\ddot{a}}{a}+H^2-\frac{2}{3}\Lambda=\frac{c}{M_{\rm P}^2}\left[\frac{\dddot{a}}{a}+3H\frac{\ddot{a}}{a}+\left(\frac{\ddot{a}}{a}\right)^2-\left(5+\frac{4b}{c}\right)H^2\frac{\ddot{a}}{a}\right], \tag{98}$$

in which we defined the Planck mass $M_{\rm P}^{-2}=8\pi G_{\rm N}$. As could have been anticipated, this solution depends on b and c, but neither on ω and a_1 since the Weyl tensor is conformally invariant, nor on a_2 and a_3 (surface terms), and we have set $a_4\to 0$ to ensure the original theory is conformally invariant.

Inflationary solutions for (98) can be found in Refs. [56, 61, 62, 63, 64]. A simple case consists of a de Sitter solution $a\propto\exp(Ht)$ with H constant, which transforms (98) into a quadratic algebraic equation for H whose solutions

$$H^2=\frac{M_{\rm P}^2}{2|b|}\left(1\pm\sqrt{1+\frac{4|b|\Lambda}{3M_{\rm P}^2}}\right)\xrightarrow[|b|\Lambda\ll M_{\rm P}^2]{}\begin{cases}H_{\rm inf}^2=M_{\rm P}^2/|b| & (+)\\ H_\Lambda^2=2\Lambda/3 & (-)\end{cases} \tag{99}$$

produce the two relevant extreme cases of present-day cosmological constant domination and initial inflation, with $H_{\rm inf}\gg H_\Lambda$.

Tensor perturbations of the kind (1) in this context are slightly different from those of ordinary GR discussed in the previous sections. In particular, the mode equation (4) is now replaced by the slightly more involved fourth order equation (see Ref. [65] for details)

$$\left(2f_1+\frac{f_2}{2}\right)\dddot{h}+\left[3H(4f_1+f_2)+4\dot{f}_1+\dot{f}_2\right]\ddot{h}+\Bigg[3H^2\left(6f_1+\frac{f_2}{2}-4f_3\right)$$
$$+H\left(16\dot{f}_1+\frac{9}{2}\dot{f}_2\right)+6\dot{H}(f_1-f_3)-\frac{16\pi^2}{3}|b|\left(H^2-\dot{H}\right)\Bigg]\ddot{h}$$
$$-(4f_1+f_2)\frac{\nabla^2\ddot{h}}{a^2}+\Bigg[2\dot{H}(2\dot{f}_1-3\dot{f}_3)-\frac{21}{2}H\dot{H}(f_2+4f_3)-\frac{3}{2}\ddot{H}(f_2+4f_3)$$
$$+3H^2\left(4\dot{f}_1+\frac{1}{2}\dot{f}_2-4\dot{f}_3\right)-9H^3(f_2+4f_3)+H\left(4\ddot{f}_1+\frac{3}{2}\ddot{f}_2+\frac{3M_{\rm P}^2}{4}\right)$$
$$+\frac{16\pi^2}{3}|b|\left(\ddot{H}+H\dot{H}-3H^3\right)\Bigg]\dot{h}-\left[H(4f_1+f_2)+4\dot{f}_1+\dot{f}_2\right]\frac{\nabla^2\dot{h}}{a^2}$$
$$+\Bigg[\frac{16\pi^2}{3}|b|\left(2\dddot{H}+12H\ddot{H}+9\dot{H}^2-6H^2\dot{H}-15H^4\right)+\frac{M_{\rm P}^2}{2}\left(2\dot{H}+3H^2\right)$$
$$-4H\dot{H}\left(8\dot{f}_1+9\dot{f}_2+30\dot{f}_3\right)-8\ddot{H}\left(\dot{f}_1+\dot{f}_2+3\dot{f}_3\right)-H^2(4\ddot{f}_1+6\ddot{f}_2+24\ddot{f}_3)$$
$$-4\dot{H}\left(\ddot{f}_1+\ddot{f}_2+3\ddot{f}_3\right)-H^3\left(8\dot{f}_1+12\dot{f}_2+48\dot{f}_3\right)$$
$$-\left(36\dot{H}H^2+18\dot{H}^2+24H\ddot{H}+4\dddot{H}\right)(f_1+f_2+3f_3)\Bigg]h$$
$$+\Big[2\left(2H^2+\dot{H}\right)(f_1+f_2+3f_3)+\frac{1}{2}H\left(4\dot{f}_1+\dot{f}_2\right)+\frac{M_{\rm P}^2}{2}-\frac{1}{2}\ddot{f}_2$$
$$-\frac{16\pi^2}{3}|b|\left(\dot{H}+5H^2\right)\Big]\frac{\nabla^2 h}{a^2}+\left(2f_1+\frac{1}{2}f_2\right)\frac{\nabla^4 h}{a^4}=0, \tag{100}$$

stemming from the variation of the second-order Lagrangian function

$$\mathscr{L}=\frac{M_{\rm P}^2}{2}R+f_1R_{\alpha\beta\mu\nu}^2+f_2R_{\alpha\beta}^2+f_3R^2-\frac{4\pi}{3}\sqrt{|b|}\sigma\Box R+\frac{1}{2}\sigma\Delta\sigma, \tag{101}$$

and we have set $\rho=\rho_{\rm h}\to 0$ and $\sigma_{\rm h}\to 0$ as the background depends only on time; the perturbation $h(\boldsymbol{x},t)$ is the amplitude of the tensor mode h_{ij} for a given polarisation. In Eqs. (100) and (101), the coefficients f_1, f_2 and f_3 are time-dependent functions that take the values

$$f_1=a_1+a_2+\frac{|b|-\omega}{2\sqrt{|b|}}\sigma,$$
$$f_2=-2a_1-4a_2+\frac{\omega-2|b|}{\sqrt{|b|}}\sigma,$$
$$f_3=\frac{a_1}{3}+a_2-\frac{3c-2|b|}{36}+\frac{3|b|-\omega}{6\sqrt{|b|}}\sigma.$$

By inspection of the combinations of f's entering Eq. (100), one notes that the equation of motion does not depend on a_2, as expected from the fact that this comes from a surface term.

Eq. (100) was obtained by assuming the value (97) for the auxiliary field $\sigma(t)$ in terms of the background Hubble variable, and so can be used for any admissible solution for the scale factor, including the inflating case of (99). Expanding in Fourier modes, i.e. replacing $\boldsymbol{\nabla}$ by $-\boldsymbol{k}^2$, in principle permits to evaluate the gravitational wave stochastic spectrum in such a theory, with a catch: contrary to GR, the mode equation is no longer that of a parametric oscillator, so that its quantisation, and consequently the vacuum initial conditions, are not that well defined.

This issue, still under discussion, can be handled by assuming that our semiclassical framework provides a perturbation to GR, so that the extra (higher derivative) terms may be neglected while quantising in a regime in which one can manage to construct a consistent Hilbert space of state. Setting quantum vacuum fluctuation initial conditions exactly then allows setting initial values for the gravitational wave amplitude and its first three time derivatives.

Moreover, the presence of the higher derivative terms potentially implies instabilities. Setting initial conditions as discussed above, one finds [66, 67] that the time development, and hence the resulting predictions, is very sensitive to the properties of the background. Assuming, for instance, a de Sitter inflation phase with constant Hubble rate $H = H_{\rm inf}$, initial trans-Planckian runaway solutions can be redshifted to become sub-Planckian and then rapidly damped by the expansion: the instabilities indeed present in the theory can end up harmless in a cosmological setup. We assume in what follows that this is indeed the case.

3.8 Primordial gravitational-wave background

Independently of the underlying quantum theory leading to the production of primordial tensor modes, one must now evolve them through the expanding universe to evaluate their current contribution. As we know GR to be valid for the most part of the FLRW evolution, we consider from now on that the higher derivative terms discussed above are either not present at all, or contribute only negligibly. In order to clearly distinguish classical from quantum effects, we include again the relevant factors of $\hbar$ when necessary.

In Sec. 3.6, we have laid out three equivalent ways to describe the evolution of perturbations for a general time-dependent background $a(\eta)$: the use of Bogoliubov transformations, mode functions and squeezing parameters. We now solve the dynamics of the gravitational wave field in a simplified model of the cosmological evolution to discuss the properties of the primordial gravitational waves generated and make a connection with observations.

3.8.1 Cosmological evolution

In FLRW the curvature of spacetime is contained in the scale factor a, whose dynamics is related to the matter content of the Universe through the Friedmann equations. In what follows, we first solve them in the standard approximation that there is always a single fluid dominating the energy budget of the Universe and that transitions between two phases are instantaneous. One can thus model the cosmological evolution as a succession of three eras: first an accelerated expansion phase for $-\infty \leq \eta \leq \eta_{\rm r}$, whose dynamics is that of a slow-roll inflation phase [68], then a radiation dominated phase for $\eta_{\rm r} \leq \eta \leq \eta_{\rm m}$ and finally a matter domination for $\eta \geq \eta_{\rm m}$. For the sake of simplicity, we ignore the late-time accelerated expansion.

The evolution of the gravitational waves contained in the universe is controlled by Eq. (4) where the expansion enters through the scale factor $a(\eta)$ and its second derivative. Connecting the scale factor and its derivative continuously across the transitions, we have

$$\frac{a(\eta)}{a_{\rm r}} = \begin{cases} \dfrac{\eta_{\rm r}^{1+\varepsilon}}{(2\eta_{\rm r}-\eta)^{1+\varepsilon}} \approx \dfrac{\eta_{\rm r}}{2\eta_{\rm r}-\eta} + \mathcal{O}(\varepsilon) & \text{for } -\infty \leq \eta \leq \eta_{\rm r}, \\ \dfrac{\eta}{\eta_{\rm r}} & \text{for } \eta_{\rm r} \leq \eta \leq \eta_{\rm m}, \\ \dfrac{\eta_{\rm m}}{2\eta_{\rm r}}\left(\dfrac{\eta^2}{\eta_{\rm m}^2}+1\right) & \text{for } \eta_{\rm m} \leq \eta, \end{cases} \tag{102}$$

where $\eta_{\rm r} > 0$. The first expression in inflation is at first order in $\varepsilon = 1 - \mathcal{H}'/\mathcal{H}^2$ the first slow-roll parameter considered time-independent and we have also given the de Sitter limit $\varepsilon = 0$. From this, one computes the time-dependent part of the frequency ω_k^2 defined in Eq. (5)

$$\frac{a''}{a} = \begin{cases} \dfrac{2+3\varepsilon}{(2\eta_{\rm r}-\eta)^2} \approx \dfrac{2}{(\eta_{\rm r}-\eta)^2} + \mathcal{O}(\varepsilon) & \text{for } -\infty \leq \eta \leq \eta_{\rm r}, \\ 0 & \text{for } \eta_{\rm r} \leq \eta \leq \eta_{\rm m}, \\ \dfrac{2}{\eta^2} & \text{for } \eta_{\rm m} \leq \eta. \end{cases} \tag{103}$$

Solving Eq. (4) with (103) yields reference mode functions in each era, namely

$$u_k^{(\rm infl.)}(\eta) = \sqrt{\frac{-(\eta-2\eta_{\rm r})\hbar\pi}{4}} H^{(1)}_{\frac{3}{2}+\varepsilon}\left[-k(\eta-2\eta_{\rm r})\right] \quad \text{for } -\infty \leq \eta \leq \eta_{\rm r}, \tag{104a}$$

$$\approx \sqrt{\frac{\hbar}{2k}} e^{-ik(\eta-2\eta_{\rm r})}\left[1 - \frac{i}{k(\eta-2\eta_{\rm r})}\right]$$

$$u_k^{(\rm r)}(\eta) = \sqrt{\frac{\hbar}{2k}} e^{-ik\eta} = u_k^{(\rm M)}(\eta) \quad \text{for } \eta_{\rm r} \leq \eta \leq \eta_{\rm m}, \tag{104b}$$

$$u_k^{(\rm m)}(\eta) = \sqrt{\frac{\hbar}{2k}} e^{-ik\eta}\left(1 - \frac{i}{k\eta}\right) \quad \text{for } \eta_{\rm m} \leq \eta, \tag{104c}$$

where in the first line, $H_\kappa^{(1)}$ is the Hankel function of the first kind of index κ and the approximation corresponds to the de Sitter limit. We refer to [69] for a recent textbook in which all details of the computations of the inflationary mode function can be found. Note that during radiation domination, the solution is given by the Minkowski mode function because $a'' = 0$. Since two solutions of (4) are related by a Bogoliubov transformation, a mode function solution of (4) for the whole cosmological evolution is related by a Bogoliubov transformation to the associate reference mode function (104) in each era.

One can construct a global solution $u_k(\eta)$ starting in the inflationary period. The reference mode function there was chosen to match the Minkowski mode function $u_k^{(\mathrm{M})}$ in the asymptotic past $\eta \to -\infty$. This gives us an "in" region in which we can set the initial condition for the state of the system in terms of a well-defined particle content. We therefore pick $u_k(\eta) = u_k^{(\mathrm{M})}(\eta)$ during inflation. The expressions for the radiation and matter domination are then

$$u_k(\eta) = \begin{cases} \alpha_k^{(\mathrm{r})} u_k^{(\mathrm{r})}(\eta) + \beta_k^{(\mathrm{r})} u_k^{\star(\mathrm{r})}(\eta) & \text{for } \eta_\mathrm{r} \leq \eta \leq \eta_\mathrm{m}, \\ \alpha_k^{(\mathrm{m})} u_k^{(\mathrm{m})}(\eta) + \beta_k^{(\mathrm{m})} u_k^{\star(\mathrm{m})}(\eta) & \text{for } \eta_\mathrm{m} \leq \eta\,, \end{cases} \tag{105}$$

where the Bogoliubov coefficients are found by requiring that the mode function and its first time-derivative are continuous across the transition. Their expressions are worked-out in full in Ref. [45]. The mode $u_k(\eta)$ is then completely determined for both polarisations and, using (38), one achieves a fully quantum description of the evolution of the gravitational wave field.

The analysis is completed once one specifies the initial state of the gravitational waves as $k\eta \to -\infty$. The standard choice is to assume that, in the far past, the inflation phase somehow wiped out any initial perturbation, leaving no graviton to start with: this is the motivation behind choosing the vacuum state for every mode. This vacuum initial state is often referred to the Bunch-Davies vacuum [25], although it should be more appropriately be called Minkowski vacuum. This choice implies that the state of the perturbation consists of a collection of independent 2-mode squeezed states as discussed in Sec. 3.4.

For scalar perturbations, the above vacuum choice turns out to be in excellent agreement with the observations of the Cosmic Microwave Background [70]. For gravitational waves, we are so far short of equivalent observations so that other states could be chosen as initial condition [71]. Although such alternative choices do not modify our description of the subsequent evolution, they change the values of the Bogoliubov coefficients and therefore the prediction on the amplitude of gravitational waves or, equivalently, the number of gravitons produced.

We have explained in Sec. 3.6 that, most of the time, this number is ambiguous due to the time-dependent part of ω_k^2. Let us explain how to make sense of it for primordial gravitational waves. First, in the sub-Hubble regime $k^2 \gg a''/a$ the frequency reduces to $\omega_k \sim k$ i.e. the mode $\boldsymbol{k}$ does not feel the expansion of space and effectively oscillates as in flat spacetime. In this sub-Hubble limit, the reference mode functions (104) reduce to the Minkowski one, and we can treat the mode as if

evolving in Minkowski. On the other hand, in the super-Hubble regime $k^2 \ll a''/a$, the mode behaves as an inverted harmonic oscillator $\omega_k \sim -a''/a < 0$. One therefore expects its amplitude to be amplified, and it is indeed where most of the squeezing happens, as illustrated in the first two panels of Fig. 5.

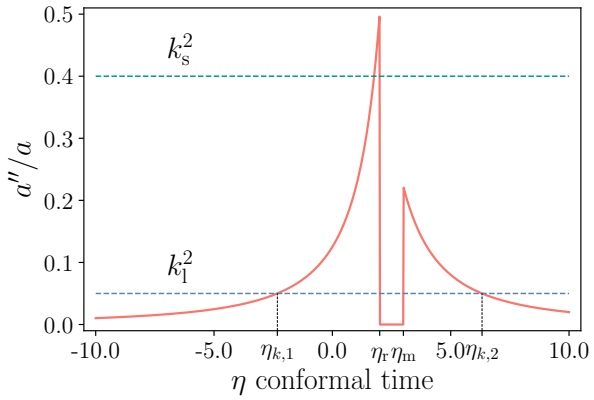

Fig. 4 Sketch of the potential for the tensor mode within the toy model (103). The full red line represents the evolution of a''/a in arbitrary units in our simplified cosmological evolution (102). The blue and green dotted lines represent two comoving frequencies $k_{\rm s}^2$ and $k_{\rm l}^2$ in arbitrary units which are constant during the evolution.

The evolution (103) of the time-dependent piece a''/a is plotted in Fig. 4 and is compared to the square of the comoving frequencies of two different modes $k_{\rm s}^2$ and $k_{\rm l}^2$. Note that at the beginning of inflation and during the radiation era, since $a'' = 0$, all modes are sub-Hubble and effectively living in Minkowski there[12]. This second aspect is due to our simplistic modelling of the transition in Eq. (102). In a realistic cosmological model, a'' is continuous and part of the modes progressively reach the sub-Hubble regime. In Fig. 4, the mode $\boldsymbol{k}_{\rm s}$ has a short wavelength and is always sub-Hubble. It is not affected by the amplification process. The mode $\boldsymbol{k}_{\rm l}$ has a larger wavelength and becomes super-Hubble during inflation after $\eta_{k,1}$, is insensitive to the expansion during radiation domination, becomes super-Hubble again during matter domination, until $\eta_{k,2}$ where it settles in the sub-Hubble regime. The modes of interest for cosmological observations are of the second type (or become and stay super-Hubble during radiation domination).

The picture that we have just sketched for these modes, putting aside radiation domination, is reminiscent of the idealized situation described in Sec. 3.6 where the "in" region corresponds to $\eta \ll \eta_{k,1}$ and the "out" region to $\eta \gg \eta_{k,2}$. For such modes, we are thus justified in talking about graviton production.

[12] Recall that in this limiting case, the relation between the dominant term in the frequency and the wavelength size compared to the Hubble radius does not hold. One cannot, strictly speaking, employ the terminology sub or super-hubble here.

Two remarks are in order here. First, modes progressively reenter the Hubble radius during the neglected current accelerated expansion. For the modes of interest here, this is of no consequence. Second, one should be careful when discussing modes responsible for the B modes of polarisation in the CMB since some of them had not yet reached the sub-Hubble regime when generating polarisation.

To close this discussion, we compute the relevant quantities describing the gravitons in the different formalisms. For simplicity we only consider an inflationary period where most of the amplification occurs. For this estimate, we neglect slow-roll corrections and model inflation by a period of de Sitter expansion ending at $\eta_{\rm r}$. After the transition to radiation domination, the mode does not feel the expansion anny more, so that its particle content can be computed. In de Sitter, the covariance matrix elements can be computed exactly using the mode function in Eqs. (104). We evaluate them at $\eta_{\rm r}$ [37]

$$\gamma_{11} = 1 + \frac{1}{k^2\eta_{\rm r}^2} \approx e^{2N}\,, \quad \gamma_{12} = -\frac{1}{k\eta_{\rm r}} \approx e^{N}\,, \quad \gamma_{22} = 1\,. \tag{106}$$

where, since we are considering a mode which is in the super-Hubble regime during inflation, we have taken the limit $k\eta_{\rm r} \ll 1$. These last expressions are given in terms of the number of e-folds N defined by $N = \ln\left[a\left(\eta\right)/a\left(\eta_k\right)\right] = \ln\left[k\left(2\eta_{\rm r} - \eta\right)\right]$ where $a\left(\eta_k\right)$ is the scale factor evaluated at Hubble crossing time $k\left(2\eta_{\rm r} - \eta_k\right) = 1$.

At this point, one notes that $\left\langle \left(\hat{h}'_{\lambda,\boldsymbol{k}}\hat{h}'_{\lambda,-\boldsymbol{k}}\right)^2 \right\rangle \propto \gamma_{22}/a^2(\eta)$, so that, for a super-Hubble mode, it decays exponentially during inflation. The fact that the matrix element $\gamma_{11} = 2k\left\langle \left(\hat{\mu}^{\rm R}_{\boldsymbol{k}}\right)^2 \right\rangle$ grows faster than γ_{12} and γ_{22} leads to squeezing in a direction close to that of the $\mu^{\rm R}_{\boldsymbol{k}}$ axis. This can be verified by computing explicitly the squeezing parameters: inverting Eq. (66), we deduce the squeezing parameters as

$$r_k = \operatorname{arcsinh}\left(\frac{1}{2k\eta_{\rm r}}\right) \quad , \quad \varphi_k = \frac{\pi}{2} - \frac{1}{2}\arctan\left(2k\eta_{\rm r}\right), \tag{107}$$

which, in the super-Hubble limit, yields

$$r_k \approx \ln\left(\frac{1}{2k\eta_{\rm r}}\right) \approx N\,, \quad \varphi_k \approx \frac{\pi}{2} - k\eta_{\rm r} \approx \frac{\pi}{2} - e^{-N}\,. \tag{108}$$

$\varphi_k \to \pi/2$ so that indeed the ellipse will be squeezed in a direction close to $\mu^{\rm R}_{\boldsymbol{k}}$.

For scales of cosmological interest, one typically expects $N = \ln\left(k\eta_{\rm r}\right) \sim 50$ at the end of inflation so that $r \approx 50$. This is to be compared with the best quantum optics experiments where one can hardly achieve $r \approx 2$; the squeezing is extreme [72]. The resulting evolution of the Wigner function is plotted for a few e-folds after Hubble exit in Fig. 5 where the very large squeezing is manifest.

Finally, we compute the number of particles created and their pair correlation: Eq. (78) in the de Sitter and super-Hubble limits gives

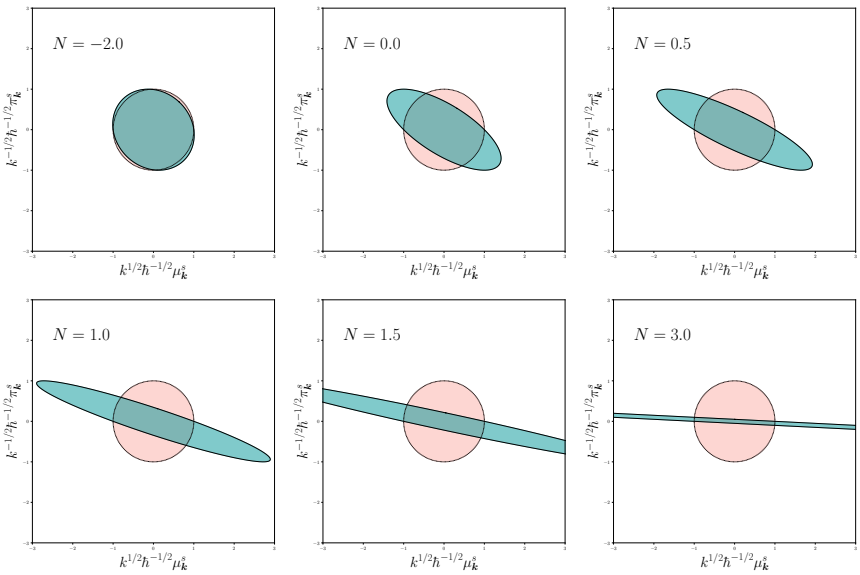

Fig. 5 Phase space ellipse in the plane $(k^{1/2}\mu^{\mathrm{s}}_{\boldsymbol{k}}, k^{-1/2}\pi^{\mathrm{s}}_{\boldsymbol{k}})$ at different instants during inflation, labelled by $N = \ln[a/a(\eta_k)]$, i.e. the number of e-folds measured from the Hubble-crossing time of the mode under consideration. On sub-Hubble scales, the ellipse remains roughly a circle, while it gets squeezed and rotates in the super-Hubble regime.

$$n_k = \frac{1}{4k^2\eta^2} = \frac{e^{2N}}{4}\,, \tag{109}$$

$$c_k = \frac{1}{4k^2\eta^2} - \frac{i}{2k\eta} \approx \frac{e^{2N}}{4}\,. \tag{110}$$

The number of pairs and their correlation grow at the same rate; squeezing necessarily creates entangled pairs. After 50 e-folds of inflation, one finds $n_k \sim 10^{43}$. This number might appear very large, but the physical field h_{ij} is diluted by the inverse of the scale factor that will keep acting even when the creation process stops, following Eq. (3). In addition, the number of gravitons is not directly observable; we observe gravitational waves or their imprint on other fields, e.g. the electromagnetic field in the CMB, but not individual gravitons. One therefore needs to compute the physical quantities that are more directly relevant in forecasting future observations.

3.8.2 Connection to observations

There is hope that observable signatures of these primordial gravitational waves will be found either in the ***B***-modes of the CMB or directly in future gravitational wave interferometers. We refer to Ref. [73] or Chapter 19, 20 and 23 in Ref. [33] for a detailed account. The waves we have described are stochastic in nature owing

to their quantum origin. They account for part of the stochastic gravitational-wave background (SGWB), the rest being produced by unresolved astrophysical sources or possibly other high-energy phenomena such as topological defects. The SGWB is usually assumed to be statistically homogeneous and isotropic, as the FLRW background metric, Gaussian, either due to the sum of a large number of independent sources or because it is sourced by a Gaussian state as considered here, and unpolarised (same content in both polarisations and polarisations are uncorrelated) [13] because there is no significant source of parity violation in the Universe [73]. All these assumptions only have to be made on the initial state as the dynamics is the same for both fields $\hat{\mu}_\lambda$ and preserves isotropy and homogeneity. They are in particular satisfied for primordial gravitational waves produced from the Bunch-Davies vacuum. A typical quantity used to characterize a stochastic ensemble of waves is their power spectrum which, within the gaussianity assumption, contains all the information. The power spectrum $\mathscr{P}_{\mathrm{T}}$ of gravitational waves h_{ij} at time η is then defined (working classically for the moment) by

$$\left\langle \mu_\lambda\left(\boldsymbol{k},\eta\right)\mu^\star_{\lambda'}\left(\boldsymbol{k}',\eta\right)\right\rangle = \frac{\pi a^2\left(\eta\right)}{32G_{\mathrm{N}}k^3}\delta^{(3)}\left(\boldsymbol{k}-\boldsymbol{k}'\right)\delta_{\lambda,\lambda'}\mathscr{P}_{\mathrm{T}}\left(k,\eta\right), \tag{111}$$

where the Dirac delta comes from homogeneity, and $\mathscr{P}_{\mathrm{T}}$ only depends on k since the background is isotropic and unpolarised. The index "T" stands for "tensor", to differentiate the latter from the scalar power spectrum $\mathscr{P}_{\mathrm{S}}$. Using (3), (15) and the orthogonality relations of the tensors below (16), one finds the two-point correlation function of the Fourier coefficients of h_{ij}

$$\left\langle h^{ij}\left(\boldsymbol{k},\eta\right)h^\star_{ij}\left(\boldsymbol{k},\eta\right)\right\rangle = \delta^{(3)}\left(\boldsymbol{k}-\boldsymbol{k}'\right)\frac{2\pi^2}{k^3}\mathscr{P}_{\mathrm{T}}\left(k,\eta\right),$$

as well as the two-point correlation of h_{ij} in real space, namely

$$\left\langle h^{ij}\left(\boldsymbol{x},\eta\right)h_{ij}\left(\boldsymbol{x},\eta\right)\right\rangle = \int \mathrm{d}\ln\left(k\right)\mathscr{P}_{\mathrm{T}}\left(k,\eta\right).$$

The power spectrum $\mathscr{P}_{\mathrm{T}}\left(k,\eta\right)$ corresponds to the typical squared amplitude of the wave, per logarithm of k, at the time η. For perturbations made of sub-Hubble modes $k \gg |\mathscr{H}|$, the time dependent term of (4) can be neglected and the energy density of gravitational waves reads [14]

$$\rho_{\mathrm{GW}} = \frac{1}{32\pi G_{\mathrm{N}}}\left\langle \dot{h}^{ij}\left(\boldsymbol{x},\eta\right)\dot{h}_{ij}\left(\boldsymbol{x},\eta\right)\right\rangle. \tag{112}$$

[13] It can be checked using (17) that the assumptions that the waves are both unpolarised $\left\langle \mu_+\mu^\star_+\right\rangle = \left\langle \mu_\times\mu^\star_\times\right\rangle$ and that polarisations uncorrelated $\left\langle \mu_+\mu^\star_\times\right\rangle = 0$ in terms of the $+,-$ helicity basis is equivalent to the same two assumptions on the $+,\times$ basis.

[14] Averaging is necessary even for a deterministic source of gravitational waves to make sense of their energy. The averaging can either be performed over a certain volume or a certain duration, see [33]. In the context of this review, the averaging in (112) refers to an ensemble average.

For sub-Hubble modes, $h_{+,\times}(\boldsymbol{k},\eta) \propto e^{i(\boldsymbol{k}.\boldsymbol{x}-k\eta)}/a(\eta)$ so that neglecting terms in $\mathscr{H}$ with respect to k we get

$$\left\langle \dot{h}^{ij}(\boldsymbol{k},\eta)\dot{h}_{ij}(\boldsymbol{k},\eta)\right\rangle \approx k^2 \frac{\left\langle h^{ij}(\boldsymbol{k},\eta)h_{ij}(\boldsymbol{k},\eta)\right\rangle}{a^2(\eta)}. \tag{113}$$

Note that, since h_{ij} dilutes as a^{-1}, ρ_{GW} dilutes as a^{-4}, i.e. sub-Hubble modes dilute as standard radiation. Expanding the energy density in Fourier space and normalising by the critical energy density $\rho_{\mathrm{c}} = 3H^2/8\pi G_{\mathrm{N}}$, we get the energy fraction per logarithm of k that is directly expressed as a function of the power spectrum

$$\Omega_{\mathrm{GW}}(k,\eta) = \frac{1}{\rho_c}\frac{\mathrm{d}\rho_{\mathrm{GW}}}{\mathrm{d}\ln k} = \frac{k^2}{12H^2a^2(\eta)}\mathscr{P}_{\mathrm{T}}(k,\eta). \tag{114}$$

The power spectrum (111) and the energy density fraction (114) are the two quantities customarily used to assess the observability and constrain the models of primordial gravitational waves. More precisely, we often estimate the *primordial* power spectrum, i.e. the power spectrum at the beginning of radiation domination. The rest of the evolution is encoded in so-called transfer functions; these can be estimated using the previous computations. For actual comparison with observations, they have to be computed numerically by solving Boltzmann-like equations.

Let us then evaluate the primordial power spectrum by considering only the initial phase of single field slow-roll inflation in the cosmological evolution Eq. (102) and assuming Bunch-Davies vacuum for both polarisations $\pm$. Using (38), the power spectrum is straightforwardly expressed in terms of the mode function for $\hat{\mu}_{\boldsymbol{k}}$

$$\mathscr{P}_{\mathrm{T}}(k,\eta) = \frac{32G_{\mathrm{N}}k^3}{\pi a^2(\eta)}\left|u_k^{(\mathrm{infl.})}(\eta)\right|^2. \tag{115}$$

Making use of (104), we get

$$\mathscr{P}_{\mathrm{T}}(k,\eta) = 8G_{\mathrm{N}}\frac{H_k^2\hbar}{(1+\varepsilon)^{2+\varepsilon}}\left[-k(\eta-2\eta_{\mathrm{r}})\right]^{3+2\varepsilon}\left|H^{(1)}_{\frac{3}{2}+\varepsilon}\left[-k(\eta-2\eta_{\mathrm{r}})\right]\right|^2, \tag{116}$$

where η_k is the Hubble crossing time $k/a(\eta_k) = H(\eta_k)$. To be consistent we expand all the quantities at first order in the slow-roll parameter ε and take the super-Hubble limit relevant for cosmological scales $|k(\eta-2\eta_{\mathrm{r}})| \ll 1$

$$\begin{aligned}\mathscr{P}_{\mathrm{T}}(k,\eta) &= \frac{2H_k^2\hbar}{\pi^2}8\pi G_{\mathrm{N}}\left[1+2(1-\log 2-\gamma_{\mathrm{E}})\varepsilon\right],\\ &= \frac{2H_\star^2\hbar}{\pi^2}8\pi G_{\mathrm{N}}\left[1+2(1-\log 2-\gamma_{\mathrm{E}})\varepsilon-2\varepsilon\log\left(\frac{k}{k_\star}\right)\right]\end{aligned} \tag{117}$$

where γ_{E} is the Euler-Mascheroni constant. Notice that in this limit the power spectrum does not depend on η, and we made the k-dependence explicit in the second line by expanding H_k around a pivot scale $k_\star$.

Current experiments have not been able to detect the primordial gravitational-wave background but the combined (non)-observations of Planck and BICEP experiments allow us to put bounds on the tensor-to-scalar ratio in single-field slow-roll inflation [74]. A discussion of its potential observability in future gravitational wave interferometers and with future CMB experiments can be found in [73, 75, 76]. Notice that different models of the very early universe would change the prediction (117): initially excited states [71], temporary departures from the single field slow-roll scenario [77] or coupling with extra fields [78] might for instance be able to generate larger signatures than single-field slow-roll inflation, while modifications of gravity in the high energy regime could also lead to changes in the spectrum at high frequencies, e.g. through introduction of a cut-off in theories of lower dimensionality in the ultraviolet [79]. Finally, we want to emphasise that the toy model of cosmological evolution of Eq. (102) makes the unrealistic assumption of an instantaneous reheating. Adding a period of reheating is known to significantly modify the resulting spectrum, e.g. the frequency at which it starts to decay, thereby modifying observational perspectives [80].

3.8.3 Quantum origin of the primordial gravitational waves

To close this part, we want to comment on how quantumness enters the prediction (117).

First, a subtle point hidden in (111) is the meaning of the averaging $\langle\rangle$. In the discussion of the dynamics of perturbations, we have been computing averages in the sense of expectation value for observables in a given quantum state. It is a basic assumption of quantum mechanics that this would be the expected average value of the physical quantity after repeated measurements of it when the system is prepared in the same state. Unfortunately, we only have one realisation of the history of the Universe. Yet, using statistical isotropy, we can treat each (sufficiently large) patch of sky as an independent realisation of the same underlying random process and compute average values over this ensemble of patches. Under an *ergodicity* assumption, the resulting correlation functions can then be compared to (117), a procedure applied to CMB data analysis [81]. Additional arguments to justify trading quantum averages for classical ones will be discussed in Sec. 4.

Second, as we repeatedly emphasised, since the linear evolution is the same in the classical and quantum settings, the quantum aspect has to be confined to the choice of initial state. The result (117) reflects the choice that the waves emerged from initial *vacuum fluctuations*. For primordial gravitational waves, we are short of observational data to test this prediction. Still, if we were to insist on having a purely classical treatment, then a classical vacuum of gravitational waves, i.e. $a_{\pm\boldsymbol{k}}(\eta_{\rm in}) = 0$ would persist throughout the evolution. There would simply be *no* primordial gravitational waves. On the contrary, initial gravitational waves would be classically amplified by cosmological expansion, but we then have to motivate a specific choice for the initial distribution of perturbations. For scalar perturbations, the CMB observations already demonstrated a tremendously good agreement with the predicted

power spectrum $\mathscr{P}_{\rm S}$ of initial vacuum fluctuations for the modes observed [74, 82]. Giving up on a quantum treatment in the inflationary paradigm would then require providing an *ad hoc* classical theory that yields the same initial conditions as the quantum vacuum. We could therefore argue that observations of the scalar sector give indirect proof that gravitational degrees of freedom should be quantised.

Yet, third, it is sometimes argued see e.g. [33, 83], that the verification of the prediction (117) would provide additional insights on the quantum aspect of gravity with respect to the observation of the scalar perturbations. In the treatment of scalar perturbations in single-field slow-roll inflation, the appropriate gauge-invariant variable is the Mukhanov-Sasaki (MS) field related to the perturbations of the inflaton $\delta\phi$ and the gravitational potential Ψ through

$$v_{\rm MS} = \frac{z}{\kappa}\left(\Psi + \mathscr{H}\frac{\delta\phi}{\phi_0'}\right), \tag{118}$$

where $z = a\sqrt{2\varepsilon}$, ε being the first slow-roll parameter, ϕ_0 the homogeneous background inflaton field and κ the reduced Planck mass. This is a scalar field whose Lagrangian is the same as (22) upon substituting $a \to z$, and up to normalisation. The MS field is then quantised in exactly the same manner as the two polarisations of the graviton and the power spectrum evaluated by initially choosing the Bunch-Davies vacuum. However, in the absence of perturbations $\delta\phi$ for the scalar field, the equation of motion of the scalar part of the metric perturbations show that they can be set to zero. This is the so-called synchronous gauge [84]. The existence of scalar perturbations then requires the presence of the scalar field $\delta\phi$ and is not intrinsic to the gravitational degrees of freedom. Even when $\delta\phi \neq 0$, in the synchronous gauge $\Psi = 0$ and only the scalar field contributes to the perturbations. In this gauge, the whole quantification process and evaluation of the power spectrum only deals with the physics of a quantum scalar field that is not related to gravitational degrees of freedom. This could therefore cast some doubt on whether some gravitational degrees of freedom were even quantised in the first place. Such ambiguity does not exist when dealing with gravitational waves. In the absence of any anisotropic stress, the gravitational waves persist, and the quantisation procedure is undeniably a perturbative quantisation of the gravitational field. Verification of (117) would then be an indirect observational proof that the gravitational field must be quantised.

Finally, to mitigate the above discussion, let us also mention an argument against our line of reasoning, as discussed, e.g. in Ref. [35]. The argument made above can be reversed, as one can also find a gauge in which the perturbation of the field vanishes altogether, with $\delta\phi = 0$, while the metric part is $\Psi \neq 0$; in this gauge, the quantisation is then over an element of the metric only. In addition, since perturbations of matter and geometry appear on each side of Einstein equations (however, note that their quantum counterpart is unknown), it is inconsistent to quantise only one degree of freedom. The observational verification of the prediction for the scalar power spectrum thus can be argued to be an indirect proof that the gravitational field should be quantised.

4 Quantum features in primordial gravitational waves ?

Given the quantum origin of primordial gravitational waves, it may seem natural to wonder about their state's quantum or classical character at present. While it is expected that we will never be able to detect the signal produced by a single graviton [85], a discrete spectrum of excitations is not the only specific feature of a quantum theory. For instance, entanglement is a *statistical* quantum feature that can be experimentally verified using Bell inequalities [86, 87]. The exciting possibility that primordial gravitational waves exhibit such features has been investigated since this idea was first put forward by Grishchuk and Sidorov in [30]. These discussions have gradually introduced many concepts borrowed from low-energy quantum physics, particularly quantum optics: squeezing, quasi-probability distribution, decoherence, quantum discord. In this section, we will review this line of research following a historical approach and trying to show the progress brought by each contribution.

This section is structured as follows. First, arguments based on the very squeezed character of the state are used to justify a classical treatment to compute cosmological observables [45]. This approach, sometimes called "decoherence without decoherence" [39], and its critics are reviewed in Sec. 4.1. It turns out, however, that the classicality identified by these works does not do away with all the quantum features of the state; the state of the perturbations could for instance violate a Bell inequality [88]. We review these "quantum information" approaches in Sec. 4.2. Lastly, taking into account the weak interactions of the perturbations is necessary as they would induce *decoherence* which might erase the quantum features exhibited at the linear level. This aspect is reviewed in Sec. 4.3.

For the most part, these works are based on analysing the state of a quantum scalar field, which can either represent the MS field of scalar perturbations or one of the polarisations of the tensor perturbations. The mechanisms and arguments being the same for both, we do not distinguish when citing works which refers to which and are only specific when necessary.

4.1 Classicalisation of perturbations without decoherence

In [30], the authors argue that the perturbations exhibit non-classical features due to the fact that the relevant quantum state is strongly squeezed. In order to make the discussion precise yet simple, we focus again on the inflationary period modeled by a de Sitter phase of expansion and assume initial Bunch-Davies vacuum[15]; the relevant equations were derived at the end of Sec. 3.8.1, and the squeezing is shown in Fig 5.

One of the arguments developed in [30] is that the trajectory in phase space of a classical system with given initial conditions is represented by a point moving on a single curve. The situation is different for a quantum system. Due to the intrinsic

[15] The reasoning can also be extended to certain non-vacuum initial states [89].

uncertainty stemming from the Heisenberg principle, the trajectory is represented by a moving surface. The quantum state that comes closest to mimicking a classical trajectory would then be a coherent state. Indeed, its trajectory in phase space is represented by a circle moving along a single curve: the system is located within a tube of minimal uncertainty around the classical trajectory. On the contrary, the surface representing an increasingly squeezed state is stretched around its centre delocalising the position of the system away from any single curve. Therefore, they argue, a very squeezed state like that of the cosmological perturbations is a very *quantum* state.

In a couple of works written in response [45, 39], the authors reproduce and complement the computations made in [30], but give a different interpretation of the result. The gist of their arguments, which we reproduce below, is that the properties of a system in an extremely squeezed state are indistinguishable from that of a classical system whose state is represented by a *classic stochastic distribution*; an argument borrowed from [90]. In other words, although the intrinsic quantum uncertainty on the outcome of a measurement dramatically spreads due to the evolution of the system, this uncertainty cannot be distinguished from a purely classical one.

To demonstrate this, let us consider the wavefunction of the perturbations in the modes $\pm\boldsymbol{k}$ decomposed in the R/I sector and given by Eq. (63). Discarding the indices "k", we recall that this is the wavefunction of a 1-mode squeezed state. We can show that for large r, it satisfies very well the conditions of the WKB approximation. For a general wavefunction $\Psi(\mu) = C(\mu)\exp[iS(\mu)/\hbar]$ the WKB approximation is valid when the amplitude C varies slowly compared to the phase S: $|\partial S/\partial\mu| \gg \left|C^{-1}\partial C/\partial\mu\right|$. Since the WKB approximation is generally understood as a semi-classical limit, this property is sometimes referred to as the "WKB-classicality" of the state. Using the wavefunction (63), we have

$$C(\mu) = \left(\frac{k}{\hbar\pi\gamma_{11}}\right)^{1/4} e^{-\frac{k\mu^2}{2\hbar\gamma_{11}}}, \tag{119a}$$

$$S(\mu) = k\mu^2\frac{\gamma_{12}}{2\gamma_{11}}, \tag{119b}$$

where we have dropped the exponent S and the index $\boldsymbol{k}$ for simplicity. We get

$$\left|\frac{C}{\partial C/\partial\mu}\frac{\partial S/\partial\mu}{\hbar}\right| = \left|\sin(2\varphi_k)\sinh(2r_k)\right|. \tag{120}$$

In the de Sitter case, using Eq. (107), one has $\sin(2\varphi_k)\sinh(2r_k) \approx e^N$; the condition is perfectly satisfied. We then compute the action of $\hat{\mu}$ and $\hat{\pi}$ on such a state

$$\hat{\mu}\Psi(\mu) = \mu\Psi(\mu), \tag{121a}$$

$$\hat{\pi}\Psi(\mu) = -i\hbar\frac{\partial\Psi}{\partial\mu} = \frac{\partial S}{\partial\mu}\left(1 - i\hbar\frac{\partial C/\partial\mu}{C\partial S/\partial\mu}\right)\Psi(\mu) \approx \frac{\partial S}{\partial\mu}(\mu)\Psi(\mu), \tag{121b}$$

where in the last line we have used Eq. (120). This last equality suggests that, neglecting sub-dominant contributions, we could attribute an unambiguous value to the "momentum" π through the relation $\pi \approx \partial S/\partial\mu$ [45] while the value of the position μ would be controlled by the probability distribution given by the μ-representation of the wavefunction, namely

$$P(\mu) = C(\mu)^2 = \left(\frac{k}{\pi\hbar\gamma_{11}}\right)^{1/2} e^{-\frac{k\mu^2}{\hbar\gamma_{11}}}\,. \tag{122}$$

To make this intuition rigorous, which is not always possible as we explain at the end of the section, we have to use a phase space representation of the state. The Wigner function $W^{\mathrm{S}}(\mu,\pi)$ can be factorised

$$\begin{aligned} W^{\mathrm{S}}(\mu,\pi) &= \sqrt{\frac{k}{\pi\hbar\gamma_{11}}} e^{-\frac{k\mu^2}{\hbar\gamma_{11}}} \sqrt{\frac{\gamma_{11}}{k\pi\hbar}} e^{-\frac{\gamma_{11}}{\hbar k}\left(\pi-\frac{\gamma_{12}}{\gamma_{11}}k\mu\right)^2}\,, \\ &= P(\mu)\sqrt{\frac{\gamma_{11}}{k\pi\hbar}} e^{-\frac{\gamma_{11}}{\hbar k}\left(\pi-\frac{\gamma_{12}}{\gamma_{11}}k\mu\right)^2}\,, \end{aligned} \tag{123}$$

where the relation $\det(\gamma) = \gamma_{11}\gamma_{22} - \gamma_{12}^2 = 1$ (we are using a pure state) was used. The first piece is the probability distribution (122). The second piece controls the value of $\pi - \gamma_{12}k\mu/\gamma_{11} = \pi - \partial S/\partial\mu$, i.e. the difference between the actual value of π and that attributed to it following the WKB-classicality approach. It can be read out from the above, or shown by a straightforward computation using covariance matrix elements, that

$$\left\langle \left(\hat{\pi} - \frac{\gamma_{12}}{\gamma_{11}}k\hat{\mu}\right)^2 \right\rangle = \frac{\hbar k}{2}\frac{1}{\gamma_{11}} \approx \frac{\hbar k}{2} e^{-2N}\,, \tag{124}$$

where we have taken the super-Hubble limit in the last equality. Since the state is Gaussian, and $\hat{\pi}$, $\hat{\mu}$ are centred, this is the only quantity that controls the error induced by replacing $\hat{\pi}$ by its WKB counterpart $\gamma_{12}k\hat{\mu}/\gamma_{11}$ in the expectation values. As inflation proceeds, this error becomes exponentially small while the fluctuations of $\hat{\mu}$ get exponentially large, and that of $\gamma_{12}k\hat{\mu}/\gamma_{11}$ tends to a constant. Therefore, to compute the expectation value of any operator which is a polynomial in $\hat{\mu}$ and $\hat{\pi}$, one can safely make the WKB replacement. We emphasise that, to have meaningful operators, the coefficients of these polynomials must not depend on the state of the system. In such polynomials, when expanding $\hat{\pi}$ as $(\hat{\pi} - \gamma_{12}k\hat{\mu}/\gamma_{11}) + \gamma_{12}k\hat{\mu}/\gamma_{11}$, the coefficients of $\hat{\mu}$ and $\hat{\pi}$ cannot conspire to yield an expression depending only on the subdominant combination $\hat{\pi} - \gamma_{12}k\hat{\mu}/\gamma_{11}$ since it explicitly depends on the squeezing parameters. The translation of this approximation in terms of the Wigner function is to take the limit of infinite r_k, with $\gamma_{11} \to \infty$, and to replace the Gaussian over $\pi - \partial S/\partial\mu$ by a Dirac delta [21, 45, 39]

$$W^{\mathrm{S}}(\mu,\pi) \approx P(\mu)\,\delta\left(\pi - \frac{\gamma_{12}}{\gamma_{11}}k\mu\right)\,. \tag{125}$$

The interpretation of this equation is straightforward: when computing expectation values using the Wigner function and Eq. (54), up to very sub-dominant contributions, we can replace π by $\partial S/\partial\mu$ in the Weyl transform and take the average on μ using the classical stochastic variable of distribution Eq. (122). In the limit of Eq. (125), the contour levels of the Wigner function are squashed from ellipses to lines, and this implies that the size of the sub-fluctuant mode has been neglected. This line-like limit of the Wigner function is visible in the last panels of Fig. 5.

We conclude with a series of remarks on this result. First, it is clear that the replacement $\hat{\pi} \to \partial S/\partial\mu$ cannot be exact as it implies $[\hat{\mu},\hat{\pi}] = 0 \neq i\hbar$, thus violating the canonical commutation relations, although those must be verified irrespective of the state of the system. Yet, the contribution of this non-vanishing commutator to the expectation value of operators $O(\hat{\mu},\hat{\pi})$ which are polynomial in $\hat{\mu}$ and $\hat{\pi}$ is negligible.

The second remark is that, as explained in [72], we want to emphasise that the Wigner function of a WKB state does *not* in general give rise to a Dirac delta; in fact, it needs not even be positive everywhere. The naive intuition is only verified here because the state is also Gaussian. In addition, the fact that the Wigner function can be negative suggests taking with a grain of salt the idea that any WKB state is understandable as an approximate classical state.

Thirdly, as stressed in [83], the distribution (125) has some undesirable features for a Wigner function. For instance, computing the purity using the function (125) and Eq. (54) yields an infinite result. This is obviously incorrect since for any quantum state $p_k \leq 1$, and, in this pure case, we had derive earlier $p_k = 1$. Geometrically, by squeezing the ellipse to a line, one looses the information on the area that encodes the purity and the non-commutation of the variables through the Heisenberg uncertainty principle. This additionally informs us that there exist quantities of interest that crucially depend on the sub-leading contributions that were neglected, and so on the sub-fluctuant mode.

The fourth point we want to stress concerns classicality. The part of the argument based on analysing the phase space distribution does not actually require large squeezing to be formulated. Indeed, even before taking any limit, the Wigner function of the state is everywhere positive and obeys the classical equations of motion (59), so that using Eq. (54), any observable can be computed using a classical stochastic distribution.

As a fifth point, let us note that the above statement has to be made more precise because it hides several subtle points. To start with, as pointed out in [37], beyond quadratic order, the Weyl transform of an observable $O(\hat{\mu},\hat{\pi})$ is, in general, not obtained by replacing the operators $\hat{\mu}$ and $\hat{\pi}$ by the corresponding phase space variables i.e. $O(\mu,\pi) \neq \tilde{O}(\mu,\pi)$. For instance

$$\widetilde{\hat{\mu}_{\boldsymbol{k}}^2\hat{\pi}_{\boldsymbol{k}}^2} + \widetilde{\hat{\pi}_{\boldsymbol{k}}^2\hat{\mu}_{\boldsymbol{k}}^2} = 2\mu_{\boldsymbol{k}}^2\pi_{\boldsymbol{k}}^2 - \hbar\,, \tag{126}$$

so that, using Eq. (54)

$$\left\langle \hat{\mu}_{\boldsymbol{k}}^2\hat{\pi}_{\boldsymbol{k}}^2 + \hat{\pi}_{\boldsymbol{k}}^2\hat{\mu}_{\boldsymbol{k}}^2 \right\rangle = 2\mathbb{E}\left(\mu_{\boldsymbol{k}}^2\pi_{\boldsymbol{k}}^2\right) - \hbar. \tag{127}$$

This extra $\hbar$ is a contribution of the commutator that the Wigner-Weyl formalism takes into account. Therefore, despite the Wigner function being everywhere positive and acting as a measure in Eq. (54), these terms introduce a slight difference with classical stochastic distributions. The culprit is the Weyl transform of the operators rather than the Wigner function. As argued above, in the large squeezing limit, these extra contributions to the Weyl transform of $\hat{\mu}$ and $\hat{\pi}$ are expected to become negligible. The second subtle point is precisely that these distortions will *not* become negligible for all observables so that the classicality argument does not apply to these. The fact that certain quantum features persist should not be a surprise since we have shown that the gravitons produced by the evolution remain in entangled pairs in the absence of other interactions [83].

The findings of this section can be summarised as follows: as long as we measure only $\hat{\mu}$ and $\hat{\pi}$, or observables which are polynomials of it, super-Hubble modes behave classically since their expectation values can be completely reproduced by a classical stochastic distribution [88, 37].

4.2 Quantum information approaches

It has to be mentioned that the authors of Ref. [45] do recognise the possibility that other operators would exhibit quantum features since squeezed states are known to possess such features in quantum optics experiments. However, they dismiss this possibility by arguing that, contrary to quantum optics, one can only perform measurements of the values of the fields $\hat{\mu}_{\boldsymbol{k}}$ and $\hat{\pi}_{\boldsymbol{k}}$ and not, say, of the number of particles $\hat{n}_k$. Therefore the 'decoherence without decoherence' argument is sufficient to claim that the perturbations are *practically* classical. Setting temporarily aside the question of their observability, we now derive examples of operators revealing non-classicality features in the state of primordial gravitational waves.

We have already mentioned that the purity of the state cannot be computed if the sub-dominant contributions of the non-vanishing commutators are dropped. In [91], the authors showed that in order to correctly compute the entropy of the state using the von Neumann entropy $S(\hat{\rho}) = -\mathrm{Tr}\left[\hat{\rho}\log(\hat{\rho})\right]$ the sub-dominant contributions have to be restored. For a 2-mode mode squeezed state , the von Neumann entropy reads [92]

$$S(\hat{\rho}) = 2f\left[\det(\gamma)\right], \tag{128}$$

where the growing function f is defined for $x \geq 1$ by

$$f(x) = \left(\frac{x+1}{2}\right)\log_2\left(\frac{x+1}{2}\right) - \left(\frac{x-1}{2}\right)\log_2\left(\frac{x-1}{2}\right). \tag{129}$$

The entropy and purity are both controlled by the determinant of the covariance matrix, which requires the inclusion of sub-dominant contributions to be correctly

evaluated. For the pure 2-mode squeezed state of perturbations, one gets $\det(\gamma) = 1$ and the definition of f gives $f(1) = 0$, so we recover that the entropy vanishes.

We have so far only shown that, for certain operators, it is not appropriate to neglect the sub-fluctuant mode. We now go further and exhibit quantities whose values *cannot* be accounted for if the system is described by a classical stochastic distribution. The prime example of such quantities is the combinations of expectation values of spin operators entering the famous Bell inequalities [86]. To design a Bell inequality, one has to exhibit a combination of operators $C\left(\hat{O}_1,...,\hat{O}_n\right)$ such that, if the expectation values of the $\hat{O}_i$s are described by a stochastic probability distribution[16], then C is bounded by a real number c

$$C(O_1,...,O_n) \leq c\,. \tag{130}$$

As a consequence, if a quantum state is such that $\left\langle C\left(\hat{O}_1,...,\hat{O}_n\right)\right\rangle > c$, then we have proven that not all expectation values of this state can be accounted for by a classical probabilistic theory.

A necessary condition for a state to violate a Bell inequality is that it is not *separable* [94]. A state $\hat{\rho}$ of a system that can be partitioned in two subsystems A and B is said to be separable in this partition if its density matrix can be written as

$$\hat{\rho} = \sum_i p_i \hat{\rho}^i_{\rm A} \bigotimes \hat{\rho}^i_{\rm B}\,, \tag{131}$$

where $p_i \geq 0$ and $\sum_i p_i \geq 0$. Such a state can be constructed using a classical protocol [94]. The interpretation of Eq. (131) is that p_i is the probability of finding the system in the sector $\hat{\rho}^i_{\rm A} \otimes \hat{\rho}^i_{\rm B}$ where the subsystems A and B are independent since the density matrix is factorised. The correlations between the subsystems are thus controlled only by the probabilities $\{p_i\}$ and deemed classical. Non-separable states are generally called *entangled* states. In general, it is very difficult to determine whether a state is separable. Fortunately, for Gaussian states, the Peres-Horodecki criterion allows us to check separability using the covariance matrix elements only [95]. This method was first applied to cosmological perturbations by Campo and Parentani in [44]. We explain their result in the terms used in this review.

We first need to choose a partition of the system. The separable character of the state or not depends on the subsystems considered; for a general discussion of the notion of partition, see [46]. Using the vectors of conjugate operators introduced in Sec. 3.5, we define a (bi)partition of the system by sorting the operators into two vectors of smaller dimensions

$$\hat{X} = \hat{X}_A \bigoplus \hat{X}_B\,. \tag{132}$$

To represent the state of the perturbations we have used the R/I partition defined by $\hat{X}_{\rm R/I} = \left(k^{1/2}\hat{\mu}^{\rm R}_{\boldsymbol{k}}, k^{-1/2}\hat{\pi}^{\rm R}_{\boldsymbol{k}}, k^{1/2}\hat{\mu}^{\rm I}_{\boldsymbol{k}}, k^{-1/2}\hat{\pi}^{\rm I}_{\boldsymbol{k}}\right)$ where the two subsystems decouple. These operators will, however, mix the creation/annihilation operators (28) defining

[16] The precise assumption is that their values are described by a local realistic theory. For a discussion of this subtle and important point we refer to [93].

the modes $\pm\boldsymbol{k}$. If we are interested in the correlations between these modes we have to build separate hermitian operators describing the mode $\boldsymbol{k}$ and $-\boldsymbol{k}$. This is readily done by considering

$$\hat{q}_{\pm\boldsymbol{k}} = \sqrt{\frac{\hbar}{2k}}\left(\hat{a}_{\pm\boldsymbol{k}} + \hat{a}^{\dagger}_{\pm\boldsymbol{k}}\right) \quad \text{and} \quad \hat{p}_{\pm\boldsymbol{k}} = -i\sqrt{\frac{\hbar k}{2}}\left(\hat{a}_{\pm\boldsymbol{k}} + \hat{a}^{\dagger}_{\pm\boldsymbol{k}}\right). \tag{133}$$

These operators define the $\pm\boldsymbol{k}$ partition $\hat{X}_{\pm\boldsymbol{k}} = \left(k^{1/2}\hat{q}_{\boldsymbol{k}}, k^{-1/2}\hat{p}_{\boldsymbol{k}}, k^{1/2}\hat{q}_{-\boldsymbol{k}}, k^{-1/2}\hat{p}_{-\boldsymbol{k}}\right)$. We compute the covariance matrix in this partition

$$\gamma = \begin{pmatrix} \gamma_{\boldsymbol{k}} & \gamma_{\boldsymbol{k},-\boldsymbol{k}} \\ \gamma_{-\boldsymbol{k},\boldsymbol{k}} & \gamma_{-\boldsymbol{k}} \end{pmatrix}, \tag{134}$$

with

$$\gamma_{\boldsymbol{k}} = \gamma_{-\boldsymbol{k}} = \cosh(2r_k)\mathbb{I}_2 = \left(n_k + \frac{1}{2}\right)\mathbb{I}_2, \tag{135}$$

where $\mathbb{I}_2$ is the 2-dimensional identity matrix and

$$\gamma_{\boldsymbol{k},-\boldsymbol{k}} = \gamma_{-\boldsymbol{k},\boldsymbol{k}} = -\sinh(2r_k)\begin{pmatrix} \cos 2\varphi_k & \sin 2\varphi_k \\ \sin 2\varphi_k & -\cos 2\varphi_k \end{pmatrix} = \begin{pmatrix} \Re\mathrm{e}(c_k) & \Im\mathrm{m}(c_k) \\ \Im\mathrm{m}(c_k) & -\Re\mathrm{e}(c_k) \end{pmatrix}. \tag{136}$$

Unlike in the R/I partition, this covariance matrix is not block-diagonal. It shows that the $\boldsymbol{k}$ and $-\boldsymbol{k}$ particles are correlated. The Peres-Horodecki applied to this covariance matrix reduces to [44]

$$\hat{\rho} \text{ separable in } \pm\boldsymbol{k} \text{ partition} \iff |c_k| \leq n_k. \tag{137}$$

This criterion lends itself to a very simple interpretation, the state will be separable if and only if the correlation of the pairs is larger than their number. When is this satisfied? The condition (137) is straightforwardly expressed in terms of the squeezing parameters. We find that the state is separable if only if $e^{-r_k} \geq 1$, i.e. for the vacuum $r_k = 0$. Therefore, the primordial gravitons pairs $\pm\boldsymbol{k}$ are always entangled. We have found a first quantum feature of their distribution. Notice that the same analysis could be repeated in the R/I partition, but since these sectors are not correlated, it would trivially lead to the conclusion that the state is always separable in this partition. This illustrates clearly the dependence of the (non)-separable character of the state on the choice of subsystems.

The state of the perturbations we have considered so far is pure. It was shown that, for any entangled pure state, one can build a Bell inequality that the state violates [94]. The separability criterion is, in this case, sufficient. How can we find operators able to violate a Bell inequality for the gravitons? The considerations of Sec. 4.1 already demonstrated that, in order to reveal the quantumness of the distribution, we have to use operators which are non-polynomials in $\hat{\mu}^{\mathrm{S}}_{\boldsymbol{k}}$ and $\hat{\pi}^{\mathrm{S}}_{\boldsymbol{k}}$. In [96],

Revzen further introduces a distinction between what he calls proper and improper operators.

Proper operators are defined as those that cannot be used to violate a CSH-type [97] Bell inequality when the Wigner function of the state is positive. He shows that any operator $\hat{O}$ whose Weyl transform $\tilde{O}$ takes values in the set of its eigenvalues is proper. Indeed, the Wigner function then provides an appropriate local hidden variable theory to describe its expectation values. Therefore, we have to use operators that do not fall in this category to build a Bell inequality that can be violated by primordial gravitational waves. In fact, these operators are not uncommon. Consider, for example, the number operator

$$\hat{n}_k = \hat{a}^\dagger_{\boldsymbol{k}}\hat{a}_{\boldsymbol{k}} = \frac{k}{2\hbar}\hat{\mu_{\boldsymbol{k}}}^2 + \frac{1}{2\hbar k}\hat{\pi_{\boldsymbol{k}}}^2 + \frac{1}{2}\,. \tag{138}$$

It has a discrete spectrum, while its Weyl transform $\widetilde{\hat{n}_k} = \frac{k}{2\hbar}\mu^2_{\boldsymbol{k}} + \frac{1}{2\hbar k}\pi^2_{\boldsymbol{k}} + \frac{1}{2}$ is a continuous function of the phase space variables. In [44], Campo and Parentani were the first to exhibit Bell inequalities violated by cosmological perturbations. They emphasise the necessity to use non-polynomial operators in the field operator and they use as a building block the probability of finding the system in a certain 2-mode coherent state

$$\begin{aligned} Q(v,w) &= \mathrm{Tr}\left(\hat{\rho}\hat{\Pi}_{\boldsymbol{k},-\boldsymbol{k}}\right)\,, \\ &= \frac{1}{\Delta_k}\exp\left\{-\frac{1}{\Delta_k}\left[(n_k+1)\left(|v|^2+|w|^2\right) - 2\Re\mathrm{e}\left(c_k^* vw\right)\right]\right\}\,, \end{aligned} \tag{139}$$

where $\Delta_k = (n_k+1)^2 - |c_k|^2$ and $\hat{\Pi}_{\boldsymbol{k},-\boldsymbol{k}} = |v,\boldsymbol{k}\rangle\langle v,\boldsymbol{k}| \otimes |w,-\boldsymbol{k}\rangle\langle w,-\boldsymbol{k}|$ projects the subsystem $\boldsymbol{k}$ (respectively $-\boldsymbol{k}$) on the coherent state associated to $v \in \mathbb{C}$ (resp. $w \in \mathbb{C}$). The bounds given on n_k and c_k in Sec. 3.4 ensure that Δ_k is a positive quantity. This real and positive function of v and w is called the Husimi Q-representation of the state [98][17]. For the purpose of building a Bell inequality, it can be simplified by re-parametrising the arbitrary phase of v to absorb that of c_k. We take $\arg v = 2\arg c_k$ so that $2\Re\mathrm{e}\left(c_k^* vw\right) = 2|c_k|\,\Re\mathrm{e}\left(v^* w\right)$. For a 2-mode squeezed state $|c_k| = \sqrt{n_k(n_k+1)}$ so that, upon rearranging,

$$Q(v,w) = \frac{1}{n_k+1}\exp\left(-\frac{|v|^2}{n_k+1}\right)\exp\left(-\left|w - v\sqrt{\frac{n_k}{n_k+1}}\right|^2\right)\,. \tag{140}$$

Since the Husimi representation is also the expectation value of an operator, it can be used in a Bell inequality. The authors then use the Bell inequality demonstrated by [99] over $Q(v,w)$

[17] Like the Wigner function, it is a phase-space representation of the state but using coherent states as a basis rather than eigenstates of the field operators. The authors discuss the quantumness of the perturbation using its properties and that of the related Glauber Sudarshan P-representation. They argue that the state not admitting a P-representation can be considered a non-classical feature. For brievity, we will not discuss these aspects here and refer to [44, 98] for details.

$$C(v,w) = [Q(0,0) + Q(v,0) + Q(0,w) - Q(v,w)] \left(\frac{n_k+1}{2}\right) \leq 1\,. \tag{141}$$

They argue that C is maximal for $w = -v$ in which case it only depends on $|v|^2$ and

$$C_{\max}\left(|v|^2\right) = \frac{1}{2}\left[1 + 2e^{-|v|^2} - e^{-2\left(1+\sqrt{\frac{n_k}{n_k+1}}\right)|v|^2}\right]. \tag{142}$$

One can show that, provided we are not in the vacuum $n_k = 0$, $C_{\max}$ is always larger than unity in the vicinity of $v = 0$, as illustrated in Fig. 7; the Bell inequality is violated. As expected, we have recovered the separability condition. In a later work [100], the authors proved that another inequality, built using operators, also defined in [101], that are complementary (in the sense that their sum is the identity) to the projectors $\hat{\Pi}_{\boldsymbol{k},-\boldsymbol{k}}$, is violated. They also build other inequalities using the (GKM and Larsson) pseudo-spin operators in the same work. They explicitly show that all these operators belong to the subclass of improper operators identified by Revzen. Since the Weyl transform of the identity is just the number 1, we can infer from their complementary with the projectors $\hat{\Pi}_{\boldsymbol{k},-\boldsymbol{k}}$ that the operators $\hat{\Pi}_{\boldsymbol{k},-\boldsymbol{k}}$ also belong to this subclass.

We now introduce a last non-classicality criterion, the quantum discord. We start by giving the intuition behind its definition and reviewing some important properties. Technical details in definitions and proofs are skipped and can be found in [102, 103]. The idea of quantum discord is also to show that correlations between two subsystems are stronger than allowed classically. Two measures of the information attached to these correlations are introduced to that end. These measures are based on the von Neumann entropy, which, as we have shown, is highly sensitive to terms that can be neglected when computing field expectation values. The first measure is the mutual information

$$\mathscr{I}(A,B) = S(A) + S(B) - S(A,B), \tag{143}$$

where $S(A,B)$ is the von-Neumann entropy of the full system while $S(A)$ and $S(B)$ are the entropies of the subsystems. The latter are defined by computing the entropy of the reduced density matrices when one of the subsystems is traced out, e.g. $\hat{\rho}_A = \mathrm{Tr}_B(\hat{\rho})$ for the subsystem A. They are also called the entanglement entropy of the state. The second measure

$$\mathscr{J}(A,B) = S(A) - S(A|B), \tag{144}$$

where $S(A|B)$ measure the information gained on A by measuring B. Its precise definition in the quantum setting must therefore include the system state after measuring the system B. It is obtained by minimising the density matrix residual entropy after having measured a complete set of projections on B, i.e. by maximising the information gain. For a quantum state, we then define the quantum discord as their difference

$$\mathscr{D}(A,B) = \mathscr{I}(A,B) - \mathscr{J}(A,B)\,, \tag{145}$$

which is shown to be in general *non-negative*. The key observation is that, by the Bayes theorem, $\mathscr{I}$ and $\mathscr{J}$ coincide for a classical system so that the discord *vanishes*. A non-vanishing discord $\mathscr{D}(A,B) > 0$ is therefore taken as a non-classical feature. As the other criteria introduced, the quantum discord depends on the choice of partition $\hat{R} = \hat{R}_A \bigoplus \hat{R}_B$. However, it does not depend on the operators chosen to represent them, i.e. it is invariant under any change of operators within the sectors A and B. We call such a quantity a *local* symplectic invariant. On the contrary, a Bell inequality is not necessarily a local symplectic invariant. A last important property of the discord is that, for a pure state, it reduces to the entanglement entropy $\mathscr{D}(A,B) = S(A) = S(B)$, and, for a pure state still, being entangled is equivalent to a non-vanishing entanglement entropy. Therefore, all criteria introduced (separability, Bell inequality, quantum discord) are equivalent for pure states. The cosmological perturbations must therefore have a non-vanishing quantum discord.

The quantum discord of cosmological perturbations was computed in [37] for the $\pm\boldsymbol{k}$ partition[18]. It reads

$$\mathscr{D}_{\pm\boldsymbol{k}} = f\left[\cosh\left(2r_k\right)\right], \tag{146}$$

where f was defined in Eq. (129). We immediately verify that the discord is non-vanishing provided that $r_k > 0$, i.e. that we are not in the vacuum. Taking the de Sitter limit of the above expression, we find $\mathscr{D}_{\pm\boldsymbol{k}} \approx 2r_k/\ln 2 \approx 2N/\ln 2$, the discord grows linearly with the number of e-folds.

The results of this section demonstrate that, as suspected, the primordial gravitational waves are only classical if we restrict our attention to field operators $\hat{\mu}$ and $\hat{\pi}$. We showed, using several criteria, that their state exhibits in principle quantum features: it is entangled, violates Bell inequalities and has a non-vanishing quantum discord. We additionally verified that these three criteria are equivalent for pure states like the 2-mode squeezed state considered here. Still, in any realistic model of the early Universe, this assumption of purity has to be given up. What has allowed us so far to simply consider a couple of modes $\pm\boldsymbol{k}$ of the field is that we have neglected all interactions of the gravitational waves, in particular their intrinsic non-linearities. We were justified in doing since the latter are weak. Yet, it is well known that even very weak interactions can lead to an erasure of non-classical features by inducing *decoherence* of the system. The most famous example of this is probably that a grain of dust whose spatial superposition would be turned into a classical superposition in a fraction of an instant simply by the scattering of photons from the CMB [105]. The importance of decoherence in the discussion of quantum features of cosmological perturbations was quickly realised [106, 107]. We now investigate how it affects the state, in general, and in particular the quantum features we have just exhibited.

[18] The quantum discord was already used in a work on cosmological perturbations in [104] but the author considered correlation of another nature, namely that of the perturbations and their environment.

4.3 Decoherence of cosmological perturbations

We start by briefly recalling some basic concepts of decoherence and refer to [108] for details. The 2-mode squeezed state of a coupled of modes $\pm\boldsymbol{k}$ is a pure state represented by the ket (46). One can easily compute its density matrix and express it in the graviton 2-mode number basis

$$\hat{\rho}_{2\mathrm{MSS}} = \frac{1}{\cosh^2(2r_k)} \sum_{n,n'=0}^{+\infty} \left[-\tanh(2r_k)\right]^{n+n'} e^{2i\left(n-n'\right)\varphi_k} \left|n_{\boldsymbol{k}}, n_{-\boldsymbol{k}}\right\rangle \left\langle n'_{\boldsymbol{k}}, n'_{-\boldsymbol{k}}\right| . \quad (147)$$

The coefficients on the diagonal $q_n = \tanh^{2n}(2r_k)/\cosh^2(2r_{\boldsymbol{k}})$ give a classical probability distribution over the 2-mode number states, while the non-diagonal reflects the quantum interferences between them. If we discard these terms, the density matrix reads

$$\hat{\rho}_{\mathrm{th.}} = \frac{1}{\cosh^2(2r_k)} \sum_{n=0}^{+\infty} \tanh^{2n}(2r_k) \left|n_{\boldsymbol{k}}, n_{-\boldsymbol{k}}\right\rangle \left\langle n_{\boldsymbol{k}}, n_{-\boldsymbol{k}}\right| . \quad (148)$$

The state now represents a classical superposition of different number states with the same probabilities as $\hat{\rho}_{2\mathrm{MSS}}$. Such states are called statistical mixtures and are indeed mixed states (except if all coefficients but one vanish) since $p_k = \sum_n q_n^2$ and $q_n \leq 1$. The general idea of decoherence is that interactions of the system with a large number of unobserved degrees of freedom, referred to as the environment, precisely diagonalises the density matrix, driving the state to a statistical mixture. Equation (148) is actually the density matrix of a thermal state with, on average, n_k particles in both modes. Since it is fully diagonal, it is considered the result of a complete decoherence process. A very important point is that the (non)-diagonal character of the matrix depends on the basis, e.g. the matrix is originally diagonal in the 2-mode squeezed state basis. The basis in which decoherence makes the density matrix diagonal is called the pointer basis. Once again, we see that the choice of basis and operators to analyse the state of the system is crucial. For cosmological perturbations, several pointer basis were considered: coherent state basis [109, 44], field amplitude basis [110, 111, 106, 107], number basis [110], and others [112][19]. Ultimately, in a realistic model, the pointer basis is given by the eigenstates of the interaction Hamiltonian selected. The basis thus bears a double physical sense: it tells us for which type of measurements the system appears classical, e.g. measures of field amplitude or of number of particles, and also to which operators of the system is the environment sensitive. In their follow-up articles [106, 107] to [39], the group of authors (Kiefer, Lesgourgues, Starobinski, Polarski) considered the effect of decoherence. They argued that the correct pointer basis should be the field amplitude basis on the ground that self-interactions of pure gravity are local in the field basis,

[19] Notice that some of these, [111, 110], predate works referred to in the last section. Decoherence was, in fact, already investigated in the context of the early Universe before the argument of 'decoherence without decoherence' was made. It was especially used to try to make sense of the solutions of quantum cosmology, where both the background and the perturbations are treated as quantum fields [113].

i.e. $H_{\rm in} \propto \hat{\mu}^n(\boldsymbol{x},\eta)\,\hat{\pi}^m(\boldsymbol{x},\eta)$. Since these interactions are contained in the Einstein-Hilbert action, they constitute a minimal and well-defined source of decoherence. They were then taken into account in a more realistic model of decoherence for the first time in [114, 115]. There, the system considered is made up of the observed large wavelengths while the environment is made-up of the rest of the short unobserved wavelengths like in stochastic inflation [116]. This approach was originally performed for scalar perturbations and was later generalised to tensor perturbations [117].

How is their influence on the state of $\pm\boldsymbol{k}$ modes concretely accounted for? In [114, 115] the process is followed in time, rather than assumed to have completed [109, 118, 112], using a master equation. Earlier papers [111, 110] had also used an equivalent formalism, the Feynman-Vernon influence functional, but only in solvable toy models with two scalar fields interacting quadratically. The two formalisms were also used in [119], using the short-long wavelengths splitting and considering a quartic self-interaction of the scalar field. To derive a master equation, one starts by postulating that the couple system-environment evolves under a Hamiltonian

$$\hat{H}_{\rm tot} = \hat{H}\otimes\hat{\mathbb{I}}_{\rm env} + \hat{\mathbb{I}}\otimes\hat{H}_{\rm env} + g\hat{H}_{\rm int}\,, \tag{149}$$

where the Hamiltonian of interaction is taken to be an integral of a product of operators acting on the system and the environment

$$\hat{H}_{\rm int} = \int \mathrm{d}^3\boldsymbol{x}\,\hat{A}(\eta,\boldsymbol{x})\otimes\hat{E}(\eta,\boldsymbol{x})\,. \tag{150}$$

Under certain assumptions, essentially perturbative coupling and a "large" enough environment unperturbed by the action of the system, the von Neumann equation over the full density matrix $\hat{\rho}_{\rm tot}$ can be reduced to a *master* equation over the reduced density matrix of the system $\hat{\rho} = \mathrm{tr}_{\rm env}(\hat{\rho}_{\rm tot})$. Master equations became a standard tool to analyse the decoherence of cosmological perturbations and are very often considered to be of the Lindblad-type, e.g. [114, 115, 108, 120],

$$\frac{\mathrm{d}\hat{\rho}}{\mathrm{d}\eta} = -i\left[\hat{H},\hat{\rho}\right] - g^2\eta_{\rm c}\int \mathrm{d}^3\boldsymbol{x}\,\mathrm{d}^3\boldsymbol{y}\,\langle\hat{E}(\eta,\boldsymbol{x})\hat{E}(\eta,\boldsymbol{y})\rangle\left[\hat{A}(\boldsymbol{x}),\left[\hat{A}(\boldsymbol{y}),\hat{\rho}\right]\right], \tag{151}$$

where $\eta_{\rm c}$ is the auto-correlation time of the environment. This is a Markovian master equation; it assumes that the environment is effectively stationary with respect to the system, i.e. $\eta_{\rm c} \ll \delta\eta$ where $\delta\eta$ is the typical time-scale of evolution of the system. In addition, the interaction term is often considered linear in the system field operators $H_{\rm int} \propto (\alpha\hat{\mu} + \beta\hat{\pi})\otimes\hat{O}_{\rm env}$, where $\hat{O}_{\rm env}$ acts only on the environment [39, 120]. It is the so-called Caldeira-Legget model [121]. Such interactions can also be identified as the dominant term when considering pure gravity [114, 117] and has the great advantage of preserving gaussianity and homogeneity. The result of the evolution can therefore be simply analysed by considering a Gaussian decohered homogeneous density matrix (GHDM). This class of state was introduced in [122, 44] to study decoherence finely, without having to assume any specific master equation, and still preserving a "partially" decohered state rather than assuming

from the on-set the density matrix diagonal. This class also encompasses the density matrices obtained by the common ansatz that its non-diagonal terms are suppressed by a Gaussian, e.g. [123, 100]. For all these reasons, we will in this section analyse the effect of decoherence using the GHDM and follow [44, 46].

To define the GHDM, we work in Fourier space. First, to avoid a preferred direction all 1-point correlation functions have to vanish. The Gaussian state is then completely characterised by its covariance matrix (58) made of 2-point correlation functions. By homogeneity, the only non-vanishing 2-point correlation functions involve $\boldsymbol{k}$ and $-\boldsymbol{k}$, and we can work with a single couple of modes $\pm\boldsymbol{k}$. *A priori* we have a 4×4 matrix, but, as mentioned below Eq. (63), homogeneity further imposes that the matrix is block diagonal in the R/I partition. We are left with a 2×2 covariance matrix like that of Eq. (64). The state is then fully characterised by the three real covariance matrix elements γ_{ij} in Eq. (65), or alternatively the number of pairs n_k and their pair correlation c_k (one complex and one real number) defined in Eq. (78). The only difference with the previous analyses is that the constraint imposed by the purity of the state $p_k=1$ is now relaxed to $p_k\leq1$, i.e. $\det(\gamma^{\mathrm{S}})=\gamma_{11}\gamma_{22}-\gamma_{12}^2\geq1$, or equivalently $|c_k|\leq\sqrt{n_k(n_k+1)}$. Notice that these numbers can still not be arbitrarily chosen in order to keep a *bona fide* quantum state with purity bounded by one. Finally, to be able to have a simple geometrical representation, we can use the purity as an effective extra squeezing parameter and write [46]

$$\gamma_{11}=p_k^{-1/2}\left[\cosh(2r_k)-\cos(2\varphi_k)\sinh(2r_k)\right], \tag{152a}$$

$$\gamma_{12}=\gamma_{21}=-p_k^{-1/2}\sin(2\varphi_k)\sinh(2r_k), \tag{152b}$$

$$\gamma_{22}=p_k^{-1/2}\left[\cosh(2r_k)+\cos(2\varphi_k)\sinh(2r_k)\right]. \tag{152c}$$

One can check that this is a fully general parametrisation of a 2×2 symmetric matrix, that indeed $\det(\gamma)=p_k^{-2}$ and that for $p_k=1$, we recover Eq. (66). How is the geometrical representation affected by this additional parameter? It is readily seen that the eigenvectors of γ are unchanged, and its eigenvalues simply increased by $p_k^{-1/2}\geq1$. The effect on the $\sqrt{2}-\sigma$ contour levels is thus simply a dilation by $p_k^{-1/4}$. This increased width of the Gaussian was already noticed as an effect of decoherence in [123] and before in a different context by [124]. An important remark is that the existence of a sub-fluctuant mode due to squeezing is not guaranteed anymore since the semi-minor axis is now of length $B_k=p_k^{-1/4}e^{-r_k}$ which can always be made larger than one, the vacuum value, provided that decoherence is strong enough at a given a value of squeezing r_k. Fig. 6 illustrates the ellipse corresponding to the state in Fig. 3 after having lost purity to $p_k=0.17$; there is no sub-fluctuant direction. We mention an alternative parametrisation, used in [44, 88], where the extent of the breaking of the relation between n_k and $|c_k|$ is used to interpolate between a 2-mode squeezed state and a thermal state at fixed n_k. We define δ_k such that

$$|c_k|=(n_k+1)(n_k-\delta_k). \tag{153}$$

$\delta_k = 0$ is a 2-mode squeezed state and $\delta_k = n_k$, the maximal value, is a thermal state. This parameter is easily related to the purity and the squeezing via

$$\delta_k = \frac{1}{2\sqrt{p_k}} \frac{1-p_k}{\cosh(2r_k) + \sqrt{p_k}}\,. \tag{154}$$

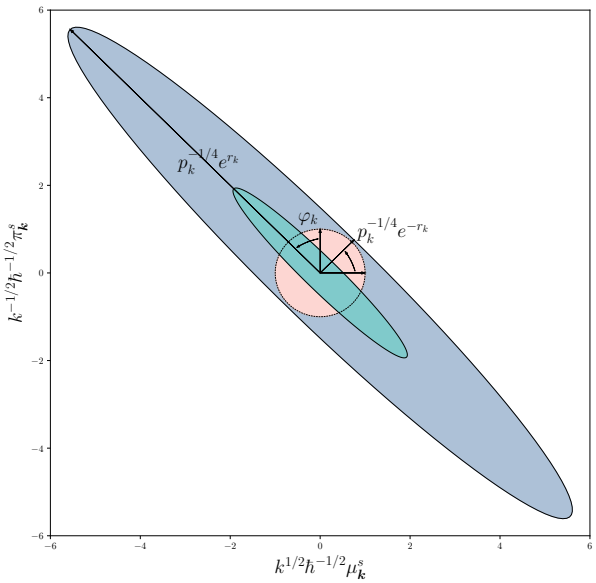

Fig. 6 $\sqrt{2}$-σ contour level of the Wigner function W^{S} for $\varphi_k = \pi/4$, $r_k = 1$, $p_k = 0.12$ (blue ellipse) or $p_k = 1$ (green ellipse) and the vacuum state $r_k = 0$ (pink circle).

Let us investigate the effect of decoherence using this class of state. To start with, how is the level of decoherence of the state estimated? Several criteria have been used in the literature: the so-called rate of de-separation [106], evaluating the suppression of non-diagonal terms [115, 114, 123], the positivity time if the initial state is assumed to be non-Gaussian [108], δ_k [44] or simply the purity p_k [120]. We will use the latter since it directly enters our definition of the GHDM (152). The purity can also be conveniently related to the entropy by Eq. (128), which still applies for decohered states. Since the purity has decreased, the entropy increases and becomes non-vanishing. For instance, a thermal state in the 2-mode particle number basis (148) gives $c_k = r_k = 0$ and $p_k = (2n_k + 1)^{-1}$.

Our focus is on how a certain level of decoherence, represented by p_k, can lead to a classical state in the sense of the criteria discussed in the previous section. As we now show, for mixed states, the different criteria are, in general, inequivalent and give different answers [122]. The separability condition Eq. (131) is also still valid for the partially decohered distribution [44]. It has a very elegant interpretation

when rewritten in terms of the effective squeezing parameter

$$B_k \hbar^{-1/2} = p_k^{-1/4} e^{-r_k} \leq 1\,, \tag{155}$$

i.e. the state becomes separable when there is no sub-fluctuant mode anymore due to a sufficient level of decoherence $p_k < e^{r_k}$. The condition can also be written as $\delta_k \geq n_k/(n_k+1)$ which, for the very large number of primordial gravitons expected $n_k \gg 1$, becomes $\delta_k \geq 1$ [44].

Let us now turn to the Bell inequality of Eq. (141). Its form, its maximisation procedure, and the formula Eq. (139) are still valid for our partially decohered state. We plot the value of $C_{\max}$ for a modest number of gravitons in each polarisation $n_k = 100$ and different values of δ_k in Fig. 7. We see that the maximum of $C_{\max}$ gradually recedes away from violation as δ_k increases, and that for $\delta_k = 0.1$, the inequality is not violated anymore. In [88], the authors give an approximation in the limit $\delta_k \ll n_k$, which is equivalent to $\cosh^2(r_k) \gg 1$, i.e. in the limit of a very squeeze state. In this limit, we have

$$C_{\max}\left(|v|^2\right) = \frac{1}{2(1+\delta_k)}\left[1 + \frac{3}{2^{4/3}} + O\left(\frac{1+\delta_k}{n_k}\right)\right]. \tag{156}$$

so that inequality is violated when

$$\delta_k < 0.095\,. \tag{157}$$

The threshold is an order of magnitude smaller than that of separability. This condition is unfortunately not easily expressed in a comparison between p_k and r_k. The perturbations loose their quantum character in the sense of the Bell inequality Eq. (141) faster than in the sense of separability. This is expected since we recall that separability is a necessary condition for Bell inequality violation, and here we see that it is not a sufficient condition anymore; the criteria are inequivalent for mixed states.

Finally, let us examine the behaviour of the quantum discord. The formula (146) was generalised in [46] for partially decohered states. A similar computation in presence of decoherence, although less general, was previously carried out in [125]. The generalisation reads

$$\mathscr{D}_{\pm\boldsymbol{k}} = f\left[p_k^{-1/2}\cosh(2r_k)\right] - 2f\left(p_k^{-1}\right) + f\left[\frac{p_k^{-1/2}\cosh(2r_k) + p_k^{-1}}{p_k^{-1/2}\cosh(2r_k) + 1}\right]. \tag{158}$$

One notes that the discord does not depend on the squeezing angle φ_k. This angle can always be modified by a local symplectic transformation, and the discord is a local symplectic invariant, so it must not depend on it. In Fig. 8, we plot this formula as a function of p_k and r_k, and draw the line delimiting separable from non-separable states. Its complexity prevents us from giving a simple threshold for the discord to be, say, larger than 1 and to compare with separability and Bell inequality. Figure 8 shows clearly that, as for separability, the value of the discord is dictated by the

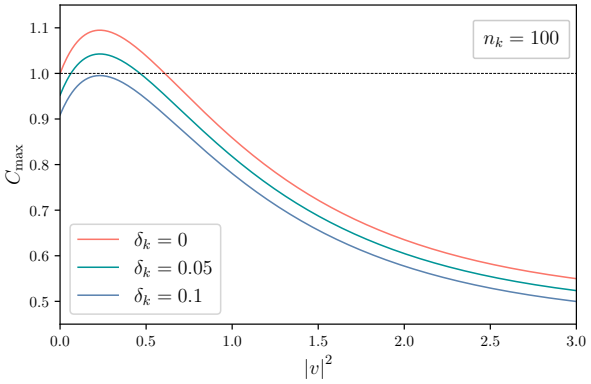

Fig. 7 $C_{\max}$ as a function of $|v|^2$ is shown in full line for different values of δ_k. The threshold of Bell inequality violation $C_{\max} = 1$ is shown in dashed black line.

result of a competition between the level of squeezing r_k and that of decoherence p_k. These two criteria, along with a Bell inequality of the type considered in [100], were recently compared in [126].

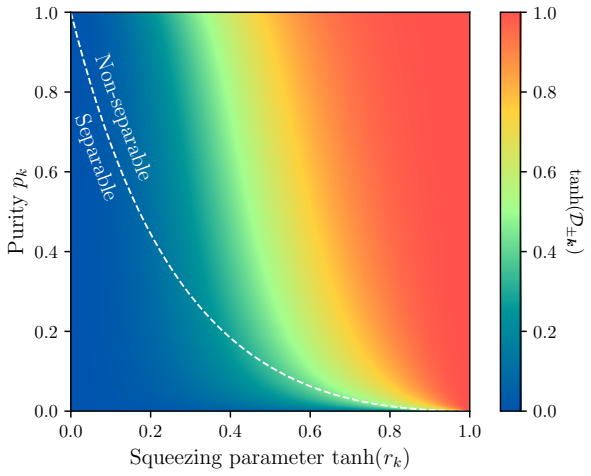

Fig. 8 Quantum discord $\mathscr{D}_{\pm \boldsymbol{k}}$ of Eq. (158) for a partially decohered state defined by Eq. (152) as a function of its squeezing r_k and a purity p_k.

The overall result of this discussion is that decoherence, if large enough, does, in the sense of different inequivalent criteria, erase the quantum features of the state. To be able to complete the analysis, the only thing necessary is to get a realistic estimation of the loss of purity in the early universe. Can we get observational constraints

on the interactions generating decoherence and on its level? Unfortunately, not for primordial gravitational waves since they were not detected yet. However, for scalar perturbations, the observation of the baryonic acoustic oscillation (BAO) actually imposes that during inflation, decoherence cannot modify too much the squeezing parameters [44] $r_k \gg 1$ and $\varphi_k \approx -\pi/2$. In particular, this implies that complete decoherence during inflation, leading to a thermal state like Eq. (148), is excluded. Indeed, the squeezing parameter r_k would vanish [106]. Note that the purity p_k is not constrained by this argument. This relation between the oscillations and strong squeezing had initially led to label the former a quantum feature [30]. As we have explained, the squeezing, in its dynamical aspect, can be understood as the presence of a growing and a decaying mode so that this result can be understood completely classically as pointed in [45]. This 'temporal coherence' of the perturbations is explained in detail (using a classical point of view) in [82]. In addition of this general argument, for precise models of decoherence, other constraints can be obtained as discussed, for instance, in Ref. [120].

Let us close this section by coming back to the important question of the observability of the features. Even in the absence of decoherence, are the operators that we have used in the discussion measurable? For the Bell inequality Eq (141) they have derived in [88], Campo and Parentani argue that each of the four terms is, in principle, measurable. However, one needs to measure a difference of order 1 between these while the intrinsic fluctuations of the factor n_k is of order n_k, which is of order 10^{86}. The measure is, in practice, impossible. The authors of [100] argue that having only access to the growing mode makes it impossible to measure two of their three pseudo-spin operators. Verifying their Bell inequality necessitates measuring at least two, and so is experimentally impossible. To address this difficulty, they suggest that one could try to build Legget-Garg inequalities [127] that rely on correlation in time of a single operator and do not require to measure two non-commuting operators at a given time. Ref. [128] also proposed a "baroque", to use the term of the author, inflationary model in which Bell operators are measured during inflation by another field rather than at later times by observer. The field stores the result in classical, robust variables that could be read out at later times by observers. Finally, the separability and quantum discord, being directly attached to properties of the density matrix, seem harder to measure. The possibility of measuring them directly in the cosmological case has not, to the best of our knowledge, been analysed. In [37], the authors took another approach and showed that if the perturbations were in a quantum non-discordant state, and reproduced the power spectrum measured for scalar perturbations, then they have to be in the thermal state (148). As we have just explained, this is ruled out. Note that this argument *assumes* that the system is described by a quantum state rather than proves it.

5 Some perspectives and critics

To conclude this review, we mention a few perspectives and possible criticisms of the previously developed issues.

First, the estimation of the minimal level of decoherence of cosmological perturbations keeps being refined see, e.g. [129, 117, 130]. Most authors conclude that decoherence has completed by the end of inflation, and the state is classical when the modes become sub-Hubble again. However, an application of the precise level of decoherence obtained to a concrete non-classicality criterion is still missing. Such computation would be essential since we have shown that the threshold for the emergence of classicality given by the different criteria depends on both the purity *and* the level of squeezing. In addition, some authors have also suggested that the use of Markovian approximation is not well-justified in the cosmological context and that a more general master equation is required to achieve a correct prediction [131, 132].

Second, the discussion of Sec. 4 applies to the tensor and scalar perturbations. However, primordial gravitational waves have the important specificity that they could be *directly* detected, not only indirectly in the temperature anisotropies of the CMB, as scalar ones. Direct detection (although futuristic see [73]) would bring about exciting possibilities to search for quantum signatures in gravitational wave detectors. Several authors, e.g. [133, 134, 135], have investigated these. The squeezed states of gravitons could produce noise in gravitational wave interferometers, and some of the authors argued that its quantum character might be revealed by measuring the decoherence it would induce between two entangled mirrors.

Another possibility that we have not discussed is to use the interactions of the perturbations, not as a mere source of decoherence, but as giving new signals in the form of non-gaussianities that could be used. Focusing on scalar perturbations, the authors of Ref. [136] showed that substituting the initial quantum vacuum fluctuations by a Gaussian stochastic field with the same two-point functions would lead to enhanced non-gaussianities akin to those generated by initial excited states. Not measuring such an enhancement was then suggested to be a sign of non-classicality of the initial state (see also [137]). With a different approach to non-gaussianities, the Wigner function of primordial gravitational waves was calculated in Ref. [138], taking in account the intrinsic non-linearities of gravity. Its regions of negativity were then explored as a means of exhibiting a signature of quantumness of the state. Other works such as Refs. [139, 140] took yet another route and provided some constraints on decoherence based on the level of non-gaussianities.

Finally, some authors criticised the standard approach of analysing correlations between $\pm\boldsymbol{k}$ modes. The authors of [141, 122] have argued that discussing correlations between $\pm\boldsymbol{k}$ modes is not appropriate as these two modes do not exist separately outside of Minkowski, in particular during inflation, and keep being mixed. Just as there is no preferred choice of vacuum (Sec. 3.6), there is no preferred choice of partition to unambiguously discuss levels of squeezing and correlations. These critics, we believe, would not apply to sub-Hubble modes, e.g. in our toy model radiation domination where $a' = 0$. Some recent works [142, 143] do not suffer from these shortcomings since they perform similar computations for quantum discord

and Bell inequalities, but use real space correlation functions. Unfortunately, their results tend to show that, even in the absence of decoherence, no quantum features appear in real space. Lastly, the formalism presented here does not address the so-called "quantum measurement problem" in cosmology. In our approach, we used an ergodicity assumption to justify equating the quantum expectation values to average values over different patches of the sky. However, one could argue that we did not discuss how the perturbations "collapsed" from a homogeneous quantum state to an inhomogeneous distribution with different values in each patch. For a discussion of this point, see [144].

To conclude, it is fair to say that the current status regarding the quest for quantum features in the primordial gravitational wave background is not entirely settled. First, on the observational side, the waves themselves, even in their classical aspects, have yet to be detected [145]. Experiments in preparation [75, 76] might manage to detect signatures of the waves in the $\boldsymbol{B}$-modes of the CMB. However, direct detection via gravitational wave interferometers seems so far out of reach [73]. On the theoretical side, in recent years, several quantum features of the quantum state for the primordial gravitational waves predicted in the simplest models have been exhibited. Unfortunately, no currently available experimental protocol has yet been designed to detect these features. In addition, the effect of decoherence has been increasingly more precisely characterised, and the latest findings tend to show that it might have erased all the potentially detectable features by the end of inflation. At this time, most analyses have been restricted to the simplest inflationary models and at the Gaussian level. More recently, some promising suggestions and proposals have been made concerning non-gaussianities, discussing the possible signatures of decoherence, or other possible hints of a quantum origin of the perturbations.

Acknowledgements

We thank Karim Benabed for insights on the possibility of detection of $\boldsymbol{B}$-modes by future missions as well as Jérôme Martin and Ilya Shapiro for enlightening discussions and remarks on the manuscript.

References

[1] V.F. Mukhanov, H.A. Feldman, R.H. Brandenberger, Phys. Rept. **215**, 203 (1992). DOI 10.1016/0370-1573(92)90044-Z

[2] P. Peter, J.P. Uzan, *Primordial cosmology*. Oxford Graduate Texts (Oxford University Press, Oxford, 2013)

[3] T.S. Pereira, C. Pitrou, J.P. Uzan, JCAP **09**, 006 (2007). DOI 10.1088/1475-7516/2007/09/006

[4] L.P. Grishchuk, Physical Review D **48**(12), 5581 (1993). DOI 10.1103/PhysRevD.48.5581
[5] B. Craps, T. De Jonckheere, A.S. Koshelev, JCAP **11**, 022 (2014). DOI 10.1088/1475-7516/2014/11/022
[6] D. Battefeld, P. Peter, Phys. Rept. **571**, 1 (2015). DOI 10.1016/j.physrep.2014.12.004
[7] R. Brandenberger, P. Peter, Found. Phys. **47**(6), 797 (2017). DOI 10.1007/s10701-016-0057-0
[8] T.J. Battefeld, R. Brandenberger, Phys. Rev. D **70**, 121302 (2004). DOI 10.1103/PhysRevD.70.121302
[9] N. Pinto-Neto, J.C. Fabris, J.D. Toniato, G.S. Vicente, S.D.P. Vitenti, Phys. Rev. D **101**(12), 123519 (2020). DOI 10.1103/PhysRevD.101.123519
[10] M. Bojowald, G.M. Hossain, Class. Quant. Grav. **24**, 4801 (2007). DOI 10.1088/0264-9381/24/18/015
[11] C. Ganguly, J. Quintin, Phys. Rev. D **105**(2), 023532 (2022). DOI 10.1103/PhysRevD.105.023532
[12] M. Shiraishi, C. Hikage, R. Namba, T. Namikawa, M. Hazumi, Phys. Rev. D **94**(4), 043506 (2016). DOI 10.1103/PhysRevD.94.043506
[13] E. Lifshitz, General Relativity and Gravitation **49**(2), 18 (2017). DOI 10.1007/s10714-016-2165-8
[14] L.H. Ford, L. Parker, Physical Review D **16**(6), 1601 (1977). DOI 10.1103/PhysRevD.16.1601
[15] Y. Takahashi, H. Umezawa, Il Nuovo Cimento **6**(6), 1324 (1957). DOI 10.1007/BF02785488
[16] L. Parker, Physical Review Letters **21**(8), 562 (1968). DOI 10.1103/PhysRevLett.21.562
[17] L. Parker, Physical Review **183**(5), 1057 (1969). DOI 10.1103/PhysRev.183.1057
[18] L. Parker, Physical Review D **3**(2), 346 (1971). DOI 10.1103/PhysRevD.3.346
[19] B.K. Berger, Annals of Physics **83**(2), 458 (1974). DOI 10.1016/0003-4916(74)90207-3
[20] Y.B. Zel'Dovich, A.A. Starobinskiĭ, Soviet Journal of Experimental and Theoretical Physics **34**(6), 1159 (1971)
[21] L.P. Grishchuk, Soviet Journal of Experimental and Theoretical Physics **40**, 409 (1975)
[22] L.P. Grishchuk, Annals of the New York Academy of Sciences **302**(1 Eighth Texas), 439 (1977). DOI 10.1111/j.1749-6632.1977.tb37064.x
[23] J.B. Hartle, Physical Review Letters **39**(22), 1373 (1977). DOI 10.1103/PhysRevLett.39.1373
[24] A.A. Starobinsky, JETP Lett. **30**, 682 (1979)
[25] T.S. Bunch, P.C.W. Davies, Proceedings of the Royal Society of London. A. Mathematical and Physical Sciences **360**(1700), 117 (1978). DOI 10.1098/rspa.1978.0060

[26] V. Rubakov, M. Sazhin, A. Veryaskin, Physics Letters B **115**(3), 189 (1982). DOI 10.1016/0370-2693(82)90641-4
[27] R. Fabbri, M. Pollock, Physics Letters B **125**(6), 445 (1983). DOI 10.1016/0370-2693(83)91322-9
[28] L. Abbott, M.B. Wise, Nuclear Physics B **244**(2), 541 (1984). DOI 10.1016/0550-3213(84)90329-8
[29] L. Abbott, D. Harari, Nuclear Physics B **264**, 487 (1986). DOI 10.1016/0550-3213(86)90494-3
[30] L.P. Grishchuk, Y.V. Sidorov, Physical Review D **42**(10), 3413 (1990). DOI 10.1103/PhysRevD.42.3413
[31] L.P. Grishchuk, Classical and Quantum Gravity **10**(12), 2449 (1993). DOI 10.1088/0264-9381/10/12/006
[32] N.D. Birrell, P.C.W. Davies, *Quantum Fields in Curved Space*, 1st edn. (Cambridge University Press, 1982). DOI 10.1017/CBO9780511622632
[33] M. Maggiore, *Gravitational Waves. Vol. 2: Astrophysics and Cosmology* (Oxford University Press, 2018)
[34] V. Mukhanov, S. Winitzki, *Introduction to Quantum Effects in Gravity*, 1st edn. (Cambridge University Press, 2007). DOI 10.1017/CBO9780511809149
[35] J. Martin, in *Planck Scale Effects in Astrophysics and Cosmology*, vol. 669, ed. by Kowalski-Glikman, G. Amelino-Camelia (Springer-Verlag, Berlin/Heidelberg, 2005), pp. 199–244. DOI 10.1007/11377306_7
[36] N.N. Bogoljubov, Il Nuovo Cimento **7**(6), 794 (1958). DOI 10.1007/BF02745585
[37] J. Martin, V. Vennin, Physical Review D **93**(2), 023505 (2016). DOI 10.1103/PhysRevD.93.023505
[38] B.L. Schumaker, C.M. Caves, Physical Review A **31**(5), 3093 (1985). DOI 10.1103/PhysRevA.31.3093
[39] D. Polarski, A.A. Starobinsky, Classical and Quantum Gravity **13**(3), 377 (1996). DOI 10.1088/0264-9381/13/3/006
[40] W.B. Case, American Journal of Physics **76**(10), 937 (2008). DOI 10.1119/1.2957889
[41] T. Curtright, D. Fairlie, C. Zachos, *A Concise Treatise on Quantum Mechanics in Phase Space* (World Scientific, New Jersey, 2014)
[42] R. Hudson, Reports on Mathematical Physics **6**(2), 249 (1974). DOI 10.1016/0034-4877(74)90007-X
[43] G. Adesso, S. Ragy, A.R. Lee, Open Systems & Information Dynamics **21**(01n02), 1440001 (2014). DOI 10.1142/S1230161214400010
[44] D. Campo, R. Parentani, Physical Review D **72**(4), 045015 (2005). DOI 10.1103/PhysRevD.72.045015
[45] A. Albrecht, P. Ferreira, M. Joyce, T. Prokopec, Physical Review D **50**(8), 4807 (1994). DOI 10.1103/PhysRevD.50.4807
[46] J. Martin, A. Micheli, V. Vennin, Journal of Cosmology and Astroparticle Physics **2022**(04), 051 (2022). DOI 10.1088/1475-7516/2022/04/051

[47] C. Bernard, A. Duncan, Annals of Physics **107**(1), 201 (1977). DOI 10.1016/0003-4916(77)90210-X
[48] M.J. Duff, Nucl. Phys. B **125**, 334 (1977). DOI 10.1016/0550-3213(77)90410-2
[49] S. Deser, M.J. Duff, C.J. Isham, Nucl. Phys. B **111**, 45 (1976). DOI 10.1016/0550-3213(76)90480-6
[50] M.J. Duff, Class. Quant. Grav. **11**, 1387 (1994). DOI 10.1088/0264-9381/11/6/004
[51] N.D. Birrell, P.C.W. Davies, *Quantum Fields in Curved Space*. Cambridge Monographs on Mathematical Physics (Cambridge Univ. Press, Cambridge, UK, 1984). DOI 10.1017/CBO9780511622632
[52] I.L. Buchbinder, S.D. Odintsov, I.L. Shapiro, *Effective Action in Quantum Gravity* (Inst. of Physics Publ, Bristol, 1992)
[53] I.L. Shapiro, Class. Quant. Grav. **25**, 103001 (2008). DOI 10.1088/0264-9381/25/10/103001
[54] K.S. Stelle, Phys. Rev. D **16**, 953 (1977). DOI 10.1103/PhysRevD.16.953
[55] N. Ohta. One-loop divergences in higher-derivative gravity (2022)
[56] A.A. Starobinsky, Phys. Lett. B **91**, 99 (1980). DOI 10.1016/0370-2693(80)90670-X
[57] R.J. Riegert, Phys. Lett. B **134**, 56 (1984). DOI 10.1016/0370-2693(84)90983-3
[58] E.S. Fradkin, A.A. Tseytlin, Phys. Lett. B **134**, 187 (1984). DOI 10.1016/0370-2693(84)90668-3
[59] I.L. Shapiro, A.G. Zheksenaev, Phys. Lett. B **324**, 286 (1994). DOI 10.1016/0370-2693(94)90195-3
[60] P.O. Mazur, E. Mottola, Phys. Rev. D **64**, 104022 (2001). DOI 10.1103/PhysRevD.64.104022
[61] I. Antoniadis, E.T. Tomboulis, Phys. Rev. D **33**, 2756 (1986). DOI 10.1103/PhysRevD.33.2756
[62] A.A. Starobinsky, in *Second Seminar on Quantum Gravity* (1981)
[63] I.L. Shapiro, J. Sola, Phys. Lett. B **530**, 10 (2002). DOI 10.1016/S0370-2693(02)01355-2
[64] A.M. Pelinson, I.L. Shapiro, F.I. Takakura, Nucl. Phys. B **648**, 417 (2003). DOI 10.1016/S0550-3213(02)00999-9
[65] J.C. Fabris, A.M. Pelinson, F. de O. Salles, I.L. Shapiro, JCAP **02**, 019 (2012). DOI 10.1088/1475-7516/2012/02/019
[66] F.d.O. Salles, I.L. Shapiro, Phys. Rev. D **89**(8), 084054 (2014). DOI 10.1103/PhysRevD.89.084054. [Erratum: Phys.Rev.D 90, 129903 (2014)]
[67] P. Peter, F.D.O. Salles, I.L. Shapiro, Phys. Rev. D **97**(6), 064044 (2018). DOI 10.1103/PhysRevD.97.064044
[68] E.D. Stewart, D.H. Lyth, Physics Letters B **302**(2-3), 171 (1993). DOI 10.1016/0370-2693(93)90379-V
[69] D. Baumann, *Cosmology*, 1st edn. (Cambridge University Press, 2022). DOI 10.1017/9781108937092

[70] Planck Collaboration, N. Aghanim *et al.*, Astronomy & Astrophysics **641**, A6 (2020). DOI 10.1051/0004-6361/201833910
[71] J. Martin, A. Riazuelo, M. Sakellariadou, Physical Review D **61**(8), 083518 (2000). DOI 10.1103/PhysRevD.61.083518
[72] J. Martin, Universe **5**(4), 92 (2019). DOI 10.3390/universe5040092
[73] C. Caprini, D.G. Figueroa, Class. Quant. Grav. **35**(16), 163001 (2018). DOI 10.1088/1361-6382/aac608
[74] Planck Collaboration, Y. Akrami *et al.*, Astronomy & Astrophysics **641**, A10 (2020). DOI 10.1051/0004-6361/201833887
[75] K. Abazajian *et al.*, The Astrophysical Journal **926**(1), 54 (2022). DOI 10.3847/1538-4357/ac1596
[76] P. Campeti, E. Komatsu, D. Poletti, C. Baccigalupi, Journal of Cosmology and Astroparticle Physics **2021**(01), 012 (2021). DOI 10.1088/1475-7516/2021/01/012
[77] J. Fumagalli, G.A. Palma, S. Renaux-Petel, S. Sypsas, L.T. Witkowski, C. Zenteno, Journal of High Energy Physics **2022**(3), 196 (2022). DOI 10.1007/JHEP03(2022)196
[78] E. Dimastrogiovanni, M. Fasiello, T. Fujita, Journal of Cosmology and Astroparticle Physics **2017**(01), 019 (2017). DOI 10.1088/1475-7516/2017/01/019
[79] J.R. Mureika, D. Stojkovic, Physical Review Letters **106**(10), 101101 (2011). DOI 10.1103/PhysRevLett.106.101101
[80] K. Nakayama, S. Saito, Y. Suwa, J. Yokoyama, Journal of Cosmology and Astroparticle Physics **2008**(06), 020 (2008). DOI 10.1088/1475-7516/2008/06/020
[81] L.P. Grishchuk, J. Martin, Physical Review D **56**(4), 1924 (1997). DOI 10.1103/PhysRevD.56.1924
[82] S. Dodelson, in *AIP Conference Proceedings*, vol. 689 (2003), vol. 689, pp. 184–196. DOI 10.1063/1.1627736
[83] J.T. Hsiang, B.L. Hu, Universe **8**(1), 27 (2022). DOI 10.3390/universe8010027
[84] M. Maggiore, Physics Reports **331**(6), 283 (2000). DOI 10.1016/S0370-1573(99)00102-7
[85] F. Dyson, International Journal of Modern Physics A **28**(25), 1330041 (2013). DOI 10.1142/S0217751X1330041X
[86] J.S. Bell, Physics Physique Fizika **1**(3), 195 (1964). DOI 10.1103/PhysicsPhysiqueFizika.1.195
[87] B. Allen, E. Flanagan, M.A. Papa, Physical Review D **61**(2), 024024 (1999). DOI 10.1103/PhysRevD.61.024024
[88] D. Campo, R. Parentani, Physical Review D **74**(2), 025001 (2006). DOI 10.1103/PhysRevD.74.025001
[89] J. Lesgourgues, D. Polarski, A. Starobinsky, Nuclear Physics B **497**(1-2), 479 (1997). DOI 10.1016/S0550-3213(97)00224-1
[90] A.H. Guth, S.Y. Pi, Physical Review D **32**(8), 1899 (1985). DOI 10.1103/PhysRevD.32.1899

[91] J. Lesgourgues, D. Polarski, A.A. Starobinsky, Classical and Quantum Gravity **14**(4), 881 (1997). DOI 10.1088/0264-9381/14/4/006
[92] T.F. Demarie, European Journal of Physics **39**(3), 035302 (2018). DOI 10.1088/1361-6404/aaaad0
[93] T. Maudlin, Journal of Physics A: Mathematical and Theoretical **47**(42), 424010 (2014). DOI 10.1088/1751-8113/47/42/424010
[94] R.F. Werner, Physical Review A **40**(8), 4277 (1989). DOI 10.1103/PhysRevA.40.4277
[95] R. Simon, Physical Review Letters **84**(12), 2726 (2000). DOI 10.1103/PhysRevLett.84.2726
[96] M. Revzen, Foundations of Physics **36**(4), 546 (2006). DOI 10.1007/s10701-005-9037-5
[97] J.F. Clauser, M.A. Horne, A. Shimony, R.A. Holt, Physical Review Letters **23**(15), 880 (1969). DOI 10.1103/PhysRevLett.23.880
[98] C.W. Gardiner, P. Zoller, *Quantum Noise: A Handbook of Markovian and Non-Markovian Quantum Stochastic Methods with Applications to Quantum Optics*, 3rd edn. Springer Series in Synergetics (Springer, Berlin ; New York, 2004)
[99] K. Banaszek, K. Wodkiewicz, Physical Review A **58**(6), 4345 (1998). DOI 10.1103/PhysRevA.58.4345
[100] J. Martin, V. Vennin, Physical Review D **96**(6), 063501 (2017). DOI 10.1103/PhysRevD.96.063501
[101] K. Banaszek, K. Wodkiewicz, Physical Review Letters **82**(10), 2009 (1999). DOI 10.1103/PhysRevLett.82.2009
[102] H. Ollivier, W.H. Zurek, Physical Review Letters **88**(1), 017901 (2001). DOI 10.1103/PhysRevLett.88.017901
[103] L. Henderson, V. Vedral, Journal of Physics A: Mathematical and General **34**(35), 6899 (2001). DOI 10.1088/0305-4470/34/35/315
[104] E.A. Lim, Physical Review D **91**(8), 083522 (2015). DOI 10.1103/PhysRevD.91.083522
[105] E. Joos, H.D. Zeh, Zeitschrift für Physik B Condensed Matter **59**(2), 223 (1985). DOI 10.1007/BF01725541
[106] C. Kiefer, D. Polarski, Annalen der Physik **510**(3), 137 (1998). DOI 10.1002/andp.2090070302
[107] C. Kiefer, D. Polarski, A.A. Starobinsky, International Journal of Modern Physics D **07**(03), 455 (1998). DOI 10.1142/S0218271898000292
[108] C. Kiefer, I. Lohmar, D. Polarski, A.A. Starobinsky, Classical and Quantum Gravity **24**(7), 1699 (2007). DOI 10.1088/0264-9381/24/7/002
[109] A.L. Matacz, Physical Review D **49**(2), 788 (1994). DOI 10.1103/PhysRevD.49.788
[110] R. Brandenberger, R. Laflamme, M. Mijić, Physica Scripta **T36**, 265 (1991). DOI 10.1088/0031-8949/1991/T36/029
[111] M.a. Sakagami, Progress of Theoretical Physics **79**(2), 442 (1988). DOI 10.1143/PTP.79.442

[112] M. Gasperini, M. Giovannini, Physics Letters B **301**(4), 334 (1993). DOI 10.1016/0370-2693(93)91159-K
[113] C. Kiefer, Classical and Quantum Gravity **4**(5), 1369 (1987). DOI 10.1088/0264-9381/4/5/031
[114] C.P. Burgess, R. Holman, D. Hoover, Physical Review D **77**(6), 063534 (2008). DOI 10.1103/PhysRevD.77.063534
[115] P. Martineau, Classical and Quantum Gravity **24**(23), 5817 (2007). DOI 10.1088/0264-9381/24/23/006
[116] A.A. Starobinsky, in *Field Theory, Quantum Gravity and Strings*, vol. 246, ed. by H. Araki, J. Ehlers, K. Hepp, R. Kippenhahn, H.A. Weidenmüller, J. Zittartz, W. Beiglböck, H.J. de Vega, N. Sánchez (Springer Berlin Heidelberg, Berlin, Heidelberg, 1988), pp. 107–126. DOI 10.1007/3-540-16452-9_6
[117] J.O. Gong, M.S. Seo, Journal of High Energy Physics **2019**(5), 21 (2019). DOI 10.1007/JHEP05(2019)021
[118] R. Brandenberger, V. Mukhanov, T. Prokopec, Physical Review Letters **69**(25), 3606 (1992). DOI 10.1103/PhysRevLett.69.3606
[119] F.C. Lombardo, D.L. Nacir, Physical Review D **72**(6), 063506 (2005). DOI 10.1103/PhysRevD.72.063506
[120] J. Martin, V. Vennin, Journal of Cosmology and Astroparticle Physics **2018**(05), 063 (2018). DOI 10.1088/1475-7516/2018/05/063
[121] A.O. Caldeira, A.J. Leggett, Physical Review Letters **46**(4), 211 (1981). DOI 10.1103/PhysRevLett.46.211
[122] D. Campo, R. Parentani, Physical Review D **78**(6), 065044 (2008). DOI 10.1103/PhysRevD.78.065044
[123] C. Kiefer, D. Polarski, A.A. Starobinsky, Physical Review D **62**(4), 043518 (2000). DOI 10.1103/PhysRevD.62.043518
[124] O. Brodier, A.M.O. de Almeida, Physical Review E **69**(1), 016204 (2004). DOI 10.1103/PhysRevE.69.016204
[125] T.J. Hollowood, J.I. McDonald, Physical Review D **95**(10), 103521 (2017). DOI 10.1103/PhysRevD.95.103521
[126] J. Martin, A. Micheli, V. Vennin. Comparing quantumness criteria (2023). DOI 10.1209/0295-5075/acc3be
[127] J. Martin, V. Vennin, Physical Review A **94**(5), 052135 (2016). DOI 10.1103/PhysRevA.94.052135
[128] J. Maldacena, Fortschritte der Physik **64**(1), 10 (2016). DOI 10.1002/prop.201500097
[129] C.P. Burgess, R. Holman, G. Tasinato, M. Williams, Journal of High Energy Physics **2015**(3), 90 (2015). DOI 10.1007/JHEP03(2015)090
[130] C.P. Burgess, R. Holman, G. Kaplanek, J. Martin, V. Vennin. Minimal decoherence from inflation (2022)
[131] T. Colas, J. Grain, V. Vennin, The European Physical Journal C **82**(12), 1085 (2022). DOI 10.1140/epjc/s10052-022-11047-9
[132] S. Brahma, A. Berera, J. Calderón-Figueroa, Journal of High Energy Physics **2022**(8), 225 (2022). DOI 10.1007/JHEP08(2022)225

[133] S. Kanno, J. Soda, Physical Review D **99**(8), 084010 (2019). DOI 10.1103/PhysRevD.99.084010
[134] M. Parikh, F. Wilczek, G. Zahariade, Physical Review D **104**(4), 046021 (2021). DOI 10.1103/PhysRevD.104.046021
[135] S. Kanno, J. Soda, J. Tokuda, Physical Review D **104**(8), 083516 (2021). DOI 10.1103/PhysRevD.104.083516
[136] D. Green, R.A. Porto, Physical Review Letters **124**(25), 251302 (2020). DOI 10.1103/PhysRevLett.124.251302
[137] D. Ghosh, A. Harsh Singh, F. Ullah, Journal of Cosmology and Astroparticle Physics **2023**(04), 007 (2023). DOI 10.1088/1475-7516/2023/04/007
[138] J.O. Gong, M.S. Seo, Journal of High Energy Physics **2020**(3), 60 (2020). DOI 10.1007/JHEP03(2020)060
[139] J. Martin, V. Vennin, Journal of Cosmology and Astroparticle Physics **2018**(06), 037 (2018). DOI 10.1088/1475-7516/2018/06/037
[140] A. Daddi Hammou, N. Bartolo, Journal of Cosmology and Astroparticle Physics **2023**(04), 055 (2023). DOI 10.1088/1475-7516/2023/04/055
[141] I. Agullo, B. Bonga, P.R. Metidieri, arXiv:2203.07066 (2022)
[142] J. Martin, V. Vennin, Journal of Cosmology and Astroparticle Physics **2021**(10), 036 (2021). DOI 10.1088/1475-7516/2021/10/036
[143] L. Espinosa-Portalés, V. Vennin, Journal of Cosmology and Astroparticle Physics **2022**(07), 037 (2022). DOI 10.1088/1475-7516/2022/07/037
[144] D. Sudarsky, International Journal of Modern Physics D **20**(04), 509 (2011). DOI 10.1142/S0218271811018937
[145] J. Fumagalli, M. Pieroni, S. Renaux-Petel, L.T. Witkowski, JCAP **07**(07), 020 (2022). DOI 10.1088/1475-7516/2022/07/020

2.3 Article: 'Discord and decoherence'

Our general strategy to evaluate the quantumness of cosmological perturbations is to consider correlations between different perturbations and see if these can be labelled quantum because they exhibit features that cannot be accounted for by a classical theory, e.g. they violate a Bell inequality [3]. The non-classicality of these correlations is expected to be affected by the interaction of the perturbations with other degrees of freedom and themselves, a phenomenon known as decoherence. In [2] reproduced below, we analysed one specific measure of the non-classicality of correlations, the quantum discord, in the cosmological context. The main result of this paper, derived in Sec. 4, is the computation of the quantum discord in the presence of a minimal decoherence model, extending known results [154]. Similarly to, [153] we show that there is a competition between the dynamics of inflation generating quantum correlations and decoherence that destroys them: the rate of interaction with the external degrees of freedom leading to decoherence must be large enough for the quantum discord to have disappeared by the end of inflation. Again, we point out that the convention used for $\hat{p}$, the field conjugated to the Mukhanov-Sasaki field $\hat{v}$ matches Eq. (1.95), and so differs from that used in [1], see Sec. 2.2 for details.

Discord and Decoherence

Jérôme Martin,[a] **Amaury Micheli,**[a,b] **Vincent Vennin**[c,a]

[a]Institut d'Astrophysique de Paris, UMR 7095-CNRS, Université Pierre et Marie Curie, 98 bis boulevard Arago, 75014 Paris, France

[b]IJCLab, CNRS/IN2P3, Université Paris-Saclay, 91405 Orsay, France

[c]Laboratoire Astroparticule et Cosmologie, CNRS Université de Paris, 10 rue Alice Domon et Léonie Duquet, 75013 Paris, France

E-mail: jmartin@iap.fr, amaury.micheli@ijclab.in2p3.fr, vincent.vennin@cnrs.fr

Abstract. In quantum information theory, quantum discord has been proposed as a tool to characterise the presence of "quantum correlations" between the subparts of a given system. Whether a system behaves quantum-mechanically or classically is believed to be impacted by the phenomenon of decoherence, which originates from the unavoidable interaction between this system and an environment. Generically, decoherence is associated with a decrease of the state purity, i.e. a transition from a pure to a mixed state. In this paper, we investigate how quantum discord is modified by this quantum-to-classical transition. This study is carried out on systems described by quadratic Hamiltonians and Gaussian states, with generalised squeezing parameters. A generic parametrisation is also introduced to describe the way the system is partitioned into two subsystems. We find that the evolution of quantum discord in presence of an environment is a competition between the growth of the squeezing amplitude and the decrease of the state purity. In phase space, this corresponds to whether the semi-minor axis of the Wigner ellipse increases or decreases, which has a clear geometrical interpretation. Finally, these considerations are applied to primordial cosmological perturbations, where we find that quantum discord can remain large even in the presence of strong decoherence.

Contents

1 Introduction

A intriguing fact in modern science is that, sometimes, it is not straightforward to decide whether a system behaves classically or quantum-mechanically. This is for instance the case in Cosmology where it is believed that the structures observed in our universe are nothing but quantum fluctuations amplified to astrophysical scales [1–3]. Even if this

hypothesis allows us to explain the properties of these structures, acquiring evidence that would establish their origin beyond any doubt turns out to be highly non-trivial. Indeed, assuming that the primordial fluctuations are stochastic rather than quantum leads to almost the same consequences up to corrections that, in practice, are very difficult to reveal experimentally [4, 5].

Recently, new methods have been developed to address the question of whether a system is classical or quantum-mechanical. A typical approach consists in dividing the system into two sub-systems and to study and characterise the nature of the correlations between these two sub-systems. As a matter of fact, there exist efficient tools to decide whether correlations are classical or quantum-mechanical in nature. Sometimes, indeed, correlations are impossible to understand in a classical framework (see, for instance, the Bell experiments [6, 7]) which establishes unambiguously their quantum origin. This strategy leads to the concept of quantum discord [8, 9]. However, the ability of quantum discord to precisely identify the quantum nature of some correlations has been challenged in the case of mixed states while, in the case of pure states, there is a one-to-one correspondence between quantum discord and entropy of entanglement [10, 11]. On the other hand, the quantum-to-classical transition of a system is generically believed to be connected to the phenomenon of decoherence [12, 13]. This mechanism, which has been observed in the laboratory [7], takes into account that any system is in fact always an open system, namely a system in interaction with other degrees of freedom that collectively constitute an environment. This interaction, when one is only interested in the properties of the system, is responsible for the appearance of classical properties.

It is therefore interesting to study how the quantum discord "responds" to the presence of decoherence in a system and to investigate how quantum discord can track the "classicalization" of a system. This is the main goal of the present paper. This study will be carried out in the generic case of a quadratic Hamiltonian. Physically, this is very relevant since many systems are described by this type of Hamiltonians. This is for instance the case for the Schwinger effect, the dynamical Casimir effect, the Hawking effect, inflationary fluctuations, etc. Technically, this is advantageous since the quantisation of these systems always leads to Gaussian states for which there exists an efficient formalism permitting the calculation of quantum discord. When it comes to concrete applications, we will consider the example of cosmological perturbations [14]. In addition to the advantages mentioned above, this will also allow us to shed new light on the question of whether their quantum origin can be observationally revealed, a long-standing question in Cosmology that has recently been the subject of many new studies [4, 15–23].

This article is organised as follows. In Sec. 2, we present a description of the quadratic systems considered in this paper and provide the formulas permitting the calculation of their quantum discord. In Sec. 3, as a warm-up, we explain how the time evolution of these systems and their quantum discord can be calculated in absence of an environment. In Sec. 4, we introduce a simple model, based on the Caldeira-Leggett model, which allows us to study and calculate quantum discord in presence of decoherence. In Sec. 5, we apply this formalism to the theory of cosmological perturbations of

quantum-mechanical origin. At the end of the article, in Sec. 6, we present our conclusions. Finally, the technical details of our calculations are given in a series of appendices. In Sec. A, we come back to the notion of partitions of a system and explain it in more details. In Sec. B, we calculate the covariance matrix of a Gaussian system for an arbitrary partition. In Sec. C, we explain how the formula giving the quantum discord used in the main text is arrived at. In Sec. D, we calculate the covariance matrix of the system in presence of an environment and derive efficient approximations for its components.

2 Quantum discord of a Gaussian field

2.1 Quantum phase space

In this work we consider the case of a real quantum scalar field with a local quadratic Hamiltonian

$$\hat{H} = \frac{1}{2}\int_{\mathbb{R}^3} \mathrm{d}^3\boldsymbol{x}\, \hat{z}^{\mathrm{T}}(\boldsymbol{x})\Lambda(\tau)\hat{z}(\boldsymbol{x})\,, \tag{2.1}$$

where $\hat{z}(\boldsymbol{x}) = \left(\hat{\phi}(\boldsymbol{x})\,, \hat{\pi}_\phi(\boldsymbol{x})\right)^{\mathrm{T}}$ contains the field $\hat{\phi}$ and its conjugate momentum $\hat{\pi}_\phi$, which satisfy the canonical commutation relations

$$\left[\hat{\phi}(\boldsymbol{x}), \hat{\pi}_\phi(\boldsymbol{y})\right] = i\delta(\boldsymbol{x}-\boldsymbol{y}). \tag{2.2}$$

We assume that the 2×2 symmetric matrix $\Lambda(\tau)$ does not depend on $\boldsymbol{x}$ but only on time τ, which can result from the invariance under spatial translations of the physical setup on which the field is introduced. For instance, the field ϕ may describe cosmological perturbations evolving on top of a homogeneous and isotropic background, as further discussed in Sec. 5, but for now the formalism we develop remains generic and applies to any system described by a (possibly infinite) collection of parametric oscillators. Note that $\Lambda_{\phi\phi}(\tau)$ can nonetheless contain gradient operators $\partial/\partial\boldsymbol{x}$ to any positive (in agreement with the locality assumption) and even (in order to preserve homogeneity and isotropy) power. If the theory does not feature higher-than two derivatives, which we assume here, then the other entries of Λ cannot contain spatial gradients. In what follows we introduce several successive canonical transformation, i.e. changes of variables that preserve the structure of the commutators (2.2), which make the expression of the Hamiltonian (2.1) simpler.

Let us perform a first canonical transformation and introduce the variables $\hat{v}(\boldsymbol{x})$ and $\hat{p}(\boldsymbol{x})$ defined as

$$\begin{aligned}\hat{\phi}(\boldsymbol{x}) &= \sqrt{\Lambda_{\pi\pi}}\,\hat{v}(\boldsymbol{x})\\ \hat{\pi}_\phi(\boldsymbol{x}) &= \left(\frac{1}{2}\frac{\Lambda'_{\pi\pi}}{\Lambda_{\pi\pi}} - \Lambda_{\phi\pi}\right)\frac{\hat{v}(\boldsymbol{x})}{\sqrt{\Lambda_{\pi\pi}}} + \frac{\hat{p}(\boldsymbol{x})}{\sqrt{\Lambda_{\pi\pi}}}\,,\end{aligned} \tag{2.3}$$

where a prime denotes derivation with respect to time, and where one can easily check that $\hat{v}$ and $\hat{p}$ obey the same commutation relations as the original fields, see Eq. (2.2).

In terms of these new variables, the Hamiltonian takes the simple form [24]

$$\hat{H} = \frac{1}{2}\int_{\mathbb{R}^3} \mathrm{d}^3\boldsymbol{x}\left[\hat{p}^2(\boldsymbol{x}) + \omega^2\hat{v}^2(\boldsymbol{x})\right] , \tag{2.4}$$

where $\omega^2 = \Lambda_{\phi\phi}\Lambda_{\pi\pi} + 1/2(\Lambda''_{\pi\pi}/\Lambda_{\pi\pi}) - 3/4(\Lambda'_{\pi\pi}/\Lambda_{\pi\pi})^2 - \Lambda'_{\phi\pi} - \Lambda^2_{\phi\pi} + \Lambda_{\phi\pi}\Lambda'_{\pi\pi}/\Lambda_{\pi\pi}$ encodes all the information about the dynamics.

We then perform a second canonical transformation, in the form of the Fourier expansion

$$\hat{v}(\boldsymbol{x}) = \frac{1}{(2\pi)^{3/2}}\int_{\mathbb{R}^3} \mathrm{d}^3\boldsymbol{k}\, e^{-i\boldsymbol{k}\cdot\boldsymbol{x}}\hat{v}_{\boldsymbol{k}} \tag{2.5}$$

and a similar expression for $\hat{p}(\boldsymbol{x})$. The fact that this defines a canonical transformation can be easily seen from combining the inverse Fourier transform, $\hat{v}_{\boldsymbol{k}} = (2\pi)^{-3/2}\int \mathrm{d}^3\boldsymbol{x}\, e^{i\boldsymbol{k}\cdot\boldsymbol{x}}\hat{v}(\boldsymbol{x})$ (and a similar expression for $\hat{p}_{\boldsymbol{k}}$) with Eq. (2.2) for the fields $\hat{v}(\boldsymbol{x})$ and $\hat{p}(\boldsymbol{x})$, which yields

$$\left[\hat{v}_{\boldsymbol{k}}, \hat{p}^\dagger_{\boldsymbol{k}'}\right] = i\delta(\boldsymbol{k} - \boldsymbol{k}') , \tag{2.6}$$

while $[\hat{v}_{\boldsymbol{k}}, \hat{v}^\dagger_{\boldsymbol{k}'}] = [\hat{p}_{\boldsymbol{k}}, \hat{p}^\dagger_{\boldsymbol{k}'}] = 0$. Plugging the Fourier expansions into the Hamiltonian (2.4), one obtains

$$\hat{H} = \int_{\mathbb{R}^{3+}} \mathrm{d}^3\boldsymbol{k}\,\hat{\mathcal{H}}_{\boldsymbol{k}} = \int_{\mathbb{R}^{3+}} \mathrm{d}^3\boldsymbol{k}\left[\hat{p}_{\boldsymbol{k}}\hat{p}^\dagger_{\boldsymbol{k}} + \omega^2\,(k,t)\,\hat{v}_{\boldsymbol{k}}\hat{v}^\dagger_{\boldsymbol{k}}\right] , \tag{2.7}$$

which defines the Hamiltonian density in Fourier space $\hat{\mathcal{H}}_{\boldsymbol{k}}$. In this expression, ω can depend on k since, as pointed out above, it may involve the gradient operator. It is important to notice that the operators $\hat{v}_{\boldsymbol{k}}$ and $\hat{p}_{\boldsymbol{k}}$ are not Hermitian. Indeed, since $\hat{v}(t,\boldsymbol{x})$ is real, one has $\hat{v}^\dagger_{\boldsymbol{k}} = \hat{v}_{-\boldsymbol{k}}$ and a similar relation for the conjugate momentum. This shows that independent degrees of freedom are labelled by half the Fourier space only, and explains why the integral is performed over $\mathbb{R}^{3+} = \mathbb{R}^2 \times \mathbb{R}^+$ in Eq. (2.7). In the helicity basis, this also allows one to decompose the fields $\hat{v}_{\boldsymbol{k}}$ and $\hat{p}_{\boldsymbol{k}}$ onto creation and annihilation operators as

$$\hat{v}_{\boldsymbol{k}} = \frac{1}{\sqrt{2k}}\left(\hat{c}_{\boldsymbol{k}} + \hat{c}^\dagger_{-\boldsymbol{k}}\right) \qquad \text{and} \qquad \hat{p}_{\boldsymbol{k}} = -i\sqrt{\frac{k}{2}}\left(\hat{c}_{\boldsymbol{k}} - \hat{c}^\dagger_{-\boldsymbol{k}}\right) , \tag{2.8}$$

where $\hat{c}_{\boldsymbol{k}}$ and $\hat{c}^\dagger_{\boldsymbol{k}'}$ obey the commutation relation $[\hat{c}_{\boldsymbol{k}}, \hat{c}^\dagger_{\boldsymbol{k}'}] = \delta(\boldsymbol{k} - \boldsymbol{k}')$. By plugging the above into Eq. (2.7), one obtains

$$\hat{H} = \int_{\mathbb{R}^{3+}} \mathrm{d}^3\boldsymbol{k}\left[\frac{k}{2}\left(\frac{\omega^2}{k^2} + 1\right)\left(\hat{c}_{\boldsymbol{k}}\hat{c}^\dagger_{\boldsymbol{k}} + \hat{c}^\dagger_{-\boldsymbol{k}}\hat{c}_{-\boldsymbol{k}}\right) + \frac{k}{2}\left(\frac{\omega^2}{k^2} - 1\right)\left(\hat{c}_{\boldsymbol{k}}\hat{c}_{-\boldsymbol{k}} + \hat{c}^\dagger_{-\boldsymbol{k}}\hat{c}^\dagger_{\boldsymbol{k}}\right)\right] . \tag{2.9}$$

In this expression, the first term does not lead to net particle creation and represents a collection of free oscillators while the second term either creates or destroys a pair of

particles with momenta $\boldsymbol{k}$ and $-\boldsymbol{k}$, and can be seen as resulting from the interaction with an exterior classical source. Note that the four combinations of ladder operators appearing in Eq. (2.9) are the only quadratic terms that are allowed by statistical isotropy, i.e. they are the only combinations that ensure momentum conservation in the particle content. Let us also notice that the form (2.9) is not the one commonly used in Cosmology [which is given by Eq. (14) of Ref. [5]]. However, it is related to it by a simple canonical transformation and is, therefore, equivalent to it.

Since $\hat{v}_{\boldsymbol{k}}$ and $\hat{p}_{\boldsymbol{k}}$ are not Hermitian, it is convenient to perform a third and last canonical transformation, and introduce the Hermitian operators corresponding to the Hermitian and anti-Hermitian parts of $\hat{v}_{\boldsymbol{k}}$ and $\hat{p}_{\boldsymbol{k}}$,

$$\hat{v}^{\mathrm{R}}_{\boldsymbol{k}} = \frac{\hat{v}_{\boldsymbol{k}} + \hat{v}^{\dagger}_{\boldsymbol{k}}}{\sqrt{2}}\,, \qquad \hat{v}^{\mathrm{I}}_{\boldsymbol{k}} = \frac{\hat{v}_{\boldsymbol{k}} - \hat{v}^{\dagger}_{\boldsymbol{k}}}{\sqrt{2}\,i}\,, \qquad \hat{p}^{\mathrm{R}}_{\boldsymbol{k}} = \frac{\hat{p}_{\boldsymbol{k}} + \hat{p}^{\dagger}_{\boldsymbol{k}}}{\sqrt{2}}\,, \qquad \hat{p}^{\mathrm{I}}_{\boldsymbol{k}} = \frac{\hat{p}_{\boldsymbol{k}} - \hat{p}^{\dagger}_{\boldsymbol{k}}}{\sqrt{2}\,i}\,. \tag{2.10}$$

The transformation (2.10) can be inverted according to $\hat{v}_{\boldsymbol{k}} = \left(\hat{v}^{\mathrm{R}}_{\boldsymbol{k}} + i\hat{v}^{\mathrm{I}}_{\boldsymbol{k}}\right)/\sqrt{2}$ and $\hat{p}_{\boldsymbol{k}} = \left(\hat{p}^{\mathrm{R}}_{\boldsymbol{k}} + i\hat{p}^{\mathrm{I}}_{\boldsymbol{k}}\right)/\sqrt{2}$, and one can readily check that these relations define a canonical transformation, namely that $[\hat{v}^{s}_{\boldsymbol{k}}, \hat{p}^{s'}_{\boldsymbol{k}'}] = i\delta(\boldsymbol{k}-\boldsymbol{k}')\delta_{s,s'}$ and that $[\hat{v}^{s}_{\boldsymbol{k}}, \hat{v}^{s'}_{\boldsymbol{k}'}] = [\hat{p}^{s}_{\boldsymbol{k}}, \hat{p}^{s'}_{\boldsymbol{k}'}] = 0$ where $s = \mathrm{R}, \mathrm{I}$. It is also clear from these expressions that $\hat{v}^{s}_{\boldsymbol{k}}$ and $\hat{p}^{s}_{\boldsymbol{k}}$ are Hermitian operators, and that the Hamiltonian reads

$$\hat{H} = \int_{\mathbb{R}^{3+}} \mathrm{d}^3\boldsymbol{k} \sum_{s=\mathrm{R},\mathrm{I}} \hat{\mathcal{H}}^{s}_{\boldsymbol{k}} = \frac{1}{2}\int_{\mathbb{R}^{3+}} \mathrm{d}^3\boldsymbol{k} \sum_{s=\mathrm{R},\mathrm{I}} \left[(\hat{p}^{s}_{\boldsymbol{k}})^2 + \omega^2(k,\tau)(\hat{v}^{s}_{\boldsymbol{k}})^2\right]\,. \tag{2.11}$$

The advantage of this last parameterisation is that it makes the Hamiltonian sum separable, see Eq. (2.11). In other words, it describes a collection of independent parametric oscillators. If the initial quantum state is factorisable in that basis, which is for instance the case for the vacuum state selected by that Hamiltonian, it remains so at later time, and the dynamical evolution does not generate correlation or entanglement between different subspaces.

2.2 Partitions

As mentioned above, the system under consideration can be factorised into independent Fourier subspaces, within which entangled pairs of particles with opposite wave-momenta are created. Our goal is to measure the amount of entanglement associated with this mechanism, and to determine whether the resulting correlations have genuinely quantum properties.

Experiments aimed at testing the quantum nature of a physical setup usually rely on probing the properties of the correlations between two of its subsystems. In Bell inequality experiments for instance, the correlations between the spin states of two entangled particles are tested against a possible local hidden-variables theory. In that case, the way the physical system is split into two subsystems is obvious: the two subsystems are simply the two space-like separated particles. One may choose to parameterise phase space by means of other combinations of the spin operators, but given that Bell experiments test for locality, it is clear that the two particles constitute a preferred partition.

The situation is however less clear for quantum fields. One may still choose to work in real space, and probe the nature of the correlations for two spatially-separated regions, see for instance Refs. [21, 25]. However, in this approach, one has to deal with mixed states, coming from the fact that when observing the field at two distinct locations in real space one implicitly traces over the configurations of the field in all other locations, making the reduced state of interest a mixed one. This problem does not occur in Fourier space since different Fourier subspaces are uncoupled. Since we want to study the effect of decoherence on the presence of quantum correlations, it seems important to first isolate the decoherence associated with the coupling to environmental degrees of freedom, from the one coming from the effective mixing effect mentioned above. This is why in this work we choose to study correlations within Fourier subspaces, leaving the combination of both mixing effects (i.e. the analysis of quantum discord in real space in the presence of an environment) for future work.

In Fourier space, there is no obvious way to split the system into two subsystems. At the technical level, this implies that the construction of Hermitian operators out of $\hat{v}_{\boldsymbol{k}}$ and $\hat{p}_{\boldsymbol{k}}$ is not unique, and that Eq. (2.10) is not the only possibility. For instance, one can consider the set of operators $\hat{q}_{\boldsymbol{k}}$ and $\hat{\pi}_{\boldsymbol{k}}$ involving ladder operators of a single mode $\boldsymbol{k}$ (and excluding $-\boldsymbol{k}$), namely [5]

$$\hat{q}_{\boldsymbol{k}} = \frac{1}{\sqrt{2k}}\left(\hat{c}_{\boldsymbol{k}} + \hat{c}^{\dagger}_{\boldsymbol{k}}\right) \qquad \text{and} \qquad \hat{\pi}_{\boldsymbol{k}} = -i\sqrt{\frac{k}{2}}\left(\hat{c}_{\boldsymbol{k}} - \hat{c}^{\dagger}_{\boldsymbol{k}}\right), \tag{2.12}$$

which are indeed Hermitian and satisfy $[\hat{q}_{\boldsymbol{k}}, \hat{\pi}_{\boldsymbol{k}'}] = i\delta(\boldsymbol{k} - \boldsymbol{k}')$. The variables (2.10) and (2.12) define two partitions (namely a partition between the real and imaginary sector, and between the $\boldsymbol{k}$ and $-\boldsymbol{k}$ sector, respectively), and these two partitions feature different correlations of different amount and nature.

Since there is no preferred partition, a generic approach is to probe the nature of the correlations in all possible partitions. This is why we now define the notion of quantum partitions at a more formal level, and see how different partitions are related to each other (we refer the reader to Appendix A for a more detailed analysis of partitions). A partition of a Fourier subspace into two subsystems 1 and 2 is encoded in the phase-space vector

$$\hat{R}_{1/2} = \left(k^{1/2}\hat{q}^{(1)}_{\boldsymbol{k}}, k^{-1/2}\hat{\pi}^{(1)}_{\boldsymbol{k}}, k^{1/2}\hat{q}^{(2)}_{\boldsymbol{k}}, k^{-1/2}\hat{\pi}^{(2)}_{\boldsymbol{k}}\right)^{\mathrm{T}}, \tag{2.13}$$

where the two first entries concern the first sector and the two last entries describe the second sector (the prefactors $k^{1/2}$ and $k^{-1/2}$ are introduced to make all entries of the $\hat{R}_{1/2}$ vector of the same dimension), and where the commutators between the entries of $\hat{R}_{1/2}$ are canonical (i.e. the only non-vanishing commutators are between the first and the second, and the third and the fourth, entries, and this commutator equals i). For instance, in the R/I partition corresponding to Eq. (2.10), one has $\hat{R}_{\mathrm{R/I}} = (k^{1/2}\hat{v}^{\mathrm{R}}_{\boldsymbol{k}}, k^{-1/2}\hat{p}^{\mathrm{R}}_{\boldsymbol{k}}, k^{1/2}\hat{v}^{\mathrm{I}}_{\boldsymbol{k}}, k^{-1/2}\hat{p}^{\mathrm{I}}_{\boldsymbol{k}})^{\mathrm{T}}$, while in the $\pm\boldsymbol{k}$ partition corresponding to Eq. (2.12), one has $\hat{R}_{\pm\boldsymbol{k}} = (k^{1/2}\hat{q}_{\boldsymbol{k}}, k^{-1/2}\hat{\pi}_{\boldsymbol{k}}, k^{1/2}\hat{q}_{-\boldsymbol{k}}, k^{-1/2}\hat{\pi}_{-\boldsymbol{k}})^{\mathrm{T}}$.

Among all possible partitions, let us note that the R/I partition plays a specific role since it is such that the Hamiltonian is sum separable [i.e. Eq. (2.11) does not

contain cross terms between the two subsectors]. In the following, in order to preserve the quadratic nature of the Hamiltonian density, we focus on partitions that are linearly related to that reference partition,

$$\hat{R}_{1/2} = T^{\mathrm{R/I}\to 1/2}\hat{R}_{\mathrm{R/I}}\,, \tag{2.14}$$

where $T^{\mathrm{R/I}\to 1/2}$ is a four-by-four matrix that encodes the change of partitions. This matrix must be such that the commutator structure is preserved, i.e. it must be a symplectic matrix. Further imposing that different parameterisations share the same vacuum state, i.e. that $T^{\mathrm{R/I}\to 1/2}$ does not mix creation and annihilation operators, in Appendix A we show that $T^{\mathrm{R/I}\to 1/2}$ must be of the form

$$T^{\mathrm{R/I}\to 1/2} = \begin{pmatrix} \cos\alpha\cos\theta & -\sin\alpha\cos\theta & -\cos\delta\sin\theta & \sin\delta\sin\theta \\ \sin\alpha\cos\theta & \cos\alpha\cos\theta & -\sin\delta\sin\theta & -\cos\delta\sin\theta \\ \cos\beta\sin\theta & -\sin\beta\sin\theta & \cos(\alpha-\beta-\delta)\cos\theta & \sin(\alpha-\beta-\delta)\cos\theta \\ \sin\beta\sin\theta & \cos\beta\sin\theta & -\sin(\alpha-\beta-\delta)\cos\theta & \cos(\alpha-\beta-\delta)\cos\theta \end{pmatrix}, \tag{2.15}$$

where α, β, δ and θ are four angles that entirely characterise the partition. For instance, the R/I partition obviously corresponds to $\alpha=\beta=\delta=\theta=0$, while the $\pm\boldsymbol{k}$ partition corresponds to $\alpha=0$, $\beta=-\pi$, $\delta=\pi/2$ and $\theta=-\pi/4$. It is also worth mentioning that the one-parameter subset of partitions studied in Ref. [5] can be obtained by setting $\alpha=0$, $\beta=3\pi/2+2\theta$ and $\delta=\pi/2$ in Eq. (2.15), leading to

$$T^{\mathrm{R/I}\to 1/2}(\theta) = \begin{pmatrix} \cos\theta & 0 & 0 & \sin\theta \\ 0 & \cos\theta & -\sin\theta & 0 \\ \sin\theta\sin(2\theta) & \sin\theta\cos(2\theta) & \cos\theta\cos(2\theta) & -\cos\theta\sin(2\theta) \\ -\sin\theta\cos(2\theta) & \sin\theta\sin(2\theta) & \cos\theta\sin(2\theta) & \cos\theta\cos(2\theta) \end{pmatrix}. \tag{2.16}$$

This subset reaches the $\pm\boldsymbol{k}$ partition since one can check that $T^{\mathrm{R/I}\to\pm\boldsymbol{k}} = T^{\mathrm{R/I}\to 1/2}(-\pi/4)$. In what follows, we will focus on the subclass (2.16) of partitions for concrete applications of our formalism, since it will be sufficient to study how the result may depend on the choice of partitions, but the formalism will be kept general enough to make it obvious how to apply it to the most generic partitions (2.15).

2.3 Covariance matrix

Since the Hamiltonian (2.1) is quadratic, the dynamics it generates is linear and admits Gaussian states as solutions.[1] Such states are entirely characterised by their two-point correlation functions. The two-point correlation functions are conventionally gathered in the real symmetric covariance matrix γ of the state defined by

$$\gamma_{ab} = \langle\{\hat{R}_a, \hat{R}_b\}\rangle\,, \tag{2.17}$$

[1] Note that this work is not restricted to pure states, so the quantum states we consider are in general represented by a density matrix $\hat{\rho}$, or equivalently by a Wigner function. Here, what "Gaussian state" means in practice is that the Wigner function is Gaussian.

where $\{.\}$ denotes the anti-commutator, namely $\{a,b\} \equiv ab + ba$. Upon a change of partition $\hat{R} \to \hat{R}' = T\hat{R}$, the covariance matrix becomes

$$\gamma' = T\gamma T^{\mathrm{T}} \,. \tag{2.18}$$

As discussed around Eq. (2.11), in the R/I partition, the two sectors decouple and have the same reduced Hamiltonian. As a consequence, if the initial state is uncorrelated and symmetric between the two sectors (which is the case of the vacuum state selected by the Hamiltonian), it remains so at any time, and the covariance matrix is of the form

$$\gamma^{\mathrm{R/I}} = \begin{pmatrix} \gamma_{11} & \gamma_{12} & 0 & 0 \\ \gamma_{12} & \gamma_{22} & 0 & 0 \\ 0 & 0 & \gamma_{11} & \gamma_{12} \\ 0 & 0 & \gamma_{12} & \gamma_{22} \end{pmatrix} , \tag{2.19}$$

which depends on three parameters only, namely

$$\gamma_{11} = 2k \left\langle \left(\hat{v}_{\boldsymbol{k}}^{\mathrm{R}}\right)^2 \right\rangle = 2k \left\langle \left(\hat{v}_{\boldsymbol{k}}^{\mathrm{I}}\right)^2 \right\rangle = k \left\langle \left\{ \hat{v}_{\boldsymbol{k}}, \hat{v}_{\boldsymbol{k}}^{\dagger} \right\} \right\rangle , \tag{2.20}$$

$$\gamma_{12} = \gamma_{21} = \left\langle \hat{v}_{\boldsymbol{k}}^{\mathrm{R}} \hat{p}_{\boldsymbol{k}}^{\mathrm{R}} + \hat{p}_{\boldsymbol{k}}^{\mathrm{R}} \hat{v}_{\boldsymbol{k}}^{\mathrm{R}} \right\rangle = \left\langle \hat{v}_{\boldsymbol{k}}^{\mathrm{I}} \hat{p}_{\boldsymbol{k}}^{\mathrm{I}} + \hat{p}_{\boldsymbol{k}}^{\mathrm{I}} \hat{v}_{\boldsymbol{k}}^{\mathrm{I}} \right\rangle = \left\langle \hat{v}_{\boldsymbol{k}} \hat{p}_{\boldsymbol{k}}^{\dagger} + \hat{p}_{\boldsymbol{k}} \hat{v}_{\boldsymbol{k}}^{\dagger} \right\rangle , \tag{2.21}$$

$$\gamma_{22} = \frac{2}{k} \left\langle \left(\hat{p}_{\boldsymbol{k}}^{\mathrm{R}}\right)^2 \right\rangle = \frac{2}{k} \left\langle \left(\hat{p}_{\boldsymbol{k}}^{\mathrm{I}}\right)^2 \right\rangle = \frac{1}{k} \left\langle \left\{ \hat{p}_{\boldsymbol{k}}, \hat{p}_{\boldsymbol{k}}^{\dagger} \right\} \right\rangle , \tag{2.22}$$

where we have also related the entries of the covariance matrix to the two-point function of the original $\hat{v}_{\boldsymbol{k}}$ and $\hat{p}_{\boldsymbol{k}}$ operators (where one can also check that $\langle \hat{v}_{\boldsymbol{k}} \hat{p}_{\boldsymbol{k}} + \hat{p}_{\boldsymbol{k}}^{\dagger} \hat{v}_{\boldsymbol{k}}^{\dagger} \rangle = 0$). Note that states represented by a covariance matrix of the form (2.19) are called Gaussian and Homogeneous Density Matrices (GHDM) in Ref. [16], where they are shown to yield the most general partial reconstruction of the state using only the knowledge of the two-point correlation function.

Making use of Eq. (2.16) and (2.18), the covariance matrix can then be written down in any partition, and we give the result in Appendix B for display convenience, where the specific case of the $\pm\boldsymbol{k}$ partition is also treated. Note that the correlators of the ladder operators introduced in Eq. (2.8) can also be expressed in terms of the entries of the covariance matrix (2.19), and one obtains

$$\left\langle \left\{ \hat{c}_{\boldsymbol{k}}, \hat{c}_{\boldsymbol{k}}^{\dagger} \right\} \right\rangle = \left\langle \left\{ \hat{c}_{-\boldsymbol{k}}, \hat{c}_{-\boldsymbol{k}}^{\dagger} \right\} \right\rangle = \frac{\gamma_{11} + \gamma_{22}}{2} \equiv 2\mathcal{N}_k + 1 \,, \tag{2.23}$$

$$\left\langle \{ \hat{c}_{\boldsymbol{k}}, \hat{c}_{-\boldsymbol{k}} \} \right\rangle = \frac{\gamma_{11} - \gamma_{22}}{2} + i\gamma_{12} \equiv 2\mathcal{C}_k \,, \tag{2.24}$$

$$\left\langle \left\{ \hat{c}_{\boldsymbol{k}}^{\dagger}, \hat{c}_{-\boldsymbol{k}}^{\dagger} \right\} \right\rangle = \frac{\gamma_{11} - \gamma_{22}}{2} - i\gamma_{12} = 2\mathcal{C}_k^* \,. \tag{2.25}$$

where other correlators vanish. These expressions also define $\mathcal{N}_k$, the number of particles in the modes $\boldsymbol{k}$ and $-\boldsymbol{k}$ (which are equal because of isotropy), and $\mathcal{C}_k$, the correlation between the modes $\pm\boldsymbol{k}$ [26].

Note that the covariance matrix contains all information about the quantum state, and any relevant quantity can be expressed in terms of its entries. For instance, the purity of the state, $\mathrm{Tr}(\hat{\rho}^2)$ is given by [27]

$$\mathrm{Tr}\left(\hat{\rho}^2\right) = \frac{1}{\sqrt{\det\gamma}} = \frac{1}{\gamma_{11}\gamma_{22} - \gamma_{12}^2}\,. \tag{2.26}$$

This quantity is comprised between 0 and 1 and measures the deviation from a pure state, for which it equals 1. In the following, the purity will be thus used as a measure of decoherence. Note that since symplectic matrices have unit determinant, the purity is invariant under changes of partitions, and more generally under any change of phase-space parameterisation.

2.4 Quantum discord

The presence of quantum correlations between two subparts of a system can be characterised by means of quantum discord [8, 9], which is briefly reviewed in Appendix C. The idea is to introduce two measures of correlation that coincide for classically correlated setups because of Bayes theorem, but that may differ for quantum systems. The first measure is the so-called mutual information, which is defined as the sum between the von-Neumann entropy of each reduced sub-systems (known as entanglement entropy), minus the entropy of the entire system. The second measure evaluates the difference between the entropy contained in the first subsystem, and the entropy contained in that same subsystem when the second subsystem has been measured, where an extremisation is performed over all possible ways to "measure" the second subsystem. Quantum discord is defined as the difference between these two measures, and thus quantifies deviations from Bayes theorem.

It is worth mentioning that for pure states, the different measures of correlations mentioned above (entanglement entropy, mutual information and quantum discord) coincide up to numerical prefactors. While this implies that correlated pure states necessarily feature quantum correlations, it also means that quantum discord does not add particular insight in measuring them, since it contains the same information as entanglement entropy, which is easier to compute. However, quantum discord becomes more clearly useful when considering mixed states, which is precisely the topic of this work. The reason is that there exist mixed states that feature classical correlations only. Contrary to pure states, mixed states can thus possess classical *and* quantum correlations, and the role of discord is to isolate the part of the correlations that is genuinely quantum.

In Appendix C, we show that for Gaussian homogeneous states such as the ones introduced above, both measures depend only on the symplectic eigenvalue of the reduced covariance matrix (i.e. of the diagonal 2-by-2 blocks of the covariance matrix),

$$\sigma(\theta) = \sqrt{\cos^2(2\theta)\left(\gamma_{11}\gamma_{22} - \gamma_{12}^2\right) + \left(\frac{\gamma_{11}+\gamma_{22}}{2}\right)^2 \sin^2(2\theta)}\,, \tag{2.27}$$

and of the symplectic eigenvalue of the full covariance matrix, which is nothing but $\sigma(0)$ [and which coincides with $(\det\gamma)^{1/4}$, see Eq. (2.19)]. This gives rise to the following

expression for quantum discord

$$\mathcal{D}(\theta) = f\left[\sigma(\theta)\right] - 2f\left[\sigma(0)\right] + f\left[\frac{\sigma(\theta)+\sigma^2(0)}{\sigma(\theta)+1}\right], \tag{2.28}$$

where the function $f(x)$ is defined for $x \geq 1$ by

$$f(x) = \left(\frac{x+1}{2}\right)\log_2\left(\frac{x+1}{2}\right) - \left(\frac{x-1}{2}\right)\log_2\left(\frac{x-1}{2}\right), \tag{2.29}$$

One can check that, for the R/I partition where $\theta = 0$, the above expressions give $\mathcal{D} = 0$, in agreement with the fact that the two subsystems are uncorrelated in this partition.

3 Discord in the absence of an environment

In Sec. 2, we have seen how the Fourier subspaces of a real scalar field can be partitioned, and how the presence of quantum correlations between its subparts can be characterised from the knowledge of its covariance matrix. In this section, we treat the situation where the field does not couple to any environmental degree of freedom, and its quantum state remains pure. We describe its time evolution using three different, though complementary, approaches: via Bogoliubov coefficients in Sec. 3.1, via squeezing parameters in Sec. 3.2 and via transport equations in Sec. 3.3. These three approaches are useful as they will lead to different insights into the case with environmental coupling, treated in Sec. 4. We finally analyse how quantum discord evolves in time in Sec. 3.4.

3.1 Bogoliubov coefficients

In the Heisenberg picture, the equation of motion for the ladder operators can be obtained from Eq. (2.9), and in matricial form they are given by

$$\frac{\mathrm{d}}{\mathrm{d}\tau}\begin{pmatrix}\hat{c}_{\boldsymbol{k}}\\ \hat{c}^\dagger_{-\boldsymbol{k}}\end{pmatrix} = \begin{pmatrix} -i\frac{k}{2}\left[\frac{\omega^2(k,\tau)}{k^2}+1\right] & -i\frac{k}{2}\left[\frac{\omega^2(k,\tau)}{k^2}-1\right] \\ i\frac{k}{2}\left[\frac{\omega^2(k,\tau)}{k^2}-1\right] & i\frac{k}{2}\left[\frac{\omega^2(k,\tau)}{k^2}+1\right] \end{pmatrix}\begin{pmatrix}\hat{c}_{\boldsymbol{k}}\\ \hat{c}^\dagger_{-\boldsymbol{k}}\end{pmatrix}. \tag{3.1}$$

This system being linear, it can be solved with a linear transformation known as the Bogoliubov transformation

$$\begin{pmatrix}\hat{c}_{\boldsymbol{k}}(\tau)\\ \hat{c}^\dagger_{-\boldsymbol{k}}(\tau)\end{pmatrix} = \begin{pmatrix} u_{\boldsymbol{k}}(\tau) & w_{\boldsymbol{k}}(\tau) \\ w^*_{-\boldsymbol{k}}(\tau) & u^*_{-\boldsymbol{k}}(\tau) \end{pmatrix}\begin{pmatrix}\hat{c}_{\boldsymbol{k}}\left(\tau_{\mathrm{in}}\right)\\ \hat{c}^\dagger_{-\boldsymbol{k}}\left(\tau_{\mathrm{in}}\right)\end{pmatrix}, \tag{3.2}$$

where $u_{\boldsymbol{k}}$ and $w_{\boldsymbol{k}}$ are the two complex Bogoliubov coefficients satisfying

$$|u_{\boldsymbol{k}}|^2 - |w_{-\boldsymbol{k}}|^2 = 1\,. \tag{3.3}$$

This condition ensures that the commutation relation $[\hat{c}_{\boldsymbol{k}}, \hat{c}^\dagger_{\boldsymbol{k}'}] = \delta(\boldsymbol{k}-\boldsymbol{k}')$ is preserved in time [which can be checked by differentiating this commutation relation with respect

to time and using Eq. (3.1)]. Solving the evolution of the system then boils down to computing the Bogoliubov coefficients. They satisfy the same differential system as the creation and annihilation operators, namely Eq. (3.1), with initial conditions $u_{\pm\boldsymbol{k}}\left(\tau_{\rm in}\right)=1$ and $w_{\pm\boldsymbol{k}}\left(\tau_{\rm in}\right)=0$. Note that because of statistical isotropy, the Bogoliubov coefficients only depend on the norm of $\boldsymbol{k}$, so $u_{\boldsymbol{k}}=u_{-\boldsymbol{k}}\equiv u_k$ and $w_{\boldsymbol{k}}=w_{-\boldsymbol{k}}\equiv w_k$.

The two first-order differential equations for the Bogoliubov coefficients can be combined into a single second-order equation for the combination $u_k+w_k^*$, namely

$$\frac{\mathrm{d}^2}{\mathrm{d}\tau^2}\left(u_k+w_k^*\right)+\omega^2(k,\tau)\left(u_k+w_k^*\right)=0\,. \tag{3.4}$$

This equation needs to be solved with the initial conditions $(u_k+w_k^*)(\tau_{\rm in})=1$ and $(u_k+w_k^*)'(\tau_{\rm in})=-ik$, where the latter comes from the relation

$$\frac{\mathrm{d}}{\mathrm{d}\tau}\left(u_k+w_k^*\right)=-ik\left(u_k-w_k^*\right), \tag{3.5}$$

which itself follows from the fact that the Bogoliubov coefficients satisfy the differential system (3.1). Note that Eq. (3.5) also implies that $u_k-w_k^*$ can be obtained from the solution of the second-order equation (3.4), hence both u_k and w_k can be reconstructed from that solution. In practice, determining the full dynamics of the system thus boils down to solving Eq. (3.4).

The evolution can also be expressed in terms of the field variables, since plugging Eq. (3.2) into Eq. (2.12) leads to

$$\hat{R}_{\rm R/I}\left(\tau\right)=T_{\rm R/I}\left(\tau\right)\hat{R}_{\rm R/I}\left(\tau_{\rm in}\right), \tag{3.6}$$

where

$$T_{\rm R/I}\left(\tau\right)=\begin{pmatrix}\Re\mathrm{e}\,\left(u_k+w_k\right) & -\Im\mathrm{m}\,\left(u_k-w_k\right) & 0 & 0\\ \Im\mathrm{m}\,\left(u_k+w_k\right) & \Re\mathrm{e}\,\left(u_k-w_k\right) & 0 & 0\\ 0 & 0 & \Re\mathrm{e}\,\left(u_k+w_k\right) & -\Im\mathrm{m}\,\left(u_k-w_k\right)\\ 0 & 0 & \Im\mathrm{m}\,\left(u_k+w_k\right) & \Re\mathrm{e}\,\left(u_k-w_k\right)\end{pmatrix}. \tag{3.7}$$

The covariance matrix can then be evaluated by means of Eq. (2.18), namely $\gamma\left(\tau\right)=T_{\rm R/I}\left(\tau\right)\gamma\left(\tau_{\rm in}\right)T_{\rm R/I}^{\rm T}\left(\tau\right)$, which gives rise to

$$\begin{aligned}\gamma_{11}\left(\tau\right)&=\frac{1}{2}\left[\gamma_{11}(\tau_{\rm in})+\gamma_{22}(\tau_{\rm in})\right]\left|u_k(\tau)+w_k^*(\tau)\right|^2\\&\quad+\Re\mathrm{e}\left\{\left[u_k(\tau)+w_k^*(\tau)\right]^2\left[\frac{\gamma_{11}(\tau_{\rm in})-\gamma_{22}(\tau_{\rm in})}{2}+i\gamma_{12}(\tau_{\rm in})\right]\right\},\end{aligned} \tag{3.8}$$

$$\begin{aligned}\gamma_{22}\left(\tau\right)&=\frac{1}{2}\left[\gamma_{11}(\tau_{\rm in})+\gamma_{22}(\tau_{\rm in})\right]\left|u_k(\tau)-w_k^*(\tau)\right|^2\\&\quad-\Re\mathrm{e}\left\{\left[u_k(\tau)-w_k^*(\tau)\right]^2\left[\frac{\gamma_{11}(\tau_{\rm in})-\gamma_{22}(\tau_{\rm in})}{2}+i\gamma_{12}(\tau_{\rm in})\right]\right\},\end{aligned} \tag{3.9}$$

$$\gamma_{12}\left(\tau\right)=\left[\gamma_{11}(\tau_{\rm in})+\gamma_{22}(\tau_{\rm in})\right]\Im\mathrm{m}\left[u_k(\tau)w_k(\tau)\right]$$

$$- \Im\mathrm{m}\left\{\left[u_k^{*2}(\tau) - w_k^2(\tau)\right]\left[\frac{\gamma_{11}(\tau_{\rm in}) - \gamma_{22}(\tau_{\rm in})}{2} - i\gamma_{12}(\tau_{\rm in})\right]\right\} . \tag{3.10}$$

Notice that, using Eqs. (2.23), (2.24) and (2.25), the above relations can be rewritten in terms of the initial number of particles $\mathcal{N}_k(\tau_{\rm in})$ and mode correlation $\mathcal{C}_k(\tau_{\rm in})$, leading to

$$\gamma_{11}(\tau) = [2\mathcal{N}_k(\tau_{\rm in}) + 1]\,|u_k(\tau) + w_k^*(\tau)|^2 + 2\,\Re\mathrm{e}\left\{[u_k(\tau) + w_k^*(\tau)]^2\,\mathcal{C}_k(\tau_{\rm in})\right\} \tag{3.11}$$

$$\gamma_{22}(\tau) = [2\mathcal{N}_k(\tau_{\rm in}) + 1]\,|u_k(\tau) - w_k^*(\tau)|^2 - 2\,\Re\mathrm{e}\left\{[u_k(\tau) - w_k^*(\tau)]^2\,\mathcal{C}_k(\tau_{\rm in})\right\} \tag{3.12}$$

$$\gamma_{12}(\tau) = 2\,[2\mathcal{N}_k(\tau_{\rm in}) + 1]\,\Im\mathrm{m}\,[u_k(\tau)w_k(\tau)] - 2\,\Im\mathrm{m}\left\{\left[u_k^{*2}(\tau) - w_k^2(\tau)\right]\mathcal{C}_k^*(\tau_{\rm in})\right\} . \tag{3.13}$$

If the initial state is chosen as the vacuum state, $\mathcal{N}_k(\tau_{\rm in}) = \mathcal{C}_k(\tau_{\rm in}) = 0$, the above expressions reduce to

$$\gamma_{11}(\tau) = |u_k(\tau) + w_k^*(\tau)|^2 , \qquad \gamma_{22}(\tau) = |u_k(\tau) - w_k^*(\tau)|^2 , \tag{3.14}$$

$$\gamma_{12}(\tau) = 2\,\Im\mathrm{m}\,[u_k(\tau)w_k(\tau)] . \tag{3.15}$$

In that case, given the initial conditions $u_k(\tau_{\rm in}) = 1$ and $w_k(\tau_{\rm in}) = 0$, these expressions also imply that $\gamma_{11}(\tau_{\rm in}) = \gamma_{22}(\tau_{\rm in}) = 1$ and $\gamma_{12}(t_{\rm in}) = 0$.

3.2 Squeezing parameters

An equivalent description of the dynamics is through the squeezing parameters $(r_k, \varphi_k, \theta_k)$ (notice that the rotation angle θ_k, which carries the index "k", should not be confused with the angle θ defining a partition), which are defined in terms of the Bogoliubov coefficients as

$$u_k(\tau) = e^{-i\theta_k}\cosh r_k, \qquad w_k(\tau) = -e^{i\theta_k + 2i\varphi_k}\sinh r_k , \tag{3.16}$$

which ensures that the condition (3.3) is automatically satisfied. Given that the Bogoliubov coefficients satisfy the differential system (3.2), one can derive equations of motion for the squeezing parameters, namely

$$\frac{\mathrm{d}r_k}{\mathrm{d}\tau} = \frac{k}{2}\left(\frac{\omega^2}{k^2} - 1\right)\sin(2\varphi_k) , \tag{3.17}$$

$$\frac{\mathrm{d}\varphi_k}{\mathrm{d}\tau} = -\frac{k}{2}\left(\frac{\omega^2}{k^2} + 1\right) + \frac{k}{2}\left(\frac{\omega^2}{k^2} - 1\right)\frac{\cos(2\varphi_k)}{\tanh(2r_k)} , \tag{3.18}$$

$$\frac{\mathrm{d}\theta_k}{\mathrm{d}\tau} = \frac{k}{2}\left(\frac{\omega^2}{k^2} + 1\right) - \frac{k}{2}\left(\frac{\omega^2}{k^2} - 1\right)\cos(2\varphi_k)\tanh r_k , \tag{3.19}$$

where one can see that θ_k does not contribute to the time evolution of r_k and φ_k. Moreover, since we have already derived the relation between the covariance matrix elements and the functions u_k and v_k, see Eq. (3.14), one can also express the components γ_{11}, γ_{22} and γ_{12} in terms of the squeezing parameters. One finds[2]

$$\gamma_{11} = \cosh(2r_k) - \cos(2\varphi_k)\sinh(2r_k), \tag{3.20}$$

[2] In the $\pm\boldsymbol{k}$ partition, where the covariance matrix is given by Eqs. (B.10)-(B.16), those expressions allow one to recover Eq. (C28) of Ref. [5].

$$\gamma_{22} = \cosh(2r_k) + \cos(2\varphi_k)\sinh(2r_k), \tag{3.21}$$
$$\gamma_{12} = -\sin(2\varphi_k)\sinh(2r_k), \tag{3.22}$$

where one can see that θ_k does not appear.

The geometrical interpretation of the squeezing parameters becomes clear when computing the Wigner function [28–30], which is the Wigner-Weyl transform of the density matrix. It can be seen as a quasi probability distribution function, in the sense that the quantum expectation value of any operator is given by the integral over phase-space of the product between the Weyl transform of that operator and the Wigner function. For a Gaussian state, it reads

$$W(R) = \frac{1}{\pi^2\sqrt{\det\gamma}} \exp\left(-R^{\mathrm{T}}\gamma^{-1}R\right) . \tag{3.23}$$

In the R/I partition, $\gamma^{\mathrm{R/I}}$ is given by Eq. (2.19), so

$$\left(\gamma^{\mathrm{R/I}}\right)^{-1} = \begin{pmatrix} \left(\gamma^{\mathrm{R}}\right)^{-1} & 0 \\ 0 & \left(\gamma^{\mathrm{I}}\right)^{-1} \end{pmatrix} \tag{3.24}$$

with

$$\left(\gamma^{\mathrm{R}}\right)^{-1} = \left(\gamma^{\mathrm{I}}\right)^{-1} = \begin{pmatrix} \cosh(2r_k) + \cos(2\varphi_k)\sinh(2r_k) & \sin(2\varphi_k)\sinh(2r_k) \\ \sin(2\varphi_k)\sinh(2r_k) & \cosh(2r_k) - \cos(2\varphi_k)\sinh(2r_k) \end{pmatrix} . \tag{3.25}$$

Since $(\gamma^{\mathrm{R/I}})^{-1}$ is block diagonal, the Wigner function factorises in that partition, i.e. $W(R) = W^{\mathrm{R}}(R^{\mathrm{R}})W^{\mathrm{I}}(R^{\mathrm{I}})$, where $R^s = (k^{1/2}v^s_{\boldsymbol{k}}, k^{-1/2}p^s_{\boldsymbol{k}})^{\mathrm{T}}$ with $s = \mathrm{R}, \mathrm{I}$. This translates the above remark that, in the R/I partition, the state is uncorrelated and separable.

Owing to the Gaussian nature of W^s, the contours of the Wigner function are ellipses in phase space, the geometrical parameters of which can be derived as follows. The quadratic form appearing in the argument of the exponential in the Wigner function can be diagonalised upon performing a phase-space rotation with angle φ_k

$$\widetilde{R}^s = \mathcal{R}(-\varphi_k)R^s = \begin{pmatrix} \cos\varphi_k & \sin\varphi_k \\ -\sin\varphi_k & \cos\varphi_k \end{pmatrix} R^s \,, \tag{3.26}$$

along which the covariance matrix becomes

$$(\widetilde{\gamma}^s)^{-1} = \mathcal{R}(-\varphi_k)(\gamma^s)^{-1}\mathcal{R}^{\mathrm{T}}(-\varphi_k) = \begin{pmatrix} e^{2r_k} & 0 \\ 0 & e^{-2r_k} \end{pmatrix} . \tag{3.27}$$

This implies that the semi-minor and the semi-major axes of the above-mentioned ellipses are tilted by the angle φ_k in phase space, and that for the $\sqrt{2}$-σ contour, their respective lengths are given by e^{r_k} and e^{-r_k}. Such an ellipse is displayed in Fig. 1, and fully describes the quantum state of the system. This leads to a simple interpretation of

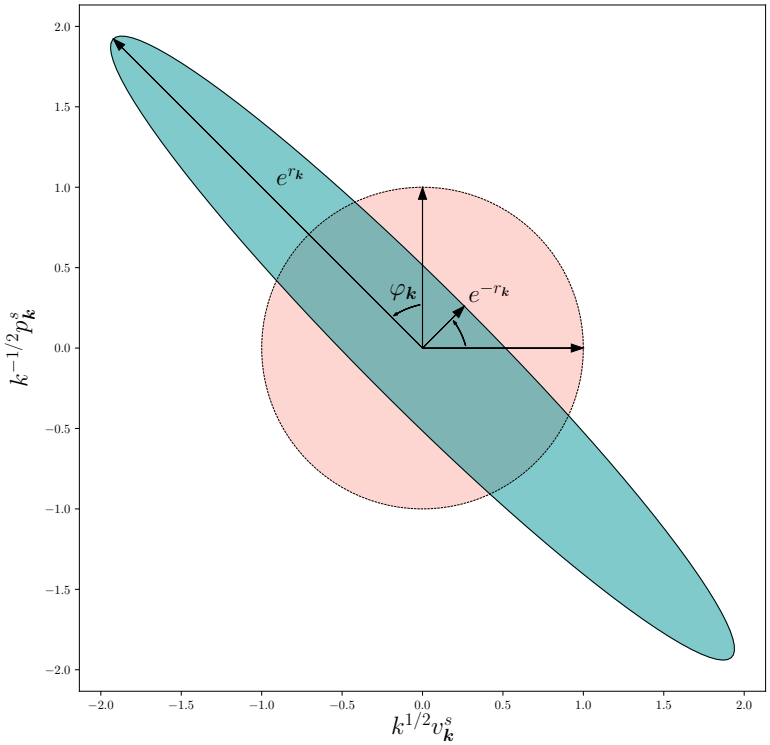

Figure 1. Phase space representation of the $\sqrt{2}$-σ contour level of the Wigner function W^s, for $\varphi_{\boldsymbol{k}} = \pi/4$, $r_{\boldsymbol{k}} = 1$ (green ellipse) compared to the pink circle corresponding to a vacuum state (coherent state) with vanishing squeezing.

the squeezing parameters: r_k controls the eccentricity of the Wigner-function contours, and φ_k its phase-space orientation.

Note that the area of the ellipse, which is proportional to the product between the semi-major and the semi-minor axes lengths, is a constant. This can be traced back to the fact that it is proportional to the determinant of the covariance matrix, which is a constant given that the time evolution is performed via a symplectic matrix in Eq. (3.6). Alternatively, it can also be seen as a consequence of Eq. (3.3). Since the determinant of the covariance matrix is related to the purity of the state via Eq. (2.26), it also simply translates the fact that the state remains pure if it does not couple to an environment.

3.3 Transport equations

The third method which allows us to follow the time evolution of the system is to establish the differential equations obeyed by the components of the covariance matrix, i.e. by the two-point functions of the system. In general, the quantum expectation value

of any operator $\hat{O}$ evolves according to the Heisenberg equation

$$\frac{\mathrm{d}\langle\hat{O}\rangle}{\mathrm{d}\tau} = \left\langle\frac{\partial\hat{O}}{\partial\tau}\right\rangle - i\left\langle\left[\hat{O},\hat{H}\right]\right\rangle. \tag{3.28}$$

For one-point correlation functions, using the Hamiltonian (2.7), this leads

$$\frac{\mathrm{d}\langle v^s_{\boldsymbol{k}}\rangle}{\mathrm{d}\tau} = \langle p^s_{\boldsymbol{k}}\rangle, \quad \frac{\mathrm{d}\langle p^s_{\boldsymbol{k}}\rangle}{\mathrm{d}\tau} = -\omega^2(k,\tau)\langle v^s_{\boldsymbol{k}}\rangle\,, \tag{3.29}$$

which is nothing but Ehrenfest's theorem. Combined together, these two equations lead to $\langle\hat{v}^s_{\boldsymbol{k}}\rangle'' + \omega^2(k,\tau)\langle\hat{v}^s_{\boldsymbol{k}}\rangle = 0$, which coincides with the equation satisfied by the combination $u_k + w_k^*$ of the Bogoliubov coefficients, see Eq. (3.4), and which is nothing but the classical equation of motion.

For two-point correlation functions, one has

$$\frac{\mathrm{d}}{\mathrm{d}\tau}\langle\hat{v}^s_{\boldsymbol{k}_1}\hat{v}^s_{\boldsymbol{k}_2}\rangle = \langle\hat{v}^s_{\boldsymbol{k}_1}\hat{p}^s_{\boldsymbol{k}_2} + \hat{p}^s_{\boldsymbol{k}_1}\hat{v}^s_{\boldsymbol{k}_2}\rangle, \tag{3.30}$$

$$\frac{\mathrm{d}}{\mathrm{d}\tau}\langle\hat{p}^s_{\boldsymbol{k}_1}\hat{v}^s_{\boldsymbol{k}_2}\rangle = \langle\hat{p}^s_{\boldsymbol{k}_1}\hat{p}^s_{\boldsymbol{k}_2}\rangle - \omega^2(k_1,\tau)\langle\hat{v}^s_{\boldsymbol{k}_1}\hat{v}^s_{\boldsymbol{k}_2}\rangle, \tag{3.31}$$

$$\frac{\mathrm{d}}{\mathrm{d}\tau}\langle\hat{v}^s_{\boldsymbol{k}_1}\hat{p}^s_{\boldsymbol{k}_2}\rangle = \langle\hat{p}^s_{\boldsymbol{k}_1}\hat{p}^s_{\boldsymbol{k}_2}\rangle - \omega^2(k_2,\tau)\langle\hat{v}^s_{\boldsymbol{k}_1}\hat{v}^s_{\boldsymbol{k}_2}\rangle, \tag{3.32}$$

$$\frac{\mathrm{d}}{\mathrm{d}\tau}\langle\hat{p}^s_{\boldsymbol{k}_1}\hat{p}^s_{\boldsymbol{k}_2}\rangle = -\omega^2(k_2,\tau)\langle\hat{p}^s_{\boldsymbol{k}_1}\hat{v}^s_{\boldsymbol{k}_2}\rangle - \omega^2(k_1,\tau)\langle\hat{v}^s_{\boldsymbol{k}_1}\hat{p}^s_{\boldsymbol{k}_2}\rangle, \tag{3.33}$$

where, as expected, the time derivative of correlators mixing R and I quantities vanish, i.e. $\mathrm{d}\langle R^s_i R^{\tilde{s}}_j\rangle/(\mathrm{d}\tau) \propto \delta(s-\tilde{s})$. Making use of Eqs. (2.20)-(2.22), this leads to the following differential system for the entries of the covariance matrix,

$$\frac{1}{k}\frac{\mathrm{d}\gamma_{11}}{\mathrm{d}\tau} = \gamma_{12} + \gamma_{21}, \tag{3.34}$$

$$\frac{1}{k}\frac{\mathrm{d}}{\mathrm{d}\tau}(\gamma_{12} + \gamma_{21}) = 2\gamma_{22} - 2\frac{\omega^2}{k^2}\gamma_{11}, \tag{3.35}$$

$$\frac{1}{k}\frac{\mathrm{d}\gamma_{22}}{\mathrm{d}\tau} = -\frac{\omega^2}{k^2}(\gamma_{12} + \gamma_{21}). \tag{3.36}$$

Let us recall that, as pointed out below Eq. (3.15), if the initial state is chosen to be the vacuum state, these equations must be solved with initial conditions $\gamma_{11}(\tau_{\rm in}) = \gamma_{22}(\tau_{\rm in}) = 1$ and $(\gamma_{12} + \gamma_{21})(\tau_{\rm in}) = 0$. One can check that, in agreement with the remark made at the end of Sec. 3.2, these equations imply that $\det\gamma^s = \gamma_{11}\gamma_{22} - \gamma_{12}\gamma_{21}$ is preserved in time. One may also note that the above three first-order differential equations lead to a single, third-order, differential equation for γ_{11}, namely

$$\frac{1}{k^3}\frac{\mathrm{d}^3\gamma_{11}}{\mathrm{d}\tau^3} + 4\frac{\omega^2}{k^2}\frac{1}{k}\frac{\mathrm{d}\gamma_{11}}{\mathrm{d}\tau} + \frac{2}{k}\frac{\mathrm{d}}{\mathrm{d}\tau}\left(\frac{\omega^2}{k^2}\right)\gamma_{11} = 0. \tag{3.37}$$

The order of that differential equation can however be reduced upon introducing the (complex) change of variable $\gamma_{11} = v_k v_k^*$. Indeed, one can show that Eq. (3.37) is satisfied

if $v_k'' + \omega^2 v_k = 0$. One recovers again the same second-order differential equation as the one satisfied by the combination of Bogoliubov coefficients $u_k + w_k^*$, see Eq. (3.4) [note that the initial conditions also match, i.e. the initial conditions give above for γ_{11}, γ_{12} and γ_{22} lead to $v_k(\tau_{\rm in}) = 1$ and $v_k'(\tau_{\rm in}) = -ik$], which also coincides with the classical equation of motion as pointed out above. This shows that the evolution of Gaussian quantum states can be entirely described by the dynamics of its classical counterpart, and that the three approaches introduced above to solve the dynamics are technically equivalent.

3.4 Quantum discord

As explained in Sec. 2.4, the computation of quantum discord boils down to the computation of the symplectic eigenvalue $\sigma(\theta)$. Setting $\theta = 0$ in Eq. (2.27) leads to $\sigma(0) = \sqrt{\det \gamma^s}$, so for a pure state, one has $\sigma(0) = 1$. Since Eq. (2.29) leads to $f(1) = 0$, the expression (2.28) for quantum discord reduces to

$$\mathcal{D} = f\left[\sigma(\theta)\right] . \tag{3.38}$$

The symplectic eigenvalue $\sigma(\theta)$ can be expressed in terms of the Bogoliubov coefficients by plugging Eq. (3.14) into Eq. (2.27), and one finds $\sigma(\theta) = \sqrt{1 + 4|u_k|^2|w_k|^2 \sin^2(2\theta)}$. Making use of Eq. (3.16), it can also be written in terms of the squeezing parameters as

$$\sigma(\theta) = \sqrt{1 + \sinh^2(2r_k)\sin^2(2\theta)} , \tag{3.39}$$

where only the squeezing amplitude r_k enters the expression. This shows that, when $\theta \neq 0$, the discord increases with the squeezing amplitude but does not depend on the squeezing angle. Let us also mention that, plugging Eq. (2.23) into Eq. (2.27), one obtains an expression that only involves the number of particles $\mathcal{N}_k$, namely

$$\sigma(\theta) = \sqrt{1 + 4\sin^2(2\theta)\mathcal{N}_k\left(\mathcal{N}_k + 1\right)} . \tag{3.40}$$

This shows that discord increases with the number of entangled particles created between the sectors $\boldsymbol{k}$ and $-\boldsymbol{k}$, as expected. This also indicates that discord is maximal when $\theta = -\pi/4$, i.e. in the partition $\pm\boldsymbol{k}$. These considerations are in agreement with the results found in Ref. [5].

4 Discord in the presence of an environment

In Sec. 3, we have described the evolution of the system and its quantum discord in the case where it is placed in a pure state, without interactions with environmental degrees of freedom. We now study how these considerations generalise to the situation where an environment is present and couples to the system. Formally, we write down the total Hamiltonian as the sum of a term acting on the system, $\hat{H}$, a term acting on the environment, $\hat{H}_{\rm env}$, and an interaction term, $\hat{H}_{\rm int}$,

$$\hat{H}_{\rm tot} = \hat{H} \otimes \hat{\mathbb{I}}_{\rm env} + \hat{\mathbb{I}} \otimes \hat{H}_{\rm env} + g\hat{H}_{\rm int}, \tag{4.1}$$

where g is a coupling constant that controls the interaction strength and we recall that $\hat{H}$ is given in Eq. (2.7). Our goal is to analyse the state of the system, which is described by the reduced density matrix

$$\hat{\rho} = \mathrm{Tr}_{\mathrm{env}}\left(\hat{\rho}_{\mathrm{tot}}\right) . \tag{4.2}$$

In practice, we assume that the interaction term is local, so it can be written as

$$\hat{H}_{\mathrm{int}}(\tau) = \int \mathrm{d}^3\boldsymbol{x}\, \hat{A}(\tau,\boldsymbol{x}) \otimes \hat{E}(\tau,\boldsymbol{x}), \tag{4.3}$$

where $\hat{A}$ is an operator acting in the Hilbert space of the system and $\hat{E}$ an operator acting in the Hilbert space of the environment.

4.1 Caldeira-Leggett model

Under the assumption that the auto-correlation time of $\hat{E}$ in the environment, which we denote τ_{c}, is much shorter than the time scale over which the system evolves, one can show that the reduced density matrix (4.2) obeys the Lindblad equation [15, 31–34]

$$\frac{\mathrm{d}\hat{\rho}}{\mathrm{d}\tau} = -i\left[\hat{H},\hat{\rho}\right] - \frac{\Gamma}{2}\int \mathrm{d}^3\boldsymbol{x}\,\mathrm{d}^3\boldsymbol{y}\, C_E(\tau;\boldsymbol{x},\boldsymbol{y})\left[\hat{A}(\boldsymbol{x}),\left[\hat{A}(\boldsymbol{y}),\hat{\rho}\right]\right], \tag{4.4}$$

where $C_E(\tau;\boldsymbol{x},\boldsymbol{y}) = \langle\hat{E}(\tau,\boldsymbol{x})\hat{E}(\tau,\boldsymbol{y})\rangle$ is the equal-time correlation function of $\hat{E}$, and $\Gamma \equiv 2g^2\tau_{\mathrm{c}}$. Let us note that the Lindblad equation generates all quantum dynamical semigroups [35], and that even though it is derived at leading order in g, it allows for efficient late-time re-summation [36].

Similarly to Eq. (3.28), the equation controlling the quantum expectation value of a given operator $\hat{O}$, namely $\langle\hat{O}\rangle = \mathrm{Tr}(\hat{\rho}\,\hat{O})$, can be obtained from the Lindblad equation, and one finds

$$\frac{\mathrm{d}\langle\hat{O}\rangle}{\mathrm{d}\tau} = \left\langle\frac{\partial\hat{O}}{\partial\tau}\right\rangle - i\left\langle\left[\hat{O},\hat{H}\right]\right\rangle \quad -\frac{\Gamma}{2}(2\pi)^{3/2}\int_{\mathbb{R}^3}\mathrm{d}^3\boldsymbol{k}\,\tilde{C}_E(\tau,\boldsymbol{k})\left\langle\left[\left[\hat{O},\hat{A}_{\boldsymbol{k}}\right],\hat{A}_{-\boldsymbol{k}}\right]\right\rangle, \tag{4.5}$$

where $\tilde{C}_E(\tau,\boldsymbol{k})$ is the Fourier transform of the correlation function [assuming statistical homogeneity, $C_E(\boldsymbol{x},\boldsymbol{y})$ depends only on $\boldsymbol{x}-\boldsymbol{y}$, so we mean the Fourier transform with respect to $\boldsymbol{x}-\boldsymbol{y}$].

These equations are difficult to solve in general, but they greatly simplify under the assumption that $\hat{A}$ is linear in the phase-space variables. The reason is that, in that case, all interactions involving the system are linear, so the state of the system remains Gaussian (although it becomes a mixed state). This allows one to still fully describe it in terms of a covariance matrix, and to generalise most of the considerations presented in Sec. 3. Such a setup is called the Caldeira-Leggett model [37–39], and in what follows we will use it to understand how decoherence may affect the presence of quantum discord within the system. For simplicity, we will consider the case where $\hat{A} = \hat{v}$, but the more generic situation where $\hat{A}$ is a linear combination of $\hat{v}$ and $\hat{p}$ can be dealt with along very similar lines, see Ref. [19].

4.2 Transport equations

Let us first follow the approach presented in Sec. 3.3 and derive transport equations from Eq. (4.5). For one-point correlation functions, one still obtains Eq. (3.29), i.e. the classical equations of motion. For two-point correlation functions, one finds

$$\frac{\mathrm{d}}{\mathrm{d}\tau}\langle\hat{v}^s_{\boldsymbol{k}_1}\hat{v}^s_{\boldsymbol{k}_2}\rangle = \langle\hat{v}^s_{\boldsymbol{k}_1}\hat{p}^s_{\boldsymbol{k}_2} + \hat{p}^s_{\boldsymbol{k}_1}\hat{v}^s_{\boldsymbol{k}_2}\rangle, \tag{4.6}$$

$$\frac{\mathrm{d}}{\mathrm{d}\tau}\langle\hat{p}^s_{\boldsymbol{k}_1}\hat{v}^s_{\boldsymbol{k}_2}\rangle = \langle\hat{p}^s_{\boldsymbol{k}_1}\hat{p}^s_{\boldsymbol{k}_2}\rangle - \omega^2(k_1,\tau)\langle\hat{v}^s_{\boldsymbol{k}_1}\hat{v}^s_{\boldsymbol{k}_2}\rangle, \tag{4.7}$$

$$\frac{\mathrm{d}}{\mathrm{d}\tau}\langle\hat{v}^s_{\boldsymbol{k}_1}\hat{p}^s_{\boldsymbol{k}_2}\rangle = \langle\hat{p}^s_{\boldsymbol{k}_1}\hat{p}^s_{\boldsymbol{k}_2}\rangle - \omega^2(k_2,\tau)\langle\hat{v}^s_{\boldsymbol{k}_1}\hat{v}^s_{\boldsymbol{k}_2}\rangle, \tag{4.8}$$

$$\frac{\mathrm{d}}{\mathrm{d}\tau}\langle\hat{p}^s_{\boldsymbol{k}_1}\hat{p}^s_{\boldsymbol{k}_2}\rangle = -\omega^2(k_2,\tau)\langle\hat{p}^s_{\boldsymbol{k}_1}\hat{v}^s_{\boldsymbol{k}_2}\rangle - \omega^2(k_1,\tau)\langle\hat{v}^s_{\boldsymbol{k}_1}\hat{p}^s_{\boldsymbol{k}_2}\rangle + \Gamma(2\pi)^{3/2}\tilde{C}_E(\tau,\boldsymbol{k}_1)\delta(\boldsymbol{k}_2-\boldsymbol{k}_1), \tag{4.9}$$

where correlators mixing R and I quantities still vanish, i.e. $\langle R^s_i R^{\tilde{s}}_j\rangle \propto \delta(s-\tilde{s})$. Compared to Eqs. (3.30)-(3.33), one can see that only the last equation gets modified, and receives an additional contribution proportional to Γ. Making use of Eqs. (2.20)-(2.22), this leads to the following differential system for the entries of the covariance matrix,

$$\frac{1}{k}\frac{\mathrm{d}\gamma_{11}}{\mathrm{d}\tau} = \gamma_{12}+\gamma_{21}, \tag{4.10}$$

$$\frac{1}{k}\frac{\mathrm{d}}{\mathrm{d}\tau}(\gamma_{12}+\gamma_{21}) = 2\gamma_{22} - 2\frac{\omega^2}{k^2}\gamma_{11}, \tag{4.11}$$

$$\frac{1}{k}\frac{\mathrm{d}\gamma_{22}}{\mathrm{d}\tau} = -\frac{\omega^2}{k^2}(\gamma_{12}+\gamma_{21}) + 2\Gamma(2\pi)^{3/2}\frac{\tilde{C}_E}{k^2}\,, \tag{4.12}$$

which should be compared with Eqs. (3.34)-(3.36). Let us recall that, under the assumption that the system is initially in the vacuum state, these equations should be solved with initial conditions $\gamma_{11}(\tau_{\rm in}) = 1$, $(\gamma_{12}+\gamma_{21})(\tau_{\rm in}) = 0$ and $\gamma_{22}(\tau_{\rm in}) = 1$.

Another important consequence of these transport equations is that they lead to the following evolution for $\det(\gamma^s) = \gamma_{11}\gamma_{22} - \gamma_{12}^2$:

$$\frac{\mathrm{d}}{\mathrm{d}\tau}\det\left(\gamma^s\right) = 2\Gamma\gamma_{11}(2\pi)^{3/2}\frac{\tilde{C}_E}{k}. \tag{4.13}$$

When $\Gamma = 0$, i.e. in the absence of an environment, one recovers the fact that this determinant is preserved, hence the system remains in a pure state. Otherwise, Eq. (4.13) indicates that the interaction with the environment induces decoherence of the system, since it makes the purity decrease away from one, see Eq. (2.26).

Finally, similarly to Eq. (3.37), one can derive a single, third-order differential equation for γ_{11}, which reads

$$\frac{1}{k^3}\frac{\mathrm{d}^3\gamma_{11}}{\mathrm{d}\tau^3} + 4\frac{\omega^2}{k^2}\frac{1}{k}\frac{\mathrm{d}\gamma_{11}}{\mathrm{d}\tau} + \frac{2}{k}\frac{\mathrm{d}}{\mathrm{d}\tau}\left(\frac{\omega^2}{k^2}\right)\gamma_{11} = 4\Gamma(2\pi)^{3/2}\frac{\tilde{C}_E}{k^2}\,. \tag{4.14}$$

As pointed out below Eq. (3.37), in the absence of a source term in the right-hand side, the solution to this equation reads $\gamma_{11} = v_k v_k^*$, where v_k satisfies the classical equation of motion $v_k'' + \omega^2 v_k = 0$. Using Green's function method, the solution in the presence of a source term is thus given by

$$\gamma_{11}(\tau) = v_k(\tau)v_k^*(\tau) - \frac{8k}{W^2}(2\pi)^{3/2}\int_{\tau_{\rm in}}^{\tau}\Gamma(\tau')\,\tilde{C}_E(\tau',k)\,\Im\mathrm{m}^{\,2}\left[v_k(\tau)v_k^*(\tau')\right]\mathrm{d}\tau', \tag{4.15}$$

where $W \equiv v_k v_k^{*\prime} - v_k^* v_k'$ is the Wronksian of the v_k mode function. Given the equation of motion that v_k satisfies, one can readily show that W is preserved in time. It can therefore be evaluated at initial time, where the initial conditions derived for v_k below Eq. (3.37) lead to $W = 2ik$. Using Eqs. (4.10) and (4.11) again, one thus obtains the following expressions for the entries of the covariance matrix,

$$\gamma_{11} = |v_k|^2 + \mathcal{I}_k, \qquad \gamma_{12} = \frac{\Re\mathrm{e}\,(v_k v_k^{*\prime})}{k} + \mathcal{J}_k, \qquad \gamma_{22} = \frac{|v_k'|^2}{k^2} + \mathcal{K}_k\,, \tag{4.16}$$

where

$$\mathcal{I}_k(\tau) = \frac{2}{k}(2\pi)^{3/2}\int_{\tau_{\rm in}}^{\tau}\Gamma(\tau')\,\tilde{C}_E(\tau',k)\,\Im\mathrm{m}^{\,2}\left[v_k(\tau')v_k^*(\tau)\right]\mathrm{d}\tau'\,, \tag{4.17}$$

$$\mathcal{J}_k(\tau) = \frac{2}{k^2}(2\pi)^{3/2}\int_{\tau_{\rm in}}^{\tau}\Gamma(\tau')\,\tilde{C}_E(\tau',k)\,\Im\mathrm{m}\left[v_k(\tau')v_k^*(\tau)\right]\Im\mathrm{m}\left[v_k(\tau')v_k^{*\prime}(\tau)\right]\mathrm{d}\tau'\,, \tag{4.18}$$

$$\mathcal{K}_k(\tau) = \frac{2}{k^3}(2\pi)^{3/2}\int_{\tau_{\rm in}}^{\tau}\Gamma(\tau')\,\tilde{C}_E(\tau',k)\Im\mathrm{m}^{\,2}\left[v_k(\tau')v_k^{*\prime}(\tau)\right]\mathrm{d}\tau'\,. \tag{4.19}$$

These formula provide an explicit expression for the covariance matrix, hence for the full quantum state of the reduced system.

4.3 Generalised squeezing parameters

We now follow the approach presented in Sec. 3.2 where the quantum state of the system is described in terms of squeezing parameters. Note that the Bogoliubov coefficients introduced in Sec. 3.1 cannot be directly generalised to the case where an environment is present, since they are related to the unitary evolution of the system. Therefore, one cannot use Eq. (3.16) to define squeezing parameters in the present situation. However, the geometrical interpretation developed around Fig. 1 can still be used to introduce generalised squeezing parameters. This will be particularly useful to understand the state purity, and quantum discord, from a phase-space geometrical perspective.

In the Caldeira-Leggett model indeed, the state is still described by a covariance matrix, that can still be diagonalised as in Eq. (3.27). The only difference is that, as mentioned around Eq. (4.13), the determinant of the covariance matrix does not remain equal to one. This introduces a new "squeezing parameter", denoted $\lambda_k \equiv \det(\gamma^s)$, such that Eq. (3.27) becomes

$$(\tilde{\gamma}^s)^{-1} = \lambda_k^{-1/2}\begin{pmatrix} e^{2r_k} & 0 \\ 0 & e^{-2r_k}\end{pmatrix}. \tag{4.20}$$

Performing the phase-space rotation of angle φ_k introduced in Eq. (3.27), this leads to the following expression for the covariance matrix in the R/I partition,

$$\gamma^s = \sqrt{\lambda_k} \begin{pmatrix} \cosh(2r_k) - \cos(2\varphi_k)\sinh(2r_k) & -\sin(2\varphi_k)\sinh(2r_k) \\ -\sin(2\varphi_k)\sinh(2r_k) & \cosh(2r_k) + \cos(2\varphi_k)\sinh(2r_k) \end{pmatrix}, \quad (4.21)$$

which generalises Eqs. (3.20)-(3.22). This shows that, in the Caldeira-Leggett model, the quantum state of the system can still be described with an ellipse in phase space, where r_k describes the eccentricity of the ellipse, φ_k its orientation, and λ_k its area (which is given by $\pi\lambda_k$).

Note that equations of motion for the generalised squeezing parameters r_k, φ_k and λ_k can also be derived, by plugging Eq. (4.21) into Eqs. (4.10)-(4.12). This leads to

$$\frac{\mathrm{d}\lambda_k}{\mathrm{d}\tau} = 2\Gamma(2\pi)^{3/2}\frac{\tilde{C}_E}{k}\lambda_k^{1/2}\left[\cosh(2r_k) - \cos(2\varphi_k)\sinh(2r_k)\right], \quad (4.22)$$

$$\frac{\mathrm{d}r_k}{\mathrm{d}\tau} = \frac{k}{2}\left(\frac{\omega^2}{k^2} - 1\right)\sin(2\varphi_k) - \frac{\Gamma}{\sqrt{\lambda_k}}\frac{(2\pi)^{3/2}}{2}\frac{\tilde{C}_E}{k}\left[\sinh(2r_k) - \cos(2\varphi_k)\cosh(2r_k)\right], \quad (4.23)$$

$$\frac{\mathrm{d}\varphi_k}{\mathrm{d}\tau} = -\frac{k}{2}\left(\frac{\omega^2}{k^2} + 1\right) + \frac{k}{2}\left(\frac{\omega^2}{k^2} - 1\right)\frac{\cos(2\varphi_k)}{\tanh(2r_k)} - \Gamma\frac{\sin(2\varphi_k)}{2\sinh(2r_k)\sqrt{\lambda_k}}(2\pi)^{3/2}\frac{\tilde{C}_E}{k}. \quad (4.24)$$

One can check that, in the limit $\Gamma \to 0$, Eqs. (3.17) are recovered, and that Eq. (4.22) is essentially a rewriting of Eq. (4.13) for the non-conservation of the determinant.

4.4 Quantum discord

Let us now turn to the main goal of this article, namely the calculation of the quantum discord in the presence of an environment. As explained in Sec. 2.4, a single quantity needs to be computed, namely $\sigma(\theta)$ given in Eq. (2.27), which in terms of the generalised squeezing parameters reads

$$\sigma(\theta) = \lambda_k^{1/2}\sqrt{1 + \sinh^2(2r_k)\sin^2(2\theta)}. \quad (4.25)$$

Plugging this expression into Eq. (2.28), one obtains an explicit formula for quantum discord in terms of three parameters only: the squeezing amplitude r_k, the state purity $\mathrm{Tr}(\hat{\rho}^2) = 1/\lambda_k$, and the partition angle θ. This formula is displayed in Fig. 2 for $\theta = -\pi/4$ (left panel, corresponding to the $\pm\boldsymbol{k}$ partition) and $\theta = 0.1$ (right panel). One can see that, as the squeezing amplitude increases, quantum discord increases, as in the case where no environment was present. When the state purity decreases, quantum discord decreases, which means that interactions with an environment tend to reduce the amount of quantum correlations. This is in agreement with the common lore that decoherence is associated with the emergence of classical properties. One can also check that quantum discord increases with the partition angle as it varies between 0 and $\pi/4$, i.e. as it interpolates between the R/I partition which is separable (hence uncorrelated) and the $\pm\boldsymbol{k}$ partition where it is maximally correlated and discordant.

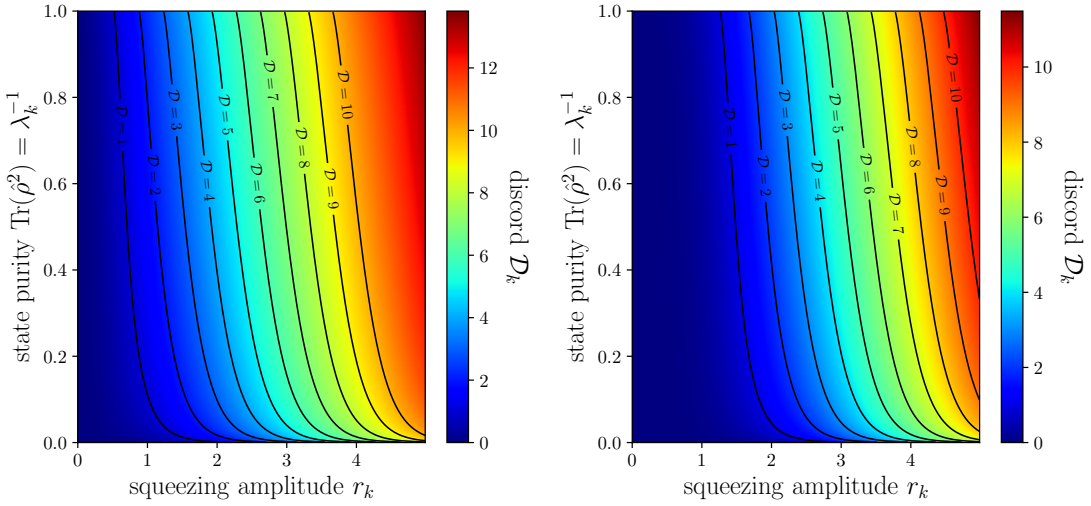

Figure 2. Quantum discord $\mathcal{D}_k$ in terms of the generalised squeezing amplitude r_k and the state purity $\mathrm{Tr}(\hat{\rho}^2) = 1/\lambda_k$, for $\theta = -\pi/4$ (left panel) and $\theta = 0.1$ (right panel). The black solid lines show a few contour lines of $\mathcal{D}_k$.

In order to gain more analytical insight in the behaviour of quantum discord, let us consider the large-squeezing limit $r_k \gg 1$ (this limit is particularly relevant to the cosmological setting considered in Sec. 5). From Eq. (2.28), it is clear that different behaviours are obtained depending on whether $\sigma(\theta)/\sigma^2(0)$ is small or large. In the large-squeezing limit, this ratio is given by

$$\frac{\sigma(\theta)}{\sigma^2(0)} \simeq \lambda_k^{-1/2} e^{2r_k} \frac{|\sin(2\theta)|}{2} \,. \tag{4.26}$$

In general, as the time evolution proceeds, r_k increases (denoting particle creation) and λ_k increases too (as an effect of decoherence). The two effects therefore compete in Eq. (4.26), and whether the ratio $\sigma(\theta)/\sigma^2(0)$ is small or large depends on the details of the dynamics. Expanding Eq. (2.28) in these two limits, one obtains

$$\mathcal{D}_k \simeq \begin{cases} \dfrac{2r_k}{\ln 2} & \text{if} \quad e^{2r_k}\,|\sin(2\theta)| \gg \sqrt{\lambda_k} \\ \lambda_k^{-1/2} e^{2r_k} \dfrac{|\sin(2\theta)|}{2\ln 2} & \text{if} \quad e^{2r_k}\,|\sin(2\theta)| \ll \sqrt{\lambda_k} \end{cases} \,. \tag{4.27}$$

This shows that quantum discord is large in the first case and small in the second case. As a consequence, whether quantum discord is large or small depends on which of squeezing or decoherence wins in the ratio (4.26). This provides a simple criterion for assessing when decoherence substantially reduces the amount of quantum correlations, namely it happens when

$$\mathrm{Tr}(\hat{\rho}^2) \ll e^{-4r_k} \,. \tag{4.28}$$

A useful geometrical interpretation of Eq. (4.26) is that, according to Eq. (4.20), the combination $\sqrt{\lambda_k}e^{-2r}$ happens to be the length of the semi-minor axis of the phase-space ellipse. The semi-minor axis increases as an effect of decoherence, which increases the overall area of the ellipse, and decreases because of quantum squeezing: this competition determines whether the semi-minor axis increases or decreases, hence it determines the fate of quantum discord.

Finally, in the same way as we have introduced generalised squeezing parameters, one can extend the definition of the number of particles $\mathcal{N}_k$ and the correlation $\mathcal{C}_k$, by plugging Eq. (4.21) into Eqs. (2.23)-(2.25), leading to

$$2\mathcal{N}_k + 1 = \sqrt{\lambda_k}\cosh(2r_k) \ , \quad 2\mathcal{C}_k = -\sqrt{\lambda_k}e^{i2\varphi_k}\sinh(2r_k) \ . \tag{4.29}$$

In terms of these parameters, one has $\sigma(\theta) = \sqrt{4(\mathcal{N}_k + 1/2)^2 - 4|\mathcal{C}_k|^2\cos^2(2\theta)}$, which allows one to express quantum discord as a function of $\mathcal{N}_k$ and $|\mathcal{C}_k|$ only.

5 Application : Cosmological perturbations

In this section, we apply the formalism developed so far to the case of cosmological perturbations. The goal is twofold. First, this will allow us to exemplify in a concrete situation how the tools introduced above work in practice. Second, as explained in Sec. 1, the presence of quantum correlations in the primordial field of cosmological perturbations, and how decoherence might partly remove them, is of great importance regarding our understanding of the origin of cosmic structures as emerging from a quantum-mechanical mechanism, and for our ability to test this aspect of the cosmological scenario.

When the universe is dominated by a single scalar-field, there is a single scalar gauge-invariant perturbation known as the Mukhanov-Sasaki variable [2, 40]. If time is parameterised by conformal time η,[3] which is related to cosmic time t by $\mathrm{d}t = a\mathrm{d}\eta$, where a is the Friedman-Lemaître-Robertson-Walker scale factor, then the Hamiltonian for the Mukhanov-Sasaki variable v is by Eq. (2.7) where

$$\omega^2(k,\eta) = k^2 - \frac{\left(a\sqrt{\epsilon_1}\right)''}{a\sqrt{\epsilon_1}} \ . \tag{5.1}$$

In this expression, a prime denotes derivation with respect to η, $\epsilon_1 = 1 - \mathcal{H}'/\mathcal{H}^2$ is the first slow-roll parameter and $\mathcal{H} = a'/a$.

In practice, we will consider the case of a de-Sitter expansion where $a(\eta) = -1/(H\eta)$ with H the Hubble parameter, since cosmological observations indicate that it is a good proxy for the dynamics of the universe expansion during the inflationary phase. In that case, $\omega^2 = k^2 - 2/\eta^2$, where η varies between $-\infty$ to 0.

[3] So far the time variable was left unspecified and denoted with the generic variable "τ". The above considerations can thus be applied to any time variable, provided the Hamiltonian is adapted accordingly. In what follows, we therefore make the identification $\tau = \eta$ and $' = \partial/\partial\eta$.

5.1 Inflationary perturbations in the absence of an environment

Following the approach presented in Sec. 3.1, let us first derive the Bogoliubov coefficients. The solution of the equation of motion (3.4) satisfied by $v_k = u_k + w_k^*$, i.e. $v_k'' + \omega^2 v_k = 0$, is given by

$$v_k(\eta) = \left(1 - \frac{i}{k\eta}\right) e^{-ik\eta}, \tag{5.2}$$

where we have made use of the initial conditions derived for v_k below Eq. (3.37), namely $v_k(\eta_{\rm in}) = 1$ and $v_k'(\eta_{\rm in}) = -ik$, at initial time $\eta_{\rm in}$ set to the infinite past, $\eta_{\rm in} = -\infty$. As explained below Eq. (3.5), this allows one to derive both Bogoliubov coefficients, and one finds

$$u_k = \left(1 - \frac{i}{k\eta} - \frac{1}{2k^2\eta^2}\right) e^{-ik\eta}, \qquad w_k^* = \frac{1}{2k^2\eta^2} e^{-ik\eta}. \tag{5.3}$$

One can easily check that these solutions satisfy Eq. (3.3), i.e. $|u_k|^2 - |w_k|^2 = 1$. Using Eq. (3.14), one can then calculate the covariance-matrix element and one obtains

$$\gamma_{11}(\eta) = 1 + \frac{1}{k^2\eta^2}, \qquad \gamma_{12}(\eta) = -\frac{1}{k^3\eta^3}, \qquad \gamma_{22}(\eta) = 1 - \frac{1}{k^2\eta^2} + \frac{1}{k^4\eta^4}. \tag{5.4}$$

As a consistency check, one can verify that these expressions are solutions of the differential system (3.34)-(3.36), and that they satisfy the initial conditions that were given for it. Finally, the squeezing parameters can be derived from Eqs. (3.20)-(3.22), which lead to

$$\cosh^2(r_k) = 1 + \frac{1}{4(k\eta)^4}, \quad \tan(2\varphi_k) = \frac{2k\eta}{1 - 2k^2\eta^2}. \tag{5.5}$$

These expressions can be inverted, and one finds[4]

$$r_k(\eta) = \frac{1}{2}\text{arccosh}\left[1 + \frac{1}{2(k\eta)^4}\right], \tag{5.6}$$

$$\varphi_k = \frac{1}{2}\arctan\left(\frac{2k\eta}{1 - 2k^2\eta^2}\right) - \frac{\pi}{2}\text{H}\left(-k\eta - \frac{1}{\sqrt{2}}\right) + \ell\pi, \tag{5.7}$$

where ℓ is an integer number and H is the Heaviside step function defined as $\text{H}(x) = 1$ when $x > 0$ and 0 otherwise. One can see that the squeezing amplitude increases as inflation proceeds, and at late time (i.e. when the wavelength of the mode under consideration is much larger than the Hubble radius, $k \ll \mathcal{H} = -1/\eta$), $r_k \simeq -2\ln(-k\eta) = 2\ln[a/a(k)]$. In this expression, $a(k)$ denotes the value of the scale factor when k crosses out the

[4]The inversion for φ_k should be done noting that from Eq. (3.17) and the fact that r_k grows during inflation, one has $\sin(2\varphi_k) < 0$. Moreover, Eq. (5.5) implies that $\tan(2\varphi_k) > 0$ if $k\eta < -1/\sqrt{2}$ and $\tan(2\varphi_k) < 0$ if $-1/\sqrt{2} < k\eta < 0$. This implies that $2\varphi_k \in [-\pi, -\pi/2]$ when $k\eta < -1/\sqrt{2}$, and that $2\varphi_k \in [-\pi/2, 0]$ when $k\eta < -1/\sqrt{2}$ (modulo 2π). The Heaviside function in Eq. (5.7) ensures that φ_k is continuous when $k\eta = -1/\sqrt{2}$.

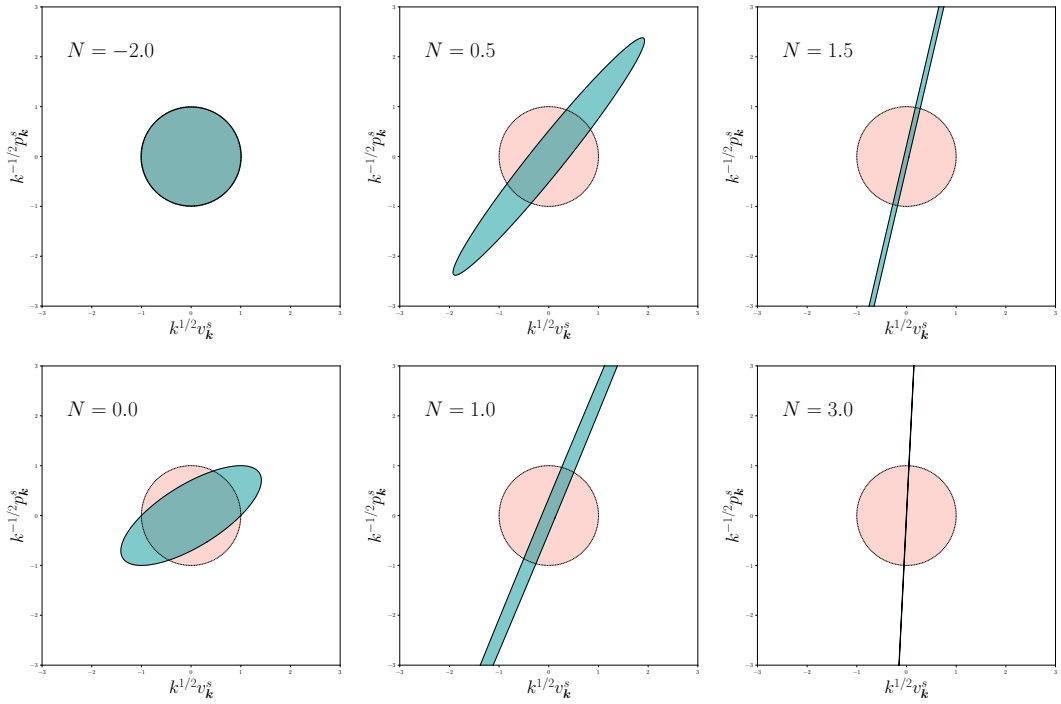

Figure 3. Phase-space ellipse in the plane $(k^{1/2}v^s_{\boldsymbol{k}}, k^{-1/2}p^s_{\boldsymbol{k}})$ (see the discussion around Fig. 1) at different instants during inflation, labelled by $N = \ln[a/a(k)]$, i.e. the number of e-folds measured from the Hubble-crossing time of the mode under consideration. On sub-Hubble scales, the ellipse remains a circle, while it gets squeezed and rotates in the super-Hubble regime.

Hubble scale, i.e. when $k\eta = -1$. For the modes observed in the cosmic microwave background, $\ln[a/a(k)] \simeq 50$ at the end of inflation, hence the squeezing amplitude is of order 100. The squeezing angle starts out from $\varphi_k = -\pi/2$ in the asymptotic past and approaches 0 at late time, where $\varphi_k \simeq k\eta \simeq -a(k)/a \simeq -e^{-r_k/2}$ [here we set $\ell = 0$ in Eq. (5.7)]. The evolution of the squeezing parameters is displayed at the level of the phase-space ellipse in Fig. 3. While the mode under consideration remains in the vacuum state, i.e. on sub-Hubble scales when $a \ll a(k)$, the squeezing amplitude is small and the ellipse is close to a circle. When the mode crosses out the Hubble radius, the ellipse gets squeezed ($r_k > 0$) and rotates. In the asymptotic future, it gets infinitely squeezed and its semi-minor axis becomes aligned with the horizontal axis ($\varphi_k \to 0$, in agreement with Fig. 1).

Regarding quantum discord, plugging Eq. (5.6) into Eq. (3.39) leads to

$$\sigma(\theta) = \sqrt{1 + \frac{1}{k^4\eta^4}\left(1 + \frac{1}{4k^4\eta^4}\right)\sin^2(2\theta)}\,, \tag{5.8}$$

which together with Eq. (3.38) leads to an explicit expression for quantum discord. In the super-Hubble regime, i.e. at late time when the squeezing amplitude is large, it can

be expanded according to

$$\mathcal{D}_k \simeq \log_2\left(\frac{|\sin(2\theta)|}{4k^4\eta^4}\right) + \frac{1}{\ln 2} \sim \frac{4}{\ln 2}\ln\left[\frac{a}{a(k)}\right] . \tag{5.9}$$

Recalling that modes of astrophysical interest are such that $r_k \sim 50$ at the end of inflation, their discord is of order 300, which makes the cosmic microwave background an extremely discordant state by laboratory-experiment standard [5].

5.2 Inflationary perturbations in the presence of an environment

Let us now generalise the above considerations to the case where cosmological perturbations interact with environmental degrees of freedom. In practice, we will use the Caldeira-Leggett model and the approach laid out in Sec. 4. Note that this framework relies on the assumption that interactions are linear in the system's variables, which is indeed the case at leading order in cosmological perturbation theory. In principle, higher-order coupling terms may also be present, which would lead to non-Gaussian states. While Lindblad equations can still be derived in that case, and the environmental imprint on the power spectrum and higher-order correlation functions can be investigated, see Refs. [19, 20], this does not allow for a straightforward calculation of quantum discord. Nevertheless, these effects are parametrically suppressed by the amplitude of primordial fluctuations, which are constrained to be small, so they can be safely neglected as a first approximation.

In practice, the relevant environmental degrees of freedom during inflation can be additional fields, (since most physical setups that have been proposed to embed inflation contain extra fields), to which the inflaton couples at least gravitationally. Because of the non-linearities of General Relativity, unobserved scales also couple to the ones of observable interest, and they may constitute another "environment". The advantage of the present formalism is that the microphysical details of the environment do not need to be further specified.

The calculation of the integrals derived in Eqs. (4.17), (4.18) and (4.19) require to specify the function $\tilde{C}_E(k)$, i.e. the Fourier transform of the equal-time environment correlator $C_E(\boldsymbol{x}-\boldsymbol{y})$. In practice, we will consider that the environment is correlated on length scales ℓ_E, i.e. that $C_E(\boldsymbol{x}-\boldsymbol{y})$ is suppressed when $a|\boldsymbol{x}-\boldsymbol{y}| \gg \ell_E$ (here $\boldsymbol{x}$ and $\boldsymbol{y}$ are comoving coordinates, which explains why the scale factor has been introduced). This implies that the Fourier transform $\tilde{C}_E(k)$ is suppressed at scales $k \ll a/\ell_E$, which in practice we model via a simple Heaviside function

$$\Gamma\tilde{C}_E(k) = (2\pi)^{-3/2}k_\Gamma^2\left(\frac{a}{a_*}\right)^{p-3}\mathrm{H}\left(1-\frac{k\ell_E}{a}\right). \tag{5.10}$$

In this expression, k_Γ sets the strength of the environmental effects and has the same dimension as a comoving wavenumber, hence the notation [the prefactor $(2\pi)^{-3/2}$ is introduced for later convenience, and in order to match the notations of Refs. [19, 20]]. The possible time dependence of Γ is accounted for in the factor $(a/a_*)^{p-3}$, where a_* denotes the scale factor at some reference time, i.e. we assume that $\Gamma\tilde{C}_E$ evolves as a

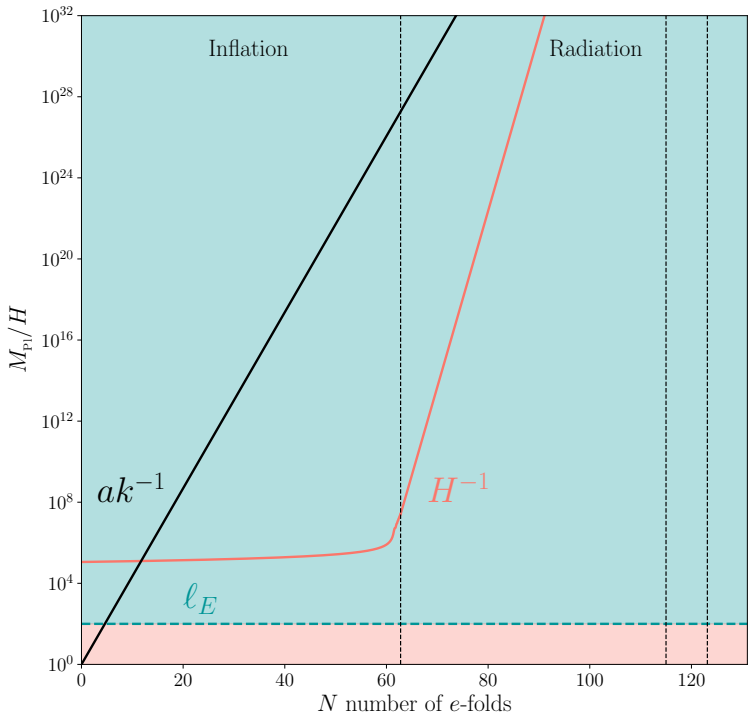

Figure 4. Schematic representation of the evolution of the different physical scales. a/k (black) represents the physical wavelength of the mode $\boldsymbol{k}$ under consideration. When a/k crosses ℓ_E (green dashed), the coherence length of the environment, decoherence starts to be effective. When a/k crosses out H^{-1} (pink), the Hubble radius, the perturbation starts to be amplified.

power of the scale factor. The model has therefore two free parameters, namely k_Γ and p.

In realistic situations, one may want to consider smoother kernels than Heaviside functions, but this only slightly affects the boundary terms in the integrals of Eqs. (4.17), (4.18) and (4.19) and does not lead to substantial modifications of the following considerations. In practice, Eq. (5.10) indicates that small-scales fluctuations are immune to environmental effects (which, conveniently, leave the vacuum state unaffected at early time). The effect of the interaction with the environment becomes relevant when the mode under consideration crosses out the correlation length ℓ_E. In practice, if the environment is comprised of heavy (i.e. with respect to the Hubble scale) degrees of freedom, one has $\ell_E < a/\mathcal{H}$, hence a given mode first crosses the environment correlation length before crossing the Hubble radius. The situation is depicted in Fig. 4.

5.2.1 Covariance matrix

With the ansatz (5.10), the integrals appearing in Eqs. (4.17), (4.18) and (4.19) can be performed exactly, and a detailed calculation is presented in Appendix D. In the

late-time limit, i.e. on super-Hubble scales, $-k\eta \to 0$, they can be approximated by

$$\gamma_{11} \simeq \frac{1}{(-k\eta)^2}\left\{1-2\left(\frac{k_\Gamma}{k}\right)^2\left[B_{11}\left(\frac{k}{k_*},p,\ell_E H\right)+A_{11}\left(\frac{k}{k_*},p\right)(-k\eta)^{8-p}\right]\right\}, \tag{5.11}$$

$$\gamma_{12} \simeq \frac{1}{(-k\eta)^3}\left\{1-2\left(\frac{k_\Gamma}{k}\right)^2\left[B_{12}\left(\frac{k}{k_*},p,\ell_E H\right)+A_{12}\left(\frac{k}{k_*},p\right)(-k\eta)^{8-p}\right]\right\}, \tag{5.12}$$

$$\gamma_{22} \simeq \frac{1}{(-k\eta)^4}\left\{1-2\left(\frac{k_\Gamma}{k}\right)^2\left[B_{22}\left(\frac{k}{k_*},p,\ell_E H\right)+A_{22}\left(\frac{k}{k_*},p\right)(-k\eta)^{8-p}\right]\right\}, \tag{5.13}$$

see Eqs. (D.38), (D.42) and (D.46), where k_* denotes the comoving scale that crosses out the Hubble radius at the reference time η_*. One can check that, in the limit $k_\Gamma \to 0$, one recovers the covariance matrix calculated in the absence of an environment, namely Eqs. (5.4). The coefficients A_{11}, B_{11}, A_{12}, B_{12}, A_{22} and B_{22} are functions of the parameters p and $\ell_E H$ and their explicit expressions can be found in Appendix D.

Let us note that the expression for γ_{11} is of observational interest as it gives the relative correction to the power spectrum of the Mukhanov-Sasaki variable, see Eq. (2.20), or of any quantity proportional to the Mukhanov-Sasaki variable such as the curvature perturbation ζ that is measured on the cosmic microwave background. Upon expanding the expression given for B_{11} in Appendix D in the regime $\ell_E H \ll 1$, one obtains

$$\begin{aligned} B_{11} \simeq \frac{1}{2}\left(\frac{k}{k_*}\right)^{p-3}\Bigg(&\frac{(\ell_E H)^{p-4}}{p-4}\left\{1-\frac{p-4}{2}(\ell_E H)\sin\left(\frac{2}{\ell_E H}\right)+\mathcal{O}\left[(\ell_E H)^2\right]\right\} \\ &-\frac{(p-3)(p-6)}{2^{4-p}}\Gamma(2-p)\cos\left(\frac{\pi}{2}p\right)\Bigg). \end{aligned} \tag{5.14}$$

It is interesting to notice that, at next-to-leading order, this expression contains non-analytical terms. However, it is likely that this non-analytical behaviour would be smoothed out if a non-sharp window function were used. On the other hand, we also have $A_{11} = -2(k/k_*)^{p-3}/[(p-8)(p-5)(p-2)]$, see Eq. (D.31). Which term dominates in B_{11} depends on the relative position of p with respect to 4, while which of the corrections in Eq. (5.11) dominates depends on whether $p < 8$ or $p > 8$. There are therefore three cases to distinguish, and one finds

$$\frac{\Delta\mathcal{P}_\zeta}{\mathcal{P}_\zeta} \simeq \begin{cases} \dfrac{(\ell_E H)^{p-4}}{4-p}\left(\dfrac{k_\Gamma}{k_*}\right)^2\left(\dfrac{k}{k_*}\right)^{p-5} & \text{if} \quad p<4, \\ 2^{p-4}(3-p)(6-p)\Gamma(2-p)\cos\left(\dfrac{\pi p}{2}\right)\left(\dfrac{k_\Gamma}{k_*}\right)^2\left(\dfrac{k}{k_*}\right)^{p-5} & \text{if} \quad 4<p<8, \\ \dfrac{4}{(p-8)(p-5)(p-2)}\left(\dfrac{k_\Gamma}{k_*}\right)^2\left(\dfrac{k}{k_*}\right)^3\left(\dfrac{\eta}{\eta_*}\right)^{8-p} & \text{if} \quad p>8. \end{cases} \tag{5.15}$$

One can check that these expressions coincide with the result obtained in Ref. [19].[5] In particular, when $p < 8$, the correction to the power spectrum freezes on large scale and is scale invariant when $p = 5$, while it continues to increase on large scales for $p > 8$. These formulas allow one to set upper bound on Γ such that the modifications to observables remain negligible, see the white dotted line in Fig. 6 below.

5.2.2 State purity

Endowed with the above expressions of the components γ_{11}, γ_{12} and γ_{22} of the covariance matrix, we are now in a position to calculate $\sigma(0)$ and the state purity. However, upon evaluating $\sigma(0)$ by plugging Eqs. (5.11)-(5.13) into Eq. (2.27), one can see that the terms controlled by k_Γ all cancel out when $\theta = 0$, which implies that Eqs. (5.11)-(5.13) must be expanded to higher order in order to get the first correction to $\sigma(0)$. Before following that route, let us note that such an expansion can be avoided by using Eq. (4.13) directly. The right hand side of this equation is proportional to k_Γ^2, so it is enough to evaluate it by using the solution (5.4) for γ_{11} in the free theory, which leads to

$$\sigma^2(0) = \det\gamma^s \simeq 1 - 2\left(\frac{k_\Gamma}{k_*}\right)^2\left(\frac{k}{k_*}\right)^{p-5}\int_{1/(\ell_E H)}^{-k\eta}\left(y^{3-p} + y^{1-p}\right)\mathrm{d}y, \tag{5.16}$$

namely

$$\sigma^2(0) \simeq 1 + 2\left(\frac{k_\Gamma}{k_*}\right)^2\left(\frac{k}{k_*}\right)^{p-5}\left[\frac{1}{p-2}\left(\frac{k}{k_*}\right)^{2-p}\left(\frac{a_*}{a}\right)^{2-p} - \frac{(\ell_E H)^{p-4}}{p-4}\right], \tag{5.17}$$

where we have kept the leading terms in $\ell_E H$ and in $-k\eta$ only. This again coincides with the result found in Ref. [19], see Eq. (4.6) of that reference, and it implies that decoherence occurs at the pivot scale k_* when

$$\frac{k_\Gamma}{k_*} \gg \begin{cases} (\ell_E H)^{2-\frac{p}{2}} & \text{if} \quad p < 2, \\ \left(\dfrac{a}{a_*}\right)^{1-\frac{p}{2}} & \text{if} \quad p > 2, \end{cases} \tag{5.18}$$

where we recall that the state purity is related to $\sigma(0)$ via Eq. (2.26). This domain is delineated by the white dashed line in Fig. 6.

Before moving on and addressing the calculation of quantum discord, let us note that the above result can be recovered from a higher-order expansion of the covariance matrix. This is done in detail in Appendix D, see Eqs. (D.30), (D.40) and (D.44). This leads to expressions for γ_{11}, γ_{12} and γ_{22} which, compared to Eqs. (5.11), (5.12) and (5.13), contain extra coefficients (i.e. beyond A_{11}, B_{11}, A_{12}, B_{12}, A_{22} and B_{22}), namely C_{11}, D_{11}, ..., C_{12}, D_{12}, ...and C_{22}, D_{22}, ..., the explicit expressions of which are given

[5] More precisely, they should be compared to Eqs. (3.35), (3.32) and (3.29) of that reference (when setting $\epsilon_{1*} = 0$ and $\nu = 3/2$ in those expressions), to which they agree up to a factor 2 that corresponds to a factor 2 difference in the definition of Γ.

in Appendix D. Of course, these coefficients are also functions of the parameters p and $\ell_E H$. Plugging the result into Eq. (2.27), one obtains that, on super-Hubble scales,

$$\begin{aligned}\sigma^2(0) = {} & \Sigma_{-6}\,(-k\eta)^{-6} + \Sigma_{-5}\,(-k\eta)^{-5} + \Sigma_{-4}\,(-k\eta)^{-4} + \Sigma_{-3}\,(-k\eta)^{-3} + \Sigma_{-2}\,(-k\eta)^{-2} \\ & + \Sigma_{-1}\,(-k\eta)^{-1} + 1 + \Sigma_0 + \Sigma_1\,(-k\eta) + \cdots + \Sigma_{2-p}\,(-k\eta)^{2-p} + \Sigma_{4-p}\,(-k\eta)^{4-p} \\ & + \Sigma_{5-p}\,(-k\eta)^{5-p} + \cdots\,. \end{aligned} \tag{5.19}$$

Each coefficient Σ_i is a combination of the coefficients A_{11}, B_{11}, ..., A_{12}, B_{12}, ... and A_{22}, B_{22} .... As a consequence, the Σ_i's are also functions of the parameters p and $\ell_E H$ and are proportional to k_Γ^2 or k_Γ^4, which guarantees that, without an environment (i.e. when $k_\Gamma \to 0$), one recovers $\sigma(0) = 1$. Then, using the explicit expressions of A_{11}, B_{11}, ..., A_{12}, B_{12}, ... and A_{22}, B_{22} ... given in Appendix D, one can show that $\Sigma_{-6} = \Sigma_{-5} = \Sigma_{-4} = \Sigma_{-3} = \Sigma_{-2} = \Sigma_{-1} = \Sigma_1 = \cdots = 0$. These relationships are direct consequences of the cancellations mentioned before, and indicate that the expansion has to be performed to very high order indeed. Therefore, at leading order in the super-Hubble limit, one has

$$\sigma^2(0) \simeq 1 + \Sigma_0 + \Sigma_{2-p}\,(-k\eta)^{2-p} + \cdots\,, \tag{5.20}$$

with

$$\begin{aligned}\Sigma_0 = {} & \left(\frac{k_\Gamma}{k}\right)^2 (-2C_{11} + 4E_{12} - 2E_{22} - 2F_{11} - 2G_{22}) \\ & + \left(\frac{k_\Gamma}{k}\right)^4 \left(-4C_{12}^2 + 4D_{11}D_{22} - 8B_{12}E_{12} + 4C_{11}E_{22} + 4B_{22}F_{11} + 4B_{11}G_{22}\right), \end{aligned} \tag{5.21}$$

$$\Sigma_{2-p} = \left(\frac{k_\Gamma}{k}\right)^2 (-2A_{11} + 4A_{12} - 2A_{22}) + \left(\frac{k_\Gamma}{k}\right)^4 (4A_{22}B_{11} - 8A_{12}B_{12} + 4A_{11}B_{22})\,. \tag{5.22}$$

As mentioned above, the coefficients appearing in the expansions of γ_{11}, γ_{12} and γ_{22} are functions of p and $\ell_E H$. However, the coefficients A_{11}, A_{12} and A_{22} only depend on p, see the explicit expressions in Appendix D, Eqs. (D.31), (D.41) and (D.45). It follows that the term proportional to k_Γ^2 in the expression of Σ_{2-p} is also a function of p only. Explicitly, one has

$$-2A_{11} + 4A_{12} - 2A_{22} = \frac{2}{p-2}\left(\frac{k}{k_*}\right)^{p-3}\,. \tag{5.23}$$

By contrast, the term proportional to k_Γ^2 in the coefficient Σ_0 contains the terms C_{11}, E_{12}, E_{22}, F_{11} and G_{22} and, as consequence, depends on p but also on $\ell_E H$. Explicitly, one finds

$$-2C_{11} + 4E_{12} - 2E_{22} - 2F_{11} - 2G_{22} = -2\left(\frac{k}{k_*}\right)^{p-3}\left[\frac{(\ell_E H)^{p-4}}{p-4} + \frac{(\ell_E H)^{p-2}}{p-2}\right]. \tag{5.24}$$

Combining the above results, one recovers Eq. (5.17), which is an important consistency check of our calculations.

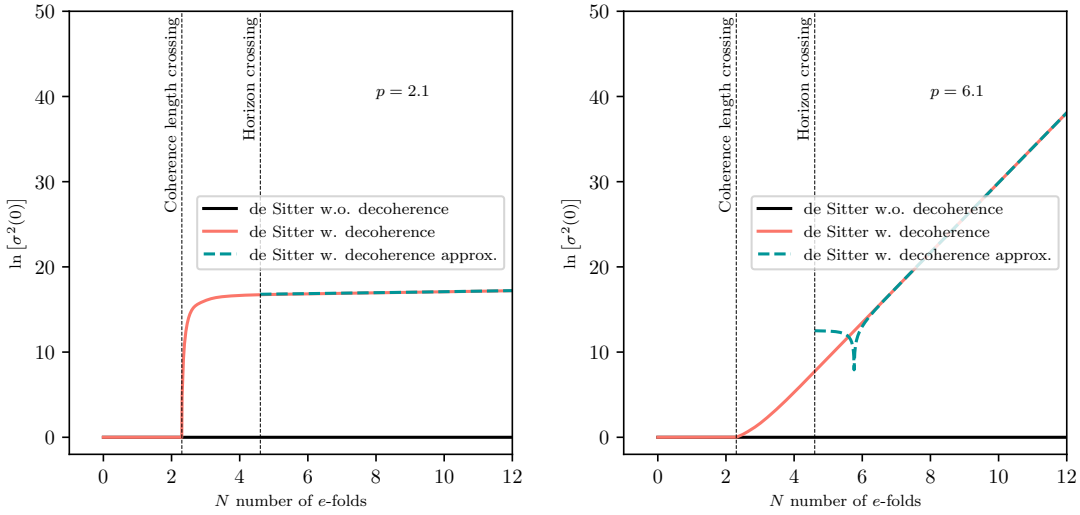

Figure 5. $\ln\left[\sigma^2(0)\right]$ with (pink) and without (black) decoherence for the de Sitter case. The approximated version (green dashed) is obtained using Eq. (5.20) for $\sigma^2(0)$. The first vertical dashed line shows the time when the mode $\boldsymbol{k}$ starts to decohere $\ell_E a/k = 1$, the second the time when the mode $\boldsymbol{k}$ exits the Hubble radius. The parameters are $\ell_E H = 0.1$, $x_\star = 1$, $p = 2.1$ (left) or $p = 6.1$ (right), and $k_\Gamma/k = 10$.

5.2.3 Quantum discord

The final step is to calculate $\sigma^2(\theta)$ and extract quantum discord. Given that we already have computed $\sigma^2(0)$, see Eq. (5.17), and since Eq. (2.27) can be rewritten as

$$\sigma(\theta) = \sqrt{\sigma^2(0) + \frac{1}{4}\left[(\gamma_{11}-\gamma_{22})^2 + 4\gamma_{12}^2\right]\sin^2(2\theta)}\,, \tag{5.25}$$

we see that we only need to estimate the second term, i.e. the one proportional to $\sin^2(2\theta)$. This is easier since no cancellation occurs in that term. In Appendix D, we find that the dominant contribution comes from γ_{22}, and that $(\gamma_{11}-\gamma_{22})^2 + 4\gamma_{12}^2 \simeq (-k\eta)^{-8}[1-(k_\Gamma/k)^2 B_{11}/2]^2$, see Eqs. (D.38), (D.42) and (D.46). This leads to

$$\sigma^2(\theta) = \left[1 - \frac{1}{2}\left(\frac{k_\Gamma}{k}\right)^2 B_{11}\right]^2 \frac{\sin^2(2\theta)}{4\,(-k\eta)^8} + \mathcal{O}\left[(-k\eta)^{-6}\right]. \tag{5.26}$$

Recalling that B_{11} does not depend on time, one can see that the effect of the environment is only to change the prefactor in $\sigma(\theta)$, while it does not affect its time behaviour $\sigma(\theta) \propto (k\eta)^{-4}$ on super-scales.

Let us now consider the ratio $\sigma^2(0)/\sigma(\theta)$ which, as explained in Sec. 4.4, determines the fate of quantum discord. If $p < 2$, the second term dominates in Eq. (5.17), hence $\sigma^2(0)$ reaches a constant on large scales. One thus has $\sigma^2(0)/\sigma(\theta) \propto a^{-4}$, which is highly

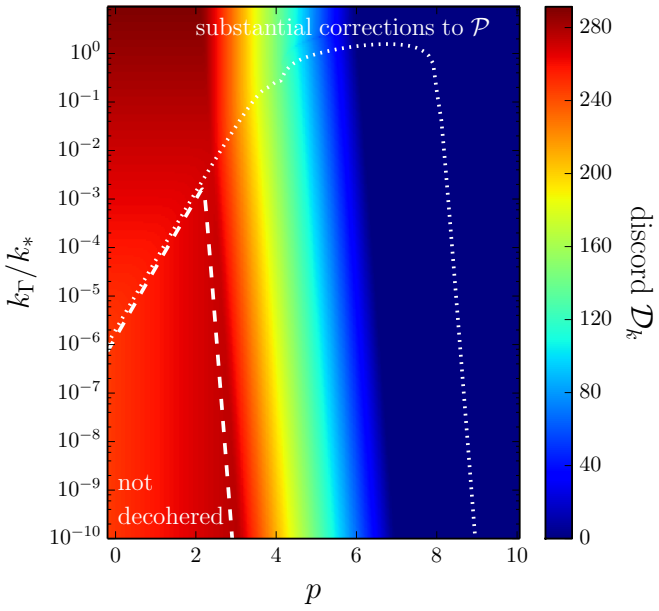

Figure 6. Quantum discord $\mathcal{D}_k$ as a function of p and k_Γ/k_*, for $k = k_*$, $-k\eta = e^{-50}$ (corresponding to the scales probed in the cosmic microwave background at the end of inflation), $\ell_E H = 10^{-3}$ and $\theta = -\pi/4$. The white dashed line is the contour line of $\mathrm{Tr}(\rho^2) = 1/2$, and above that line the quantum state is decohered. The white dotted line is the contour line of $\Delta\mathcal{P}_\zeta/\mathcal{P}_\zeta = 1$, above which the power spectrum is spoilt by environmental effects. These two contours essentially correspond to Fig. 6 of Ref. [19]; but, in Fig. 6 of Ref. [19], the region where there is a substantial change of the spectral index is displayed, as opposed to the region where there is a substantial change of $\mathcal{P}_\zeta$ in the above figure. This is the reason why, in Fig. 6 of Ref. [19], there is a feature at $p = 5$, for which the corrections are scale-invariant, which does not appear in the above figure. One of the main result of the present paper is the value of the quantum discord in the parameter space $(p, k_\Gamma/k_*)$. Let us also notice that the "not decohered" region invades the whole figure for sufficiently small values of k_Γ. Here, it looks bounded because, due to the logarithmic scale used, k_Γ is "cut" at $k_\Gamma/k_* = 10^{-10}$.

suppressed on super-Hubble scales, and which gives rise to $\mathcal{D}_k \propto 4\log_2[a/a(k)]$. This shows that quantum discord is large in that case, and one recovers the result obtained in Eq. (5.9). If $p \geq 2$, the first term dominates in Eq. (5.17), hence $\sigma^2(0) \propto a^{p-2}$ on super-Hubble scales. As a consequence, $\sigma^2(0)/\sigma(\theta) \propto a^{p-6}$, the time behaviour of which depends on whether $p < 6$ or $p > 6$ as illustrated by Fig. 5 . If $p < 6$, $\sigma^2(0)/\sigma(\theta)$ decays, and one has $\mathcal{D}_k \propto (6-p)\log_2[a/a(k)]$, so the discord remains large. If $p > 6$, $\sigma^2(0)/\sigma(\theta)$ increases on super-Hubble scales, and upon expanding Eq. (2.28) in that regime one finds that $\mathcal{D}_k \propto [a/a(k)]^{6-p}$, so it becomes highly suppressed. The behaviour of $\mathcal{D}_k$ on each side of the threshold is illustrated by Fig. 7

These considerations can be checked in Fig. 6, where quantum discord is displayed as a function of p and k_Γ/k_*. It confirms that the pivotal value of p from the point of view of quantum discord is $p = 6$: discord remains large on super-Hubble scales when $p < 6$,

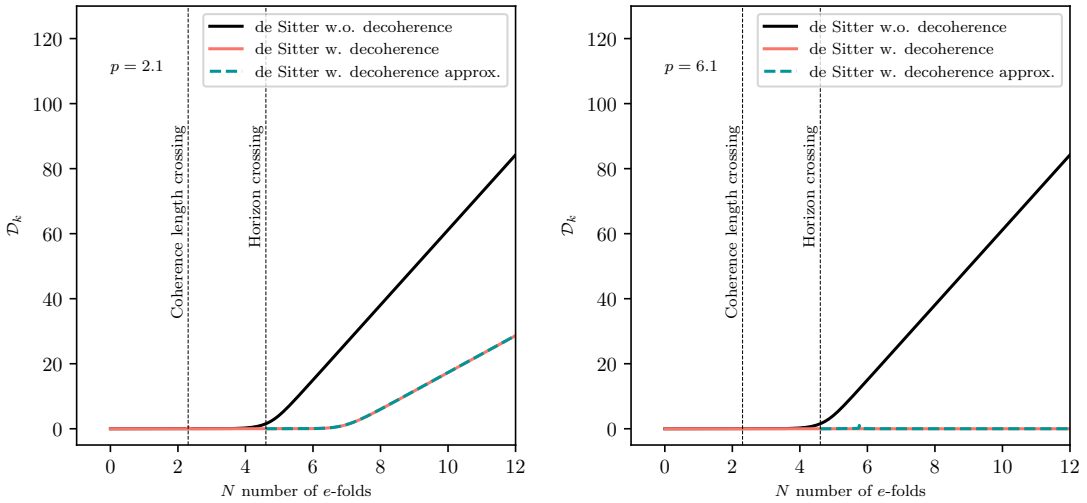

Figure 7. Quantum discord $\mathcal{D}_k$ with (pink) and without (black) decoherence for the de Sitter case. The approximated version (green dashed) is obtained using the first order approximations (5.11), (5.12) and (5.13) for γ_{ij} and the expression (5.20) for $\sigma^2(0)$ to obtain $\sigma^2(\theta)$ in (5.25). The quantity $\sigma^2(0)$ and $\sigma^2(\theta)$ are then used in the expression (2.28) for the discord. The first vertical dashed line shows the time when the mode $\boldsymbol{k}$ starts to decohere $\ell_E a/k = 1$, the second the time when the mode $\boldsymbol{k}$ exits the Hubble radius. The parameters are $\ell_E H = 0.1$, $x_\star = 1$, $p = 2.1$ (left) or $p = 6.1$ (right), and $k_\Gamma/k = 10$.

and is highly suppressed otherwise. Note however that the above formulas only describe the time behaviour at large scales, and do not incorporate the constant prefactors that can otherwise be readily established from combining the above results. These prefactors depend on both $\ell_E H$ and Γ (through k_Γ), and they explain why the discord shown in Fig. 6 does not depend only on p (for instance, even for $p > 6$, one can get a substantial discord by considering extremely low values of k_Γ, in agreement with the fact that in the limit $\Gamma \to 0$, one recovers the results of Sec. 5.1). Nonetheless, for reasonable values of the coupling constant Γ, the result is mostly determined by the value of p.

In Fig. 6, we have also displayed the region in parameter space where decoherence does not occur (below the white dashed line, see Sec. 5.2.2) and the region where substantial corrections to the power spectrum are obtained (above the white dotted line, see Sec. 5.2.1). One can see that when the coupling to the environment is not strong enough to make the system decohere, quantum discord is always large on super-Hubble scales. This corresponds to the bottom left corner in Fig. 6. In the opposite corner, namely the top-right region in Fig. 6, the coupling with the environment is so strong that it both decoheres the system very efficiently, while it prevents its quantum discord from growing. An important remark is that, between these two regimes, there are regions where quantum discord remains large even though the system decoheres and even when imposing that the observed power spectrum is unaffected by environmental effects.

6 Conclusions

In this work, we have studied how quantum discord behaves in the presence of an environment. When a quantum system couples to environmental degrees of freedom, the entanglement between the open system and the environment leads to decoherence of the system, which is usually associated with the loss of certain quantum features displayed by the system. Since discord characterises how "genuinely quantum" the correlations between subparts of the system are, it is naturally expected that decoherence leads to a suppression of discord. The goal of this work was to study this effect on generic grounds, since any practical experiment aiming at revealing the presence of quantum effects is a priori subject to such environmental limitations.

For simplicity, we have considered the case of a quantum scalar field with (homogeneous and isotropic) quadratic Hamiltonian, which boils down to a collection of independent pairs of quantum parametric oscillators, one for each pair of opposite Fourier modes. We have shown that, in general, quantum discord depends on the precise way these systems are partitioned into two subsystems. We have found a generic parameterisation that describes all possible partitions, which has allowed us to derive quantum discord for any partitioning. Note that the way a given physical system should be split into two subsystems is sometimes obvious: for instance, for two particles located in each polariser of a Bell's inequality experiment, the two sub-systems are clearly the two space-like separated particles. However, the Fourier sub-sector of a quantum field does not feature such a clear preferred partitioning, and it is therefore necessary to study how the result depends on the partition in general.[6]

In the absence of interactions with an environment, the system is placed in a Gaussian state known as the two-mode squeezed state, which can be equivalently described in terms of Bogoliubov coefficients, squeezing parameters, or covariance matrix. In that case, we recovered the formula derived in Ref. [5] for quantum discord, which we nonetheless extended to any partitioning.

In the case where an environment is present and couples to the system, for explicitness, we have assumed that the coupling is linear in the phase-space variables describing the system, and that it can be cast in terms of a Lindblad equation (this is the so-called Caldeira-Leggett model). In this context, the state remains Gaussian (though not pure anymore), so it can still be described in terms of a covariance matrix, for which we have derived the modified evolution equation. We have shown that generalised squeezing parameters can also still be defined, from their geometrical phase-space interpretation. A third parameter describing the area of the elliptic contours of the

[6] An alternative approach is to study correlations between the field configuration at two separated positions in real space (as opposed to between opposite Fourier modes). In that case, a natural partitioning is available (namely the two real-space locations), and the relevant bipartite system is mixed even if the full quantum field is in a pure state. This is because, when considering the field configuration at two locations, one implicitly traces over the configuration of the field at every other location, to which the bipartite system is a priori entangled. The formalism developed in this work is still relevant for that case, since it merely boils down to the calculation of quantum discord in a mixed Gaussian state. This is the topic of Refs. [21, 25].

Wigner function should be added to the usual squeezing amplitude and squeezing angle, which respectively correspond to the eccentricity and orientation of these ellipses. This "third squeezing parameter" equals one for a pure state and is larger than one otherwise, and it is directly related to the inverse purity of the state. We have thus derived the modified evolution equations for these three "squeezing parameters", which represent an alternative description of the state with an intuitive geometrical interpretation [41].

We have then computed quantum discord in this model, both in terms of the covariance matrix and in terms of the generalised squeezing parameters. As in the case of pure states, we have found that quantum discord does not depend on the squeezing angle, but only involves the squeezing amplitude, the state purity and the partition parameters. More precisely, in a given partitioning, quantum discord increases as the length of the semi-minor axis of the phase-space ellipse decreases, which provides a simple geometrical interpretation of discord. This implies that discord increases with both the squeezing amplitude and the state purity. In general, as the time evolution proceeds, the squeezing amplitude increases (denoting particle creation) and the state purity decreases (because of decoherence), so the two effects compete. The details of how quantum discord is affected by an environment thus depend on the rate at which these two parameters vary, which has to be discussed on a model-by-model basis. Those findings are consistent with the work of Ref. [18] where the authors considered a model corresponding to p=5 in our parametrisation. They computed an upper bound on the discord which despite decoherence grows in time, albeit at a reduced rate, in line with the discussion of Sec. 5.2.3.

To go beyond those generic considerations, we have finally applied our framework to the case of primordial cosmological perturbations. This case study is of particular interest not only because it provides a useful illustration of the tools introduced in this work, but also since the possible presence of quantum correlations in cosmic structures, and the potential of decoherence to make them undetectable, is of great importance for our understanding of their origin. Assuming that the coupling parameter Γ between the system (here cosmological perturbations) and the environment (possibly heavier fields, smaller-scale degrees of freedom, etc.) grows as a power of the scale factor a of the universe, $\Gamma \propto a^p$, whether or not decoherence leads to a suppression of discord (i.e. whether or not the phase-space semi-minor axis increases) crucially depends on p. More precisely, if $p < 6$, discord remains large on large scales, and is strongly suppressed otherwise. Let us also note that for $p < 2$, decoherence cannot proceed without substantially affecting the observed power spectrum of the cosmological density field, so in the region of parameter space that is in agreement with current observations, environmental effects are mostly irrelevant. For $2 < p < 6$, there exists a regime where the state decoheres but remains strongly discordant, while preserving its power spectrum.

Those considerations imply that there is no simple relationship between decoherence and discord: one can find situations where the state of the system becomes decohered and non-discordant, where it becomes decohered but remains discordant, where it remains pure and discordant, or where it is pure and non discordant (this case does not appear in cosmology but may be encountered in other contexts, see the discussion

around Fig. 2). As a consequence, although decoherence may affect our ability to reveal the presence of quantum correlations within a given quantum system, this effect cannot be simply assessed by considering the amount of decoherence (i.e. the state purity). One alternative criterion may be the quantum discord discussed in this work, although its relationship with concrete observables is not clear, in particular in the context of mixed states [42]. This is why a next natural step would be to apply the present framework to investigate violations of Bell-inequalities in the presence of environmental effects, using the techniques developed in Refs. [17, 43–46]. In this way, one may be able to better understand the relationship between discord, decoherence, Bell inequalities violation, and maybe other criteria such as Peres-Horodecki separability [47], in a broad context.

Acknowledgments

A. Micheli is supported by the French National Research Agency under the Grant No. ANR-20-CE47-0001 associated with the project COSQUA. We thank Ashley Wilkins for pointing out a typo in the labels of Fig. 3 in a previous version of the manuscript.

A Partitions

As explained in Sec. 2.2, when studying the nature of the correlations present within a given (classical or quantum) system, one first has to split this system into two (or more) sub-systems, and then to analyse how these sub-systems are correlated. This way to divide the system into several sub-systems is called a "partition", and in this appendix we formally study how partitions can be defined on generic grounds, and how different partitions are related to each other.

A.1 Quantum phase space

In this article, we consider continuous-variable systems, i.e. systems described by Hermitian operators satisfying canonical commutation relation. It can be, for instance, the positions $\hat{q}_i$ and momenta $\hat{\pi}_i$ of n particles (with $i = 1 \cdots n$), with $[\hat{q}_i, \hat{\pi}_j] = i\delta_{ij}$. This can also correspond to the Fourier modes of a quantum field, see Sec. 2.1. The quantum state of the system is an element of the Hilbert space

$$\mathcal{E} = \bigotimes_{i=1\cdots n} \mathcal{E}_i \,, \tag{A.1}$$

where $\mathcal{E}_i$ is the Hilbert space associated to the i^{th} particle. It can be described by the vector

$$\hat{R} = (\hat{q}_1, \hat{\pi}_1, \cdots, \hat{q}_i, \hat{\pi}_i, \cdots, \hat{q}_n, \hat{\pi}_n)^{\mathrm{T}} \,. \tag{A.2}$$

In terms of the components of the vector $\hat{R}$, the commutation relations can be written as[7]

$$\left[\hat{R}_a, \hat{R}_b\right] = i J^{(n)}_{ab} \,, \tag{A.3}$$

where $J^{(n)}$ is the $2n \times 2n$ block-diagonal matrix

$$J^{(n)} = \begin{pmatrix} J^{(1)} & & \\ & \ddots & \\ & & J^{(1)} \end{pmatrix} \quad \text{with} \quad J^{(1)} = \begin{pmatrix} 0 & 1 \\ -1 & 0 \end{pmatrix} . \tag{A.4}$$

An alternative description of the system is by means of the creation and annihilation operators $\hat{c}_i$ and $\hat{c}_i^\dagger$, defined by

$$\hat{q}_i = \frac{1}{\sqrt{2}} \left(\hat{c}_i + \hat{c}_i^\dagger\right) , \quad \hat{\pi}_i = -\frac{i}{\sqrt{2}} \left(\hat{c}_i - \hat{c}_i^\dagger\right) . \tag{A.5}$$

They can be assembled into the vector

$$\hat{C} = (\hat{c}_1, \cdots, \hat{c}_i, \cdots, \hat{c}_n, \hat{c}_1^\dagger, \cdots, \hat{c}_i^\dagger, \cdots, \hat{c}_n^\dagger)^{\mathrm{T}} . \tag{A.6}$$

Contrary to the vector $\hat{R}$, notice that $\hat{C}$ is not arranged such that the variables describing the subsystem i directly follow each other, and the reason for this choice will be made clear below.[8]

The relation between $\hat{R}$ and $\hat{C}$ is linear and can thus be written in matricial form as $\hat{R} = M^{(n)} \cdot \hat{C}$, where $M^{(n)}$ is an unitary matrix that can be obtained from Eq. (A.5).[9] For instance, with $n = 2$, one has

$$M^{(2)} = \frac{1}{\sqrt{2}} \begin{pmatrix} 1 & 0 & 1 & 0 \\ -i & 0 & i & 0 \\ 0 & 1 & 0 & 1 \\ 0 & -i & 0 & i \end{pmatrix} . \tag{A.8}$$

[7] Hereafter, the indices $a, b, c, \cdots$ label the components of the vectors $\hat{R}$, while the indices $i, j, k, \cdots$ label the degrees of freedom of the system. For instance, for a two-"particle" system, one has $\hat{R} = (\hat{q}_1, \hat{\pi}_1, \hat{q}_2, \hat{\pi}_2)^{\mathrm{T}}$, so $\hat{R}_1 = \hat{q}_1$, $\hat{R}_2 = \hat{\pi}_1$, $\hat{R}_3 = \hat{q}_2$ and $\hat{R}_4 = \hat{\pi}_2$.

[8] In practice, one may also consider the vector $\hat{\overline{C}} = (\hat{c}_1, \hat{c}_1^\dagger, \cdots, \hat{c}_n, \hat{c}_n^\dagger)^{\mathrm{T}}$ which is related to $\hat{C}$ through $\hat{\overline{C}} = P^{(n)} \cdot \hat{C}$, where $P^{(n)}$ is a permutation matrix that can be readily written down.

[9] In general, the matrix $M^{(n)}$ can be computed as follows. One first writes $\hat{R} = \overline{M}^{(n)} \hat{\overline{C}}$, where $\hat{\overline{C}}$ was introduced in footnote 8 and where $\overline{M}^{(n)}$ is a simple block-diagonal matrix :

$$\overline{M}^{(n)} = \begin{pmatrix} \overline{M}^{(1)} & & \\ & \ddots & \\ & & \overline{M}^{(1)} \end{pmatrix} , \quad \text{where} \quad \overline{M}^{(1)} = \frac{1}{\sqrt{2}} \begin{pmatrix} 1 & 1 \\ -i & i \end{pmatrix} . \tag{A.7}$$

Since $\overline{M}^{(n)} = M^{(n)} \cdot P^{(n)}$, one has $M^{(n)} = \overline{M}^{(n)} P^{(n),\mathrm{T}}$ since permutation matrices are orthogonal. This allows one to compute $M^{(n)}$ from the above expression for $\overline{M}^{(n)}$. This also allows one to show that $M^{(n)}$ is unitary: one can check that $\overline{M}^{(1)} \overline{M}^{(1),\dagger} = \mathbb{I}_2$ and so $\overline{M}^{(n)} \cdot \overline{M}^{(n),\dagger} = \mathbb{I}_{2n}$, which in turns implies that $M^{(n)} \cdot M^{(n),\dagger} = \mathbb{I}_{2n}$, using the fact that $P^{(n)}$ is orthogonal.

The commutation relations can be expressed as

$$\left[\hat{C}_a, \hat{C}_b\right] = \Omega^{(n)}_{ab}\,, \tag{A.9}$$

with $\Omega^{(n)} = iM^{(n),-1} \cdot J^{(n)} \cdot M^{(n),-1,\mathrm{T}}$, i.e.

$$\Omega^{(n)} = \begin{pmatrix} 0 & \mathbb{I}_n \\ -\mathbb{I}_n & 0 \end{pmatrix}, \tag{A.10}$$

where $\mathbb{I}_n$ is the identity matrix of size n.

A.2 Partitioning

For $n \geq 2$, the degrees of freedom can always be split into two subsets A and B. This defines a partition and allows us to see the whole system as a bipartite system. An important point is that one can define several partitions for the same system. As an introductory (and elementary) example, let us consider the case $n = 4$ where $\hat{R} = (\hat{q}_1, \hat{\pi}_1, \hat{q}_2, \hat{\pi}_2, \hat{q}_3, \hat{\pi}_3, \hat{q}_4, \hat{\pi}_4)^{\mathrm{T}}$. For instance, one can choose the subsystem A to be made of the first two degrees of freedom and to be described by $\hat{R}^{(A)} = (\hat{q}_1, \hat{\pi}_1, \hat{q}_2, \hat{\pi}_2)^{\mathrm{T}}$, and the subsystem B to contain the third and fourth degrees of freedom, $\hat{R}^{(B)} = (\hat{q}_3, \hat{\pi}_3, \hat{q}_4, \hat{\pi}_4)^{\mathrm{T}}$. Then, the vector $\hat{R}$ can be written as $\hat{R} = (\hat{R}^{(A)}, \hat{R}^{(B)})^{\mathrm{T}}$. This definition of $\hat{R}$, namely the way we order its components, is, implicitly, a definition of a partition. Obviously, other partitions are possible, for instance the one defined by $\hat{R}^{(A)\prime} = (\hat{q}_1, \hat{\pi}_1, \hat{q}_3, \hat{\pi}_3)^{\mathrm{T}}$ and $\hat{R}^{(B)\prime} = (\hat{q}_2, \hat{\pi}_2, \hat{q}_4, \hat{\pi}_4)^{\mathrm{T}}$ with $\hat{R}' = (\hat{R}^{(A)\prime}, \hat{R}^{(B)\prime})^{\mathrm{T}}$.

More generally, changing the partition can be viewed as performing a canonical transformation on the system (i.e. a transformation that preserves the commutator structure). A linear canonical transformation is a transformation $\hat{R} \to \hat{R}' = T\hat{R}$, where T is a real matrix since $\hat{R}$ and $\hat{R}'$ are Hermitian, which preserves the commutators, i.e. such that $[\hat{R}'_a, \hat{R}'_b] = [\hat{R}_a, \hat{R}_b]$ (hereafter we drop the index n for notational convenience). This leads to the condition

$$TJT^{\mathrm{T}} = J\,, \tag{A.11}$$

which defines the group of symplectic matrices T [24, 48, 49]. In particular, any symplectic matrix has determinant 1 [48],

$$\det T = 1\,. \tag{A.12}$$

In the simple example mentioned above, one can check that the transformation matrix T is indeed symplectic. Let us note that canonical transformations can also be defined at the level of the vectors $\hat{C}$, since $\hat{R} \to T\hat{R}$ leads to $\hat{C} \to S\hat{C}$ with

$$S = M^{-1}TM = M^{\dagger}TM \tag{A.13}$$

(where, in the last equation, we have used that M is unitary, see footnote 9). Using the definition of Ω given below Eq. (A.9), Eqs. (A.11) and (A.13) lead to the condition

$$S\Omega S^{\mathrm{T}} = \Omega\,, \tag{A.14}$$

which also implies that

$$\det S = 1\,. \tag{A.15}$$

Another useful property for the matrix S comes from the ordering of the entries of the vector $\hat{C}$ in Eq. (A.6), which leads to $\hat{C}^\dagger = A \cdot \hat{C}$, where $\hat{C}^\dagger$ is defined as $(\hat{C}^\dagger)_a = (\hat{C}_a)^\dagger$ and where $A = \begin{pmatrix} 0 & \mathbb{I}_n \\ \mathbb{I}_n & 0 \end{pmatrix}$. Since $\hat{R}^\dagger = \hat{R}$, the adjoint of the relation $\hat{R} = M\hat{C}$ gives rise to $M^* A = M$. Evaluating the complex conjugate of $S = M^{-1}TM$, this leads to

$$S^* = ASA\,, \tag{A.16}$$

where we have used that $A^2 = \mathbb{I}_n$ and that $T^* = T$ (since $\hat{R}$ and $\hat{R}'$ are both Hermitian).

It is worth pointing out that there are canonical transformations that do not mix the two subsystems (they are called "local" transformations) and hence do not change the partition. A simple example is $\hat{R}' = (\hat{q}_2, \hat{\pi}_2, \hat{q}_1, \hat{\pi}_1, \hat{q}_3, \hat{\pi}_3, \hat{q}_4, \hat{\pi}_4)^{\mathrm{T}}$ where we have simply flipped the ordering of the two first degrees of freedom. As a less trivial example, let us define $\hat{Q}^{\pm}_{ij} = (\hat{q}_i \pm \hat{q}_j)/\sqrt{2}$ and $\hat{\Pi}^{\pm}_{ij} = (\hat{\pi}_i \pm \hat{\pi}_j)/\sqrt{2}$ so that $[\hat{Q}^{\pm}_{ij}, \Pi^{\pm}_{ij}] = i$, thus ensuring that the corresponding transformation can be described by a symplectic matrix. Clearly, $\hat{R}' = (\hat{Q}^{+}_{12}, \hat{\Pi}^{+}_{12}, \hat{Q}^{-}_{12}, \hat{\Pi}^{-}_{12}, \hat{q}_3, \hat{\pi}_3, \hat{q}_4, \hat{\pi}_4)^{\mathrm{T}}$ corresponds to the same partition as $\hat{R} = (\hat{q}_1, \hat{\pi}_1, \hat{q}_2, \hat{\pi}_2, \hat{q}_3, \hat{\pi}_3, \hat{q}_4, \hat{\pi}_4)^{\mathrm{T}}$ since we still have 1 and 2 in subsystem A and 3 and 4 in subsystem B. Therefore, partition changes are described by only a subclass of symplectic matrices (namely those that are not $n\times n$-block diagonal).

In order for two parameterisations of the system to share the same vacuum state, let us first impose that S does not mix creation and annihilation operators. This implies that S is block diagonal (which is the reason why the ordering made in Eq. (A.6) was indeed convenient). The condition (A.16) then imposes that the two blocks are complex conjugate to each other, so S can be written as

$$S = \begin{pmatrix} s^{(n)} & 0 \\ 0 & s^{(n)*} \end{pmatrix}\,. \tag{A.17}$$

The symplectic condition (A.14) leads to $s^{(n)\dagger} s^{(n)} = \mathbb{I}_n$, i.e. the matrices $s^{(n)}$ belong to the unitary group $U(n)$. This discussion shows that the space of partitions is essentially the group $U(n)$, so any parameterisation of that group, which has dimension n^2, leads to a parameterisation of all possible partitions, by means of the above formulas. For instance, with $n = 2$, matrices of $U(2)$ can be written in the form

$$s^{(2)} = \begin{pmatrix} e^{i\alpha}\cos\theta & -e^{i\delta}\sin\theta \\ e^{i\beta}\sin\theta & e^{i(\delta+\beta-\alpha)}\cos\theta \end{pmatrix}, \tag{A.18}$$

where α, β, δ and θ are four arbitrary real numbers, which thus parameterise all possible partitions. The matrix T can be also written in terms of these parameters by making use of Eq. (A.13) together with Eqs. (A.8) and (A.17), leading to

$$T = \begin{pmatrix} \cos\alpha\cos\theta & -\sin\alpha\cos\theta & -\cos\delta\sin\theta & \sin\delta\sin\theta \\ \sin\alpha\cos\theta & \cos\alpha\cos\theta & -\sin\delta\sin\theta & -\cos\delta\sin\theta \\ \cos\beta\sin\theta & -\sin\beta\sin\theta & \cos(\alpha-\beta-\delta)\cos\theta & \sin(\alpha-\beta-\delta)\cos\theta \\ \sin\beta\sin\theta & \cos\beta\sin\theta & -\sin(\alpha-\beta-\delta)\cos\theta & \cos(\alpha-\beta-\delta)\cos\theta \end{pmatrix}. \tag{A.19}$$

As a consistency check, one can verify that such a matrix is indeed symplectic, namely that it satisfies Eq. (A.11). However, note that the group of real 4×4 symplectic matrices, usually denoted $\mathrm{Sp}(4,\mathbb{R})$, is of dimension 10 [49]. Therefore, partition changes, that are described by 4 parameters, only correspond to a subgroup (isomorphic to U(2), and corresponding to the "rotation" generators of table 2 in Ref. [49]) of the symplectic group.

Note that, in agreement with the group structure of $U(n)$, changes of partitions can be composed according to

$$T^{1/2\to1'/2'} = T^{1/2\to1''/2''}\cdot T^{1''/2''\to1'/2'}\,, \tag{A.20}$$

and that

$$T^{1/2\to1'/2'} = \left(T^{1'/2'\to1/2}\right)^{-1}\,, \tag{A.21}$$

with similar expressions for $S^{1/2\to1'/2'}$.

B Covariance matrix in arbitrary partition

The covariance matrix γ in a given phase-space parameterisation $\hat{R}$ is defined by Eq. (2.17). Since $\hat{R}_a\hat{R}_b = (\{\hat{R}_a,\hat{R}_b\}+[\hat{R}_a,\hat{R}_b])/2$, Eqs. (A.3) and (2.17), give rise to

$$\langle\hat{R}_a\hat{R}_b\rangle = \frac{1}{2}\gamma_{ab} + \frac{i}{2}J^{(n)}_{ab}\,, \tag{B.1}$$

where the matrix $J^{(n)}$ has been defined in Eq. (A.4). Furthermore, since $\hat{R}_a$ and $\hat{R}_b$ are Hermitian, $\{\hat{R}_a,\hat{R}_b\}$ is also Hermitian, and Eq. (2.17) implies that γ is a real symmetric matrix. Note that the correlators of the ladder operators introduced in Eq. (A.6), and arranged into the vector $\hat{C} = M^{(n),-1}\hat{R}$, can also be expressed in terms of the covariance matrix:

$$\left\langle\left\{\hat{C}_a,\hat{C}_b\right\}\right\rangle = M^{(n),-1}_{ac}\gamma_{cd}M^{(n),*}_{db} \tag{B.2}$$

where we have used that $M^{(n)}$ is unitary, see footnote 9.

In the Fourier subspaces of a real scalar field, the covariance matrix is given by Eq. (2.19) in the R/I partition. Making use of Eq. (2.16) and (2.18), the covariance matrix can then be computed in all partitions, and one finds

$$\gamma = \begin{pmatrix}\gamma_A & \gamma_C\\ \gamma_C & \gamma_B\end{pmatrix}, \tag{B.3}$$

with

$$\gamma_A = \begin{pmatrix}\gamma_{11}\cos^2\theta+\gamma_{22}\sin^2\theta & \gamma_{12}\cos(2\theta)\\ \gamma_{12}\cos(2\theta) & \gamma_{22}\cos^2\theta+\gamma_{11}\sin^2\theta\end{pmatrix}, \tag{B.4}$$

$$\gamma_B = \begin{pmatrix} \gamma_B|_{11} & \gamma_B|_{12} \\ \gamma_B|_{21} & \gamma_B|_{22} \end{pmatrix}, \tag{B.5}$$

$$\gamma_C = \begin{pmatrix} \frac{1}{2}(\gamma_{11}-\gamma_{22})\sin^2(2\theta) + \frac{1}{2}\gamma_{12}\sin(4\theta) & -\frac{1}{4}(\gamma_{11}-\gamma_{22})\sin(4\theta) + \gamma_{12}\sin^2(2\theta) \\ -\frac{1}{4}(\gamma_{11}-\gamma_{22})\sin(4\theta) + \gamma_{12}\sin^2(2\theta) & -\frac{1}{2}(\gamma_{11}-\gamma_{22})\sin^2(2\theta) - \frac{1}{2}\gamma_{12}\sin(4\theta) \end{pmatrix}, \tag{B.6}$$

where the components of γ_B are given by

$$\gamma_B|_{11} = \frac{1}{2}\gamma_{11} + \frac{1}{2}\gamma_{22} + \frac{1}{2}(\gamma_{11}-\gamma_{22})\cos(2\theta)\cos(4\theta) - \gamma_{12}\cos(2\theta)\sin(4\theta), \tag{B.7}$$

$$\gamma_B|_{12} = \gamma_B|_{21} = \gamma_{12}\cos(2\theta)\cos(4\theta) + \frac{1}{2}(\gamma_{11}-\gamma_{22})\cos(2\theta)\sin(4\theta), \tag{B.8}$$

$$\gamma_B|_{22} = \frac{1}{2}\gamma_{11} + \frac{1}{2}\gamma_{22} - \frac{1}{2}(\gamma_{11}-\gamma_{22})\cos(2\theta)\cos(4\theta) + \gamma_{12}\cos(2\theta)\sin(4\theta). \tag{B.9}$$

For instance, recalling that the $\pm\boldsymbol{k}$ partition is reached by setting $\theta = \pi/4$, the correlation functions in the "$\boldsymbol{k}$"-sector are given by

$$k\left\langle \hat{q}_{\boldsymbol{k}}^2 \right\rangle = \frac{1}{2}\gamma_A|_{11} + \frac{i}{2}J_{11}^{(2)} = \frac{\gamma_{11}+\gamma_{22}}{4}, \tag{B.10}$$

$$\frac{\left\langle \hat{\pi}_{\boldsymbol{k}}^2 \right\rangle}{k} = \frac{1}{2}\gamma_A|_{22} + \frac{i}{2}J_{22}^{(2)} = \frac{\gamma_{11}+\gamma_{22}}{4} \tag{B.11}$$

$$\langle \hat{q}_{\boldsymbol{k}}\hat{\pi}_{\boldsymbol{k}} \rangle = \gamma_A|_{12} + \frac{i}{2}J_{12}^{(2)} = \frac{i}{2}, \quad \langle \hat{\pi}_{\boldsymbol{k}}\hat{q}_{\boldsymbol{k}} \rangle = \gamma_A|_{21} + \frac{i}{2}J_{21}^{(2)} = -\frac{i}{2}, \tag{B.12}$$

and we have the same results in the "$-\boldsymbol{k}$"-sector since, for $\theta = -\pi/4$, one has $\gamma_A = \gamma_B = (\gamma_{11}+\gamma_{22})\mathrm{diag}(1,1)/2$. The correlation functions mixing $\boldsymbol{k}$ and $-\boldsymbol{k}$ modes depend on the matrix γ_C, and are given by

$$k\left\langle \hat{q}_{\boldsymbol{k}}\hat{q}_{-\boldsymbol{k}} \right\rangle = \frac{1}{2}\gamma_C|_{11} + \frac{i}{2}J_{13}^{(2)} = \frac{1}{4}(\gamma_{11}-\gamma_{22}) \tag{B.13}$$

$$\frac{1}{k}\left\langle \hat{\pi}_{\boldsymbol{k}}\hat{\pi}_{-\boldsymbol{k}} \right\rangle = \frac{1}{2}\gamma_C|_{22} + \frac{i}{2}J_{24}^{(2)} = -\frac{1}{4}(\gamma_{11}-\gamma_{22}) \tag{B.14}$$

$$\langle \hat{q}_{\boldsymbol{k}}\hat{\pi}_{-\boldsymbol{k}} \rangle = \frac{1}{2}\gamma_C|_{12} + \frac{i}{2}J_{14}^{(2)} = \frac{1}{2}\gamma_{12}, \quad \langle \hat{\pi}_{-\boldsymbol{k}}\hat{q}_{\boldsymbol{k}} \rangle = \frac{1}{2}\gamma_C|_{21} + \frac{i}{2}J_{41}^{(2)} = \frac{1}{2}\gamma_{12}, \tag{B.15}$$

$$\langle \hat{q}_{-\boldsymbol{k}}\hat{\pi}_{\boldsymbol{k}} \rangle = \frac{1}{2}\gamma_C|_{12} + \frac{i}{2}J_{32}^{(2)} = \frac{1}{2}\gamma_{12}, \quad \langle \hat{\pi}_{\boldsymbol{k}}\hat{q}_{-\boldsymbol{k}} \rangle = \frac{1}{2}\gamma_C|_{21} + \frac{i}{2}J_{23}^{(2)} = \frac{1}{2}\gamma_{12}\,. \tag{B.16}$$

C Quantum discord for Gaussian homogeneous states

In this appendix we explain how the quantum discord can be used as a tool to assess the presence of quantum correlations between two subsystems. In Secs. C.1 and C.2, we first present a brief introduction to the main ideas behind quantum discord and give its mathematical definition. In Secs. C.3 and C.4, we then derive the expression of quantum discord for Gaussian homogeneous states we use in the main text, i.e. Eq. (2.28) .

C.1 Classical correlations

Let us consider two systems A and B, and denote by $\{a_i\}$ and $\{b_j\}$ their possible respective configurations. The probability to find the system A in the configuration a_i is noted p_i, and similarly for p_j. How uncertain the state of system A is can be characterised by the von Neumann entropy which is defined by the following expression

$$S(A) = -\sum_i p_i \log_2(p_i)\,. \tag{C.1}$$

One can check that $S(A) = 0$ corresponds indeed to the situation where all a_i vanish but one (so the state of A is certain), and that, in general, $S(A) \geq 0$. A similar expression for $S(B)$ can be introduced, and this can also be done for the joint system

$$S(A,B) = -\sum_{i,j} p_{ij} \log_2(p_{ij}), \tag{C.2}$$

where p_{ij} denotes the joint probability to find the system A in configuration a_i and the system B in configuration b_j. Then, the mutual information between A and B can be measured by

$$\mathcal{I}(A,B) = S(A) + S(B) - S(A,B)\,. \tag{C.3}$$

The fact that $\mathcal{I}(A,B)$ measures the presence of correlations between A and B can be seen by noting that if A and B are uncorrelated, then the mutual information vanishes. Indeed, if $p_{ij} = p_i p_j$, then $\mathcal{I} = -\sum_i p_i \log_2(p_i) - \sum_j p_j \log_2(p_j) + \sum_{i,j} p_i p_j [\log_2(p_i) + \log_2(p_j)] = 0$, where we have used that $\sum_i p_i = \sum_j p_j = 1$. More generally, p_{ij} can be expressed by means of Baye's theorem

$$p_{i,j} = p_j p_{i|j}\,, \tag{C.4}$$

where $p_{i|j}$ denotes the conditional probability to find A in configuration a_i knowing that B is in configuration b_j. Plugging Eq. (C.4) into the definition (C.3), one obtains $\mathcal{I} = -\sum_i p_i \log_2(p_i) - \sum_j p_j \log_2(p_j) + \sum_{i,j} p_j p_{i|j} [\log_2(p_j) + \log_2(p_{i|j})] = -\sum_i p_i \log_2(p_i) + \sum_{i,j} p_j p_{i|j} \log_2(p_{i|j})$ where we have used that $\sum_i p_{i|j} = 1$. This justifies the introduction of the following quantity

$$S(A|B) = -\sum_j p_j \sum_i p_{i|j} \log_2(p_{i|j})\,, \tag{C.5}$$

which stands for the conditional entropy contained in A after finding the system B in configuration b_j, averaged over all possible configurations for B. The above calculation thus suggests an alternative expression for mutual information, namely

$$\mathcal{J}(A,B) = S(A) - S(A|B)\,. \tag{C.6}$$

It also shows that, in classical systems, $\mathcal{I} = \mathcal{J}$.

C.2 Quantum correlations

We now want to reproduce the above discussion in a quantum-mechanical context. This implies to construct quantum analogues of $\mathcal{I}$ and $\mathcal{J}$. The full quantum system can be described by its density matrix $\hat{\rho}_{A,B}$, where information about the subsystem A is obtained by tracing over the degrees of freedom contained in B, i.e.

$$\hat{\rho}_A = \mathrm{Tr}_B \left(\hat{\rho}_{A,B} \right) , \tag{C.7}$$

and similarly for $\hat{\rho}_B$. The von Neumann entropy can then be written as

$$S(A) = -\mathrm{Tr} \left[\hat{\rho}_A \log_2 \left(\hat{\rho}_A \right) \right] , \tag{C.8}$$

with similar expressions for $S(B)$ and $S(A,B)$. This allows us to evaluate $\mathcal{I}(A,B)$ with Eq. (C.3). In order to evaluate $\mathcal{J}(A,B)$, one needs to introduce the notion of entropy after performing a (quantum) measurement, $S(A|B)$. To this end, let us introduce $\hat{\Pi}_j$, a complete set of projectors on subsystem B, and denote by $|b_j\rangle$ the quantum states on which they project. One thus has $\hat{\Pi}_j = \hat{\mathbb{I}}_A \otimes |b_j\rangle\langle b_j|$. It is important to notice that such complete sets of projectors $\hat{\Pi}_j$ (or equivalently, of states $|b_j\rangle$) are not unique. For instance, for a spin particle, one can consider $|+\rangle_{\vec{e}}$ and $|-\rangle_{\vec{e}}$ along any unit vector $\vec{e}$. We will come back to this point below. The probability to find B in the state b_j is given by $p_j = \mathrm{Tr}(\hat{\rho}\hat{\Pi}_j)$, and a measurement of B that returns the result b_j projects the state into $\hat{\rho} \to \hat{\Pi}_j \hat{\rho} \hat{\Pi}_j / p_j$. This leads us to introduce

$$\hat{\rho}_{A|\hat{\Pi}_i} = \mathrm{Tr}_B \left(\frac{\hat{\Pi}_j \hat{\rho} \hat{\Pi}_j}{p_j} \right) , \tag{C.9}$$

which describes the state of A after measuring B and finding b_j as a result of the measurement, and in terms of which the conditional entropy is given by

$$S(A|B) = \sum_j p_j S \left(\hat{\rho}_{A|\hat{\Pi}_i} \right) . \tag{C.10}$$

This is the analogue of Eq. (C.5), and these formulas then allow one to evaluate $\mathcal{J}(A,B)$ with Eq. (C.6). Quantum discord is finally defined as

$$\delta(A,B) = \min_{\{\hat{\Pi}_i\}} \left[\mathcal{I}(A,B) - \mathcal{J}(A,B) \right] . \tag{C.11}$$

In this expression, we have minimised over all possible complete sets of projectors. This ensures that a non-vanishing discord signals genuine quantum correlations, for any projection basis.

C.3 Mutual information $\mathcal{I}$

For a Gaussian state, which is entirely characterised by its covariance matrix γ, the von Neumann entropy is given by [50]

$$S(\hat{\rho}) = \sum_{i=1}^{n} f(\sigma_i), \tag{C.12}$$

where the function $f(x)$ is defined for $x \geq 1$ by Eq. (2.29) in the text and σ_i are the symplectic eigenvalues of the covariance matrix, that is to say the quantities σ_i such that $\mathrm{Sp}(J^{(n)}\gamma) = \{i\sigma_1, -i\sigma_1, \cdots, i\sigma_n, -i\sigma_n\}$.

For a partition of the kind (2.16), the full covariance matrix can be obtained from (2.18) and Eq. (2.19). One can show that a Gaussian state remains Gaussian after partial tracing over, with a covariance matrix given by the relevant entries of the full covariance matrix. In other words, $\hat{\rho}_A$ is still a Gaussian state with covariance matrix γ_A given in Eq. (B.4), and $\hat{\rho}_B$ is still a Gaussian state with covariance matrix γ_B given in Eq. (B.5). This leads to $\mathrm{Sp}(J^{(1)}\gamma_A) = \mathrm{Sp}(J^{(1)}\gamma_B) = \{i\sigma(\theta), -i\sigma(\theta)\}$ where $\sigma(\theta)$ has been defined in the text Eq. (2.27).

Moreover, for the full system, one obtains $\mathrm{Sp}(J^{(2)}\gamma) = \{i\sigma(0), -i\sigma(0), i\sigma(0), -i\sigma(0)\}$ with $\sigma^2(0) = \gamma_{11}\gamma_{22} - \gamma_{12}^2$. Combining the above results, one obtains

$$\mathcal{I} = 2f\left[\sigma(\theta)\right] - 2f\left[\sigma(0)\right]. \tag{C.13}$$

Note that because of Heisenberg's uncertainty principle, $\sigma(0) \geq 1$ since $\sigma^2(0)$ is the determinant of the covariance matrix written in the R or I subspace, see Eq. (2.19). This also guarantees that $\sigma(\theta) \geq 1$ since Eq. (2.27) implies that $\sigma(\theta) \geq \sigma^2(0)$. This ensures that the function f can be safely applied to $\sigma(0)$ and $\sigma(\theta)$.

C.4 Mutual information $\mathcal{J}$

The calculation of $\mathcal{J}$ is less straightforward and we will follow the approach presented in Ref. [51]. It relies on noting that the mutual information $\mathcal{J}$ (like $\mathcal{I}$) is invariant under local canonical transformations, which means that correlation measures do not depend on the way each subsystem is parameterised internally. As a consequence, it is convenient to first perform local canonical transformations that bring the covariance matrix into the simple form

$$\gamma = \begin{pmatrix} \mathfrak{A} & \mathfrak{C} \\ \mathfrak{C}^{\mathrm{T}} & \mathfrak{B} \end{pmatrix}, \tag{C.14}$$

with $\mathfrak{A} = \mathfrak{a}\mathbb{I}_2$, $\mathfrak{B} = \mathfrak{b}\mathbb{I}_2$ and $\mathfrak{C} = \mathrm{diag}\,(\mathfrak{c}, \mathfrak{d})$.

This can be achieved by performing two transformations. The first local transformation is realised by

$$T = \begin{pmatrix} T_A & 0 \\ 0 & T_B \end{pmatrix}, \tag{C.15}$$

with $T_A = \sqrt{\sigma(\theta)}\,\mathbb{I}_2\gamma_A^{-1/2}$ and $T_B = \sqrt{\sigma(\theta)}\,\mathbb{I}_2\gamma_B^{-1/2}$. One can check that T_A and T_B, hence T, satisfy Eq. (A.11), so they generate symplectic transformations. Making use of Eq. (2.18), the covariance matrix becomes

$$\gamma' = \begin{pmatrix} \sigma(\theta)\mathbb{I}_2 & \gamma_C \\ \gamma_C & \sigma(\theta)\mathbb{I}_2 \end{pmatrix}, \tag{C.16}$$

where we used the fact that $\gamma_C^{\mathrm{T}} = \gamma_C$. It is interesting to notice that the off-diagonal block matrix γ_C has been left unchanged by the transformation.

The second step uses the singular-value-decomposition theorem. The theorem states that, if M is a two-dimensional real matrix, then it can always be written as $M = U\Sigma V^{\mathrm{T}}$ where U and V are orthogonal (namely $UU^{\mathrm{T}} = U^{\mathrm{T}}U = VV^{\mathrm{T}} = V^{\mathrm{T}}V = \mathbb{I}_2$) and Σ is a diagonal matrix (in fact, the theorem is valid for complex matrices of arbitrary dimension but we do not need this general version here). The diagonal entries of Σ are the singular values of M and are always positive. Since U and V are orthogonal [they belong to the O(2) group], they have determinant $+1$ or -1, hence they can be written in the form

$$\mathfrak{M}^{+} = \begin{pmatrix} \cos\psi & -\sin\psi \\ \sin\psi & \cos\psi \end{pmatrix} \quad \text{or} \quad \mathfrak{M}^{-} = \begin{pmatrix} -\cos\psi & \sin\psi \\ \sin\psi & \cos\psi \end{pmatrix} \tag{C.17}$$

depending on the value of their determinant. One can check that the first matrix (with determinant 1) is symplectic, i.e. it satisfies Eq. (A.11), while the second matrix (with determinant -1) is not, in agreement with the fact that symplectic matrices have always determinant $+1$ (and in dimension 2, being symplectic is equivalent to having determinant 1) [52].

Our goal is to use the singular value decomposition theorem to define a four-dimensional symplectic transformation, expressed in terms of the two-dimensional matrices U and V that diagonalise γ_C, without affecting the diagonal blocks of γ'. We will show that, quite intuitively, this is possible if U and V are symplectic themselves, that is to say if they have determinant $+1$. However, let us note that since Eq. (B.6) leads to $\det\gamma_C = -[\gamma_{12}^2 + (\gamma_{11} - \gamma_{22})^2/4]\sin^2(2\theta) < 0$, the equation $\gamma_C = U\Sigma V^{\mathrm{T}}$ implies that the determinants of U and V are of opposite signs, hence they cannot be both equal to $+1$. This issue can be dealt with by introducing the matrix $\tilde{\gamma}_C = \sigma_3\gamma_C$, where $\sigma_3 = \mathrm{diag}(1, -1)$ is the third Pauli matrix. Since $\det\sigma_3 = -1$, one has $\det\tilde{\gamma}_C > 0$. One can then apply the singular-value-decomposition theorem to $\tilde{\gamma}_C$, i.e. $\tilde{\gamma}_C = \tilde{U}\tilde{\Sigma}\tilde{V}^{\mathrm{T}}$, where the determinants of $\tilde{U}$ and $\tilde{V}$ are now the same. If they are both -1, one can simply multiply $\tilde{U}$ and $\tilde{V}$ by σ_3 (which does not change the form of the singular-value decomposition since $\sigma_3\tilde{\Sigma}\sigma_3 = \tilde{\Sigma}$ given that $\tilde{\Sigma}$ is diagonal) such that one can assume that $\tilde{U}$ and $\tilde{V}$ have determinant $+1$ without loss of generality. This implies that they are symplectic and that they satisfy Eq. (A.11). Let us then consider the transformation generated by the matrix

$$T = \begin{pmatrix} \tilde{U} & 0 \\ 0 & \tilde{V}^{\mathrm{T}} \end{pmatrix}. \tag{C.18}$$

One can check that it is symplectic, given that $\tilde{U}$ and $\tilde{V}$ are. Plugging Eqs. (C.16) and (C.18) into Eq. (2.18), the covariance matrix becomes

$$\gamma'' = \begin{pmatrix} \sigma(\theta)\mathbb{I}_2 & \tilde{U}\gamma_C\tilde{V} \\ \tilde{V}^{\mathrm{T}}\gamma_C\tilde{U}^{\mathrm{T}} & \sigma(\theta)\mathbb{I}_2 \end{pmatrix}, \tag{C.19}$$

where we have used that $\tilde{U}$ and $\tilde{V}$ are orthogonal. Since $\gamma_C = \sigma_3\tilde{\gamma}_C$ and $\tilde{\gamma}_C = \tilde{U}\tilde{\Sigma}\tilde{V}^{\mathrm{T}}$, the off-diagonal block reads $\tilde{U}\gamma_C\tilde{V} = \tilde{U}\sigma_3\tilde{U}\tilde{\Sigma}$. One can then check explicitly that matrices of the form $\mathfrak{M}^+$ in Eq. (C.17) satisfy $\sigma_3\mathfrak{M}^+ = (\mathfrak{M}^+)^{\mathrm{T}}\sigma_3$, so $\tilde{U}\sigma_3\tilde{U} = \sigma_3$ and one obtains

$$\gamma'' = \begin{pmatrix} \sigma(\theta)\mathbb{I}_2 & \sigma_3\tilde{\Sigma} \\ \sigma_3\tilde{\Sigma} & \sigma(\theta)\mathbb{I}_2 \end{pmatrix}. \tag{C.20}$$

We have thus reached our goal, since γ'' is of the form (C.14) with $\mathfrak{a} = \mathfrak{b} = \sigma(\theta)$ and $\mathfrak{C} = \sigma_3\tilde{\Sigma}$ is a diagonal matrix that we denote $\mathrm{diag}(\mathfrak{c}, \mathfrak{d})$.

Let us now explain how the numbers $\mathfrak{c}$ and $\mathfrak{d}$ can be obtained in practice. Since $\tilde{\gamma}_C = \tilde{U}\tilde{\Sigma}\tilde{V}^{\mathrm{T}}$, the eigenvalues of $\tilde{\gamma}_C\tilde{\gamma}_C^{\mathrm{T}}$ are the same as those of $\tilde{\Sigma}^2$, i.e. $\mathrm{Sp}(\tilde{\gamma}_C\tilde{\gamma}_C^{\mathrm{T}}) = \{\mathfrak{c}^2, \mathfrak{d}^2\}$. Making use of Eq. (B.6), the eigenvalues of $\tilde{\gamma}_C\tilde{\gamma}_C^{\mathrm{T}}$ can be computed explicitly, and this leads to

$$\mathfrak{c} = -\mathfrak{d} = \frac{1}{2}\sqrt{(\gamma_{11} - \gamma_{22})^2 + 4\gamma_{12}^2}\,|\sin(2\theta)|\,. \tag{C.21}$$

Here, we have used the fact that $\mathfrak{c}$ and $\mathfrak{d}$ are of opposite signs since, as mentioned already $\det\gamma_C < 0$. In terms of the function $\sigma(\theta)$ given in Eq. (2.27), this can also be written as $\mathfrak{c} = -\mathfrak{d} = \sqrt{\sigma^2(\theta) - \sigma^2(0)}$.

The mutual information $\mathcal{J}$ for covariance matrices of the form (C.14) is computed in Ref. [51], where it is shown that the result depends on the sign of $(1 + \det\mathfrak{B})\det^2\mathfrak{C}(\det\mathfrak{A} + \det\gamma) - (\det\gamma - \det\mathfrak{A}\det\mathfrak{B})^2$. Using that $\mathfrak{c} = -\mathfrak{d}$, this quantity is given by $\mathfrak{c}^4(\mathfrak{a} - \mathfrak{a}\mathfrak{b}^2 + \mathfrak{b}\mathfrak{c}^2)^2$, which is necessarily positive. In that case, $\mathcal{J}$ is given by [51]

$$\max_{\{\hat{\Pi}_i\}}\mathcal{J} = f\left[\sigma(\theta)\right] - f\left[\frac{\sigma^2(0) + \sigma(\theta)}{1 + \sigma(\theta)}\right], \tag{C.22}$$

where we have used that $\sigma^2(0) > 1$, see the discussion below Eq. (C.13).

Plugging Eqs. (C.13) and (C.22) into Eq. (C.11), one finally obtains the formula Eq. (2.28) for the quantum discord.

D Covariance matrix for cosmological perturbations in the Caldeira-Leggett model

In this appendix, we compute the covariance matrix of inflationary perturbations, given by Eqs. (4.16) and (4.17), (4.18), (4.19) in the Caldeira-Leggett model described by the ansatz (5.10).

D.1 Exact calculation

Recalling that the mode function is given by Eq. (5.2), the quantity $\Im\mathrm{m}^2\left[v_{\boldsymbol{k}}(\eta)v_{\boldsymbol{k}}^*(\eta')\right]$ appearing in the integrand of Eq. (4.17) can be written as

$$\mathrm{Im}^2\left[v_{\boldsymbol{k}}(\eta)v_{\boldsymbol{k}}^*(\eta')\right] = \frac{1}{k^4\eta^2\eta'^2}\Big[k(\eta' - \eta)\cos(k\eta - k\eta') + (1 + k^2\eta\eta')\sin(k\eta - k\eta')\Big]^2. \tag{D.1}$$

Introduce the dimensionless variables $x = -k\eta$ and $x' = -k\eta'$ for notational convenience, and recalling that $a = -1/(H\eta)$ where $H = \mathcal{H}/a$ in the de Sitter space time, Eq. (4.16) gives rise to

$$\gamma_{11}(\eta) = v_{\boldsymbol{k}}(\eta)v^*_{\boldsymbol{k}}(\eta) - 2\left(\frac{k_\Gamma}{k}\right)^2 \int_{1/(\ell_E H)}^{x} \left(\frac{x_*}{x'}\right)^{p-3} \frac{1}{x^2 x'^2}\big[(x-x')\cos(x'-x) + (1+xx')\sin(x'-x)\big]^2 \mathrm{d}x' \tag{D.2}$$

$$= v_{\boldsymbol{k}}(\eta)v^*_{\boldsymbol{k}}(\eta) - 2\left(\frac{k_\Gamma}{k}\right)^2 \left[I_{11}^{(1)} + I_{11}^{(2)} + I_{11}^{(3)}\right], \tag{D.3}$$

with

$$\begin{aligned}
I_{11}^{(1)} &= \frac{x_*^{p-3}(1+x^2)}{2x^2} \int_{1/(\ell_E H)}^{x} x'^{1-p}(1+x'^2)\mathrm{d}x' \,, \\
I_{11}^{(2)} &= \frac{x_*^{p-3}}{4x^2} e^{-2ix} \int_{1/(\ell_E H)}^{x} e^{2ix'} x'^{1-p} \left[(x-x')^2 - 2i(x-x')(1+xx') - (1+xx')^2\right] \mathrm{d}x' \,, \\
I_{11}^{(3)} &= \frac{x_*^{p-3}}{4x^2} e^{2ix} \int_{1/(\ell_E H)}^{x} e^{-2ix'} x'^{1-p} \left[(x-x')^2 + 2i(x-x')(1+xx') - (1+xx')^2\right] \mathrm{d}x' \,,
\end{aligned} \tag{D.4}$$

where the time η_* and k_* have been defined after Eqs. (5.10) and (5.11), (5.12), (5.13). Our goal is now to calculate the three above integrals.

The calculation of the first integral is straightforward and one obtains the following expression

$$I_{11}^{(1)} = \frac{x_*^{p-3}(1+x^2)}{2x^2}\left[\frac{x^{2-p}}{2-p} + \frac{x^{4-p}}{4-p} - \frac{(\ell_E H)^{p-2}}{2-p} - \frac{(\ell_E H)^{p-4}}{4-p}\right]. \tag{D.5}$$

Of course, the result is not defined for the particular values $p = 2$ or $p = 4$. In these cases, instead of power law solutions, we just have logarithms.

The calculation of the second term is more complicated but can still be done in terms of special functions. After straightforward manipulations, one arrives at

$$I_{11}^{(2)} = \frac{x_*^{p-3}}{4x^2} e^{-2ix}\left[(x^2 - 1 - 2ix)(A_{1-p} - A_{3-p}) - (4x + 2ix^2 - 2i)A_{2-p}\right], \tag{D.6}$$

with

$$A_\alpha \equiv \int_{1/(\ell_E H)}^{x} e^{2ix'} x'^{\alpha} \mathrm{d}x' = -2^{-1-\alpha}(-i)^{-1-\alpha}\left[\Gamma\left(1+\alpha, -2ix\right) - \Gamma\left(1+\alpha, -\frac{2i}{\ell_E H}\right)\right], \tag{D.7}$$

where $\Gamma(a,z) = \int_z^{+\infty} t^{a-1}e^{-t}\mathrm{d}t$ is the incomplete Gamma function [53, 54]. The third term, $I_{11}^{(3)}$, is just given by $I_{11}^{(3)} = I_{11}^{(2)*}$. The resulting time evolution of $\gamma_{11}(\eta)$, with the choices $\ell_E H = 0.1$, $x_* = 0.1$, $p = 2.1$ and $k_\Gamma/k = 10$, is displayed in Fig. 8.

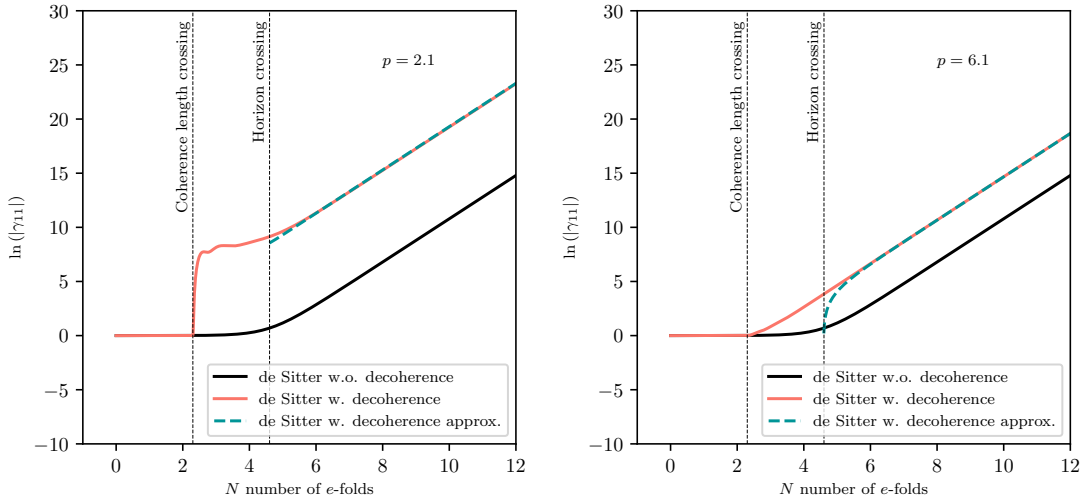

Figure 8. $\ln(|\gamma_{11}|)$ with (pink) and without (black) decoherence for the de Sitter case. The approximated version (green dashed) is obtained using the first order approximations (5.11). The first vertical dashed line shows the time when the mode $\boldsymbol{k}$ starts to decohere $\ell_E a/k = 1$, the second the time when the mode $\boldsymbol{k}$ exits the Hubble radius. The parameters are $\ell_E H = 0.1$, $x_\star = 1$, $p = 2.1$ (left) or $p = 6.1$ (right), and $k_\Gamma/k = 10$.

The next step consists in evaluating γ_{12}. Instead of using Eq. (4.16) and performing a similar calculation as above, one can use the transport equations (4.10), (4.11) and (4.12). This leads to

$$\gamma_{12} = \frac{1}{2k}\frac{\mathrm{d}}{\mathrm{d}\eta}\left(v_{\boldsymbol{k}}v_{\boldsymbol{k}}^*\right) + \left(\frac{k_\Gamma}{k}\right)^2 \int_{-\infty}^{\eta}\left(\frac{a}{a_*}\right)^{p-3} \mathrm{H}\left(1 - \frac{k\ell_E}{a}\right)\frac{\partial}{\partial\eta}\mathrm{Im}^2\left[v_{\boldsymbol{k}}(\eta)v_{\boldsymbol{k}}^*(\eta')\right]\mathrm{d}\eta'. \tag{D.8}$$

Instead of $\mathrm{Im}^2\left[v_{\boldsymbol{k}}(\eta)v_{\boldsymbol{k}}^*(\eta')\right]$ in the integrand, as was the case for γ_{11}, we now have the derivative of it. Explicitly, written in terms of the variables x and x', it can be expressed as

$$\begin{aligned}\frac{\partial}{\partial\eta}\mathrm{Im}^2\left[v_{\boldsymbol{k}}(\eta)v_{\boldsymbol{k}}^*(\eta')\right] = {}& \frac{k}{x^3x'^2}(1+x'^2) - \frac{i}{2x^3x'^2}e^{-2ix}e^{2ix'}k(-i+x)\left[-1+x(-i+x)\right] \\ & \times (i+x')^2 + \frac{i}{2x^3x'^2}e^{2ix}e^{-2ix'}k(i+x)\left[-1+x(i+x)\right](-i+x')^2.\end{aligned} \tag{D.9}$$

As a consequence, γ_{12} takes the following form

$$\gamma_{12} = \frac{1}{2k}\frac{\mathrm{d}}{\mathrm{d}\eta}\left[v_{\boldsymbol{k}}(\eta)v_{\boldsymbol{k}}^*(\eta)\right] - 2\left(\frac{k_\Gamma}{k}\right)^2\left[I_{12}^{(1)} + I_{12}^{(2)} + I_{12}^{(3)}\right], \tag{D.10}$$

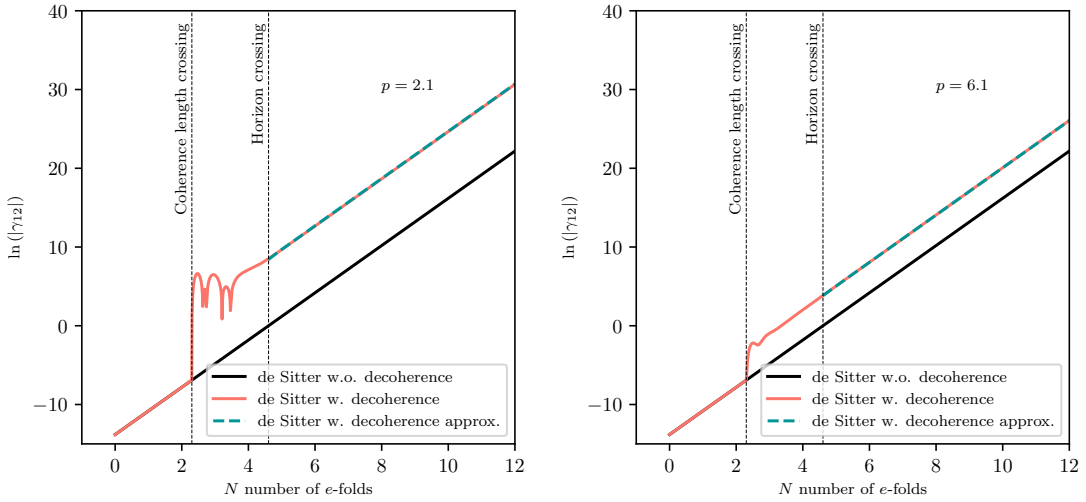

Figure 9. $\ln(|\gamma_{12}|)$ with (pink) and without (black) decoherence for the de Sitter case. The approximated version (green dashed) is obtained using the first order approximations (5.12). The first vertical dashed line shows the time when the mode $\boldsymbol{k}$ starts to decohere $\ell_E a/k = 1$, the second the time when the mode $\boldsymbol{k}$ exits the Hubble radius. The parameters are $\ell_E H = 0.1$, $x_\star = 1$, $p = 2.1$ (left) or $p = 6.1$ (right), and $k_\Gamma/k = 10$.

with

$$I_{12}^{(1)} = \frac{1}{2}\frac{x_*^{p-3}}{x^3}\int_{1/(\ell_E H)}^{x} x'^{1-p}(1+x'^2)\mathrm{d}x', \tag{D.11}$$

$$I_{12}^{(2)} = -\frac{ix_*^{p-3}}{4x^3}e^{-2ix}(-i+x)\left[x(-i+x)-1\right]\int_{1/(\ell_E H)}^{x} e^{2ix'}x'^{1-p}(i+x')^2\mathrm{d}x', \tag{D.12}$$

$$I_{12}^{(3)} = \frac{ix_*^{p-3}}{4x^3}e^{2ix}(i+x)\left[x(i+x)-1\right]\int_{1/(\ell_E H)}^{x} e^{-2ix'}x'^{1-p}(-i+x')^2\mathrm{d}x'. \tag{D.13}$$

These integrals are very similar to those appearing in the expression (D.2) of γ_{11} and they can be computed with the same techniques. We obtain

$$I_{12}^{(1)} = \frac{1}{2}\frac{x_*^{p-3}}{x^3}\left[\frac{x^{2-p}}{2-p}+\frac{x^{4-p}}{4-p}-\frac{(\ell_E H)^{p-2}}{2-p}-\frac{(\ell_E H)^{p-4}}{4-p}\right], \tag{D.14}$$

$$I_{12}^{(2)} = -\frac{ix_*^{p-3}}{4x^3}e^{-2ix}(-i+x)\left[x(-i+x)-1\right]\left(-A_{1-p}+2iA_{2-p}+A_{3-p}\right), \tag{D.15}$$

and $I_{12}^{(3)} = I_{12}^{(2)*}$. In Fig. 9, we have plotted γ_{12} with the same parameter values as in Fig. 8, namely $\ell_E = 0.1$, $x_* = 0.1$, $p = 2.1$ and $k_\Gamma/k = 10$.

Finally, the component γ_{22} remains to be evaluated. As done above for the component γ_{12}, one can use the transport equations to calculate γ_{22} from the expression of

γ_{11}. This leads to the following expression

$$\gamma_{22} = \frac{1}{2k^2}\frac{\mathrm{d}^2}{\mathrm{d}\eta^2}\left(v_{\boldsymbol{k}}v_{\boldsymbol{k}}^*\right) + \frac{1}{k}\left(\frac{k_\Gamma}{k}\right)^2 \int_{-\infty}^{\eta}\left(\frac{a}{a_*}\right)^{p-3} \mathrm{H}\left(1-\frac{k\ell_E}{a}\right)\frac{\partial^2}{\partial\eta^2}\mathrm{Im}^2\left[v_{\boldsymbol{k}}(\eta)v_{\boldsymbol{k}}^*(\eta')\right]\mathrm{d}\eta' + \frac{\omega^2}{k^2}\gamma_{11}. \tag{D.16}$$

As expected, the integrand in the above formula now contains the second derivative of $\mathrm{Im}^2\left[v_{\boldsymbol{k}}(\eta)v_{\boldsymbol{k}}^*(\eta')\right]$. Concretely, this quantity can be written as

$$\begin{aligned}\frac{\partial^2}{\partial\eta^2}\mathrm{Im}^2\left[v_{\boldsymbol{k}}(\eta)v_{\boldsymbol{k}}^*(\eta')\right] = {}& \frac{3k^2}{x^4x'^2}(1+x'^2) \\ & + \frac{k^2}{2x^4x'^2}e^{-2ix}e^{2ix'}\left\{3+2x\left[3i+x(-3-2ix+x^2)\right]\right\}(i+x')^2 \\ & + \frac{k^2}{2x^4x'^2}e^{2ix}e^{-2ix'}\left\{3+2x\left[-3i+x(-3+2ix+x^2)\right]\right\}(-i+x')^2.\end{aligned} \tag{D.17}$$

This leads to

$$\gamma_{22} = \frac{1}{2k^2}\frac{\mathrm{d}^2}{\mathrm{d}\eta^2}\left[v_{\boldsymbol{k}}(\eta)v_{\boldsymbol{k}}^*(\eta)\right] - 2\left(\frac{k_\Gamma}{k}\right)^2\left[I_{22}^{(1)}+I_{22}^{(2)}+I_{22}^{(3)}\right] + \frac{\omega^2}{k^2}\gamma_{11} \tag{D.18}$$

$$= \frac{1}{2k^2}\frac{\mathrm{d}^2}{\mathrm{d}\eta^2}\left[v_{\boldsymbol{k}}(\eta)v_{\boldsymbol{k}}^*(\eta)\right] + \frac{\omega^2}{k^2}v_{\boldsymbol{k}}(\eta)v_{\boldsymbol{k}}^*(\eta) - 2\left(\frac{k_\Gamma}{k}\right)^2\left\{I_{22}^{(1)}+I_{22}^{(2)}+I_{22}^{(3)}++\frac{\omega^2}{k^2}\left[I_{11}^{(1)}+I_{11}^{(2)}+I_{11}^{(3)}\right]\right\}, \tag{D.19}$$

with

$$I_{22}^{(1)} = \frac{3}{2}\frac{x_*^{p-3}}{x^4}\int_{1/(\ell_E H)}^{x} x'^{1-p}(1+x'^2)\mathrm{d}x', \tag{D.20}$$

$$I_{22}^{(2)} = \frac{x_*^{p-3}}{4x^4}e^{-2ix}\left\{3+2x\left[3i+x(-3-2ix+x^2)\right]\right\}\int_{1/(\ell_E H)}^{x} e^{2ix'}x'^{1-p}(i+x')^2\mathrm{d}x', \tag{D.21}$$

$$I_{22}^{(3)} = \frac{x_*^{p-3}}{4x^4}e^{2ix}\left\{3+2x\left[-3i+x(-3+2ix+x^2)\right]\right\}\int_{1/(\ell_E H)}^{x} e^{-2ix'}x'^{1-p}(-i+x')^2\mathrm{d}x'. \tag{D.22}$$

Again, the integrals $I_{22}^{(1)}$, $I_{22}^{(2)}$ and $I_{22}^{(3)}$ can be computed with the same tools used above. This leads to the following expressions

$$I_{22}^{(1)} = \frac{3}{2}\frac{x_*^{p-3}}{x^4}\left[\frac{x^{2-p}}{2-p}+\frac{x^{4-p}}{4-p}-\frac{(\ell_E H)^{p-2}}{2-p}-\frac{(\ell_E H)^{p-4}}{4-p}\right] \tag{D.23}$$

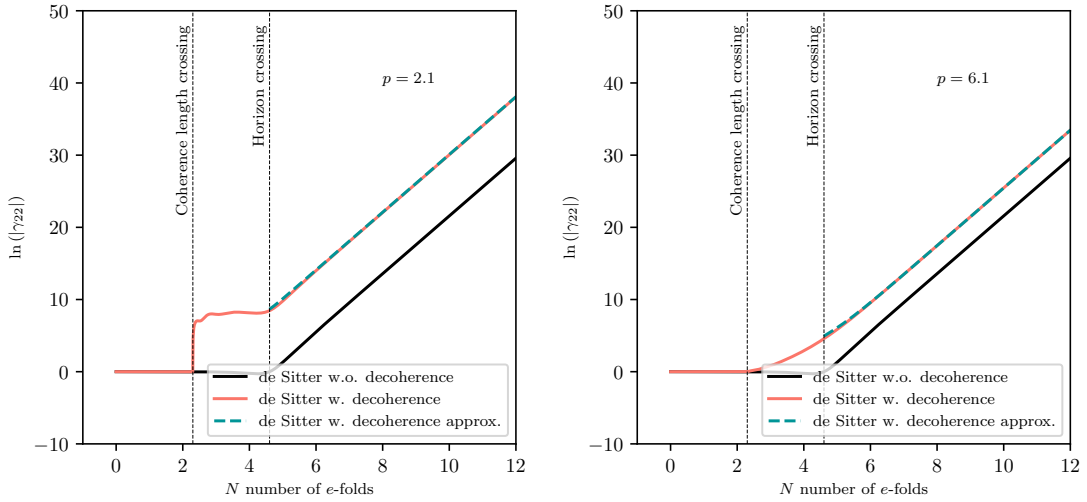

Figure 10. $\ln(|\gamma_{22}|)$ with (pink) and without (black) decoherence for the de Sitter case. The approximated version (green dashed) is obtained using the first order approximations (5.13). The first vertical dashed line shows the time when the mode $\boldsymbol{k}$ starts to decohere $\ell_E a/k = 1$, the second the time when the mode $\boldsymbol{k}$ exits the Hubble radius. The parameters are $\ell_E H = 0.1$, $x_\star = 1$, $p = 2.1$ (left) or $p = 6.1$ (right), and $k_\Gamma/k = 10$.

$$I_{22}^{(2)} = \frac{x_*^{p-3}}{4x^4} e^{-2ix} \left\{3 + 2x\left[3i + x(-3 - 2ix + x^2)\right]\right\} \left(-A_{1-p} + 2iA_{2-p} + A_{3-p}\right), \quad \text{(D.24)}$$

and $I_{22}^{(3)} = I_{22}^{(2)*}$. The quantity γ_{22} is represented in Fig. 10 for the same values of the parameters as above, that is to say $\ell_E H = 0.1$, $x_* = 1$, $p = 2.1$, and $k_\Gamma/k = 10$.

D.2 Approximations

The above results allow one to fully study the time evolution of the system, since they give exact and explicit expressions for the elements of the covariance matrix. However, the corresponding formulas are not particularly insightful and it is therefore useful to approximate them and to extract the leading behaviours of γ_{11}, γ_{12} and γ_{22} in the late time, i.e. super-Hubble, limit. This is the goal of this sub-section.

Let us start with the first component, γ_{11}. We write the function A_α in terms of its real and imaginary parts, $A_\alpha = A_\alpha^{\mathrm{R}} + iA_\alpha^{\mathrm{I}}$. Then, it follows that

$$\begin{aligned} I_{11}^{(2)} + I_{11}^{(3)} = {} & \frac{x_*^{p-3}}{2x^2}\left[\left(x^2-1\right)\left(A_{1-p}^{\mathrm{R}} - A_{3-p}^{\mathrm{R}} + 2A_{2-p}^{\mathrm{I}}\right)\right. \\ & \left. + 2x\left(A_{1-p}^{\mathrm{I}} - A_{3-p}^{\mathrm{I}} - 2A_{2-p}^{\mathrm{R}}\right)\right]\cos(2x) \\ & + \frac{x_*^{p-3}}{2x^2}\left[\left(x^2-1\right)\left(A_{1-p}^{\mathrm{I}} - A_{3-p}^{\mathrm{I}} - 2A_{2-p}^{\mathrm{R}}\right)\right. \\ & \left. - 2x\left(A_{1-p}^{\mathrm{R}} - A_{3-p}^{\mathrm{R}} + 2A_{2-p}^{\mathrm{I}}\right)\right]\sin(2x). \end{aligned} \quad \text{(D.25)}$$

Since $I_{11}^{(3)} = I_{11}^{(2)*}$, the quantity $I_{11}^{(2)} + I_{11}^{(3)}$ must be real and one can check that it is indeed the case. Then, upon Taylor expanding the real and imaginary parts of the function A_α, defined in Eq. (D.7), around $x = 0$, one obtains

$$\begin{aligned} A_\alpha^{\rm R} \simeq \mathcal{A}_\alpha^{\rm R}(\ell_E H) + x^{1+\alpha}\Bigg[&\frac{1}{\alpha+1} - \frac{2x^2}{3+\alpha} + \frac{2x^4}{3(5+\alpha)} - \frac{4x^6}{45(7+\alpha)} \\ &+ \frac{2x^8}{315(9+\alpha)} - \frac{4x^{10}}{14175(11+\alpha)} + \frac{4x^{12}}{467775(13+\alpha)} - \frac{8x^{14}}{42567525(15+\alpha)} \\ &+ \frac{2x^{16}}{638512875(17+\alpha)} - \frac{4x^{18}}{97692469875(19+\alpha)} + \cdots\Bigg], \end{aligned} \tag{D.26}$$

where

$$\begin{aligned} \mathcal{A}_\alpha^{\rm R}(\ell_E H) = 2^{-1-\alpha}\Gamma(1+\alpha)\sin\left(\frac{\pi\alpha}{2}\right) - i\,2^{-2-\alpha}\Bigg[&e^{-i\pi\alpha/2}\Gamma\left(1+\alpha, \frac{2i}{\ell_E H}\right) \\ &- e^{i\pi\alpha/2}\Gamma\left(1+\alpha, -\frac{2i}{\ell_E H}\right)\Bigg]. \end{aligned} \tag{D.27}$$

The same type of calculations lead to the following expression for the imaginary part

$$\begin{aligned} A_\alpha^{\rm I} \simeq \mathcal{A}_\alpha^{\rm I}(\ell_E H) + x^{2+\alpha}\Bigg[&\frac{2}{2+\alpha} - \frac{4x^2}{3(4+\alpha)} + \frac{4x^4}{15(6+\alpha)} - \frac{8x^6}{315(8+\alpha)} \\ &+ \frac{4x^8}{2835(10+\alpha)} - \frac{8x^{10}}{155925(12+\alpha)} + \frac{8x^{12}}{6081075(14+\alpha)} - \frac{16x^{14}}{638512875(16+\alpha)} \\ &+ \frac{4x^{16}}{10854718875(18+\alpha)} - \frac{8x^{18}}{1856156927625(20+\alpha)} + \cdots\Bigg], \end{aligned} \tag{D.28}$$

where

$$\begin{aligned} \mathcal{A}_\alpha^{\rm I}(\ell_E H) = -2^{-1-\alpha}\Gamma(1+\alpha)\cos\left(\frac{\pi\alpha}{2}\right) + 2^{-2-\alpha}\Bigg[&e^{-i\pi\alpha/2}\Gamma\left(1+\alpha, \frac{2i}{\ell_E H}\right) \\ &+ e^{i\pi\alpha/2}\Gamma\left(1+\alpha, -\frac{2i}{\ell_E H}\right)\Bigg]. \end{aligned} \tag{D.29}$$

The next step consists in using the above approximations for the real and imaginary parts of A_α in Eq. (D.25) which, together with the exact expressions of $I_{11}^{(1)}$ (which is already given in terms of power-laws) leads to an approximation for the term $I_{11}^{(1)} + I_{11}^{(2)} + I_{11}^{(3)}$. The corresponding expression reads

$$\begin{aligned} I_{11}^{(1)} + I_{11}^{(2)} + I_{11}^{(3)} \simeq x^{-p}\left[A_{11}x^6 + \mathcal{O}\left(x^8\right)\right] + \frac{B_{11}}{x^2} + C_{11} + D_{11}x + E_{11}x^3 + F_{11}x^4 \\ + G_{11}x^5 + H_{11}x^6 + \mathcal{O}\left(x^7\right), \end{aligned} \tag{D.30}$$

where

$$A_{11} = -\frac{2x_*^{p-3}}{(p-8)(p-5)(p-2)} \tag{D.31}$$

$$B_{11} = \frac{x_*^{p-3}}{2}\left[\frac{(\ell_E H)^{p-4}}{p-4} + \frac{(\ell_E H)^{p-2}}{p-2} - \mathcal{A}^{\mathrm{R}}_{1-p} - 2\mathcal{A}^{\mathrm{I}}_{2-p} + \mathcal{A}^{\mathrm{R}}_{3-p}\right], \tag{D.32}$$

$$C_{11} = B_{11}, \tag{D.33}$$

$$D_{11} = \frac{x_*^{p-3}}{3}\left(-\mathcal{A}^{\mathrm{I}}_{1-p} + 2\mathcal{A}^{\mathrm{R}}_{2-p} + \mathcal{A}^{\mathrm{I}}_{3-p}\right), \tag{D.34}$$

$$E_{11} = \frac{2}{5}D_{11}, \tag{D.35}$$

$$F_{11} = \frac{x_*^{p-3}}{9}\left(\mathcal{A}^{\mathrm{R}}_{1-p} + 2\mathcal{A}^{\mathrm{I}}_{2-p} - \mathcal{A}^{\mathrm{R}}_{3-p}\right), \tag{D.36}$$

$$G_{11} = -\frac{6}{35}D_{11}, \quad H_{11} = -\frac{1}{5}F_{11}. \tag{D.37}$$

We combine the above with Eq. (D.2) to obtain an approximation of γ_{11} which can be expressed as

$$\gamma_{11} = \frac{1}{x^2}\left[1 - 2\left(\frac{k_\Gamma}{k}\right)^2 B_{11}\right] + \mathcal{O}\left(x^0\right) - 2\left(\frac{k_\Gamma}{k}\right)^2 A_{11}x^{6-p} + \mathcal{O}\left(x^{8-p}\right). \tag{D.38}$$

Which of the two terms in the expression dominates depends on the value of p. This asymptotic expression of γ_{11} is represented by the green dashed line in Fig. 8. We see that it matches very well the exact result.

Let us now derive an approximation for the matrix element γ_{12}. Compared to what has been done above for γ_{11}, the calculation proceeds in a similar fashion. The expression of $I^{(1)}_{12}$ is already explicit, see Eq. (D.14). The two remaining terms, $I^{(2)}_{12}$ and $I^{(3)}_{12}$, have similar expressions in terms of the real and imaginary parts of A_α as $I^{(2)}_{11}$ and $I^{(3)}_{11}$. This leads to

$$\begin{aligned} I^{(2)}_{12} + I^{(3)}_{12} = \frac{x_*^{p-3}}{2x^3}\Big[&(1-2x^2)\left(-A^{\mathrm{R}}_{1-p} - 2A^{\mathrm{I}}_{2-p} + A^{\mathrm{R}}_{3-p}\right) \\ &- x(2-x^2)\left(-A^{\mathrm{I}}_{1-p} + 2A^{\mathrm{R}}_{2-p} + A^{\mathrm{I}}_{3-p}\right)\Big]\cos(2x) \\ &+ \frac{x_*^{p-3}}{2x^3}\Big[(1-2x^2)\left(-A^{\mathrm{I}}_{1-p} + 2A^{\mathrm{R}}_{2-p} + A^{\mathrm{I}}_{3-p}\right) \\ &+ x(2-x^2)\left(-A^{\mathrm{R}}_{1-p} - 2A^{\mathrm{I}}_{2-p} + A^{\mathrm{R}}_{3-p}\right)\Big]\sin(2x). \end{aligned} \tag{D.39}$$

Using this result and expanding consistently the result, one obtains the following expression

$$I^{(1)}_{12} + I^{(2)}_{12} + I^{(3)}_{12} \simeq x^{-p}\left[A_{12}x^5 + \mathcal{O}\left(x^7\right)\right] + \frac{B_{12}}{x^3} + C_{12} + D_{12}x^2 + E_{12}x^3$$

$$+ F_{12}x^4 + G_{12}x^5 + H_{12}x^6 + \mathcal{O}\left(x^7\right), \tag{D.40}$$

with

$$A_{12} = -\frac{x_*^{p-3}(p-6)}{(p-8)(p-5)(p-2)}, \tag{D.41}$$

and $B_{12} = B_{11}$, $C_{12} = -D_{11}/2$, $D_{12} = -3D_{11}/5$, $E_{12} = -2F_{11}$, $F_{12} = 3D_{11}/7$, $G_{12} = 3F_{11}/5$ and $H_{12} = -2D_{11}/27$. Using Eq. (D.10) we get

$$\gamma_{12} = \frac{1}{x^3}\left[1 - 2\left(\frac{k_\Gamma}{k}\right)^2 B_{12}\right] + \mathcal{O}\left(x^0\right) - 2\left(\frac{k_\Gamma}{k}\right)^2 \left[A_{12}x^{5-p} + \mathcal{O}\left(x^{7-p}\right)\right], \tag{D.42}$$

Again, which of the two terms dominates in the above equation depends on the value of p. The approximation (D.42) is represented in Fig. 9 and we notice that, in its domain of validity (namely, on large scales), it is very accurate.

Let us finally consider the matrix element γ_{22}. In order to establish its large scale expansion, the considerations presented before can be repeated once more. The term $I_{22}^{(1)}$ has already the adequate form, see Eq. (D.23). As a consequence, the only calculation that is needed is to express $I_{22}^{(2)} + I_{22}^{(3)}$ in terms of the real and imaginary parts of A_α. One obtains

$$\begin{aligned} I_{22}^{(2)} + I_{22}^{(3)} = {} & \frac{x_*^{p-3}}{2x^4}\Big[\left(3 - 6x^2 + 2x^4\right)\left(-A_{1-p}^{\mathrm{R}} - 2A_{2-p}^{\mathrm{I}} + A_{3-p}^{\mathrm{R}}\right) \\ & - \left(6x - 4x^3\right)\left(-A_{1-p}^{\mathrm{I}} + 2A_{2-p}^{\mathrm{R}} + A_{3-p}^{\mathrm{I}}\right)\Big]\cos(2x) \\ & + \frac{x_*^{p-3}}{2x^4}\Big[\left(3 - 6x^2 + 2x^4\right)\left(-A_{1-p}^{\mathrm{I}} + 2A_{2-p}^{\mathrm{R}} + A_{3-p}^{\mathrm{I}}\right) \\ & + \left(6x - 4x^3\right)\left(-A_{1-p}^{\mathrm{R}} - 2A_{2-p}^{\mathrm{I}} + A_{3-p}^{\mathrm{R}}\right)\Big]\sin(2x). \end{aligned} \tag{D.43}$$

The next step consists in inserting the expressions (D.26) and (D.28) of the real and imaginary parts of A_α in the above formula. This leads to the following equation for the correction

$$\begin{aligned} I_{22}^{(1)} + I_{22}^{(2)} + I_{22}^{(3)} + \frac{\omega^2}{k^2}\left[I_{11}^{(1)} + I_{11}^{(2)} + I_{11}^{(3)}\right] = {} & x^{-p}\left[A_{22}x^4 + \mathcal{O}\left(x^6\right)\right] + \frac{B_{22}}{x^4} + \frac{C_{22}}{x^2} \\ & + \frac{D_{22}}{x} + E_{22} + F_{22}x + G_{22}x^2 + H_{22}x^3 + I_{22}x^4 + J_{22}x^5 + K_{22}x^6 + \mathcal{O}\left(x^7\right), \end{aligned} \tag{D.44}$$

with

$$A_{22} = -\frac{[26 + p(p-11)]x_*^{p-3}}{(p-8)(p-5)(p-2)}, \tag{D.45}$$

and $B_{22} = B_{11}$, $C_{22} = -B_{11}$, $D_{22} = -2D_{11}$, $E_{22} = B_{11}$, $F_{22} = 7D_{11}/5$, $G_{22} = 4F_{11}$, $H_{22} = -34D_{11}/35$, $I_{22} = -8F_{11}/5$, $J_{22} = 218D_{11}/945$ and $K_{22} = 43F_{11}/175$. Finally, we obtain the following approximation for γ_{22}

$$\gamma_{22}(\eta) = \frac{1}{x^4}\left[1 - 2\left(\frac{k_\Gamma}{k}\right)^2 B_{22}\right] + \mathcal{O}\left(\frac{1}{x^2}\right) - 2\left(\frac{k_\Gamma}{k}\right)^2 A_{22}x^{4-p} + \mathcal{O}\left(x^{6-p}\right). \quad \text{(D.46)}$$

This approximation (D.46) is plotted in Fig. 10 and we notice that it fits very well the exact result. Summarising, we have obtained, for each component of the covariant matrix, precise and simple approximations valid on large scales.

An interesting feature of the above calculations is the relationships that exist between the coefficients of the expansions of γ_{11}, γ_{12} and γ_{22}. This can be understood as follows. Combining Eqs. (4.10) and (4.12), one has

$$-\frac{\mathrm{d}\gamma_{22}}{\mathrm{d}x} = \frac{\omega^2}{k^2}\frac{\mathrm{d}\gamma_{11}}{\mathrm{d}x} + 2\left(\frac{k_\Gamma}{k}\right)^2 x_*^{p-3}x^{3-p}. \quad \text{(D.47)}$$

Then, one can insert Eqs. (D.38) and (D.46) in the above formula and this leads to

$$\frac{4}{x^5} - 2\left(\frac{k_\Gamma}{k}\right)^2\left[\frac{4B_{22}}{x^5} - (4-p)A_{22}x^{3-p}\right] = -\frac{2}{x^3} + \frac{4}{x^5} - 2\left(\frac{k_\Gamma}{k}\right)^2\left[-\frac{2B_{11}}{x^3}\right.$$
$$\left. + (6-p)A_{11}x^{5-p} + \frac{4B_{11}}{x^5} - 2(6-p)A_{11}x^{3-p}\right] + 2\left(\frac{k_\Gamma}{k}\right)^2 x_*^{p-3}x^{3-p}. \quad \text{(D.48)}$$

At this stage, one has to remember that the expressions used above are valid in the long time limit only. Therefore, the term $-2/x^3$ (first term on the right hand side) can be neglected compared to $4/x^5$ (second term in the right hand side) and, indeed, the equation is satisfied in the limit $k_\Gamma \to 0$. Applying the same reasoning for the terms proportional to k_Γ^2, one deduces that $B_{22} = B_{11}$, a relation already established before but whose origin is now understood, and

$$(4-p)A_{22} = 2(6-p)A_{11} + x_*^{p-3}. \quad \text{(D.49)}$$

One checks that this equation is satisfied by A_{11} and A_{22} given in Eqs. (D.31) and (D.45). Of course, the above considerations are just an example illustrating the origin of the relationships between the coefficients. A systematic generalisation of these calculations, with more terms in the expansions, would allow us to derive all the relationships among the coefficients.

References

[1] A.A. Starobinsky, *Spectrum of relict gravitational radiation and the early state of the universe*, *JETP Lett.* **30** (1979) 682.

[2] V.F. Mukhanov and G.V. Chibisov, *Quantum Fluctuations and a Nonsingular Universe*, *JETP Lett.* **33** (1981) 532.

[3] L.P. Grishchuk and Y.V. Sidorov, *Squeezed quantum states of relic gravitons and primordial density fluctuations*, *Phys. Rev. D* **42** (1990) 3413.

[4] D. Polarski and A.A. Starobinsky, *Semiclassicality and decoherence of cosmological perturbations*, *Class. Quant. Grav.* **13** (1996) 377 [gr-qc/9504030].

[5] J. Martin and V. Vennin, *Quantum Discord of Cosmic Inflation: Can we Show that CMB Anisotropies are of Quantum-Mechanical Origin?*, *Phys. Rev. D* **93** (2016) 023505 [1510.04038].

[6] J.S. Bell, *On the Einstein-Podolsky-Rosen paradox*, *Physics Physique Fizika* **1** (1964) 195.

[7] M. Brune, E. Hagley, J. Dreyer, X. Maitre, A. Maali, C. Wunderlich et al., *Observing the Progressive Decoherence of the 'Meter' in a Quantum Measurement*, *Phys. Rev. Lett.* **77** (1996) 4887.

[8] L. Henderson and V. Vedral, *Classical, quantum and total correlations*, 0105028.

[9] H. Ollivier and W.H. Zurek, *Quantum Discord: A Measure of the Quantumness of Correlations*, *Phys. Rev. Lett.* **88** (2001) 017901.

[10] A. Bera, T. Das, D. Sadhukhan, S. Singha Roy, A. Sen De and U. Sen, *Quantum discord and its allies: a review of recent progress*, *Reports on Progress in Physics* **81** (2018) 024001 [1703.10542].

[11] A. Datta, *A Condition for the Nullity of Quantum Discord*, *arXiv e-prints* (2010) arXiv:1003.5256 [1003.5256].

[12] W.H. Zurek, *Pointer Basis of Quantum Apparatus: Into What Mixture Does the Wave Packet Collapse?*, *Phys. Rev. D* **24** (1981) 1516.

[13] W.H. Zurek, *Environment induced superselection rules*, *Phys. Rev. D* **26** (1982) 1862.

[14] V.F. Mukhanov, H.A. Feldman and R.H. Brandenberger, *Theory of cosmological perturbations. Part 1. Classical perturbations. Part 2. Quantum theory of perturbations. Part 3. Extensions*, *Phys. Rept.* **215** (1992) 203.

[15] C.P. Burgess, R. Holman and D. Hoover, *Decoherence of inflationary primordial fluctuations*, *Phys.Rev.* **D77** (2008) 063534 [astro-ph/0601646].

[16] D. Campo and R. Parentani, *Decoherence and entropy of primordial fluctuations. i. formalism and interpretation*, *Phys. Rev. D* **78** (2008) 065044.

[17] S. Choudhury, S. Panda and R. Singh, *Bell violation in the Sky*, *Eur. Phys. J. C* **77** (2017) 60 [1607.00237].

[18] T.J. Hollowood and J.I. McDonald, *Decoherence, discord and the quantum master equation for cosmological perturbations*, *Phys. Rev. D* **95** (2017) 103521 [1701.02235].

[19] J. Martin and V. Vennin, *Observational constraints on quantum decoherence during inflation*, *JCAP* **05** (2018) 063 [1801.09949].

[20] J. Martin and V. Vennin, *Non Gaussianities from Quantum Decoherence during Inflation*, *JCAP* **06** (2018) 037 [1805.05609].

[21] J. Martin and V. Vennin, *Real-space entanglement in the Cosmic Microwave Background*, 2106.15100.

[22] S.-Y. Lin, C.-H. Chou and B.L. Hu, *Quantum entanglement and entropy in particle creation*, *Phys. Rev. D* **81** (2010) 084018 [1001.4922].

[23] J.-T. Hsiang and B.-L. Hu, *Intrinsic Entropy of Squeezed Quantum Fields and Nonequilibrium Quantum Dynamics of Cosmological Perturbations*, 2110.02757.

[24] J. Grain and V. Vennin, *Canonical transformations and squeezing formalism in cosmology*, *JCAP* **02** (2020) 022 [1910.01916].

[25] J. Martin and V. Vennin, *Real-space entanglement of quantum fields*, 2106.14575.

[26] S. Robertson, F. Michel and R. Parentani, *Assessing degrees of entanglement of phonon states in atomic Bose gases through the measurement of commuting observables*, *Phys. Rev. D* **96** (2017) 045012 [1705.06648].

[27] G. Adesso, S. Ragy and A.R. Lee, *Continuous variable quantum information: Gaussian states and beyond*, *Open Systems & Information Dynamics* **21** (2014) 1440001.

[28] R. Simon, E.C.G. Sudarshan and N. Mukunda, *Gaussian-wigner distributions in quantum mechanics and optics*, *Phys. Rev. A* **36** (1987) 3868.

[29] R. Simon, E. Sudarshan and N. Mukunda, *Gaussian wigner distributions: A complete characterization*, *Physics Letters A* **124** (1987) 223 .

[30] W.B. Case, *Wigner functions and weyl transforms for pedestrians*, *American Journal of Physics* **76** (2008) 937 [https://doi.org/10.1119/1.2957889].

[31] C. Cohen-Tannoudji, J. Dupont-Roc and G. Grunberg, *Atom - Photon Interactions: Basic Process and Appilcations*, Wiley-Interscience (1992).

[32] M. Le Bellac, *Quantum Physics*, Cambridge University Press (2006).

[33] P. Pearle, *Simple Derivation of the Lindblad Equation*, *Eur. J. Phys.* **805** (2012) [1204.2016].

[34] R.d.J.N. Carlos Alexandre Brasil, Felipe Fernandes Fanchini, *A simple derivation of the Lindblad equation*, *Rev. Bras. Ensino Fís.* **35** (2012) [1110.2122].

[35] G. Lindblad, *On the Generators of Quantum Dynamical Semigroups*, *Commun. Math. Phys.* **48** (1976) 119.

[36] G. Kaplanek and C.P. Burgess, *Hot Accelerated Qubits: Decoherence, Thermalization, Secular Growth and Reliable Late-time Predictions*, *JHEP* **03** (2020) 008 [1912.12951].

[37] A.O. Caldeira and A.J. Leggett, *Influence of dissipation on quantum tunneling in macroscopic systems*, *Phys. Rev. Lett.* **46** (1981) 211.

[38] A.O. Caldeira and A.J. Leggett, *Quantum tunneling in a dissipative system*, *Annals Phys.* **149** (1983) 374.

[39] A.O. Caldeira and A.J. Leggett, *Path integral approach to quantum Brownian motion*, *Physica A* **121** (1983) 587.

[40] H. Kodama and M. Sasaki, *Cosmological Perturbation Theory*, *Prog. Theor. Phys. Suppl.* **78** (1984) 1.

[41] Y.-R. Chen, H.-Y. Hsieh, J. Ning, H.-C. Wu, H.L. Chen, Y.-L. Chuang et al., *Experimental Reconstruction of Wigner Distribution Currents in Quantum Phase Space*, 2111.08285.

[42] P. Giorda and M.G.A. Paris, *Gaussian Quantum Discord*, *Phys. Rev. Lett.* **105** (2010) 020503 [1003.3207].

[43] J. Martin and V. Vennin, *Bell inequalities for continuous-variable systems in generic squeezed states*, *Phys. Rev. A* **93** (2016) 062117 [1605.02944].

[44] J. Martin and V. Vennin, *Leggett-Garg Inequalities for Squeezed States*, *Phys. Rev. A* **94** (2016) 052135 [1611.01785].

[45] J. Martin and V. Vennin, *Obstructions to Bell CMB Experiments*, *Phys. Rev. D* **96** (2017) 063501 [1706.05001].

[46] K. Ando and V. Vennin, *Bipartite temporal Bell inequalities for two-mode squeezed states*, *Phys. Rev. A* **102** (2020) 052213 [2007.00458].

[47] R. Simon, *Peres-horodecki separability criterion for continuous variable systems*, *Phys. Rev. Lett.* **84** (2000) 2726.

[48] H. Goldstein, C. Poole and J. Safko, *Classical Mechanics*, Addison Wesley (2002).

[49] T. Colas, J. Grain and V. Vennin, *Four-mode squeezed states: two-field quantum systems and the symplectic group* $\mathrm{Sp}(4,\mathbb{R})$, 2104.14942.

[50] A.S. Holevo and R.F. Werner, *Evaluating capacities of Bosonic Gaussian channels*, *arXiv e-prints* (1999) quant [quant-ph/9912067].

[51] G. Adesso and A. Datta, *Quantum versus Classical Correlations in Gaussian States*, *Phys. Rev. Lett.* **105** (2010) 030501 [1003.4979].

[52] H. Goldstein, C. Poole and J. Safko, *Classical Mechanics*, Addison Wesley (2002).

[53] I.S. Gradshteyn and I.M. Ryzhik, *Table of Integrals, Series, and Products*, Academic Press, New York and London (1965).

[54] M. Abramowitz and I.A. Stegun, *Handbook of Mathematical Functions with Formulas, Graphs, and Mathematical Tables*, Dover, New York City, ninth dover printing, tenth gpo printing ed. (1964).

2.4 Article: 'Comparing quantumness criteria'

As shown in the review [1], many quantumness criteria have been used to assess the degree of non-classicality of cosmological perturbations in slightly different situations. In [3] reproduced in this section, we thoroughly compare three such criteria over a general class of states, the two-mode squeezed thermal states, which cover most of the decohered states considered in the literature on inflationary perturbations and beyond. The analysis is kept at a very general level, and the paper is presented as one of quantum information. We supplement our general analysis with the study of the effect on an initial two-mode squeezed states of two simple Gaussian channels i.e. transformations of the state that needs not be unitary, modelling losses and noise in a measurement process. Therefore, although the initial motivation behind this work is the study of cosmological perturbations, the comparison also applies to the study of the experiment [130] in which we expect the state of correlated quasi-particles to be mixed and quasi-Gaussian, see Sec 3.6.

Comparing quantumness criteria

Jérôme Martin[1], Amaury Micheli,[2,1] and Vincent Vennin[3,1]

[1] *Institut d'Astrophysique de Paris, CNRS & Sorbonne Université, UMR 7095 98 bis boulevard Arago, 75014 Paris, France*
[2] *Université Paris-Saclay, CNRS/IN2P3, IJCLab, 91405, Orsay, France*
[3] *Laboratoire de Physique de l'Ecole Normale Supérieure, ENS, CNRS, Université PSL, Sorbonne Université, Université Paris Cité, F-75005 Paris, France*

Abstract –Measuring the quantumness of a system can be done with a variety of methods. In this article we compare different criteria, namely quantum discord, Bell inequality violation and non-separability, for systems placed in a Gaussian state. When the state is pure, these criteria are equivalent, while we find that they do not necessarily coincide when decoherence takes place. Finally, we prove that these criteria are essentially controlled by the semi-minor axis of the ellipse representing the state's Wigner function in phase space.

Introduction. – The characterisation of "classicality" and "quantumness" in quantum systems has become a topic of major importance in several branches of modern physics. Indeed, maybe surprisingly, it is not always trivial to establish whether a system behaves "classically" or "quantum-mechanically". This question is especially important when one tries to understand the nature of a physical phenomenon.

For instance, in cosmology, it is well-known that primordial perturbations are very well reproduced [20] by vacuum quantum fluctuations, amplified by gravitational instability [8, 33, 35, 60, 61, 75] during an early epoch of accelerated expansion named inflation [5, 32, 46, 47, 69, 74]. However, the quantum origin of those primordial perturbations has never been tested directly and, in practice, they are mostly treated by astronomers as classical, stochastic fluctuations. The reason why this is possible is that, under peculiar circumstances, and for certain observables, a quantum system can be mimicked by a classical one [45, 51, 53]. However, if a genuine quantum signature could be detected in cosmological observables, that would shed light on fundamental issues such as the need to quantise gravitational degrees of freedom or the emergence of classicality at cosmological scales [7, 49, 55, 59, 64, 78].

The same need to distinguish classical from quantum processes appears in analogue gravity, where phenomena involving gravitational physics are mapped to condensed-matter systems. In these setups, particles can either be created by quantum channels or by the classical amplification of a thermal bath [12]. The latter mechanism is always present when conducting

experiments at finite temperature. A quantum test is a way to tell the two populations apart and to demonstrate the existence of a quantum channel in these experiments [12, 40, 68, 76].

In quantum technologies, the distinction between quantum and classical behaviours is also central, since "quantumness" is a crucial resource e.g. in quantum computing [43] and quantum cryptography [21, 66].

This has led various notions of "quantumness" to be put forward. One possible approach is to consider correlations between sub-parts of a given system, and to determine whether or not they can be reproduced by classical random variables. This route gave rise to the celebrated Bell inequalities [6, 18, 29], quantum steering [83], different measures of entanglement (non-separability [81], multipartite entanglement [38], entanglement witnesses [37], *etc.*), quantum discord [11, 36, 63], *etc.*.

Another possible approach, leading to a second class of criteria, is to make use of phase-space formulations of quantum mechanics. For instance, the non-positivity of the Wigner function [82] or the absence of the P-representation [28, 77] have been viewed as criteria signalling the quantumness of a system [26, 80].

How these different criteria are related is a non-trivial question. In pure states, it is known that quantum discord reduces to entanglement entropy [11], which only vanishes in separable states, and that all non-separable states violate a Bell inequality [81]. For mixed states however, these relations become more elusive (for instance non-separability is only a necessary condition for Bell-inequality violation [81]).

In this article, our goal is to investigate the relations between different criteria in a subclass of quantum states where explicit calculations can be performed. We want to determine in which cases they lead to the same conclusion regarding the quantumness of a system, and in which cases they differ. In practice, we consider two continuous degrees of freedom placed in two-mode squeezed thermal states and analyse the link between three quantum criteria: non-separability, quantum discord and a Bell inequality.

Gaussian states. – Let us consider two continuous degrees of freedom q_1 and q_2, with conjugated momenta p_1 and p_2, arranged into the phase-space vector $\hat{\boldsymbol{R}}_{1/2} = (\hat{q}_1, \hat{p}_1, \hat{q}_2, \hat{p}_2)^{\mathrm{T}}$ with $[\hat{q}_i, \hat{p}_j] = i\delta_{ij}$. Their quantum state is represented by the density matrix $\hat{\rho}$. For a given quantum operator $\hat{O}$, the Weyl transform

$$\tilde{O}(\boldsymbol{R}_{1/2}) \equiv \int \mathrm{d}u_1\, \mathrm{d}u_2\, e^{-ip_1u_1 - ip_2u_2} \times \left\langle q_1 + \frac{u_1}{2}, q_2 + \frac{u_2}{2} \middle| \hat{O} \middle| q_1 - \frac{u_1}{2}, q_2 - \frac{u_2}{2} \right\rangle \quad (1)$$

yields a scalar function in phase space. The Wigner function W is the Weyl transform of the density matrix [16], $W = \tilde{\rho}/(2\pi)^2$, and is such that the expectation value of any quantum operator $\hat{A}$ is given by the phase-space average of its Weyl transform against the Wigner function,

$$\left\langle \hat{A} \right\rangle = \int \tilde{A}\left(\boldsymbol{R}_{1/2}\right) W(\boldsymbol{R}_{1/2})\, \mathrm{d}^4\boldsymbol{R}_{1/2}\,. \quad (2)$$

This is why the Wigner function is often referred to as a "quasi-probability" distribution function.

A Gaussian state is defined as a state whose Wigner function is Gaussian. All information about the state is then contained in the covariance matrix

$$\gamma_{ab} = \langle \{\hat{R}_a, \hat{R}_b\} \rangle\,, \quad (3)$$

where $\hat{R}_a$ refers to the components of the vector $\hat{\boldsymbol{R}}_{1/2}$, $\{\hat{A}, \hat{B}\} = \hat{A}\hat{B} + \hat{B}\hat{A}$ is the anti-commutator and the Wigner function reads

$$W(\boldsymbol{R}_{1/2}) = \frac{1}{\pi^2\sqrt{\det\boldsymbol{\gamma}}} \exp\left(-\boldsymbol{R}_{1/2}^{\mathrm{T}}\boldsymbol{\gamma}^{-1}\boldsymbol{R}_{1/2}\right)\,. \quad (4)$$

Let us also introduce the purity $p \equiv \mathrm{Tr}(\hat{\rho}^2)$, which determines whether the state is pure ($p = 1$) or mixed ($p < 1$). For a Gaussian state, the purity is directly related to the determinant of the covariance matrix [2]

$$p = \frac{1}{\sqrt{\det\boldsymbol{\gamma}}}\,. \quad (5)$$

Two-mode squeezed vacuua (TMSV) are Gaussian states whose covariance matrix depend on two parameters only, r and φ, respectively called squeezing amplitude and squeezing angle, and reads [9, 17, 70]

$$\boldsymbol{\gamma}^{\mathrm{TMSV}} \equiv \begin{pmatrix} \boldsymbol{\gamma}^{11} & \boldsymbol{\gamma}^{12} \\ \boldsymbol{\gamma}^{21} & \boldsymbol{\gamma}^{22} \end{pmatrix} , \tag{6}$$

with

$$\boldsymbol{\gamma}^{11} = \boldsymbol{\gamma}^{22} \equiv \cosh(2r)\mathbb{1}_2 , \tag{7}$$

and

$$\boldsymbol{\gamma}^{12} = \boldsymbol{\gamma}^{21} \equiv -\sinh 2r \begin{pmatrix} \cos 2\varphi & \sin 2\varphi \\ \sin 2\varphi & -\cos 2\varphi \end{pmatrix} . \tag{8}$$

TMSV are ubiquitous in modern physics : they appear in quantum optics [9, 17, 70], cold atoms [22, 62] as well as in the study of inflation [3, 19, 30, 31] and Hawking radiation [4, 34]. Using Eq. (5) one can check that they are pure. In general, TMSV may become mixed as an effect of decoherence [42, 84, 85]. We will consider the class of two-mode squeezed thermal states which are defined as Gaussian states with covariance matrices of the form

$$\boldsymbol{\gamma} = \frac{\boldsymbol{\gamma}^{\mathrm{TMSV}}}{\sqrt{p}} , \tag{9}$$

where one can check from Eq. (5) that p is indeed the purity of the state. These states arise for instance for cosmological perturbations linearly coupled to an environment while preserving statistical homogeneity [15, 50], or when an initial TMSV interacts with two identical independent thermal baths [23, 48], or when the modes are sent through a pure-loss or an additive Gaussian noise channel [25]. The two latter channels are described by simple transformations of the covariance matrix, respectively given by $\boldsymbol{\gamma} = \eta\boldsymbol{\gamma}^{\mathrm{TMSV}} + (1-\eta)\,\mathbb{1}_4$ where the efficiency parameter $0 \leq \eta \leq 1$ encodes the level of loss/damping experienced across the channel, and $\boldsymbol{\gamma} = \boldsymbol{\gamma}^{\mathrm{TMSV}} + \Delta\mathbb{1}_4$ where $\Delta \geq 0$ encodes the level of noise. Both matrices can then be put in the form (9), with effective squeezing and purity parameters given in Eqs. (66) and (70) of the Appendix where these two channels are studied in details.

In the following we work in terms of these effective squeezing and purity parameters, such that all setups mentioned above are encompassed in the analysis. Decoherence is expected to play a key role in the emergence of classicality, and this simply parameterised class of states will allow us to study how different criteria respond to it.

Under a canonical transformation, $\hat{\boldsymbol{R}} \to \boldsymbol{T}\hat{\boldsymbol{R}}$, where $\boldsymbol{T}$ is a symplectic matrix (i.e. it preserves commutation relations), the covariance matrix changes according to $\boldsymbol{\gamma} \to \boldsymbol{T}\boldsymbol{\gamma}\boldsymbol{T}^{\mathrm{T}}$. This implies that the covariance matrix depends on the set of canonical variables used to describe a system.

For instance, there exists a partition $\hat{\boldsymbol{R}}_{\mathrm{D}}$ where the covariance matrix is block diagonal,

$$\gamma^{\mathrm{D}} = \frac{1}{\sqrt{p}} \begin{pmatrix} \gamma^{\mathrm{OMSV}} & 0 \\ 0 & \gamma^{\mathrm{OMSV}} \end{pmatrix} , \tag{10}$$

with

$$\gamma^{\mathrm{OMSV}} \equiv \begin{pmatrix} \gamma_{qq} & \gamma_{qp} \\ \gamma_{pq} & \gamma_{pp} \end{pmatrix} \tag{11}$$

and

$$\gamma_{qq} = [\cosh(2r) - \cos(2\varphi)\sinh(2r)] , \tag{12}$$

$$\gamma_{pq} = \gamma_{\mathrm{qp}} = -\sin(2\varphi)\sinh(2r), \tag{13}$$

$$\gamma_{pp} = [\cosh(2r) + \cos(2\varphi)\sinh(2r)] , \tag{14}$$

such that the Wigner function factorises according to $W^{\mathrm{D}}(\boldsymbol{R}^{\mathrm{D}}) = \bar{W}(q_1^{\mathrm{D}}, p_1^{\mathrm{D}})\bar{W}(q_2^{\mathrm{D}}, p_2^{\mathrm{D}})$. In this basis, the quantum state is nothing but the product of two identical and uncorrelated one-mode squeezed (thermal) states. If $p = 1$ they are one-mode squeezed vacuua (OMSV).

This also implies that quantumness criteria, which characterise the correlations between two subsystems, obviously depend on the way the system is partitioned (for instance, the way quantum discord depends on the choice of partition has been studied in Refs. [50, 52]).

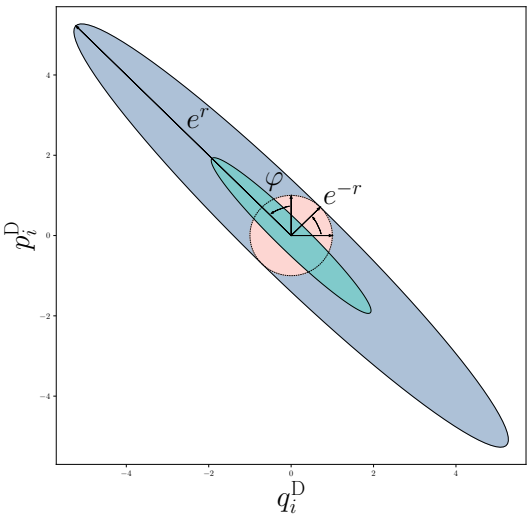

Fig. 1: Phase-space $\sqrt{2}$-σ contour levels of the Wigner function $\bar{W}$. The pink circle corresponds to a vacuum state (coherent state) with $p = 1$ and vanishing squeezing parameter $r = 0$. The green ellipse represents a pure state $p = 1$, slightly squeezed $r = 1$ along the diagonal $\varphi = \pi/4$. The blue ellipse represents a state with the same squeezing parameter $r = 1$ but with purity $p = e^{-4} \approx 0.018$ such that its semi-minor axis is of the same size as in the vacuum state.

In practice, their often exists a "preferred" basis of operators corresponding to separately measurable physical degrees of freedom [56, 57] The factorised partition (10) is nonetheless useful as it provides a simple geometric representation of the quantum state: the contours of $\bar{W}$ are ellipses in the phase space $(q_i^{\mathrm{D}}, p_i^{\mathrm{D}})$, as displayed in Fig. 1. Their eccentricity is controlled by r, φ is the angle between the q_i^{D}-axis and the semi-minor axis, and the area contained in the ellipses is proportional to $1/p$.

Quantumness criteria. – Since the quantum states we consider are fully characterised by the three parameters r, φ and p, let us express the three quantumness criteria in terms of these parameters, in order to compare them.

Quantum Discord. A first way to characterise the presence of quantum correlations between two sub-parts of a system is by quantum discord [36, 63]. The idea is to introduce two measures of correlation that coincide for classically correlated setups thanks to Bayes' theorem, but that may differ for quantum systems. The first measure is the so-called mutual information $\mathcal{I}$, which is the sum between the von-Neumann entropy of both reduced sub-systems, minus the entropy of the entire system. The second measure $\mathcal{J}$ evaluates the difference between the entropy contained in the first subsystem, and the entropy contained in that same subsystem when the second subsystem has been measured, where an extremisation is performed over all possible ways to "measure" the second subsystem. $\mathcal{J}$ can be shown to be always less than $\mathcal{I}$. Quantum discord $\mathcal{D}$ is defined as the difference between these two measures and is thus a positive quantity that only vanishes for classical systems.

For Gaussian states, $\mathcal{I}$, $\mathcal{J}$ and $\mathcal{D}$ can be expressed in terms of the local symplectic invariants of the covariance matrix [2].[1] It is shown in [1, 27, 65] that, for covariance matrices of the form (9), quantum discord depends on r and p only and is given by

$$\mathcal{D}(p,r) = f\left[\sigma(p,r)\right] - 2f\left(p^{-1/2}\right) + f\left[\frac{\sigma(p,r)+p^{-1}}{\sigma(p,r)+1}\right], \tag{15}$$

where the function $f(x)$ is defined for $x \geq 1$ by

$$f(x) \equiv \left(\frac{x+1}{2}\right)\log_2\left(\frac{x+1}{2}\right) - \left(\frac{x-1}{2}\right)\log_2\left(\frac{x-1}{2}\right), \tag{16}$$

[1] This means that quantum discord is invariant under local symplectic transformations, i.e. those mixing q_i with p_i but not with q_j and p_j. This explains why φ does not appear in the final expression (15), since it can be changed arbitrarily by performing phase-space rotations in each sector.

and

$$\sigma(p,r) = \frac{\cosh(2r)}{\sqrt{p}}\,. \tag{17}$$

Note that in the partition (10), where the covariance matrix is block-diagonal, the two subsystems are uncorrelated hence quantum discord vanishes.

Bell Inequality. Another way to characterise the presence of quantum correlations is via Bell inequalities [10]. When violated, they allow one to exclude classical and realistic local theories [58]. Usually designed for discrete observables [18](such as spins), they can also be applied to continuous variables by means of pseudo-spin operators [6, 29] or via projections on coherent states [14]. In this paper we will use the pseudo-spin operators introduced in Ref. [29]

$$\hat{\sigma}_x^i = \int_{-\infty}^{\infty} \mathrm{sign}(q_i)\,|q_i\rangle\langle q_i|\,\mathrm{d}q_i\,, \tag{18}$$

$$\hat{\sigma}_y^i = -i\int_{-\infty}^{\infty} \mathrm{sign}(q_i)\,|q_i\rangle\langle -q_i|\,\mathrm{d}q_i\,, \tag{19}$$

$$\hat{\sigma}_z^i = -\int_{-\infty}^{\infty} |q_i\rangle\langle -q_i|\,\mathrm{d}q_i\,. \tag{20}$$

One can check that these operators satisfy the SU(2) commutation relations

$$\left[\hat{\sigma}_\mu^i, \hat{\sigma}_\nu^j\right] = 2i\epsilon_{\mu\nu\lambda}\hat{\sigma}_\lambda^i\delta^{ij}\,, \tag{21}$$

where $\epsilon_{\mu\nu\lambda}$ is the totally anti-symmetric tensor.

From these operators we can build a Bell inequality [29, 54]

$$\langle\hat{B}\rangle = 2\sqrt{\langle\hat{\sigma}_z^1\hat{\sigma}_z^2\rangle^2 + \langle\hat{\sigma}_x^1\hat{\sigma}_x^2\rangle^2} \leq 2. \tag{22}$$

In order to compute the two-point correlation functions of the operators $\hat{\sigma}_x$ and $\hat{\sigma}_z$, one can derive their Weyl transform and make use of Eq. (2). Since $\hat{\sigma}_\mu^1$ and $\hat{\sigma}_\mu^2$ act on different degrees of freedom, the Weyl transform of their product factorises as

$$\widetilde{\sigma_\mu^1\sigma_\nu^2} = \widetilde{\sigma_\mu^1}\,\widetilde{\sigma_\nu^2}\,, \tag{23}$$

and in the appendix we show that

$$\widetilde{\sigma_z^i} = -\pi\delta(q_i)\delta(p_i), \quad \widetilde{\sigma_x^i} = \mathrm{sgn}(q_i)\,, \tag{24}$$

where δ stands for the Dirac distribution. Together with Eq. (2), this leads to

$$\left\langle\hat{\sigma}_z^i\hat{\sigma}_z^j\right\rangle = p\,, \tag{25}$$

$$\left\langle\hat{\sigma}_x^i\hat{\sigma}_x^j\right\rangle = -\frac{2}{\pi}\arcsin\left[|\cos(2\varphi)|\tanh(2r)\right]\,. \tag{26}$$

Inserting Eqs. (25) and (26) into Eq. (22) leads to

$$\langle\hat{B}\rangle = 2\sqrt{p^2 + \frac{4}{\pi^2}\arcsin^2\left[\cos(2\varphi)\tanh(2r)\right]}\,. \tag{27}$$

Compared to quantum discord given in Eq. (15), one can see that the mean value of the Bell operator $\langle\hat{B}\rangle$ depends on the squeezing angle φ in addition to the squeezing amplitude r and the purity p. This is expected since the operators given in Eq. (18) are not invariant under local symplectic transformations.

Non-separability. Finally we consider quantum separability. A state is said to be separable in a certain partition if its density matrix can be written as a statistical mixture of products of density matrices over the two sub-systems, i.e.

$$\hat{\rho} = \sum_i \alpha_i\hat{\rho}_1^i \bigotimes \hat{\rho}_2^i, \tag{28}$$

where α_i are real coefficients. In general, proving that a state is separable is a non-trivial task, yet, for Gaussian states, the so-called Peres-Horodecki criterion was proven to be necessary and sufficient [72]. In the appendix we show how to evaluate this criterion for Gaussian states, in a one-parameter family of partitions that contains both Eq. (9) and Eq. (10). In the partition corresponding to Eq. (10), the state is, as expected, always separable, while for Eq. (9) we find that the state is separable if and only if

$$e^{-2r} \geq \sqrt{p}\,. \tag{29}$$

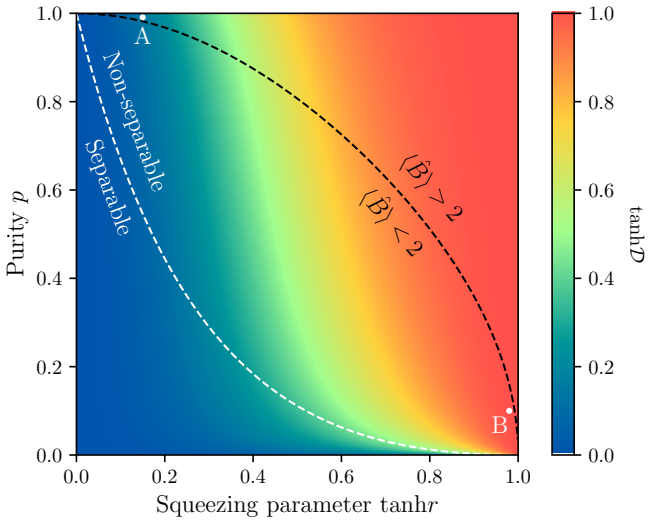

Fig. 2: Hyperbolic tangent of the quantum discord $\tanh\mathcal{D}$ computed from Eq. (15) as a function of the purity p and the hyperbolic tangent of the squeezing parameter $\tanh r$. The dashed white (respectively black) line represents the threshold of separability (respectively Bell inequality violation) defined as the equality case in Eq. (29) [respectively Eq. (27)].

Results & Discussion. – Let us first make connection with the phase-space approaches mentioned in the introduction. We point out that the thermal squeezed states considered here always have a *positive* Wigner phase-space probability distribution, which could make them appear classical. Yet, as demonstrated, these states can exhibit quantum features. We refer to Refs. [24, 49, 67] for detailed discussions of this point. Additionally, for these states, the absence of a Glauber-Sudarshan P-representation, which is considered as a sign of non-classicality, is actually equivalent to the non-separability of the state [13, 44] whose conditions has been computed in Eq. (29).

We now compare the three different criteria for deciding whether a system behaves quantum-mechanically or not: the quantum discord (15), the violation of Bell inequalities (27) and the non-separability of the state (29). As mentioned above, the squeezing angle φ can be adjusted by rotating the measurement direction in phase space. This is why, for the Bell inequality (27), which is the only criterion depending on φ, we choose to optimise φ in order to get the maximal violation. It corresponds to setting $\varphi = 0$. All three criteria thus depend on r and p only, and are shown in Fig. 2. The colour encodes the value of quantum discord as given by Eq. (15), the black dashed line corresponds to the threshold for Bell-inequality violation, Eq. (27), while the white line stands for the non-separability criterion as given in Eq. (29).

One can check that, for pure state ($p = 1$), all criteria are equivalent: except from the vacuum state ($r = 0$), all states have non-vanishing quantum discord, are non separable and violate the Bell inequality. In this sense, for a pure Gaussian state, any correlation is quantum in nature. For mixed states ($p < 1$), non-separability is a necessary but non-sufficient condition for the Bell-inequality violation [81] (i.e. the white line is below the black line), and non-discordant states are separable [11] (i.e. the dark blue region is below

the white line).

These results also confirm that decoherence (i.e. smaller value for p) is associated to the emergence of classicality. Indeed, for a given squeezing amplitude r, there always exists a value of the purity parameter p below which the Bell inequality is not violated, the state is separable and quantum discord is smaller than a given threshold. The required amount of decoherence (i.e. the critical value for the purity parameter p), increases (decreases) with the squeezing amplitude. This is because, as r increases, the two subsystems get more entangled, hence it takes more decoherence to erase quantum features. In [48], the authors had considered a similar class of states and studied the robustness of non-classicality measures against decoherence induced by coupling to thermal baths. In this special case it was also found that the state becomes classical in the sense that quantum discord asymptotes zero at large decoherence, and that separability vanishes once decoherence reaches a certain finite threshold.

Our findings also prompt some reservations about the physical relevance of the numerical value of quantum discord. Discord is measured in information bits and, a priori, one may think that it is an extensive quantity, namely the larger the discord the more "quantum" the state. However, one notices in Fig. 2 that the value of quantum discord at which the separability or Bell criteria are crossed may be small or large, depending on the squeezing amplitude. For instance, if the state is almost pure $p \sim 1$ and the squeezing weak $r \leq 1$, then one can achieve a non-separable state and/or a Bell inequality violation while keeping a small quantum discord, see point "A"; or for large squeezing and small purity we can both have a large quantum discord and still satisfy the Bell inequality, see point "B". This suggests that the numerical value of discord itself has no clear interpretation, at least in this setup and in terms of the other quantumness criteria.

The behaviour of these three criteria can be further understood in the phase-space representation. Ignoring the orientation φ (which we have set to its optimal value $\varphi = 0$ for Bell inequality violation), the ellipses of Fig. 1 have been parameterised so far using their area, via p, and their eccentricity, via r. Alternatively, one can describe them by means of their semi-major, a, and semi-minor, b, axes, related to r and p by

$$a = e^r p^{-1/4}, \quad b = e^{-r} p^{-1/4}. \tag{30}$$

In particular, we expect b, the size of semi-minor axis, to play a physical role since it encodes the presence or absence of a sub-fluctuant direction in phase space with respect to the vacuum.

Using Eq. (30) all criteria can be expressed in terms of a and b. The non-separability criterion assumes an extremely simple form as Eq. (29) is straightforwardly recast to $b \geq 1$. The fact that the state is non-separable is then equivalent to the existence of a sub-fluctuant direction in phase space (for instance, in Fig. 1 the state represented by the green ellipse is non-separable while the one represented by the blue ellipse is separable). The expression of quantum discord and the Bell operator in terms of a and b is not particularly illuminating but in the large-squeezing and small-purity limit, i.e. $a \gg b \gg 1/a$, in the appendix we show that the discord also becomes a function of b only (i.e. of the sub-fluctuant mode), namely

$$\mathcal{D}(a,b) \to g\left(1+2b^2\right) + \log_2\left(1+\frac{1}{2b^2}\right), \tag{31}$$

where $g(x)$ is bounded and defined in Eq. (64).

All criteria are displayed as a function of a and b in Fig. 3, where one can check that $\langle \hat{B} \rangle$ and $\mathcal{D}$ become independent of a in the large-squeezing limit.

Conclusions. – In this letter, we compared three different criteria, quantum discord, Bell inequality violation and non-separability, aimed at assessing whether a system behaves quantum-mechanically or not. We have found that, even in a simple class of Gaussian states, these criteria are inequivalent, i.e. a state can be, at the same time, "quantum" according to one criterion and "classical" according to another one. However,

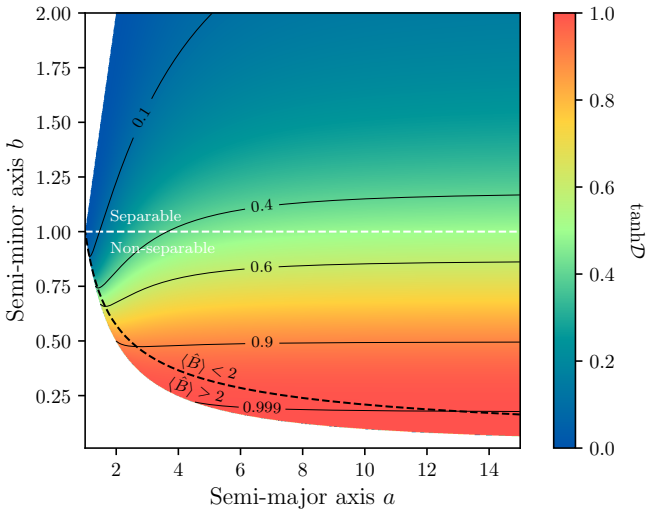

Fig. 3: Same criteria as in Fig. 2, as a function of the semi-major a and semi-minor b axes of the phase-space ellipses depicted in Fig. 1. The solid black lines are contour levels of quantum discord. The white region corresponds to either $a < b$ or $p > 1$, which are both non physical. In the large squeezing limit, $b \ll a$, $\langle \hat{B} \rangle = 2$ (black dashed line) is equivalent to $b = [\pi/(8a^3)]^{1/5}$.

in the large squeezing limit these criteria were found to be mainly controlled by the amplitude of the sub-fluctuant mode. There is no natural threshold for the value of quantum discord at which the other two criteria are crossed, and we found that decoherence always leads to more classical states regardless of the criterion being used.

This analysis could be extended to non-Gaussian states [79], which are known to behave differently under quantum criteria (for instance, according to Hudson theorem [39] their Wigner functions are necessarily non-positive if they are pure).

* * *

We thank Scott Robertson for interesting discussions and useful suggestions. A. Micheli is supported by the French National Research Agency under the Grant No. ANR-20-CE47-0001 associated with the project COSQUA.

REFERENCES

[1] Gerardo Adesso and Animesh Datta. Quantum versus Classical Correlations in Gaussian States. *Physical Review Letters*, 105(3):030501, July 2010.

[2] Gerardo Adesso, Sammy Ragy, and Antony R. Lee. Continuous variable quantum information: Gaussian states and beyond. *Open Systems & Information Dynamics*, 21(01n02):1440001, June 2014.

[3] Ivan Agullo, Béatrice Bonga, and Patricia Ribes Metidieri. Does inflation squeeze cosmological perturbations? *arXiv:2203.07066*, March 2022.

[4] Ivan Agullo, Anthony J. Brady, and Dimitrios Kranas. Event horizons are tunable factories of quantum entanglement. 9 2022.

[5] Andreas Albrecht and Paul J. Steinhardt. Cosmology for Grand Unified Theories with Radiatively Induced Symmetry Breaking. *Phys. Rev. Lett.*, 48:1220–1223, 1982.

[6] Konrad Banaszek and Krzysztof Wodkiewicz. Quantum Nonlocality in Phase Space. *Physical Review Letters*, 82(10):2009–2013, March 1999.

[7] Shreya Banerjee, Sayantani Bera, and Tejinder P. Singh. Quantum discord as a tool for comparing collapse models and decoherence. *Physics Letters A*, 380(45):3778–3785, November 2016.

[8] James M. Bardeen, Paul J. Steinhardt, and Michael S. Turner. Spontaneous Creation of Almost Scale - Free Density Perturbations in an Inflationary Universe. *Phys. Rev. D*, 28:679, 1983.

[9] S. M. Barnett and P. M. Radmore. *Methods in Theoretical Quantum Optics*. Clarendon Press Publication, Oxford, 1997.

[10] J. S. Bell. On the Einstein Podolsky Rosen paradox. *Physics Physique Fizika*, 1(3):195–200, November 1964.

[11] Anindita Bera, Tamoghna Das, Debasis Sadhukhan, Sudipto Singha Roy, Aditi Sen De, and Ujjwal Sen. Quantum discord and its allies: A review. *Reports on Progress in Physics*, 81(2):024001, February 2018.

[12] Xavier Busch, Renaud Parentani, and Scott Robertson. Quantum entanglement due to a modulated dynamical Casimir effect. *Phys. Rev. A*, 89(6):063606, 2014.

[13] David Campo and Renaud Parentani. Inflationary spectra and partially decohered distributions. *Physical Review D*, 72(4):045015, August 2005.

[14] David Campo and Renaud Parentani. Inflationary spectra and violations of Bell inequalities. *Physical Review D*, 74(2):025001, July 2006.

[15] David Campo and Renaud Parentani. Decoherence and entropy of primordial fluctuations. I. Formalism and interpretation. *Physical Review D*, 78(6):065044, September 2008.

[16] William B. Case. Wigner functions and Weyl transforms for pedestrians. *American Journal of Physics*, 76(10):937–946, October 2008.

[17] Carlton M. Caves and Bonny L. Schumaker. New formalism for two-photon quantum optics. 1. Quadrature phases and squeezed states. *Phys. Rev.*, A31:3068–3092, 1985.

[18] John F. Clauser, Michael A. Horne, Abner Shimony, and Richard A. Holt. Proposed Experiment to Test Local Hidden-Variable Theories. *Physical Review Letters*, 23(15):880–884, October 1969.

[19] Thomas Colas, Julien Grain, and Vincent Vennin. Four-mode squeezed states: two-field quantum systems and the symplectic group $\mathrm{Sp}(4,\mathbb{R})$. *Eur. Phys. J. C*, 82(1):6, 2022.

[20] Planck Collaboration. Planck 2018 results. X: Constraints on inflation. *Astronomy & Astrophysics*, 641:A10, September 2020.

[21] Artur K. Ekert. Quantum cryptography based on Bell's theorem. *Physical Review Letters*, 67(6):661–663, August 1991.

[22] J. Estève, C. Gross, A. Weller, S. Giovanazzi, and M. K. Oberthaler. Squeezing and entanglement in a Bose-Einstein condensate. *Nature*, 455(7217):1216–1219, October 2008.

[23] Alessandro Ferraro, Stefano Olivares, and Matteo G. A. Paris. Gaussian states in continuous variable quantum information, March 2005.

[24] Alessandro Ferraro and Matteo G. A. Paris. Nonclassicality Criteria from Phase-Space Representations and Information-Theoretical Constraints Are Maximally Inequivalent. *Physical Review Letters*, 108(26):260403, June 2012.

[25] Marco G. Genoni, Ludovico Lami, and Alessio Serafini. Conditional and unconditional Gaussian quantum dynamics. *Contemporary Physics*, 57(3):331–349, July 2016.

[26] Marco G. Genoni, Mattia L. Palma, Tommaso Tufarelli, Stefano Olivares, M. S. Kim, and Matteo G. A. Paris. Detecting quantum non-Gaussianity via the Wigner function. *Phys. Rev. A*, 87(6):062104, June 2013.

[27] Paolo Giorda and Matteo G. A. Paris. Gaussian Quantum Discord. *Physical Review Letters*, 105(2):020503, July 2010.

[28] Roy J. Glauber. Coherent and Incoherent States of the Radiation Field. *Physical Review*, 131(6):2766–2788, September 1963.

[29] G. Gour, F. C. Khanna, A. Mann, and M. Revzen. Optimization of Bell's Inequality Violation For Continuous Variable Systems. *Physics Letters A*, 324(5-6):415–419, April 2004.

[30] Julien Grain and Vincent Vennin. Canonical transformations and squeezing formalism in cosmology. *Journal of Cosmology and Astroparticle Physics*, 2020(02):022–022, February 2020.

[31] L. P. Grishchuk and Y. V. Sidorov. Squeezed quantum states of relic gravitons and primordial density fluctuations. *Physical Review D*, 42(10):3413–3421, November 1990.

[32] Alan H. Guth. The Inflationary Universe: A Possible Solution to the Horizon and Flatness

Problems. *Phys. Rev. D*, 23:347–356, 1981.

[33] Alan H. Guth and S. Y. Pi. Fluctuations in the New Inflationary Universe. *Phys. Rev. Lett.*, 49:1110–1113, 1982.

[34] S. W. Hawking. Particle Creation by Black Holes. *Commun. Math. Phys.*, 43:199–220, 1975. [Erratum: Commun.Math.Phys. 46, 206 (1976)].

[35] S. W. Hawking. The Development of Irregularities in a Single Bubble Inflationary Universe. *Phys. Lett. B*, 115:295, 1982.

[36] L. Henderson and V. Vedral. Classical, quantum and total correlations. 2001.

[37] Michal Horodecki, Pawel Horodecki, and Ryszard Horodecki. On the necessary and sufficient conditions for separability of mixed quantum states. *Phys. Lett. A*, 223:1, 1996.

[38] Ryszard Horodecki, Paweł Horodecki, Michał Horodecki, and Karol Horodecki. Quantum entanglement. *Reviews of Modern Physics*, 81(2):865–942, June 2009.

[39] R.L. Hudson. When is the wigner quasi-probability density non-negative? *Reports on Mathematical Physics*, 6(2):249–252, 1974.

[40] J.-C. Jaskula, G. B. Partridge, M. Bonneau, R. Lopes, J. Ruaudel, D. Boiron, and C. I. Westbrook. Acoustic Analog to the Dynamical Casimir Effect in a Bose-Einstein Condensate. *Physical Review Letters*, 109(22):220401, November 2012.

[41] Hyunseok Jeong, Jinhyoung Lee, and M. S. Kim. Dynamics of Nonlocality for A Two-Mode Squeezed State in Thermal Environment. *Physical Review A*, 61(5):052101, March 2000.

[42] E. Joos and H. D. Zeh. The Emergence of classical properties through interaction with the environment. *Z. Phys. B*, 59:223–243, 1985.

[43] Richard Jozsa and Noah Linden. On the role of entanglement in quantum computational speed-up. *Proceedings of the Royal Society of London. Series A: Mathematical, Physical and Engineering Sciences*, 459(2036):2011–2032, August 2003.

[44] M. S. Kim, F. A. M. de Oliveira, and P. L. Knight. Properties of squeezed number states and squeezed thermal states. *Physical Review A*, 40(5):2494–2503, September 1989.

[45] J. Lesgourgues, David Polarski, and Alexei A. Starobinsky. Quantum to classical transition of cosmological perturbations for nonvacuum initial states. *Nucl. Phys. B*, 497:479–510, 1997.

[46] Andrei D. Linde. A New Inflationary Universe Scenario: A Possible Solution of the Horizon, Flatness, Homogeneity, Isotropy and Primordial Monopole Problems. *Phys. Lett. B*, 108:389–393, 1982.

[47] Andrei D. Linde. Chaotic Inflation. *Phys. Lett. B*, 129:177–181, 1983.

[48] Paulina Marian, Iulia Ghiu, and Tudor A Marian. Decay of Gaussian correlations in local thermal reservoirs. *Physica Scripta*, 90(7):074041, June 2015.

[49] Jérôme Martin. Cosmic Inflation, Quantum Information and the Pioneering Role of John S Bell in Cosmology. *Universe*, 5(4):92, April 2019.

[50] Jérôme Martin, Amaury Micheli, and Vincent Vennin. Discord and decoherence. *Journal of Cosmology and Astroparticle Physics*, 2022(04):051, April 2022.

[51] Jerome Martin and Vincent Vennin. Quantum Discord of Cosmic Inflation: Can we Show that CMB Anisotropies are of Quantum-Mechanical Origin? *Phys. Rev. D*, 93(2):023505, 2016.

[52] Jérôme Martin and Vincent Vennin. Quantum discord of cosmic inflation: Can we show that CMB anisotropies are of quantum-mechanical origin? *Physical Review D*, 93(2):023505, January 2016.

[53] Jerome Martin and Vincent Vennin. Obstructions to Bell CMB Experiments. *Phys. Rev. D*, 96(6):063501, 2017.

[54] Jerome Martin and Vincent Vennin. Obstructions to Bell CMB Experiments. *Physical Review D*, 96(6):063501, September 2017.

[55] Jérôme Martin and Vincent Vennin. Cosmic Microwave Background Constraints Cast a Shadow On Continuous Spontaneous Localization Models. *Phys. Rev. Lett.*, 124(8):080402, 2020.

[56] Jerome Martin and Vincent Vennin. Real-space entanglement in the Cosmic Microwave Background. *Journal of Cosmology and Astroparticle Physics*, 2021(10):036, October 2021.

[57] Jerome Martin and Vincent Vennin. Real-space entanglement of quantum fields. *Physical Review D*, 104(8):085012, October 2021.

[58] Tim Maudlin. What Bell did. *Journal of Physics A: Mathematical and Theoretical*, 47(42):424010, October 2014.

[59] Amaury Micheli and Patrick Peter. Quantum cosmological gravitational waves?, November 2022.

[60] Viatcheslav F. Mukhanov and G. V. Chibisov. Quantum Fluctuations and a Nonsingular Universe. *JETP Lett.*, 33:532–535, 1981.

[61] Viatcheslav F. Mukhanov and G. V. Chibisov. The Vacuum energy and large scale structure of the universe. *Sov. Phys. JETP*, 56:258–265, 1982.

[62] A. Nunnenkamp, K. Børkje, J. G. E. Harris, and S. M. Girvin. Cooling and squeezing via quadratic optomechanical coupling. *Phys. Rev. A*, 82(2):021806, August 2010.

[63] Harold Ollivier and Wojciech H. Zurek. Quantum Discord: A Measure of the Quantumness of Correlations. *Phys. Rev. Lett.*, 88:017901, 2001.

[64] Nelson Pinto-Neto, Grasiele Santos, and Ward Struyve. Quantum-to-classical transition of primordial cosmological perturbations in de Broglie–Bohm quantum theory. *Phys. Rev. D*, 85:083506, 2012.

[65] Stefano Pirandola, Gaetana Spedalieri, Samuel L. Braunstein, Nicolas J. Cerf, and Seth Lloyd. Optimality of Gaussian Discord. *Physical Review Letters*, 113(14):140405, October 2014.

[66] S. Pironio, A. Acín, S. Massar, A. Boyer de la Giroday, D. N. Matsukevich, P. Maunz, S. Olmschenk, D. Hayes, L. Luo, T. A. Manning, and C. Monroe. Random numbers certified by Bell's theorem. *Nature*, 464(7291):1021–1024, April 2010.

[67] M. Revzen, P. A. Mello, A. Mann, and L. M. Johansen. Bell's Inequality Violation (BIQV) with Non-Negative Wigner Function. *Physical Review A*, 71(2):022103, February 2005.

[68] Scott Robertson, Florent Michel, and Renaud Parentani. Assessing degrees of entanglement of phonon states in atomic Bose gases through the measurement of commuting observables. *Physical Review D*, 96(4):045012, August 2017.

[69] K. Sato. First Order Phase Transition of a Vacuum and Expansion of the Universe. *Mon. Not. Roy. Astron. Soc.*, 195:467–479, 1981.

[70] Bonny L. Schumaker and Carlton M. Caves. New formalism for two-photon quantum optics. 2. Mathematical foundation and compact notation. *Phys. Rev.*, A31:3093–3111, 1985.

[71] Alessio Serafini, Fabrizio Illuminati, Matteo G. A. Paris, and Silvio De Siena. Entanglement and purity of two-mode Gaussian states in noisy channels. *Physical Review A*, 69(2):022318, February 2004.

[72] R. Simon. Peres-Horodecki separability criterion for continuous variable systems. *Physical Review Letters*, 84(12):2726–2729, March 2000.

[73] R. Simon, E.C.G. Sudarshan, and N. Mukunda. Gaussian wigner distributions: A complete characterization. *Physics Letters A*, 124(4):223 – 228, 1987.

[74] Alexei A. Starobinsky. A New Type of Isotropic Cosmological Models Without Singularity. *Phys. Lett. B*, 91:99–102, 1980.

[75] Alexei A. Starobinsky. Dynamics of Phase Transition in the New Inflationary Universe Scenario and Generation of Perturbations. *Phys. Lett. B*, 117:175–178, 1982.

[76] Jeff Steinhauer. Observation of quantum Hawking radiation and its entanglement in an analogue black hole. *Nature Physics*, 12(10):959–965, October 2016.

[77] E. C. G. Sudarshan. Equivalence of Semiclassical and Quantum Mechanical Descriptions of Statistical Light Beams. *Physical Review Letters*, 10(7):277–279, April 1963.

[78] Daniel Sudarsky. Shortcomings in the Understanding of Why Cosmological Perturbations Look Classical. *Int. J. Mod. Phys. D*, 20:509–552, 2011.

[79] Mattia Walschaers. Non-Gaussian Quantum States and Where to Find Them. *PRX Quantum*, 2(3):030204, September 2021.

[80] J. Weinbub and D. K. Ferry. Recent advances in Wigner function approaches. *Applied Physics Reviews*, 5(4):041104, December 2018.

[81] Reinhard F. Werner. Quantum states with Einstein-Podolsky-Rosen correlations admitting a hidden-variable model. *Physical Review A*, 40(8):4277–4281, October 1989.

[82] Eugene P. Wigner. On the quantum correction for thermodynamic equilibrium. *Phys. Rev.*, 40:749–760, 1932.

[83] H. M. Wiseman, S. J. Jones, and A. C. Doherty. Steering, Entanglement, Nonlocality, and the EPR Paradox. *Physical Review Letters*, 98(14):140402, April 2007.

[84] W. H. Zurek. Pointer Basis of Quantum Apparatus: Into What Mixture Does the Wave

Packet Collapse? *Phys. Rev. D*, 24:1516–1525, 1981.

[85] W. H. Zurek. Environment induced superselection rules. *Phys. Rev. D*, 26:1862–1880, 1982.

Appendix. – In the two first sections of this appendix we present the technical details relevant for computing the expectation value of the Bell operator and the separability criterion for Gaussian states. In the third section, we show that, in the limit $r \gg 1$ and $p \ll 1$, quantum discord is only controlled by b, the size of the semi-minor axis introduced in the main text. In the last section we analyse the effect of two specific Gaussian noisy channels, namely the pure-loss and the additive-noise channels, on the non-classicality of a TMSV using the criteria identified in the text.

Weyl transform of spin operators and expectation value of Bell operator. We start by presenting the computation of the Weyl transform of the spin operators defined in Eq. (18). The Weyl transform of an operator has been defined in Eq. (1). We apply this formula to $\hat{\sigma}_z^i$, the spin operator of the $i^{\rm rm}$ subsystem along z

$$\widetilde{\sigma_z^i}\left(q_i,p_i\right) = \int_{-\infty}^{\infty} e^{ip_i y}\left\langle q_i+\frac{y}{2}\right|\left(-\int_{-\infty}^{\infty}|x\rangle\langle -x|\,\mathrm{d}x\right)\left|q_i-\frac{y}{2}\right\rangle \mathrm{d}y \tag{32}$$

$$= -\int_{-\infty}^{\infty} e^{ip_i y}\int_{-\infty}^{\infty}\delta\left(q_i+\frac{y}{2}-x\right)\delta\left(q_i-\frac{y}{2}+x\right)\mathrm{d}x\,\mathrm{d}y \tag{33}$$

$$= -\delta\left(2q_i\right)\int_{-\infty}^{\infty} e^{ip_i y}\mathrm{d}y \tag{34}$$

$$= -\pi\delta\left(q_i\right)\delta\left(p_i\right)\,, \tag{35}$$

which is the formula given in Eq. (24). This readily gives Eq. (25). Proceeding similarly for the spin operator along x we get

$$\widetilde{\sigma_x^i}\left(q_i,p_i\right) = \int_{-\infty}^{\infty} e^{ip_i y}\left\langle q_i+\frac{y}{2}\right|\left(-\int_{-\infty}^{\infty}\mathrm{sign}\left(x\right)|x\rangle\langle -x|\,\mathrm{d}x\right)\left|q_i-\frac{y}{2}\right\rangle \mathrm{d}y \tag{36}$$

$$= \int_{-\infty}^{\infty} e^{ip_i y}\int_{-\infty}^{\infty}\mathrm{sign}\left(x\right)\delta\left(q_i+\frac{y}{2}-x\right)\delta\left(x-q_i+\frac{y}{2}\right)\mathrm{d}x\,\mathrm{d}y \tag{37}$$

$$= \int_{-\infty}^{\infty} e^{ip_i y}\,\mathrm{sign}\left(q_i-\frac{y}{2}\right)\delta\left(y\right)\mathrm{d}y \tag{38}$$

$$= \mathrm{sign}\left(q_i\right)\,, \tag{39}$$

which is the (second) formula given in Eq (24). Using Eq. (2) and the Gaussian Wigner function (4), the expectation value of $\hat{\sigma}_z^1\hat{\sigma}_z^2$ can then be obtained as

$$\left\langle\hat{\sigma}_x^1\hat{\sigma}_x^2\right\rangle = \int\frac{\mathrm{sign}\left(q_1\right)\mathrm{sign}\left(q_2\right)}{\pi^2\sqrt{\det\gamma}}\exp\left(-R_{1/2}^{\rm T}\gamma^{-1}R_{1/2}\right)\mathrm{d}q_1\,\mathrm{d}p_1\,\mathrm{d}q_2\,\mathrm{d}p_2 \tag{40}$$

$$= \int\frac{\mathrm{sign}\left(q_1\right)\mathrm{sign}\left(q_2\right)}{\pi\sqrt{\gamma_{qq}\gamma_{pp}}}\exp\left[-\frac{\left(q_1+q_2\right)^2}{2\gamma_{qq}}-\frac{\left(q_1-q_2\right)^2}{2\gamma_{pp}}\right]\mathrm{d}q_1\,\mathrm{d}q_2 \tag{41}$$

$$= -\frac{2}{\pi}\arctan\left[\frac{\cos(2\varphi)\sinh(2r)}{\sqrt{1+\sin^2\left(2\varphi\right)\sinh\left(2r\right)}}\right] \tag{42}$$

$$= -\frac{2}{\pi}\arcsin\left[\left|\cos(2\varphi)\right|\tanh(2r)\right]\,, \tag{43}$$

where in the second line we have performed the integration over p_1 and p_2, and in the third line over q_1 and q_2 after having inserted the expression of γ_{qq} and γ_{pp} given by Eqs.(12) and (14). The last result is nothing but Eq. (26).

Separability criterion. In this section we derive Eq. (29) of the main text, i.e. the condition for a Gaussian state to be separable. In the partition leading to Eq. (9), the result is known, see for instance [15]. Here we extend this result to the one-parameter family of partitions considered in Ref. [50]: starting from $\hat{\boldsymbol{R}}_{\rm D}$, it is obtained by performing the canonical transformation $\hat{\boldsymbol{R}}_{\rm D} \to S(\theta)\hat{\boldsymbol{R}}_{\rm D}$ where $S(\theta)$ is the symplectic matrix

$$S\left(\theta\right) = \begin{pmatrix} \cos\theta & 0 & 0 & \sin\theta \\ 0 & \cos\theta & -\sin\theta & 0 \\ \sin\theta\sin(2\theta) & \sin\theta\cos(2\theta) & \cos\theta\cos(2\theta) & -\cos\theta\sin(2\theta) \\ -\sin\theta\cos(2\theta) & \sin\theta\sin(2\theta) & \cos\theta\sin(2\theta) & \cos\theta\cos(2\theta) \end{pmatrix}. \tag{44}$$

This class of partitions is parameterised by the angle θ. The partition (9) corresponds to $\theta = -\pi/4$, while the factorised partition, i.e. the one leading to Eq. (10), corresponds to $\theta = 0$. For arbitrary θ the covariance matrix reads

$$\gamma = \begin{pmatrix} \gamma_A & \gamma_C \\ \gamma_C & \gamma_B \end{pmatrix}, \tag{45}$$

with

$$\gamma_A = \begin{pmatrix} \gamma_{11}\cos^2\theta + \gamma_{22}\sin^2\theta & \gamma_{12}\cos(2\theta) \\ \gamma_{12}\cos(2\theta) & \gamma_{22}\cos^2\theta + \gamma_{11}\sin^2\theta \end{pmatrix}, \tag{46}$$

$$\gamma_B = \begin{pmatrix} \gamma_B|_{11} & \gamma_B|_{12} \\ \gamma_B|_{21} & \gamma_B|_{22} \end{pmatrix}, \tag{47}$$

$$\gamma_C = \begin{pmatrix} \frac{1}{2}(\gamma_{11}-\gamma_{22})\sin^2(2\theta) + \frac{1}{2}\gamma_{12}\sin(4\theta) & -\frac{1}{4}(\gamma_{11}-\gamma_{22})\sin(4\theta) + \gamma_{12}\sin^2(2\theta) \\ -\frac{1}{4}(\gamma_{11}-\gamma_{22})\sin(4\theta) + \gamma_{12}\sin^2(2\theta) & -\frac{1}{2}(\gamma_{11}-\gamma_{22})\sin^2(2\theta) - \frac{1}{2}\gamma_{12}\sin(4\theta) \end{pmatrix}, \tag{48}$$

and where the components of γ_B are given by

$$\gamma_B|_{11} = \frac{1}{2}\gamma_{11} + \frac{1}{2}\gamma_{22} + \frac{1}{2}(\gamma_{11}-\gamma_{22})\cos(2\theta)\cos(4\theta) - \gamma_{12}\cos(2\theta)\sin(4\theta), \tag{49}$$

$$\gamma_B|_{12} = \gamma_B|_{21} = \gamma_{12}\cos(2\theta)\cos(4\theta) + \frac{1}{2}(\gamma_{11}-\gamma_{22})\cos(2\theta)\sin(4\theta), \tag{50}$$

$$\gamma_B|_{22} = \frac{1}{2}\gamma_{11} + \frac{1}{2}\gamma_{22} - \frac{1}{2}(\gamma_{11}-\gamma_{22})\cos(2\theta)\cos(4\theta) + \gamma_{12}\cos(2\theta)\sin(4\theta). \tag{51}$$

For a general covariance matrix the Peres-Horodecki criterion for separability can be written as [73]

$$\det\gamma_A\det\gamma_B + (|\det\gamma_C| - 1)^2 - \mathrm{Tr}\left[\gamma_A J^{(1)}\gamma_C J^{(1)}\gamma_B J^{(1)}\gamma_C^{\rm T}J^{(1)}\right] \geq \det\gamma_A + \det\gamma_B\,, \tag{52}$$

where the matrix $J^{(1)}$ is defined by $J^{(1)} \equiv \begin{pmatrix} 0 & 1 \\ -1 & 0 \end{pmatrix}$. Using the above expressions, straightforward

manipulations lead to

$$\det\gamma_A = \det\gamma_B = \frac{1}{p}\left[\cosh^2(2r) - \cos^2(2\theta)\sinh^2(2r)\right] = \frac{1}{p} - \det\gamma_C, \tag{53}$$

$$\det\gamma_C = -\frac{1}{p}\sinh^2(2r)\sin^2(2\theta), \tag{54}$$

$$\mathrm{Tr}\left[\gamma_A J^{(1)}\gamma_C J^{(1)}\gamma_B J^{(1)}\gamma_C^{\mathrm{T}} J^{(1)}\right] = -2\det\gamma_C\left(\frac{1}{p} - \det\gamma_C\right). \tag{55}$$

Combining the above results, the general criterion (52) can be written as a condition on $\det(\gamma_C)$ only, which is always negative as can be seen in Eq. (54). One obtains

$$\left(\frac{1}{p} - \det\gamma_C\right)^2 + (\det\gamma_C + 1)^2 + 2\det\gamma_C\left(\frac{1}{p} - \det\gamma_C\right) \geq 2\left(\frac{1}{p} - \det\gamma_C\right). \tag{56}$$

Using Eq. (54) the above reduces to

$$\frac{1}{p^2} - \frac{2}{p} + 1 + 4\det\gamma_C \geq 0\,. \tag{57}$$

Using Eq. (54) again, one finds

$$\left(\frac{1}{\sqrt{p}} - \sqrt{p}\right)^2 \geq 4\sinh^2(2r)\sin^2(2\theta)\,. \tag{58}$$

In the partition leading to Eq. (9), the above expression can be evaluated with $\theta = -\pi/4$, a value for which the previous formula reduces to

$$\left(\frac{1}{\sqrt{p}} - \sqrt{p}\right)^2 \geq \left(\frac{1}{e^{-2r}} - e^{-2r}\right)^2. \tag{59}$$

Given that both $\sqrt{p}$ and e^{-2r} are smaller than one, and since $y \to y - 1/y$ is a strictly increasing function, this finally leads to

$$\frac{e^{-2r}}{\sqrt{p}} \geq 1\,, \tag{60}$$

which corresponds to Eq. (29).

Quantum discord in the large-squeezing limit. Using Eqs. (30), we can re-write the expression (15) of the quantum discord in terms of the lengths of the semi-major, a, and semi-minor axis, b. Eq. (15) only depends on the quantity σ, defined by Eq. (17), and p. Therefore, we need to express these two quantities in terms of a and b and one obtains

$$\sigma = \frac{1}{2}\left(a^2 + b^2\right), \quad p = \frac{1}{a^2 b^2}. \tag{61}$$

Combining Eq. (15) and the two above formula, we get the following expression for the quantum discord as a function of a and b only

$$\mathcal{D}(a,b) = f\left[\frac{1}{2}\left(a^2 + b^2\right)\right] - 2f\left(ab\right) + f\left(\frac{a^2 + b^2 + 2a^2b^2}{a^2 + b^2 + 2}\right). \tag{62}$$

Under this form the quantum discord is expressed as a sum of terms which have no definite sign and are unbounded. In order to see that $\mathcal{D}$ is only controlled by b in the large-squeezing (i.e. $a \gg b$) and small-purity (i.e. $ab = 1/\sqrt{p} \gg 1$) limit, we rewrite the above as

$$\mathcal{D}(a,b) = g\left[\frac{1}{2}\left(a^2+b^2\right)\right] - 2g\left(ab\right) + g\left(\frac{a^2+b^2+2a^2b^2}{a^2+b^2+2}\right) + \log_2\left[\frac{(a^2+b^2)(a^2+b^2+2a^2b^2)}{2a^2b^2(a^2+b^2+2)}\right], \quad (63)$$

where we have defined the function $g(x)$ by

$$g(x) = f(x) - \log_2\left(\frac{x}{2}\right) - \frac{1}{\ln 2}. \quad (64)$$

The function $g(x)$ is defined as the difference between $f(x)$ and its asymptotic value at large argument. One can check that $g(x)$ is a negative, strictly increasing function, which is bounded by its limits $\lim_{x\to 1^+} g(x) = -1/\ln 2 + 1 \approx -0.44$ and $\lim_{x\to+\infty} g(x) = 0$. The large-squeezing regime corresponds to $b \gg a$. Since $ab \geq 1$ for the purity to be smaller than one, large squeezing requires $a \gg 1$, i.e. the semi-major axis must be much larger than its vacuum value. The first term in Eq. (63) therefore vanishes in this limit. In addition, for small purity $ab = 1/\sqrt{p} \gg 1$, the second term vanishes as well. We are thus left with the last two terms, which, in this limit, read

$$\mathcal{D}(a,b) \to g\left(1+2b^2\right) + \log_2\left(1+\frac{1}{2b^2}\right). \quad (65)$$

Therefore, the value of the discord only depends on the size of the semi-minor axis b as can be seen in the lower-right corner of Fig. 3. Note that asymptotic expression behaves as expected in the limit of a large semi-minor axis, $b \gg 1$, where $\mathcal{D}$ goes to 0. In the opposite limit, namely, $b \ll 1$, the first term goes to a finite value while the second one vanishes.

Pure-loss and additive-noise channels. Consider now the effect of a pure-loss channel of efficiency η on a TMSV whose covariance matrix is given by Eq. (6). The resulting covariance matrix, $\eta\boldsymbol{\gamma}^{\mathrm{TMSV}} + (1-\eta)\,\mathbb{1}_4$, can be recast in the form of Eq. (9) using the following effective squeezing parameters and purity

$$r' = \frac{1}{2}\mathrm{arctanh}\left[\frac{\eta\sinh(2r)}{\eta\cosh(2r)+1-\eta}\right], \quad \varphi' = \varphi, \quad p = \frac{1}{1+4\sinh^2(r)\,\eta\,(1-\eta)}. \quad (66)$$

We check that, in the limit $\eta \to 1$ (no loss), the rescaled squeezing parameters coincide with the original ones and $p = 1$. Using this mapping we can express the quantum discord, the non-separability and the Bell violation criteria with the help of the formulas derived in the main text. We plot these three criteria in Fig. 4, where we set $\varphi = 0$ to optimise for the violation of the Bell inequality.

First, we notice that, at fixed value of r, the discord increases with η, which is intuitive since we expect the quantumness of the state to be more and more preserved as the loss decreases. Of course, on the other hand, at fixed efficiency, the discord increases as r increases.

Second, the criterion for separability (52), expressed in terms of r and η, reads

$$-16\eta^2\sinh^2(r)\left[1+\eta\,(2-\eta)\sinh^2(r)\right] \geq 0, \quad (67)$$

which can only be satisfied if $r = 0$. This means that, after having gone through the loss channel, an initial non-separable state will always remain non-separable irrespective of its efficiency as expected for such pure damping [71].

Third, in Fig. 4, we have also represented the threshold for violation of Bell inequality, see the black dashed line. In terms of r and η, it is given by the following expression,

$$\langle \hat{B} \rangle = 2\sqrt{\frac{1}{\left[1+4\sinh^2(r)\,\eta\,(1-\eta)\right]^2} + \frac{4}{\pi^2}\arcsin^2\left[\frac{\eta\sinh(2r)}{\eta\cosh(2r)+1-\eta}\right]}\,, \tag{68}$$

This threshold is discontinuous at $r = 0$. Indeed, for $r = 0$, the system is in the vacuum which does not violate the Bell inequality $\left\langle \hat{B} \right\rangle = 2$. For small but non-vanishing value of the squeezing parameter, we can expand the expression of $\langle \hat{B} \rangle$,

$$\langle \hat{B} \rangle \sim 2 + 8r^2\eta\left[\left(\frac{2}{\pi^2}+1\right)\eta - 1\right]\,, \tag{69}$$

and, as a consequence, the threshold of violation for the Bell inequality corresponds to $\eta \geq \left(1+2\pi^{-2}\right)^{-1} \sim 0.83$, which is independent of the squeezing parameter r. We now consider the large r behaviour of the threshold. The figure shows that for large initial squeezing the level of loss required to prevent the violation of the Bell inequality *decreases*. This is consistent with the results of [41] where the authors consider a TMSV interacting with two thermal baths, and showed that the violation of the Bell inequality considered in [6] decreases with the initial squeezing. Since a large squeezing also implies stronger correlation, and larger value of the Bell operator initially, this fact might appear surprising at first. However, this picture overlooks that the decoherence caused this pure-channel is more efficient for strongly squeezed states. Indeed, Eq. (66) shows that for a channel with fixed efficiency η, increasing the initial squeezing r of the TMSV will exponentially suppress its purity p after the channel. This decoherence is suppressing the first term in Eq. (68), while the stronger correlation increase the second term. The fact that the threshold of Bell inequality violation goes to $\eta = 1$ shows that this increase is not sufficient to compensate the decoherence encoded in the first term. We can check this behaviour by approximating the curve $\langle \hat{B} \rangle = 2$ in the vicinity of $r \gg 1$ and $\eta \sim 1$. One finds $\eta \sim 1 - (\pi/8)^{2/5} e^{-6r/5}$, see the white dashed line in Fig. 4. This confirms the above described behaviour, which illustrates the "fragility" of a strongly squeezed state.

Finally, we repeat the same analyses for the additive-noise channel whose covariance matrix, as already mentioned above, is given by $\boldsymbol{\gamma} = \boldsymbol{\gamma}^{\mathrm{TMSV}} + \Delta \mathbb{1}_4$, where $\Delta \geq 0$ represents the noise level. Using the following parameters

$$r' = \frac{1}{2}\mathrm{arctanh}\left[\frac{\sinh(2r)}{\cosh(2r)+\Delta}\right], \quad \varphi' = \varphi\,, \quad p = \frac{1}{1+2\Delta\cosh(2r)+\Delta^2}\,, \tag{70}$$

it can also be put under the form of Eq. (9). Of course, we check that, when $\Delta \to 0$, $r' = r$, $\varphi' = \varphi$ and $p = 1$. The exact expressions of the quantum discord, the average value of the Bell operator and the non-separability threshold can be obtained using this mapping. Starting from Eq. (29), one can check that the state is separable if and only if

$$\Delta \geq 1 - e^{-2r}\,. \tag{71}$$

The expressions of the Bell violation threshold and the quantum discord can also be derived but are involved and not very enlightening. We do not reproduce them here. We only want to point out that a phenomenon similar to that observed in the pure-loss channel for large initial squeezing also happens for the additive-noise channel. Namely, as squeezing gets large, the amount of noise required to destroy the violation of the Bell inequality is reduced. All these results are summarised in Fig. 5.

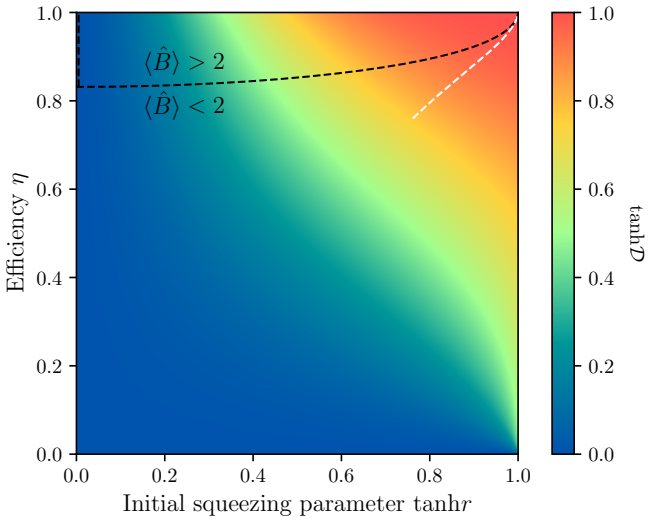

Fig. 4: Hyperbolic tangent of the quantum discord $\tanh \mathcal{D}$ computed from Eq. (15) as a function of the efficiency η and the hyperbolic tangent of the initial squeezing parameter $\tanh r$. The dashed black line represents the threshold of separability Bell inequality violation defined as the equality case in Eq. (27). The vertical piece overlaps and follow the line $r = 0$ and is represented shifted towards a non-vanishing value of r to be visible. The dashed white line shows the approximation for the threshold valid for $r \gg 1$, plotted for $r \geq 1$.

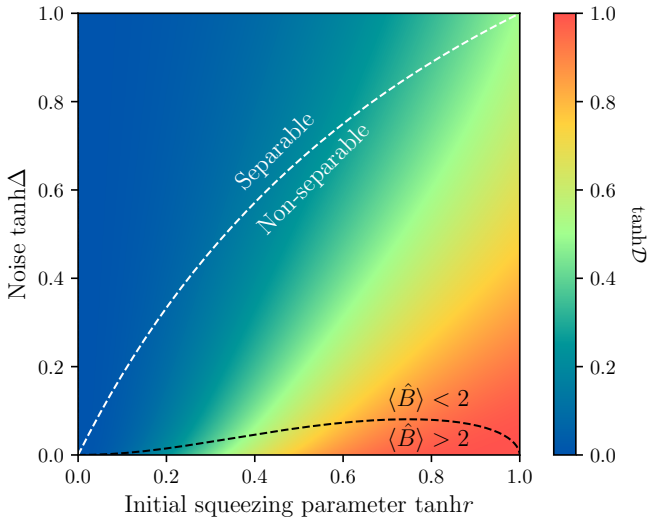

Fig. 5: Hyperbolic tangent of the quantum discord $\tanh \mathcal{D}$ computed from Eq. (15) as a function of the noise Δ and the hyperbolic tangent of the initial squeezing parameter $\tanh r$. The dashed white (respectively black) line represents the threshold of separability (respectively Bell inequality violation) defined as the equality case in Eq. (29) [respectively Eq. (27)].

3 - An analogue preheating experiment with BEC

3.1 Content of this chapter

This chapter is devoted to analysing the analogue preheating experiment [130], which is the second topic of the PhD. In Sec. 3.2, we present the original experimental set-up, its goal and what was (not) observed in its first run. Then, in Sec. 3.3, we present the model we use to describe it and review the results obtained in previous publications on the re-analysis of the experiment [155, 132, 156, 157, 133]. The latest publication [4] is reproduced in Sec. 3.4. It contains part of the original results obtained during this PhD on the analysis of the experiment. It presents a general decay mechanism for phonons in a 1D Bose gas via Beliaev-Landau channels and its application to resonant phonons in a parametric amplification set-up akin to that of [130]. Given the importance of numerical simulations in this latest analysis, we devote Sec. 3.5 to a more detailed explanation of the algorithm used. Finally, Sec. 3.6 presents preliminary results on the decay, via similar Beliaev-Landau processes, of phononic pair-correlation of the type generated during parametric amplification. These results will be the object of a future publication. We conclude that these processes are sufficient to explain the absence of entanglement in [130], which is the main result of the second part of this PhD.

3.2 Presentation of the experiment

In [130], the authors report on the results of their experiment of an analogue Dynamical Casimir Effect (DCE) [158, 159, 160]. The dynamical Casimir effect refers to the production of particles expected for a quantum field confined in a space region when the boundaries of this region are varied in time. This creation can be understood on the same basis as the cosmological pair production [161] discussed in Sec. 2.2: an 'in' vacuum before the expansion, and an 'out' vacuum after the expansion, are related by a Bogoliubov transformation [158]. Analogues of the DCE were experimentally observed in super-conducting circuits [162, 163], where the index of the medium is modulated to mimic changing boundary conditions, and in an optical system [164]. In [130], the authors prepared a gas of approximately

10^5 meta-stable Helium atoms[1] $^4\mathrm{He}^\star$ cooled down to 200nK. The atoms are placed in a magnetic trap of an elongated cigar shape in the vertical direction, see Fig. 3.1. The trapping potential is divided between a radial and vertical (longitudinal) part

$$V_{\text{ext}}(\boldsymbol{x}) = \frac{1}{2}m\omega_\perp^2 r^2 + \frac{1}{2}m\omega_z^2 z^2\,, \tag{3.1}$$

where m is the mass of the Helium atoms, $r^2 = x^2 + y^2$, $\omega_\perp$ is the radial trapping frequency and ω_z is the vertical trapping frequency. For the anisotropic trap of this experiment the authors report $\omega_\perp/2\pi = 1500$ Hz while $\omega_z/2\pi = 7$ Hz, so that $\omega_\perp \gg \omega_z$ and the gas is effectively one-dimensional.

The experimenter can change these trapping frequencies during the experiment, and two types of time dependence were investigated in [130]. The first is a quench of the frequencies by a factor $\sqrt{2}$ i.e. the trap is suddenly made tighter. In the second experiment, the trap frequencies are modulated according to $\omega^2 = \omega_0^2[1 + A\sin(\omega_{\text{m}}t)]$ for frequencies $\omega_{\text{m}}/2\pi \in [900, 5000]$ Hz and $A = 0.1$, which is the peak-to-peak modulation amplitude of ω. In both cases, due to the already strong trapping in the radial direction, the frequency change does not excite the atoms radially but leads to longitudinal excitations. These excitations are sound waves on top of the condensed atoms for long enough wavelengths. This mechanism of longitudinal waves generation via parametric resonance was also used in [165]. As we will show in detail in Sec. 3.3.2-c the excitations can generally be interpreted as quasi-particles. A modulation at frequency ω_{m} is expected to lead to a parametric creation of them in pairs of frequencies $\omega_{1/2}$ such that $\omega_{\text{m}} = \omega_1 + \omega_2$. To preserve the isotropy of the gas, they have to be of opposite momentum $\pm\boldsymbol{k}$, and so are of the same frequency $\omega_{\boldsymbol{k}}$. Even in the case where no quasi-particles are present in the initial state, owing to the quantum nature of the gas, pairs are going to be produced out of the vacuum, a mechanism very reminiscent of preheating. Note that, in agreement with a remark made in Sec. 1.2.4, since any time dependence would lead to quasi-particle creation, an analogy could also be made with inflation by expanding the trap rather than modulating it. A distinctive feature of this creation out of the vacuum is that we expect the pairs to be entangled [155].

In [130], the authors showed that the modulation produced quasi-particles in pairs of opposite momentum $\pm\boldsymbol{k}$. In addition, they showed that these pairs are

[1] This number of atoms could be inaccurate due to the detector's saturation when the condensed part of the gas reaches it. Compared with the current experiment run, it is likely overestimated, and we will take the value of 1.5×10^4 for numerical applications below. This number is obtained by inferring the one-dimensional density of the condensed gas n_0 from the speed of sound and trap frequency reported in [130]. Since most atoms are initially in the condensate, we assimilate this density to the total density of the gas $n_{1\text{D}}$. The number of atoms is then obtained by assuming that the longitudinal size of the gas is given by twice the Thomas-Fermi radius, see below. We thank Victor Gondret for the discussions on this point.

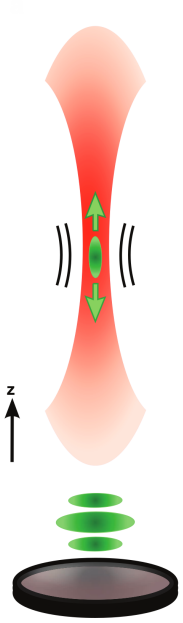

Figure 3.1: Representation of the trapped cold atoms used for the analogue Dynamical Casimir effect. This figure is adapted from [130] with only a change of colors.

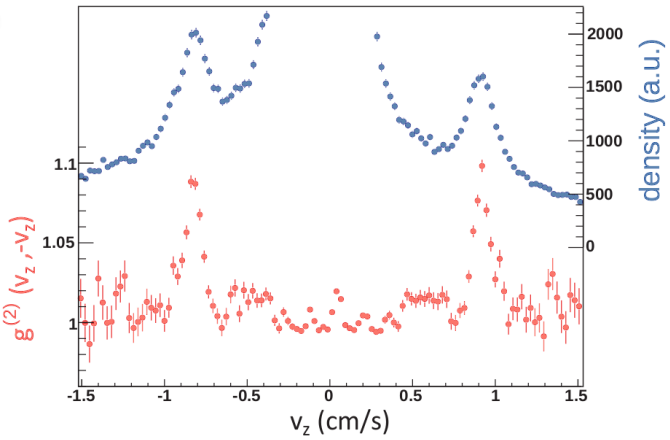

Figure 3.2: In red, 2-point correlation function $g_k^{(2)}$ of Eq. (3.64) as measured after opening the trap in the experiment [130]. This figure is adapted from [130] with only a change of colors.

correlated, yet, the correlations were not strong enough to demonstrate that the pairs were entangled. In contrast, in other analogue DCE experiments [163, 164], the authors explicitly demonstrated that the generated pairs of photons were in an entangled state, thereby proving that they had been created out of the vacuum; a genuine quantum effect. Subsequent analyses [155, 132, 156, 157, 133] tried to account for the absence of entanglement and the non-linear processes at play in [130]. The emergence of entanglement in the early-time dynamics was studied in [155, 132] using simple quadratic models. The authors pointed out the analogy with the parametric creation during preheating. Then, in [156], the authors accounted more precisely for the interplay between the change in the trapping frequency and the production of excitations, with a focus on entanglement in [157]. In the latest paper of the series [133], the authors numerically analysed the redistribution of energy of the generated pairs via interactions between quasi-particles and their backreaction on the condensate. They also dealt with the late-time processes drawing an analogy with the processes following preheating in the early Universe. We point out that the focus of [156, 157, 133] was on the quench experiment rather than the modulation. Still, following a quench, the gas would exhibit 'breathing' oscillations in the radial direction, and these oscillations would, in turn, lead to pair creation in well-defined resonant modes. We come back to this point in Sec. 3.3.2-a.

In the next section Sec. 3.3, we present the mathematical formalism that they used to describe the experiment, which is independent of the type of modulation considered. Similarly, the computations presented in Sec. 3.4 apply generically to any quasi-particles in a 1D Bose gas, irrespective of their production mechanism.

3.3 Modelling the experiment

In Sec 3.3.1, we start by defining a condensed state in the standard description of a gas using quantum field theory. Then, in Sec. 3.3.2, we describe the general dynamics of a weakly interacting gas in a (quasi-)condensed state, including when the radial trapping frequency is varied. In Sec. 3.3.3, we briefly examine the specific case of a modulation of the radial trapping frequency, draw the link with preheating and explain how relevant information about the created quasi-particles is experimentally accessed. Finally, in Sec. 3.3.4, we amend the standard BdG approximation presented in Sec. 3.3.2 for the specific case of a one-dimensional gas.

3.3.1 Condensed state

The standard mathematical description of a mono-atomic Bose gas of Helium atoms uses a quantum field theory for a complex scalar field $\hat{\Psi}(\boldsymbol{x})$ dubbed the

atomic field. An extensive presentation of this formalism can be found in [166], and we briefly recap essential aspects. The atomic field $\hat{\Psi}(\boldsymbol{x})$ is defined as the operator whose action on any quantum state describing the system $|\Psi\rangle$ removes one atom at position $\boldsymbol{x}$ i.e. it is a destruction operator in real space. Similarly, its hermitian conjugate $\hat{\Psi}^\dagger(\boldsymbol{x})$ is a creation operator in real space. We impose that they satisfy the canonical commutation relation

$$\left[\hat{\Psi}\left(\boldsymbol{x}\right), \hat{\Psi}^\dagger\left(\boldsymbol{x}'\right)\right] = \delta\left(\boldsymbol{x} - \boldsymbol{x}'\right) , \tag{3.2}$$

while the atomic field commutes with itself at any point $\left[\hat{\Psi}\left(\boldsymbol{x}\right), \hat{\Psi}\left(\boldsymbol{x}'\right)\right] = 0$. The atomic density at $\boldsymbol{x}$ is given by

$$\hat{\rho}\left(\boldsymbol{x}\right) = \hat{\Psi}^\dagger\left(\boldsymbol{x}\right)\hat{\Psi}\left(\boldsymbol{x}\right) , \tag{3.3}$$

which is a hermitian operator. The total number of atoms in the system N is obtained by integrating the density field over space. We can also define the phase $\hat{\theta}$ of the gas by writing the atomic field

$$\hat{\Psi}\left(\boldsymbol{x}\right) = e^{i\hat{\theta}}\sqrt{\hat{\rho}\left(\boldsymbol{x}\right)} . \tag{3.4}$$

Mathematical problems are attached to the definition of a phase operator [167, 168]. We briefly discuss them in Sec. 3.3.4-b. The decomposition in density and phase of Eq. (3.4) is called the Madelung form [169]. It will prove helpful later when dealing with a one-dimensional gas for which no true condensed state can emerge, and we can only have a *quasicondensate* [170]. For three, and even two-dimensional, systems, there exists a temperature $T_{\text{cond.}}$ below which the gas can be placed in a condensed state. In a condensed state, a single-particle state, typically the ground state of the gas, is macroscopically occupied, i.e. the number of particles in this state N_0 is such that when the total number of particles N diverges in the thermodynamical limit, the fraction $n_0 = N_0/N$ remains finite [166]. Such a state is characterised by long-range order for some correlations [166], typically the one-body correlation function g_1 defined by

$$g_1\left(\boldsymbol{x}\,,\,\boldsymbol{x}'\right) = \left\langle \hat{\Psi}^\dagger\left(\boldsymbol{x}\right)\hat{\Psi}\left(\boldsymbol{x}'\right)\right\rangle . \tag{3.5}$$

If we consider a homogeneous system, g_1 only depends on the difference $\boldsymbol{x} - \boldsymbol{x}'$ and for a condensate state is expected in the thermodynamical limit to behave as

$$g_1\left(\boldsymbol{x}\,,\,\boldsymbol{x}'\right) \xrightarrow[|\boldsymbol{x}-\boldsymbol{x}'|\to+\infty]{} n_0 \neq 0 . \tag{3.6}$$

For a condensed gas, given that a macroscopic amount of particles are in the same state, we consider them as a separate gas for which we define the operator $\hat{\Psi}_0$ that

destroys a particle of the macroscopically occupied state. The density of particles in this state is then given by

$$n_0 = \left\langle \hat{\Psi}_0^\dagger \hat{\Psi}_0 \right\rangle . \tag{3.7}$$

For condensed states, where the number of particles N_0 is huge, removing or adding a particle in this macroscopically occupied state should keep the system's state roughly the same. The action of $\hat{\Psi}_0$ can then be approximated as a multiplication by a complex function Ψ_0 such that

$$\hat{\Psi}_0 \left|\Psi\right\rangle \approx \Psi_0 \left|\Psi\right\rangle , \tag{3.8}$$

and similarly for its hermitian conjugate. Therefore we treat this operator as a complex function

$$\hat{\Psi}_0 \left(\boldsymbol{x}\right) \approx \Psi_0 \left(\boldsymbol{x}\right) \hat{\mathbb{1}} , \tag{3.9}$$

where $\hat{\mathbb{1}}$ is the identity operator. If we consider all particles to be in the macroscopically occupied state, then removing an atom from the gas corresponds to removing an atom from the macroscopically occupied state hence

$$\hat{\Psi} \left(\boldsymbol{x}\right) \approx \Psi_0 \left(\boldsymbol{x}\right) \hat{\mathbb{1}} , \tag{3.10}$$

and the total density n then equals the condensed density n_0. Assuming that the condensed state is homogeneous, it trivially exhibits non-diagonal long-range order

$$g_1 \left(\boldsymbol{x} , \boldsymbol{x}'\right) \approx n_0 \neq 0 . \tag{3.11}$$

Still, we need to refine the above prescription as only part of the atoms are in the macroscopically occupied state. The standard approach is to split the atomic field between a condensed part and a perturbation [166]

$$\hat{\Psi} = \Psi_0 \left(\hat{\mathbb{1}} + \delta\hat{\Psi}\right) , \tag{3.12}$$

where $\delta\hat{\Psi}$ is the atomic field for the non-condensed part. Notice that here we have defined the perturbations in a relative manner using the condensed wavefunction as a pre-factor. It is more common to use absolute perturbation $\hat{\Psi} = \Psi_0\hat{\mathbb{1}} + \delta\hat{\Psi}$. The Bogoliubov-de Gennes approximation (BdG) consists in assuming the contribution of the non-condensed part to be a perturbation on top of the condensate $|\delta\hat{\Psi}| \ll 1$. Note the similarity with the analysis that lead to the introduction of the acoustic metric in Sec. 1.3.2, where we considered the perturbations of a fluid around a background flow. We now write a Hamiltonian describing the dynamics of this atomic field.

3.3.2 Dynamics of the gas

For dilute Bose gas as in [130], the interactions are dominated by two-body contact interactions, which are described by the pseudo-potential [166]

$$\hat{V}(\boldsymbol{x}) = \frac{g}{2}\hat{\Psi}^{\dagger}(\boldsymbol{x})\,\hat{\Psi}^{\dagger}(\boldsymbol{x})\,\hat{\Psi}(\boldsymbol{x})\,\hat{\Psi}(\boldsymbol{x})\,, \tag{3.13}$$

where the interaction constant can be related to the s-wave scattering length $g = 4\pi\hbar^2 a_s/m$. The trapping potential is given by Eq. (3.1), and we can write down the Hamiltonian for the gas

$$\hat{H} = \int \mathrm{d}\boldsymbol{x}\left[\frac{\hbar^2}{2m}\vec{\nabla}\hat{\Psi}^{\dagger}\cdot\vec{\nabla}\hat{\Psi} + V_{\mathrm{ext}}(\boldsymbol{x})\,\hat{\Psi}^{\dagger}\hat{\Psi} + \frac{g}{2}\hat{\Psi}^{\dagger}\hat{\Psi}^{\dagger}\hat{\Psi}\hat{\Psi}\right]. \tag{3.14}$$

Its Heisenberg equation of motion derived using Eq. (3.2) reads

$$i\hbar\partial_{\mathrm{t}}\hat{\Psi} = -\frac{\hbar^2}{2m}\Delta\hat{\Psi} + V_{\mathrm{ext}}(\boldsymbol{x})\,\hat{\Psi} + g\hat{\Psi}^{\dagger}\hat{\Psi}\hat{\Psi}\,. \tag{3.15}$$

One can check that the number of atoms given by

$$N\hat{\mathbb{1}} = \int \hat{\Psi}^{\dagger}\hat{\Psi}\mathrm{d}\boldsymbol{x} \tag{3.16}$$

is conserved for an evolution via Eq. (3.15). We solve Eq. (3.15) by splitting the atomic field into condensed and perturbation parts as in Eq. (3.12), and use the BdG approximation to write first an equation for the condensed part neglecting the non-condensed part which is the classical version of Eq. (3.15)

$$i\hbar\partial_{\mathrm{t}}\Psi_0 = -\frac{\hbar^2}{2m}\Delta\Psi_0 + V_{\mathrm{ext}}(\boldsymbol{x})\,\Psi_0 + g\left|\Psi_0\right|^2\Psi_0\,. \tag{3.17}$$

This equation is called the Gross-Pitaevskii equation (GPE).

The BdG approximation is only valid for weakly interacting gas, so before moving on to the computation of the dynamics of the gas, we do some order of magnitude computations for the gas in [130] to ensure that the approximations we applied are valid. First, we approximate the gas to have the geometry of a cylinder. The radius of the cylinder is directly given by the trapping frequency $a_\perp = \sqrt{\hbar/m\omega_\perp}$, see Sec. 3.3.2-a. The length of the gas is more complicated to compute. Applying the analysis of [170], see in particular Fig. 5, given the number of atoms $N \approx 10^4$, and the radial extension $a_\perp$ of [130], shows the gas is in the Thomas-Fermi regime. Then, the vertical condensed density profile has an extension of twice the Thomas-Fermi radius given by

$$R_{\mathrm{TF}} = a_z\left(3\frac{a_z a_s}{a_\perp^2}N\right)^{1/3}, \tag{3.18}$$

where $a_z = \sqrt{\hbar/m\omega_z}$. Due to the second term in brackets, this extension is much larger than the naive expectation a_z. While in the Thomas-Fermi regime the density profile is not homogeneous, in the rest, we neglect the vertical trapping and consider a homogeneous profile of length L. The length is estimated using the above to $L \approx 2R_{\mathrm{TF}}$. We then compute the gas parameter na_s^3, where $n \approx N/(2R_{\mathrm{TF}}\pi a_\perp^2)$ is the number density of atoms, and a_s is the s-wave scattering length for ^{4}He atoms in 2^3S_1 meta-stable state. It is measured [171] to be $a_s = 7.5\,\mathrm{nm}$. The condition for a weakly interacting 3D gas is that the gas parameter is much smaller than unity, i.e. that the typical distance between atoms $n^{-1/3}$ is larger than the s-wave scattering length. We find $na_s^3 \approx 2 \times 10^{-6}$, so we are well within this regime. It is also useful to compute the gas parameter in 1D $n_{1\mathrm{D}}a_s = Na_s/(2R_{\mathrm{TF}}) \approx 0.19$, which is used as a parameter in the papers analysing the experiment e.g. [133]. Following [170], the gas is in the weakly interacting regime in one-dimension when the interaction energy per particle is much less than the characteristic kinetic energy of particles. This condition translates in the requirement that the Lieb-Liniger interaction constant [172] $\gamma = mg_1/(\hbar n_{1\mathrm{D}})$, where g_1 is the one-dimensional interaction constant, is much less than one $\gamma \ll 1$. For our radially confined gas we find [173, 170] $g_1 = g/(2a_\perp^2)$, which is derived in Eq. (3.31) below. We then have $\gamma = 2a_s/(n_{1\mathrm{D}}a_\perp^2) \approx 4 \times 10^{-4}$. Again, we are in a weakly interacting regime. Having checked the consistency of our treatment, we describe the behaviour of the condensed part of the gas.

3.3.2-a Condensate

The wave function of the condensed part, which will act as a background for the excitations on top, is shaped by the trap's effect and the interaction between atoms. We want to account for the effect of the change in the trap size on the solution of this equation. We follow the method and the approximations made in [156, 157, 133]. First, we expect the physics to be mainly one-dimensional in the vertical direction due to the anisotropy of the trap $\omega_\perp \gg \omega_z$. We thus separate the condensate wavefunction in a vertical part $\phi_0(z,t)$ and radial part $\psi_0(r,\theta,t)$ such that

$$\Psi_0 = \frac{1}{\sqrt{2\pi}}\psi_0\left(r,\theta,t\right)\phi_0\left(z,t\right)\,, \tag{3.19}$$

where we choose the normalisation of these fields such that ϕ_0 is normalised as the wavefunction of 1D condensate

$$\int_{-\infty}^{+\infty}\left|\phi_0\left(z,t\right)\right|^2\mathrm{d}z = N_0\,, \tag{3.20a}$$

$$\int_0^{+\infty}\left|\psi_0\left(r,\theta,t\right)\right|^2 r\mathrm{d}r = 1\,, \tag{3.20b}$$

where N_0 is the number of atoms in the condensate. The factorisation ansatz. (3.19) can only describe cylindrically symmetric condensates whose radial profile is the same along their vertical extension. It can still provide a good approximation of the ground state of the gas, as shown in [156] by comparing its profile to a numerically computed one. Again, we appeal to the strong anisotropy of the trap $\omega_\perp \gg \omega_z$ to neglect the effect of the vertical trapping. To still give the gas a finite extension, we assume it is confined in a box of length L in the vertical direction. In addition, we assume the condensed part of the gas to be homogeneous in the vertical direction i.e. $\phi_0 = n_0 = N_0/L$ where n_0 is the linear density of the condensate along the vertical direction. Finally, homogeneity for a finite-size gas requires working with periodic boundary conditions. The GPE over the radial direction then reads

$$i\hbar\partial_t\psi = -\frac{\hbar^2}{2m}\frac{1}{r}\frac{\partial}{\partial r}\left(r\frac{\partial\psi}{\partial r}\right) + \frac{\hbar^2}{2ma_\perp^4}r^2\psi + \frac{\hbar^2}{m}2n_0a_s\left|\psi\right|^2\psi\,, \tag{3.21}$$

where the factor of n_0 is inherited from the vertical homogeneous profile entering the non-linear interaction term, and we recall that $a_\perp = \sqrt{\hbar/m\omega_\perp}$. Assuming that the gas is stationary before any change in the trap frequency, we have

$$\psi_0\left(r,\theta,t\right) = \tilde{\psi}\left(r\right)e^{-i\frac{\mu}{\hbar}t}\,, \tag{3.22}$$

where μ is the chemical potential i.e. the energy per atom. The stationary GPE now reads

$$\mu\tilde{\psi} = -\frac{\hbar^2}{2m}\frac{1}{r}\frac{\partial}{\partial r}\left(r\frac{\partial\tilde{\psi}}{\partial r}\right) + \frac{\hbar^2}{2ma_\perp^4}r^2\tilde{\psi} + \frac{\hbar^2}{m}2n_0a_s\left|\tilde{\psi}\right|^2\tilde{\psi}\,. \tag{3.23}$$

To find the ground state's wave function in which the gas condenses, we have to minimise the right-hand side of this wave function. It can be done approximately by using a Gaussian ansatz for the radial profile

$$\tilde{\psi} = \frac{\sqrt{2}}{\sigma}e^{-\frac{r^2}{2\sigma^2}}\,, \tag{3.24}$$

where σ controls the extension of the gas. If we neglect the interaction of the gas $g = 0$, then the Gaussian profile is an exact solution The extension is then $\sigma = a_\perp$, and the chemical potential is $\mu = \hbar\omega_\perp$, completely controlled by the trap frequency. This justifies the intuition that $a_\perp$ is an estimate of the radial size of the condensate in the trap. To compute the modifications to these values due to interactions, we insert the ansatz (3.24) in Eq. (3.23) and integrate over the radial direction

$$\mu = \frac{m\omega_\perp^2}{2}\sigma^2 + \frac{\hbar^2}{2m\sigma^2}\left(1 + 4n_0a_s\right)\,. \tag{3.25}$$

The first term is due to the trap. It favours smaller extensions, where the atoms lie in the centre of the trap with minimal potential energy, while the second term, due both to quantum pressure and the interactions, favours larger extensions, where the atoms are far apart from each other. Minimising the right-hand side over σ we find [174, 156] the extension of the ground state $\sigma_0 = a_\perp(1+4n_0a_s)^{1/4}$ and the associated energy $\mu_0 = \hbar\omega_\perp(1+4n_0a_s)^{1/2}$. We found an approximate wavefunction for the condensate when the trap frequency is constant

$$\Psi_0 = \sqrt{\frac{n_0}{2\pi\sigma_0^2}}\, e^{-\frac{r^2}{2\sigma_0^2}} e^{-i\frac{\mu_0}{\hbar}t}\,. \tag{3.26}$$

We now have to consider the change in the radial trapping frequency. In [130], both the vertical and radial trapping frequencies are quenched (or modulated). Nevertheless, since the radial trapping frequency is much tighter, the change of the radial frequency injects much more energy for the same ratio of final and initial frequencies. Therefore, we neglect changes in the vertical size. For a time-dependent harmonic radial trap $\omega_\perp(t)$ one can build an exact solution of the equation of motion for a time-varying trap from a stationary solution at fixed trap frequency $\omega_{\perp,0}$ [175]. Starting from our approximate stationary solution of Eq. (3.26), we can then build the approximate time-dependent solution

$$\Psi_0\left(r,t\right) = \sqrt{\frac{n_0}{2\pi\sigma^2(t)}}\, e^{-\frac{r^2}{2\sigma^2(t)}} e^{i\left[\frac{mr^2}{2\hbar}\frac{\dot\sigma}{\sigma} - \frac{\mu_0}{\hbar}\int_0^t \frac{\sigma_0^2}{\sigma^2(t')}\mathrm{d}t'\right]}\,, \tag{3.27}$$

where the radial extension of the gas σ is now time-dependent and satisfies the Ermakov-Pinney [176, 177] differential equation

$$\ddot\sigma + \omega_\perp^2(t)\sigma = \frac{\sigma_0^4\omega_{\perp,0}^2}{\sigma^3}\,. \tag{3.28}$$

The trap modulation's effect has been accounted for by a change in the geometry of the condensate. Notice that when the trap is held at $\omega_{\perp,0}$, then $\sigma = \sigma_0$. It is instructive to solve Eq. (3.28) for the two types of change considered in [130]: a quench and a modulation. A quench of the radial trapping frequency from $\omega_\perp$ to $\omega_{\perp,\mathrm{f}}$ will lead to oscillations of the radial size of the gas at $2\omega_{\perp,\mathrm{f}}$, see lower panel of Fig. 3.3. In the case of a modulation at ω_m, if it is slow enough i.e. $\omega_\mathrm{m} \ll \omega_\perp$, the radial size will dominantly oscillate at ω_m. However if the modulation is fast $\omega_\mathrm{m} \gg \omega_\perp$ then the behaviour of σ has two characteristic frequencies ω_m and $2\omega_\perp$, see upper panel of Fig. 3.3. The oscillations at $2\omega_\perp$ are present in the slow case, but suppressed. Notice that the equation also has resonances, for instance, at $\omega_\mathrm{m} = 2\omega_\perp$ where σ grows exponentially. For the benchmark value in [130] $\omega_\mathrm{m} \approx 1.5\omega_\perp$, shown in the upper panel of Fig. 3.3, we are in an intermediate regime where we do expect to have oscillations at ω_m and $2\omega_\perp$, two similar frequencies.

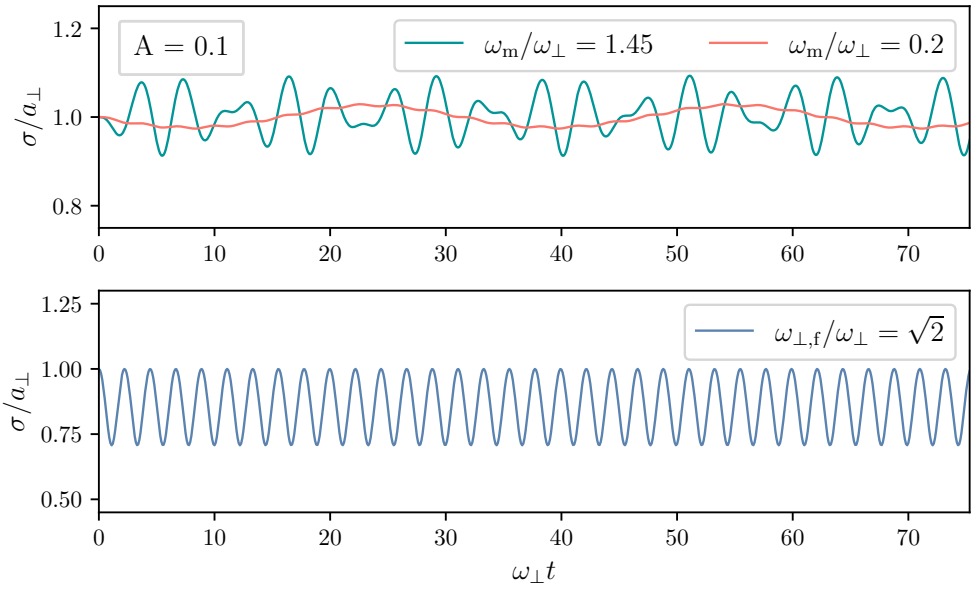

Figure 3.3: (Upper panel) Behaviour of σ, the radial extension of the condensate, under a modulation of the transverse trapping frequency $\omega_\perp$ according to $\omega_\perp^2 = \omega_\perp^2 [1 + A \sin(\omega_m t)]$. σ is adimensionalised by the transverse size $a_\perp$ associated to $\omega_\perp$, and the time is adimensionalised by $\omega_\perp$. The green curve matches the benchmark values used in [130], $A = 0.1$ and $\omega_m = 1.45\omega_\perp$. σ features oscillations at two frequencies $2\omega_\perp$ and ω_m. The red curve corresponds to $\omega_m \ll \omega_\perp$, σ then predominantly features oscillations at ω_m, while the breathing oscillations at $2\omega_\perp$ are suppressed. (Lower panel) Behaviour of σ, the radial extension of the condensate, under a quench of the transverse trapping frequency $\omega_\perp \to \omega_{\perp,f}$. Following the quench σ oscillates at a frequency $2\omega_{\perp,f}$.

We now compute the dynamics of the perturbation and show that it only depends on that of the trap indirectly, through that of the condensate. In particular, the perturbations undergo parametric amplification at half the frequency of oscillations of the condensate. Here we will neglect the backreaction of perturbations on the condensate and refer to [133] for treatment of that point.

3.3.2-b Perturbations

First, we will neglect excitations with nodes in the radial direction so that

$$\hat{\Psi} = \Psi_0 (r, t) \left[\hat{\mathbb{1}} + \delta\hat{\Psi}(z, t) \right] . \tag{3.29}$$

Notice that we are dealing with a relative perturbation here, so the absolute perturbations have an r dependence given by the profile of the condensate. Following [133], this approximation can be justified by computing the dispersion relation $\omega(k, n)$ of the three-dimensional excitations, perturbing Eq. (3.15) around Eq. (3.26), where k is the wavenumber in the vertical direction and n is a quantum number labelling excitations in the radial direction. This procedure was done analytically in the non-interacting limit and numerically for excitations with no azimuthal dependence in [156]. The authors found that azimuthally symmetric excitations with a non-trivial radial part typically have an energy $2\omega_\perp$ larger than the longitudinal ones. Therefore, at the initial time, the thermal radial excitations will be negligible in numbers compared to the longitudinal ones. Additionally, anticipating the rest of the section, for a modulation at ω_m we expect parametric resonance to occur in modes with a frequency half that of driving $\omega_\mathrm{m}/2$, and possibly at the trap frequency $\omega_\perp$. On the other hand, for a quench, we expect oscillation at the trap frequency $\omega_\perp$. For the benchmark value $\omega_\mathrm{m} = 1.5\omega_\perp$, both of these frequencies are lower than the frequency of the first radial mode, which will thus not be excited. We will neglect the radial excitations from now on. We proceed by inserting Eq. (3.29) in Eq. (3.14) and collect the terms of second order in $\delta\hat{\Psi}$ to form a Hamiltonian at first non-trivial order for the perturbations $\hat{H}^{(2)}$. At this stage, a slight technical complication comes from using relative perturbations in Eq. (3.29). $\hat{\Psi}^{(\dagger)}$ are canonically conjugate operators, see Eq. (3.2), and $\sqrt{n_0}\delta\hat{\Psi}^{(\dagger)}$ inherit this property (after integration over the radial profile) so that

$$\left[\delta\hat{\Psi} (\boldsymbol{x}) , \delta\hat{\Psi}^{(\dagger)} (\boldsymbol{x}') \right] = \frac{1}{n_0} \delta (\boldsymbol{x} - \boldsymbol{x}') . \tag{3.30}$$

However, the time-dependent factor of Ψ_0 in front of $\delta\hat{\Psi}$ in the expansion of $\hat{\Psi}$ will lead to an additional term $i\hbar\dot{\Psi}_0\delta\hat{\Psi}$ in the equation of motion at the first order of $\delta\hat{\Psi}$ which is therefore not directly the Heisenberg equation derived from $\hat{H}^{(2)}$. This extra factor corresponds to implementing a canonical transformation $\delta\hat{\Psi} \to \Psi_0\delta\hat{\Psi}$ with a time-dependent factor which, as well-known, leads to a modified

Hamiltonian. The computations are performed in Appendix. C.1, and we give the resulting Hamiltonian (that we still call $\hat{H}^{(2)}$ for simplicity)

$$\hat{H}^{(2)} = \int_0^L n_0 \left[\frac{\hbar^2}{2m} \frac{\partial \delta\hat{\Psi}^\dagger}{\partial z} \frac{\partial \delta\hat{\Psi}}{\partial z} + g_1 n_0 \delta\hat{\Psi}^\dagger \delta\hat{\Psi} + \frac{g_1 n_0}{2} \left(\delta\hat{\Psi}^{\dagger\,2} + \delta\hat{\Psi}^2 \right) \right] \mathrm{d}z \,, \tag{3.31}$$

where we have integrated over the radial profile, and $g_1(t) = g/2\pi\sigma^2(t)$ is the effective 1D interaction constant. Eq. (3.31) is exactly the BdG Hamiltonian for a one-dimensional gas whose interaction constant is made time-dependent. In general, the interaction constant of a Bose gas can be controlled using a Fesbach resonance, as in [141]. However, here the interaction constant is an effective one coming from the dimensional reduction, and the time dependence is due to the trap. We can compute the associated Heisenberg equation of motion, which could have directly computed by perturbing Eq. (3.15) as in [156]

$$i\hbar \partial_t \delta\hat{\Psi} = -\frac{\hbar^2}{2m} \partial_z^2 \delta\hat{\Psi} + g_1(t) n_0 \left(\delta\hat{\Psi} + \delta\hat{\Psi}^\dagger \right) . \tag{3.32}$$

This equation is solved by decomposing the perturbation in Fourier modes

$$\delta\hat{\Psi}(z,t) = \frac{1}{\sqrt{N_0}} \sum_{k \in 2\pi\mathbb{Z}^\star/L} e^{ikz} \hat{a}_k \,. \tag{3.33}$$

where $\hat{a}_k$ is the adimensional annihilation operator for atoms with momentum $\hbar k$. The $k = 0$ term is removed to make the number of condensed atoms conserved, and the total number of atoms conserved at first order in perturbations[2]. The creation/annihilation operators satisfy the canonical commutation relation

$$\left[\hat{a}_k, \hat{a}_{k'}^\dagger \right] = \delta_{k,k'} \,, \tag{3.34a}$$

$$\left[\hat{a}_k, \hat{a}_{k'} \right] = 0 \,, \tag{3.34b}$$

where $\delta_{k,k'}$ is the Kronecker delta. We have

$$N = \int \mathrm{d}z \, \langle \hat{\rho} \rangle = N_0 + \sum_{k \in 2\pi\mathbb{Z}^\star/L} \left\langle \hat{a}_k^\dagger \hat{a}_k \right\rangle \,, \tag{3.35}$$

where the second piece gives the number of excited atoms not in the condensate. This piece is referred to as the *depletion*. We then write the Hamiltonian (3.31) in Fourier modes

$$\hat{H}^{(2)} = \sum_{k \in 2\pi\mathbb{Z}^\star/L} \left(\frac{\hbar^2 k^2}{2m} + g_1 n_0 \right) \hat{a}_k^\dagger \hat{a}_k + \frac{g_1 n_0}{2} \left(\hat{a}_k^\dagger \hat{a}_{-k}^\dagger + \hat{a}_k \hat{a}_{-k} \right) . \tag{3.36}$$

[2]Notice that thanks to this, the Hamiltonian (3.14) vanishes at first order in perturbation, and the quadratic Hamiltonian (3.31) is the first non-trivial contribution.

The linear Heisenberg equation of motion (3.32) can also be recast as an equation over $\hat{a}_k$ and $\hat{a}^\dagger_{-k}$. We have

$$i\hbar\,\partial_t \begin{pmatrix} \hat{a}_k \\ \hat{a}^\dagger_{-k} \end{pmatrix} = \underbrace{\begin{pmatrix} \frac{\hbar^2k^2}{2m} + g_1 n_0 & g_1 n_0 \\ -g_1 n_0 & -\frac{\hbar^2k^2}{2m} - g_1 n_0 \end{pmatrix}}_{=M_k} \begin{pmatrix} \hat{a}_k \\ \hat{a}^\dagger_{-k} \end{pmatrix} . \tag{3.37}$$

Notice that, just as for cosmological perturbations, see Sec. 1.2.3-c, as a consequence of homogeneity of the Hamiltonian (3.14) these equations preserve the total momentum only mixing operators having the same action, raising or lowering the total momentum by k. Hence, only the mode $\pm k$ are coupled at quadratic order.

3.3.2-c Dynamics in the absence of external drive

Let us first consider the time-independent case where the trap frequency is held at a fixed value $\omega_{\perp,0}$ so that $\sigma = \sigma_0$. For a free system $g = 0$, M_k is diagonal and atoms of different momenta evolve independently. In the presence of interactions, $g \neq 0$, there is a non-trivial mixing between $\pm\hbar k$ atoms. At the level of the Hamiltonian, this manifests in the fact that Eq. (3.36) is not diagonal in the atom number basis. Therefore, the ground state of the interacting gas does not only contain atoms at rest, a part of them will be moving; this is the so-called quantum depletion [166]. To quantify this depletion we need to diagonalise the Hamiltonian or equivalently the matrix M_k of Eq. (3.37). As for cosmological perturbations, see Sec. 2.2, this is done via a Bogoliubov transformation

$$\begin{pmatrix} \hat{a}_k \\ \hat{a}^\dagger_{-k} \end{pmatrix} = \underbrace{\begin{pmatrix} u_k & v_k \\ v^*_{-k} & u^*_{-k} \end{pmatrix}}_{=P_k} \begin{pmatrix} \hat{b}_k \\ \hat{b}^\dagger_{-k} \end{pmatrix} , \tag{3.38}$$

where we have defined the Bogoliubov coefficients that satisfy the standard relations $|u_k|^2 - |v_k|^2 = |u_{-k}|^2 - |v_{-k}|^2 = 1$ and $u_k v_{-k} = u_{-k} v_k$ for the pairs $(\hat{b}_{\pm k}, \hat{b}^\dagger_{\pm k})$ to be canonically conjugated. These operators define the quasi-particles of the system, often called *phonons*, although this term is sometimes reserved only for low-lying excitations. We here use these words interchangeably. We then pick P_k to diagonalise M_k, and we find the expressions of the two Bogoliubov coefficients [166]

$$u_k = \sqrt{\frac{\left(\frac{\hbar^2k^2}{2m} + g_1 n_0\right) + \hbar\omega_k}{2\hbar\omega_k}} = \frac{\sqrt{\frac{\hbar^2k^2}{4m} + g_1 n_0} + \sqrt{\frac{\hbar^2k^2}{4m}}}{\sqrt{2\hbar\omega_k}} , \tag{3.39}$$

$$v_k = -\sqrt{\frac{\left(\frac{\hbar^2k^2}{2m} + g_1 n_0\right) - \hbar\omega_k}{2\hbar\omega_k}} = -\frac{\sqrt{\frac{\hbar^2k^2}{4m} + g_1 n_0} - \sqrt{\frac{\hbar^2k^2}{4m}}}{\sqrt{2\hbar\omega_k}} , \tag{3.40}$$

where we have defined the frequency

$$\omega_k = c|k|\sqrt{1+\frac{\xi^2 k^2}{4}}\,, \tag{3.41}$$

the speed of sound $c^2 = g_1 n_0/m$ and the healing length $\xi = \hbar/mc$. Eq. (3.41) is the standard Bogoliubov-de Gennes dispersion relation [166]. The diagonalised dynamics then reads

$$\partial_t \begin{pmatrix} \hat{b}_k \\ \hat{b}^\dagger_{-k} \end{pmatrix} = \begin{pmatrix} -i\omega_k & 0 \\ 0 & i\omega_k \end{pmatrix} \begin{pmatrix} \hat{b}_k \\ \hat{b}^\dagger_{-k} \end{pmatrix}\,, \tag{3.42}$$

and so

$$\hat{b}_k(t) = e^{-i\omega_k t}\hat{b}_k(0)\,. \tag{3.43}$$

Using the phononic creation and annihilation operators, we rewrite the Hamiltonian, which is now diagonal

$$\hat{H}^{(2)} = \sum_{k\in 2\pi\mathbb{Z}^\star/L} \hbar\omega_k \hat{b}^\dagger_k \hat{b}_k\,. \tag{3.44}$$

The phonons describe the gas (at the first order in perturbation) as a collection of free quasi-particles of energy $\hbar\omega_k$. We can get a physical understanding of the nature of these excitations by considering two limits. In the large wavenumber limit $k\xi \gg 1$, we have $\omega_k \sim \hbar k^2/2m$, the dispersion of free atoms, and the Bogoliubov coefficients give $u_k \to 1$ and $v_k \to 0$: the quasi-particles are close to free atoms. On the other hand, for $k\xi \ll 1$, we have $\omega_k \sim c|k|$, the dispersion of sound waves, and the Bogoliubov coefficients becomes equal $u_k \sim v_k \sim \sqrt{mc/(2\hbar|k|)}$: the low wavenumber excitations are that of a fluid. It is in this hydrodynamic regime that the analogy of analogue gravity is usually formulated, see Sec. 1.3.

3.3.2-d Dynamics in the presence of an external drive

We now consider the case where the interaction constant $g_1(t)$ is varied, or equivalently as considered in [178, 155, 132] the speed of sound $c(t)$ is varied. We follow the analysis of [132]. The passage matrix P_k defined in Eq. (3.38) is time-dependent, and then the equation of motion for the phononic operators reads

$$\partial_t \begin{pmatrix} \hat{b}_k \\ \hat{b}^\dagger_{-k} \end{pmatrix} = \begin{pmatrix} -i\omega_k(t) & \frac{\omega_k}{2\omega_k} \\ \frac{\omega_k}{2\omega_k} & i\omega_k(t) \end{pmatrix} \begin{pmatrix} \hat{b}_k \\ \hat{b}^\dagger_{-k} \end{pmatrix}\,, \tag{3.45}$$

where we have used $|u_k|^2 - |v_k|^2 = 1$, and the fact that only $c(t)$ is varied here while the mass is kept constant. The anti-diagonal term comes from the time dependence of the passage matrix. It shows that, in addition to the adiabatic change of

frequency $\omega_k(t)$ in the phase, the evolution leads to a non-trivial mixing between the phononic modes $\pm k$, and so a quasi-particle creation. Notice the similarity with Eq. (32) of [1], reproduced in Sec. 2.2, for cosmological perturbations. This equation is then similarly solved by introducing a Bogoliubov transformation with coefficients $\alpha_k(t)$ and $\beta_k(t)$ such that

$$\begin{pmatrix} \hat{b}_k(t) \\ \hat{b}^\dagger_{-k}(t) \end{pmatrix} = \begin{pmatrix} \alpha_k(t) e^{-i\int_{t_{\rm in}}^t \omega_k {\rm d}t'} & \beta_k^\star(t) e^{-i\int_{t_{\rm in}}^t \omega_k {\rm d}t'} \\ \beta_k(t) e^{i\int_{t_{\rm in}}^t \omega_k {\rm d}t'} & \alpha_k^\star(t) e^{i\int_{t_{\rm in}}^t \omega_k {\rm d}t'} \end{pmatrix} \begin{pmatrix} \hat{b}_k(t_{\rm in}) \\ \hat{b}^\dagger_{-k}(t_{\rm in}) \end{pmatrix} , \tag{3.46}$$

where $\alpha_k(t_{\rm in}) = 1$, $\beta_k(t_{\rm in}) = 0$ and $\hat{b}_k^{(\dagger)}(t_{\rm in})$ corresponds to the operators of Eq. (3.38) evaluated at some time $t_{\rm in}$. In Eq. (3.46), we have factored out the adiabatic evolution of the phase, and Eq. (3.45) is then equivalent to

$$\dot{\alpha_k} = \frac{\dot{\omega_k}}{2\omega_k} \beta_k e^{2i\int_{t_{\rm in}}^t \omega_k {\rm d}t'} , \tag{3.47}$$

$$\dot{\beta_k} = \frac{\dot{\omega_k}}{2\omega_k} \alpha_k e^{-2i\int_{t_{\rm in}}^t \omega_k {\rm d}t'} . \tag{3.48}$$

We consider a situation where the frequency of the trap is varied during a finite duration such that $\omega_\perp(t) \xrightarrow[t\to-\infty]{} \omega_{\perp,{\rm in}}$ and $\omega_\perp(t) \xrightarrow[t\to+\infty]{} \omega_{\perp,{\rm out}}$. In these two asymptotic regions, the Bogoliubov coefficients $u_k^{\rm in,out}$ and $v_k^{\rm in,out}$ are time-independent, so the phonons defined by the creation and annihilation operators $\hat{b}_{\pm k}^{(\dagger)\,{\rm in,out}}$ of Eq. (3.38), evaluated in the asymptotic regions, have a well-defined number. These pairs of in and out operators are related by a Bogoliubov transformation. This can be seen by fixing $t_{\rm in} \to -\infty$ in Eq. (3.46). Then the operators $\hat{b}_{\pm k}^{(\dagger)}(t)$ in the asymptotic future will correspond to $\hat{b}_{\pm k}^{(\dagger)\,{\rm out}}$ (up to the running phase that we factorised out) so

$$\hat{b}_{\pm k}^{\rm out} = \alpha_k(+\infty) \hat{b}_{\pm k}^{\rm in} + \beta_k^\star(+\infty) \hat{b}_{\mp k}^{\dagger\,{\rm in}} . \tag{3.49}$$

The dynamics is then completely fixed by solving Eq. (3.47) for the specific variation of $\omega_k(t)$ we consider. In principle, for a given variation of $\omega_\perp(t)$, we should first solve Eq. (3.28) to get the evolution of $\sigma(t)$, which we then use as an input to solve Eq. (3.47). In practice, in [4], we made the simplifying assumption that the modulation of $\omega_\perp(t)$ induces a modulation of $\omega_k(t)$ at the same frequency, which we recall is only valid for a slow enough modulation.

3.3.3 Parametric amplification

3.3.3-a Link with preheating

To exhibit the link between the creation of phonons in the Bose gas and the preheating mechanism described in Sec. 1.2.4, we focus on the case where, for

example following a quench, the speed of sound oscillates at a certain frequency

$$c^2(t) = c_0^2 \left[1 + a \sin\left(\omega_m t\right)\right] , \tag{3.50}$$

so that

$$\omega_k^2(t) = \omega_{k,0}^2 \left[1 + \mathcal{A}_k \sin\left(\omega_m t\right)\right] , \tag{3.51}$$

where $\mathcal{A}_k = a(1 + k^2\xi^2/4)^{-1}$, we recall that ξ is the healing length defined below Eq. (3.41). This modulation type was considered in [132]. To derive a Mathieu's equation, inspired by [179], we consider the perturbations of the density and phase fields. Using the form (3.4), after integration over the radial profile, we expand the field in density $\delta\hat{\rho}$ and phase $\delta\hat{\theta}$ perturbations assumed small

$$\hat{\Psi} = n_0 \sqrt{\hat{\mathbb{1}} + \frac{\delta\hat{\rho}}{n_0}}\, e^{i\delta\hat{\theta}} \approx n_0 \left(\mathbb{1} + \frac{\delta\hat{\rho}}{2n_0} + i\delta\hat{\theta}\right) . \tag{3.52}$$

Equating with Eq. (3.29), and taking the hermitian and anti-hermitian part, we get

$$\delta\hat{\rho}\,(z,t) = n_0 \left(\delta\hat{\Psi} + \delta\hat{\Psi}^\dagger\right) , \tag{3.53a}$$

$$\delta\hat{\theta}\,(z,t) = -\frac{i}{2} \left(\delta\hat{\Psi} - \delta\hat{\Psi}^\dagger\right) . \tag{3.53b}$$

We use the same conventions as [1] for the Fourier transform of these quantities (chosen to make them adimensional)

$$\delta\hat{\rho} = \sqrt{\frac{n_0}{L}} \sum_{k\neq 0} e^{ikx} \hat{\rho}_k \,, \tag{3.54a}$$

$$\delta\hat{\theta} = \frac{1}{\sqrt{L n_0}} \sum_{k\neq 0} e^{ikx} \hat{\theta}_k \,, \tag{3.54b}$$

where we recall L is the length of the gas. In Fourier space, the relation with the perturbations of the atomic field then reads

$$\hat{\rho}_k = \hat{a}_k + \hat{a}_{-k}^\dagger = (u_k + v_k) \left(\hat{b}_k + \hat{b}_{-k}^\dagger\right) , \tag{3.55a}$$

$$\hat{\theta}_k = -\frac{i}{2} \left(\hat{a}_k - \hat{a}_{-k}^\dagger\right) = -\frac{i}{2} \left(u_k - v_k\right) \left(\hat{b}_k - \hat{b}_{-k}^\dagger\right) , \tag{3.55b}$$

where in the second equality we have written the expressions in terms of phononic operators. First, notice that in a thermal state of atoms (or phonons), the above expressions show explicitly that the average density and phase fluctuations vanish $\langle\delta\hat{\theta}\rangle = \langle\delta\hat{\rho}\rangle = 0$. Second, notice that $(i\hbar\delta\hat{\theta}, \delta\hat{\rho})$ form a canonically conjugated pair.

Finally, expressing $u_k + v_k = \sqrt{\hbar k^2/2m\omega_k}$, notice that the normalisation (similar to that of a relativistic scalar field) has a time-dependent piece due to ω_k. Now using Eq. (3.45) we can write the equation of motion of the density perturbation modes

$$\ddot{\hat{\rho}}_k + \omega_k^2 \hat{\rho}_k = 0\,. \tag{3.56}$$

For a modulation of the frequency as in Eq. (3.51), Eq. (3.56) is exactly a Mathieu's equation as that found for a scalar field excited by the oscillations of the inflaton in preheating, see Eq. (1.139). Notice that Eq. (1.139) was obtained in the regime where the expansion of space is negligible. Having an analogue of the equation in the presence of expansion could maybe be achieved by considering the expansion of the vertical part, which would redshift the modes as in [138]. Following the standard analysis of Mathieu's equation [74] we thus expect an exponential creation of density fluctuations and pairs of phonons in some resonant bands.

To conclude this part, we compare two other studies of analogue preheating systems [**?** 145]. On the one hand, the setting of the numerical study [146] is very similar to the one of [130] in that it considers a 1D Bose gas whose longitudinal modes are sourced by initial excitations in the radial modes. The main difference is that while in [146] only the first excited radial mode is populated, in [130], the gas is driven to oscillate in a quasi-classical manner in the radial direction. The radial excitation is then treated as a second quantum field in the former, while it is taken to be a classical background in the latter. Consequently, the longitudinal modes are excited via a tachyonic instability triggered by the excited radial mode in [146], while they are excited via parametric resonances due to the coherent radial oscillations in [130]. On the other hand, the experiment [145] is based on a quite different set-up which uses 2D interface waves. The system is placed on a moving platform, which oscillates to trigger a parametric amplification of the waves. In contrast to [146, 145], the excitations are classical in nature, and the amplification is seeded by environmental noise rather than vacuum or thermal one. The authors follow the amplification of the modes from their initial exponential growth to its saturation and the redistribution towards other modes of the system, leading to the growth of secondaries. In Sec. 3.4, we consider the effect of damping in a 1D Bose gas due to interaction with a thermal population of quasi-particles. Our analysis focuses on linear damping when the population of the decaying mode is relatively small. In contrast, the system of Ref. [146] features linear damping but not due to interaction with other modes, and the authors focus on damping triggered by the largeness of the amplitude of the resonant mode leading to non-linear damping.

3.3.3-b Growth and decay of phonon numbers and correlation

In [132], the authors analysed analytically and numerically the generation of phonons and the correlation between them in the presence of an effective dissipation rate. Let us first review the results in the absence of dissipation. Assuming that we start from a thermal state (including possibly the vacuum), the initial state is Gaussian, and the evolution via Eq. (3.47) leads to another Gaussian state. For the homogeneous system we consider, the covariance matrix for the modes $\pm k$ is then completely characterised by the 2-point functions

$$n_{\pm k} = \left\langle \hat{b}^\dagger_{\pm k} \hat{b}_{\pm k} \right\rangle , \tag{3.57a}$$

$$c_k = \left\langle \hat{b}_{\pm k} \hat{b}_{\mp k} \right\rangle , \tag{3.57b}$$

where $n_{\pm k}$ is the number of phonons in the mode $\pm k$ and c_k the correlation in between them. Notice that c_k is a complex quantity and, by definition, $c_k = c_{-k}$. We assume that the system is isotropic $n_k = n_{-k}$ for simplicity. Using the relation (3.49), we can relate this quantity before and after the variation of the speed of sound. We have

$$n_k^{\text{out}} = \left(|\alpha_k|^2 + |\beta_k|^2 \right) n_k^{\text{in}} + |\beta_k|^2 , \tag{3.58a}$$

$$c_k = \alpha_k \beta_k^\star \left(2 n_k^{\text{in}} + 1 \right) , \tag{3.58b}$$

where we have used $c_k^{\text{in}} = 0$ and $\langle \hat{b}_k \hat{b}^\dagger_{-k} \rangle = 0$ in a homogeneous thermal state.

We see that generically phonons are created by the variation of the sound speed, the extent of which is controlled by the magnitude of the Bogolibuov coefficients and the initial population. There are two types of contributions, the one proportional to the initial population n_k^{in}, a stimulated creation, and the spontaneous creation, which would be present even if $n_k^{\text{in}} = 0$. Spontaneous production can occur from an initial vacuum state, and it arises in the computation from the non-commutation of the creation/annihilation operators; it is a genuine quantum process. One cannot distinguish a phonon created via a stimulated or a spontaneous process, these two channels add phonons in the mode $\pm k$ in a common quantum state. Still [132], a way to check those phonons were created out of the vacuum is to check that their state is entangled, also referred to as 'non-separable', see Sec. 2.4 for details on this notion. For an isotropic and homogeneous Gaussian state, the non-separability condition is equivalent to the inequality [132, 180]

$$\Delta_k = n_k - |c_k| < 0 . \tag{3.59}$$

After the modulation, we have

$$\Delta_k^{\text{out}} = \frac{-|\beta_k| \left(|\alpha_k| + |\beta_k| \right) + n_k^{\text{in}}}{\left(|\alpha_k| + |\beta_k| \right)^2} , \tag{3.60}$$

which makes clear the effect of the different contributions. If we start from the vacuum, then $\Delta_k^{\rm out} < 0$, and the phonons are in an entangled state. On the other hand, if we start to increase $n_k^{\rm in}$, then Δ_k will also increase, and it can make the state separable if $2n_k^{\rm in}+1 > (|\alpha_k|+|\beta_k|)^2$. Therefore, *only* creation out of the vacuum via a spontaneous process can generate an entangled state, while stimulated creation will dilute this entanglement. In addition, with the form (3.60), one can check that for a fixed value of $n_k^{\rm in}$, $\Delta_k^{\rm out}$ is monotonically decreasing as $|\beta_k|$ increases. For very large $|\beta_k|$, it goes to $\Delta_k^{\rm out} \to -1/2$. Therefore, the resonant modes of the parametric amplification, which have the largest values of $|\beta_k|$, will exhibit the smallest values of $\Delta_k^{\rm out}$.

The authors of [132] solved Eq. (3.47) for the modulation of Eq. (3.51) and showed that, as expected from the Mathieu's equation, Eq. (3.56), the Bogoliubov coefficients only grows exponentially in some resonant bands and oscillate out of this band. They also analysed the evolution of Δ_k for different modes. As an illustration we plot in Fig. 3.4 the evolution of n_k and $|c_k|$ obtained for a small quench of the trapping frequency $\omega_{\perp,\rm f}/\omega_\perp = 1.048$, that results in a modulation of ω_k at a frequency $2\omega_\perp$. The ratio $\omega_{\perp,\rm f}/\omega_\perp$ determines the amplitude a of the oscillations of c^2 in Eq. (3.50), which will be small in this case, putting us in the narrow resonance regime, see Sec. 1.2.4. The instantaneous Bogoliubov coefficients of Eq. (3.46) are numerically computed by first solving Eq. (3.28) and using the result as an input for a numerical resolution of Eq. (3.45). We then compute n_k and $|c_k|$ from Eqs. (3.58a)-(3.58b) as a function of time for a non-vanishing initial temperature $k_{\rm B}T/mc^2 = 1$. We chose these values to make the entanglement generation clear and visible. We comment on more realistic values below. Fig. 3.4 shows the generation of an entangled state for the modes $\pm k$ at late times i.e. $|c_k| > n_k$.

In [132], the authors solved Eq. (3.47) for a modulation lasting 50 oscillations, close to the value of $N_{\rm m} \approx 54.4$ used in the second experiment of [130]. They estimated the initial temperature value $k_{\rm B}T/\hbar\omega_\perp = 1$. They concluded the simple quadratic model overestimates the intensity of correlations, predicting that the state should have been entangled. To illustrate this conclusion, we plot in Fig. 3.5 the evolution of n_k and $|c_k|$ following a modulation of the trapping frequency. We used values estimated from [130]. We considered a modulation at the benchmark value of $\omega_{\rm m}/2\pi = 2170\,{\rm Hz}$, lasting $N_{\rm m} \approx 54.4$ oscillations. We used values of the speed of sound and temperature computed from the estimates derived in Sec. 3.2, which gives $c \approx 8\,{\rm mm/s}$ and $k_{\rm B}T/mc^2 \approx 6.5$. In this respect, the value of $k_{\rm B}T/\omega_k = 1$, at resonance, used in [132] seems too low. It would correspond to $k_{\rm B}T/mc^2 \approx 2.3$. Still, it is in the appropriate range for the current run of the experiment where $k_{\rm B}T/mc^2 \approx 1$. Another difference with the computations of [132] is that, in Fig. 3.5, we solved Eq. (3.28) to deduce the change in the speed of sound due to

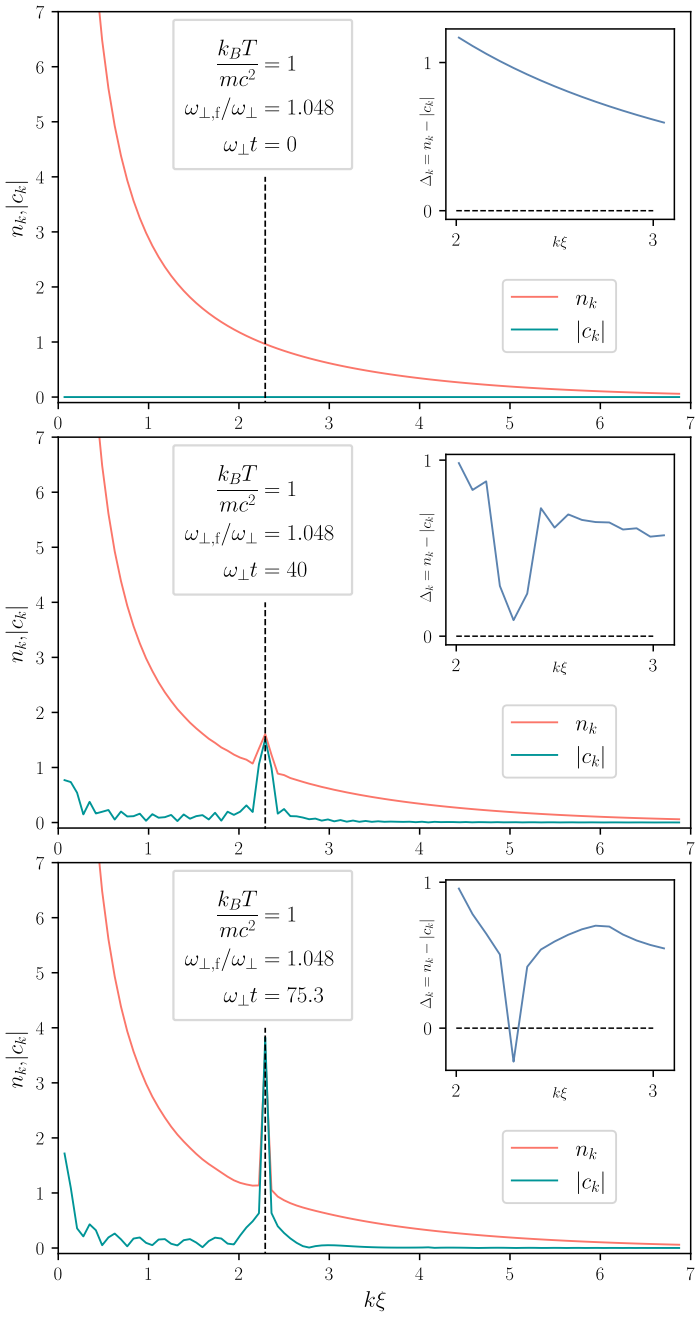

Figure 3.4: Evolution of the number of quasi-particles n_k and their pair-correlation $|c_k|$, as predicted by Eqs. (3.58a)-(3.58b), following a quench of the trap frequency. The vertical dashed line is located at the discrete mode k_j whose frequency is closest to half the final trap frequency $2\omega_{k_j} = \omega_{\perp,\mathrm{f}}$. We are in the narrow resonance regime where resonant modes are located close to this sub-harmonic mode. We consider a gas of length $L/a_\perp = 256$.

the modulation, rather than using the effective form Eq. (3.51). The oscillation of σ is a combination of several oscillations at different frequencies as shown for instance in the upper panel of Fig. 3.3. In the context of preheating [181, 182, 183], it is known that such non-ideal modulation results in a modified structure of the Mathieu equation resonance bands, for instance by broadening them [3] In our particular case, Fig. 3.5 shows two resonant peaks, one around $\omega_k = \omega_\perp$, and one around $\omega_k = \omega_\mathrm{m}/2$. As reported in [132], and at odds with the experimental results of [130], Fig. 3.5 shows that the phononic states of the two pairs of modes are entangled at late time. For comparison, we have plotted the result of the same modulation on the initial state of phonons at a lower temperature $k_\mathrm{B}T/mc^2 = 1$, close to current experimental values. We observe that the state becomes entangled at earlier times and that the lower bound $\delta_k = -0.5$ is quickly saturated. Note that despite this saturation, the entanglement will be harder to detect when the number of excitations is very large, see discussion below Eq. (3.64).

The authors of [132] suggested as a tentative explanation for the absence of entanglement that some dissipative processes, ignored here, might have weakened the correlations. They then introduce a model of dissipation that preserves the Gaussianity and isotropy of the state of the modes so that they are still described by n_k and c_k. Therefore, the resulting state is in the same class as the ones considered for the cosmological perturbations in Sec. 2. The authors then derived an evolution equation for n_k and c_k parameterised by a dissipation rate Γ, such that n_k and c_k both decay at a rate 2Γ. They show that a large enough Γ can prevent the generation of entanglement and, in some cases, even stop the exponential growth of the number of phonons. Note that in Fig. 3.5 the number of phonons in the resonant modes is much larger than that reported in [130]. Thus, in addition to prevent the generation of entanglement, we do expect dissipation to significantly reduced the number of phonons reduced. The authors of [132] give a threshold $\Gamma/\omega_k \geq 4.2\%$[4] above which they estimated the dissipation sufficient to explain the absence of entanglement in [130].

However, the treatment of [132] was effective. In Sec. 3.4, by analysing the non-linear evolution of the gas, we exhibit a micro-physically derived dissipation mechanism due to Beliaev-Landau scatterings present in any one-dimensional Bose gas. In Sec. 3.6, we explain that the same processes are expected to affect correlations in just the same proportion so that due to these scatterings, n_k and c_k decay approximately at the same rate. We then compare the magnitude of this rate with the bounds given in [132]. Notice that we limit our investigations to the

[3] Quasi-particle interactions can also lead to broadened peak as shown in Sec. 3.4. However, note that in this case the other modes in the peak are still non-resonant and are fed by the decay of excitations in the resonant modes.

[4] We use our convention here where n_k and c_k decay at Γ_k, while their decay rate is $2\Gamma_k$ in [132].

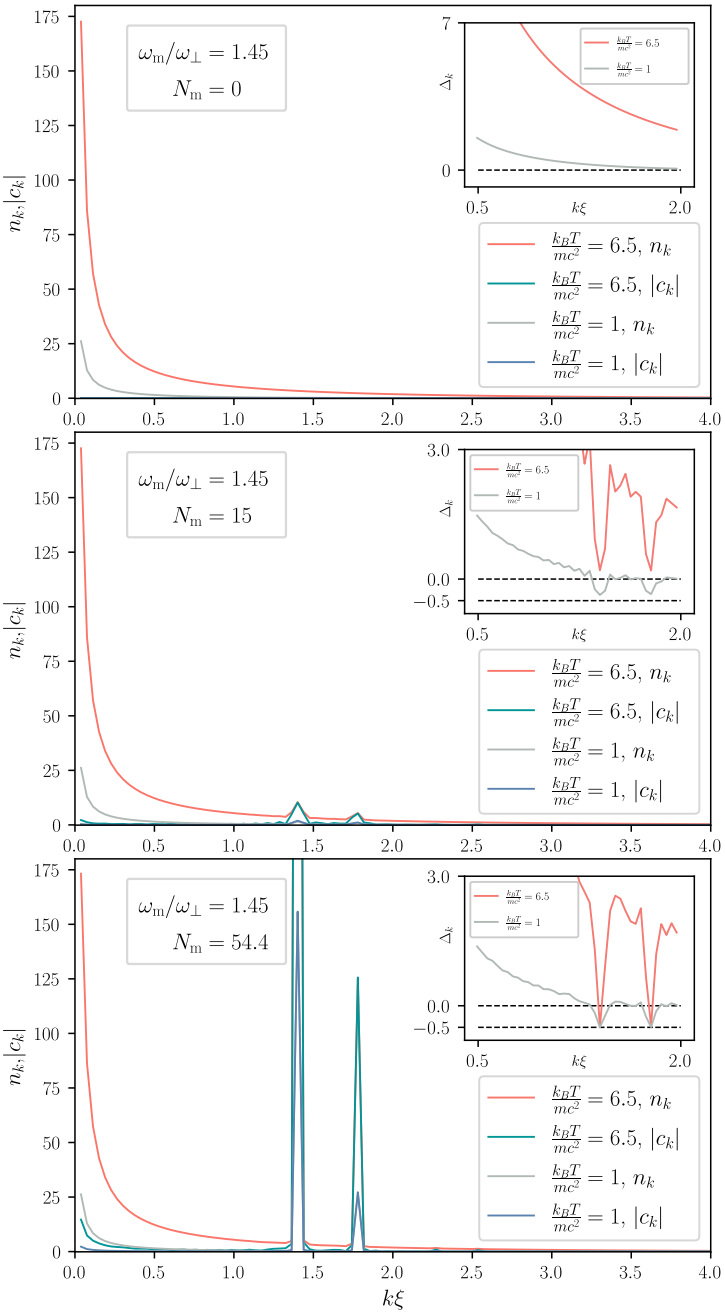

Figure 3.5: Evolution of the number of quasi-particles n_k and their pair-correlation $|c_k|$ as a function of time during modulation of the trap frequency at ω_m with amplitude $A = 0.1$, as predicted by Eqs. (3.58a)-(3.58b). At final time the number of phonons in the first peak is $n_k = 8.3 \times 10^2$, outside of the frame of the figure. We consider a gas of length $L/a_\perp = 256$.

effect of the dissipation on the growth of the resonant modes. The loss of entanglement and slowing down of the exponential growth are only the first effects of non-linearities. They will be followed by substantial growth of non-resonant modes and back-reaction on the condensate oscillations, which will be damped. These later stages are very reminiscent of the very non-linear regime following preheating. They were numerically analysed in [133]. As preparation for deriving the phonon scattering rate in Sec. 3.6, we explain in the next sub-section, Sec. 3.3.4, why the formalism used so far is not adapted for 1D gases and develop a more suitable one.

We close this sub-section by considering how the non-separability criteria of Eq (3.59) can be experimentally accessed.

3.3.3-c Density-density correlation

In [156, 157], the authors showed that the 2-point density-density correlation function, a quantity experimentally measured in [111] for instance, can be used to demonstrate the non-separability of the phonon pairs. We define the connected 2-point density correlation function at equal time following [157]

$$\begin{aligned} G^{(2)}\left(z,z';t\right) &= \left\langle \hat{\rho}\left(z,t\right)\hat{\rho}\left(z',t\right)\right\rangle - \left\langle \hat{\rho}\left(z,t\right)\right\rangle \left\langle \hat{\rho}\left(z',t\right)\right\rangle \,, \\ &= \left\langle \delta\hat{\rho}\left(z,t\right)\delta\hat{\rho}\left(z',t\right)\right\rangle \,, \end{aligned} \tag{3.61}$$

where we have used that $\langle\delta\hat{\rho}\rangle = 0$ to get the second line. Taking the Fourier transform and expanding in terms of quasi-particles, we get

$$\begin{aligned} G^{(2)}\left(k,k';t\right) &= \int_0^L\int_0^L G^{(2)}e^{-ikz}e^{-ik'z'}\left(z,z';t\right)\mathrm{d}z\mathrm{d}z' \,, \\ &= n_0 L\left\langle \delta\hat{\rho}_k\delta\hat{\rho}_{k'}\right\rangle \,, \\ &= \left(u_k+v_k\right)^2\left[2n_k+1+2\Re\left(c_k\right)\right]\delta_{k,-k'} \,, \end{aligned} \tag{3.62}$$

where the Kronecker delta comes from the homogeneity of the state. The only non-trivial information then comes from the anti-diagonal 2-point function $G^{(2)}(k,-k) = G^{(2)}_k$. Evaluating the above in the out asymptotic region, where the quasi-particles are evolving freely, we have

$$G^{(2)}_k\left(t\right) = G^{(2)\,\mathrm{out\,vac}}_k\left[2n^{\mathrm{out}}_k+1+2\Re\left(c^{\mathrm{out}}_k e^{-i2\omega^{\mathrm{out}}_k t}\right)\right] \,, \tag{3.63}$$

where we have introduced the out vacuum value $G^{(2)\,\mathrm{vac}}_k = (u^{\mathrm{out}}_k + v^{\mathrm{out}}_k)^2$. If at any time t, $G^{(2)}_k$ is less than its vacuum value then it implies $|c^{\mathrm{out}}_k| > n^{\mathrm{out}}_k$ i.e. the state of the quasi-particles is non-separable. The density-density correlation can be directly accessed in an experimental set-up allowing for *in situ* measurements, e.g. [111].

In the case of [130], the phononic distribution is measured by opening the trap and letting the atomic cloud expand and fall on a measuring device. The velocities are inferred from the expansion of the cloud, a method called Time Of Flight measurement (TOF), and one can show that, in the limit of an adiabatic opening, the state of the phonons is mapped to the atoms [156], a phenomenon known as phonon evaporation [130]. Using this procedure, the authors were able to measure the following quantity

$$g^{(2)} = \frac{\left\langle \hat{b}^\dagger_{-k}\hat{b}^\dagger_k\hat{b}_k\hat{b}_{-k}\right\rangle}{\left\langle \hat{b}^\dagger_k\hat{b}_k\right\rangle\left\langle \hat{b}^\dagger_{-k}\hat{b}_{-k}\right\rangle} = 1 + \frac{|c_k|^2}{n_k^2}\,, \tag{3.64}$$

where we performed Wick contractions to get the second equality. The condition of entanglement (3.59) is now recast as $g^{(2)} > 2$. Note that measuring $g^{(2)} > 2$, or likewise $G^{(2)}_k < G^{(2)\,\mathrm{vac}}_k$, is not a non-classicality criteria in the sense of Ref. [184]. Indeed, we could find a classical model of the system giving $G^{(2)}_k < G^{(2)\,\mathrm{vac}}_k$. A Bell inequality would be necessary to rule out a whole class of alternative classical theories. Still, our aim is slightly different here. We already know that the correct description of the system is a quantum one. Adopting this description, we want to show that the system is in a particular type of *quantum* states, the entangled states, which is sufficient to demonstrate vacuum amplification.

We reproduce in Fig. 3.2 the measured values in [130]. We see that across the spectrum, and in particular around the resonant mode, $g^{(2)} < 2$. Therefore, as previously stated, one cannot claim that the phonons produced in the experiment were in an entangled state. Notice that with the values of n_k and $|c_k|$ shown in Fig. 3.5, although the state is entangled since $\Delta^{\mathrm{out.}}_k$ is negative, we would have $g^{(2)} \approx 2$ at the resonant modes i.e. the threshold value between a separable and an entangled state. This convergence to 2 is due to the normalisation of $g^{(2)}$ by the number of phonons n_k. It illustrates the notion of visibility of the entanglement [157, 133]. Even if the state is entangled, it can be difficult to tell if we have to compare two very large numbers, n_k and $|c_k|$, while their difference is bounded from below by $-1/2$. Therefore, the visibility of entanglement in the experiment is optimal when we create a small number of excitations [133]. Consequently, as illustrated in Fig. 3.5, where entanglement is reached with fewer excitations created for the smallest of the two temperatures, we should use the lowest possible initial temperature for optimal visibility.

Having completed our review of the previous theoretical endeavours to analyse the experiment results, we will present the progress made during this PhD. First, we discuss the Madelung perturbation scheme, which is at the core of the analysis conducted in [1] reproduced in Sec. 3.4.

3.3.4 Madelung approximation of 1D gas

In this section, we examine more closely the BdG approximation, presented in Sec. 3.3.2-b, in the case of one-dimensional gas. We show that it is not valid anymore if the length of the gas L is larger than a critical size r_0 defined in Eq. (3.76). We then present a perturbative scheme based on the Madelung form (3.4), which remains valid for long one-dimensional quasi-condensates.

3.3.4-a Failure of BdG in 1D gas

Assuming that we are in a static situation $g = \text{cst}$, the approximate ground state of the system is given by the vacuum of phonons $n_k = c_k = 0$ for any k. The number of depleted atoms in the mode k then reads

$$\left\langle \hat{a}_k^\dagger \hat{a}_k \right\rangle = |v_k|^2 \sim_{k\to 0} \frac{g_1 n_0}{2\hbar c k}\,, \tag{3.65}$$

where we have taken the small wavenumber limit. The total number of atoms N given by Eq. (3.35) is always larger than that in the condensate N_0, so the total density n always larger than n_0. We want to compute the value of the total density of the gas in the thermodynamic limit $L \to +\infty$ for a condensate of fixed density n_0. The extra contribution is given by the number of depleted atoms normalised by L, which by using the formula for Riemann sums, reads

$$\frac{1}{L}\sum_{k\in 2\pi\mathbb{Z}^\star/L} \left\langle \hat{a}_k^\dagger \hat{a}_k \right\rangle \xrightarrow[L\to+\infty]{} \frac{1}{2\pi}\int_{-\infty}^{+\infty} \left\langle \hat{a}_k^\dagger \hat{a}_k \right\rangle \mathrm{d}k = +\infty\,. \tag{3.66}$$

The right-hand side is an IR divergent integral since its integrand behaves as k^{-1}. In the large L limit, the Bogoliubov approximate predicts an unphysical infinite density. This failure of the approximation is directly related to the general Mermin-Wagner-Hohenberg theorem [185] stating the absence of long-range order in one and two-dimensional systems. The theorem can be proven using general inequalities on the number of excitation resulting in a divergence of some physical quantities, see Sec. 7.4 of [166]. In the specific case of Bose gas, it implies that there can be no genuine condensate in reduced dimensions, only *quasi*-condensate.

The physical reason behind this failure is that one-dimensional Bose gas exhibits large phase fluctuations [166]. One can check that by computing the phase-phase correlation in a thermal state of phonons using Eq. (3.55b), see Sec. 3.3.4-c. Because of these fluctuations, any pre-existing order will be gradually destroyed. Thinking in terms of numbers rather than operators, the condition $|\delta\Psi| \ll 1$ of the BdG approximation requires that the atomic field Ψ, a complex number, is close to Ψ_0. This condition requires that the modulus and the phase of Ψ are close to that of Ψ_0 i.e. the density *and* the phase perturbations around the condensate are small. The latter condition is not satisfied for a 1D gas of arbitrary length. A finite length L of the gas regulates the unbouded growth of the phase fluctuations,

but the $|\delta\Psi|$ term would become more and more problematic as L is increased. To avoid this problem, we can formulate a perturbation theory for one-dimensional gas in the Madelung form of Eq. (3.4), where we expand the relative density perturbation, but not the phase one that cannot be assumed small. We followed this strategy in [4] to define quasi-particles and calculate their interaction rate, and we now give more details on this approach.

3.3.4-b Quantum hydrodynamics and quasi-condensate

Before making any computations using the density and phase formalism, we have to say a few words about the technical difficulties hidden there. Indeed, the analysis in density and phase can only describe long enough wavelength fluctuations. As a consequence, as mentioned below the definition Eq. (3.4), the phase operator cannot be mathematically well-defined. It is physically intuitive that the notion of fluid ceases to make sense when looking at scales shorter than the inter-particle distance: the density is infinite at points where atoms are located and vanishing elsewhere. The authors of [168] showed that in order to make the effective character of the theory manifest and make the mathematical treatment rigorous, it is necessary to discretise space in boxes of size $\mathrm{d}x$, which provides a UV cut-off to the theory. Using this discrete theory, we want to describe a quasi-condensed gas which exhibits small density fluctuations i.e. the variance of its density is smaller than its average value $\mathrm{Var}(\hat{\rho})/\langle\hat{\rho}\rangle \ll 1$. Following [168], it is instructive to write the variance in this discrete theory explicitly

$$\begin{aligned}\mathrm{Var}\left(\hat{\rho}\right) &= \left\langle\hat{\rho}^2\right\rangle - \left\langle\hat{\rho}\right\rangle^2 \\ &= \left\langle\hat{\Psi}^\dagger\left(\boldsymbol{x}\right)\hat{\Psi}^\dagger\left(\boldsymbol{x}\right)\hat{\Psi}\left(\boldsymbol{x}\right)\hat{\Psi}\left(\boldsymbol{x}\right)\right\rangle + \frac{\left\langle\hat{\rho}\left(\boldsymbol{x}\right)\right\rangle}{\mathrm{d}x} - \left\langle\hat{\rho}\left(\boldsymbol{x}\right)\right\rangle^2 ,\end{aligned} \tag{3.67}$$

where we have used the commutation relation of the discrete theory $[\hat{\Psi}\left(\boldsymbol{x}\right), \hat{\Psi}^\dagger\left(\boldsymbol{x}'\right)] = \delta_{\boldsymbol{x},\boldsymbol{x}'}/\mathrm{d}x$. We then have

$$\frac{\mathrm{Var}\left(\hat{\rho}\right)}{\left\langle\hat{\rho}\right\rangle^2} = \frac{1}{\left\langle\hat{\rho}\right\rangle\mathrm{d}x} + \frac{\left\langle:\delta\hat{\rho}(x)^2:\right\rangle}{\left\langle\hat{\rho}\right\rangle^2} . \tag{3.68}$$

The density fluctuations thus contain two terms. The first one comes from the commutator; it depends on the discretisation and would be infinite in a continuous theory. Therefore, to suppress the density fluctuations, we must choose a box size large enough to ensure that $\langle\hat{\rho}\rangle\,\mathrm{d}x \gg 1$ i.e. the occupation number in each box is large. The second term in Eq. (3.68) is the normal-ordered (with respect to the atomic field) relative density fluctuations and regular in a well-behaved continuous theory. It encodes information about the state considered rather than the discretisation, and we must consider states where it is small. Under these first two requirements, we can define an approximate phase operator [168]. Additional

requirements are necessary to describe well the physics of long wavelength fluctuations. The size of the boxes must be smaller than the healing length, to capture the departure of excitation from exact sound waves, and smaller than the thermal de Broglie wavelength $\lambda_{\mathrm{T}} = \sqrt{2\pi\hbar^2/mk_{\mathrm{B}}T}$, for the energy cut-off $\hbar^2/m\mathrm{d}x^2$ to be larger than the typical energy of thermal fluctuations $k_{\mathrm{B}}T$. In this framework, the authors of [168] then develop a perturbation theory around a classical solution of the equation of motion given by $\rho_0(x)$ and $\theta_0(x)$. Assuming that the density fluctuations about this solution are small $|\delta\hat{\rho}(x)| \ll \rho_0$, and that the phase fluctuations are slow $|\partial_x\delta\hat{\theta}|\mathrm{d}x \ll 1$, they compute one and two-body correlation functions and show that no divergence occurs when taking the limit $\mathrm{d}x \to 0$. This rigorous procedure is quite technical, and in [4], we skipped over these aspects when introducing the density and phase representation. Nonetheless, no divergence appears in the computations, the spectrum of the quadratic theory found does match that derived in [168], and the decay processes that we have identified involve only thermal fluctuations located at very long wavelengths, where the effective density and phase treatment is expected to be valid. The density and phase representation is also used in the numerical simulations of the one-dimensional gas we performed to confirm our analytical results. There, we represented the system using a grid and chose the space-step $\mathrm{d}x$ to respect the prescription of [168]. At the end of this section and in the next Sec. 3.5, we give additional details on the physics of quasi-condensate and the method used to simulate it, that we omitted in [4].

3.3.4-c Phase and density fluctuations

We follow Sec. 3.4 and perform the canonical transformation to density and phase using Eq. (3.4) while ignoring previously mentioned technical difficulties. We first consider a classical theory of fields, where the transformation is indeed canonical, and all quantities are well-defined. We then quantise the density and phase by imposing

$$\left[\hat{\rho}\left(x\right)\,,\,\hat{\theta}\left(x'\right)\right] = i\,\delta\left(x-x'\right)\,. \tag{3.69}$$

We reproduce the Hamiltonian (3) of [4]

$$\hat{H} = \int_0^L \mathrm{d}x\left[\frac{\hbar^2}{2m}\frac{\partial\hat{\theta}}{\partial x}\hat{\rho}\frac{\partial\hat{\theta}}{\partial x} + \frac{\hbar^2}{8m\hat{\rho}}\left(\frac{\partial\hat{\rho}}{\partial x}\right)^2 + \frac{g}{2}\hat{\rho}^2\right]\,, \tag{3.70}$$

where we dropped infinite commutators coming from the kinetic and interaction term. The latter could be renormalised by an (infinite) chemical potential shift. Notice that we have not expanded the exponential of the phase to obtain the above. We then assume we are in a state where the density and phase are perturbations around homogeneous and stationary solutions of the classical equations of motion, given by $\rho_0(x)$ and $\theta_0(x)$

$$\hat{\Psi} = e^{i\theta_0 + i\delta\hat{\theta}}\sqrt{\rho_0 + \delta\hat{\rho}}\,, \tag{3.71}$$

with small relative density fluctuations $|\delta\hat{\rho}(x)|\rho_0^{-1}$, and slow phase fluctuations i.e. $|\partial_x\delta\hat{\theta}|$ small. The Hamiltonian Eq. (3.70) is then expanded in a perturbation series, see Eq. (5) of [4]. The result of this expansion is given in Eq. (6) of [4]. We diagonalise the quadratic term of this expansion to Eq. (3.46) by introducing quasi-particle creation/ annihilation operators defined in Eq. (10) of [4]. Notice that both the energy spectrum defined by this procedure, see Eq. (9) of [4], and the link between quasi-particles and density/phase, see Eq. (10) of [4], have the same form as that obtained in the BdG approach, Eq. (3.41) and Eq. (3.55b)[5]. However, one subtle difference is that n_0 in the BdG expressions is replaced by ρ_0, the background density, in the Madelung perturbation scheme. Since $\langle\delta\hat{\rho}\rangle = 0$, one can check by computing the number of atoms in the gas via Eq. (3.35) that ρ_0 is, in fact, the *total* density of atoms, while n_0 was the density of condensed atoms only. The Madelung perturbation scheme is thus, by construction, immune to the appearance of divergences in the total number of atoms. Up to this substitution, the two approaches only differ in how the atomic field is reconstructed from the phonons. In BdG, the density and phase perturbations are treated as additive perturbations of the atomic field, while in the density and phase picture, the reconstruction is non-linear, see Eq. (3.71).

Using these new quasi-particles, we can define an approximate thermal state of the system by assuming a thermal distribution $\langle\hat{b}_k^\dagger\hat{b}_k\rangle = n_k^{\mathrm{th}}$, where

$$n_k^{\mathrm{th}} = \frac{1}{e^{\hbar\omega_k/k_{\mathrm{B}}T} - 1}\,. \tag{3.72}$$

We can then compute the phase and density fluctuations in this state. We have

$$\begin{aligned}\chi\left(x-x'\right) = \left\langle\delta\hat{\theta}\left(x\right)\delta\hat{\theta}\left(x'\right)\right\rangle &= \frac{1}{4\rho_0 L}\sum_{k\neq 0} e^{ik(x-x')}\left(u_k - v_k\right)^2\left(2n_k^{\mathrm{th}}+1\right)\,,\\ &\approx \frac{1}{8\pi\rho_0}\int_{-\infty}^{+\infty} e^{ik(x-x')}\left(u_k - v_k\right)^2\left(2n_k^{\mathrm{th}}+1\right)\mathrm{d}k\,,\end{aligned} \tag{3.73}$$

where in the second line, we have taken the continuum limit. Although the integral is taken over the whole range of wavenumbers, there should be a UV cut-off since the hydrodynamical theory is not valid for arbitrarily large wavenumbers, and the integral is divergent in this limit where $u_k - v_k \to 1$. This divergence gives rise to a Dirac delta and we study the finite part of the integral. We want to extract this integral's physical large wavelength content, which will correspond to the large separation $s = |x - x'|$ regime. For that, we expand the integrand in the limit of

[5]The published equation reproduced in Sec. 3.4 has a factor 1/2 too many in the definition of C_k given below Eq. (10).

small k. The lowest order term gives

$$\frac{\left(u_k - v_k\right)^2}{4}\left(2n_k^{\mathrm{th}} + 1\right) \sim_{k\to 0} \frac{k_{\mathrm{B}}T}{mc^2}\frac{1}{k^2 a_\perp^2}\,. \tag{3.74}$$

The phase fluctuations thus diverge for large wavelengths, the limit in which we expect the theory to be valid. In addition, the term in Eq. (3.74) gives the integral a finite UV contribution, so we do not need to introduce a cut-off to regularise it. Notice that the dominant fluctuations are of thermal origin, as made manifest by the factor of T, while vacuum fluctuations would contribute in $1/k$ [166]. In one dimension, the integral in Eq. (3.73) does not pick up any factor of k from the differential element and therefore exhibits an IR divergence. The divergence can be renormalised by removing the coincident point fluctuation $\chi(0)$ [166]. We then have

$$\chi\left(s\right) - \chi\left(0\right) \approx \frac{1}{\pi\rho_0}\int_0^{+\infty}\left[\cos\left(ks\right) - 1\right]\frac{k_{\mathrm{B}}T}{mc^2}\frac{\mathrm{d}k}{k^2} = -\frac{s}{r_0}\,, \tag{3.75}$$

where

$$r_0 = \frac{2\hbar^2\rho_0}{k_{\mathrm{B}}Tm}\,, \tag{3.76}$$

gives the characteristic scale for the growth of phase fluctuations. To compare, we compute the density fluctuations

$$\left\langle\delta\hat{\rho}\left(x\right)\delta\hat{\rho}\left(x'\right)\right\rangle \approx \frac{\rho_0}{2\pi L}\int_{-\infty}^{+\infty} e^{ik(x-x')}\left(u_k + v_k\right)^2\left(2n_k^{\mathrm{th}} + 1\right)\mathrm{d}k\,. \tag{3.77}$$

We again have a UV divergence giving rise to a Dirac delta as $u_k + v_k \to 1$ for $k\xi \gg 1$. However, in the long wavelength limit, we find

$$\left(u_k + v_k\right)^2\left(2n_k^{\mathrm{th}} + 1\right) \sim_{k\to 0} \frac{k_{\mathrm{B}}T}{mc^2}\,, \tag{3.78}$$

the density fluctuations are not growing in the IR. The integral in Eq. (3.77) will be regular in this limit, giving a contribution decaying in $1/s$. In this sense, the density fluctuations are suppressed compared to the phase ones.

Finally, we use these results to compute the behaviour of the one-body correlation, defined in Eq. (3.5), for a quasi-condensate at thermal equilibrium. We will neglect the density fluctuations, and we have [166]

$$\begin{aligned} g_1\left(x, x'\right) &= \left\langle\sqrt{\hat{\rho}\left(x\right)}\, e^{-i\left[\hat{\theta}(x) - \hat{\theta}(x')\right]}\sqrt{\hat{\rho}\left(x'\right)}\right\rangle\,, \\ &\approx \rho_0\left\langle e^{-i\left[\hat{\theta}(x) - \hat{\theta}(x')\right]}\right\rangle\,, \\ &= \rho_0 e^{-\frac{\left\langle\left[\hat{\theta}(x) - \hat{\theta}(x')\right]^2\right\rangle}{2}}\,, \\ &= \rho_0 e^{\chi(s) - \chi(0)} = \rho_0 e^{-\frac{s}{r_0}}\,. \end{aligned} \tag{3.79}$$

To compute the expression on the third line, we first expanded the exponential and dropped the odd powers that are vanishing by expansion in creation/annihilation operators

$$\left\langle e^{-i\left[\hat{\theta}(x)-\hat{\theta}(x')\right]}\right\rangle = \sum_{j=0}^{+\infty} \frac{(-1)^j}{(2j)!} \left\langle \left[\hat{\theta}\left(x\right) - \hat{\theta}\left(x'\right)\right]^{2j} \right\rangle . \tag{3.80}$$

Each term in the expansion can be computed using Wick contractions and counting the number of pairs. In general

$$\left\langle \hat{X}^{2j} \right\rangle = \frac{(2j)!}{2^j j!} \left\langle \hat{X}^2 \right\rangle^j . \tag{3.81}$$

Using this relation and the expansion Eq. (3.80), we obtain the third line of Eq. (3.79). The above computation is only valid for distances s large compared to the healing length ξ and the thermal length λ_{T}. A refined version can be found in [168], which agrees with Eq. (3.79) in the large s limit. Eq. (3.79) shows that even if the density fluctuations are small, there can be no long-range order in one dimension due to large phase fluctuations.[6] Notice, however, that if we consider a system of finite size L, as we do here, then the Mermin-Wagner theorem does not strictly apply, and the total number of depleted atoms remains finite. Eq. (3.79) indicates that when $L/r_0 \ll 1$, the effect of the phase fluctuation is not visible, and the gas effectively appears as condensed. Using the estimates computed in Sec. 3.3.1, in particular, for the vertical size of the condensate in the Thomas-Fermi regime, and the value of the temperature estimated in Sec. 3.3.2-d, we compute the value of L/r_0 in [130]. We find $r_0/L \approx 3 \times 10^{-2}$ i.e. we are in the quasi-condensate regime where phase fluctuations are large.

We reproduce our work [4] in the next section, Sec. 3.4. In this work, we also use the perturbation theory based on the Madelung form for numerical simulations. More details about the workings of these simulations are given in Sec. 3.5.

3.4 Article: 'Phonon decay in one-dimensional atomic Bose quasi-condensates via Beliaev-Landau damping'

[6] This results still holds for zero temperature. The computation is different and lead to a power-law decay [168].

Phonon decay in 1D atomic Bose quasicondensates via Beliaev-Landau damping

Amaury Micheli[1,2] and Scott Robertson[3,1]

[1] *Université Paris-Saclay, CNRS/IN2P3, IJCLab, 91405 Orsay, France*
[2] *Sorbonne Université, CNRS, UMR 7095, Institut d'Astrophysique de Paris, 98 bis bd Arago, 75014 Paris, France*
[3] *Université Paris-Saclay, Institut d'Optique Graduate School, CNRS, Laboratoire Charles Fabry, 91127 Palaiseau, France*

(Dated: December 23, 2022)

In a 1D Bose gas, there is no non-trivial scattering channel involving three Bogoliubov quasiparticles that conserves both energy and momentum. Nevertheless, we show that such 3-wave mixing processes (Beliaev and Landau damping) account for their decay via interactions with thermal fluctuations. Within an appropriate time window where the Fermi Golden Rule is expected to apply, the occupation number of the initially occupied mode decays exponentially and the rate takes a simple analytic form. The result is shown to compare favorably with simulations based on the Truncated Wigner Approximation. It is also shown that the same processes slow down the exponential growth of phonons induced by a parametric oscillation.

I. INTRODUCTION

Ultracold gases have proved to be a fruitful arena for both theoretical and experimental research. In particular, the propagation of elementary excitations on top of a macroscopic condensed background provides an accessible realisation of a quantum field in an effective curved spacetime [1, 2]. This can be exploited to, *e.g.*, mimic a black-hole horizon so as to induce the analogue of Hawking radiation (as recently achieved in [3]). It can also be used as a platform for realising an analogue of preheating, or the Dynamical Casimir Effect, which is a topic of current interest [4–6]. The degree of experimental control, combined with the intrinsically quantum nature of ultracold gases, makes them well-suited for such experiments.

In studies of this kind, an important issue concerns the effect of dissipation on the expected signal. Dissipation arises in closed systems as an effective phenomenon due to quasiparticle interactions [7, 8]. This entails the existence of an intrinsic quasiparticle decay. In 3D Bose gases, the principle mechanisms behind this decay are the 3-wave mixing processes of Beliaev and Landau damping [9, 10]. However, in 1D Bose gases with only two-body contact interactions (*i.e.*, of the Lieb-Liniger model [11]), two objections have been raised against the possibility of such processes. The first is that the integrability of the model prevents quasiparticle decay in principle, and that integrability-breaking perturbations must therefore be included before damping can occur [12–14]. The second is that quasiparticle decay requires the existence of non-trivial scattering channels conserving both momentum and energy, a criterion that has been routinely applied in many systems of all dimensionalities [15–19]. As there are no such channels involving three collinear Bogoliubov excitations due to their gapless and convex spectrum, it has been concluded that 3-wave mixing in 1D cannot induce decay [12, 18, 20].

In this paper, we wish to push back a little against these conclusions. First, integrability does not seem to prevent relaxation within a physical model, but only thermalization: the system tends towards an equilibrium state with rather more structure than a thermal state [21], described by a generalized Gibbs ensemble [22], see [23] for a recent application to the Lieb-Liniger gas. In addition, in the context of 1D Bose gases, this relaxation could even be necessary in order to comply with the Mermin-Wagner-Hohenberg theorem [24, 25], as it provides a mechanism by which the long-range order induced by a sufficiently narrowband excitation spectrum is washed away.

Second, we wish to show and emphasise that the apparent absence of an elastic scattering channel does not necessarily preclude any quasiparticle decay. In the Fermi Golden Rule (FGR), the Dirac delta enforcing energy conservation is typically interpreted in a binary way: either an energy-conserving channel exists and quasiparticle decay occurs, or there is no such channel and the quasiparticle is stable. However, the Dirac delta is an idealization of a narrow distribution with a small but finite width, so we must consider those final states that are *in the vicinity* of the exactly energy-conserving one. In particular, in 1D quasicondensates, the trivial 3-wave mixing channel involving the zero-energy mode is not physical itself. Yet the divergent thermal population of nearby infrared modes yields a well-defined contribution to the FGR decay rate. As anticipated, this mechanism leads to a broadening of the excitation spectrum and, within an appropriate time interval, the occupation of the initially occupied mode decays exponentially at a constant rate. The calculation of this rate is our main result.

The paper is organized as follows. In Sec. II, we recall the Lieb-Liniger model of a 1D Bose gas, including its hydrodynamical description in the weakly-interacting regime, and define the quasiparticles whose decay we are interested in. In Sec. III, we present a derivation of the intrinsic quasiparticle decay rate, as well as the outline of a more precise formulation that includes the main deviations from exponential decay. In Sec. IV, we show that the decay rate extracted from numerical simulations is in good agreement with the prediction of Sec. III, both

in the relaxation of an initial injection of phonons and in the slowing of exponential growth induced by a parametric oscillation (the latter example being inspired by experiments [4]). We conclude and make links with other works in Sec. V, while some further details are relegated to Appendices.

II. SETTINGS

Here we recall the necessary preliminaries for describing a 1D Bose gas. The quasicondensate nature, and the appropriateness of the hydrodynamical description, are introduced. The quasiparticles are defined in the hydrodynamical framework. A brief description of the numerical procedure adopted for simulating the dynamics of the gas is also given, and some preliminary numerical observations of the quasiparticle decay are presented.

A. Quasicondensate description

Consider a 1D gas of identical bosons of mass m with only two-body contact interactions and no atom losses, described by the Hamiltonian

$$\hat{H} = \int_0^L dx \left\{ \frac{\hbar^2}{2m} \partial_x \hat{\Psi}^\dagger \, \partial_x \hat{\Psi} + \frac{g}{2} \hat{\Psi}^{\dagger 2} \hat{\Psi}^2 \right\} , \qquad (1)$$

where $\hat{\Psi}$ is the atomic field and g is the 1D interaction constant. We impose periodic boundary conditions, so that the gas effectively lives on a torus of length L. The gas is "trapped" by the finiteness of the torus, but its dynamics and statistics are completely homogeneous. This allows an equivalent description using Fourier modes, each characterized by a wave number $k = 2\pi n/L$ for $n \in \mathbb{Z}$. Each Fourier amplitude $\hat{\Psi}_k$ is the annihilation operator for atoms of momentum $\hbar k$. The state of the system is fully characterized by the expectation values of the $\hat{\Psi}_k^{(\dagger)}$ and all their products.

A condensate occurs when one of the states of the system (typically the lowest-energy state $k = 0$) contains a macroscopic fraction of the total atom number $N_{\rm at}$ or, equivalently, when the gas demonstrates long-range order: the one-particle density matrix $g_1(x - x') = \left\langle \hat{\Psi}^\dagger(x) \, \hat{\Psi}(x') \right\rangle$ has a finite limit when $|x - x'| \to \infty$ [26]. However, the Mermin-Wagner-Hohenberg theorem [24, 25] precludes the apparition of such long-range order in a 1D system, essentially because the excitations of the system induce large fluctuations in the relative phase of $\hat{\Psi}$ between widely separated points. The one-particle density matrix then decays exponentially: $g_1(x - x') \approx \exp(-|x - x'|/r_0)$, where the coherence length r_0 is given by [25]

$$\frac{r_0}{\xi} = \left(\frac{k_B T}{mc^2} \right)^{-1} 2\rho_0 \xi \, . \qquad (2)$$

A *quasi*-condensed state can however be achieved in a 1D Bose gas at sufficiently low temperature [27]. As indicated above, the quasicondensate is characterized by large relative phase fluctuations over large distances, while the density fluctuations remain small. It is therefore appropriate to adopt these as the field variables. They are related to the atomic field via the Madelung transformation: $\hat{\Psi} = e^{i\hat{\theta}} \sqrt{\hat{\rho}}$. The representation in terms of the density and phase fields is known as the *hydrodynamical* description, since $\hat{\theta}$ acts like a potential for the flow velocity: $\hat{v} = \frac{\hbar}{m} \partial_x \hat{\theta}$. At the classical level where these are all c-numbers, this is an exact canonical transformation, with ρ and θ being conjugate variables. At the quantum level, this is approximately true as long as the discreteness of the atoms can be neglected, which requires a sufficiently weak interaction and coarse-graining over sites containing many atoms [28]. We may then write the hydrodynamical version of Eq. (1), up to some irrelevant term coming from normal ordering:

$$\hat{H} = \int_0^L dx \left\{ \frac{\hbar^2}{2m} \frac{\partial \hat{\theta}}{\partial x} \hat{\rho} \frac{\partial \hat{\theta}}{\partial x} + \frac{\hbar^2}{8m\hat{\rho}} \left(\frac{\partial \hat{\rho}}{\partial x} \right)^2 + \frac{g}{2} \hat{\rho}^2 \right\} , \qquad (3)$$

while imposing the canonical commutation relation

$$\left[\hat{\rho}(x) \, , \, \hat{\theta}(x') \right] = i \, \delta(x - x') \, . \qquad (4)$$

B. Perturbative expansion of Hamiltonian

We wish to study elementary excitations, which requires a well-defined splitting of the total field into a background plus perturbations. The background is defined as the homogeneous solution of the classical equation associated to the Hamiltonian (1) (*i.e.*, the Gross-Pitaevskii equation [25]), working in the rest frame of the gas. The density ρ_0 is then constant (the total number of atoms is $N_{\rm at} = \rho_0 L$) and the phase $\theta_0 = -g\rho_0 t/\hbar$. The density fluctuations $\delta\hat{\rho}$ around this background are assumed small while only the spatial variation of the phase fluctuations $\partial_x \delta\hat{\theta}$ is assumed small. We then expand the Hamiltonian in $(\delta\hat{\rho}, \partial_x \delta\hat{\theta})$

$$\hat{H} = E_0 \hat{\mathbb{1}} + \hat{H}_2 + \hat{H}_3 + \sum_{i \geq 0} \hat{H}_{4+i} \, , \qquad (5)$$

where the zeroth-order term $E_0 = g\rho_0^2 L/2$ is the energy of the homogeneous background, before any fluctuations are included. Since the background is an exact solution of the classical equation of motion, the first-order term

vanishes identically. The higher orders are given by

$$\hat{H}_2 = \int_0^L \left[\frac{\hbar^2 \rho_0}{2m} \left(\frac{\partial \delta\hat{\theta}}{\partial x} \right)^2 + \frac{\hbar^2}{8m\rho_0} \left(\frac{\partial \delta\hat{\rho}}{\partial x} \right)^2 + \frac{g}{2} \delta\hat{\rho}^2 \right] \mathrm{d}x \,,$$
$$\hat{H}_3 = \int_0^L \left[\frac{\hbar^2}{2m} \frac{\partial \delta\hat{\theta}}{\partial x} \delta\hat{\rho} \frac{\partial \delta\hat{\theta}}{\partial x} - \frac{\hbar^2}{8m\rho_0} \left(\frac{\partial \delta\hat{\rho}}{\partial x} \right)^2 \frac{\delta\hat{\rho}}{\rho_0} \right] \mathrm{d}x \,,$$
$$\hat{H}_{4+i} = (-1)^i \int_0^L \frac{\hbar^2}{8m\rho_0} \left(\frac{\partial \delta\hat{\rho}}{\partial x} \right)^2 \left(\frac{\delta\hat{\rho}}{\rho_0} \right)^{(2+i)} \mathrm{d}x \,, \tag{6}$$

for $i \geq 0$.

A couple of remarks are in order here. Notice first that the quasicondensate perturbative scheme clearly differs from the standard Bogoliubov treatment since the standard non-linear term $\hat{\Psi}^{\dagger\,2}\hat{\Psi}^2$ is fully included in the quadratic Hamiltonian, while the infinite series of perturbative corrections comes entirely from the kinetic term. Second, Eq. (6) indicates that each order is suppressed by an additional factor of $\delta\hat{\rho}/\rho_0$ which suggests that $\langle \delta\rho^2 \rangle / \rho_0^2$ can be used as a measure of the importance of taking these higher orders into account. For the typical values of parameters used in this work we have $\langle \delta\hat{\rho}^2 \rangle / \rho_0^2 \sim 10^{-3}$ so that we will consider only the second-order term $\hat{H}_2$ and the first perturbation Hamiltonian $\hat{H}_3$.

C. Quasiparticle definition

Working in the canonical ensemble, the atom number N_{at} is a fixed parameter, and therefore so is the background density ρ_0. The zero mode of the density fluctuations thus vanishes identically: $\delta\hat{\rho}_{k=0} = 0$. Consequently, the conjugate variable $\delta\hat{\theta}_{k=0}$ is non-dynamical and can be ignored. The fluctuations $\delta\hat{\rho}$ and $\delta\hat{\theta}$ on top of this background are then composed of the non-zero Fourier modes $\delta\hat{\rho}_k$ and $\delta\hat{\theta}_k$:

$$\delta\hat{\rho}(x) = \sqrt{\frac{\rho_0}{L}} \sum_{k\neq 0} e^{ikx} \delta\hat{\rho}_k \,, \quad \delta\hat{\theta}(x) = \frac{1}{\sqrt{\rho_0 L}} \sum_{k\neq 0} e^{ikx} \delta\hat{\theta}_k \,. \tag{7}$$

With this writing $\delta\hat{\rho}_k$ and $\delta\hat{\theta}_k$ are dimensionless, and they satisfy $\left[\delta\hat{\rho}_k \,,\, \delta\hat{\theta}_{k'} \right] = i\, \delta_{k,-k'}$. Since $\delta\hat{\rho}(x)$ and $\delta\hat{\theta}(x)$ are Hermitian operators, the Fourier components satisfy $\delta\hat{\rho}_{-k} = \delta\hat{\rho}_k^\dagger$ and $\delta\hat{\theta}_{-k} = \delta\hat{\theta}_k^\dagger$. $\hat{H}_2$ can be diagonalized into normal modes, called *phonons* [1], represented by operators $\hat{\varphi}_k^{(\dagger)}$ such that

$$\hat{H}_2 = \sum_{k\neq 0} \hbar\omega_k \left(\hat{\varphi}_k^\dagger \hat{\varphi}_k + \frac{1}{2} \right) \,, \tag{8}$$

where the phonon frequency

$$\omega_k = c\,|k| \sqrt{1 + \frac{1}{4} k^2 \xi^2} \,, \tag{9}$$

with $c = \sqrt{g\rho_0/m}$ the speed of sound and $\xi = \hbar/mc$ the healing length. In the limit $k\xi \to 0$, we have an exactly linear dispersion relation like that of the Luttinger liquid. The phononic operators are related to the density and phase fluctuations by

$$\hat{\varphi}_k = \frac{1}{\sqrt{2}} \left(C_k^{-1}\, \delta\hat{\rho}_k + i\, C_k\, \delta\hat{\theta}_k \right) \,, \tag{10}$$

where $C_k^2 = \hbar k^2 / (2m\omega_k)$. The use of inverse coefficients C_k and C_k^{-1} ensures that the transformation is canonical and hence that the phonon operators satisfy the bosonic commutation relation $\left[\hat{\varphi}_k \,,\, \hat{\varphi}_{k'}^\dagger \right] = \delta_{k,k'}$.

ξ and the associated healing time, $t_\xi = \xi/c$, provide natural units in which to express quantities adimensionally. There are three dimensionless parameters describing the system: the 1D density $\rho_0\xi$, the length L/ξ, and the temperature $k_B T/mc^2$ (where $mc^2 = \hbar/t_\xi$ is the chemical potential $\partial E_0/\partial N_{\mathrm{at}}$). The interaction strength is characterised by $\gamma_{\mathrm{LL}} = 1/(\rho_0\xi)^2$, the dimensionless Lieb-Liniger constant [11, 27]. Numerical simulations presented in this work typically have $\gamma_{\mathrm{LL}} \sim 10^{-5} - 10^{-3}$, placing us firmly in the weakly-interacting regime. We also choose a grid spacing Δx such that $\rho_0 \Delta x \sim 20$ atoms per site, justifying our use of the hydrodynamical description.

Just as for the atom operators $\hat{\Psi}_k$, the phonon operators $\hat{\varphi}_k$ provide a complete description of the system, whose state is fully characterized by the expectation values of the $\hat{\varphi}_k^{(\dagger)}$ and all their products. Since the $\hat{\varphi}_k$ come close to diagonalizing the full Hamiltonian $\hat{H}$, the phonons are close to the exact normal modes of the system and their mutual interactions are relatively weak. The phonons therefore provide the most natural basis in which to examine the state of the system and interpret its dynamical behavior. However, the simplicity of the full Hamiltonian (1) makes the atom basis more convenient for numerical treatments of the evolution.

D. Quasiparticle interactions

Turning now to $\hat{H}_3$, and neglecting terms of the form $\varphi^\dagger\hat{\varphi}^\dagger\hat{\varphi}^\dagger$ $(\hat{\varphi}\hat{\varphi}\hat{\varphi})$ which cause the unbalanced appearance (disappearance) of three phonons typically associated with strong violation of energy conservation, the relevant part of the interaction Hamiltonian takes the form

$$\hat{V}_3 = \frac{1}{\sqrt{N_{\mathrm{at}}}} \sum_{\substack{p,q\neq 0 \\ p+q\neq 0}} \hbar V_3(p,q) \left\{ \hat{\varphi}_p^\dagger \hat{\varphi}_q^\dagger \hat{\varphi}_{p+q} + \hat{\varphi}_{p+q}^\dagger \hat{\varphi}_p \hat{\varphi}_q \right\} \,, \tag{11}$$

[1] In this paper, we use the term "phonon" to refer to a quasiparticle of any wavelength, and *not* just to those well within the linear part of the dispersion relation (9).

where

$$V_3(p,q) = \sqrt{\frac{\hbar}{32m}}\sqrt{\frac{|pq(p+q)|}{v_p^{\rm ph}v_q^{\rm ph}v_{p+q}^{\rm ph}}}\Bigg\{-\left(\frac{\hbar}{2m}\right)^2\left[p^2+pq+q^2\right] + v_p^{\rm ph}v_q^{\rm ph} + v_q^{\rm ph}v_{p+q}^{\rm ph} + v_p^{\rm ph}v_{p+q}^{\rm ph}\Bigg\}, \tag{12}$$

and $v_k^{\rm ph} = \omega_k/k$ is the phase velocity at k.

$\hat{V}_3$ describes the decomposition of a single phonon into two phonons, as well as the inverse process where two phonons combine into one. Note that it is momentum-conserving, reflecting the homogeneity of the system, and that if p is held fixed and $q \to 0$, $V_3(p,q)$ vanishes as $\sqrt{q}$. A similar writing of $\hat{V}_3$ can be found in [13], in a form that is equivalent to the one given here.

E. Numerical simulations

The system is modeled numerically using the truncated Wigner approximation (TWA) [29] (see Appendix C for more details). The operators $\hat{\Psi}$ are replaced by classical variables Ψ, and products of these variables are identified with the corresponding fully symmetrized quantum operators. A series of *ab initio* Monte Carlo simulations are performed, with quantum indeterminacy appearing through the statistical ensemble describing the initial state. The field is then evolved according to the dynamics of Hamiltonian (1). This is repeated for a large number of independent initial realisations, so as to get good statistics when computing averages.

The phenomenon of interest is illustrated in Fig. 1, which shows the typical evolution observed in numerical simulations. Starting from a thermal state, the occupation number of a mode is increased by δn, to be considered as the initial number of phonons in the probe. Indeed, throughout this paper we shall adopt the following decomposition:

$$n_k = n_k^{\rm th} + \delta n_k\,, \tag{13}$$

where $n_k = \left\langle \hat{\varphi}_k^\dagger \hat{\varphi}_k \right\rangle$ is the full phonon spectrum and $n_k^{\rm th}$ is the (thermal) spectrum in the absence of any probe. Further details of the simulations are given in Sec. IV. The figure shows n_k at a series of different times. We see that $n_k^{\rm probe}$, the population of the initially occupied mode, decays. The observed behaviour is essentially linear, in the sense that the relative change $\delta n_k(t)/\delta n$ is independent of δn, the number of phonons injected in the probe. Moreover, it is clear that the spectrum of the probe has broadened. Summing over nearby modes (those within the vertical dotted lines), the total n is found to be constant in time. The phonons seem not to have been lost, but rather to have been kicked into neighboring modes. Note that the broadening is essentially symmetric: the phonons are just as likely to be kicked towards a higher momentum as a lower one. The small shifts in momentum suggest that the evolution is primarily driven by interactions with infrared phonons from the thermal bath.

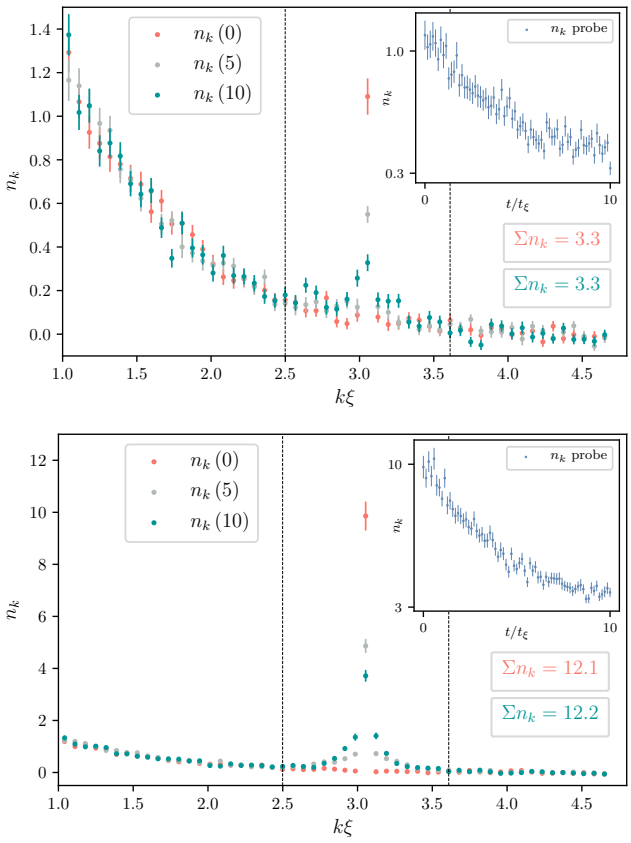

Figure 1. Snapshots of the phonon number spectrum at times $t/t_\xi = 0, 5, 10$ assuming an initial thermal state at temperature $k_B T/mc^2 = 2$ on top of which an additional $\delta n = 1$ (top) or $\delta n = 10$ (bottom) phonons are added in the mode $k\xi = 3.1$. The size of the system is $L/\xi = 90.5$ and its atomic density $\rho_0\xi = 49.9$. The averages are calculated from an ensemble of 400 independent realisations, while the error bars represent the standard deviation. There are 256 points on the grid. The inset shows a more time-resolved evolution of the population in the probe mode. The total number of phonons within the vertical dotted lines is given for the initial and final times, and is seen to be conserved.

III. THEORETICAL DERIVATION

In this section, we provide an analytical description of the dissipative process at play. In Sec. III A, we derive the decay rate using the FGR; as this applies to a discrete eigenstate in interaction with a continuum, we expect it to describe the decay of the population of a singularly occupied mode (*i.e.*, when the spectrum is sufficiently narrow). In Sec. III B, we sketch a formalism which takes us beyond such an approximation, using response functions

to model the dynamics of the spectrum more accurately and to describe the deviations from purely exponential behavior. A fuller treatment of this formalism is given in Appendix A, while a comprehensive analysis of the main deviations observed numerically is given in Appendix B.

A. Using the Fermi Golden Rule

Given an initial eigenstate $|i\rangle$ that couples to a continuum of final eigenstates $|\nu_f\rangle$ via a time-independent weak perturbation Hamiltonian $\hat{H}'$, the FGR gives the transition rate into the continuum [30]:

$$dW_{i\to f} = \frac{2\pi}{\hbar}\left|\langle\nu_f|\,\hat{H}'\,|i\rangle\right|^2 \delta\left(E_f - E_i\right)\, d\nu_f\,, \qquad (14)$$

where E_i and E_f are the energies of the initial and final states, the latter being labeled by the dimensionless number ν_f. The Dirac delta imposes energy conservation, *i.e.* the rate is evaluated as a matrix element between states with the same (unperturbed) energy. The total rate is found by integrating over ν_f.

Consider a singularly occupied phonon mode k, which decays due to interactions with the thermal population of phonons. Each available momentum is a multiple of $2\pi/L$. For sufficiently large kL the thermal distribution of phonons, as well as the states available to decay to, can be approximated as a continuum from the point of view of the mode k. We thus expect the FGR (14) to be applicable. We need only determine the relevant perturbation and corresponding initial and final states.

In the phonon basis, the role of the perturbation entering the FGR is played by $\hat{V}_3$ of Eq. (11). It describes two distinct processes involving the annihilation of a probe phonon at wave number k :

- Phonons of wave-numbers k and q combine to produce a single phonon with wave number $k+q$. The relevant term is $\hat{\varphi}^\dagger_{k+q}\hat{\varphi}_q\hat{\varphi}_k$, taking $|i\rangle = |n_q, n_k, n_{k+q}\rangle$ to $|f\rangle = |n_q - 1, n_k - 1, n_{k+q} + 1\rangle$, and the corresponding squared matrix element is $\frac{1}{N_{\rm at}}\hbar^2\left|2\,V_3\left(k,q\right)\right|^2 \times n_k n_q\left(n_{k+q}+1\right)$. The factor 2 comes from the $p \leftrightarrow q$ symmetry of the sum in Eq. (11). The factors of n come from the action of the phonon operators on the state $|i\rangle$, with the 'n' and '+1' terms encoding stimulated and spontaneous processes, respectively. The energy difference is $E_f - E_i = \hbar\,\delta\omega_L = \hbar\left(\omega_{k+q} - \omega_q - \omega_k\right)$; at small q, this gives $\delta\omega_L \approx v^{\rm gr}_k q - c\,|q| = q\left(v^{\rm gr}_k \mp c\right)$, where $v^{\rm gr}_k = d\omega_k/dk$ is the group velocity at k.
- k decays to two phonons, with wave numbers $k-q$ and q. The relevant term is $\hat{\varphi}^\dagger_{k-q}\hat{\varphi}^\dagger_q\hat{\varphi}_k$, taking $|i\rangle = |n_q, n_{k-q}, n_k\rangle$ to $|f\rangle = |n_q + 1, n_{k-q} + 1, n_k - 1\rangle$, and the corresponding squared matrix element is $\frac{1}{N_{\rm at}}\hbar^2\left|2\,V_3\left(k-q,q\right)\right|^2 \times n_k\left(n_q+1\right)\left(n_{k-q}+1\right)$. The energy difference is $E_f - E_i = \hbar\,\delta\omega_B = \hbar\left(\omega_{k-q} + \omega_q - \omega_k\right)$; at small q, this gives $\delta\omega_B \approx -q\left(v^{\rm gr}_k \mp c\right) = -\delta\omega_L$.

The two scattering processes described above lead to the well-known Landau and Beliaev damping of phonons in BECs: the former is associated with the absorption of a thermal phonon, the latter with a splitting into two phonons. [2] The associated frequency differences are thus labeled $\delta\omega_L$ and $\delta\omega_B$.

Imposing also energy conservation $\delta\omega_{L,B}\left(q;k\right) = 0$, as demanded by the Dirac delta in Eq. (14), we encounter the problem anticipated above: the only exact solution respecting both momentum *and* energy conservation is the trivial one, $q = 0$. [3] In the vicinity of this channel, the interaction vanishes as $\left|V_3(k,q)\right|^2 \propto q$. However, the frequency ω_q also vanishes as $\omega_q \to c\,|q|$, and therefore the thermal population $n_q \approx k_B T/\hbar\omega_q$ simultaneously diverges. It therefore makes sense to refer to the product $\left|V_3(k,q)\right|^2 n_q$ as an effective interaction strength for the corresponding channel, as it has a finite limit as $q \to 0$, and it is this finite limit that is picked up by the Dirac delta in Eq. (14). Although the delta is centered at $q = 0$, it does not actually matter that the trivial elastic channel is unphysical and thus removed from the dynamics: the Dirac delta is a placeholder for a steadily narrowing distribution of final states in the vicinity of this channel (see Appendix A). As long as there are sufficiently many modes within this distribution, the single removed mode at $q = 0$ has a relative measure of zero. This allows the application of the FGR, as if the limiting processes at $q \to 0^\pm$ were physically allowed. [4]

The Dirac delta in Eq. (14) also serves to multiply by the density of available states with respect to the energy. Since the available states are evenly spaced in momentum, in a window of size Δq the number of states is $\Delta N = L/2\pi \times \Delta q \approx L/2\pi\hbar \times \left|dq/d\left(\delta\omega_{L/B}\right)\right| \times \Delta E$. Recalling from above that, for small q, we have $\delta\omega_L \approx -\delta\omega_B \approx q\left(v^{\rm gr}_k \mp c\right)$, this gives the following density of states:

$$\rho_E\left(k\right) \equiv \frac{dN}{dE} = \frac{1}{2\pi\hbar}\,\frac{L}{v^{\rm gr}_k \mp c}\,. \qquad (15)$$

For ease of notation we restrict to $k > 0$, so that $v^{\rm gr}_k \mp c$ is always positive. Due to isotropy, $-k$ will behave in

---

[2] While Beliaev damping often occurs spontaneously (as it is a $1 \to 2$-phonon process), we are concerned here with a regime of sufficiently high temperature in which it is stimulated by the presence of a large number of thermal infrared phonons.

[3] Notice that for a Luttinger liquid where $\xi = 0$ the problem is exactly the opposite as there is an infinite number of elastic scattering channels leading to a divergence of the FGR decay rate [31, 32].

[4] One important modification with respect to the standard case arises because the effective interaction strength $\left|V_3(k,q)\right|^2 n_q$ is discontinuous across the resonant channel $q = 0$. This obliges us to consider separately the coupling with positive and negative q, leading to two applications of the FGR where each channel picks up "half" of the Dirac delta around $q = 0$. This factor is cancelled by the co-occurrence of the Landau and Beliaev channels, which contribute equally to the decay rate.

exactly the same way as k. We recall that the sign in the denominator is related to the sign of q, the momentum of the infrared phonons with which the interaction takes place. The abrupt change in the velocity as q crosses zero means that there are two distinct limits to be taken: $q \to 0$ from above and from below. Putting everything together, we thus derive two decay rates, corresponding to the coupling with positive and negative q:

$$\Gamma_{\pm}(k) = \frac{\lim_{q\to 0^{\pm}} \left[\frac{L}{N_{\rm at}} |2\,V_3(k,q)|^2\, n_q\right]}{(v_k^{\rm gr} \mp c)}\,. \tag{16}$$

Inserting the explicit form of $V_3(k,q)$ yields:

$$\Gamma_{\pm} t_{\xi} = \frac{k_B T}{mc^2}\frac{1}{\rho_0 \xi} f_{\pm}(k\xi) \tag{17}$$

where

$$f_{\pm}(k\xi) = \frac{1}{2}\frac{(k\xi)^2}{\left(v_k^{\rm ph}/c\right)^2}\frac{\left(v_k^{\rm ph}/c \pm 1/2\right)^2}{v_k^{\rm gr}/c \mp 1}\,. \tag{18}$$

The total decay rate presented in the figures is $\Gamma_k = \Gamma_+ + \Gamma_-$.

Equation (17) constitutes our main result: an explicit expression for the rate at which the population of a singularly populated mode will decay, due to interactions with thermal phonons.

Since at small q we have $\delta\omega_L \approx -\delta\omega_B \approx v_k^{\rm gr} q - c\,|q|$, at fixed $|q|$ the magnitude of the frequency difference is smaller when q has the same sign as k. We therefore expect that such modes provide the dominant contribution to the decay, while the coupling to modes of the opposite sign induces a subdominant correction. So the Landau channel tends to kick a phonon at k into a higher-energy mode, while the Beliaev channel acts in the opposite direction. Since the two channels contribute equally, there is no preference for a phonon at k to be kicked towards either a higher or lower momentum. This explains the approximate symmetry of the broadening observed in Fig. 1.

B. Using response functions

Here, we give the outline of a more precise description of how a perturbation to the phonon number spectrum δn_k evolves. For brevity, we shall avoid details here, though they can be found in Appendix A. However, the writing will allow us to point out significant deviations from the exponential decay rate of Eq. (17), which are studied in more detail in Appendix B.

The time-derivative of δn_k depends both on δn_k and on phonon correlations, the most important of which are the 3-point correlations induced by the Beliaev and Landau processes described above: $C^{(3)}_{p,q} = \langle \hat{\varphi}^{\dagger}_p \hat{\varphi}^{\dagger}_q \hat{\varphi}_{p+q} \rangle$. Neglecting other connected correlation functions, the equations of motion can be written entirely in terms of n_k, though they become integro-differential equations that include response functions, which encode how the system "remembers" and responds to its past behaviour. Neglecting any self-interaction of the perturbation, we linearize the equations in δn_{k+q}:

$$\begin{aligned}\partial_t(\delta n_k) = &-\int_0^t dt'\, D_k(t-t')\,\delta n_k(t') \\ &+\int_0^t dt' \sum_{q\neq -k} M_{k,k+q}(t-t')\,\delta n_{k+q}(t')\,.\end{aligned} \tag{19}$$

The first term on the right-hand side of (19), governed by D_k, describes the essential behavior of δn_k, when back-reaction from its near-neighbors can be neglected and finite-size effects can also be ignored (see below). $D_k(t-t')$ decays to zero within a time scale $t_{\rm crit}$, and its integral approaches Γ_k of Eq. (17). As long as $t \gg t_{\rm crit}$ and δn_k does not vary much on time scales of order $t_{\rm crit}$, its value at t can be taken outside the integral, and the first term becomes $-\Gamma_k\,\delta n_k$. This is the regime in which the analysis of the previous subsection applies. We can thus expect deviations when δn_k varies significantly over times of order $t_{\rm crit}$. This can happen either when $\partial_t(\delta n_k)$ is particularly large, or for a time $t_{\rm crit}$ after a sudden injection of phonons. The latter case will be relevant for some of our numerical simulations.

The second term of Eq. (19), governed by $M_{k,k+q}$, describes the influence of other modes on the evolution of n_k. These typically act to slow down the decay of n_k, because some of the phonons in neighboring modes will be kicked into the mode of interest. This is particularly relevant in situations where k is at the center of a peak with a finite width, and in such a scenario we expect the net decay rate to be smaller than that predicted by Eq. (17). Note that this is not in contradiction with the FGR, which applies when a single discrete mode loses energy to a continuum of modes; this picture becomes less applicable when the mode losing energy is itself part of a continuum. Generally, the effect of this back-reaction term is difficult to take fully into account, but in certain situations (particularly in the case of parametric resonance) we can make approximations and derive the expected qualitative behavior for the decay rate as a function of the peak width.

C. Suppression due to finite size of system

The second term of Eq. (19) includes a contribution from $q = 0$, which will be present even when neighboring modes are not significantly populated. This $q = 0$ term slows down the decay, but it is proportional to $1/L$ and vanishes entirely in the limit $L \to \infty$ where we have a continuum in k-space. The primary function of this term is to account for the finite resolution in k by keeping track of those phonons which, in the continuum limit, would be lost to nearby modes within $1/L$ of the main

decaying mode. With the finite resolution induced by the finiteness of L, these phonons remain in the same bin as the decaying mode. Therefore, their contribution to the variation of n_k is removed, and the net decay is effectively slowed down.

In Appendix B we derive the slowing down of the decay rate induced by this contribution. On sufficiently short time scales, it enters as a quadratic correction to the exponential decay:

$$\delta n_k \approx \delta n_k(0)\, e^{-\Gamma_k t + \frac{1}{2}\gamma_k t^2}\,, \tag{20}$$

where

$$\gamma_k t_\xi^2 = \frac{k_B T}{mc^2}\,\frac{1}{\rho_0 L}\, g\,(k\xi) \tag{21}$$

and where we have defined

$$g\,(k\xi) = \frac{(k\xi)^2}{v_{\rm ph}^2(k)/c^2}\left\{\left(\frac{v_{\rm ph}(k)}{c}-\frac{1}{2}\right)^2+\left(\frac{v_{\rm ph}(k)}{c}+\frac{1}{2}\right)^2\right\}. \tag{22}$$

The finite-size effect grows in importance as time progresses, on a time scale $t_{\rm fs}$ such that $\gamma_k t_{\rm fs}^2 = \Gamma_k t_{\rm fs}$ (where the decay in Eq. (20) slows to zero). Its relevance therefore depends on how $t_{\rm fs}$ compares to the typical time-scale of decay Γ_k^{-1}, *i.e.*, the relevant quantity is

$$\begin{aligned}\Gamma_k t_{\rm fs} = \frac{\Gamma_k^2}{\gamma_k} &= \frac{2L}{r_0}\,\frac{f^2\,(k\xi)}{g\,(k\xi)}\\ &\approx \frac{L}{r_0} \quad \text{when} \quad k\xi \gg 1\,.\end{aligned} \tag{23}$$

In the second line we have taken the large wavenumber limit, where our exponential prediction for the decay is most accurate (see Sec. IV below). r_0 is the (one-body) coherence length of the quasicondensate defined in Eq. (2). So, when $L/r_0 \ll 1$, the decay proceeds hardly at all before it is stopped by the finite-size effect. On the other hand, when $L/r_0 \gg 1$, the decay is significant before the slowing-down kicks in, and the finite-size effect becomes irrelevant.

As mentioned in Sec. II A, when considering a quasicondensate over distances larger than r_0 the long-range order characterising condensation is lost due to large thermal fluctuations in the phase. Conversely, if we restrict attention to distances much shorter than r_0, the one-body correlation is preserved and the gas looks like a "true" condensate. Equation (23) then shows that if we consider a small enough system that appears as a true condensate, the decay will be strongly suppressed by finite-size effects. In effect, the decay processes we have identified manifest in position space as an x-dependent drift in the phase of the excited phonon, whose variance becomes significant only over distances larger than r_0. Therefore, the decay is only effective when we reach the quasicondensate regime $L \gg r_0$.

This correspondence is further explored in Appendix B, where it is also shown that binning modes in momentum space yields an evolution that is very similar to that on a shorter torus. We thus conclude that the system size L appearing in Eq. (23) can be generalized to the size of any subsection of a larger system. If this size is small compared to r_0, local measurements will be insensitive to the decay.

IV. NUMERICAL CONFIRMATION

We have run several numerical simulations in order to test our prediction for the phonon damping rate. The essentials of the numerical method have already been described in Sec. II E, and more details can be found in Appendix C.

The simulations fall into two types. First, we perform a series of simulations like that of Fig. 1, where a number of phonons is injected into a single mode k, and the evolution of the phonon number spectrum is followed in time. This setup allows us to study the response of a thermal system to a single perturbation, the addition of phonons in the mode k. We use it to demonstrate that the thermal processes discussed in the previous section are indeed the main culprit involved in the scattering of injected phonons, and to check that the scaling properties of the decay rate match those predicted by Eq. (17). Moreover, this controlled scenario enables us to track precisely how phonons scatter to other modes (as shown in Fig. 1), informing our study of the decay process and its generalization to a peak of finite width (see Sec. IV B below, and Appendix B).

The second series of simulations is inspired by the parametric resonance experiments of [4] and theoretically studied in [8, 33]: starting from a thermal state, a sinusoidal modulation of the 1D atomic interaction strength is applied, inducing exponential growth of the phonon occupation number within a resonance window. (This can be achieved experimentally by modulating the transverse stiffness of the trap [4, 7, 8].) The phonon damping is then observed as a reduction in the rate of exponential growth. As suggested above, the finite width of the resonant peak induces a deviation from the decay rate (17), which strictly speaking is only applicable in the limit of a singularly occupied mode. However, this deviation occurs in a controlled fashion, and is found to be consistent with the back-reaction term appearing in Eq. (19).

A. Initial injection of phonons

In the first run of simulations, the initial state is taken to be a thermal state for the quadratic Hamiltonian $\hat{H}_2$, with the possible addition of a probe in a single phonon mode of wave vector k. When the probe is present, it is given an initial occupation number δn on top of the thermal distribution by simply multiplying the amplitude of the relevant mode by a constant factor. This ensures that the phonon modes are initially independent of each other,

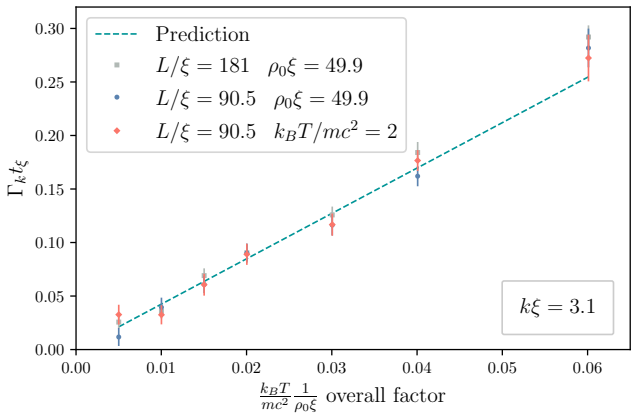

Figure 2. Best fit values for $\hbar\Gamma_k$ extracted from the TWA simulations, as a function of $k_BT/\rho_0\xi$. All points are extracted from simulations performed using an addition of $\delta n = 3$ phonons on average. We used 400 realisations, a grid spacing $\Delta x/\xi = 0.35$, and a time window $t/t_\xi \in [0, 10]$ with 140 time steps. For the grey and blue points the temperature varies $k_BT/mc^2 \in [0.25, 3]$, while for the red points the density varies in $\rho_0\xi \in [33, 399]$. The parameters that are fixed in each run are listed in the legend.

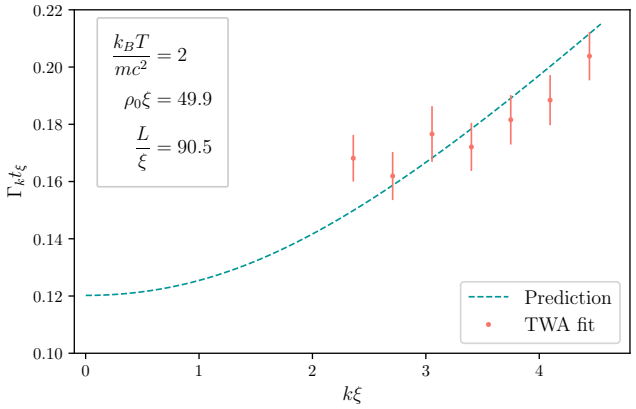

Figure 3. Best fit values for $\hbar\Gamma_k$ extracted from the TWA simulations, as a function of $k\xi$. All other physical parameters are fixed at the values shown, while numerical parameters are the same as in Fig. 2. Numerically extracted values are shown only for $k\xi \gtrsim 2.5$. For lower $k\xi$, significant deviations appear due to the longer response time. (A fuller treatment of this regime is given in Appendix B.)

and separately exhibit Gaussian statistics. Each realisation is then evolved twice, with and without the probe, to take account of the slight degree of time-dependence that occurs even when the probe is absent. The spectra are calculated independently at different times in the interval $t/t_\xi \in [0\,,\,10]$, and the probe spectrum $\delta n_k(t)$ is defined as the difference between the two, in accordance with Eq. (13). $\delta n_k(t)$ is then fitted to the template $A\exp\left(-\Gamma t + \gamma t^2/2\right)$ of Eq. (20), the fitted value of Γ being the extracted decay rate. As mentioned in Sec. III C above, the t^2 correction is related to the limited resolution in k-space induced by the finite length of the condensate, coming from the $q = 0$ term in the second line of Eq. (19). It is included here as it makes a small but noticeable difference to the fit. More details on the extraction of the γ term are given in Appendix B.

In Fig. 2 we demonstrate the linearity of the best-fit values of Γ in the overall prefactor in Eq. (17), at fixed $k\xi$. The numerical results are in good agreement with the prediction. We illustrate that varying T at fixed $\rho\xi$ (and *vice versa*) yields the expected behaviour, and moreover that the fitted decay rate is unaffected by a change in L, as expected from prediction (17). Any L-dependence of the observed behavior would then appear in the other fitting parameters like γ.

In Fig. 3 we show instead the dependence of these best-fit values for Γ on the probe mode $k\xi$, with the prefactor in Eq. (17) fixed. The numerical observations agree well with the predicted behaviour at modestly high $k\xi \gtrsim 2.5$. At lower $k\xi$, we expect significant deviations, for as noted in Sec. III B, the FGR becomes valid only after a critical time $t_{\rm crit}$ (see also [30, 34]). We show in Appendix B that $t_{\rm crit}$ diverges like $1/\left(k\xi\right)^3$ as $k\xi \to 0$, and for $k\xi \lesssim 2.5$ it is not reached within the sampled time frame. In this regime, the decay proceeds quadratically in time rather than exponentially, with a lifetime that is significantly longer than predicted by (17). This early-time behavior at small $k\xi$ is examined in more detail in Appendix B.

B. Slowing of exponential growth

In our second set of simulations, the initial state is simply a thermal state for the quadratic Hamiltonian $\hat{H}_2$, with no additional component added by hand. Instead, during the evolution, parametric resonance is induced by a sinusoidal modulation of the 1D atomic interaction parameter:

$$g(t) = g\left(1 + a\sin\left(\omega_p t\right)\right) . \tag{24}$$

As $c^2(t) \propto g(t)$, this translates into a sinusoidal modulation of the squared phonon frequencies:

$$\begin{aligned}\omega_k^2(t) &= c^2k^2\left[1 + a\sin\left(\omega_p t\right) + \frac{1}{4}k^2\xi^2\right] \\ &= \omega_k^2\left(1 + A_k\sin\left(\omega_p t\right)\right) ,\end{aligned} \tag{25}$$

where $A_k = a/\left(1 + k^2\xi^2/4\right)$. This is exactly the situation modeled in [33]. The result is an exponential growth of the number of phonons within a resonant frequency window centered at $\omega_p/2$. In the absence of any damping mechanism, the analysis in Appendix A of [33] shows that, for the exactly resonant mode at $\omega_k = \omega_p/2$, the occupation number is parametrically amplified according to

$$n_k(t) \approx n_k^{\rm in} + \left(2n_k^{\rm in} + 1\right)\sinh^2\left(\frac{1}{2}G_k t\right) , \tag{26}$$

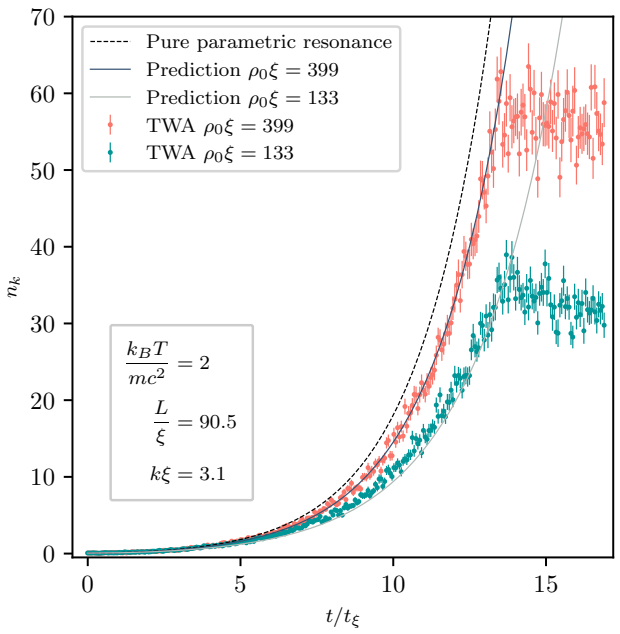

Figure 4. Mean occupation of the resonant mode as a function of time, as extracted from TWA simulations. We take an initial thermal state at temperature $k_BT/mc^2 = 2$, and a modulation of amplitude $a = 0.5$ at frequency $\omega_p = 2\omega_k$ where $k\xi = 3.1$ (so that the modulation of ω_k^2 has amplitude $A_k = 0.15$) lasting 24 periods, *i.e.*, $13.5\,t_\xi$. The size of the system is $L/\xi = 90.5$ and its atomic density is $\rho_0\xi = 399$ for the red dots and $\rho_0\xi = 133$ for the green ones. The dashed black line is the estimate Eq. (26), where $n_{\rm in}$ has been set to the thermal value. The solid lines correspond to the corrected estimate Eq. (27), with Γ_k as predicted by Eq. (17). Each data point is calculated independently, averaged over 400 realizations.

where the growth rate $G_k = A_k\omega_k/2$. Since the initial state is thermal, the initial occupation number $n_k^{\rm in}$ is simply the thermal population of the mode.

When including the effects of phonon interactions, the Beliaev-Landau scattering with the thermal population acts simultaneously with the parametric amplification, kicking phonons out of the resonant mode as they are being produced. The damping mechanism thus acts much like the phenomenological damping introduced in [33], and is therefore expected to reduce the growth rate. This is illustrated in Fig. 4, where $n_k(t)$ of the exactly resonant mode is extracted from the numerical simulations and shown for two different values of $\rho_0\xi$. We clearly see that the exponential growth rate is lower than predicted by Eq. (26), and that it is further reduced as $\rho_0\xi$ is reduced, so that Γ_k of Eq. (17) is accordingly increased.

We may use the difference between the observed growth rate and the "pure" growth rate of Eq. (26) as a measure of the damping. [5] Assuming that the damping acts straightforwardly as a reduction of the growth rate, we make a slight generalization of Eq. (26) and propose the following ansatz for the occupation number of the resonant mode:

$$n_k(t) = n_k^{\rm in} + \left(2n_k^{\rm in} + 1\right)\sinh^2\left[\frac{1}{2}\left(G_k - \Gamma_k\right)t\right] . \quad (27)$$

Figure 4 shows that this ansatz, taken together with the assumption that Γ_k is as predicted by Eq. (17), accounts very well for the reduced growth observed in TWA simulations with respect to that of Eq. (26). We stress that this reduction rapidly leads to a sizeable change in the number of produced phonons. For example, considering the red data points in Fig. 4 (corresponding to $k\xi = 3.1$, $k_BT/mc^2 = 2$, and $\rho_0\xi = 399$), the relative damping is $\Gamma_k/G_k = 5\%$, yet the reduction with respect to the non-damped case is very clear, and we are thus able to extract quite precise values for the damping rate.

We now perform a more systematic examination of the numerically observed reduction of the growth rate. Proceeding as for the first set of simulations, we fit $n_k(t)$ for the exactly resonant mode to Eq. (27), where Γ_k is now treated as a fitting parameter. This is done for two different wave vectors, one in the high-k regime ($k\xi = 3.1$) where the first set of simulations worked reasonable well, and one in the low-k regime ($k\xi = 1.0$) where they did not. The temperature is fixed at $k_BT/mc^2 = 2$, and the 1D density $\rho_0\xi$ is varied. The extracted values of Γ_k are shown in Fig. 5 alongside the prediction of Eq. (17).

A few remarks are in order concerning these results. We begin by focusing on the high-k mode ($k\xi = 3.1$), the first and third data points of which correspond to the simulations shown in Fig. 4. While the extracted decay rate tends towards prediction (17) at large $\rho_0\xi$, there is a clear trend for it to fall further away from this prediction as $\rho_0\xi$ is decreased. We attempt to explain this behavior by appealing to the finite width of the resonant peak. Examining the evolution of the number spectrum shows that, to a good approximation, the shape of the resonant peak saturates such that $n_k \sim R_k e^{Gt}$ at sufficiently late time, for some profile R_k and some growth rate G. This is in contrast to the results of the "pure" parametric resonance with no phonon interactions, where the growth rate is k-dependent and largest at exact resonance [33], so that the width of the peak approaches zero as $t \to \infty$. In the present case, in addition to the saturation of the profile, we observe that larger interaction strengths are associated with wider peaks, see Fig. 6. It thus seems likely that n_k is also being fed by phonons in neighboring modes through the last term on

[5] Similar simulations were performed in [8] where, although the focus was on nonlinear effects at large n_k, hints of an n_k-independent damping rate were seen at sufficiently early times (see in particular Fig. 6 and footnote 10). Given the parameters used ($k\xi \sim 1$, $k_BT/mc^2 \sim 1/2$, $\rho_0\xi \sim 400$), this intrinsic decay rate has $\hbar\Gamma_k/mc^2$ equal to a few times 10^{-3}, in agreement with prediction (17).

the right-hand side of Eq. (19). We investigate this effect by adopting a Lorentzian ansatz for the profile of δn_k. Figure 6 shows how our ansatz compares with the numerically observed number spectrum. Under this assumption, we solve Eq. (19) self-consistently to extract the net growth rate. The details of this calculation are given in Appendix B, but the corrected predictions for the decay rate are shown by the blue dots in Fig. 5. For $k\xi = 3.1$ this corrected prediction is found to be in very good agreement with the extracted rate.

For the low-k mode ($k\xi = 1.0$) there remains a clear discrepancy even when accounting for the finite width of the peak. Part of the explanation lies in the non-Lorentzianity of the profile visible in Fig. 6, making the correction less valid. However, note that the extracted decay rate does not tend well to prediction (17) at large $\rho_0\xi$, as it seems to approach a line with a different slope. We believe this to be a consequence of the large critical time in the low-k regime: in effect, the occupation number is growing a little too fast for the system to have time to react, and the amount of damping is thus lower than expected.

The parametric resonance simulations described here yield results that corroborate and complement those found using straightforward phonon injection. In the high-k regime where the critical response time is sufficiently short, the observed deviations from prediction (17) are well described via corrections due to the finite width of the peak, which only appear in the case of parametric resonance. On the other hand, at low k where the critical time is long, the phonon injection method yields a non-exponential behavior that has not been shown here (see instead Appendix B), whereas the parametric resonance approach still gives a damping rate that has the same qualitative behavior as in the high-k regime (see the near-linear behavior of the red dots in the lower panel of Fig. 5). Moreover, the method of parametric resonance for exciting phonons has some interesting advantages over that of phonon injection. Most notably, the damping mechanism manifests in a rather more dramatic way, as is evident from the difference in the final phonon numbers shown in Fig. 4. It is also of considerable experimental relevance: while the injection of phonons is conceptually simple, it is not very practical, whereas parametric resonance is a way of exciting phonons that has already been implemented in experiments [4]. On the conceptual side, the method of parametric resonance bypasses the finite-size effect. In Sec. IV A, it arises due to the discretization of a time-dependent continuous profile, the "binned" mode of interest containing both the exponentially decaying mode and the nearby modes within π/L that are growing in time. Here, the profile is fixed (the only time-dependence being an overall exponential factor e^{Gt}), and the discretization is therefore irrelevant.

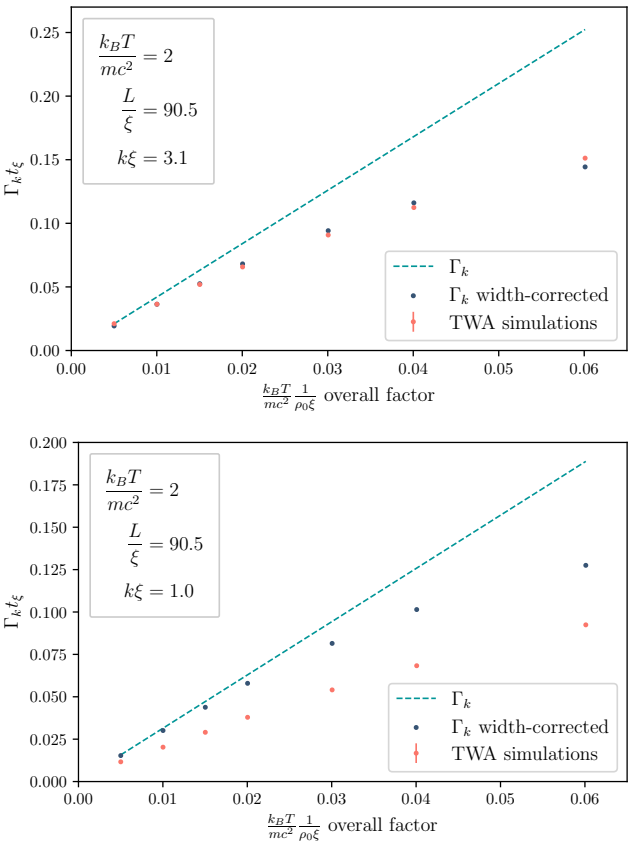

Figure 5. Best fit values for $\hbar\Gamma_k$ extracted from the TWA simulations as a function of $k_BT/\rho_0\xi$. (We divide by mc^2 to adimensionalize.) The temperature is kept fixed to $k_BT/mc^2 = 2$ and only the density is varied $\rho_0\xi \in [33, 399]$. The parameters that are fixed in each run are listed in the legend. All points are extracted from simulations performed using a continuous modulation of amplitude $a = 0.5$ at frequency $\omega_p = 2\omega_k$ where $k\xi = 3.1$ (top) and $k\xi = 1.0$ (bottom); the corresponding amplitudes for the modulation of ω_k^2 are $A_k = 0.15$ (top) and $A_k = 0.39$ (bottom). We use $n_r = 400$ realisations, a spatial grid with spacing $\Delta x/\xi = 0.35$. The fit is performed using the template Eq. (27) over a time window $t/t_\xi \in [0, 13.5]$ (top) and $t/t_\xi \in [0, 22.5]$ (bottom) with 224 (top) and 280 (bottom) time steps. The green dashed line represents the FGR prediction Eq. (17) while the blue dots are the corrected predictions taking into account the effect of a finite width of the resonant peak, see Appendix B. The peak is assumed to be of Lorentzian shape and its parameters are extracted by a procedure described in Fig. 6.

V. CONCLUDING REMARKS

We have identified a mechanism whereby interactions with a thermal bath of phonons, through Landau and Beliaev damping mechanisms, yields exponential decay of a singularly occupied phonon mode. It is effectively described by an application of the FGR with the resonant channel being the trivial one, in the limit $q \to 0$. The result was numerically verified using TWA simulations,

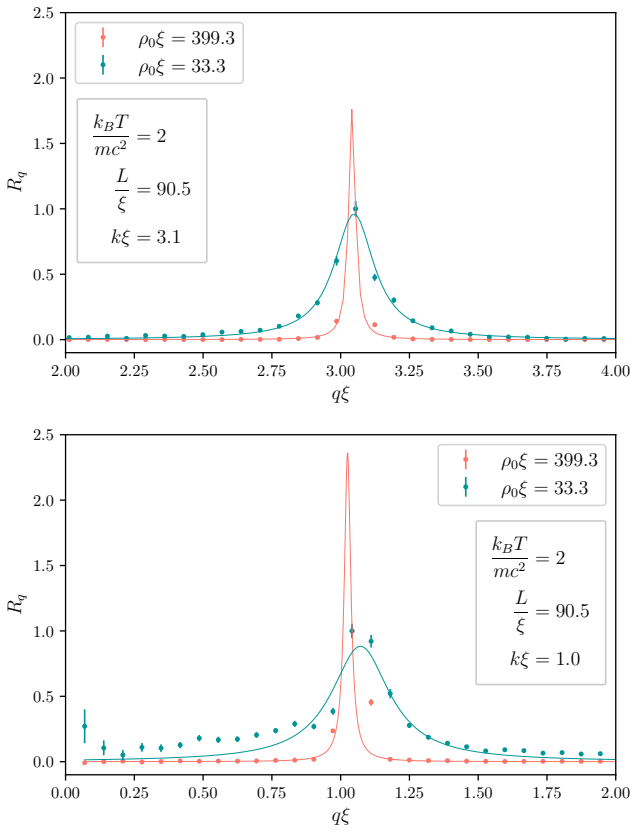

Figure 6. Snapshots of the ratio $R_q = \frac{\delta n_q}{\delta n_k}$ as a function of $q\xi$ at time $t/t_\xi = 13.5$ (top) and $t/t_\xi = 22.5$ (bottom). The spectrum is plotted for $\rho_0\xi = 399$ (red) and $\rho_0\xi = 33$ (green). They are obtained by a continuous modulation of the type Eq. (24) with $a = 0.5$ and at the appropriate frequency so that $k\xi = 3.1$ (top) or $k\xi = 3.1$ (bottom) are exactly at the resonance. A Lorentzian is fitted to the distribution taking into account the first five neighbours on each side of the central resonant mode letting the overall amplitude, width and center be free fitting parameters. The best-fit value of the width is then used to correct the prediction of the decay rate, blue dots in Fig. 5. The averages are calculated from an ensemble of 400 independent realisations, while the error bars represent the standard deviation. There are 256 points on the grid.

following both the decay of a mode excited "by hand" and the reduced growth of a parametrically resonant mode. The prediction works particularly well in the higher-k regime, where the critical response time is relatively short and the discreteness of the thermal population is invisible to the mode in question. We also observe a reduction of the damping rate due to the finite width of the peak.

While this limit yields a non-vanishing rate only in 1D (since in higher dimensions the IR divergence of the thermal population is tamed by the volume element in k-space), it seems generally applicable to 1D systems with an approximately linear excitation spectrum in the limit of small k. We thus believe that it could appear as an additional contribution to the decay of excitations in such systems, such as the 1D dipolar gas considered in [19].

Comparing with higher dimensionality D [35], there are some clear similarities: prediction (17) exhibits an increasing dependence on $k\xi$, is proportional to $\gamma_{\rm LL}^{D/2}$, and is linear in T (as found in higher dimensions when $k_BT/mc^2 \gtrsim 1$).

The experimental relevance of this decay mechanism was exemplified by numerically studying the parametric growth of phonons in the gas, as experimentally tested in [4]. We have demonstrated that the numerically observed reduction of the growth rate can be quantitatively explained assuming that the phonons generated by the parametric process simultaneously decay by thermal Landau-Beliaev processes.

These thermal scatterings of phonons are expected to occur generally in 1D quasicondensate experiments. They can produce important deviations to the dynamics of phonons and should therefore be taken into account in designing and analysing analogue gravity experiments on this platform.

Finally, let us comment on the absence of entanglement between the induced peaks in the experimental observations of [4]. In their phenomenological treatment of dissipation, the authors of [33] showed that a dissipative rate $\Gamma/\omega_k \sim 4.2\%$ [6] would be sufficient to explain this negative result. Using the relevant parameters ($k\xi \sim 1$, $k_BT/\hbar\omega_k \sim 1$, $\rho_0\xi \sim 60$), Eq. (17) gives $\Gamma/\omega_k \sim 5\%$. The decay mechanism identified here thus provides a possible microphysical basis to this scenario. The precise dynamics of the entanglement will be the subject of a future work.

ACKNOWLEDGMENTS

We thank Christos Charmousis, Alessandro Fabbri, Denis Boiron, Chris Westbrook, and especially Florent Michel for interesting discussions and useful suggestions. We are particularly grateful to our friend and mentor Renaud Parentani, who was responsible for the genesis of this work and whose guidance and input in its initial stages proved invaluable. We would like to dedicate the paper to his memory. This work was supported by the French National Research Agency via Grant No. ANR-20-CE47-0001 associated with the project COSQUA (Cosmology and Quantum Simulation).

[6] Since we focus directly on the phonon number n_k rather than the amplitudes $\hat{\varphi}_k$, there is a difference of a factor 2 between the dissipative rate defined in [33] and the one defined here.

[1] L. J. Garay, J. R. Anglin, J. I. Cirac, and P. Zoller, Sonic analog of gravitational black holes in Bose-Einstein condensates, Phys. Rev. Lett. **85**, 4643 (2000).

[2] C. Barceló, S. Liberati, and M. Visser, Analogue gravity, Living Rev. Relativity **14**, 3 (2011).

[3] J. R. M. de Nova, K. Golubkov, V. I. Kolobov, and J. Steinhauer, Observation of thermal Hawking radiation and its temperature in an analogue black hole, Nature **569**, 688 (2019).

[4] J. C. Jaskula, G. B. Partridge, M. Bonneau, R. Lopes, J. Ruaudel, D. Boiron, and C. I. Westbrook, Acoustic analog to the dynamical Casimir effect in a Bose-Einstein condensate, Phys. Rev. Lett. **109**, 220401 (2012).

[5] V. S. Barroso, A. Geelmuyden, Z. Fifer, S. Erne, A. Avgoustidis, R. J. A. Hill, and S. Weinfurtner, Primary thermalisation mechanism of early universe observed from faraday-wave scattering on liquid-liquid interfaces (2022).

[6] S. Butera and I. Carusotto, Numerical studies of back-reaction effects in an analog model of cosmological preheating (2022).

[7] M. Pylak and P. Zin, Influence of the interaction between quasiparticles on parametric resonance in Bose-Einstein quasicondensates, Phys. Rev. A **98**, 043603 (2018).

[8] S. Robertson, F. Michel, and R. Parentani, Nonlinearities induced by parametric resonance in effectively 1D atomic Bose condensates, Phys. Rev. D **98**, 056003 (2018).

[9] L. Pitaevskii and S. Stringari, Landau damping in dilute Bose gases, Phys. Lett. A **235**, 398 (1997).

[10] P. O. Fedichev, G. V. Shlyapnikov, and J. T. M. Walraven, Damping of low-energy excitations of a trapped Bose-Einstein condensate at finite temperatures, Phys. Rev. Lett. **80**, 2269 (1998).

[11] E. H. Lieb and W. Liniger, Exact analysis of an interacting Bose gas. I. The general solution and the ground state, Phys. Rev. **130**, 1605 (1963).

[12] S. Tan, M. Pustilnik, and L. I. Glazman, Relaxation of a high-energy quasiparticle in a one-dimensional Bose gas, Phys. Rev. Lett. **105**, 090404 (2010).

[13] Z. Ristivojevic and K. A. Matveev, Decay of Bogoliubov excitations in one-dimensional Bose gases, Phys. Rev. B **94**, 024506 (2016).

[14] A. Imambekov, T. L. Schmidt, and L. I. Glazman, One-dimensional quantum liquids: Beyond the Luttinger liquid paradigm, Rev. Mod. Phys. **84**, 1253 (2012).

[15] H. J. Maris, Phonon-phonon interactions in liquid helium, Rev. Mod. Phys. **49**, 341 (1977).

[16] S. Tsuchiya and A. Griffin, Damping of Bogoliubov excitations in optical lattices, Phys. Rev. A **70**, 023611 (2004).

[17] S. S. Natu and S. Das Sarma, Absence of damping of low-energy excitations in a quasi-two-dimensional dipolar Bose gas, Phys. Rev. A **88**, 031604 (2013).

[18] M. Van Regemortel, W. Casteels, I. Carusotto, and M. Wouters, Spontaneous Beliaev-Landau scattering out of equilibrium, Phys. Rev. A **96**, 053854 (2017).

[19] H. Kurkjian and Z. Ristivojevic, Damping of elementary excitations in one-dimensional dipolar Bose gases, Phys. Rev. Research **2**, 033337 (2020).

[20] Z. Ristivojevic and K. A. Matveev, Decay of Bogoliubov quasiparticles in a nonideal one-dimensional Bose gas, Phys. Rev. B **89**, 180507 (2014).

[21] T. Kinoshita, T. Wenger, and D. S. Weiss, A quantum Newton's cradle, Nature **440**, 900 (2006).

[22] M. Rigol, V. Dunjko, V. Yurovsky, and M. Olshanii, Relaxation in a completely integrable many-body quantum system: An *ab initio* study of the dynamics of the highly excited states of 1D lattice hard-core bosons, Phys. Rev. Lett. **98**, 050405 (2007).

[23] I. Bouchoule, J. Dubail, L. Dubois, and D. M. Gangardt, Relaxation of phonons in the lieb-liniger gas by dynamical refermionization (2022).

[24] P. C. Hohenberg, Existence of long-range order in one and two dimensions, Phys. Rev. **158**, 383 (1967).

[25] L. Pitaevskii and S. Stringari, Bose-Einstein Condensation and Superfluidity (Oxford University Press, 2016).

[26] O. Penrose and L. Onsager, Bose-Einstein condensation and liquid helium, Phys. Rev. **104**, 576 (1956).

[27] D. S. Petrov, D. M. Gangardt, and G. V. Shlyapnikov, Low-dimensional trapped gases, J. Phys. IV France **116**, 5 (2004).

[28] C. Mora and Y. Castin, Extension of Bogoliubov theory to quasicondensates, Phys. Rev. A **67**, 053615 (2003).

[29] M. J. Steel, M. K. Olsen, L. I. Plimak, P. D. Drummond, S. M. Tan, M. J. Collett, D. F. Walls, and R. Graham, Dynamical quantum noise in trapped Bose-Einstein condensates, Phys. Rev. A **58**, 4824 (1998).

[30] C. Cohen-Tannoudji, B. Diu, and F. Laloë, Mécanique Quantique - Tome 2 (EDP Sciences, 2020).

[31] A. F. Andreev, The hydrodynamics of two- and one-dimensional fluids, Zh. Eksp. Teor. Fiz. **78**, 2064 (1980), [Sov. Phys. JETP **51**, 1038 (1980)].

[32] K. V. Samokhin, Lifetime of excitations in a clean Luttinger liquid, J. Phys. Condens. Matter **10**, L533 (1998).

[33] X. Busch, R. Parentani, and S. Robertson, Quantum entanglement due to a modulated dynamical Casimir effect, Phys. Rev. A **89**, 063606 (2014).

[34] A. Peres, Nonexponential decay law, Ann. Phys. (N.Y.) **129**, 33 (1980).

[35] V. Pastukhov, Damping of Bogoliubov excitations at finite temperatures, J. Phys. A **48**, 405002 (2015).

[36] F. A. Bayocboc and K. V. Kheruntsyan, Frequency beating and damping of breathing oscillations of a harmonically trapped one-dimensional quasicondensate (2022).

[37] A. Sinatra, C. Lobo, and Y. Castin, The truncated Wigner method for Bose-condensed gases: Limits of validity and applications, J. Phys. B **35**, 3599 (2002).

[38] J. Ruostekoski and A. D. Martin, The truncated Wigner method for Bose gases, in Quantum Gases (Imperial College Press, 2013) pp. 203–214.

[39] A. D. Martin and J. Ruostekoski, Quantum and thermal effects of dark solitons in a one-dimensional Bose gas, Phys. Rev. Lett. **104**, 194102 (2010).

[40] I. Carusotto and C. Ciuti, Spontaneous microcavity-polariton coherence across the parametric threshold: Quantum Monte Carlo studies, Phys. Rev. B **72**, 125335 (2005).

[41] J. Huber, P. Kirton, and P. Rabl, Phase-space methods for simulating the dissipative many-body dynamics of collective spin systems, SciPost Phys. **10**, 45 (2021).

[42] T. Curtright, D. Fairlie, and C. Zachos, A Concise Treatise on Quantum Mechanics in Phase Space

(World Scientific, New Jersey, 2014).

[43] G. P. Agrawal, Nonlinear Fiber Optics (Academic Press, 2007).

Appendix A FULLER DERIVATION OF EVOLUTION OF δn_k

In this appendix we derive Eq. (19), a more precise equation of motion for the phonon spectrum, and we show how the FGR emerges despite there being no exactly elastic scattering channel. We then analyze more fully the deviations with respect to the FGR result.

A Equations of motion for phonon operators

We start by computing the Heisenberg equation of motion for $\hat{\varphi}_k$. The one for $\hat{\varphi}_k^\dagger$ is easily deduced by taking the adjoint. We consider only the dynamics under the quadratic (8) and cubic (11) Hamiltonians, neglecting higher orders. We have :

$$\partial_t \hat{\varphi}_k = -i \left\{ \omega_k \hat{\varphi}_k + \frac{1}{\sqrt{N_{\rm at}}} \sum_{q\neq 0,-k} 2V_3(k,q) \hat{\varphi}_q^\dagger \hat{\varphi}_{k+q} + \frac{1}{\sqrt{N_{\rm at}}} \sum_{q\neq 0,k} V_3(k-q,q) \hat{\varphi}_{k-q} \hat{\varphi}_q \right\} . \tag{28}$$

Considering then the full number operator $\hat{n}_k = \hat{\varphi}_k^\dagger \hat{\varphi}_k$, we have

$$\begin{aligned} \partial_t \hat{n}_k &= \hat{\varphi}_k^\dagger \cdot \partial_t \hat{\varphi}_k + \partial_t \hat{\varphi}_k^\dagger \cdot \hat{\varphi}_k \, , \\ &= -\frac{i}{\sqrt{N_{\rm at}}} \sum_{q\neq 0,-k} 2V_3(k,q) \hat{\varphi}_k^\dagger \hat{\varphi}_q^\dagger \hat{\varphi}_{k+q} - \frac{i}{\sqrt{N_{\rm at}}} \sum_{q\neq 0,k} V_3(k-q,q) \hat{\varphi}_k^\dagger \hat{\varphi}_{k-q} \hat{\varphi}_q + \text{h.c.} \, . \end{aligned} \tag{29}$$

On the right-hand side of the equation of motion for $\hat{n}_k$ appears the momentum preserving 3-phonon operator $\hat{\varphi}_k^\dagger \hat{\varphi}_q^\dagger \hat{\varphi}_{k+q}$, the same that appears in $\hat{V}_3$. We are thus compelled to consider the dynamics of this operator as well. It is useful to define $\hat{\varphi}_p^\dagger \hat{\varphi}_q^\dagger \hat{\varphi}_{p+q} = \hat{c}_3(p,q) \exp\left[-i\left(\omega_{p+q} - \omega_p - \omega_q\right) t\right]$, where the oscillations are made explicit. These operators obey

$$\begin{aligned} & e^{-i(\omega_{p+q}-\omega_p-\omega_q)t} \partial_t \hat{c}_3(p,q) = \partial_t \hat{\varphi}_p^\dagger \cdot \hat{\varphi}_q^\dagger \hat{\varphi}_{p+q} + \hat{\varphi}_p^\dagger \cdot \partial_t \hat{\varphi}_q^\dagger \cdot \hat{\varphi}_{p+q} + \hat{\varphi}_p^\dagger \hat{\varphi}_q^\dagger \cdot \partial_t \hat{\varphi}_{p+q} + i\left(\omega_{p+q} - \omega_p - \omega_q\right) \hat{\varphi}_p^\dagger \hat{\varphi}_q^\dagger \hat{\varphi}_{p+q} \\ & = \frac{2i}{\sqrt{N_{\rm at}}} V_3(p,q) \hat{\varphi}_{p+q}^\dagger \hat{\varphi}_{p+q} \\ & + \frac{2i}{\sqrt{N_{\rm at}}} \sum_{\lambda\neq 0,-p} V_3(p,\lambda) \hat{\varphi}_{p+\lambda}^\dagger \hat{\varphi}_q^\dagger \hat{\varphi}_\lambda \hat{\varphi}_{p+q} + \sum_{\lambda\neq 0,-q} V_3(q,\lambda) \hat{\varphi}_p^\dagger \hat{\varphi}_{q+\lambda}^\dagger \hat{\varphi}_\lambda \hat{\varphi}_{p+q} - \sum_{\lambda\neq 0,-(p+q)} V_3(p+q,\lambda) \hat{\varphi}_p^\dagger \hat{\varphi}_q^\dagger \hat{\varphi}_\lambda^\dagger \hat{\varphi}_{p+q+\lambda} \\ & + \frac{i}{\sqrt{N_{\rm at}}} \sum_{\lambda\neq 0,p} V_3(p-\lambda,\lambda) \hat{\varphi}_\lambda^\dagger \hat{\varphi}_{p-\lambda}^\dagger \hat{\varphi}_q^\dagger \hat{\varphi}_{p+q} + \sum_{\lambda\neq 0,q} V_3(q-\lambda,\lambda) \hat{\varphi}_p^\dagger \hat{\varphi}_\lambda^\dagger \hat{\varphi}_{q-\lambda}^\dagger \hat{\varphi}_{p+q} - \sum_{\lambda\neq 0,p+q} V_3(p+q-\lambda,\lambda) \hat{\varphi}_p^\dagger \hat{\varphi}_q^\dagger \hat{\varphi}_{p+q-\lambda} \hat{\varphi}_\lambda \, . \end{aligned} \tag{30}$$

The extra term on the first line involving the amplitudes for the $p+q$ mode comes from rearranging the one term which is not initially in normal order.

B Equations of motion for average values

We want to take average values in both equations of motion above and derive the evolution of $n_k = \langle \hat{n}_k \rangle$. However, in order to get a closed system we have to make some approximations. We assume that the state is initially homogeneous; it will remain so as our Hamiltonian is momentum-conserving. We also assume that the initial state is Gaussian, and that the only deviation from Gaussianity to evolve is a non-vanishing value of $\hat{c}_3(p,q)$, *i.e.*, every connected correlation function of order higher than three is negligible. Therefore, when taking average values on the right hand-side of Eq. (30), the 4-point functions reduce to products of 2-point functions which have to respect the homogeneity of the state:

$$\left\langle \hat{\varphi}_p^\dagger \hat{\varphi}_q^\dagger \hat{\varphi}_{p+q-\lambda} \hat{\varphi}_\lambda \right\rangle = n_p n_q \delta_{q,\lambda} + n_p n_q \delta_{p,\lambda} + c_q^\star c_\lambda \delta_{p,-q} \, , \tag{31}$$

where $c_p = \langle \hat{\varphi}_p \hat{\varphi}_{-p} \rangle$. The quantities $n_{\pm p}$ and c_p – respectively, the population and 2-mode correlation of the modes $\pm p$ – are the only non-vanishing 2-point functions in a homogeneous state. We shall further assume, for simplicity, that the c_p are all vanishing. [7] The equation of motion for n_p and $c_3(p,q) = \langle \hat{c}_3(p,q) \rangle$ then reads :

$$\begin{aligned} \partial_t n_k &= \frac{1}{\sqrt{N_{\rm at}}} \sum_{q \neq 0,-k} 4V_3(k,q) \Im \left[c_3(k,q) e^{-i\delta\omega_L(q;k)t} \right] - \frac{1}{\sqrt{N_{\rm at}}} \sum_{q \neq 0,k} 2V_3(k-q,q) \Im \left[c_3(k-q,q) e^{i\delta\omega_B(q;k)t} \right] , \\ \partial_t c_3(p,q) &= 2i \frac{V_3(p,q)}{\sqrt{N_{\rm at}}} \left[n_{p+q} \left(n_p + n_q + 1 \right) - n_p n_q \right] e^{i(\omega_{p+q} - \omega_p - \omega_q)t} . \end{aligned} \tag{32}$$

We can reduce this to a single equation of motion for n_k by writing $c_3(p,q)$ explicitly in terms of n_k:

$$c_3(p,q)(t) = 2i \, \frac{V_3\left(p,q\right)}{\sqrt{N_{\rm at}}} \int_0^t dt' \, N_{p,q}\left(t'\right) e^{i(\omega_{p+q} - \omega_p - \omega_q)t'} , \tag{33}$$

where $N_{p,q} = n_{p+q}\left(n_p + n_q + 1\right) - n_p n_q$. Equation (33) can now be substituted directly into the equation of motion for n_k:

$$\begin{aligned} \partial_t n_k = 8 \sum_{q \neq 0,-k} \frac{\left|V_3\left(k,q\right)\right|^2}{N_{\rm at}} \int_0^t dt' \, N_{k,q}\left(t'\right) \cos\left[\left(\omega_{k+q} - \omega_k - \omega_q\right)\left(t - t'\right)\right] \\ -4 \sum_{q \neq 0,k} \frac{\left|V_3\left(k-q,q\right)\right|^2}{N_{\rm at}} \int_0^t dt' \, N_{k-q,q}\left(t'\right) \cos\left[\left(\omega_k - \omega_{k-q} - \omega_q\right)\left(t - t'\right)\right] . \end{aligned} \tag{34}$$

Note that the terms depending on the various populations can be rewritten as the difference between the direct process mentioned in the text below Eq. (11) and the corresponding reverse process. For instance in the first sum, corresponding to the Landau scattering, we have

$$n_{p+q}\left(n_p + n_q + 1\right) - n_p n_q = \left(n_p + 1\right)\left(n_q + 1\right) n_{p+q} - \left(n_{p+q} + 1\right) n_q n_p . \tag{35}$$

On the right-hand side the $+1$ terms are associated only with the decay products and allow for spontaneous processes, while the ns encode the stimulated part. This generalizes the matrix elements given in the main text, which only include one direction where an excitation at p is removed by the interaction.

Equations (32) and (34) are the key equations governing the system, given our simplifying approximations. They are entirely equivalent if $c_3(p,q)$ is set to zero at $t = 0$, though Eqs. (34) can be straightforwardly modified in a more general case. Since Eqs. (32) are Markovian, they are much more suitable for numerical integration. On the other hand, Eq. (34) is a nonlinear, non-Markovian equation for the full phonon spectrum n_k. However, if analyzed using appropriate approximations, we will show that it encodes both the exponential decay of the phononic population, its first deviations and the corrections to the growth of population in a parametric resonance process.

C Dynamics of a probe on top of a quasicondensate

Up to this point, we have assumed homogeneity and quasi-Gaussianity of the state but worked with the full phonon spectrum n_q. As explained in the main text, the presence of a near-thermal population in the IR modes is instrumental in the decay process that we study. Therefore, as done in Eq. (13), we split n_q into a thermal background $n_q^{\rm th} = 1/\left[\exp\left(\hbar\omega_q / k_B T\right) - 1\right]$ plus a perturbation δn_q. Physically this setup allows us to analyze the response of a quasicondensate at temperature T to the addition of phonons around a certain mode k. This can either be done "by hand", as we have done in the first set of simulations presented in the text, or by a parametric amplification as in the second set, see Sec. IV. As illustrated by Fig. 1 of the main text, we expect these δn probe phonons to redistribute across the system and want to compute the ensuing decay rate.

Notice that the background thermal population $n_q^{\rm th}$ is not strictly stationary due to the addition of the interaction term $\hat{V}_3$, but as a first approximation we will assume it to be a solution of the equation of motion. Since we expect

[7] This is not actually the case for the 2-mode squeezed state generated by the parametric resonance considered in the second set of simulations. Yet, we achieve a quantitative agreement with the TWA simulations for large enough value of $k\xi$. We relegate the analysis of the influence of the correlation on the decay to a future work dedicated to the dynamics of entanglement in this context.

the relevant interactions to be between the peak and the thermal population, and not of the peak on itself, we insert $n_k = n_k^{\rm th} + \delta n_k$ in Eq. (34) and linearise in δn. We have

$$\begin{aligned} N_{p,q} &= N_{p,q}^{\rm th} + \delta n_{p+q}\left(n_p^{\rm th} + n_q^{\rm th} + 1\right) + \delta n_p\left(n_{p+q}^{\rm th} - n_q^{\rm th}\right) + \delta n_q\left(n_{p+q}^{\rm th} - n_p^{\rm th}\right) + O\left(\delta n^2\right) , \\ &= N_{p,q}^{\rm th} + \delta N_{p,q} + O\left(\delta n^2\right) , \end{aligned} \tag{36}$$

with $N_{p,q}^{\rm th}$ the specific combination of populations evaluated with thermal populations and

$$\delta N_{k,q} = \delta n_k\left(n_{k+q}^{\rm th} - n_q^{\rm th}\right) + \delta n_{k+q}\left(n_k^{\rm th} + n_q^{\rm th} + 1\right) + \delta n_q\left(n_{k+q}^{\rm th} - n_k^{\rm th}\right) , \tag{37}$$

$$\delta N_{k-q,q} = \delta n_k\left(n_{k-q}^{\rm th} + n_q^{\rm th} + 1\right) + \delta n_{k-q}\left(n_k^{\rm th} - n_q^{\rm th}\right) + \delta n_q\left(n_k^{\rm th} - n_{k-q}^{\rm th}\right) . \tag{38}$$

Inserting back in the equations of motion we get

$$\begin{aligned} \partial_t \delta n_k &= 8\sum_{q\neq 0,-k} \frac{|V_3(k,q)|^2}{N_{\rm at}} \int_0^t dt'\, \delta N_{k,q} \cos\left[\left(\omega_{k+q} - \omega_k - \omega_q\right)(t-t')\right] \\ &\quad - 4\sum_{q\neq 0,k} \frac{|V_3(k-q,q)|^2}{N_{\rm at}} \int_0^t dt'\, \delta N_{k-q,q} \cos\left[\left(\omega_k - \omega_{k-q} - \omega_q\right)(t-t')\right] , \\ &= -\int_0^t dt'\, D_k(t-t')\, \delta n_k(t') + \int_0^t dt' \sum_{q\neq -k} M_{k,k+q}(t-t')\, \delta n_{k+q}(t') . \end{aligned} \tag{39}$$

In the last line we have split the RHS into two terms, defining a "diagonal" response function $D_k(t-t')$ that acts only on $\delta n_k(t')$, and a "matrix" response function that includes contributions from other modes $\delta n_{k+q}(t')$. Notice that when defining the response functions we have included the term $q = 0$, by extending the summand to its finite limit as q goes to 0, in both the diagonal and the matrix function; one can check that they exactly cancel out. This inclusion allows to separate clearly the exponential decay from its deviations, as laid out below. The last equality in Eq. (39) gives Eq. (19) of the main text.

D Diagonal response function and exponential decay

Considering first the diagonal response function, we have explicitly:

$$\begin{aligned} D_k(\tau) = 8\sum_{q\neq -k} |V_3(k,q)|^2 \left(n_q^{\rm th} - n_{k+q}^{\rm th}\right) \cos\left[\left(\omega_{k+q} - \omega_k - \omega_q\right)\tau\right] \\ + 8\sum_{q\leq k/2} |V_3(k-q,q)|^2 \left(n_q^{\rm th} + n_{k-q}^{\rm th} + 1\right) \cos\left[\left(\omega_k - \omega_{k-q} - \omega_q\right)\tau\right] , \end{aligned} \tag{40}$$

where we have used the $q \to k-q$ symmetry in the second sum to fold it on $q \leq k/2$ adding a factor 2. We want to show that $D_k(\tau)$ reduces to a Dirac delta, and for this purpose it is convenient to first consider its integral. We define

$$I_k(\tau) = \int_0^\tau d\tau'\, D_k(\tau') \qquad \Longleftrightarrow \qquad D_k(\tau) = I_k'(\tau) , \quad I_k(0) = 0 . \tag{41}$$

Since $D_k(\tau)$ is an even function ($D_k(-\tau) = D_k(\tau)$), we find that $I_k(\tau)$ is odd:

$$I_k(-\tau) = \int_0^{-\tau} d\tau'\, D_k(\tau') = \int_0^\tau d(-\tau')\, D_k(-\tau') = -\int_0^\tau d\tau'\, D_k(\tau') = -I_k(\tau) . \tag{42}$$

Explicitly, we note that $\int_0^\tau \cos(\Omega\tau')\, d\tau' = \tau\,\mathrm{sinc}(\Omega\tau)$. Therefore,

$$\begin{aligned} I_k(\tau) = 8\sum_{q\neq -k} |V_3(k,q)|^2 \left(n_q^{\rm th} - n_{k+q}^{\rm th}\right) \tau\,\mathrm{sinc}\left[\left(\omega_{k+q} - \omega_k - \omega_q\right)\tau\right] \\ + 8\sum_{q\leq k/2} |V_3(k-q,q)|^2 \left(n_q^{\rm th} + n_{k-q}^{\rm th} + 1\right) \tau\,\mathrm{sinc}\left[\left(\omega_k - \omega_{k-q} - \omega_q\right)\tau\right] . \end{aligned} \tag{43}$$

It is also useful to take the continuous (large L) limit, replacing $\frac{1}{\Delta q}\sum_q \Delta q \to \frac{L}{2\pi}\int dq$

$$I_k(\tau) = \frac{4L}{\pi}\int_{-\infty}^{+\infty} dq\ |V_3(k,q)|^2 \left(n_q^{\rm th} - n_{k+q}^{\rm th}\right)\ \tau\,\mathrm{sinc}\left[(\omega_{k+q}-\omega_k-\omega_q)\,\tau\right] + \frac{4L}{\pi}\int_{-\infty}^{k/2} dq\ |V_3(k-q,q)|^2 \left(n_q^{\rm th} + n_{k-q}^{\rm th}+1\right)\ \tau\,\mathrm{sinc}\left[(\omega_k-\omega_{k-q}-\omega_q)\,\tau\right]\ . \quad (44)$$

Considering the large τ limit of Eq. (44), the sinc functions in the integrand become highly peaked around $q=0$, and to a good approximation can be replaced by Dirac deltas proportional to $\delta(q)$. However, the limit must be taken with care since the general term has a discontinuity as q goes to 0. We split the integrals for negative and positive momenta and in the limit of large τ we have $\int_0^\epsilon f(x)\tau\,\mathrm{sinc}(\tau\,\delta\omega_{L/B}(q))\mathrm{d}q \to f(0^+)\int_0^\infty \tau\,\mathrm{sinc}(\tau\,\delta\omega'_{L/B}(0^+)\,q)\mathrm{d}q = \frac{\pi}{2}\,f(0^+)/\left|\delta\omega'_{L/B}(0^+)\right|$, and similarly on the other side. Explicitly, for $\tau\to\infty$

$$\begin{aligned}
\int_{-\epsilon}^{\epsilon} |V_3(k,q)|^2 \left(n_q^{\rm th} - n_{k+q}^{\rm th}\right)\ \tau\,\mathrm{sinc}\left[\delta\omega_L(q)\tau\right]\ dq &= \frac{\pi}{2}\left(\lim_{q\to 0^-} + \lim_{q\to 0^+}\right)|V_3(k,q)|^2\,\frac{n_q^{\rm th}}{|\delta\omega'_L(q)|}\,,\\
\int_{-\epsilon}^{\epsilon} |V_3(k-q,q)|^2 \left(n_{k-q}^{\rm th} + n_q^{\rm th}+1\right)\ \tau\,\mathrm{sinc}\left[\delta\omega_B(q)\tau\right]\ dq &= \frac{\pi}{2}\left(\lim_{q\to 0^-} + \lim_{q\to 0^+}\right)|V_3(k-q,q)|^2\,\frac{n_q^{\rm th}}{|\delta\omega'_B(q)|}\,.
\end{aligned} \quad (45)$$

In both integrals, in the limit q to 0, $n_{k\pm q}^{\rm th}$ and 1 are negligible compared to $n_q^{\rm th}$ that diverges as $1/q$. In addition, we have $\left|\delta\omega'_{L/B}(0^\pm)\right| = |v_{\rm gr}(k)\mp c|$. Combining the above two limits we get the formula (17) for the decay rate of phonon of momentum k. Therefore

$$I_k(\tau) = \int_0^\tau D_k(\tau')\ d\tau' \to \pm\Gamma_k \qquad \text{as} \qquad \tau\to\pm\infty\,, \quad (46)$$

where the opposite limit is obtained by anti-symmetry. I_k is asymptotically constant in both directions and only varies in the vicinity of $\tau=0$. As a consequence D_k is peaked around $\tau=0$. We now assume that D_k is sufficiently peaked compared to the variation of δn_k so that the integral in Eq. (39) only picks out its instantaneous value $\delta n_k(t)$

$$\begin{aligned}
\int_0^t dt'\ D_k(t-t')\ \delta n_k(t') &\approx \delta n_k(t)\int_0^t dt'\ D_k(t-t')\ ,\\
&= \delta n_k(t)\, I_k(t)\,.
\end{aligned} \quad (47)$$

The equation of motion becomes

$$\partial_t \delta n_k = -\delta n_k(t)\, I_k(t) + \int_0^t dt' \sum_{q\neq -k} M_{k,k+q}(t-t')\ \delta n_{k+q}(t')\ . \quad (48)$$

Let us now consider the ideal situation where at initial time every mode but a single mode k is exactly thermal: $n_q(0) = n_q^{\rm th} + \delta n\,\delta_{k,q}$ where δn is the number of phonons added in mode k on top of the quasicondensate. This corresponds to the situation analyzed in Sec. IV A. Then we may neglect the matrix response function (since $\delta n_q \ll \delta n_k$):

$$\partial_t \delta n_k = -\delta n_k(t)\, I_k(t)\,. \quad (49)$$

Finally we take a large time limit to have $I_k(t)\to\pm\Gamma_k$ so that in this limit n_k obeys

$$\partial_t \delta n_k = -\delta n_k(t)\,\Gamma_k\,, \quad (50)$$

i.e., the population of the mode k decays exponentially at the rate predicted by Eq. (17).

E Matrix response function: the slowing effect of a finite width

It remains to give the form of $M_{k,k+q}$ and describe its effects. It reads:

$$\begin{aligned}
M_{k,k+q}(t-t') = {}& 8\,|V_3(k,q)|^2\left(n_q^{\rm th}+n_k^{\rm th}+1\right)\cos\left[(\omega_{k+q}-\omega_k-\omega_q)(t-t')\right]\\
&+8\,|V_3(k+q,-q)|^2\left(n_q^{\rm th}-n_k^{\rm th}\right)\cos\left[(\omega_k-\omega_{k+q}-\omega_q)(t-t')\right]\\
&+8\,|V_3(k,k+q)|^2\left(n_{2k+q}^{\rm th}-n_k^{\rm th}\right)\cos\left[(\omega_{2k+q}-\omega_k-\omega_{k+q})(t-t')\right]\mathbb{1}_{q\neq -2k}
\end{aligned} \quad (51)$$

Firstly, a couple of technical remarks. Notice that there is an indicator function in the last term, stating that this piece should not be evaluated at $q = -2k$. Also, the $q = 0$ term has been included to compensate for the inclusion of the opposite term in $D_k\,(t - t')$. Therefore, even in the case where only a single mode is significantly occupied, the matrix response function can never be completely neglected and (50) has to be amended. This first limitation is dealt with in Appendix B below.

$M_{k,k+q}$ represents the indirect interaction of phonons in the modes k and $k + q$ through the thermal population. Equation (51) shows that there are three such processes. The first term corresponds to the conversion between phonons of wavevectors k and q and that of wavevector $k + q$, which we write symbolically as $(k\,,\,q) \leftrightarrow k + q$. Similarly, the second term encodes processes of the form $(k + q\,,\,-q) \leftrightarrow k$, and the third term $(k + q\,,\,k) \leftrightarrow 2k + q$. Even though the perturbation is initially localised in the mode k, the decay process will generate a non-zero δn_q in the vicinity of both $q = 0$ and $q = k$. We shall assume that the perturbation spectrum is relatively narrow around these two points. Equation (48) then implies that we need only consider the values of $M_{k,k+q}$ for $k + q \approx k$ and $k + q \approx 0$.

Consider first $k + q \approx 0$. In the second and third terms of (51), the factor of $|V_3|^2$ and the combination of thermal populations independently vanish in the limit $k + q \to 0$, making these terms negligible. In the first term, only the factor of $|V_3|^2$ tends to zero, but the rapid oscillations of the cosine function at frequencies close to $2\omega_k$ will greatly suppress its contribution to the integral of (48). Therefore, the back-reaction from the decay products at very low momenta is expected to be negligible.

On the other hand, for $k + q \approx k$ only the contribution of the third term in (51) is expected to be negligible, for the frequency of the cosine function is large (roughly $\omega_{2k} - 2\omega_k$) and suppresses its contribution. We are then left with contributions coming from the first and second terms. Their frequency differences are small, preventing any averaging out due to rapid oscillations, and can be written to first order in q. Their coefficients have non-vanishing limit since the vanishing of $|V_3|^2$ is compensated by the divergence of the thermal population, and can be approximated by their low-q limits. Finally, we get [8]

$$M_{k,k+q}\,(t - t') \approx \frac{8}{N_{\rm at}} \lim_{q\to 0^+} \left[|V_3(k,q)|^2\, n_q^{\rm th}\right] \cos\left[q\,(v_{\rm gr}(k) - c)\,(t - t')\right] + \frac{8}{N_{\rm at}} \lim_{q\to 0^-} \left[|V_3(k,q)|^2\, n_q^{\rm th}\right] \cos\left[q\,(v_{\rm gr}(k) + c)\,(t - t')\right] . \quad (52)$$

Equation (52) will be used to compute the correction to the FGR prediction of the decay rate due to the finite width of the peak, *i.e.*, to the back-reaction of neighbouring modes.

Appendix B DEVIATIONS FROM FGR RESULT

We turn in this appendix to the deviations with respect to the simple exponential decay predicted by the FGR. Each of these deviations is described by equation of motion (39).

A Non-exponential decay of IR phonons

1 *Numerical observations*

It was shown in the main text that, in the first set of simulations where an initial probe is simply injected into a single phonon mode, the numerically observed decay of modes with a large enough momentum ($k\xi \geq 2.5$) is very well described by an exponential decay at a rate given by Eq. (17). In Fig. 7, a more complete set of results is shown, in which the template $\delta n_k(t) = A\exp\left(-\Gamma t + \gamma t^2/2\right)$ is fitted to the behavior of a larger set of initial momenta. This figure demonstrates that there are significant deviations at lower $k\xi$, with the values of Γ_k extracted from the simulations going to zero as $k\xi \to 0$ instead of the predicted finite limit. These deviations are due to the fact that the FGR result is only valid within a certain time window [30, 34].

We review the last approximation made in the passage from Eq. (49) to Eq. (50), which is that t be large enough for $I_k(t)$ to be equal to its asymptotic value, or equivalently (as shown in Eqs. (45)-(46)), being able to replace

[8] Notice that we dropped the terms $n_k^{\rm th}$ and $+1$ compared to $n_q^{\rm th}$ which is divergent as $q \to 0$. However, if we work in the discrete setting and consider a small $k \sim j2\pi/L$, then one could argue that q can never be less than $2\pi/L$ so that $n_q^{\rm th}$ is always finite and of the order of $n_k^{\rm th}$. Still, in the limit $k \approx 0$, these terms come with opposite signs and practically cancel out unlike the ones in $n_q^{\rm th}$.

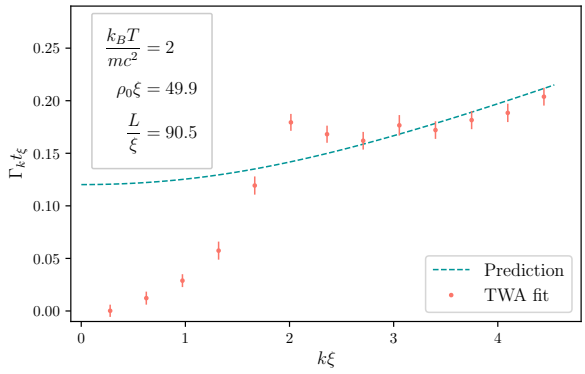

Figure 7. Best fit values for $\hbar\Gamma_k$ extracted from the TWA simulations as a function of $k\xi$. The window shown here is larger than that of Fig. 3 while all physical parameters are fixed at the same values.

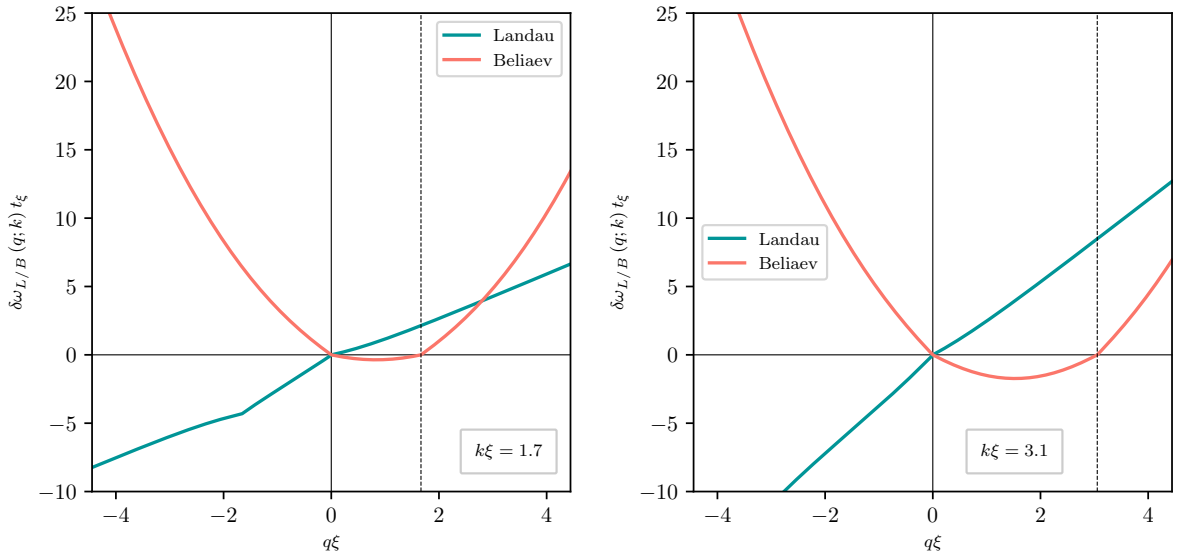

Figure 8. Plots of the Rabi frequencies associated to Landau and Beliaev damping processes $\delta\omega_{L,B}(q;k)$ as a function of q for $k\xi = 1.7$ (left.) and $k\xi = 3.1$ (right.). The value of k is shown by the vertical dashed line.

$t\,\mathrm{sinc}\left(\delta\omega_{L/B}t\right)/\pi$ by a δ function. This requires that $\delta\omega_{L/B}(k,q)\,t$, which vanishes for the elastic scattering channel $q = 0$, should nevertheless reach a large enough value in its vicinity so that the most significant part of the sinc is squeezed into the region of constant effective interaction strength. We may introduce a critical response time, t_{crit}, which marks the time after which this condition is satisfied. This critical time depends on k, so that, for a fixed time window $t/t_\xi \in [0, 10]$ over which the fit is performed, those k for which $t_{\mathrm{crit}}/t_\xi \ll 10$ will be in the FGR regime, while those k for which $t_{\mathrm{crit}}/t_\xi \gg 10$ will be in an early-time regime long before the FGR can be applied.

Examples of $\delta\omega_{L/B}(q,k)t_\xi$ are plotted in Fig. 8, for $k\xi = 1.7$ and 3.1. The key observation is that $|\delta\omega_B|$ is the most significantly constrained, especially in the window $q \in [0, k]$ where the decay processes are expected to be most efficient (as the effective interaction strength is largest there). It is this restriction on $|\delta\omega_B|$ that is most clearly responsible for the failure of the approximation. $|\delta\omega_B|$ reaches a maximum $\delta\omega_B^{(\mathrm{max})} = \omega_k - 2\omega_{k/2}$ at $q = k/2$. At lowest order in $k\xi$, we have $\delta\omega_B^{(\mathrm{max})}t_\xi \approx \frac{3}{32}(k\xi)^3$. The critical response time can be (somewhat arbitrarily) defined via $\delta\omega_B^{(\mathrm{max})}t_{\mathrm{crit}} = 2\pi$, but the key point is that it increases quickly at low momentum: $t_{\mathrm{crit}}/t_\xi \propto (k\xi)^{-3}$. Since the fitting window of Fig. 7 extends only up to $t/t_\xi = 10$, we require at least $10\,\delta\omega_B^{(\mathrm{max})}t_\xi \approx (k\xi)^3 \geq 2\pi$, which imposes $k\xi \geq 2$. This estimate is in close correspondence with the onset of deviations seen for $k\xi \sim 2$ in Fig. 7. Moreover, as the total duration of the simulation is varied, the estimated threshold for $k\xi$ will vary only slowly, as $(t/t_\xi)^{-1/3}$.

At lower $k\xi$, we are well outside the validity regime of the FGR, in an early-time regime where a t^2 behavior is

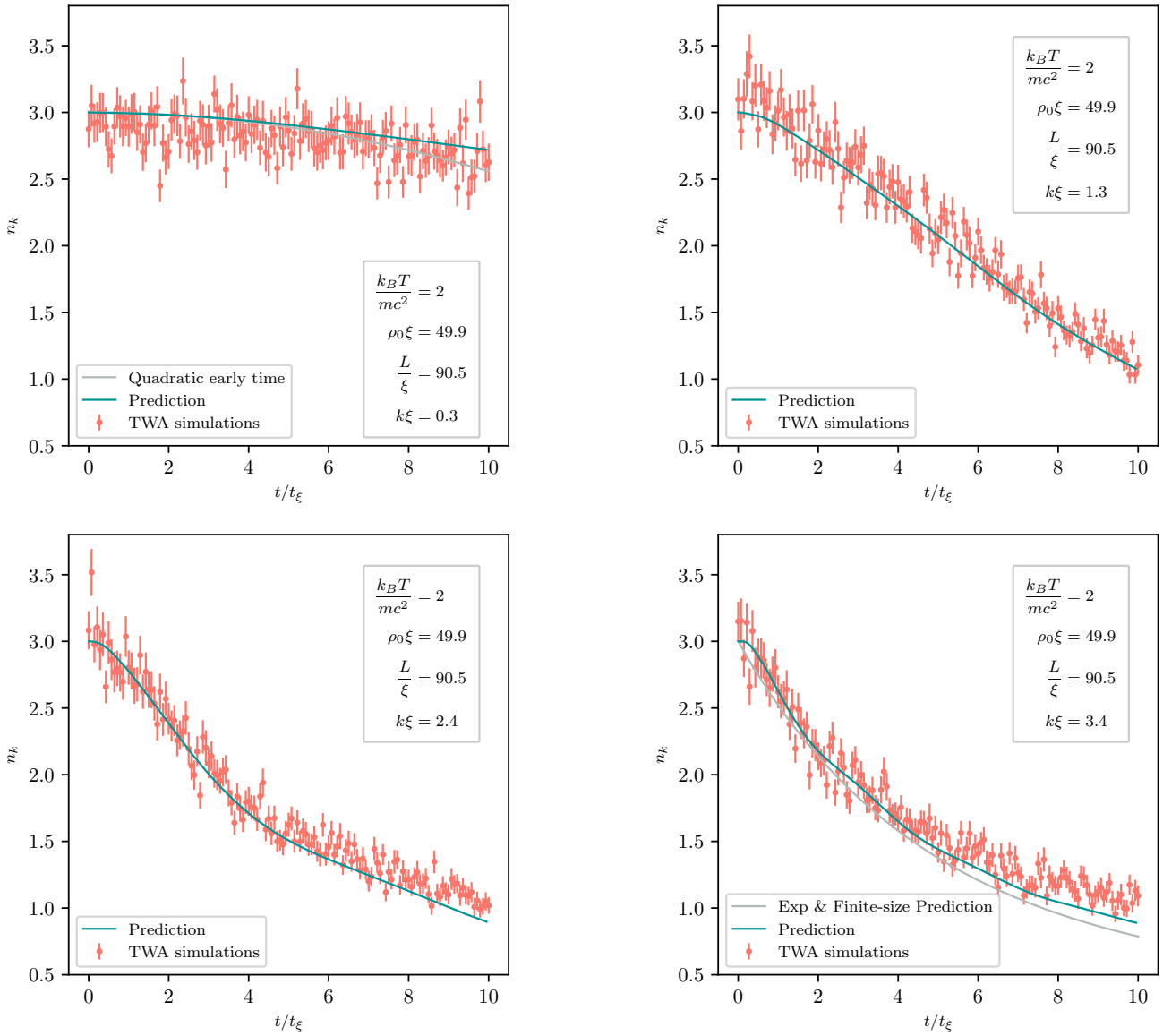

Figure 9. Number of phonons n_k in the mode $k\xi = 0.3$ (top left), $k\xi = 1.3$ (top right), $k\xi = 2.4$ (bottom left), $k\xi = 3.4$ (bottom left) as a function of time t/t_ξ for $k_BT/mc^2 = 2$, $\rho_0\xi = 49.9$, $L/\xi = 90.5$ and $n_r = 400$ realisations. Each plots is comprised of $n_t = 140$ points. The red dots correspond to the result of the TWA simulations. The green line is obtained by taking the difference of the prediction of Eq. (53) for the background thermal population and the full population. The gray line in the top left panel corresponds to the prediction for an early-time quadratic decay given by Eq. (54), while in the bottom right panel it corresponds to the prediction of an exponential decay at the rate given by Eq. (17) of the text with corrections given by Eq. (20).

expected [34] (see below). Furthermore, for very low-lying modes $k \sim 2\pi/L$, the range $q \in [0\,, k]$ will be poorly sampled. We thus expect a strong suppression of the Beliaev component of the decay as $k\xi \to 0$ due to the small number of available modes to decay to, in accordance with similar remarks made in [9, 10]. While such low-lying k mode can still decay via a Landau process we expect that in this regime the system becomes sensitive to the discreteness of excitations and this process would thus require a separate analysis (see, *e.g.*, Ref. [36]).

We expect that these low-k modes can still be well described by Eq. (34). However, we shall adopt an early-time approximation, assuming that $N_{p,q}(t)$ varies sufficiently slowly for it to be taken out of the time-integral as an overall prefactor. We get

$$\begin{aligned}\partial_t n_k = 8 \sum_{q\neq 0,-k} \left\{ \frac{|V_3(k,q)|^2}{N_{\rm at}} \left[n_{k+q}\left(n_k+n_q+1\right) - n_k n_q\right] t\,\mathrm{sinc}\left[\delta\omega_L(q;k)t\right]\right\} \\ - 8 \sum_{0<q\leq k/2} \left\{ \frac{|V_3(k-q,q)|^2}{N_{\rm at}} \left[n_k\left(n_{k-q}+n_q+1\right) - n_{k-q} n_q\right] t\,\mathrm{sinc}\left[\delta\omega_B(q;k)t\right]\right\},\end{aligned} \tag{53}$$

where we have used the symmetry $k \to k-q$ in the second term to sum over only half the momenta, compensating with the inclusion of a factor 2. This equation is then numerically solved twice: once using only the thermal population as an initial state, and a second time using the thermal population plus the δn phonons added in the mode k. We then take the difference to obtain the green curves in Fig. 9. This procedure correct for small variations of the background thermal population. A good agreement is found with the TWA simulations even for large values of $k\xi$.

Let us try to get an analytical estimate for the behavior of the low-lying modes. Their critical time being very large, it is appropriate to consider the early-time limit of Eq. (49) where $\delta n_k(t) \approx \delta n_k(0)$ and $\mathrm{sinc}\left(\delta\omega\,\tau\right) \sim 1$, therefore $I_k\left(\tau\right) = \alpha_k \tau$ for a certain constant α_k. This gives

$$\delta n_k(t) = \delta n_k(0)\left(1 - \alpha_k t^2/2\right), \tag{54}$$

where we now have to calculate α_k.

We cannot simultaneously set all the sinc functions in Eq. (44) to 1, as the $+1$ term in the second sum would then lead to a divergence. Indeed, for large q the frequency difference diverges and the sinc decay accordingly quickly. We typically consider the evolution of the system over time scales of the order of t_ξ. Considering $k\xi \sim 0.3$, we want to sort every mode q in two categories. Either $\delta\omega_{L/B}(q,k)t_\xi \ll 1$, then this mode can be considered to experience an early time behaviour and the related sinc can be set to 1, or $\delta\omega_{L/B}(q,k)t_\xi \gg 1$ then the sinc should be set to 0. We simply exclude the latter modes from the sum.

On the one hand, as noted above for the Beliaev-type channels it is clear from Fig. 8 that the modes $q \in [0,k]$ oscillate at frequencies smaller than the others and should be the one kept in the sum. On the other hand there is no clear separation for the Landau-type scatterings. However, the terms associated to $\delta\omega_L$ in Eq. (44) are already suppressed at large q by an exponentially decaying thermal population n_q in factor. The inclusion of them in the sum should then be irrelevant for the resulting numerical prediction and we include all the modes in the first sum. We then get:

$$\alpha_k = \frac{8}{N_{\rm at}} \left\{ \sum_{q\neq 0,-k} |V_3(k,q)|^2 \left(n_q^{\rm th} - n_{k+q}^{\rm th}\right) + \sum_{0<q\leq k/2} |V_3(k-q,q)|^2 \left(n_{k-q}^{\rm th} + n_q^{\rm th} + 1\right) \right\}. \tag{55}$$

In Fig. 10 we compare this prediction with the best-fit value of α for the template $A\left(1-\alpha t^2/2\right)$ applied to the TWA simulations with A and α as fitting parameters. We considered the smallest values of k of Fig. 3 in the text and used the same time-window $t/t_\xi \in [0,10]$. The agreement is good for very small k and deviations appear around $k\xi = 0.5$. This can be understood using Fig. 9. For $k\xi = 0.3$ the decay is satisfyingly described by the quadratic prediction Eq. (55), while for $k\xi = 3.4$ it is well described by the exponential prediction of Eq. (17) plus the finite size-correction examined in the next section. On the other hand for the intermediate values $k\xi = 1.4$ and $k\xi = 2.4$, corresponding to the second and third panels, the decay from $t/t_\xi = 0$ to $t/t_\xi = 10$ is neither quadratic nor exponential all the way. $k\xi = 2.4$ is precisely the value around which our prediction of exponential decay seems to break down in Fig. 7.

B Finite-size effect

1 Description of effect

The inequivalent curves in Fig. 11 plotted for $L/\xi = 90.5$ and $L/\xi = 181$ demonstrate that the dynamics of n_k in the TWA simulations is not completely insensitive to the size of the system L. Therefore, the L-independent exponential decay rate of Eq. (17) cannot fit exactly the result of the simulations.

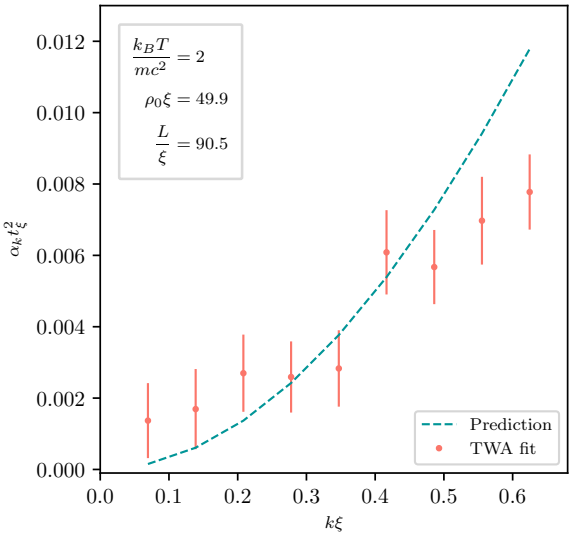

Figure 10. Red dots are the best fit values for $\alpha_k t_\xi^2$ extracted from the TWA simulations using a template of the form of Eq. (54). The green dashed line is the prediction for $\alpha_k t_\xi^2$ of equation Eq. (55). The simulation parameters are $k_BT/mc^2 = 2$, $\rho_0\xi = 49.9$ and $L/\xi = 90.5$ with $n_r = 400$. The fits are performed over a time-window $t/t_\xi \in [0, 5]$, which is half the time-window used in for the fits of Γ_k in Figs. 2 and 3, but with the same number of points $n_t = 140$.

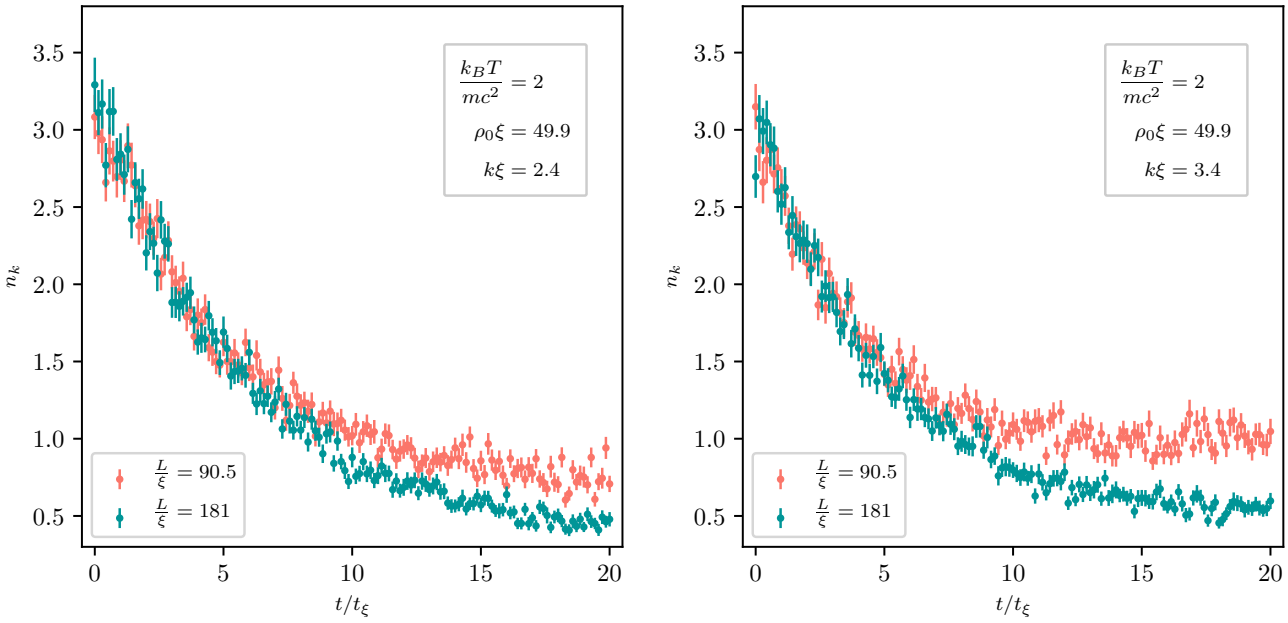

Figure 11. Number of phonons n_k in the mode $k\xi = 2.4$ (left.), $k\xi = 3.1$ (right.) as a function of time t/t_ξ for $k_BT/mc^2 = 2$, $\rho_0\xi = 49.9$ and $n_r = 400$ realisations. The red dots correspond to $L/\xi = 90.5$ and the green ones to $L/\xi = 181$.

The key to understanding this effect is the $q = 0$ contribution to the matrix part of the response function. For a singularly occupied mode, this is the only term in the matrix part that plays any significant role. Recall that it must be included simultaneously in both the diagonal and matrix parts, so that there is no net change in the total response function. If these $q = 0$ terms were not included, the effect would be related to the *absence* of the $q = 0$ term in the *diagonal* response function.

What effect does this term have? Considering the case where a certain number of phonons are injected at $t = 0$,

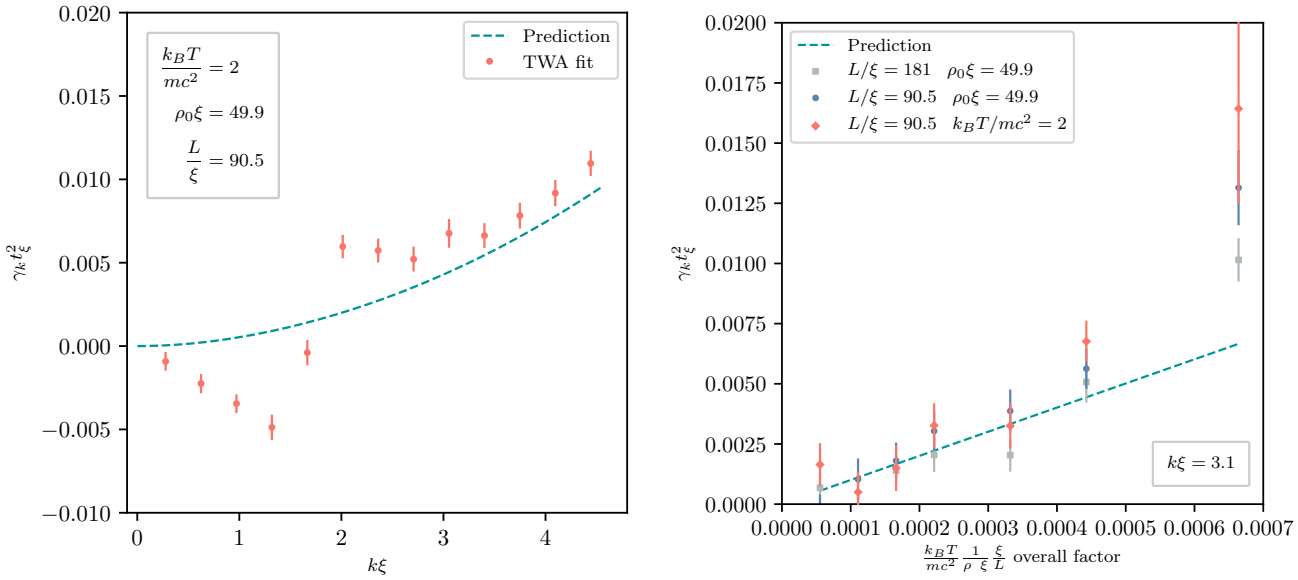

Figure 12. (Left) Plot of $\gamma_k t_\xi^2$ as a function of $k\xi$. The parameters and data used are the same as Fig. 3. (Right) Plot of $\gamma_k t_\xi^2$ as a function of k_BT/mc^2, $\rho_0\xi$ and L/ξ. The parameters and data used are the same as Fig. 2. In both panels the red dots are the best fit values extracted from the TWA simulations using Eq. (20) as a template. The green dashed line is the prediction of equation Eq. (21).

and working in the regime where the diagonal response function reduces to a Dirac delta, we have

$$\begin{aligned}\partial_t\left(\delta n_k\right) &= -\Gamma_k\,\delta n_k + \int_0^t dt'\, M_{k,k}\left(t-t'\right)\,\delta n_k\left(t'\right)\\ &= -\Gamma_k\,\delta n_k + \gamma_k \int_0^t dt'\,\delta n_k\left(t'\right)\,,\end{aligned} \tag{56}$$

where we have made it manifest that $\gamma_k \equiv M_{k,k}$ does not depend on $t-t'$:

$$\gamma_k = 8\left(\lim_{q\to 0^+} + \lim_{q\to 0^-}\right)\frac{|V_3(k,q)|^2}{N_{\rm at}} n_q^{\rm th}\,. \tag{57}$$

At fixed density, $N_{\rm at}$ is proportional to L, so $\gamma_k \propto 1/L$. Performing computations explicitly we get Eq. (21) of the main text.

It is clear from Eq. (56) that there is some push-back on the decay. The simplest solution is when δn_k does not vary much over the duration of interest, so that we can pull it out of the integral:

$$\partial_t\left(\delta n_k\right) \approx \left(-\Gamma_k + \gamma_k t\right)\delta n_k\,, \tag{58}$$

with solution given by Eq. (20) of the main text. In this approximation, the γ_k term simply provides a constant deceleration to the decay rate. [9] In numerical simulations, we have used Eq. (20) as a template to extract the fitted

[9] Here a time dependence of the rate appears through the L-dependence i.e. the finite size effect. The reader might wonder why we never mentioned possible deviations to the exponential decay solely due to the finiteness of t and hence the sinc being not exactly a Dirac delta in Eq. (44). The finite t deviation can be obtained by expanding the effective interaction strength around $q = 0$. Indeed, a Dirac delta would pick up only the value at $q = 0$, first term in the expansion, while a sinc is still sensitive to the deviations from the value at $q = 0$ which are encoded by the higher order terms. We can then proceed by integration by part in Eq. (44) to find that each term in q^n corresponds to a term decaying as $1/t^n$. A careful analysis shows that by combining both integrals the next to leading order term in the expansion around $q = 0$ is in q^2 and not linear in q as one might have expected. The first deviation is then in $1/t^2$. The reason is that since $n_q^{\rm th} + n_{k-q}^{\rm th} + 1 \approx 1/q + 1/2 + n_k^{\rm th}$ and $n_q^{\rm th} - n_{k+q}^{\rm th} \approx 1/q - 1/2 - n_k^{\rm th}$, the contribution coming from both integrals cancel exactly. Hence, the convergence of the sinc to a Dirac delta is effectively faster than one might expect and not a limitation to our result. Notice that since this term is not continuous we have to perform different expansions on both sides.

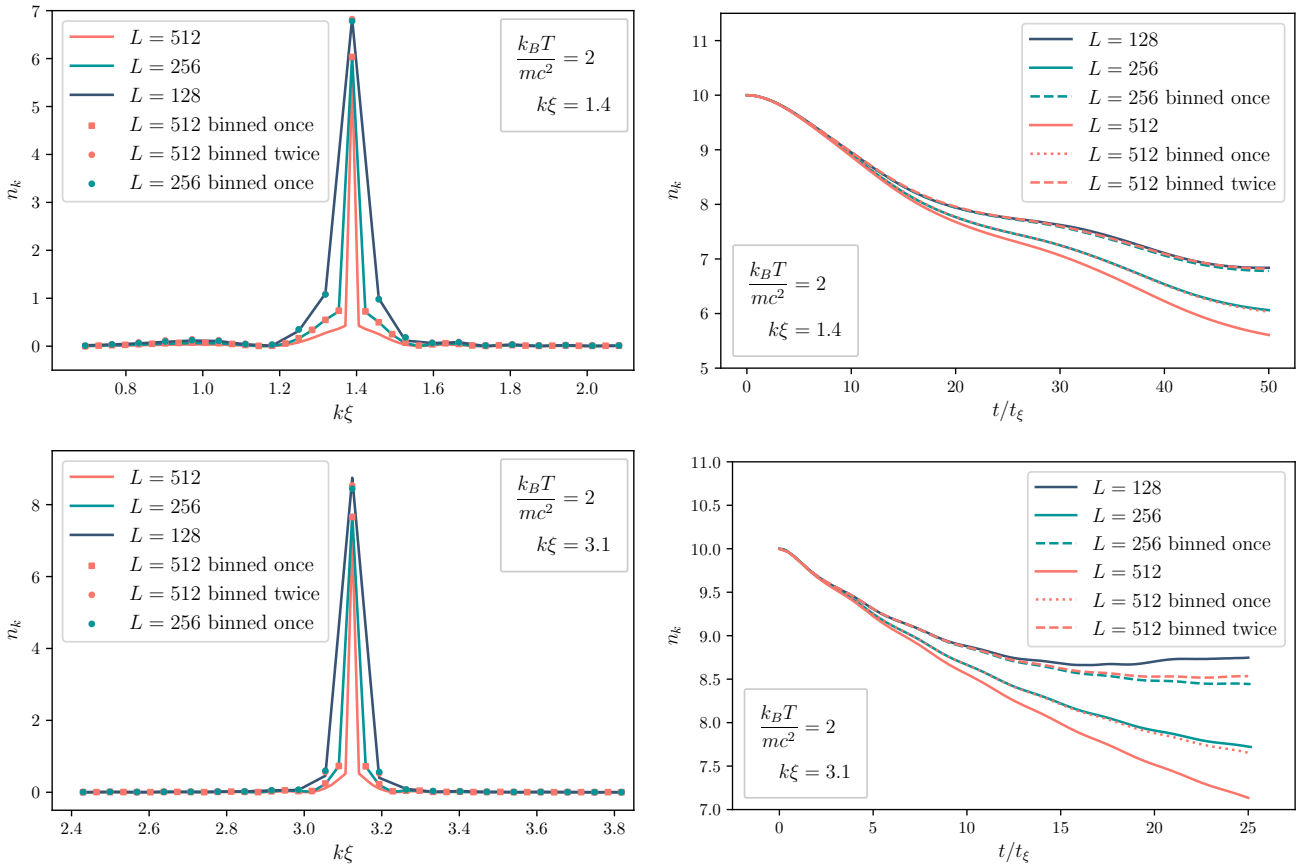

Figure 13. Number of non-thermal phonons δn_k as of function of $k\xi$ at $t/t_\xi = 50$ (top left.), and $t/t_\xi = 25$ (bottom left.), when $\delta n = 10$ phonons were initially added in the mode $k\xi = 1.4$ (top left.), or $k\xi = 3.1$ (bottom left.). This number is shown in full line for different values of density of the grid $\Delta k = 2\pi/L$ where $L = 128$ (blue), $L = 256$ (green) and $L = 512$ (red). The number of modes in the simulation for $L = 512$ is then halved by merging nearby modes into a single bin via Eq. (59) and shown in red squares. Equation (59) is then applied on the set of modes for $L = 256$ and repeated via Eq. (60) on the new set of modes to have the same set of modes as $L = 128$ shown respectively the red and green dots. They are almost everywhere superimposed so that they can hardly be distinguished. The evolution as a function of t/t_ξ of the population in the probe mode is shown in full lines on the right figures for $k\xi = 1.4$ (top right.) and $k\xi = 3.1$ (bottom right.). The result of the binning procedure from $L = 512$ to the set of modes of $L = 256$ is shown in red dotted line. The result of the second binning and the binning of $L = 256$ to the set of modes of $L = 128$ is shown in red and green dashed lines. The initial thermal state used corresponds to $k_BT/mc^2 = 2$. The evolution is performed using the same numerical strategy as described for the green curves of Fig. 9 for $\rho_0\xi = 49.9$.

values of Γ_k shown in the figures of the main text. The values of γ_k extracted from the same fits in the time window $t/t_\xi \in [0, 10]$ are plotted in Fig. 12, along with the prediction of Eq. (21). It demonstrates a reasonable agreement in the same regime of validity as the one of exponential decay ($k\xi \leq 2.5$) shown in Fig. 3. At smaller $k\xi$, the system exhibits the t^2 behavior described above, and this becomes reflected in the fitting parameters. In particular, γ_k moves over into the t^2 coefficient $-\alpha_k$, and we see indeed that its sign changes.

That said, there is a difference between how γ_k and α_k enter the expression of $n_k(t)$, respectively, linearly and exponentially. In particular, while the early t^2 behavior is described by the single fitting parameter α_k, the inclusion of γ_k as a correction to the exponential decay means that it is one of two fitting parameters. The time window of fit is large enough so that the difference between these two templates (applied on the same data) is visible, as illustrated by a direct comparison of Fig. 10 with Fig. 12.

2 Relation to finite size and resolution in k-space

Is there an intuitive way to link this apparent deceleration to the finite size of the system? As our calculations are based in Fourier space, the size of the system enters through the discreteness of the available modes. To some extent, the discretized description should simply provide a finite-resolution view of the continuous-mode (infinite-L) case.

We have investigated this by numerically solving Eqs. (32) directly. We inject a number of phonons in a single mode, and allow the system to evolve in time, for three different values of L. We then compare the evolution by appropriately binning the phonon number spectrum n_k when the k-space resolution is higher, so that each simulation is ultimately represented using the same set of discrete modes. This procedure can also be seen as restricting attention to a section of length D of the system so that the relevant momenta are $2\pi\, n/D$ rather than $2\pi\, n/L$, for $n \in \mathbb{Z}$. The precise relationship between the two sets of modes is equivalent to a choice of window in position space, over which the Fourier transform of the field is taken. We take a more heuristic approach here.

For example, to map the data for a simulation of a system of length L onto the set of modes applicable to a system or section of length $L/2$, the phonons in every second mode must be reallocated to neighbouring modes. We do this by dividing them symmetrically into their two nearest neighbours, half the phonons going into the mode above, half into the mode below. So:

$$n_k^{\text{binned}} = \frac{1}{2} n_{k-\Delta k} + n_k + \frac{1}{2} n_{k+\Delta k}\,. \tag{59}$$

Similarly, to map onto a set of modes applicable to a system of length $L/4$, we adopt the following binning procedure:

$$n_k^{\text{binned}} = \frac{1}{2} n_{k-2\Delta k} + n_{k-\Delta k} + n_k + n_{k+\Delta k} + \frac{1}{2} n_{k+2\Delta k}\,. \tag{60}$$

Results are shown in Fig. 13, for two different values of k. Interestingly, the binning procedure applied to larger-L data gives a very good approximation to the data for smaller-L. This suggests that there is no new (relevant) physics due to the discretization in k-space, in the sense that we can solve for a continuous k-space (*i.e.*, in the limit of infinite L) and then simply apply a suitable binning procedure to see how the discretized system behaves. Similarly, the (relevant) physics on a section of length L of a system of infinite size is the same as that of a finite-size system of the same length.

This binning procedure provides an intuitive explanation for the apparent deceleration of the decay encoded in Eq. (56). For, while the singularly occupied mode decays exponentially, the lost phonons are kicked into nearby modes, whose occupation numbers grow in time. This is what is captured by the second term of Eq. (56): it represents the growth of those modes in the continuous spectrum that are very near k, but which, due to the finite resolution in k-space, are included in the same bin. By local conservation of the number of phonons described in the text, if we bin all modes within the width of the peak into a single mode, we effectively suppress the decay, *i.e.*, if we consider a sufficiently short section we will not witness the decay of the phononic excitations. The time-scale comparison of Eq. (23) shows that the relevant length scale is the coherence length of the quasicondensate r_0. For shorter distances we do not expect to be able to resolve the decay of the phonons and the broadening of the peak in momentum space.

Of course, we do not expect the good correspondence shown in Fig. 13 between simulations of different L to last indefinitely. Eventually, the relevant components of the system – namely, the thermal spectrum and the probe – will be able to tell that they are on a finite torus, rather than a finite section of an infinite-size system, and we can then expect the different simulations to diverge significantly. The critical time can be conceptualized as the re-crossing of the relevant components, which would not re-cross if the system were truly infinite in length. There are two such times, corresponding to the re-crossing of the probe with the positive and negative wave vector components of the thermal spectrum, which propagate and speeds c and $-c$, respectively. Then the re-crossing times are

$$t_+^{\text{rec}} = \frac{L}{v_{\text{gr}}(k) - c}\,, \qquad t_-^{\text{rec}} = \frac{L}{v_{\text{gr}}(k) + c}\,. \tag{61}$$

Since these are simply proportional to L, it makes sense that the simulation with smallest L should be the first to show deviations, as we see in the lower-right panel of Fig. 13. (In this example, $t_-^{\text{rec}}/t_\xi = 30.1$.) However, the deviations remain small, likely due to the weaker coupling between the probe and the negative part of the thermal spectrum. We expect more significant differences after time t_+^{rec}; indeed, we have observed some recurrence of δn_k on this time scale.

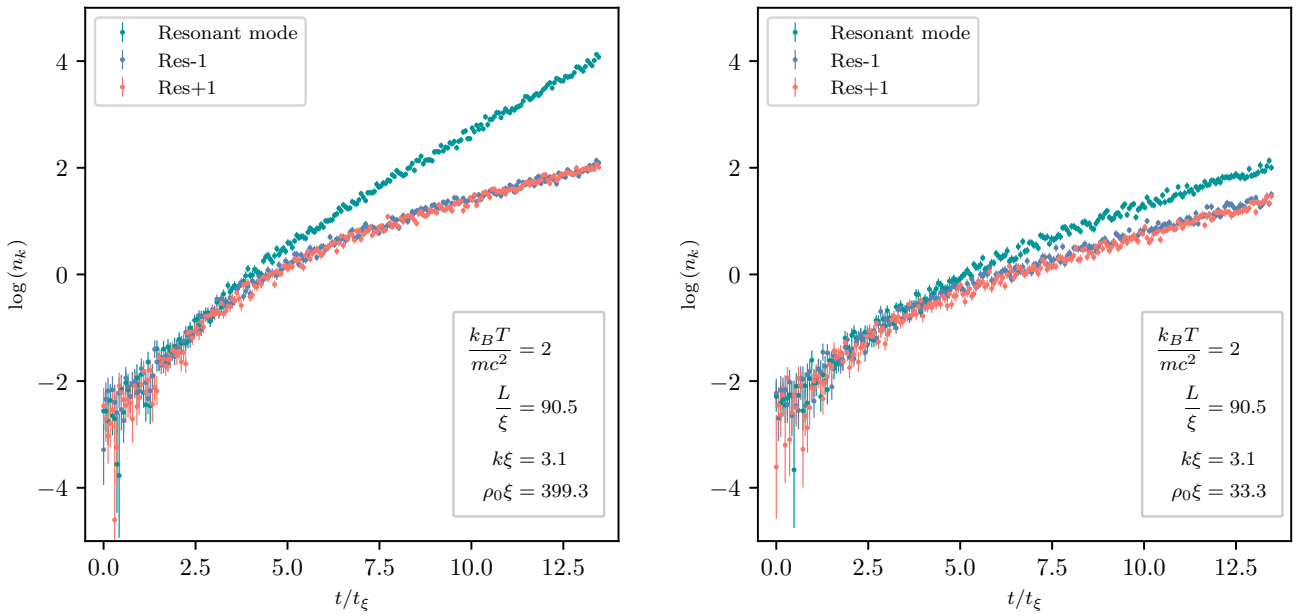

Figure 14. Logarithm of the mean occupation of the resonant mode (green) and its nearest neighbours on either sides (red, blue) as a function of time extracted from the TWA simulations. The parameters for the initial state, the amplitude and the duration of the modulation are the same as in Fig. 4. We see a quicker convergence of the growth rates within the peak on the right plot, which is due to a smaller atomic density resulting in a larger effective interaction strength.

C Finite width of the resonant peak

Here we will discuss the corrections to the decay rate induced by a finite peak width. In particular, we will show how the approximate corrections shown in Fig. 5 were calculated.

The reduction of the decay rate is induced by the off-diagonal part of the matrix response function. Phonons next to the mode of interest also decay due to interaction with the thermal population, and some of these are thus transferred into the mode of interest. Since they can only contribute positively to the occupation number of the main mode, they decelerate the decay of n_k, thereby effectively reducing the decay rate Γ_k.

In our first set of simulations, we impose a very narrow initial peak, and this effect does not have a chance to build up significantly. By contrast, in the second set of simulations where the peak is induced via parametric resonance, it naturally has a finite width which is observed to depend on the interaction strength. We thus see signs of the overall decay rate being smaller than the predicted value at larger interaction strengths, as seen in Fig. 5.

We wish to predict the expected reduction in Γ_k given the observed peak width. To this end we employ Eq. (19) with two key assumptions. First, we modify the equation to include a source term that induces exponential growth, modeling the parametric resonance. This is achieved by adding $G_k\,\delta n_k$ to the right-hand side, where G_k is the predicted growth rate in the absence of any phonon-phonon interactions:

$$G_k = \frac{1}{2} A_k \omega_k \,, \tag{62}$$

which is consistent with Eq. (26) for sufficiently large t. Second, we assume that a steady state is reached where the occupation numbers of all relevant nearby modes grow at the same net rate, $G_{\rm net}$. Therefore, the shape of the peak is assumed constant, and evolves in time simply according to

$$\delta n_k(t) = f_k\, e^{G_{\rm net} t} \,. \tag{63}$$

This appears to be consistent with numerical observations see Fig. 14.

Incorporating these assumptions in Eq. (19) for the occupation number of the resonant mode yields a consistency

equation that determines the expected net growth rate, $G_{\rm net}$:

$$\begin{aligned}\partial_t\left(\delta n_k\right) = G_{\rm net}\,\delta n_k &= \left(G_k-\Gamma_k\right)\delta n_k + \int_0^t dt' \sum_{q\neq -k} M_{k,k+q}\left(t-t'\right)\,\delta n_{k+q}\left(t'\right)\\ &\approx \left(G_k-\Gamma_k\right)\delta n_k + \int_0^t dt' \int dq\,\frac{L}{2\pi}\,M_{k,k+q}\left(t-t'\right)\,\frac{\delta n_{k+q}\left(t'\right)}{\delta n_k\left(t'\right)}\,\frac{\delta n_k\left(t'\right)}{\delta n_k(t)}\,\delta n_k(t)\\ &= \left(G_k-\Gamma_k\right)\delta n_k + \delta n_k(t)\int_0^t dt' \int dq\,\frac{L}{2\pi}\,M_{k,k+q}\left(t-t'\right)\,R_{k+q}\,e^{-G_{\rm net}\left(t-t'\right)}\,,\end{aligned} \tag{64}$$

where in the second line we have taken the continuum limit to replace the sum over wave vectors q by an integral. The exponential suppression in $t-t'$ allows us to replace the lower limit of the t' integral by $-\infty$, which in turn allows us to write the integral independently of t and to divide through the whole equation by $\delta n_k(t)$:

$$G_{\rm net} = G_k-\Gamma_k + \int_0^\infty d\tau \int dq\,\frac{L}{2\pi}\,M_{k,k+q}\left(\tau\right)\,R_{k+q}\,e^{-G_{\rm net}\tau}\,. \tag{65}$$

This self-consistency equation can be solved for $G_{\rm net}$, given that we know G_k, Γ_k, and the profile shape R_{k+q}. If we assume that the peak is narrow enough so that only small q are relevant, we may replace $M_{k,k+q}$ with its small-q limit, given in Eq. (52). This gives

$$\begin{aligned}G_{\rm net} &\approx G_k-\Gamma_k + \int_0^\infty d\tau \int dq\,\left\{f_+\cos\left[q\left(v_{\rm gr}(k)-c\right)\tau\right] + f_-\cos\left[q\left(v_{\rm gr}(k)+c\right)\tau\right]\right\}\,R_{k+q}\,e^{-G_{\rm net}\tau}\\ &= G_k-\Gamma_k + \int dq\left\{f_+\,\frac{G_{\rm net}}{G_{\rm net}^2+q^2\left(v_{\rm gr}(k)-c\right)^2} + f_-\,\frac{G_{\rm net}}{G_{\rm net}^2+q^2\left(v_{\rm gr}(k)+c\right)^2}\right\}R_{k+q}\,,\end{aligned} \tag{66}$$

where we have defined

$$f_\pm = \frac{4}{\pi}\,\frac{L}{N_{\rm at}}\lim_{q\to 0^\pm}\left\{\left|V_3\left(k,q\right)\right|^2 n_q^{\rm th}\right\}\,. \tag{67}$$

All that remains is to plug in a suitable profile R_{k+q} for the profile of the peak. Over a significant range of parameters, we observe numerically that the profile is fairly well described by a Lorentzian:

$$R_{k+q} = \frac{1}{\left(q/\sigma\right)^2+1}\,. \tag{68}$$

Adopting this as an ansatz and plugging it into the integral above, we find

$$G_{\rm net} - \Gamma_+ g\left(\frac{G_{\rm net}}{\left(v_{\rm gr}(k)-c\right)\sigma}\right) - \Gamma_- g\left(\frac{G_{\rm net}}{\left(v_{\rm gr}(k)+c\right)\sigma}\right) = G_k-\Gamma_k\,, \tag{69}$$

where $\Gamma_\pm$ are the predicted decay rates given in Eq. (17) (recall that $\Gamma_k=\Gamma_++\Gamma_-$), and where we have defined

$$g(x) = \frac{1}{1+x}\,. \tag{70}$$

The effective decay rate $\Gamma_{\rm eff}$ is then defined as $\Gamma_{\rm eff} = G - G_{\rm net}$, thus capturing the reduction of the growth rate due to phonon-phonon interactions. Note that Eq. (69) yields the expected behavior in the limits of very narrow and very broad peaks:

- When the peak is very narrow, we take $\sigma\to 0$ so that the argument of $g(x)$ becomes very large, and we can set $g(x)$ to 0. Then we just get $G_{\rm net} = G_k-\Gamma_k$, so $\Gamma_{\rm eff}=\Gamma_k$; this is exactly our prediction for the decay rate of a narrow peak.
- Conversely, when the peak is very broad so that we can send $\sigma\to\infty$, the argument of $g(x)$ becomes very small and we can replace $g(x)$ by 1. Since $\Gamma_k=\Gamma_++\Gamma_-$, Eq. (69) tells us that $G_{\rm net}=G_k$, *i.e.*, there is no reduction of the growth rate. This corroborates our expectation that the broadness of the peak tends to suppress the decay rate.

To determine the corrected decay rates shown in Fig. 5, we first perform a fit of a Lorentzian profile to the occupation numbers around the resonant peak (including five data points on either side of the resonant mode), in order to extract the width σ. This is then used in Eq. (69) on order to determine the expected net growth rate $G_{\rm net}$, and thereby the effective decay rate $\Gamma_{\rm eff}$.

Appendix C MONTE-CARLO SIMULATIONS : TRUNCATED WIGNER APPROXIMATION (TWA)

In order to assess the validity of our predictions we compare them to the results of *ab initio* Monte-Carlo simulations of the system. To simulate the evolution of our quasicondensate we use the Truncated Wigner Approximation (TWA) also known as the classical field approximation. This method is based on the description of the state of the system by means of a quasi-probability distribution, the Wigner function. The TWA has been repeatedly used to describe Bose gas [29, 37], specifically one-dimensional quasicondensate [38, 39], as well as a wide variety of other systems (polaritons, spins etc.) [40, 41]. We will restrict our presentation of the TWA to the necessary minimum and we refer to [29] for further details.

A TWA in a nutshell

The Wigner function $W(\Psi,\Psi^\star)$ is a quasi-probability distribution in phase space defined by a bijective transformation of the density matrix $\hat{\rho}$. Under this transformation the von Neumann equation of motion on the density matrix then translates into a partial differential equation for W [42]. For the Hamiltonian (1) the equation reads

$$i\hbar\dot{W}(\Psi,\Psi^\star) = -\int_{-\infty}^{+\infty}\left\{\frac{\delta}{\delta\Psi}\left[\frac{1}{2m}\partial_x^2\Psi + g\left(|\Psi|^2-1\right)\Psi\right] - \frac{1}{4}\frac{\delta^3}{\delta^2\Psi\delta\Psi^\star}\Psi\right\}W(\Psi,\Psi^\star) + c.c.\,, \tag{71}$$

where the derivatives act on the element inside of the brackets multiplied by $W(\Psi,\Psi^\star)$, see Eq. (23) of [29]. The truncation giving its name to the Truncated Wigner Approximation consists in neglecting terms with three derivatives or more. The resulting equation is then solved by using the method of characteristics. Practically, the Wigner function at time t is found by first sampling the Wigner function at initial time i.e. drawing a set of values $\Psi_i(x,t=0)$ according to the initial Wigner function and evolving these realizations under an equation of motion which is simply the classical counterpart of the Heisenberg equation of motion of $\hat{\Psi}$ under the Hamiltonian (1)

$$i\hbar\dot{\Psi} = -\frac{1}{2m}\partial_x^2\Psi + g|\Psi|^2\Psi\,. \tag{72}$$

The resulting $\Psi_i(x,t)$ represent a sampling of the Wigner function of the state at time t. This sample can be used to compute average values of observables $\langle A(\varphi_k)\rangle_{\rm TWA}$ built from φ_k. It can be shown that expectation values computed treating the Wigner function as a *bona fide* probability distribution are equal to quantum expectation values of the associated operator when the expression is completely symmetrized in $\hat{\varphi}_k$ and $\hat{\varphi}_k^\dagger$. We will not discuss here the conditions of validity of this truncation and of its numerical implementation; some considerations can be found in [18, 28, 29].

B Numerical implementation

The numerical implementation of the TWA is a straightforward application of the above program. The evolution is performed using a discretized version of Eq. (72) and a split-step Fourier algorithm [43]. The initial state is taken to be thermal at a temperature T, up to the addition of a few "probe" phonons in the mode k for the first set of simulations. The exact thermal state of the system is approximated by the one associated to the quadratic Hamiltonian $\hat{H}_2$ *i.e.*, the phonon modes are completely uncorrelated to each other and their number spectrum is set equal to the Bose-Einstein distribution at temperature T. The realisations of the atomic field are built from n_r realisations of the phonon modes φ_k. These are themselves built drawing independently $\Re[\varphi_k]$ and $\Im[\varphi_k]$ according to a centered Gaussian distribution with variance

$$\sigma_k^2 = \frac{1}{2}\left(n_k+\frac{1}{2}\right) = \frac{1}{4}\coth\left(\frac{\hbar\omega_k}{2k_BT}\right)\,. \tag{73}$$

It is then straightforward to check that the TWA averages reproduce the averages of the symmetrized quantum operators in a thermal state:

$$\langle\varphi_k\rangle_{\rm TWA} = \langle\varphi_k^*\rangle_{\rm TWA} = 0\,, \tag{74}$$

$$\langle\varphi_k^*\varphi_k\rangle_{\rm TWA} = n_k^{\rm th}+\frac{1}{2} = \frac{1}{2}\left\langle\left\{\hat{\varphi}_k,\hat{\varphi}_k^\dagger\right\}\right\rangle\,, \tag{75}$$

where $\left\{\hat{A},\hat{B}\right\} = \hat{A}\hat{B} + \hat{B}\hat{A}$ is the anti-commutator. Since this is not the exact thermal state we let the system evolve for a certain duration to be as close as possible to a stationary state that we use as an initial state. For the first set of simulations phonons are then injected in the mode k by transforming its amplitude $\varphi_k(0)$ according to

$$\varphi_k(0) \to \sqrt{1 + \frac{\delta n}{n_k^{\rm th} + \frac{1}{2}}}\varphi_k(0)\,, \tag{76}$$

so that $\varphi_k(0)$ still has Gaussian statistics but with a variance corresponding to $n_k = n_k^{\rm th} + \delta n$. We then evolve under Eq. (72) both the realisations with and without the addition of probe phonons using the same code. We repeat this process for the n_r realisations. Finally we compute the average values for n_q with and without the probe at any time and take the difference to get the evolution of the average value $\delta n_q(t)$.

This method closely mirrors the step of the derivation of the decay rate laid out around Eq. (39) where we subtract the evolution of the background thermal population to single out the evolution of the probe. However the TWA encodes also the deviations to the linear case considered in our equations. For the second set of simulations we simply evolve the initial quasi-stationary state according to (72) where g is modulated according to (25), and proceed to the same type of averaging as in the first set. We want to stress that in any figure of this work, for both set of simulations, a data point at time $t + {\rm d}t$ is *not* obtained simply by evolving the realisations at t time by an extra-step ${\rm d}t$ as this would result in strongly correlated data points. We rather start the whole evolution process from new realisations of the initial state and evolve them until $t + {\rm d}t$.

3.5 Simulating 1D Bose gas using TWA

The numerical simulations we performed are based on the Truncated Wigner Approximation (TWA) [186, 187], the general procedure of which is explained in Appendix C of [4], reproduced in the previous section. TWA allows simulating the gas's evolution beyond the BdG approximation where quasi-particles are considered free and there is no backreaction on the gas's condensed part. The strategy is to treat the atomic field $\hat{\Psi}$ as a stochastic variable Ψ. At the initial time, we draw realisations of the atomic field Ψ_i, which we evolve using the full Heisenberg equation of motion, corresponding exactly to the GPE for these classical fields. Notice that, in the TWA, the non-classical aspects are confined to the stochasticity of the initial state, while the dynamics is entirely classical. The TWA, therefore, misses part of the quantum dynamics [188]. Still, in [4], it completely captured the scattering processes we were studying. Due to the stochasticity of the initial state, the TWA differs from the resolution of the GPE describing the mean atomic field. The procedure we just described can be justified by a truncation of the equation of motion for the full Wigner function, see Appendix C of [4], and exactly solves the quantum dynamics for a Gaussian state evolved via a quadratic Hamiltonian. Our goal is to use the TWA to simulate the evolution of a gas initially in thermal equilibrium, which undergoes a change in interaction constant g leading to the creation of quasi-particles, as in [130], or to follow the evolution of a thermal state in which we initially add a few quasi-particles in some modes. These simulations allow us to probe how the gas reacts to the introduction of quasi-particles in a weakly non-linear regime and to follow the propagation of these perturbations to other modes. We summarise the main steps of the algorithm in Fig. 3.6. We give more details about each of these steps in the dedicated sub-sections below.

3.5.1 A - Initial state preparation

3.5.1-a Space discretisation

We assume that our gas is contained in a one-dimensional box of size L. Additionally, to represent the system, we need to discretise space with a space step $\mathrm{d}x$, and we have n_x sites such that $L = n_x \times \mathrm{d}x$. This discretisation of real space induces a UV cut-off in Fourier space i.e. we do not encode the physics of scales smaller than $|k| \geq \pi/\mathrm{d}x$. In our case, this UV cut-off is not a limitation since we are mainly interested in the behaviour of long wavelengths. As detailed in Sec. 3.3.4-b, for the discretisation to still capture the relevant physics, we have to make sure that the space step is small enough i.e. $\mathrm{d}x \ll \xi$ and $\mathrm{d}x \ll \lambda_\mathrm{T}$. We typically work at the limit of validity of these conditions where $\mathrm{d}x \sim \lambda_\mathrm{T}$ and $\mathrm{d}x \sim \xi/3$. Decreasing the steps did not noticeably improved the results and require more computation time to run the simulations. We also have to make sure that the space step is

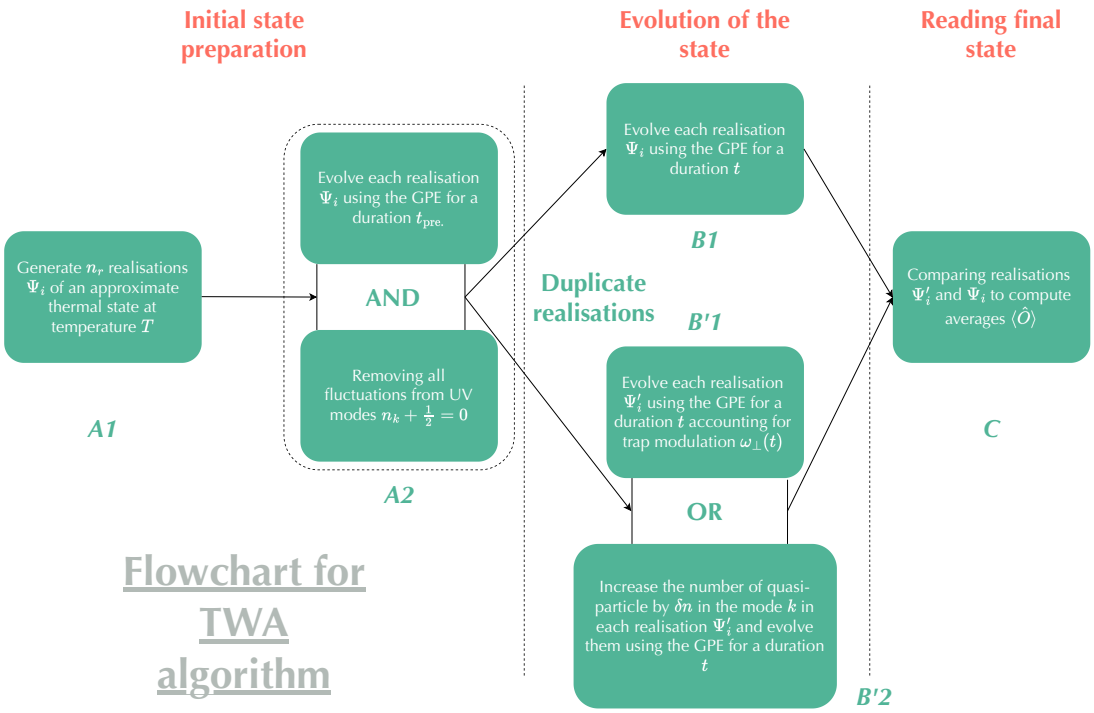

Figure 3.6: Steps of the TWA algorithm used in [4].

large enough so that the total number of atoms $\rho_0 \mathrm{d}x \gg 1$ in each site is large. For the smallest density values used in [4] we have roughly $\rho_0 \mathrm{d}x = 10$ atoms per site so that the condition is always satisfied. Combining these two series of conditions gives a range in which we can choose $\mathrm{d}x$. It thus puts a limit on the number of UV modes we can include in the simulation for a given value of the size of the system L and of the density n_0.

The condition of a large occupation in each site is a requirement to build an approximate phase operator and for the density fluctuation to remain small [168], see Eq. (3.68). This requirement can be understood easily in the case of TWA simulations. The density fluctuations are not *a priori* a normal-ordered combination, and in any state, it contains a sum of commutators encoding the vacuum fluctuations of each mode. In principle, this number is infinite, and we have to regularise it by normal ordering. In TWA simulations, each mode comes with a certain level of vacuum fluctuations included by a stochastic noise, see Sec. 3.5.1-b below, and these will contribute to every observable. If we include too many modes, the density fluctuations will grow out of control. These vacuum fluctuations are also effectively encoded via a non-zero value of the classical field as any other mode excitation. Therefore, they are not protected against scattering processes affecting the excitation of the system i.e. the 'vacuum fluctuations' can decay in a TWA code. These processes can lead to a negative occupation number of the highest UV modes and are thus another reason not to include too many UV modes [126].

3.5.1-b A1 - Thermal state

We want to use the thermal state of the system as an initial state to mimic the setting of [130]. Initialising the atomic field in an actual thermal state of the system would require knowing the exact energy spectrum and the associated eigenfunctions of the system. In general, this is impossible. We instead start from an approximate thermal state using the energy spectrum computed from the quadratic order Hamiltonian $\hat{H}_2$ of Eq. (3.44). Notice that at this stage, using BdG, or Madelung, perturbation theory gives the same energy spectrum. Nevertheless, the quasi-particles are related to the atomic field differently in these two schemes. They thus define different approximate thermal states for the system. As expected, the phase and density approach leads to a more stationary and better-behaved state. We come back to this point in Sec. 3.5.3-b.

A thermal state for the quadratic Hamiltonian is a number state $|\{n_k^{\mathrm{th}}\}\rangle$ where n_k^{th} is the thermal state given in Eq. (3.72), and ω_k is the BdG quasi-particles dispersion relation (3.41). In the stochastic treatment the operators $\hat{b}_k$ are treated as stochastic c-numbers b_k. The probability distribution attached to them is given by the Wigner function of the system's state. The thermal state is a Gaussian state meaning that its Wigner function is a Gaussian and is entirely characterised by its covariance matrix as detailed in [1] reproduced in Sec. 2.2. By analogy with a

harmonic oscillator, we can define pseudo-position $\hat{q}_k$, and pseudo-momentum operator $\hat{p}_k$, for each quasi-particle mode related to the hermitian and anti-hermitian part of the operator similar to Eq. (60) of [1]. This gives us a phase-space representation of the state. We can then use the stochastic phase-space variables q_k and p_k. Their statistics are given by the Wigner function of the modes $\pm k$ i.e. a two-dimensional Gaussian probability distribution parameterised by the covariance matrix of the quantum state. For a thermal state, q_k and p_k are independent and they have equal variance $\langle \hat{q}_k^2 \rangle = \langle \hat{p}_k^2 \rangle = n_k^{\rm th} + 1/2$ see Eq. (C.3) of [4]. In general, the stochastic phase-space variables satisfy [189].

$$\langle f\left(q_k, p_k\right)\rangle_W = \langle f_{\rm sym}\left(\hat{q}_k, \hat{p}_k\right)\rangle \ , \tag{3.82}$$

where the left-hand side is an average performed with the Wigner function, f is a polynomial and $f_{\rm sym}$ is a writing of the polynomial totally symmetric in its arguments, e.g. for $f(q,p) = q^2p^2$ we have $f_{\rm sym}(\hat{q},\hat{p}) = (\hat{q}^2\hat{p}^2 + \hat{q}\hat{p}^2\hat{q} + \hat{q}\hat{p}\hat{q}\hat{p} + \hat{p}\hat{q}\hat{p}\hat{q} + \hat{p}\hat{q}^2\hat{p} + \hat{p}^2\hat{q}^2)/6$. The left-hand side average in Eq. (3.82) can be approximated by drawing a large number n_r of independent realisations of the stochastic phase-space variables $\{q_{k,i}, p_{k,i}\}_{i\in[1,n_r]}$. Typically we use $n_r = 500$ in the simulations of [4]. Going back to phonon numbers we have in particular $\langle b_k^\star b_k\rangle_W = n_k^{\rm th} + 1/2$ see Eqs. (74)-(75) in Appendix C of [4]. The $1/2$ present in each mode encodes the vacuum fluctuations. To read out the average number of particles in each mode, we must subtract this half. Note then that the total decay of the excitation in a mode k, leading to a vanishing value for $b_{k,i}$, would indeed imply a *negative* number of quasi-particles in the mode as explained in Sec. 3.5.1-a.

Using this stochastic picture based on the Wigner function, we can exactly represent the initial thermal state of quasi-particles. We only include a finite number of modes in our simulation, but the requirement $\mathrm{d}x \ll \lambda_{\rm T}$ ensures that we sample the thermally occupied ones. Finally, from each realisation of the series $\{b_{k_j}\}_{j\in[-\pi n_x/L, \pi n_x/L]\setminus\{0\}}$, where $k_j = 2\pi j/L$, we build a realisation of the atomic field by taking for each point x_l on the grid [190]

$$\delta\rho_i\left(x_l\right) = \sqrt{\frac{\rho_0}{L}} \sum_{j\in\left[-\frac{\pi n_x}{L}, \frac{\pi n_x}{L}\right]\setminus\{0\}} e^{ik_j x_l}\left(u_{k_j} + v_{k_j}\right)\left(b_{k_j,i} + b_{k_j,i}^\star\right) \ , \tag{3.83a}$$

$$\delta\theta_i\left(x_l\right) = \frac{1}{2} \sum_{j\in\left[-\frac{\pi n_x}{L}, \frac{\pi n_x}{L}\right]\setminus\{0\}} e^{ik_j x_l}\left(u_{k_j} - v_{k_j}\right)\left(b_{k_j,i} - b_{k_j,i}^\star\right) \ , \tag{3.83b}$$

$$\Psi_i\left(x_l\right) = \sqrt{\rho_0 + \delta\rho_i\left(x_l\right)}\exp\left[\delta\theta_i\left(x_l\right)\right] \ . \tag{3.83c}$$

Notice that with the above, the average density of atoms in each realisation is fixed by construction to ρ_0. Eq. (3.83c) also shows that the formalism cannot accommodate arbitrarily large density fluctuations, or the number under the square

root might become negative. First, this requires that space discretisation is chosen as described in Sec. 3.5.1-a to limit the vacuum fluctuations. Second, we have to consider a physical situation where the gas we model is in the quasi-condensate regime so that the normal-ordered relative density fluctuations remain small [168, 170]. This condition requires a small enough temperature and a large enough density. For the values of parameters used in [4], the fluctuations are, at maximum, typically an order of magnitude smaller than the background density.

3.5.1-c Thermal state in BdG

The reconstruction Eq. (3.83c) is based on the density and phase perturbation theory that, we have argued in Sec. 3.3.4, is the most appropriate to use for 1D gas. In a previous paper [133] on the analysis of [130], the authors had used TWA simulations of the gas but relied on the BdG approximation instead. The thermal state of quasi-particles was similarly sampled, but the realisations of the initial state of the atomic field were then built using

$$\Psi_i\left(x_l\right) = \frac{n_0}{\sqrt{L}} \sum_{j\in\left[-\frac{\pi n_x}{L},\frac{\pi n_x}{L}\right]\backslash\{0\}} e^{ik_j x_l}\left(u_{k_j} b_{k_j,i} + v_{k_j} b^{\star}_{k_j,i}\right) . \tag{3.84}$$

For a given temperature value T, interaction constant g_1 and background condensed density n_0, the perturbation $\delta\Psi$ gives a non-vanishing density of depleted atoms. The state's average density of depleted atoms δn is computed from the n_r realisations. Therefore, with the prescription of Eq. (3.84), the average total number of atoms in the system will fluctuate for different values of the parameters. In [133], in order to keep the total number of atoms fixed in average, irrespective of the parameters chosen, the density of condensed atoms is corrected to $n_0 - \delta n$ and the full field taken to be

$$\Psi_i\left(x_l\right) = \sqrt{\frac{n_0 - \delta n}{n_0}}\,\delta\Psi_i\left(x_l\right) . \tag{3.85}$$

It is clear that this procedure is not entirely consistent with the BdG procedure since we first take the condensate density to be n_0 to draw the realisations of the phononic operators $b_{k,i}$, but we then modify the condensate density to $n_0 - \delta_n$ to build the field. In addition the procedure can quickly run into problems if the density of depleted atoms δn grows too much, as it typically does in one-dimension, see Sec. 3.3.4. However, even the safer prescription of Eq. (3.84) leads to divergences in the density-density correlation function and to a poorer approximation of the actual thermal state of the gas compared to Eq. (3.83c). To illustrate these aspects, we compared in Sec. 3.5.3-b the evolution of the system's Gaussian entropy for the two constructions when the system is left to evolve without external action.

3.5.1-d A2 - Modifying initial state

We can apply a couple of modifications to the initial state we have constructed to get around some of the limitations of the simulation. First, the thermal state of the quasi-particles we use as an initial state is not strictly stationary. Therefore, we expect a certain degree of state evolution even without external perturbation. We can allow this initial state to evolve for some time to limit that effect, hoping it will get closer to a stationary state before perturbing it [133]. However, when the initial state is constructed using Eq. (3.83c) this initial evolution did not dramatically change the system's response when introducing quasi-particles directly or by a modulation.

Second, we have already mentioned that only a few UV modes should be present in the simulation. The vacuum fluctuations of these modes can decay, leading to *negative* occupation, and even if we do not probe these UV modes, their decay products can be located nearby IR modes of interest for our simulations. We allow ourselves to remove all fluctuations in the modes with k larger than a certain k_{CO} to avoid this pollution of the IR modes. How do we pick this cut-off wavenumber?

In the preparation of [4], we identified spurious Beliaev-Landay decay channels for the UV modes. These will be the topic of a future publication, but a brief computation is sufficient to understand their origin. The energy and momentum conservation for 3-body scattering, such as Beliaev-Landau processes, read

$$p + q = k \,, \tag{3.86a}$$

$$\omega_p + \omega_q = \omega_k \,. \tag{3.86b}$$

The momentum-conservation condition of Eq. (3.86a) arises when looking at the third-order Hamiltonian in Fourier space. It comes from the requirement that $e^{i\mathrm{d}x(p+q-k)} = 1$. Since we work with a discrete space, the space step is finite $\mathrm{d}x = \pi/k_{\mathrm{max}}$. The conservation condition is then actually generalised to $p + q - k = m \times 2k_{\mathrm{max}}$, where m can be any integer i.e. Fourier space is also effectively periodic of period $2k_{\mathrm{max}}$. A quick analysis shows that for $(p, q) \in [-k_{\mathrm{max}}, k_{\mathrm{max}}]$ the momentum conservation condition can be satisfied for $m = 0$, the usual condition, but also for $m = \pm 1$, leading to additional spurious channels. The dispersion relation should now be extended to a periodic one $\omega_{k+2mk_{\mathrm{max}}} = \omega_k$, see Fig. 3.7.

Let us now consider the energy conservation for fixed $p > 0$. When p, q and $p + q$ lie within $[-k_{\mathrm{max}}, k_{\mathrm{max}}]$ the conservation is only satisfied for $q = 0$. However, when $p + q > k_{\mathrm{max}}$, one can find a solution with non-vanishing q. In particular choosing $p = q$ we can always find a solution $p_\star > k_{\mathrm{max}}/2$ to Eq. (3.86b). Since $2p_\star > k_{\mathrm{max}}$, if we restrict attention to modes within $[-k_{\mathrm{max}}, k_{\mathrm{max}}]$, $2p_\star$ is mapped to $2p_\star - 2k_{\mathrm{max}}$. The scattering process thus appears as the combination of two quasi-particles with positive momentum $p_\star$ to create one with negative, typically UV, momentum $2p_\star - 2k_{\mathrm{max}}$, see Fig. 3.7. The reverse process also happens, giving

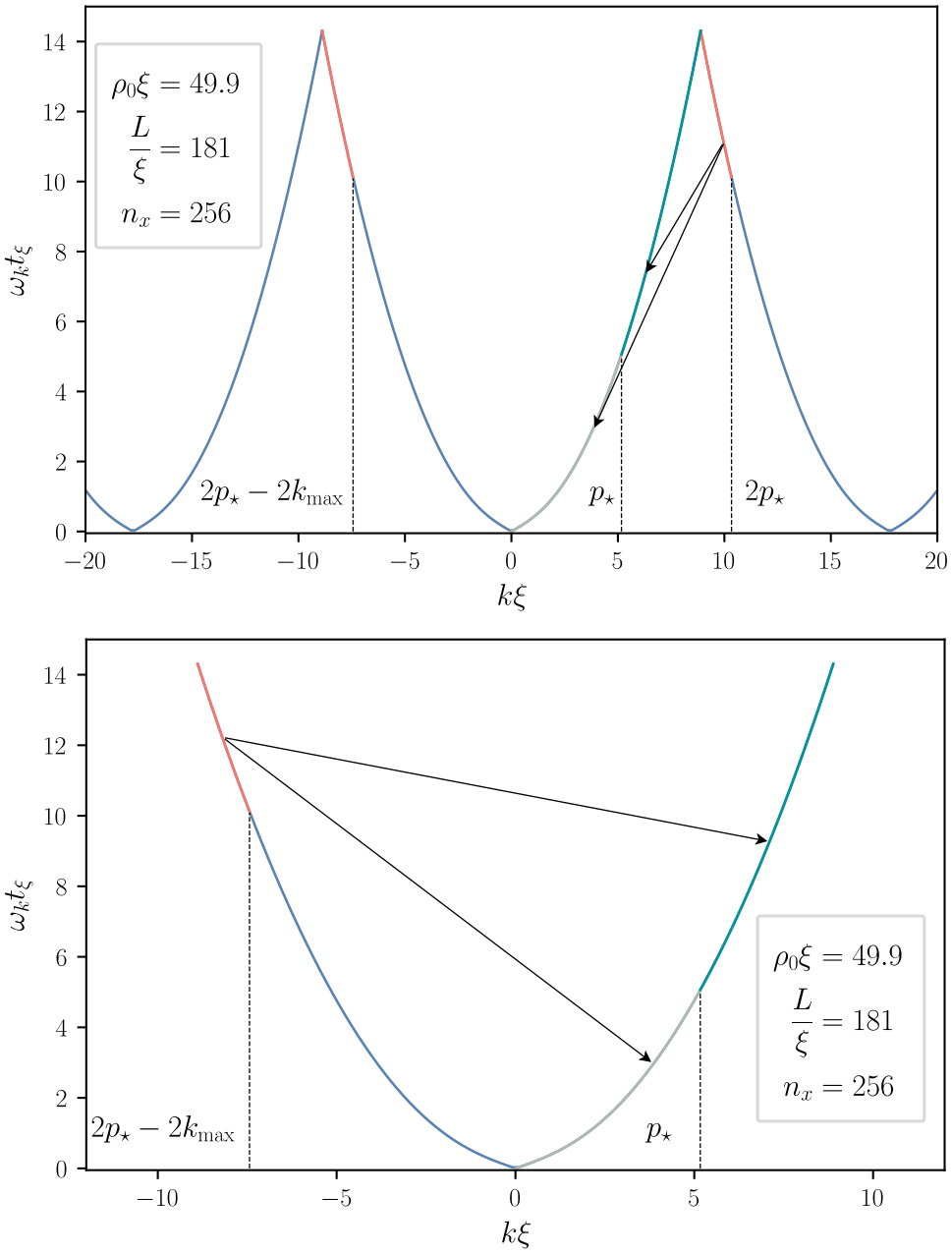

Figure 3.7: (Top panel) Periodic Bogoliubov-de Gennes dispersion relation given in Eq. (3.41) for a grid of size $n_x = 256$. The red region for $k_{\max} < k < 2p_\star$ shows the UV modes decaying towards the green and grey regions, indicated by the two arrows. The second red region for $-k_{\max} < k < 2p_\star - 2k_{\max}$ corresponds to the first one translated by $-2k_{\max}$.

a channel for UV modes to decay towards IR modes. The spurious processes will also happen between a quasi-particle with $p > p_\star$ combining with one with $q < p_\star$. Therefore, to completely suppress the direct and reverse processes, one can pick the cut-off momentum to be $k_{\rm CO} = p_\star$. We used this choice in [4] to avoid the decay of quasi-particles injected in the gas by spurious Beliaev-Landau channels, which would deteriorate quantitative comparison with our predictions for the physical channel.

3.5.2 B - Evolution

One can map the Heisenberg evolution equation to an exact evolution equation for the Wigner function. In the TWA, this equation is truncated at its lowest non-trivial order, see Sec. 3.4, and the resulting equation is solved by evolving the realisation of the atomic field Ψ_i using a space and time discrete version GPE Eq. (3.17). While we use the density and phase perturbation picture to build the initial realisations, evolving them using the equation of motion over the atomic field given in Eq. (3.15) proves more convenient. In the absence of external potential $V_{\rm ext}$, the latter only has two terms which are easy to integrate using a split-step Fourier algorithm.

3.5.2-a Split-step Fourier evolution

We start by describing how we relate a realisation of the atomic field made of the numbers $\Psi_i(x_l;t)$ to the realisation at time $\Psi_i(x_l;t+\mathrm{d}t)$, where $\mathrm{d}t$ is our time-step. Since we neglect the external potential $V_{\rm ext}$, there are two pieces to evaluate on the right-hand side of the GPE to determine the time-derivative at t: the kinetic and self-interaction terms. First, consider the interaction term. It is local in real space and depends only on $\Psi_i(x_l)$. Assuming that any change of $g(t)$ happens over time scales much larger than $\mathrm{d}t$, and forgetting about the kinetic term, the evolution would be

$$\Psi_i\left(x_l;t+\mathrm{d}t\right) = e^{-\frac{i}{\hbar}g(t)|\Psi_i(x_l;t)|^2\mathrm{d}t}\Psi_i\left(x_l;t\right) . \tag{3.87}$$

Notice that this evolution takes into account the evolution of the stationary background part $e^{-ig\rho_0\mathrm{d}t/\hbar}$ since $|\Psi_i|^2$ contains the average density ρ_0. Second, consider the kinetic term. It is not local in real space and would require to use finite differences to be evaluated at x_l, which involves the field at nearby points $x_l \pm m\times \mathrm{d}x$, with m an integer. However, working in Fourier space, this term is 'local' because its expression for $\Psi_i(k_j)$ only depends on $\Psi_i(k_j)$. If we temporarily drop the interaction term the evolution can then be solved in Fourier space by

$$\Psi_i\left(k_j;t+\mathrm{d}t\right) = e^{-\frac{i}{\hbar}\frac{\hbar^2k_j^2}{2m}\mathrm{d}t}\Psi_i\left(k_j;t\right) . \tag{3.88}$$

The split-step Fourier algorithm [191] we use to evolve the realisations makes use of both these simplifications. We first evaluate the evolution due to the interaction

term (3.87) for half a step $\mathrm{d}t/2$. We then do a discrete Fourier transform of the resulting Ψ_i and perform the evolution due to the kinetic term for a full step $\mathrm{d}t$ (3.88). Finally, we go back to real space and perform another evolution of half a step for the interaction term $\mathrm{d}t/2$. The error of the resulting evolution is expected to be of the third order in the time-step [191].

3.5.2-b Time discretisation

The time-step $\mathrm{d}t$ cannot be chosen independently of the space-step $\mathrm{d}x$. We have to make sure that the highest frequency modes $\omega_{\pm k_{\max}}$ do not evolve too quickly between two time-steps so that we correctly describe their evolution. Approximating $\omega_{\pm k_{\max}}$ as being in the free particle regime we have

$$\omega_{\pm k_{\max}}\mathrm{d}t \ll 2\pi \iff \frac{\hbar}{m}\frac{\pi \mathrm{d}t}{4\mathrm{d}x^2} \ll 1\,. \tag{3.89}$$

We have observed that choosing a too large time-step not only leads to a poor description of large frequency modes but can also lead to dramatic resonant behaviour around $\omega_k \approx \pi/\mathrm{d}t$, where we witness a spontaneous exponential growth of the number of quasi-particles. The condition (3.89) ensures that this latter frequency is not present in the system.

3.5.2-c Duplicating realisations

We want to observe the evolution of a perturbation on top of the initial thermal state, particularly how initial quasi-particles injected in the system in a given mode k redistribute. In order to isolate precisely the effect of introducing the perturbation, we can compare the evolution from the same initial state with and without the external perturbation. Recall that our initial thermal state is not exactly stationary, so we expect a small degree of evolution even without perturbation. The algorithm we use is stochastic in drawing initial realisations of the atomic field but deterministic in its evolution. If we draw n_r realisations Ψ_i, compute the evolution without perturbation, then draw n_r more Ψ_i', compute the evolution with perturbation and compare $\Psi_i(t_{\text{fin.}})$ and $\Psi_i'(t_{\text{fin.}})$ there will always be additional difference owing to the different initial states. A large number of realisation n_r already suppresses these differences. However, we can make the comparison more efficient by duplicating the first n_r realisations Ψ_i. We then use one realisation for the evolution with perturbation, corresponding to B'2 or B'1 in Fig. 3.6, and the other without perturbation, B in Fig. 3.6. This trick allows us to have clean numerical results where we can track precisely the (dis)appearance of quasi-particles in the mode k and their redistribution to other modes even if the transfers are small, see Fig.13 of [4].

3.5.2-d B'1 - Modulation of transverse trapping frequency

Modelling the effect of time-dependent trapping frequency $\omega_\perp(t)$ is straightforward with the reduction we have described in Sec. 3.3.2: it is modelled by a time-dependent 1D interaction constant $g(t)$. Although the link between the evolution of the interaction constant and that of the trapping frequency is complicated, see Eq. (3.28). In [4], we made the simplifying assumption that modulating the trapping frequency at ω_m results directly in a modulation of g at the same frequency. This modulation is simply implemented by changing the value of $g(t)$ in the integration of the kinetic term (3.88).

3.5.2-e B'2 - Injection of quasi-particles in a mode k

Another series of simulations performed in [4] consists in adding quasi-particles, on top of the thermal population, in a given mode k. To do so, we modified the statistics of the state of this mode k. In [4], we added δn quasi-particles in the mode k by enhancing the values of the stochastic numbers $b_{k,i}$ that were drawn

$$b'_{k,i} = b_{k,i}\sqrt{1+\frac{\delta n}{n_k^\mathrm{th}+0.5}}\,. \tag{3.90}$$

It is straightforward to check that the resulting $b'_{k,i}$ still follow a thermal distribution. Nevertheless, the average number of quasi-particles has been enhanced to $n_k^\mathrm{th}+\delta n$. A thermal state corresponds to a completely incoherent distribution, so we have added excitations *incoherently* i.e. $\langle b_k^2\rangle_W = 0$ before and after the addition. This incoherence would not have been achieved if we had added $\sqrt{\delta n}$ to each realisation $b_{k,i} \to b_{k,i} + \sqrt{\delta n}$. The price to pay for this is that the number of injected quasi-particles is also stochastic and only δn on average.

Note that the result of parametric amplification of the initial thermal distribution considered in Sec. 3.3.3 would lead to a different state. First, it generates quasi-particles in at least *two* resonant modes $\pm k$. Second, the quasi-particles generated in the two modes are correlated: $c_k = \langle b_k b_{-k}\rangle_W \neq 0$ after the amplification, see Sec. 3.3.2-d. The evolution of the correlation c_k is crucial to understand how entanglement can be lost in [130]. Preliminary results on this point are presented in Sec. 3.6. TWA simulations also guided these results. We injected quasi-particles *coherently* in the initial state by replacing the initial thermal state of the modes $\pm k$ with a Two-Mode Squeezed Vacuum (TMSV) state, see [3] definitions. This injection is a proxy for the effect of a parametric amplification on the modes $\pm k$. It is more computationally effective than solving the dynamics in the presence of modulation and also much more straightforward as it leaves the other modes $k' \neq k$ unaffected. A TMSV is a Gaussian state, and we can also faithfully represent it using stochastic variables drawn from a Gaussian probability distribution. The major difference with the initial state is that we deal with a four-dimensional probability distribution for $q_{\pm k}$ and $p_{\pm k}$. An easy way to build realisations of

these stochastic numbers is to transform the TMSV into two independent equally distributed One-Mode Squeezed Vacuum (OMSV) state for modes described by $(\hat{q}_{\mathrm{R/I}}, \hat{p}_{\mathrm{R/I}})$, see Sec. 2.4. We draw realisations for the numbers $q_{\mathrm{R/I}}$ and $p_{\mathrm{R/I}}$) which are then linearly related to $q_{\pm k}$ and $p_{\pm k}$. Note that the state after the two-mode squeezing of modes in a thermal state is not strictly speaking a TMSV but a two-mode squeezed thermal state because it is a mixed state, see Sec. 2.4. This correction could be implemented in a future version of the code by replacing the OMSV of the fictitious modes with a one-mode squeezed thermal state whose degree of mixedness is fixed by the initial thermal population.

3.5.2-f Independent time-step

In our simulations, we compute approximate values for quantum operators using its correspondence to stochastic averages computed using the Wigner function, see Eq. (3.82). We approximate the stochastic averages by performing averages over a finite number of independent realisations n_r. We estimate the error in our approximated average by computing the variance of this quantity in our n_r realisations. The standard deviation then gives the error bars we show in our plots in [4], e.g. in Fig. 1.

Say we want to follow a quantity in time, for instance, the number of phonons n_k in a mode k and want to compare the evolution of this quantity with our prediction, for instance, an exponential decay of the population $n_k \propto e^{-\Gamma_k t}$. Then we will fit the data points at different times using a curve matching the predicted form with a few fitting parameters. The fitting procedure will give an estimated error on the fitting parameters from the error bars given at each point t_i. However, correctly estimating the errors requires knowing how the points at different times t and $t + \mathrm{d}t$ are correlated, which requires a detailed study for each quantity. To use the usual fitting procedures, which assume that the data points are independent of each other, we re-draw n_r different realisations and repeat the complete evolution until t_i to evaluate the quantity at this time. It ensures that the data at each time point are independent.

3.5.3 C - Reading final state

The primary quantity that we compute from the realisations of the atomic field $\Psi_i(x_l)$ are the values of the phononic creation/annihilation operators $b_{k,i}$. Computing them requires knowing the density and the phase field at every point x_l. While computing the density field from the atomic field is straightforward $\rho(x_l) = |\Psi_i(x_l)|^2$, it is not so for the phase field. Indeed, the atomic field only retains the value of the phase up to 2π. A straightforward reading of the argument of the phase field can then lead to a large jump of the phase field from one point to another, while we need a continuous field to build the quasi-particles. For this reason, we construct, in parallel to the atomic field's values, the phase field's

value. To avoid large phase jumps, we proceed iteratively. First, in the initial state, we set the phase at the site $x_l = 0$ to the value of the argument of the atomic field there. Then, assuming that the phase difference between two neighbouring sites x_l and $x_l + \mathrm{d}x$ is less than π, we compute the argument $\Psi(x_l + \mathrm{d}x)/\Psi(x_l)$ and set $\theta(x_l + \mathrm{d}x) = \theta(x_l) + \arg[\Psi(x_l + \mathrm{d}x)/\Psi(x_l)]$. Having constructed a phase field devoid of large jumps for the initial state, we can repeat the same method for the time evolution. At any point $t + \mathrm{d}t$ we set the phase of the field to be $\theta(x_l; t + \mathrm{d}t) = \theta(x_l; t) + \arg[\Psi(x_l; t + \mathrm{d}t)/\Psi(x_l; t)]$. With this reconstructed phase field, we then build the stochastic number b_k by inverting the transformation of Eqs. (3.55a)-(3.55b). From this number, we can compute the average values of the quantities studied in [4], all constructed from a combination of these operators.

3.5.3-a Following the external perturbation

Once both the realisations with $\Psi_i'(x_l)$ and without perturbation $\Psi_i(x_l)$ are obtained, we can read out the effect of the perturbation by taking the difference of the two before averaging $\delta\Psi_i = \Psi_i' - \Psi_i$, rather than after. The intuition behind this can be formulated as follows. The result of the unperturbed evolution is only a function of the initial background state $\Psi_i(t) = f[\Psi_i(0); t]$. This piece can be removed from the evolution of the perturbed evolution

$$\Psi_i'(t) = \Psi_i(t) + \delta\left[\Psi_i(0), \delta\Psi_i(0); t\right], \tag{3.91}$$

where due to the non-linear evolution the perturbation $\delta\Psi_i$ at time t depends on both its initial value $\delta\Psi_i(0)$ and that of the background $\Psi_i(0)$. Therefore $\Psi_i(t)$ and $\delta\Psi_i(t)$ could be correlated $\langle\Psi_i(t)\delta\Psi_i(t)\rangle \neq 0$ even if initially incoherent $\langle\Psi_i(0)\delta\Psi_i(0)\rangle = 0$. We are not interested in this correlation between the background and perturbation but solely in the evolution of the perturbation due to the background. For instance, we may ask how many quasi-particles initially contained in $\delta\Psi_i(0)$ were lost at time t by interaction with the background. To extract this number, we first compute $\delta\Psi_i(t)$ and then extract the number of quasi-particles via $\langle\delta\Psi_i^\dagger(t)\delta\Psi_i(t)\rangle$, rather than computing $\langle\Psi_i^{\dagger,\prime}(t)\Psi_i'(t)\rangle - \langle\Psi_i^\dagger(t)\Psi_i(t)\rangle = \langle\delta\Psi_i^\dagger(t)\delta\Psi_i(t)\rangle + \langle\delta\Psi_i^\dagger(t)\Psi_i(t)\rangle + \langle\delta\Psi_i(t)\Psi_i^\dagger(t)\rangle$. The additional terms in the above expression need not vanish, and their magnitude *a priori* depends on that of the background, which can be large. Therefore, they could be a noise source, and we favour the first expression where they are absent. This comparison method is generically used in the plots of [4] unless otherwise specified.

3.5.3-b Madelung vs BdG

In this part, we illustrate the superiority of the Madelung perturbation scheme over the BdG one when performing numerical simulations. The distinction between the BdG and Madelung formalisms can be relevant at two stages. First, as already explained, when building the initial state: à la BdG as in Eq. (3.84), or using the

Madelung scheme as in Eq. (3.83c). We will refer to the first as the BdG state and the second as the Madelung state. Still, for a given value of the atomic field Ψ_i, we can use these expressions the other way around to define BdG quasi-particles and Madelung quasi-particles. In the following, to be consistent, when we refer to quasi-particles of the BdG state, we mean BdG quasi-particles, and similarly, we only extract Madelung quasi-particles from the Madelung state. We produced the data presented using a former version of the code that contained no error bars on the data points and where the time steps were not independent. However, the difference between the two schemes is clear enough without needing these refinements. To compare the two states, we compare the evolution of several quantities without any external perturbation (initial injection of quasi-particles or modulation) computed in the BdG and the Madelung states. We use the same set of realisations to build the two initial states to ensure that they only differ in the method used to construct them.

First, in Fig. 3.8, we compare the number of quasi-particles extracted from the BdG and Madelung states at two different times. At the initial time, both states give a spectrum matching the prediction for an exact Bose-Einstein distribution at temperature T given in Eq. (3.72). This has to be the case by construction. The Madelung state stays close to the prediction as a function of time for both series of values. On the other hand, Fig. 3.8 shows that, in the BdG state, n_k suffers from a significant degree of non-stationarity. For larger interactions, lower panel, the non-stationarity of the BdG state becomes more dramatic and propagates towards more UV modes. Note that additional snapshots would reveal oscillations rather than a continuous growth of these modes. We point out that the non-stationarity could be partially cured at lower interaction/temperature by 'reading' the BdG state with Madelung phonons, but the non-stationarity still appears at larger interaction/temperature. The fact that the non-stationarity persists shows that it is not only due to how we extract the quasi-particles from the BdG state; the BdG state itself is plagued with non-stationarity.

In the current version of the algorithm, the primary quantity used in the computation are the phononic amplitudes computed from the Madelung state $b_{k,i}$. Previously, the primary quantity was the atomic field Ψ_i itself. The number of quasi-particles n_k, and their pair-correlation c_k, were deduced from evaluating the density-density correlation function assuming Gaussianity using the formula (3.62). This procedure mimics an experimental 'in-situ' measurement of these quantities. Given the importance of $G^{(2)}_{k,-k}$, we compared its values computed in the BdG and the Madelung states. The results are shown in Fig. 3.9. We compare the values estimated in the simulations to the predicted values of $G^{(2)}_{k,-k}$ for a thermal state of Madelung quasi-particles at temperature T. It is given by Eq. (3.63), where $n_k = n_k^{\text{th}}$ is a thermal distribution given in Eq. (3.72), while $c_k = 0$. In the up-

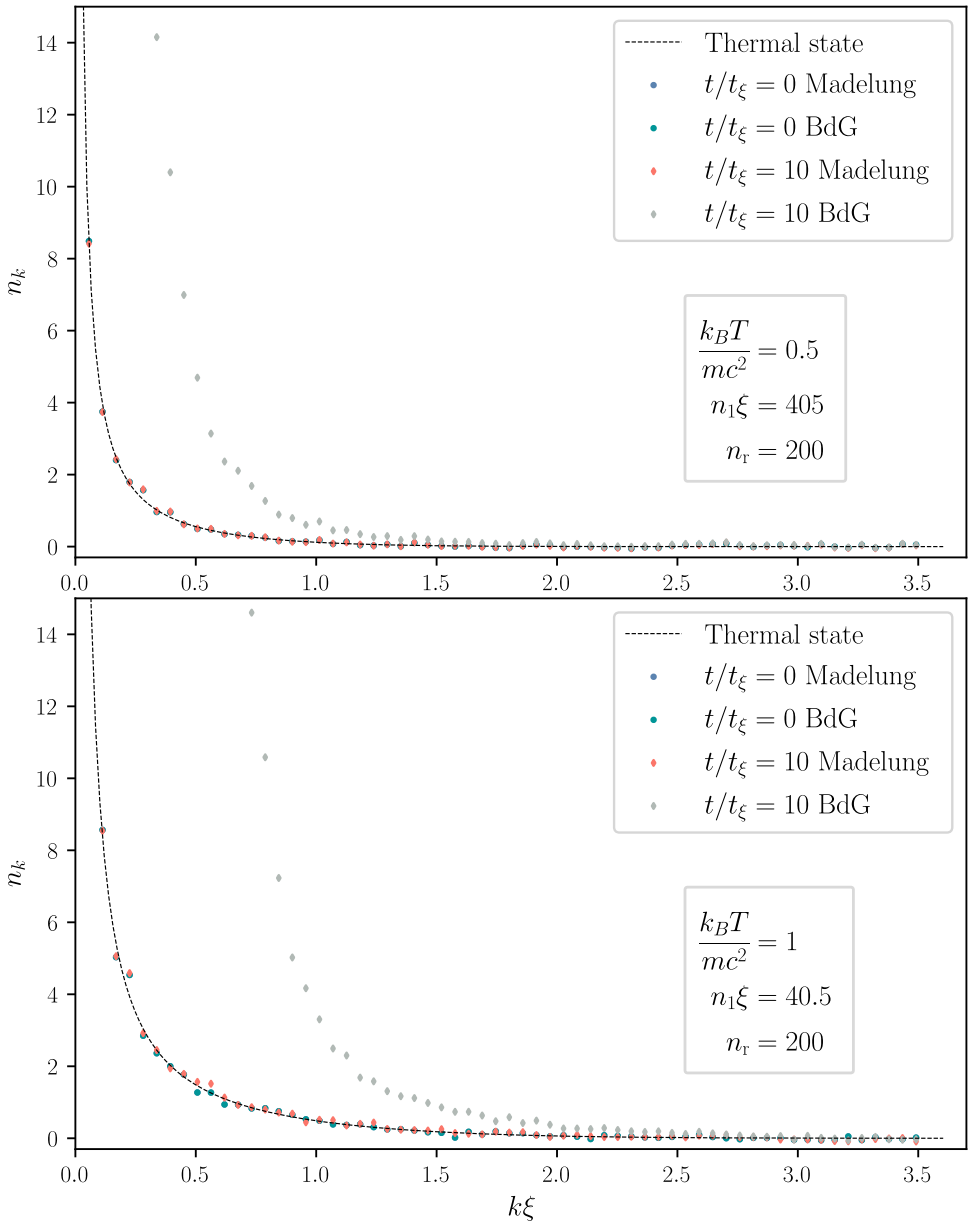

Figure 3.8: Average number of phonons (3.57a) as a function of the wavenumber $k\xi$, for the Madelung and the BdG states, at two different times. This number is compared to a thermal distribution (3.72) of phonons associated with the temperature T shown in dashed lines. The two panels differ by the values of the temperature of the initial phonon distribution $k_B T/mc^2 = 0.5$ for the upper panel, $k_B T/mc^2 = 1$ for the lower panel, and the value of the density of the background $\rho_0\xi = 405$ for the upper, and $\rho_0\xi = 40.5$ for the lower panel. Recall that lower densities imply larger interactions.

per panel of Fig. 3.9, corresponding to lower interaction/temperature, $G^{(2)}_{k,k}$ for the BdG state is manifestly non-stationary in the IR part of the spectrum. In the lower panel corresponding to larger interaction and temperature, already at the initial time, almost no point of the BdG state lies on the prediction of Eq. (3.63). At later times, its IR values decrease but are still far off the expected values. On the other hand, the Madelung state is again observed to be stationary around the expected value for both series of parameters.

Finally, to quantify the level of non-stationarity, we can compute a Gaussian approximate value of the entropy of the state. This corresponds to the best estimate of the entropy based on 2-point functions [192], and would match the exact entropy when the state is Gaussian. This entropy will be computed using the state of the quasi-particles and we will assume each pairs of modes $\pm k \neq 0$ to be independent of each other. The von Neumann entropy for one such pair reads [133]

$$S_{\boldsymbol{k}} = \left(n_k^{\text{eff}} + 1\right) \ln\left(n_k^{\text{eff}} + 1\right) - n_k^{\text{eff}} \ln\left(n_k^{\text{eff}}\right) \,, \tag{3.92}$$

where we defined the quantity

$$\left(n_k^{\text{eff}} + \frac{1}{2}\right)^2 = \left(n_k + \frac{1}{2}\right)^2 - |c_k|^2 \,. \tag{3.93}$$

We can then compute the total entropy of the state by summing this over all modes in the simulation

$$S_{\text{tot}} = \sum_{k>0} S_{\boldsymbol{k}} \,. \tag{3.94}$$

In Fig. 3.10, we show the evolution of the total entropy. (3.94) as a function of time for the two initial states. As expected from the evolution of the number of quasi-particles in Fig. 3.8, since the BdG state is more evidently non-stationary for lower background density and larger temperature, its entropy grows to even larger values. On the other hand, the entropy of the Madelung state is constant for both series of temperature and background density.

We conclude that to make reliable predictions in numerical simulations, one should relinquish the BdG state and use the Madelung state instead.

3.5.4 Improvements compared to previous versions

Since a similar algorithm was used in [133] to study the evolution of the same 1D Bose gas numerically, we quickly summarise the improvements made over the code used then. The primary improvement is using the density and phase perturbations in the Madelung form rather than the BdG approximation. It made the code more stable and reliable, especially at higher interactions, see Sec. 3.5.3-b. Second, we have also implemented the possibility of directly extracting the value of $b_{k,i}$, and

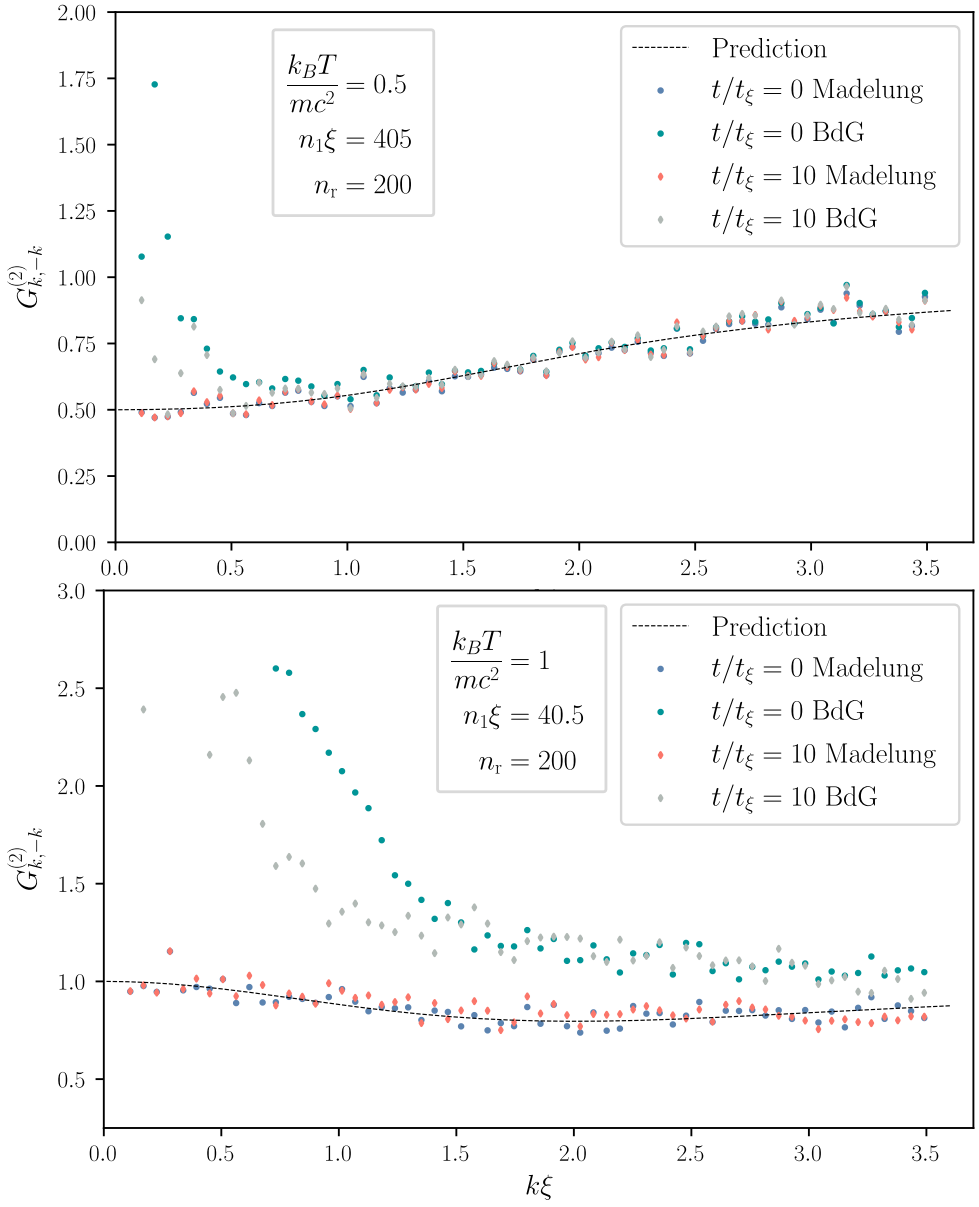

Figure 3.9: Density-density correlation (3.62) as a function of the wavenumber $k\xi$, for the Madelung and the BdG states, at two different times. The results of the numerical simulations are compared to the prediction (3.63) for a thermal state of phonons, where $n_k = n_k^{\rm th}$ and $c_k = 0$. As in Fig. 3.8, the two panels differ by the values of the temperature and density.

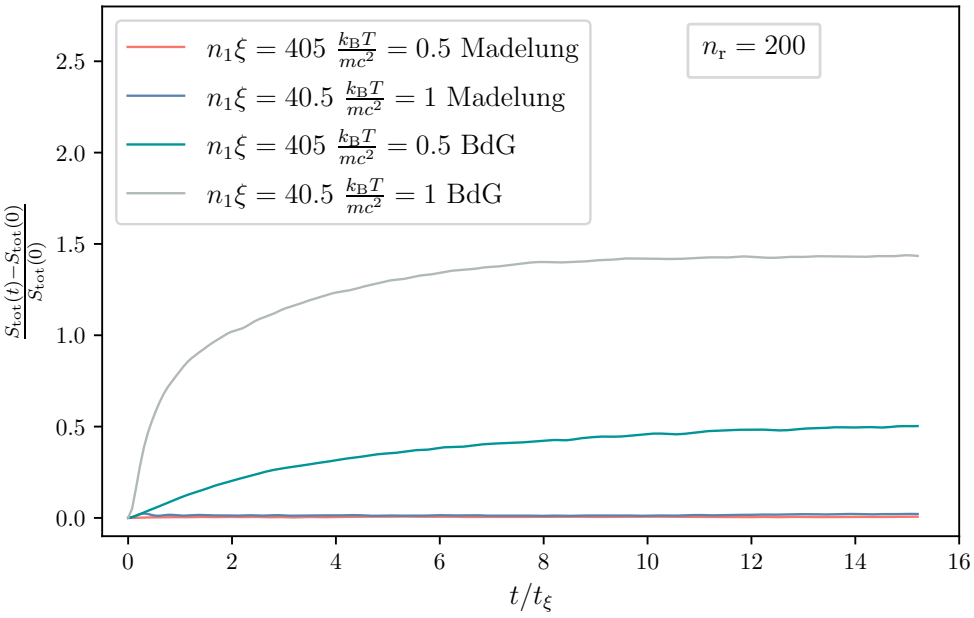

Figure 3.10: Gaussian approximation of the total entropy, given in Eq. (3.94), computed for the Madelung and the BdG states, as a function of time t/t_ξ.

compute the number of quasi-particles n_k and their correlation c_k. Thanks to this, we can directly manipulate the number of phonons in the system, allowing for the simulation series where we inject phonons in a precisely controlled manner. Third, we have implemented the duplication of realisations to visualise the effect of an external perturbation better. Finally, we eliminated several noise sources by identifying and removing spurious decay of UV modes.

3.6 Absence of entanglement during parametric resonance

In the analysis of the evolution of entanglement made in [132], the authors assumed that the pair-correlation c_k, and the particle numbers $n_{\pm k}$ decay at the same rate. Note that under this assumption, starting in a state where $|c_k| > n_k$, in the absence of an external drive, entanglement would *persist*. No pure decoherence process affects the correlation without changing the number of particles. Still, the authors found that, in the context of parametric resonance, a large enough rate $\Gamma_k/\omega_k \approx 4.2\%$ would prevent the appearance of an entangled state starting from a thermal state. Due to the simultaneity of parametric resonance and dissipation

processes, there seems to be a non-trivial effect preventing entanglement formation. Therefore, the growth rates of n_k and c_k are not simply reduced by the decay rate, as suggested by the form used in [4] when studying n_k alone. In [132], the authors assumed $\rho_0\xi = 0.6$ and $k_{\rm B}T/\hbar\omega_k = 1$ and in the conclusion of [4] we computed for these values that $\Gamma_k/\omega_k \approx 5\%$. We thus concluded that the Beliaev-Landau processes are sufficient to explain the absence of entanglement [130]. To draw this conclusion, we implicitly assumed that c_k would also decay at the rate Γ_k. The evolution of pair correlation is the topic of current investigations, and we close this chapter by briefly reporting on our latest findings.

3.6.1 Decay of correlations

In [4], we analysed the effects of Beliaev-Landau scattering processes on the number of quasi-particles $n_k = \langle \hat{b}_k^\dagger \hat{b}_k \rangle$. We derived an equation of motion for a small perturbation of the number of particles δn_k in the mode k. The strategy is to start from the full Heisenberg equation of motion of $\hat{b}_k$, given by Eq. (A1) of [4], and compute an equation of motion for n_k with and without perturbation. Under the assumption that the only relevant non-Gaussian connected correlation functions are $C^{(3)}_{p,q} = \langle \hat{b}_p^\dagger \hat{b}_q^\dagger \hat{b}_{p+q} \rangle$ we can write a system of differential equations over n_k and $C^{(3)}_{p,q}$. We re-expressed the latter as an integro-differential equation for δn_k, Eq. (19) of [4], which involves the perturbation of all modes δn_q. Finally, neglecting the inverse processes that partially restore the initial δn_k i.e. the terms in δn_q for $q \neq k$, we checked that our equation predicts the same decay rate as the Fermi Golden rule taken between two number states of quasi-particles.

Assume now that we excite quasi-particles in the modes $\pm k$ by an amount $\delta n_{\pm k}$, in a correlated fashion such that $\delta c_k = \langle \hat{b}_{-k} \hat{b}_k \rangle \neq 0$. We can repeat the same steps to derive equations of motion for $\delta n_{\pm k}$ and δc_k. The equation for δc_k features an extra non-Gaussian correlation function $D^{(3)}_{p,q} = \langle \hat{b}_p \hat{b}_q \hat{b}_{-p-q} \rangle$. Neglecting all other connected correlation functions, we find a system of coupled integro-differential equations over δn_k and δc_k. These equations also *a priori* features the whole spectrum of δn_q and δc_q. Nevertheless, an analysis of the magnitude of each term shows that those mixing δn_k and δc_k are sub-dominant; the dynamics of the number of phonons and their correlation are independent. δn_k still obeys Eq. (19) of [4], while δc_k obeys an equation of the same form with a different response function. Neglecting finite size effects and reverse processes, δn_k still decays at a rate Γ_k given by Eq. (17) of [4] that we repeat here

$$\Gamma_k t_\xi = \frac{k_{\rm B}T}{mc^2} \frac{1}{\rho_0 \xi} \left[f_- \left(k\xi \right) + f_+ \left(k\xi \right) \right] . \tag{3.95}$$

Finally, under the same assumptions, we find that $|\delta c_k|$ decays at the same rate Γ_k.

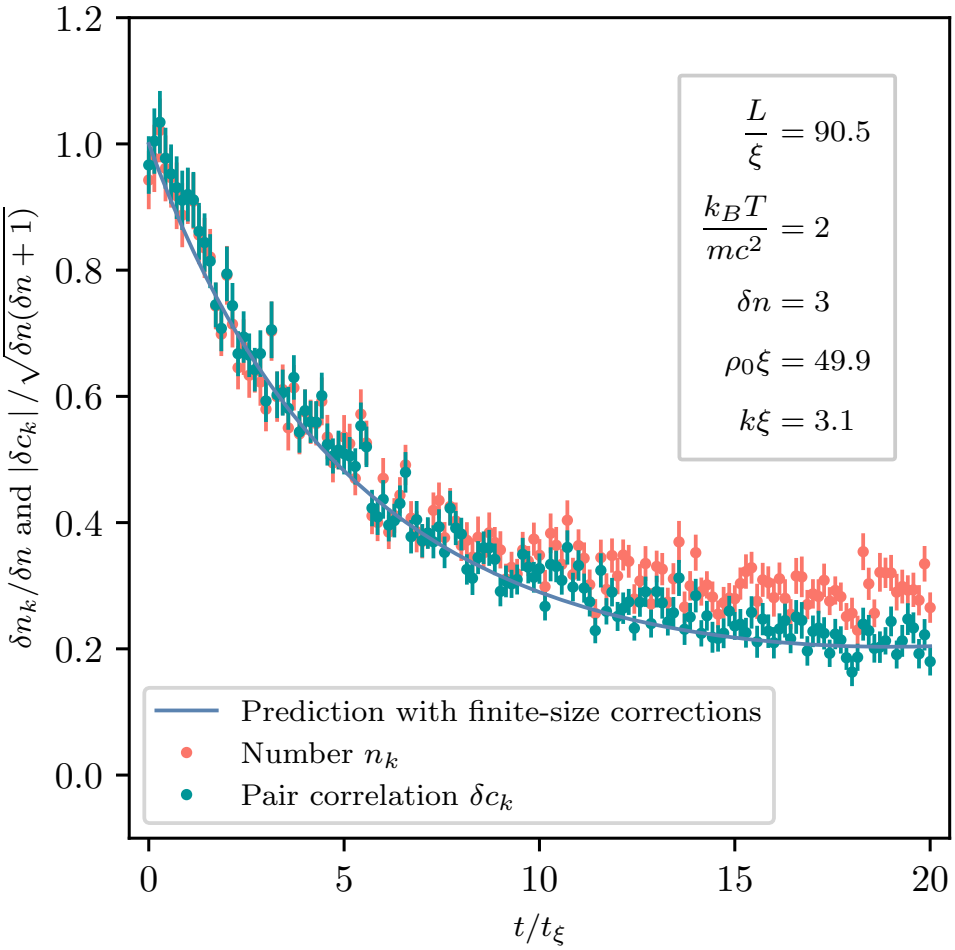

Figure 3.11: Evolution of the number of quasi-particles n_k in the modes $\pm k$ and of their pair correlation $|c_k|$, as a function of time. At the initial time, the modes' state is considered a TMSV with δn quasi-particles on average. The coloured dots shows the result of TWA simulations. The blue shows an exponential decay at a rate given by Eq. (3.95) (corrected for finite size-effect see Eq. (20) of [4]).

In Fig. 3.11, we show the evolution of $|\delta c_k|$ and δn_k from an initial TMSV. We normalised their values by their expected initial values $\delta n_k(0) = \delta n$ and $|\delta c_k|(0) = \sqrt{\delta n(\delta n + 1)}$. These two series are compared to the prediction of an exponential decay at rate Γ_k given by Eq. (3.95) (corrected for finite size-effect, see Eq. (20) of [4]) and we observe an excellent agreement, at least at early-times. The fact that correlation and number of particles decay at least at the same rate is physically reasonable: when a quasi-particle is lost in one of the modes $\pm k$, the pair-correlation c_k is lost. One could expect other pure decoherence processes to affect pair-correlation leaving the number of quasi-particles n_k unaffected. Indeed, we see signs of such processes at late times in Fig. 3.11. However, they are sub-dominant, and would only speed up the decoherence process. They are thus not expected to change our conclusion that the Beliaev-Landau dissipative processes are sufficient to explain the absence of entanglement.

In conclusion, our latest numerical and analytical analyses support the minimal assumptions of an equal dissipation for quasi-particle numbers and pair correlation made in [132]. With this extra piece of the puzzle, the claim of [4] that Beliaev-Landau scatterings are sufficient to explain the absence of entanglement in [130] is then adequately justified.

4 - Conclusion and perspectives

This PhD was dedicated to time-dependent situations relevant to cosmology that are described using quantum field theory in curved spacetimes. We studied the appearance and disappearance of quantum features in these contexts.

In the first part of this manuscript, we reported on our study of such quantum aspects in the cosmological perturbations, which are expected to have emerged from the quantum vacuum. Our goal was to assess the robustness of quantum features in the state of the perturbations to decoherence phenomena. To do so, we focused on the non-classicality of bi-partite correlation in the state of the cosmological perturbations, arguably the simplest manifestation of its quantum nature. We have measured the efficiency of decoherence on the cosmological perturbations using the quantum discord [2] and a GMKR-type Bell inequality [3]. We showed that these measures reveal a competition between decoherence and squeezing to determine the character (quantum or classical) of the bi-partite correlations between opposite Fourier modes. This phenomenon is already known for other criteria, e.g. separability or another Bell inequality [193, 153]. We systematically compared three such quantumness criteria in a context broader than that of cosmological perturbations [3]. Although they all qualitatively exhibit the competition between squeezing and decoherence, the precise threshold of classicality depends on the chosen measure. Finally, we tried to clarify and condense the discussions on this question in a review [1]. The precise decoherence level in the early Universe is still being determined. Therefore, we cannot yet assess definitively whether the correlations were already classical at the end of inflation. Nevertheless, a lower bound was recently obtained in [194].

As a continuation of the above programme and a direct application of the PhD results, we give a quick evaluation of the expected level of quantumness left at the end of inflation. The authors of [194] found that the purity of a mode $\boldsymbol{k}$ that crossed out the Hubble radius $N - N_\star$ e-folds before the end of inflation is given by

$$p_k = \frac{1}{\sqrt{1+\Xi_k}}\,, \tag{4.1}$$

where

$$\Xi_k = 1.6\times 10^4 \times \left(\frac{A_{\rm S}}{2.2\times 10^{-9}}\right)^{(} - 1) \left(\frac{E_\star}{M_{\rm Pl}c^2}\right)^8 e^{3(N-N_\star)}\,. \tag{4.2}$$

Although the exact number depends on the details of reheating and the energy scale of inflation, we expect that for modes corresponding to cosmological scales today $N - N_\star \geq 30$, so that the exponentially is typically dominant in the above

expression. The purity then scales as $p_k \propto e^{-3(N-N_\star)/2}$. To assess the entanglement of the state, we need to compare this number to the exponential of twice the squeezing parameter r [3]. Using the conventions of [2] for the conjugated momentum and taking the de Sitter limit, we have $r_k \sim 2(N - N_\star)$. Taking the ratio with the square root of the purity, we have $e^{2r}/\sqrt{p} \sim e^{13(N-N_\star)/4}$, which grows with $N - N_\star$. Thus, irrespective of the energy scale of inflation, if the mode crosses the Hubble radius early enough during inflation, the state of the pair $\pm\boldsymbol{k}$ will still be entangled at the end of inflation! A more precise illustration is given in Fig. 4.1, where we plotted the value of the quantum discord and the threshold of separability as a function of $N - N_\star$ and the energy scale of inflation $E_\star$. Fig. 4.1 shows that modes $\pm\boldsymbol{k}$ such that $N - N_\star \geq 30$, in particular cosmological scales, are still entangled at the end of inflation and have a large quantum discord. We thus observe that entanglement can persist despite an exponential suppression of the purity in the number of e-folds. This suppression led the authors of [194] to conclude that modes were all 'decohered' on cosmological scales. Nevertheless, the above shows the necessity to consider the competition between squeezing and decoherence to conclude on the classicalisation of the perturbations.

It is thus not obvious that by the end of inflation, the cosmological perturbations are in an entirely classical state. Since the quantum character of the perturbations might have persisted until the end of inflation, one may then want to ask whether it can be experimentally demonstrated. Except for the conclusion of Sec. 2.2, we did not deal with this question in the manuscript, and we say a few words about it now.

We believe that, in the context of single field slow-roll inflation, with a Gaussian state, the prospects of experimental demonstrating the quantum origin of the perturbations are scarce. First, in this scenario, there are only two fields that carry all information on the quantum state of the Universe, the Mukhanov-Sasaki field $\hat{v}$ and the tensor perturbations $\hat{h}$. Let us first discuss the scalar perturbations. In the single field scenario, where $\hat{v}$ is not substantially perturbed by other fields that would bear traces of its state, we only have access to n-point functions of $\hat{v}$ which are imprinted on CMB's photons via the Sachs-Wolfe effect [54]. However, in the Gaussian case, all correlation functions of $\hat{v}$, and its conjugated field (which we do not measure), can be reproduced to an excellent approximation by a classical stochastic process [1]. They are thus insufficient to demonstrate the quantum origin of the state. On the other hand, tensor perturbations have yet to be detected. Some authors have analysed the effect of a gravitational wave impinging on a gravitational interferometer [195, 196]. They showed that a squeezed state of the perturbations would induce noise in the detector akin to that of a Gaussian stochastic process. Therefore, a naive measure of the amplitude of these waves can only lead to an indirect proof of their quantum origin, as for scalar perturbations,

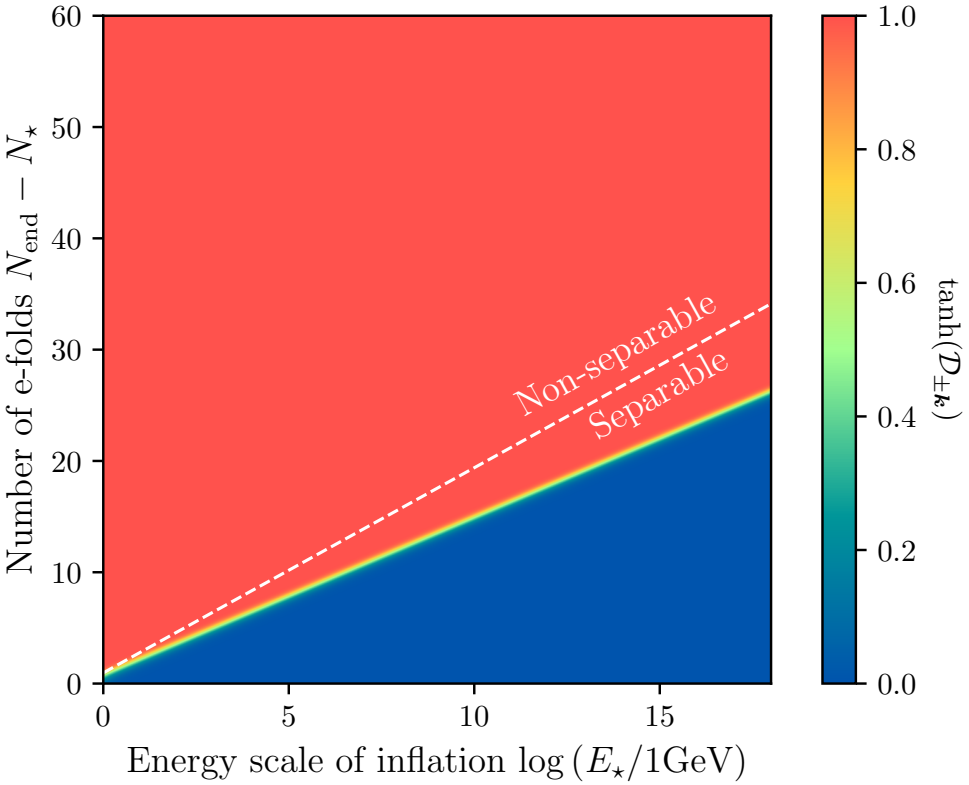

Figure 4.1: Hyperbolic tangent of the quantum discord $\tanh(\mathcal{D}_{\pm\boldsymbol{k}})$ of the correlation between modes $\pm\boldsymbol{k}$ as a function of the energy scale of inflation $E_\star$ and the number of e-folds from the time the modes crossed out the Hubble radius to the end of inflation $N - N_\star$. The white dashed line shows the separability threshold. We refer to [3] reproduced in Sec. 2.4 for details on these quantities. The quantum discord given in Eq. (2.28) of [2] for $\theta = -\pi/4$, depends on the squeezing parameter r and the purity p. The squeezing parameter is estimated using the de Sitter behaviour given in Eq. (5.6) of [2], while the purity is estimated using Eq. (4.1).

by measuring the k-dependence of their power-spectrum, see Sec. 1.2.3-d. Still, if we were to measure the noise of primordial gravitational waves in interferometers, then we would be measuring directly waves produced during inflation, as opposed to measuring CMB's photons, produced much later, in the case of scalar perturbations or B-mode detection, see Sec. 2.2. In principle, we can then access the complete state of these waves, and one could potentially design some intelligent measurement protocol to reveal their quantum nature, e.g. [197]. Unfortunately, this remaining window of opportunity might also be closed due to the smallness of the amplitude of the primordial gravitational waves. Even if the tensor to scalar ratio, see Sec. 1.2.3-d, is close to the current upper bound $r < 0.036$ at 95% [66], the waves would not be in the sensitivity of Big-Bang Observer (BBO), the most futuristic interferometer planned [198].

Before discussing possibilities to go beyond the current modelling, note that, in this work, we performed computations solely in Fourier space. Since each pair of modes $\pm\boldsymbol{k}$ is independent of the others, the only correlations to consider in Fourier space are between the two members of the pair. Nevertheless, it could be objected, see Sec. 2.2, that checking for a Bell inequality violation for non-local degrees of freedom is meaningless since the objects are not well separated. In addition, since the correlations in real space potentially depend on the state of *all* Fourier modes, one may hope to escape the no-go theorem on n-points functions of $\hat{v}$ and its conjugate field. Some authors have analysed how correlations in Fourier space manifest when correlating regions in real space [199, 200, 201]. Unfortunately, they found that, already in the absence of decoherence, Bell inequalities are never violated and that the quantum discord was very small, albeit non-vanishing.

With the work done in this PhD, we made a point that the presence of decoherence does not straightforwardly make the cosmological perturbations classical at the end of inflation. However, as long as the quantum features are concealed in operators for which no clear measurement protocol, even for a tabletop system, can be given, it could be seen as a moot point. Therefore, we believe that in the next studies, more attention should be given to operational approaches describing what could *actually* be measured. For instance, in the spirit of [202], it would be worth investigating whether some of the possible non-Gaussian signals can, under reasonable assumptions, not be attributed to a classical theory and how multi-partite [203] entanglement could manifest there.

In the other part of this PhD, we progressed on analysing the analogue preheating experiment [130]. We demonstrated the existence of scattering processes for quasi-particles of 1D quasi-condensate [4], addressing some claims to the contrary in parts of the literature. We improved a TWA simulation algorithm to study these processes, making it more precise and reliable.

A first continuation of this PhD work would be to quantitatively explain the

spectrum of phonons reported in [130]. Comparing these experimental results with the dissipation-less prediction of Fig. 3.5, we see a few differences. First, we predict two narrow and distinct peaks, while only a broad one was observed experimentally. Several things can be brought up to explain it. It could be that the two peaks are too close to be well resolved in the experiment. Additionally, although the modulation in our model is already not simply the sum of two oscillations, one associated with each peak, any supplementary noise in this modulation could affect the peak structure [181, 182, 183]. Finally, the peaks will also broaden due to the dissipation processes we identified. Therefore, they could appear as a single broad peak in the experimental data. Second, the number of phonons observed is much less than predicted. Again, the dissipation processes could provide a sufficient reduction to explain it. As a first estimation, we can compare the growth G_k and decay rate Γ_k expected for our resonant modes. Based on [132], and using the decay rate given in Eq. (17) of [4], for the values $c = 8$ mm/s, $k_{\mathrm{B}}T/mc^2 \approx 6.5$ and $n_{1\mathrm{D}}a_s \approx 0.19$ of [130] used in Fig. 3.5, we find $\Gamma_k/G_k \sim 15.6$ for the first resonant mode. In this regime, we expect the growth of the resonant modes to saturate and the final number of phonons to be strongly reduced with respect to that shown in Fig. 3.5. Nevertheless, the comparison should be done precisely at the level of the full spectrum.

A natural next step in the analysis is to use the TWA simulations to simulate the current experimental set-up's precise conditions and test whether our equations accounting for the dissipative effects, Eq. (19) of [4], allow us to predict the evolution of entanglement correctly. These equations should also be compared with the effective equations of motion used in [132] to understand the fine details of decoherence during the parametric amplification process. In this respect, the latest results shown in Fig. 3.11 indicate that decoherence channels are present in the system, even without parametric resonance. Note that, in this figure, the pair-correlation follows quite closely the predicted exponential decay, while the decay of the number of phons n_k seems to slow down. Our current understanding is that this slowing down is due to inverse processes, i.e. decay products recombining to the initial excitation. These inverse processes appear to be more efficient in regenerating the number of excitations n_k in the two modes $\pm k$ than their correlation c_k. This result still requires a finer analysis, but it would constitute a nice illustration of the fragility of quantum correlations compared to other quantities, such as the number of excitations. From a broader perspective, it would be interesting to investigate how general this decoherence mechanism via differentiated inverse process rate is. Is it a specific feature of the unusual decay process we studied, which involves many modes as decay products, or a general one?

In addition, the model still requires some improvements. We should consider the trapping of the gas that breaks periodic boundary conditions so that the nature

of the eigenmodes is altered. In particular, the notion of direction of the mode $\pm\boldsymbol{k}$ loses its meaning as it is reflected back and forth. It should then be analysed how our non-separability witnesses are affected by these changes in the mode structure. For instance, the quantity $\langle \hat{b}_{\boldsymbol{k}} \hat{b}^{\dagger}_{-\boldsymbol{k}} \rangle$, which encodes the mixes in between the two directions $\pm\boldsymbol{k}$ and was neglected in previous works, should be taken into account.

Finally, as a more long-term goal, following-up on [133], we would like to extend the analysis of the experiment to later times when it enters a very non-linear regime. Several other groups have studied, numerically and experimentally, this regime in similar set-ups, e.g. [148, 145, 146]. First, as done in [145, 146], we should be able to predict and experimentally observe the generation of secondaries in our system. Second, the authors [148] report the numerical observation of fragmentation of the initially coherent condensate in different incoherent regions of space due to the back-reaction of the amplified quantum fluctuations. It is unclear, but worth studying, if there are signatures of this fragmentation in the distribution of excitations in Fourier space beyond the mere decrease of the condensate occupation. If so, we might observe it using the TOF method used in the current set-up, making it possible to experimentally study the back-reaction from a quantum field on a classical one expected in preheating. A last question we wish to investigate is whether the initial bi-partite $\pm\boldsymbol{k}$ entanglement that is distilled to other degrees of freedom in the system can still be captured experimentally by analysing well-chosen quantities in this regime. As a first example, at early times, since the relevant Beliaev-Landau scattering processes only involve nearby modes, it may seem natural to believe that part of the entanglement is distilled to them. It is then an experimentally relevant question to know whether this distilled entanglement can be recovered in the Fourier analysis by simply correlating larger boxes i.e. larger than $\delta k \sim 2\pi/L$. More generically, it would be interesting to follow the distillation of entanglement from the two resonant modes to more, in a similar way that the number of excitations initially injected in the resonant modes can be tracked down. Nevertheless, the problem appears much more challenging. Indeed, while following which modes are excited or not only requires computing the 2-point function n_k, measuring the formation of muti-partite entanglement requires accessing higher order n-point function since c_k only encodes pair-correlation.

Appendices

A Geodesics and time dilation in FLRW

A.1 Geodesics in an expanding Universe

The Christoffel symbols of the metric (1.17) in spherical co-moving coordinates read

$$\Gamma^t_{rr} = \frac{\dot{a}a}{1-\mathcal{K}r^2}, \qquad \Gamma^t_{\theta\theta} = \dot{a}ar^2, \qquad \Gamma^t_{\phi\phi} = \dot{a}ar^2\sin^2\theta,$$
$$\Gamma^r_{tr} = \Gamma^\theta_{t\theta} = \Gamma^\phi_{t\phi} = H, \qquad \Gamma^r_{rr} = \frac{\mathcal{K}r}{1-\mathcal{K}r^2}, \qquad \Gamma^r_{\theta\theta} = -r\left(1-\mathcal{K}r^2\right),$$
$$\Gamma^r_{\phi\phi} = -r\left(1-\mathcal{K}r^2\right)\sin^2\theta, \quad \Gamma^\theta_{\theta r} = \Gamma^\phi_{\phi r} = \frac{1}{r}, \quad \Gamma^\theta_{\phi\phi} = -\sin\theta\cos\theta, \quad \Gamma^\phi_{\phi\theta} = -\frac{\sin\theta}{\cos\theta}.$$

We give the solution of the geodesic equation over the energy-momentum vector (1.16) for massive and massless particles. We consider geodesics that are purely radial at initial time $P^\theta = P^\phi = 0$, which can always be arranged by rotating the system of coordinates. The geodesic then remains radial at any time, and we find that as a function of cosmic time, its components read

$$P^t(t) = \frac{E(t)}{c} = mc\sqrt{1+\left[\frac{a_0}{a(t)}\right]^2 2\left(\frac{p_0}{mc}\right)^2}, \tag{4.3}$$
$$P^r(t) = \left[\frac{a_0}{a(t)}\right]^2 \frac{p_0}{a_0}\sqrt{1-\mathcal{K}r^2(t)}, \tag{4.4}$$

where p_0 is the physical 3-momentum at the present time. At an earlier time t we have $p = [a_0/a(t)]p_0$ i.e. the physical momentum decays with the expansion as a^{-1}. Notice that test bodies at rest in the co-moving coordinates, i.e. $p = 0$ at any time, follow spacetime's geodesics; they are said to be *co-moving*. For massless particles, in particular photons, we similarly have

$$P^t(t) = \frac{E(t)}{c} = \frac{a_0}{a}p_0\,, \tag{4.5}$$
$$P^r(t) = \left[\frac{a_0}{a(t)}\right]^2 \sqrt{1-\mathcal{K}r^2(t)}\frac{p_0}{a_0}\,. \tag{4.6}$$

In this case, the physical momentum and the energy evolve as a^{-1}. For photons, this translates into a redshift of their frequencies, see Sec. 1.1.2-b.

A.2 Time dilation in an expanding Universe

In a spacetime described by the metric (1.17), time duration as measured by observers at different times will differ. Consider an emitter E sending signals to a receptor R. We assume that E and R are co-moving observers $\underline{U}^{\mathrm{E/R}} = (c, 0, 0, 0)$. By redefining the co-moving coordinates, one can always arrange for E to be located at the coordinates' origin and R to be located at $(r_{\mathrm{R}}, 0, 0)$. Assume that E sends a first light signal from $(ct_{\mathrm{E}}, 0, 0, 0)$ received by R at $(ct_{\mathrm{R}}, r_{\mathrm{R}}, 0, 0)$, and then a second signal just after at $(ct_{\mathrm{E}} + c\delta t_{\mathrm{E}}, 0, 0, 0)$ which is received at $(ct_{\mathrm{R}} + c\delta t_{\mathrm{R}}, 0, 0, 0)$. The relation between the arrival time and the distance covered by these light signals is found by setting $\mathrm{d}^2 s = 0$ in Eq. (1.17). We find

$$r_{\mathrm{R}} = c \int_{t_{\mathrm{E}}}^{t_{\mathrm{R}}} \frac{\mathrm{d}t'}{a(t')} = c \int_{t_{\mathrm{E}}+\delta t_{\mathrm{E}}}^{t_{\mathrm{R}}+\delta t_{\mathrm{R}}} \frac{\mathrm{d}t'}{a(t')} \,. \tag{4.7}$$

By taking the difference between these last two relations and exploiting the infinitesimal character of the time intervals, we find

$$\delta t_{\mathrm{R}} = \frac{a\left(t_{\mathrm{R}}\right)}{a\left(t_{\mathrm{E}}\right)} \delta t_{\mathrm{E}} \,, \tag{4.8}$$

assuming that the scale factor increases with cosmic time, there is a time dilation $\delta t_{\mathrm{R}} > \delta t_{\mathrm{E}}$. In particular, assuming that E sends a continuous monochromatic light signal to R and taking δt_{E} to be the interval in between two crests of the light signals i.e. the period of the signal, then the above relation gives the same relation as Eq. (1.20) for the redshift of the signal. This time dilation can then be understood as the physical reason behind the redshift derived from the machinery of null geodesics.

B Stress-energy tensor and R^2 inflation

B.1 Stress-energy tensor of a scalar field

We first derive Jacobi's formula for the variation of the determinant of a matrix with respect to one of its coordinates. We have

$$g = \sum_{\mu_1,\ldots,\mu_n} \epsilon_{\mu_1,\ldots,\mu_n} g_{1\mu_1} \ldots g_{n\mu_n} \,, \tag{4.9}$$

where $\epsilon_{\mu_1,\ldots,\mu_n}$ is the Levi-Civita tensor in n-dimensions. Notice that one cannot forget about the sum by putting the indices up. It would imply having the coefficient of the inverse of metric, which would be wrong. Using the formula (4.9), we

have

$$\omega^{\alpha\beta} = \frac{\delta g}{\delta g_{\alpha\beta}} = \sum_s \sum_{\mu_1,\ldots,\mu_{s-1},\mu_{s+1},\ldots,\mu_n} \epsilon_{\mu_1,\ldots,\mu_n} g_{1\mu_1}\cdots g_{s-1\mu_{s-1}} \delta^{\alpha}{}_{s} \delta^{\beta}{}_{\mu_s} g_{s+1\mu_{s+1}}\cdots g_{n\mu_n} \tag{4.10}$$

Then one can check that $\omega^{\alpha\beta} g_{\beta\gamma} = g\delta^{\alpha}{}_{\gamma}$ and we get Jacobi's formula

$$\frac{\delta g}{\delta g_{\alpha\beta}} g g^{\alpha\beta} \,. \tag{4.11}$$

Now using that $g^{\alpha\beta} g_{\beta\gamma} = \delta^{\alpha}{}_{\gamma}$ we get

$$\delta g_{\mu\nu} = -g_{\mu\alpha} g_{\nu\beta} \delta g^{\alpha\beta} \,. \tag{4.12}$$

Combining the above

$$T_{\mu\nu} = L_{\rm m} g_{\mu\nu} - 2\frac{\delta L_{\rm m}}{\delta g^{\mu\nu}} \,. \tag{4.13}$$

For the scalar field action, this gives Eq. (1.67).

B.2 Slow-roll at first-order in R^2-inflation

In this appendix, we analyse briefly the case of slow-roll R^2 inflation.

B.2-a A potential for R^2 inflation.

This model was originally introduced by Starobinsky in [38] by considering a modification to Einstein-Hilbert action due to quantum corrections. The relevant piece reads

$$S_{R^2} = \frac{1}{2\kappa c} \int \sqrt{-g} \left(R + \frac{\hbar^2}{6m^2c^2} R^2 \right) \mathrm{d}^4\boldsymbol{x} \,, \tag{4.14}$$

where m is a mass scale. The usual Einstein-Hilbert action only has two degrees of freedom; the two polarisations of the gravitons, see Sec. 2.2. The theory described by the action (4.14) has, in fact, an extra scalar degree of freedom. This action can be recast as Einstein-Hilbert action plus an action for a scalar field ϕ [204]. We first introduce an auxiliary field χ with the action

$$S'_{R^2} = \frac{1}{2\kappa c} \int \sqrt{-g} \left(R + \frac{\hbar^2}{3m^2c^2} \chi R - \frac{\hbar^2}{6m^2c^2} \chi^2 \right) \mathrm{d}^4\boldsymbol{x} \,. \tag{4.15}$$

The Euler-Lagrange equation for χ gives $\chi = R$ so that the equations of motion are the same as that of Eq. (4.14). By re-parameterising the scalar field via $\varphi = 1 + \frac{\hbar^2}{3m^2c^2}\chi$ the action reads

$$S'_{R^2} = \frac{1}{2\kappa c} \int \sqrt{-g} \left[\varphi R - \frac{3m^2c^2}{2\hbar^2} (\varphi - 1)^2 \right] \mathrm{d}^4\boldsymbol{x} \,. \tag{4.16}$$

This action is a sub-case of Brans-Dicke's theory of gravity. Under a conformal transformation of the metric $g = \Omega^2 \tilde{g}$ the action transforms to

$$S'_{R^2} = \frac{1}{2\kappa c} \int \sqrt{-\tilde{g}} \left[\Omega^2 \varphi \left(\tilde{R} - 6\Omega^{-1} \tilde{\Box} \Omega \right) - \Omega^4 \frac{3m^2c^2}{2\hbar^2} (\varphi - 1)^2 \right] \mathrm{d}^4 \boldsymbol{x} \,. \tag{4.17}$$

To cast the gravitational part of the action in the Einstein-Hilbert form, we pick $\Omega^2 \varphi = 1$, or $\Omega = \varphi^{-1/2}$, and reparameterise $\varphi = \exp\left(\sqrt{\frac{2}{3}}\sqrt{\kappa}\phi\right)$. Then

$$6\Omega^{-1}\tilde{\Box}\Omega = 2\kappa \frac{1}{2} \partial_\mu \phi \partial_\nu \phi - \sqrt{\frac{6\kappa}{2}} \partial_\mu \partial_\nu \phi \,, \tag{4.18}$$

and dropping the boundary term in the action, we finally get

$$S'_{R^2} = \frac{1}{2\kappa c} \int \sqrt{-\tilde{g}}\, \tilde{R} \mathrm{d}^4 \boldsymbol{x} - \frac{1}{c} \int \sqrt{-\tilde{g}} \left[\frac{1}{2} \partial_\mu \phi \partial_\nu \phi + V_{\mathrm{S}}(\phi) \right] \mathrm{d}^4 \boldsymbol{x} \,, \tag{4.19}$$

where the potential V_{S} is defined in Eq. (1.82). The actions given by Eq. (4.14) and Eq. (4.19) are equivalent. The latter form is that of a scalar field minimally coupled to general relativity, which corresponds to the form used in Sec. 1.2.2. This form makes manifest the presence of an extra scalar degree of freedom compared to the Einstein-Hilbert action.

B.2-b Slow-roll

We now derive the equation of evolution of the field in the first-order in slow-roll parameters. It is useful first to rewrite the equations of motion using N, the number of e-folds, as a time variable rather than cosmic time. The Klein-Gordon equation can be recast has

$$\frac{\mathrm{d}^2\phi}{\mathrm{d}N^2} + (3 - \epsilon_1) \frac{\mathrm{d}\phi}{\mathrm{d}N} + \frac{V'(\phi)c^2}{H^2} = 0 \,. \tag{4.20}$$

The second slow-roll parameter then assumes the simple form

$$\epsilon_2 = 2 \left(\frac{\mathrm{d}\phi}{\mathrm{d}N} \right)^{-1} \frac{\mathrm{d}^2\phi}{\mathrm{d}N^2} \,, \tag{4.21}$$

which in turn allows us to rewrite the Klein-Gordon equation as

$$\left(3 - \epsilon_1 + \frac{\epsilon_2}{2}\right) \frac{\mathrm{d}\phi}{\mathrm{d}N} + \frac{V'(\phi)c^2}{H^2} = 0 \,. \tag{4.22}$$

Under this form, it is clear that neglecting the two first slow-roll parameters, we have

$$\frac{\mathrm{d}\phi}{\mathrm{d}N} \approx -\frac{V'(\phi)c^2}{3H^2} \approx -\frac{1}{\kappa}\frac{V'}{V} \,, \tag{4.23}$$

where we used Eq. (1.80) in the second equality. The expression of the first flow function in the slow-roll regime (1.79) shows that the first slow-roll condition $\epsilon \ll 1$, imposes to be in the large-field regime $\sqrt{k}\,\phi$. In this limit, defining the number of e-folds to be 0 at the start of inflation $N = \ln(a_{\rm in}/a)$ and the initial value of the field to be $\phi_{\rm in}$, the equation of motion is easily integrated to Eq. (1.83). We can then express $\dot{\phi}$, ϵ_1 and H as a function of the number of e-folds

$$\dot{\phi}(N) = -\frac{mc^2\sqrt{\kappa}}{4\hbar}\sqrt{\frac{3}{8}}\frac{1}{N_e - N}\,, \tag{4.24a}$$

$$\epsilon_1(N) = \frac{3}{4}\frac{1}{\left(N_e - N - \frac{3}{4}\right)^2}\,, \tag{4.24b}$$

$$H(N) = \frac{mc^2}{2\hbar}\left(1 - \frac{3}{4}\frac{1}{N_e - N}\right)\,. \tag{4.24c}$$

Recasting the equation for $\dot{\phi}$ we get the expression of the slow-roll trajectory in the $\left(\phi, \dot{\phi}\right)$-plane

$$\dot{\phi} = -\frac{mc^2\sqrt{\kappa}}{\hbar}\sqrt{\frac{2}{3}}e^{-\sqrt{\frac{2}{3}}\sqrt{\kappa}\phi}\,, \tag{4.25}$$

which is plotted in Fig. 1.5. Solving for $\epsilon_1(N) = 1$ we find that inflation lasts roughly $N_e - N - \frac{3}{4} - \sqrt{\frac{3}{4}}$.

C Perturbations of a 1D weakly interacting Bose gas

C.1 Canonical transformation for relative perturbations

For an Hamiltonian system with Hamiltonian H described by a conjugated pair (p, q)

$$\{p, q\} = 1\,, \tag{4.26}$$

a generating function is a function that generates a canonical transformation to another conjugated pair of variables (P, Q) :

$$\{P, Q\} = 1\,. \tag{4.27}$$

Hamilton's equations also describe the time evolution of the new pair but with respect to a possibly new Hamiltonian K computed from the generating function. If the transformation is time-independent, then $H = K$. A type-2 generating

function F_2 depends on the old position q and the new momentum P and gives the transformation laws

$$Q = \frac{\partial F_2}{\partial P}\,, \tag{4.28}$$

$$p = \frac{\partial F_2}{\partial q}\,, \tag{4.29}$$

and

$$K = H + \frac{\partial F_2}{\partial t}\,. \tag{4.30}$$

We want to use this formalism to describe the relative perturbations defined in sub-section Sec. 3.3.2-b. We consider a classical version of the system, where the atomic field Ψ is a complex function. We want to write a generating function for the transformation $\psi \to e^{-i\mu t/\hbar}\psi$, where we defined $\psi = \sqrt{n_0}\delta\hat{\Psi}$ to shorten the notations in this appendix. The canonical pair used to describe the system is initially $(\psi, i\hbar\psi^\star)$ (the additional factor of $i\hbar$ appears in the classical counterpart theory), and the final one $(\psi', i\hbar\psi^{\star\prime}) = (e^{-i\mu t/\hbar}\psi, i\hbar e^{i\mu t/\hbar}\psi^\star)$. Notice that we have one degree of freedom at each position $\boldsymbol{x}$, so implicitly, we perform the canonical transformation separately for each point. If we define the following type-2 generating function

$$F_2\left(\psi, \psi^{\star\prime}, t\right) = e^{-i\mu t/\hbar} i\hbar\psi^{\star\prime}\psi\,, \tag{4.31}$$

the associated equations of transformation are

$$\psi' = \frac{\partial F_2}{\partial i\hbar\psi^{\dagger\prime}} = e^{i\mu t}\psi\,, \tag{4.32}$$

$$i\hbar\Psi^\dagger = \frac{\partial F_2}{\partial \psi} = e^{i\mu t} i\hbar\psi^{\dagger\prime}\,, \tag{4.33}$$

which are equivalent to a $\psi \to e^{-i\mu t/\hbar}\psi$. Therefore, F_2 given by Eq. (4.31) is a generating function for the transformation we want to perform and the Hamiltonian density for the new variable is given by

$$K(x) = H(x) + \frac{\partial F_2}{\partial t} = H(x) + e^{i\mu t/\hbar}\frac{\partial e^{-i\mu t/\hbar}}{\partial t} i\hbar\psi^\star\psi\,. \tag{4.34}$$

Starting from Eq. (3.15) and expanding at second order in $\delta\hat{\Psi}$ we get

$$\begin{aligned}\hat{H}^{(2)} = \int \mathrm{d}\boldsymbol{x} \Bigg[|\Psi_0|^2 \frac{\hbar^2}{2m}\frac{\partial\delta\hat{\Psi}^\dagger}{\partial z}\frac{\partial\delta\hat{\Psi}}{\partial z} + \left(\frac{\hbar^2}{2m}\left|\frac{\partial\Psi_0}{\partial r}\right|^2 + \frac{1}{2}\omega_\perp^2 r^2 |\Psi_0|^2 + g|\Psi_0|^4\right)\delta\hat{\Psi}^\dagger\delta\hat{\Psi} \\ + g|\Psi_0|^4\hat{\Psi}^\dagger\delta\hat{\Psi} + \frac{g}{2}|\Psi_0|^4\left(\delta\hat{\Psi}^{\dagger\,2} + \delta\hat{\Psi}^2\right)\Bigg]\,,\end{aligned} \tag{4.35}$$

where, in the second term, we have isolated a combination of terms corresponding to the right-hand side of the GPE, Eq. (3.17). Performing the transformation, Eq. (4.34) cancels this term. The remaining Hamiltonian is integrated over r and θ to give Eq. (3.31), where we have reused the name $\hat{H}^{(2)}$ for this modified Hamiltonian in the main text.

Bibliography

[1] Amaury Micheli and Patrick Peter. Quantum cosmological gravitational waves?, November 2022. [Cited in Structure, 1.2.3-b, 1.2.3-d, 2.1, 2.2, 2.3, 2.4, 3.3.2-d, 3.3.3-a, 3.3.3-c, 3.5.1-b, 4, and 4]

[2] Jérôme Martin, Amaury Micheli, and Vincent Vennin. Discord and decoherence. *Journal of Cosmology and Astroparticle Physics*, 2022(04):051, April 2022. [Cited in Structure, 2.1, 2.2, 2.3, 4, 4, and 4.1]

[3] Jérôme Martin, Amaury Micheli, and Vincent Vennin. Comparing quantumness criteria. *Europhysics Letters*, 142(1):18001, April 2023. [Cited in Structure, 2.1, 2.2, 2.3, 2.4, 3.5.2-e, 4, 4, and 4.1]

[4] Amaury Micheli and Scott Robertson. Phonon decay in one-dimensional atomic Bose quasicondensates via Beliaev-Landau damping. *Physical Review B*, 106(21):214528, December 2022. [Cited in Structure, 1.2.4-a, 3.1, 3.3.2-d, 3.3.4-a, 3.3.4-b, 3.3.4-c, 3.3.4-c, 3.3.4-c, 3.5, 3.6, 3.5.1-a, 3.5.1-b, 3.5.1-b, 3.5.1-b, 3.5.1-d, 3.5.1-d, 3.5.2-c, 3.5.2-d, 3.5.2-e, 3.5.2-f, 3.5.3, 3.5.3-a, 3.6, 3.6.1, 3.11, 3.6.1, and 4]

[5] Steven Weinberg. *Cosmology*. Oxford University Press, Oxford ; New York, 2008. [Cited in 1.1, 1.1.1, 1.1.1, 1.1.1, 1.1.2-a, 1.1.2-b, 1.1.2-d, and 1.1.3-b]

[6] Daniel Baumann. *Cosmology*. Cambridge University Press, 1 edition, June 2022. [Cited in 1.1, 1.1.1, 1.1.1, 1, 1.1.1, 1.1, 1.1.2-c, 1.1.2-d, 4, 1.1.3-b, 1.1.3-b, 1.1.3-b, 7, 1.1.4-a, 1.2.2-b, and 1.2.3-d]

[7] Albert Einstein. Die Feldgleichungen der Gravitation. *Sitzungsberichte der Königlich Preussischen Akademie der Wissenschaften*, pages 844–847, January 1915. [Cited in 1.1.1]

[8] Steven Weinberg. *Gravitation and Cosmology: Principles and Applications of the General Theory of Relativity*. Wiley, New York, 1972. [Cited in 1.1.1 and 1.1.2-a]

[9] Masanori Iye, Kazuaki Ota, Nobunari Kashikawa, et al. A galaxy at a redshift z = 6.96. *Nature*, 443(7108):186–188, September 2006. [Cited in 1.1.2-b]

[10] Planck Collaboration, P. A. R. Ade, N. Aghanim, et al. Planck 2013 results. XVI. Cosmological parameters. *Astronomy & Astrophysics*, 571:A16, November 2014. [Cited in 1.1 and 1.1.3-c]

[11] Planck Collaboration, N. Aghanim, Y. Akrami, et al. Planck 2018 results. VI. Cosmological parameters. *Astronomy & Astrophysics*, 641:A6, September 2020. [Cited in 1.1, 1.2, 1.1.3-a, and 1.2.3-e]

[12] G. Lemaître. Un Univers homogène de masse constante et de rayon croissant rendant compte de la vitesse radiale des nébuleuses extra-galactiques. *Annales de la Société Scientifique de Bruxelles*, 47:49–59, January 1927. [Cited in 1.1.2-b and 1.1.3-c]

[13] Edwin Hubble. A relation between distance and radial velocity among extra-galactic nebulae. *Proceedings of the National Academy of Sciences*, 15(3):168–173, March 1929. [Cited in 1.1.2-b and 1.1.3-c]

[14] D. J. Fixsen. The Temperature of the Cosmic Microwave Background. *The Astrophysical Journal*, 707(2):916–920, December 2009. [Cited in 1.2, 1.1.3-c, 1.3, and 1.3.1]

[15] Howard Georgi and S. L. Glashow. Unity of All Elementary-Particle Forces. *Physical Review Letters*, 32(8):438–441, February 1974. [Cited in 1.1.3-b]

[16] Cyril Pitrou, Alain Coc, Jean-Philippe Uzan, and Elisabeth Vangioni. Precision big bang nucleosynthesis with improved Helium-4 predictions. *Physics Reports*, 754:1–66, September 2018. [Cited in 1.1.3-b and 1.1.3-c]

[17] R. A. Alpher, H. Bethe, and G. Gamow. The Origin of Chemical Elements. *Physical Review*, 73(7):803–804, April 1948. [Cited in 1.1.3-b]

[18] R. H. Dicke, P. J. E. Peebles, P. G. Roll, and D. T. Wilkinson. Cosmic Black-Body Radiation. *The Astrophysical Journal*, 142:414, July 1965. [Cited in 1.1.3-c]

[19] A. A. Penzias and R. W. Wilson. A Measurement of Excess Antenna Temperature at 4080 Mc/s. *The Astrophysical Journal*, 142:419, July 1965. [Cited in 1.1.3-c]

[20] Gianfranco Bertone, Dan Hooper, and Joseph Silk. Particle Dark Matter: Evidence, Candidates and Constraints. *Physics Reports*, 405(5-6):279–390, January 2005. [Cited in 1.1.3-c]

[21] Adam G. Riess, Alexei V. Filippenko, Peter Challis, et al. Observational Evidence from Supernovae for an Accelerating Universe and a Cosmological Constant. *The Astronomical Journal*, 116(3):1009–1038, September 1998. [Cited in 1.1.3-c]

[22] S. Perlmutter, G. Aldering, G. Goldhaber, et al. Measurements of Omega and Lambda from 42 High-Redshift Supernovae. *The Astrophysical Journal*, 517(2):565–586, June 1999. [Cited in 1.1.3-c]

[23] Alan H. Guth. Inflationary universe: A possible solution to the horizon and flatness problems. *Physical Review D*, 23(2):347–356, January 1981. [Cited in 1.1.3-c, 1.1.4-b, 1.2, and 1.2.1-c]

[24] G. F. Smoot, C. L. Bennett, A. Kogut, et al. Structure in the COBE differential microwave radiometer first-year maps. *The Astrophysical Journal*, 396:L1, September 1992. [Cited in 1.1.4-a, 1.3, and 1.3.1]

[25] Ya.B. Zeldovich and M.Yu. Khlopov. On the concentration of relic magnetic monopoles in the universe. *Physics Letters B*, 79(3):239–241, November 1978. [Cited in 1.1.4-c]

[26] John P. Preskill. Cosmological Production of Superheavy Magnetic Monopoles. *Physical Review Letters*, 43(19):1365–1368, November 1979. [Cited in 1.1.4-c]

[27] Alan H. Guth and S. H. H. Tye. Phase Transitions and Magnetic Monopole Production in the Very Early Universe. *Physical Review Letters*, 44(10):631–635, March 1980. [Cited in 1.1.4-c]

[28] Martin B. Einhorn, D. L. Stein, and Doug Toussaint. Are grand unified theories compatible with standard cosmology? *Physical Review D*, 21(12):3295–3298, June 1980. [Cited in 1.1.4-c]

[29] Hunmoo Jeon and Michael J. Longo. Search for Magnetic Monopoles Trapped in Matter. *Physical Review Letters*, 75(8):1443–1446, August 1995. [Cited in 1.1.4-c]

[30] Particle Data Group, R L Workman, V D Burkert, et al. Review of Particle Physics. *Progress of Theoretical and Experimental Physics*, 2022(8):083C01, August 2022. [Cited in 1.1.4-c]

[31] Planck Collaboration, R. Adam, P. A. R. Ade, et al. *Planck* 2015 results: I. Overview of products and scientific results. *Astronomy & Astrophysics*, 594:A1, October 2016. [Cited in 1.3 and 1.2.3]

[32] A. D. Linde. A new inflationary universe scenario: A possible solution of the horizon, flatness, homogeneity, isotropy and primordial monopole problems. *Physics Letters B*, 108(6):389–393, February 1982. [Cited in 1.2 and 1.2.2]

[33] Andreas Albrecht and Paul J. Steinhardt. Cosmology for Grand Unified Theories with Radiatively Induced Symmetry Breaking. *Physical Review Letters*, 48(17):1220–1223, April 1982. [Cited in 1.2 and 1.2.2]

[34] Jinn-Ouk Gong. Multi-field inflation and cosmological perturbations. *International Journal of Modern Physics D*, 26(01):1740003, January 2017. [Cited in 1.2.2]

[35] Oskar Klein. Quantentheorie und fünfdimensionale Relativitätstheorie. *Zeitschrift für Physik*, 37(12):895–906, December 1926. [Cited in 1.2.2-a]

[36] W. Gordon. Der Comptoneffekt nach der Schrödingerschen Theorie. *Zeitschrift für Physik*, 40(1-2):117–133, January 1926. [Cited in 1.2.2-a]

[37] Andrew R. Liddle, Paul Parsons, and John D. Barrow. Formalizing the slow-roll approximation in inflation. *Physical Review D*, 50(12):7222–7232, December 1994. [Cited in 1.2.2-b]

[38] Alexei A. Starobinsky. A New Type of Isotropic Cosmological Models Without Singularity. *Phys. Lett. B*, 91:99–102, 1980. [Cited in 1.2.2-b, 1.2.3, and B.2-a]

[39] Jérôme Martin, Christophe Ringeval, and Vincent Vennin. Encyclopædia Inflationaris. *Physics of the Dark Universe*, 5–6:75–235, December 2014. [Cited in 1.2.2-b, 10, and 1.2.3-e]

[40] William E. East, Matthew Kleban, Andrei Linde, and Leonardo Senatore. Beginning inflation in an inhomogeneous universe. *Journal of Cosmology and Astroparticle Physics*, 2016(09):010–010, September 2016. [Cited in 1.2.2-b]

[41] Katy Clough, Eugene A. Lim, Brandon S. DiNunno, et al. Robustness of Inflation to Inhomogeneous Initial Conditions. *Journal of Cosmology and Astroparticle Physics*, 2017(09):025–025, September 2017. [Cited in 1.2.2-b]

[42] Katy Clough, Raphael Flauger, and Eugene A. Lim. Robustness of Inflation to Large Tensor Perturbations. *Journal of Cosmology and Astroparticle Physics*, 2018(05):065–065, May 2018. [Cited in 1.2.2-b]

[43] Josu C. Aurrekoetxea, Katy Clough, Raphael Flauger, and Eugene A. Lim. The Effects of Potential Shape on Inhomogeneous Inflation. *Journal of Cosmology and Astroparticle Physics*, 2020(05):030–030, May 2020. [Cited in 1.2.2-b]

[44] Jolyon K. Bloomfield, Patrick Fitzpatrick, Kiriakos Hilbert, and David I. Kaiser. A Bumpy Start to a Smooth Ride: Onset of Inflation amid Backreaction from Inhomogeneities. *Physical Review D*, 100(6):063512, September 2019. [Cited in 1.2.2-b]

[45] David Garfinkle, Anna Ijjas, and Paul J. Steinhardt. Initial conditions problem in cosmological inflation revisited. *Physics Letters B*, 843:138028, August 2023. [Cited in 1.2.2-b]

[46] Robert Brandenberger. Initial conditions for inflation — A short review. *International Journal of Modern Physics D*, 26(01):1740002, January 2017. [Cited in 1.2.2-b]

[47] V. F. Mukhanov and G. V. Chibisov. Quantum fluctuations and a nonsingular universe. *ZhETF Pisma Redaktsiiu*, 33:549–553, May 1981. [Cited in 1.2.3 and 1.2.3-b]

[48] V. F. Mukhanov and G. V. Chibisov. Energy of vacuum and the large-scale structure of the universe. *Zhurnal Eksperimentalnoi i Teoreticheskoi Fiziki*, 83:475–487, August 1982. [Cited in 1.2.3]

[49] S.W. Hawking. The development of irregularities in a single bubble inflationary universe. *Physics Letters B*, 115(4):295–297, September 1982. [Cited in 1.2.3]

[50] A.A. Starobinsky. Dynamics of phase transition in the new inflationary universe scenario and generation of perturbations. *Physics Letters B*, 117(3-4):175–178, November 1982. [Cited in 1.2.3]

[51] Alan H. Guth and So-Young Pi. Fluctuations in the New Inflationary Universe. *Physical Review Letters*, 49(15):1110–1113, October 1982. [Cited in 1.2.3]

[52] James M. Bardeen, Paul J. Steinhardt, and Michael S. Turner. Spontaneous creation of almost scale-free density perturbations in an inflationary universe. *Physical Review D*, 28(4):679–693, August 1983. [Cited in 1.2.3 and 1.2.3-b]

[53] V.A. Rubakov, M.V. Sazhin, and A.V. Veryaskin. Graviton creation in the inflationary universe and the grand unification scale. *Physics Letters B*, 115(3):189–192, September 1982. [Cited in 1.2.3]

[54] R. K. Sachs and A. M. Wolfe. Perturbations of a Cosmological Model and Angular Variations of the Microwave Background. *The Astrophysical Journal*, 147:73, January 1967. [Cited in 1.2.3, 1.2.3-b, 1.2.3-d, and 4]

[55] V Mukhanov, R. Brandenberger, and H.A. Feldman. Theory of cosmological perturbations. *Physics Reports*, 215(5-6):203–333, June 1992. [Cited in 1.2.3-a, 1.2.3-a, 1.2.3-b, 1.2.3-b, 1.2.3-b, 1.2.3-b, 9, and 1.2.3-e]

[56] Michele Maggiore. *Gravitational Waves. Vol. 2: Astrophysics and Cosmology*. Oxford University Press, March 2018. [Cited in 1.2.3-a and 1.2.3-a]

[57] Daniel Baumann. TASI Lectures on Inflation, November 2012. [Cited in 1.2.3-a and 1.2.3-a]

[58] L. P. Grishchuk. Cosmological rotation of quantum-mechanical origin and anisotropy of the microwave background. *Physical Review D*, 48(12):5581–5593, December 1993. [Cited in 1.2.3-a]

[59] James M. Bardeen. Gauge-invariant cosmological perturbations. *Physical Review D*, 22(8):1882–1905, October 1980. [Cited in 1.2.3-b]

[60] Hideo Kodama and Misao Sasaki. Cosmological Perturbation Theory. *Progress of Theoretical Physics Supplement*, 78:1–166, 1984. [Cited in 1.2.3-b]

[61] Jérôme Martin and Dominik J. Schwarz. The influence of cosmological transitions on the evolution of density perturbations. *Physical Review D*, 57(6):3302–3316, March 1998. [Cited in 1.2.3-b]

[62] Jerome Martin. Inflationary Cosmological Perturbations of Quantum-Mechanical Origin. In Kowalski-Glikman and Giovanni Amelino-Camelia, editors, *Planck Scale Effects in Astrophysics and Cosmology*, volume 669, pages 199–244. Springer-Verlag, Berlin/Heidelberg, 2005. [Cited in 1.2.3-c and 1.2.3-d]

[63] L. P. Grishchuk and Jérôme Martin. Best Unbiased Estimates for the Microwave Background Anisotropies. *Physical Review D*, 56(4):1924–1938, August 1997. [Cited in 1.2.3-d and 1.2.3-d]

[64] Planck Collaboration, Y. Akrami, F. Arroja, et al. *Planck* 2018 results: IX. Constraints on primordial non-Gaussianity. *Astronomy & Astrophysics*, 641:A9, September 2020. [Cited in 1.2.3-d and 1.2.3-e]

[65] T. S. Bunch and P. C. W. Davies. Quantum field theory in de Sitter space: Renormalization by point-splitting. *Proceedings of the Royal Society of London. A. Mathematical and Physical Sciences*, 360(1700):117–134, March 1978. [Cited in 1.2.3-d]

[66] BICEP/Keck Collaboration, P. A. R. Ade, Z. Ahmed, et al. BICEP / Keck XIII: Improved Constraints on Primordial Gravitational Waves using Planck, WMAP, and BICEP/Keck Observations through the 2018 Observing Season. *Physical Review Letters*, 127(15):151301, October 2021. [Cited in 1.2.3-e and 4]

[67] A.D. Dolgov and A.D. Linde. Baryon asymmetry in the inflationary universe. *Physics Letters B*, 116(5):329–334, October 1982. [Cited in 1.2.4-a]

[68] Jennie H. Traschen and Robert H. Brandenberger. Particle production during out-of-equilibrium phase transitions. *Physical Review D*, 42(8):2491–2504, October 1990. [Cited in 1.2.4-a]

[69] Andreas Albrecht, Paul J. Steinhardt, Michael S. Turner, and Frank Wilczek. Reheating an Inflationary Universe. *Physical Review Letters*, 48(20):1437–1440, May 1982. [Cited in 1.2.4-a]

[70] Mustafa A. Amin, Mark P. Hertzberg, David I. Kaiser, and Johanna Karouby. Nonperturbative Dynamics Of Reheating After Inflation: A Review. *International Journal of Modern Physics D*, 24(01):1530003, January 2015. [Cited in 1.2.4-a]

[71] A. D. Dolgov and D. P. Kirilova. Production of particles by a variable scalar field. *Soviet Journal of Nuclear Physics*, 51:172–177, January 1990. [Cited in 1.2.4-a]

[72] Lev Kofman, Andrei Linde, and Alexei A. Starobinsky. Reheating after Inflation. *Physical Review Letters*, 73(24):3195–3198, December 1994. [Cited in 1.2.4-a]

[73] Lev Kofman, Andrei Linde, and Alexei Starobinsky. Towards the Theory of Reheating After Inflation. *Physical Review D*, 56(6):3258–3295, September 1997. [Cited in 1.2.4-a, 1.2.4-b, and 1.2.4-b]

[74] Ivana Kovacic, Richard Rand, and Si Mohamed Sah. Mathieu's Equation and Its Generalizations: Overview of Stability Charts and Their Features. *Applied Mechanics Reviews*, 70(2):020802, March 2018. [Cited in 1.2.4-b and 3.3.3-a]

[75] Julian Schwinger. On Gauge Invariance and Vacuum Polarization. *Physical Review*, 82(5):664–679, June 1951. [Cited in 1.2.4-b]

[76] S. W. Hawking. Black hole explosions? *Nature*, 248(5443):30–31, March 1974. [Cited in 1.2.4-b and 1.3.1]

[77] S. W. Hawking. Particle creation by black holes. *Communications In Mathematical Physics*, 43(3):199–220, August 1975. [Cited in 1.2.4-b, 1.3.1, 1.3.1, and 13]

[78] W. G. Unruh. Notes on black-hole evaporation. *Physical Review D*, 14(4):870–892, August 1976. [Cited in 1.3.1 and 1.3.1]

[79] R. Abbott, T. D. Abbott, F. Acernese, et al. Population of Merging Compact Binaries Inferred Using Gravitational Waves through GWTC-3. *Physical Review X*, 13(1):011048, March 2023. [Cited in 1.3.1]

[80] Ya. B. Zel'dovich and I. D. Novikov. The Hypothesis of Cores Retarded during Expansion and the Hot Cosmological Model. *Soviet Astronomy*, 10:602, February 1967. [Cited in 13]

[81] B. J. Carr and S. W. Hawking. Black Holes in the Early Universe. *Monthly Notices of the Royal Astronomical Society*, 168(2):399–415, August 1974. [Cited in 13]

[82] CERN Yellow Reports: Monographs. CERN Yellow Reports: Monographs, Vol. 6 (2020): Linac4 design report. page 14MB, September 2020. [Cited in 1.3.1]

[83] J. S. Bell. On the Einstein Podolsky Rosen paradox. *Physics Physique Fizika*, 1(3):195–200, November 1964. [Cited in 1.3.1]

[84] W. G. Unruh. Experimental Black-Hole Evaporation? *Physical Review Letters*, 46(21):1351–1353, May 1981. [Cited in 1.3.1, 1.3.1, 1.3.2, and 1.3.2]

[85] Renaud Parentani. What did we learn from studying acoustic black-holes? *International Journal of Modern Physics A*, 17(20):2721–2725, August 2002. [Cited in 1.3.1 and 1.3.3]

[86] Jerome Martin and Robert H. Brandenberger. The Trans-Planckian Problem of Inflationary Cosmology. *Physical Review D*, 63(12):123501, May 2001. [Cited in 1.3.1]

[87] Jens C. Niemeyer. Inflation with a Planck-scale frequency cutoff. *Physical Review D*, 63(12):123502, May 2001. [Cited in 1.3.1]

[88] J. C. Niemeyer and R. Parentani. Trans-Planckian dispersion and scale-invariance of inflationary perturbations. *Physical Review D*, 64(10):101301, October 2001. [Cited in 1.3.1]

[89] Carlos Barcelo, Stefano Liberati, and Matt Visser. Analogue Gravity. *Living Reviews in Relativity*, 8(1):12, December 2005. [Cited in 1.3.2, 1.3.2, 1.3.2, 1.3.2, and 1.3.3]

[90] Petr O. Fedichev and Uwe R. Fischer. Observer dependence for the phonon content of the sound field living on the effective curved space-time background of a Bose-Einstein condensate. *Physical Review D*, 69(6):064021, March 2004. [Cited in 1.3.2 and 1.3.4-a]

[91] M. J. Jacquet, S. Weinfurtner, and F. König. The next generation of analogue gravity experiments. *Philosophical Transactions of the Royal Society A: Mathematical, Physical and Engineering Sciences*, 378(2177):20190239, August 2020. [Cited in 1.3.3]

[92] Carla R. Almeida and Maxime J. Jacquet. Analogue gravity and the Hawking effect: Historical perspective and literature review, December 2022. [Cited in 1.3.3]

[93] W. G. Unruh. Sonic analogue of black holes and the effects of high frequencies on black hole evaporation. *Physical Review D*, 51(6):2827–2838, March 1995. [Cited in 1.3.3]

[94] R. Brout, S. Massar, R. Parentani, and Ph. Spindel. Hawking radiation without trans-Planckian frequencies. *Physical Review D*, 52(8):4559–4568, October 1995. [Cited in 1.3.3]

[95] Ted Jacobson. Trans-Planckian redshifts and the substance of the space-time river. *Progress of Theoretical Physics Supplement*, 136:1–17, 1999. [Cited in 1.3.3]

[96] G. E. Volovik. Simulation of Quantum Field Theory and Gravity in Superfluid He-3. *Low Temperature Physics*, 24(2):127–129, February 1998. [Cited in 1.3.3 and 1.3.4-a]

[97] N. B. Kopnin and G. E. Volovik. Critical velocity and event horizon in pair-correlated systems with "relativistic" fermionic quasiparticles. *Journal of Experimental and Theoretical Physics Letters*, 67(2):140–145, January 1998. [Cited in 1.3.3]

[98] T. A. Jacobson and G. E. Volovik. Effective spacetime and Hawking radiation from a moving domain wall in a thin film of 3He-A. *Journal of Experimental and Theoretical Physics Letters*, 68(11):874–880, December 1998. [Cited in 1.3.3]

[99] L. J. Garay, J. R. Anglin, J. I. Cirac, and P. Zoller. Sonic Analog of Gravitational Black Holes in Bose-Einstein Condensates. *Physical Review Letters*, 85(22):4643–4647, November 2000. [Cited in 1.3.3]

[100] U. Leonhardt and P. Piwnicki. Relativistic Effects of Light in Moving Media with Extremely Low Group Velocity. *Physical Review Letters*, 84(5):822–825, January 2000. [Cited in 1.3.3]

[101] Ralf Schützhold and William G. Unruh. Hawking Radiation in an Electromagnetic Waveguide? *Physical Review Letters*, 95(3):031301, July 2005. [Cited in 1.3.3]

[102] Ralf Schützhold and William G. Unruh. Gravity wave analogues of black holes. *Physical Review D*, 66(4):044019, August 2002. [Cited in 1.3.3]

[103] Thomas G. Philbin, Chris Kuklewicz, Scott Robertson, et al. Fiber-Optical Analog of the Event Horizon. *Science*, 319(5868):1367–1370, March 2008. [Cited in 1.3.3]

[104] Germain Rousseaux, Christian Mathis, Philippe Maïssa, et al. Observation of negative-frequency waves in a water tank: A classical analogue to the Hawking effect? *New Journal of Physics*, 10(5):053015, May 2008. [Cited in 1.3.3]

[105] Jonathan Drori, Yuval Rosenberg, David Bermudez, et al. Observation of Stimulated Hawking Radiation in an Optical Analogue. *Physical Review Letters*, 122(1):010404, January 2019. [Cited in 1.3.3]

[106] Silke Weinfurtner, Edmund W. Tedford, Matthew C. J. Penrice, et al. Measurement of stimulated Hawking emission in an analogue system. *Physical Review Letters*, 106(2):021302, January 2011. [Cited in 1.3.3]

[107] L.-P. Euvé, F. Michel, R. Parentani, et al. Observation of Noise Correlated by the Hawking Effect in a Water Tank. *Physical Review Letters*, 117(12):121301, September 2016. [Cited in 1.3.3]

[108] D. Faccio, S. Cacciatori, V. Gorini, et al. Analogue gravity and ultrashort laser pulse filamentation. *EPL (Europhysics Letters)*, 89(3):34004, February 2010. [Cited in 1.3.3]

[109] H. S. Nguyen, D. Gerace, I. Carusotto, et al. Acoustic Black Hole in a Stationary Hydrodynamic Flow of Microcavity Polaritons. *Physical Review Letters*, 114(3):036402, January 2015. [Cited in 1.3.3]

[110] M. Človečko, E. Gažo, M. Kupka, and P. Skyba. Magnonic Analog of Black- and White-Hole Horizons in Superfluid He 3 - B. *Physical Review Letters*, 123(16):161302, October 2019. [Cited in 1.3.3]

[111] Jeff Steinhauer. Observation of quantum Hawking radiation and its entanglement in an analogue black hole. *Nature Physics*, 12(10):959–965, October 2016. [Cited in 1.3.3, 3.3.3-c, and 3.3.3-c]

[112] Juan Ramón Muñoz de Nova, Katrine Golubkov, Victor I. Kolobov, and Jeff Steinhauer. Observation of thermal Hawking radiation and its temperature in an analogue black hole. *Nature*, 569(7758):688–691, May 2019. [Cited in 1.3.3]

[113] Roberto Balbinot, Alessandro Fabbri, Serena Fagnocchi, et al. Nonlocal density correlations as a signature of Hawking radiation from acoustic black holes. *Physical Review A*, 78(2):021603, August 2008. [Cited in 1.3.3]

[114] Elizabeth A. Donley, Neil R. Claussen, Simon L. Cornish, et al. Dynamics of collapsing and exploding Bose-Einstein condensates. *Nature*, 412(6844):295–299, July 2001. [Cited in 1.3.4-a]

[115] Esteban Calzetta and Bei Lok Hu. BEC Collapse, Particle Production and Squeezing of the Vacuum, June 2003. [Cited in 1.3.4-a]

[116] E. Calzetta and B. L. Hu. BEC Collapse and Dynamical Squeezing of Vacuum Fluctuations. *Physical Review A*, 68(4):043625, October 2003. [Cited in 1.3.4-a]

[117] E. A. Calzetta and B. L. Hu. Early Universe Quantum Processes in BEC Collapse Experiments. *International Journal of Theoretical Physics*, 44(10):1691–1704, October 2005. [Cited in 1.3.4-a]

[118] Carlos Barcelo, Stefano Liberati, and Matt Visser. Analogue models for FRW cosmologies. *International Journal of Modern Physics D*, 12(09):1641–1649, October 2003. [Cited in 1.3.4-a]

[119] Carlos Barcelo, Stefano Liberati, and Matt Visser. Probing semiclassical analogue gravity in Bose–Einstein condensates with widely tunable interactions. *Physical Review A*, 68(5):053613, November 2003. [Cited in 1.3.4-a and 1.3.4-b]

[120] Petr O. Fedichev and Uwe R. Fischer. "Cosmological" quasiparticle production in harmonically trapped superfluid gases. *Physical Review A*, 69(3):033602, March 2004. [Cited in 1.3.4-a and 1.3.4-b]

[121] Petr O. Fedichev and Uwe R. Fischer. Gibbons-Hawking Effect in the Sonic de Sitter Space-Time of an Expanding Bose-Einstein-Condensed Gas. *Physical Review Letters*, 91(24):240407, December 2003. [Cited in 1.3.4-a]

[122] Silke E. Ch Weinfurtner. Analog model for an expanding universe. *General Relativity and Gravitation*, 37(9):1549–1554, September 2005. [Cited in 1.3.4-a]

[123] Michael Uhlmann, Yan Xu, and Ralf Schützhold. Aspects of cosmic inflation in expanding Bose–Einstein condensates. *New Journal of Physics*, 7:248–248, November 2005. [Cited in 1.3.4-a]

[124] Uwe Fischer and Ralf Schützhold. Quantum simulation of cosmic inflation in two-component Bose-Einstein condensates. *Physical Review A*, 70(6):063615, December 2004. [Cited in 1.3.4-a]

[125] Piyush Jain, Silke Weinfurtner, Matt Visser, and C. W. Gardiner. Analogue model of a FRW universe in Bose-Einstein condensates: Application of the classical field method. *Physical Review A*, 76(3):033616, September 2007. [Cited in 1.3.4-a]

[126] Mathias Van Regemortel, Wim Casteels, Iacopo Carusotto, and Michiel Wouters. Spontaneous Beliaev-Landau scattering out of equilibrium. *Physical Review A*, 96(5):053854, November 2017. [Cited in 1.3.4-a and 3.5.1-a]

[127] Silke Weinfurtner, Piyush Jain, Matt Visser, and C. W. Gardiner. Cosmological particle production in emergent rainbow spacetimes. *Classical and Quantum Gravity*, 26(6):065012, March 2009. [Cited in 1.3.4-a]

[128] Paul M. Alsing, Jonathan P. Dowling, and G. J. Milburn. Ion Trap Simulations of Quantum Fields in an Expanding Universe. *Physical Review Letters*, 94(22):220401, June 2005. [Cited in 1.3.4-a]

[129] Ralf Schützhold, Michael Uhlmann, Lutz Petersen, et al. Analogue of Cosmological Particle Creation in an Ion Trap. *Physical Review Letters*, 99(20):201301, November 2007. [Cited in 1.3.4-a]

[130] J.-C. Jaskula, G. B. Partridge, M. Bonneau, et al. Acoustic Analog to the Dynamical Casimir Effect in a Bose-Einstein Condensate. *Physical Review Letters*, 109(22):220401, November 2012. [Cited in 1.3.4-b, 1.3.4-c, 2.4, 3.1, 3.2, 3.2, 1, 3.1, 3.3.2, 3.3.2, 3.3.2-a, 3.3.2-a, 3.3, 3.3.3-a, 3.3.3-b, 3.3.3-b, 3.3.3-c, 3.3.3-c, 3.3.4-c, 3.5, 3.5.1-b, 3.5.1-c, 3.5.2-e, 3.6, 3.6.1, and 4]

[131] I. Carusotto, R. Balbinot, A. Fabbri, and A. Recati. Density correlations and analog dynamical Casimir emission of Bogoliubov phonons in modulated atomic Bose-Einstein condensates. *The European Physical Journal D*, 56(3):391–404, February 2010. [Cited in 1.3.4-b]

[132] Xavier Busch, Renaud Parentani, and Scott Robertson. Quantum entanglement due to modulated Dynamical Casimir Effect. *Physical Review A*, 89(6):063606, June 2014. [Cited in 1.3.4-b, 1.3.4-c, 3.1, 3.2, 3.3.2-d, 3.3.3-a, 3.3.3-b, 3.3.3-b, 3.3.3-b, 3.3.3-b, 3.3.3-b, 4, 3.6, 3.6.1, and 4]

[133] Scott Robertson, Florent Michel, and Renaud Parentani. Nonlinearities induced by parametric resonance in effectively 1D atomic Bose condensates. *Physical Review D*, 98(5):056003, September 2018. [Cited in 1.3.4-b, 3.1, 3.2, 3.3.2, 3.3.2-a, 3.3.2-a, 3.3.2-b, 3.3.3-b, 3.3.3-c, 3.5.1-c, 3.5.1-c, 3.5.1-d, 3.5.3-b, 3.5.4, and 4]

[134] Chen-Lung Hung, Victor Gurarie, and Cheng Chin. From Cosmology to Cold Atoms: Observation of Sakharov Oscillations in a Quenched Atomic Superfluid. *Science*, 341(6151):1213–1215, September 2013. [Cited in 1.3.4-b]

[135] A. D. Sakharov. The Initial Stage of an Expanding Universe and the Appearance of a Nonuniform Distribution of Matter. *Soviet Journal of Experimental and Theoretical Physics*, 22:241, January 1966. [Cited in 1.3.4-b]

[136] Leonid P Grishchuk. Cosmological Sakharov oscillations and quantum mechanics of the early Universe. *Physics-Uspekhi*, 55(2):210–216, February 2012. [Cited in 1.3.4-b]

[137] Cheng-An Chen, Sergei Khlebnikov, and Chen-Lung Hung. Observation of Quasiparticle Pair Production and Quantum Entanglement in Atomic Quantum Gases Quenched to an Attractive Interaction. *Physical Review Letters*, 127(6):060404, August 2021. [Cited in 1.3.4-b]

[138] S. Eckel, A. Kumar, T. Jacobson, et al. A Rapidly Expanding Bose-Einstein Condensate: An Expanding Universe in the Lab. *Physical Review X*, 8(2):021021, April 2018. [Cited in 1.3.4-b and 3.3.3-a]

[139] Stephen Eckel and Theodore Jacobson. Phonon redshift and Hubble friction in an expanding BEC. *SciPost Physics*, 10(3):064, March 2021. [Cited in 1.3.4-b]

[140] S. Banik, M. Gutierrez Galan, H. Sosa-Martinez, et al. Accurate Determination of Hubble Attenuation and Amplification in Expanding and Contracting Cold-Atom Universes. *Physical Review Letters*, 128(9):090401, February 2022. [Cited in 1.3.4-b]

[141] Celia Viermann, Marius Sparn, Nikolas Liebster, et al. Quantum field simulator for dynamics in curved spacetime. *arXiv:2202.10399*, February 2022. [Cited in 1.3.4-b and 3.3.2-b]

[142] Pisin Chen and Gerard Mourou. Accelerating Plasma Mirrors to Investigate the Black Hole Information Loss Paradox. *Physical Review Letters*, 118(4):045001, January 2017. [Cited in 1.3.4-b]

[143] Matthias Wittemer, Frederick Hakelberg, Philip Kiefer, et al. Phonon Pair Creation by Inflating Quantum Fluctuations in an Ion Trap. *Physical Review Letters*, 123(18):180502, October 2019. [Cited in 1.3.4-b]

[144] Jeff Steinhauer, Murad Abuzarli, Tangui Aladjidi, et al. Analogue cosmological particle creation in an ultracold quantum fluid of light. *Nature Communications*, 13(1):2890, May 2022. [Cited in 1.3.4-b]

[145] Vitor S. Barroso, August Geelmuyden, Zack Fifer, et al. Primary thermalisation mechanism of Early Universe observed from Faraday-wave scattering on liquid-liquid interfaces. *arXiv:2207.02199*, July 2022. [Cited in 1.3.4-b, 1.3.4-c, 3.3.3-a, and 4]

[146] T. V. Zache, V. Kasper, and J. Berges. Inflationary preheating dynamics with two-species condensates. *Physical Review A*, 95(6):063629, June 2017. [Cited in 1.3.4-c, 3.3.3-a, and 4]

[147] Aleksandr Chatrchyan, Kevin T. Geier, Markus K. Oberthaler, et al. Analog cosmological reheating in an ultracold Bose gas. *Physical Review A*, 104(2):023302, August 2021. [Cited in 1.3.4-c]

[148] Salvatore Butera and Iacopo Carusotto. Numerical studies of back-reaction effects in an analog model of cosmological pre-heating. *arXiv:2207.00311*, July 2022. [Cited in 1.3.4-c and 4]

[149] Ke Wang, Han Fu, and K. Levin. Simulating Cosmological Evolution by Quantum Quench of an Atomic BEC, April 2023. [Cited in 1.3.4-c]

[150] L. P. Grishchuk and Y. V. Sidorov. Squeezed quantum states of relic gravitons and primordial density fluctuations. *Physical Review D*, 42(10):3413–3421, November 1990. [Cited in 2.2]

[151] Ivan Agullo, Béatrice Bonga, and Patricia Ribes Metidieri. Does inflation squeeze cosmological perturbations? *arXiv:2203.07066*, March 2022. [Cited in 2.2]

[152] Tomislav Prokopec and Gerasimos I Rigopoulos. Decoherence from isocurvature perturbations in inflation. *Journal of Cosmology and Astroparticle Physics*, 2007(11):029–029, November 2007. [Cited in 2.2]

[153] Julian Adamek, Xavier Busch, and Renaud Parentani. Dissipative fields in de Sitter and black hole spacetimes: Quantum entanglement due to pair production and dissipation. *Physical Review D*, 87(12):124039, June 2013. [Cited in 2.2, 2.3, and 4]

[154] Jérôme Martin and Vincent Vennin. Quantum discord of cosmic inflation: Can we show that CMB anisotropies are of quantum-mechanical origin? *Physical Review D*, 93(2):023505, January 2016. [Cited in 2.3]

[155] Xavier Busch and Renaud Parentani. Dynamical Casimir effect in dissipative media: When is the final state nonseparable? *Physical Review D*, 88(4):045023, August 2013. [Cited in 3.1, 3.2, and 3.3.2-d]

[156] Scott Robertson, Florent Michel, and Renaud Parentani. Controlling and observing nonseparability of phonons created in time-dependent 1D atomic Bose condensates. *Physical Review D*, 95(6):065020, March 2017. [Cited in 3.1, 3.2, 3.3.2-a, 3.3.2-a, 3.3.2-a, 3.3.2-b, 3.3.2-b, 3.3.3-c, and 3.3.3-c]

[157] Scott Robertson, Florent Michel, and Renaud Parentani. Assessing degrees of entanglement of phonon states in atomic Bose gases through the measurement of commuting observables. *Physical Review D*, 96(4):045012, August 2017. [Cited in 3.1, 3.2, 3.3.2-a, 3.3.3-c, and 3.3.3-c]

[158] Gerald T. Moore. Quantum Theory of the Electromagnetic Field in a Variable-Length One-Dimensional Cavity. *Journal of Mathematical Physics*, 11(9):2679–2691, September 1970. [Cited in 3.2]

[159] Bryce S. DeWitt. Quantum field theory in curved spacetime. *Physics Reports*, 19(6):295–357, August 1975. [Cited in 3.2]

[160] S. A. Fulling and P. C. W. Davies. Radiation from a Moving Mirror in Two Dimensional Space-Time: Conformal Anomaly. *Proceedings of the Royal Society of London. Series A, Mathematical and Physical Sciences*, 348(1654):393–414, 1976. [Cited in 3.2]

[161] L. Parker. Particle Creation in Expanding Universes. *Physical Review Letters*, 21(8):562–564, August 1968. [Cited in 3.2]

[162] C. M. Wilson, G. Johansson, A. Pourkabirian, et al. Observation of the dynamical Casimir effect in a superconducting circuit. *Nature*, 479(7373):376–379, November 2011. [Cited in 3.2]

[163] Pasi Lähteenmäki, G. S. Paraoanu, Juha Hassel, and Pertti J. Hakonen. Dynamical Casimir effect in a Josephson metamaterial. *Proceedings of the National Academy of Sciences*, 110(11):4234–4238, March 2013. [Cited in 3.2 and 3.2]

[164] Stefano Vezzoli, Arnaud Mussot, Niclas Westerberg, et al. Optical analogue of the dynamical Casimir effect in a dispersion-oscillating fibre. *Communications Physics*, 2(1):84, July 2019. [Cited in 3.2 and 3.2]

[165] P. Engels, C. Atherton, and M. A. Hoefer. Observation of Faraday Waves in a Bose-Einstein Condensate. *Physical Review Letters*, 98(9):095301, February 2007. [Cited in 3.2]

[166] L. P. Pitaevskiĭ and S. Stringari. *Bose-Einstein Condensation*. Number 116 in Oxford Science Publications. Clarendon Press, Oxford ; New York, 2003. [Cited in 3.3.1, 3.3.1, 3.3.1, 3.3.2, 3.3.2-c, 3.3.2-c, 3.3.2-c, 3.3.4-a, 3.3.4-c, and 3.3.4-c]

[167] F. D. M. Haldane. Effective Harmonic-Fluid Approach to Low-Energy Properties of One-Dimensional Quantum Fluids. *Physical Review Letters*, 47(25):1840–1843, December 1981. [Cited in 3.3.1]

[168] Christophe Mora and Yvan Castin. Extension of Bogoliubov theory to quasicondensates. *Physical Review A*, 67(5):053615, May 2003. [Cited in 3.3.1, 3.3.4-b, 3.3.4-b, 3.3.4-c, 6, 3.5.1-a, and 3.5.1-b]

[169] E. Madelung. Eine anschauliche Deutung der Gleichung von Schrödinger. *Die Naturwissenschaften*, 14(45):1004–1004, November 1926. [Cited in 3.3.1]

[170] D. S. Petrov, D. M. Gangardt, and G. V. Shlyapnikov. Low-dimensional trapped gases. *Journal de Physique IV (Proceedings)*, 116:5–44, October 2004. [Cited in 3.3.1, 3.3.2, 3.3.2, and 3.5.1-b]

[171] S. Moal, M. Portier, J. Kim, et al. Accurate Determination of the Scattering Length of Metastable Helium Atoms Using Dark Resonances between Atoms and Exotic Molecules. *Physical Review Letters*, 96(2):023203, January 2006. [Cited in 3.3.2]

[172] Elliott H. Lieb and Werner Liniger. Exact Analysis of an Interacting Bose Gas. I. The General Solution and the Ground State. *Physical Review*, 130(4):1605–1616, May 1963. [Cited in 3.3.2]

[173] M. Olshanii. Atomic Scattering in the Presence of an External Confinement and a Gas of Impenetrable Bosons. *Physical Review Letters*, 81(5):938–941, August 1998. [Cited in 3.3.2]

[174] F Gerbier. Quasi-1D Bose-Einstein condensates in the dimensional crossover regime. *Europhysics Letters (EPL)*, 66(6):771–777, June 2004. [Cited in 3.3.2-a]

[175] Yu. Kagan, E. L. Surkov, and G. V. Shlyapnikov. Evolution of a Bose-condensed gas under variations of the confining potential. *Physical Review A*, 54(3):R1753–R1756, September 1996. [Cited in 3.3.2-a]

[176] James E. Lidsey. Cosmic Dynamics of Bose-Einstein Condensates. *Classical and Quantum Gravity*, 21(4):777–785, February 2004. [Cited in 3.3.2-a]

[177] P.G.L. Leach and S.K. Andriopoulos. The Ermakov equation: A commentary. *Applicable Analysis and Discrete Mathematics*, 2(2):146–157, 2008. [Cited in 3.3.2-a]

[178] D E Bruschi, N Friis, I Fuentes, and S Weinfurtner. On the robustness of entanglement in analogue gravity systems. *New Journal of Physics*, 15(11):113016, November 2013. [Cited in 3.3.2-d]

[179] Xavier Busch, Iacopo Carusotto, and Renaud Parentani. Spectrum and entanglement of phonons in quantum fluids of light. *Physical Review A*, 89(4):043819, April 2014. [Cited in 3.3.3-a]

[180] David Campo and Renaud Parentani. Inflationary spectra and partially decohered distributions. *Physical Review D*, 72(4):045015, August 2005. [Cited in 3.3.3-b]

[181] V. Zanchin, A. Maia Jr., W. Craig, and R. Brandenberger. Reheating in the Presence of Noise. *Physical Review D*, 57(8):4651–4662, April 1998. [Cited in 3.3.3-b and 4]

[182] V. Zanchin, A. Maia Jr., W. Craig, and R. Brandenberger. Reheating in the Presence of Inhomogeneous Noise. *Physical Review D*, 60(2):023505, June 1999. [Cited in 3.3.3-b and 4]

[183] Matthew P. DeCross, David I. Kaiser, Anirudh Prabhu, et al. Preheating after multifield inflation with nonminimal couplings, II: Resonance Structure. *Physical Review D*, 97(2):023527, January 2018. [Cited in 3.3.3-b and 4]

[184] Andreas Finke, Piyush Jain, and Silke Weinfurtner. On the observation of nonclassical excitations in Bose-Einstein condensates. *New Journal of Physics*, 18(11):113017, November 2016. [Cited in 3.3.3-c]

[185] P. C. Hohenberg. Existence of Long-Range Order in One and Two Dimensions. *Physical Review*, 158(2):383–386, June 1967. [Cited in 3.3.4-a]

[186] M. J. Steel, M. K. Olsen, L. I. Plimak, et al. Dynamical quantum noise in trapped Bose-Einstein condensates. *Physical Review A*, 58(6):4824–4835, December 1998. [Cited in 3.5]

[187] Alice Sinatra, Carlos Lobo, and Yvan Castin. The truncated Wigner method for Bose condensed gases: Limits of validity and applications. *Journal of Physics B: Atomic, Molecular and Optical Physics*, 35(17):3599–3631, September 2002. [Cited in 3.5]

[188] Anatoli Polkovnikov. Phase space representation of quantum dynamics. *Annals of Physics*, 325(8):1790–1852, August 2010. [Cited in 3.5]

[189] C. W. Gardiner and P. Zoller. *Quantum Noise: A Handbook of Markovian and Non-Markovian Quantum Stochastic Methods with Applications to Quantum Optics*. Springer Series in Synergetics. Springer, Berlin ; New York, 3rd ed edition, 2004. [Cited in 3.5.1-b]

[190] J. Ruostekoski and A. D. Martin. Truncated Wigner method for Bose gases, September 2012. [Cited in 3.5.1-b]

[191] G. P. Agrawal. *Nonlinear Fiber Optics*. Elsevier/Academic Press, Amsterdam, fifth edition edition, 2013. [Cited in 3.5.2-a]

[192] David Campo and Renaud Parentani. Decoherence and entropy of primordial fluctuations. I. Formalism and interpretation. *Physical Review D*, 78(6):065044, September 2008. [Cited in 3.5.3-b]

[193] David Campo and Renaud Parentani. Inflationary spectra and violations of Bell inequalities. *Physical Review D*, 74(2):025001, July 2006. [Cited in 4]

[194] C. P. Burgess, R. Holman, Greg Kaplanek, et al. Minimal decoherence from inflation, November 2022. [Cited in 4 and 4]

[195] Sugumi Kanno, Jiro Soda, and Junsei Tokuda. Noise and decoherence induced by gravitons. *Physical Review D*, 103(4):044017, February 2021. [Cited in 4]

[196] Maulik Parikh, Frank Wilczek, and George Zahariade. Signatures of the Quantization of Gravity at Gravitational Wave Detectors. *Physical Review D*, 104(4):046021, August 2021. [Cited in 4]

[197] Sugumi Kanno, Jiro Soda, and Junsei Tokuda. Indirect detection of gravitons through quantum entanglement. *Physical Review D*, 104(8):083516, October 2021. [Cited in 4]

[198] Chiara Caprini and Daniel G. Figueroa. Cosmological Backgrounds of Gravitational Waves. *Classical and Quantum Gravity*, 35(16):163001, August 2018. [Cited in 4]

[199] Jerome Martin and Vincent Vennin. Real-space entanglement in the Cosmic Microwave Background. *Journal of Cosmology and Astroparticle Physics*, 2021(10):036, October 2021. [Cited in 4]

[200] Jerome Martin and Vincent Vennin. Real-space entanglement of quantum fields. *Physical Review D*, 104(8):085012, October 2021. [Cited in 4]

[201] Llorenç Espinosa-Portalés and Vincent Vennin. Real-space Bell inequalities in de Sitter. *Journal of Cosmology and Astroparticle Physics*, 2022(07):037, July 2022. [Cited in 4]

[202] Daniel Green and Rafael A. Porto. Signals of a Quantum Universe. *Physical Review Letters*, 124(25):251302, June 2020. [Cited in 4]

[203] Ryszard Horodecki, Paweł Horodecki, Michał Horodecki, and Karol Horodecki. Quantum entanglement. *Reviews of Modern Physics*, 81(2):865–942, June 2009. [Cited in 4]

[204] Thomas P. Sotiriou. F(R) Gravity and scalar-tensor theory. *Classical and Quantum Gravity*, 23(17):5117–5128, September 2006. [Cited in B.2-a]